Doctoral Dissertations   Graduate School

12-2013

Development of a Monitoring Framework for the Detection of Diversion of Intermediate Products in a Generic Natural Uranium Conversion Plant

Jennifer L. Ladd-Lively
University of Tennessee - Knoxville, Jladdche@yahoo.com

To the Graduate Council:

I am submitting herewith a dissertation written by Jennifer L. Ladd-Lively entitled "Development of a Monitoring Framework for the Detection of Diversion of Intermediate Products in a Generic Natural Uranium Conversion Plant." I have examined the final electronic copy of this dissertation for form and content and recommend that it be accepted in partial fulfillment of the requirements for the degree of Doctor of Philosophy, with a major in Chemical Engineering.

Tse-Wei Wang, Major Professor

We have read this dissertation and recommend its acceptance:

Robert M. Counce, Alan Icenhour, Paul Frymier, John Begovich

Accepted for the Council:

Carolyn R. Hodges

Vice Provost and Dean of the Graduate School

(Original signatures are on file with official student records.)

Development of a Monitoring Framework for the Detection of Diversion of Intermediate Products in a Generic Natural Uranium Conversion Plant

A Dissertation Presented for the
Doctor of Philosophy
Degree
The University of Tennessee, Knoxville

Jennifer L. Ladd-Lively
December 2013

ACKNOWLEDGEMENTS

ABSTRACT

The objective of this work is the development of an on-line monitoring and data analysis framework that could detect the diversion of intermediate products such as uranium dioxide, uranium tetrafluoride, and uranium hexafluoride in a natural uranium conversion plant (NUCP) using a multivariate statistical approach. This was an initial effort to determine the feasibility of this approach for safeguards applications. This study was limited to a 100 metric ton of uranium (MTU) per year NUCP using the wet solvent extraction method for the purification of uranium ore concentrate. A key component in the multivariate statistical methodology was the Principal Component Analysis (PCA) approach for the analysis of data, development of the base model, and evaluation of future operations. The PCA approach was implemented through the use of singular value decomposition of the data matrix. Component mole balances were used to model each of the process units in the NUCP. The decision framework developed in this research could be used to determine whether or not a diversion of material has occurred at an NUCP as part of an International Atomic Energy Agency (IAEA) safeguards system. The IAEA goal for NUCPs of this size is to have a 50% probability of detecting the diversion of 10 MTU over a period of one year; this was also used as the goal of detection for the monitoring framework. An initial sensitivity analysis was also performed on the relationship between the component molar flow rates (state variables) and the process parameters. This sensitivity study identified a few parameters to which some of the state variables were highly sensitive. Several faulty scenarios were developed to test the monitoring framework after the base case or "normal operating conditions" of the PCA model was established. In nearly all of the scenarios, the monitoring framework was able to detect the fault. The detection limit varied depending on the scenario, but it satisfied the limit stated above in nearly of the all cases. For the cases that the goal was not achieved, additional scaling may be able to lower the detection limit to satisfy the goal. Overall this study was successful at meeting the stated objective.

TABLE OF CONTENTS

LIST OF FIGURES

LIST OF TABLES

ABREVIATIONS AND SYMBOLS

ADU	ammonium diuranate
AUC	ammonium uranyl carbonate
CO_2	carbon dioxide
DBP	dibutyl phosphate
DOE	U.S. Department of Energy
EMIS	electromagnetic isotope separation
F_2	fluorine gas
HF	hydrogen fluoride
IAEA	International Atomic Energy Agency
INMM	Institute of Nuclear Materials Management
KOH	potassium hydroxide
MBP	mono-butyl phosphate
MSPC	multivariate statistical process control
MT	metric ton
MTU/yr	metric ton of uranium per year
NH_3	ammonia
$(NH_4)HCO_3$	ammonium bicarbonate
$(NH_4)_2U_2O_7$	ammonium diuranate
$(NH_4)_4UO_2(CO_3)_3$	ammonium uranyl carbonate
NUCP	natural uranium conversion plant
ORNL	Oak Ridge National Laboratory
PCA	Principal Component Analysis

PC	principal component
PLS	Partial Least Squares
SPC	statistical process control
SPE	squared prediction error
SQ	Significant Quantity
SVD	singular value decomposition
TBP	tributyl phosphate
UF_4	uranium tetrafluoride
UF_6	uranium hexafluoride
UOC	uranium ore concentrate
UO_2	uranium dioxide
$UO_2(NO_3)_2$	uranyl nitrate (UN)
UO_3	uranium trioxide
UO_4	uranyl peroxide
U_3O_8	triuranium octoxide
Xss	steady-state value of a state variable

1. INTRODUCTION

The objective of this work is the development of an on-line monitoring and data analysis framework that would be capable of detecting the diversion or introduction of intermediate products [e.g., uranium dioxide (UO_2), uranium tetrafluoride (UF_4), and uranium hexafluoride (UF_6)] in a natural uranium conversion plant (NUCP) using a multivariate statistical approach. The decision framework developed in this research could be used to determine whether or not a diversion of material has occurred at an NUCP. This monitoring framework can be used by the International Atomic Energy Agency (IAEA) in a safeguards system. This study was developed for a 100 metric ton of uranium per year (MTU/yr) NUCP using the wet solvent extraction method for the purification of uranium ore concentrate.

1.1 BACKGROUND AND MOTIVATION

This section provides the background necessary to understand the motivation of the research discussed in this dissertation. Included in this section is a brief overview of the nuclear fuel cycle, methods for the conversion of uranium ore concentrate to uranium hexafluoride, and the current IAEA safeguards policy for natural uranium conversion plants.

1.1.1 Overview of the Nuclear Fuel Cycle

The work discussed here applies to the upstream conversion process of the nuclear fuel cycle of which the final product is UF_6. A short overview of the nuclear fuel cycle is provided to describe where in the cycle conversion takes place.

The nuclear fuel cycle is a series of industrial processes in which uranium is recovered from the earth for use in nuclear reactors for power production or for the production of nuclear weapons. The activities associated with the nuclear fuel cycle (Figure 1.1) include: uranium mining and milling, conversion of triuranium octoxide (U_3O_8) to gaseous uranium hexafluoride (UF_6), enrichment in the ^{235}U isotope, fuel fabrication, energy production at power reactors, spent fuel storage, and finally direct disposal or reprocessing and recycling of the spent fuel. The nuclear fuel cycle is well known and discussed in detail by Benedict, Pigford, and Levi 1981; Cochran and Tsoulfanidis 1990; and Moghissi, Godbee, and Hobert 1992.

Figure 1.1. The Nuclear Fuel Cycle. The step where safeguarding is being discussed here is the 'Conversion' process. (Source: International Atomic Energy Agency (IAEA), http://www.iaea.org/OurWork/ST/NE/NEFW/Technical_Areas/NFC/home.html).

1.1.2 Methods of Converting Uranium Ore to Uranium Hexafluoride

The uranium oxide product of the uranium mining and milling process is not directly usable for enrichment or fuel fabrication and must undergo additional processing. Conversion plants purify the uranium ore received from the mining and milling operation of the nuclear fuel cycle and then convert it to a gaseous form prior to shipment to an enrichment plant. According to the IAEA Nuclear Fuel Cycle Information System (http://www-nfcis.iaea.org), operating conversion plants are located worldwide with a total estimated design capacity of ~175,000 MTU/yr. The actual production rate is less than half the design capacity which supports more than 400 nuclear power plants. Conversion plants can be classified into three categories based on production capacity: small (100 MTU/yr), medium (1,000 MTU/yr), or large (10,000 MTU/yr). These plants use some variation of the two processes discussed in this section. The work reported here is focused specifically on a 100 MTU/yr NUCP using the wet solvent extraction process.

The following is a review of common conversion methods used in various NUCPs. Moghissi, Godbee, and Hobert 1992 states that the reason for conversion is "uranium concentrate from milling operations is free of the bulk of the ore components, but is still far from pure enough for use in fuel." The uranium ore concentrate (UOC) from the mining and milling operation contains at least 75% U_3O_8. The UOC becomes the feed material to a conversion plant. At the conversion plant the UOC is submitted to a series of operations which remove impurities and eventually convert the U_3O_8 to gaseous UF_6 which is then in the necessary form for subsequent isotopic enrichment by the gaseous diffusion or gas centrifuge process (Moghissi, Godbee, and Hobert 1992). Two methods are available for purification from the uranium ore concentrate (dry hydrofluor process or wet solvent extraction process). The wet solvent extraction method is the most common method and will be discussed below.

The wet process uses solvent extraction to purify the U_3O_8 feed material before eventual conversion to UF_6. This method separates impurities by preferentially extracting the uranium into an organic solvent, leaving other constituents in the aqueous phase. The method generally consists of the following operations:

a) Preprocess handling, weighing, sampling, and storage;
b) Digestion in hot nitric acid;
c) Countercurrent solvent extraction with tributyl phosphate (TBP) in kerosene;
d) Reextraction of uranium as uranyl nitrate solution [$UO_2(NO_3)_2$];
e) Calcination to uranium trioxide (UO_3), precipitation of ammonium diuranate (ADU), or precipitation of ammonium uranyl carbonate (AUC);
f) Fluidized-bed reduction with hydrogen from cracked ammonia to UO_2;
g) Fluidized-bed hydrofluorination in a two-stage countercurrent reactor to form UF_4 using anhydrous hydrogen fluoride (HF); and

h) Flame reactor fluorination to UF_6 by reaction with fluorine gas (F_2) (Moghissi, Godbee, and Hobert 1992).

The actual wet conversion method employed by an NUCP is based on the size of the plant. Figure 1.2 shows a simplified flow diagram of the conversion process; the left side represents the processing steps most frequently used in small-scale chemical conversion plants while the right side shows the processes used in medium and large plants. A generic production process for natural uranium conversion using the wet method begins with yellowcake dissolution with nitric acid, followed by purification using solvent extraction techniques, and then evaporation to produce a concentrated, purified uranyl nitrate solution. For small plants, ammonia or ammonium hydroxide/carbon dioxide are used to convert uranyl nitrate to a precipitate of ADU or AUC, respectively. After precipitation, calcination in the presence of hydrogen produces UO_2 powder. Precipitation processes can be operated in a continuous mode, but are well suited to batch production techniques typical of small-scale plants. Medium and large plants typically utilize a denitration process which is more commonly used in continuous operations where higher production capabilities are required. The denitration process uses heat to dehydrate and denitrate the purified uranyl nitrate solution and produce UO_3, followed by oxide reduction with hydrogen to produce UO_2. Then irrespective of the size of the plant, the UO_2 is hydrofluorinated to UF_4 using HF. The UF_4 can then be fluorinated into UF_6 using F_2. However, the UF_4 can also be reduced to uranium metal using magnesium or calcium and heat (Faulkner et al. 2004). Additionally, other intermediate materials could be diverted from the process or clandestinely produced and/or obtained material could be substituted into the process. For example, as shown in Figure 1.2, clandestinely produced UF_6 (green arrow) could be fed into the process at the precipitation step or UO_2 from the calcination or oxide reduction steps could be diverted for reactor fuel production.

1.1.3 Current IAEA Safeguards Policy for Conversion Plants

The objective of IAEA safeguards is outlined in paragraph 28 of INFCIRC/153 (corrected) (IAEA 1972).

> The objective of safeguards is the timely detection of diversion of significant quantities of *nuclear material* from peaceful nuclear activities to the manufacture of nuclear weapons or of other nuclear explosive devices or for purposes unknown, and deterrence of such diversion by the risk of early detection.

Operating in accordance with international agreements, the IAEA has had limited ability to monitor the front end of the nuclear fuel cycle because safeguards programs have been constrained to control nuclear materials at the start of the uranium enrichment processes, with UF_6 as its feedstock and designated as the chemical form of interest (Ferrada 2004). Since the final product of an NUCP is UF_6, IAEA accountability data begins at the final step of the NUCP process when the product is declared.
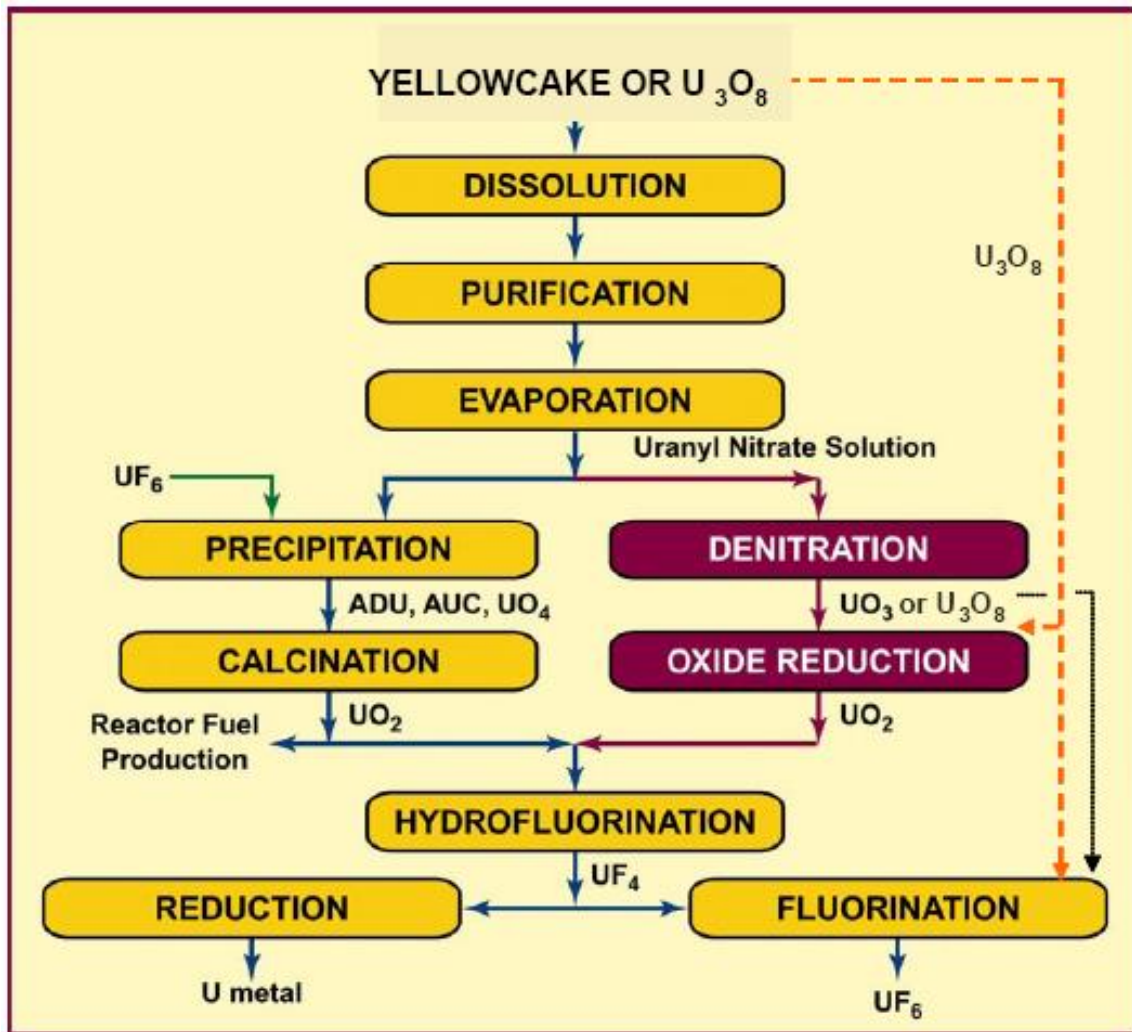
Figure 1.2. Simplified Flow Diagram of the Wet Solvent Extraction Process Used to Convert Yellowcake to UF$_6$ or U Metal. Note that the left side represents the processing steps most frequently used in small-scale chemical conversion plants. (Source: R. L. Faulkner, J. M. Begovich, J. J. Ferrada, R. D. Spence, J. M. Whitaker, W. J. Bicha, and L. G. Loden. 2004. "Oak Ridge Efforts to Enhance Conversion Plant Safeguards." *Proceedings 45th Annual Meeting of Institute of Nuclear Materials Management (INMM)*, July 18–22, 2004, Orlando.)

Without information to ascertain a uranium mass balance between the yellowcake feed stock and the final product, there are no assurances that the declared product was the total possible uranium produced by an NUCP.

Traditionally, only the final product materials (UO_2, UF_6, and U metal) of the NUCPs, and not intermediate materials, have been considered as being materials subject to the full safeguards procedures. However, IAEA policy in this area was recently revised. IAEA now considers all highly purified uranium compounds as candidates for safeguarding which includes the intermediate products of an NUCP (Doo et al. 2003). This revised policy gives the IAEA the possibility of detecting a diversion or undeclared production of nuclear material for clandestine uranium enrichment or plutonium production facilities at the NUCP. The following provides an overview of the current safeguards policy as it applies to NUCPs.

Doo et al. 2003 outlines a new approach developed by the IAEA for safeguards at NUCPs. Current IAEA policy, as stated in paragraph 34(c) of INFCIRC/153 (corrected) (IAEA 1972), considers any purified aqueous uranium solution or any purified uranium oxides to be considered nuclear material of a composition and purity suitable for isotopic enrichment or fuel fabrication, respectively;

> When any *nuclear material* of a composition and purity suitable for fuel fabrication or for being isotopically enriched leaves the plant or the process stage in which it has been produced, or when such *nuclear material*, or any other *nuclear material* produced at a later stage in the nuclear fuel cycle, is imported into the State, the *nuclear material* shall become subject to the other safeguards procedures specified in the Agreement.

Additionally, paragraph 34(c) of INFCIRC/153 (corrected) requires that full safeguards procedures should be applied no later than the first point in the conversion process at which such material leaves the process stage or the plant in which it is produced. This may not be practicable or economical. In such cases, the procedures should be applied at the first practicable point earlier (i.e., "upstream") in the plant which could be as early as the UOC input at the beginning of the conversion process. However, the IAEA has not been consistent with the technical interpretation of this requirement or the implementation of safeguards at NUCPs.

Additional information about IAEA safeguards can be found in "IAEA Safeguards Glossary, 2001 Edition" (IAEA 2002), "Safeguards Techniques and Equipment, 2003 Edition" (IAEA 2003), and "IAEA Safeguards: Staying Ahead of the Game" (IAEA 2007).

1.1.4 Motivation

Due to the revision in IAEA policy for uranium conversion plants, the U.S. Department of Energy (DOE) is interested in developing instruments, tools, strategies, and methods that could be of use to the IAEA in the application of safeguards to the front end of the fuel cycle (Boyer et al. 2004, Faulkner et al. 2004). Some of the DOE studies are discussed in Chapter 2. According to Boyer et al. 2004, DOE's Office of Nonproliferation and International Security is using a systematic approach to identify the functions of a safeguards system needed for NUCPs having a range of throughputs, the safeguards that could be applied, the attractive diversion possibilities, and the effectiveness of the safeguards system.

The work discussed in this dissertation could be applied if on-line process monitoring is utilized for safeguarding uranium conversion plants. Although a simple accounting system for assessing uranium inputs and outputs will provide some assurance that undeclared material is not leaving an NUCP, the use of on-line monitoring instruments can validate accountability data and significantly improve a safeguards program. On-line monitoring methods also offer an effective means for detecting the processing of undeclared materials in a model NUCP. The purpose of on-line monitoring is to determine the uranium flow through a particular process stage.

1.2 PROBLEM STATEMENT AND OBJECTIVES

This section outlines the purpose, the importance, and the scope and limitations of the study.

1.2.1 Purpose of the Study

The objective of this work was to develop an on-line monitoring and data analysis framework that will be capable of detecting the diversion or introduction of intermediate products (e.g., UO_2, UF_4, and UF_6) in an NUCP using a multivariate statistical approach. The intermediate products are of interest for international safeguards because the products are all suitable uranium feed stocks for producing special nuclear materials. Under current safeguards procedures, these intermediate products could supply feed material for virtually any nuclear weapons program without detection by the IAEA, which has not historically begun safeguards until the purified UF_6 product was declared as feed stock for enrichment plants (IAEA 1968). According to Faulkner et al 2004, "The function of a safeguards system at a uranium chemical conversion plant is in general terms to verify that no useful nuclear material is being diverted for use in a nuclear weapons program." The IAEA now considers all highly purified uranium compounds as candidates for safeguarding (Doo et al. 2003).

1.2.2 Importance of the Study

The monitoring and decision framework developed in this research could be used to determine whether or not a diversion or addition of material has occurred at an NUCP. This monitoring framework can be used by the IAEA in a safeguards system. The work reported here can also be used to determine optimum sensor placement to provide the best possible safeguards monitoring system and to determine sensitivity of certain measurements to changes in concentrations of intermediate compounds. The goal of IAEA safeguards is the timely detection of a diversion of a significant quantity (SQ) of nuclear material. For facilities that process only natural uranium, the IAEA has declared that 10 MT of natural uranium is a SQ with a timeliness period of one year and a detection probability of 50%. In other words, the IAEA goal for NUCPs is to have a 50% probability of detecting the diversion of 10 MTU over a period of one year. The detection goal of the monitoring and decision framework reported here was set at 10% of the uranium throughput of the plant (i.e., 10 MTU) based on the IAEA limit discussed above.

Multivariate statistical process monitoring and fault detection approach considers all the process variables simultaneously instead of analyzing individual variables, one at a time. Because all the process variables are correlated, examining and analyzing each process variable behavior over time individually may not indicate a shift and/or a change in its relationship with the behavior of other process variables. A fault may not manifest itself in detectable variations in a few process variables, or in any variable to beyond its normal range of variation, but would often result in the coordinated change in clusters of correlated variables that move together in a certain direction depending on their inter-relationships. The univariate (i.e., one at a time) approach does not reflect the interactions between process variables. It is not possible to develop individual confidence interval for a process variable independent of those for others because of the correlation among them. Monitoring the behavior of one variable at a time most often misses the detection of a fault and the nature of the fault if a fault has been detected in that variable. Multivariate statistical analysis of measured process variables as a whole gives the potential of detection of variation of a process from its 'normal' behavior, thus the detection of a possible fault that has occurred.

1.2.3 Scope and Limitations

This was an initial effort to determine the feasibility of this approach for safeguards. This study was developed for a 100 MTU/yr NUCP using the wet solvent extraction method for the purification of UOC. The data needed for the decision model were obtained from subject matter experts in uranium processing and conversion plant operations. Ideal and steady-state operation was assumed. All intermediate process variables were assumed to be available where required. Principal Component Analysis (PCA) methodology was used to analyze the process data to develop an empirical model; and various multivariate diagnostic plots were developed for monitoring and analysis. In future work, relaxing the requirement of on-line accessibility of all intermediate process variable values will be

investigated. Since all state variables are correlated, only a small subset of the variable values need to be known at all times to provide the necessary operating data for analysis.

The small-sized plant (100 MTU/yr) was selected since a diversion of 10 wt-% uranium throughput is significant. Additionally, medium and large size plants use the denitration method as opposed to precipitation. However, this approach would work no matter the throughput of the model plant. Additionally, this work assumes that the plant was operating continuously and was at steady-state. If the plant is experiencing transient dynamics, one should wait until the operation has reached steady state before monitoring continues. Small-sized plants typically operate in a batch-wise manner but larger plants operate continuously. The throughput was chosen for the detection limit not the operating style. Again, this approach should work on plants with larger throughputs as well. This approach could be applied to any chemical process and is not limited in application to just the natural uranium conversion process.

1.3 ORIGINAL CONTRIBUTIONS

To date, no report of the application of multivariate statistical methodology, such as PCA, in an NUCP operation or as a safeguards monitoring approach has been found in the open literature. Work and results reported here are among the first attempts of this kind.

Multivariate statistical process monitoring and fault detection began to gain attention in the early 1990s. Some recent applications of PCA include process monitoring, fault diagnostics, gross error detection, multivariate statistical process control, data rectification, disturbance detection and isolation, gene expression analysis, facial recognition, signal processing, factor analysis, chemometrics, and chemical processes data analysis (Brauner and Shacham 2000; Valle, Li, and Qin 1999; Bakshi 1998). In chemical engineering, PCA is used to monitor batch and continuous processes to monitor product quality control, missing value replacement, identify and reconstruct sensor and/or process faults, and detect disturbances (Valle, Li, and Qin 1999). PCA is also being applied to nuclear processes (Hines, Upadhyaya, and Henkel 2008) and to nuclear forensics (Robel, Kristo, and Heller 2009).

There have been significant research efforts in safeguarding uranium conversion plants since the change in the IAEA policy. Much of this work has focused on development and placement of instrumentation.

1.4 ORGANIZATION OF DISSERTATION

This work is described in the next four chapters. Chapter two provides a literature survey which includes background information related to process monitoring along with fault and diversion detection, as well as provides additional information on current efforts for safeguarding conversion plants. Chapter two

also presents an overview of PCA, the workhorse of the multivariate statistical method. Additionally, Chapter two provides an overview of previous research related to these fields. Chapter three presents a description of the methodology used to develop and test the monitoring framework. Chapter four presents the detailed results of the development of the base case model with sensitivity analysis. Chapter four also details the results of the monitoring framework's ability to detect the diversion scenarios selected for testing. Chapter five presents the conclusions reached during this research and recommendations for future work.

2. LITERATURE REVIEW

This chapter provides a review of the literature pertinent to this research effort. This section is broken down into three subsections. Each subsection provides an overview of the topic and a review of the historical and current efforts related to that subject area. Since the objective of this work is the development of an on-line monitoring and data analysis framework that would detect the diversion of intermediate products from a natural uranium conversion plant (NUCP) using Principal Component Analysis (PCA), those subsections cover process monitoring and fault detection, safeguards and diversion in conversion plants, and PCA.

2.1 PROCESS MONITORING AND FAULT DETECTION

This section discusses both process monitoring and the use of multivariate statistical process control (MSPC) for fault detection.

MacGregor and Kourti 1995 presented an overview on both traditional and MSPC methods for monitoring and diagnosing process operating performance. MSPC began to gain attention in the early 1990s. As computers continued to increase in power, speed, and storage capacity, process computers were routinely collecting measurements on large numbers of process variables. These data led to the development of multivariate statistical methods for the analysis, monitoring, and diagnosis of process operating performance. Manufacturers used these methods to improve process performance, reduce downtime, and reduce costs. The objective of statistical process control (SPC) is to monitor the performance of a process over time in order to verify that the process is remaining in a state of statistical control. That is when certain process or product variables remain close to the desired values and the only source of variation is the normal variation which affects the process all of the time and is essentially unavoidable within the current process. In the case of this work, that is the base case model which allows for a set amount of variation in the input variables.

SPC charts are used to monitor key product variables in order to detect the occurrence of any event that is "off-normal" or having a "special" or "assignable" cause. "By finding assignable causes, long-term improvements in the process and in product quality can be achieved by eliminating the causes or improving the process or its operating procedures" (MacGregor and Kourti 1995). In most industries, traditional univariate control charts such as Shewhart, CUSUM, and EWMA, are used to separately monitor key measurements on the final product which in some way define the quality of that product. The problem with a univariate approach is that the variables are not independent and any one of them alone cannot adequately define product quality. Product quality is only defined by the correct simultaneous values of all the measured properties and is therefore a multivariate property.

11

PCA is one of the multivariate statistical projection methods presented in MacGregor and Kourti 1995. (The mathematical basis of PCA is presented in Section 2.3.) When the number of measured quality variables is large, then the variables are likely highly correlated with one another and their covariance matrix is nearly singular. A common procedure for reducing the dimensionality of the quality variables is PCA. Most of the variability in the data is captured in the first few principal components, so two or three principal components are often sufficient to explain most of the predictable variations in the product. Multivariate control charts are based on Hotelling's T^2. However, monitoring product quality via T_A^2 based on the first few (A) principal components is not sufficient as this will only detect whether or not the variation in the quality variables represented by the first A principal components is greater than can be explained by normal variation. If a completely new type of fault occurs which was not present in the reference data used to develop the PCA model, then new principal components will appear and the new observations will move off the plane. These new faults can be detected by computing the squared prediction error (SPE) of the residuals of new observations when fitted with the PCA model developed for 'normal' operation. This statistic is also referred to as the Q-statistic or distance to the model, and it represents the squared perpendicular distance of a new multivariate observation from the reference hyperplane. When the process is operating under normal conditions, the value of SPE or Q should be small. Under normal operating conditions, SPE represents unstructured fluctuations (noise) that cannot be accounted for by the model. A high value of SPE means that the projection model is not valid for that observation. Therefore, a very effective set of multivariate control charts is a T^2 chart on the A dominant orthogonal principal components plus a SPE chart. Control limits for both charts are developed from the 'normal' operation data profile.

According to MacGregor and Kourti 1995, traditionally, massive amounts of process data are being collected and stored in databases for most industrial processes, but very little analysis and interpretation of these data are being performed. The lack of analysis is due to the overwhelming size of the databases and the very ill-conditioned nature of the routine operating data being collected. Additionally, the signal-to-noise ratio can be poor in these data, and there are often significant amounts of missing data. However, all of these problems can be addressed by multivariate statistical projection methods, such as PCA. Uranium conversion plants also collect large amounts of routine process data which may or may not be available to IAEA inspectors. If the detection framework developed in this work was extended to be used as part of a monitoring system for safeguards, additional instrumentation would be required to monitor the plant operations.

The main approach of statistical quality control methods developed throughout the statistical literature has been to monitor only product quality data while ignoring all of the data on the process variables. For SPC, both process data and quality data must be considered. There are often hundreds of process variables which are measured much more frequently and usually more accurately than the product quality data. Additionally, any faults that occur will also impact the process data. In the case of this work, product quality could be thought of as the uranium concentration or the uranium assay. The most practical approaches to MSPC appear to be those based on multivariate statistical projection methods

such as PCA and Partial Least Squares (PLS). These methods are ideal for handling the large number of highly correlated and noisy process variable measurements that are being collected by process computers on a routine basis, and these methods can also handle missing data.

MacGregor and Kourti 1995 provided the following overview for monitoring processes using MSPC. Kourti 2002 presents additional information on process analysis techniques and the use of MSPC for fault detection. MacGregor and Kourti 1995 state that an essential part of SPC is to establish multivariate control charts to detect special events or faults and to diagnose possible causes. These are referred to as diagnostic plots in this work. The philosophy used for the univariate or multivariate Shewhart charts can be used for the development of MSPC procedures based on projection methods. This philosophy starts with choosing an appropriate reference set which defines the normal operating conditions for the particular process of interest. Therefore, a PCA model is built based on data collected during normal process operations; any periods containing abnormal variations that one would like to detect in the future are omitted. It is of critical importance to the successful application of this procedure that an appropriate reference set be selected. This work follows the same philosophy; a PCA model was built based on normal operating conditions and was used to test abnormal conditions using the T^2 and SPE charts.

According to Martin, Morris, and Zhang 1996, SPC is a tool for achieving and maintaining product quality. Classical univariate statistical techniques monitor one quality variable at a time and are not appropriate for analyzing process data where variables are highly correlated. This results in minimal information being derived on the interactions between variables which are very important in complex processes. These limitations can be addressed through the application of MSPC. The bases of MSPC are the projection techniques of PCA and projection to latent structures since both approaches are used to reduce the dimensionality of the problem by forming a new set of latent variables (principal components) to obtain an enhanced understanding of the process behavior.

Two types of information are typically monitored on a process: (1) quality measurements (e.g., color, texture, strength, weight, size, moisture content, material properties, etc.) and (2) process information (e.g., temperature, pressure, flow rates, speed, etc.). For this application, these would be the uranium content or assay (quality) and the process information (e.g., temperature, pressure, flow rates, etc.). Only a limited number of quality variables are taken at a much lower frequency compared to the large number of variables that are monitored in process measurements. According to Martin, Morris, and Zhang 1996, "MSPC methods address some of the limitations of univariate monitoring techniques by considering all the data simultaneously and extracting information on the directionality of the process variations, that is the behavior of one variable relative to the others." Projection techniques, such as PCA, allow for the efficient handling of large amounts of monitored process data which includes measurement errors and is ill-conditioned and highly correlated.

PCA reduces the dimensionality of the process data set by defining a series of new variables, called principal components, each of which is a linear combination of the original measured variables and would explain the maximal amount of variability embedded in the data. In other words, PCA defines a few linear combinations which can be used to summarize the data with minimal loss of information. "The primary objectives of PCA are data summarization, classification of variables, outlier detection, early warning of potential malfunctions and 'fingerprinting' for fault identification" (Martin, Morris, and Zhang 1996).

The variables that contribute the most to the individual principal components are determined based on the loadings vectors, or the principal components. Information on the clustering of the samples and the identification of transitions between different operating regimes is obtained from the scores, or the projections of the samples onto the set of principal components.

The scales used to measure the variables are of critical importance to PCA. If a set of data contains measurements of completely different types (e.g., pressures, temperatures, flow rates), then the structure of the principal components derived from this data set will depend essentially upon the arbitrary set of units of measurement. If there are large numerical differences between the variances of the data, those variables whose variances are large will tend to dominate the first few principal components even if those variables are not actually important in the detection of process malfunctions. Therefore, care needs to be taken when scaling the data. Additionally, different scaling of the process variables can produce different results thus different interpretation of results.

According to Martin, Morris, and Zhang 1996, there are "three possible ways to scale the data: select 'natural units' by ensuring all the variables measured are of the same type; variables can be mean-centered; or the variables can be scaled to zero mean and unit variance." The principal components are then calculated based upon the new scaled matrix. For this work, the third scaling option was used. In addition, differential weighted scaling was also applied in this work to some of the key process variables to bring out the variations of these variables in the presence of a much larger set of intermediate process variables whose values are of less interest in monitoring.

"One of the features of PCA is that the less important components often describe the noise in the data" (Martin, Morris, and Zhang 1996). Therefore, a smaller number (in comparison to the original variables) of principal components are required to explain the variability in the data, and it is desirable to exclude these less important components. Also according to Martin, Morris, and Zhang 1996, "the number of principal components that provide an adequate description of the data can be assessed using a number of techniques." In this work, a Scree test was applied. In practice two or three principal components are frequently sufficient for MSPC.

As mentioned before, the primary requirement for the development of MSPC charts is the acquisition of data that are representative of normal process operation. This 'normal operating' data set can be obtained from historical databases or designed experiments. A predictive model based on normal

operating data can be constructed using either PCA or PLS. Future behavior is then compared to this 'in-control' model. "The basis of the success of this approach is the recognition that many of the measurements are highly correlated and thus different combinations of the variables may define the same underlying disturbances or events occurring in the process" (Martin, Morris, and Zhang 1996). Therefore, it can be assumed that when the process is operating within normal conditions, the dimensionality of the process can be substantially reduced to a few principal components.

This information is typically presented graphically in terms of time series plots, as well as two and three dimensional representations of the principal components. According to Martin, Morris, and Zhang 1996, "the three most common forms of monitoring charts are those of the scores against time, two and three dimensional plots of the scores, and the squared prediction error (SPE). The SPE is sum of the squared difference between the observed values and the predicted values from the reference model. The SPE plot provides a way to identify a previously unidentified event, (i.e., a change that is not included in the model). Typically, principal components one and two and the calculated value of the SPE are plotted in a three-dimensional diagram.

As stated by Martin, Morris, and Zhang 1996, "a process malfunction can lead to one of the following two situations." First, the fault can change the correlation structure between the measured process variables meaning that the nominal PCA model is no longer valid and significant prediction errors will result which can be detected from the SPE plot. Second, the process malfunction may not alter the correlation structure among the process variables, in which case, the SPE will remain within the control limits but the scores will move outside the boundary of normal operation. The variables which primarily determine the direction of the individual principal components are those that have the largest absolute loadings (i.e., those that contribute the heaviest to the individual principal components). If a fault is identified, then the principal component that is no longer behaving as expected based on the reference model may be used to determine why the process has moved away from the nominal operating region.

Valle, Li, and Qin 1999 discussed the difficulties in selecting the correct number of principal components for a MSPC model and presented an overview and comparison of ten methods to determine the number of principal components, including the Scree test mentioned above as the method selected for this work. A key issue in developing a PCA model is the selection of an adequate number of principal components to represent the system in an optimal way. If too few principal components are selected, a poor model will be obtained resulting in an incomplete representation of the process. On the contrary, if too many principal components are selected, the model will be over-parameterized and will include noise. The Scree test is an empirical procedure to guide the selection of the number of principal components to retain using the cumulative percent variance. The method looks for a "knee" or "elbow" point in the cumulative percent variance plotted against the number of principal components. The break point corresponds to the number of principal components to represent the process.

Kourti 2002 reminded us "that these methods [PCA and PLS] will not be able to unequivocally identify the cause of any problem (because of the highly correlated and non-causal nature of the data). However, they can almost always identify unusual operating periods and can usually isolate the region of the plant and the group of process variables that are related to the problem. Thus, they are a powerful tool for focusing the attention of the operations engineers to a much smaller area, allowing them to better use their engineering knowledge to diagnose the cause of any abnormal situations and thereby improve the process." This same philosophy applies to using MSPC as a safeguards tool where it is IAEA inspectors who would be using the information to determine the location and cause of a fault and to determine if it resulted in a deliberate diversion of uranium.

Process monitoring is beginning to be applied to nuclear processes as discussed in Hines, Upadhyaya, and Henkel 2008. The nuclear process applications have been mostly for on-line safety-related sensor calibration monitoring. Process monitoring for safeguards monitoring of a uranium enrichment facility has also been explored by Hines, Upadhyaya, and Henkel 2008.

2.2 SAFEGUARDS AND DIVERSION IN CONVERSION PLANTS

As discussed in Chapter 1, the IAEA policy for safeguards in conversion plants has been revised. According to Doo et al. 2003, IAEA now considers all highly purified uranium compounds as candidates for safeguarding which includes the intermediate products of an NUCP. The revision of the safeguards policy resulted in significant amounts of research in the area of the application of safeguards to uranium conversion plants. Much of that research was conducted by the U.S. Department of Energy (DOE), which is interested in developing instruments, tools, strategies, and methods that could be of use to the IAEA in the application of safeguards to the front end of the fuel cycle (Boyer et al. 2004, Faulkner et al. 2004). The following is a review of the available literature on the studies in the area of conversion plant safeguards and diversion scenarios.

Doo et al. 2003 identified the following as potential diversion pathways in an NUCP: "uranium oxides, UF_6 product or uranium intermediates at NUCPs may be produced without declaration to the IAEA and diverted without efforts at concealment; or a diversion may be concealed by falsification of records to understate feed, overstate process losses, or overstate in-process inventories; or by substitution of dummy materials."

Four companion papers were presented at the 45th Annual Meeting of Institute of Nuclear Materials Management (INMM) in 2004. The first paper authored by Boyer et al. 2004 discussed an international safeguards approach for an NUCP and suggested that one approach for safeguarding conversion plants could be the use of "unattended process monitoring equipment to measure the flows of uranium through various unit processes." In traditional safeguards, the plant operator makes a declaration of the material balance for the plant and the IAEA verifies that declaration through verification of plant design

16

information, auditing of records and reports, and independent measurement of a portion of the nuclear materials that comprise the flows and inventories of the declared material balance. However, verification of the declared material balance has many limitations and in general will not detect the processing of undeclared feed to produce undeclared product. Therefore, additional safeguards measures are required to detect undeclared processing. Traditional IAEA methods (e.g., application of containment and surveillance measures) could provide some detection capability. The IAEA has revised their approach to NUCP safeguards to include more short notice random inspections during the year to gain more flexibility and unpredictability in conducting inspections. The IAEA has made increasing use of unattended monitoring to verify operations at safeguarded facilities, which could offer an effective method for detecting the processing of undeclared materials in an NUCP (Boyer et al. 2004).

In an ideal situation, safeguards would involve the continuous presence of IAEA inspectors at the plant and the installation of unattended monitors on each of the process vessels, but in practice, such intensive and intrusive approaches are not feasible because of cost, shortage of IAEA manpower, difficulty in operator acceptance, and existing political constraints (Boyer et al. 2004). Boyer et al. 2004 proposed that a safeguards approach capable of detecting the processing of undeclared materials in a small NUCP might include the following components:

- IAEA unattended monitoring instruments to measure the uranium content of intermediate process flow streams at key points in the process, primarily to detect the processing of undeclared feed;
- IAEA verification of the declared uranium balance, primarily to detect the diversion of declared uranium; and
- Operator declarations of specified nuclear material quantities and operating parameters on a daily basis.

Boyer et al. 2004 identified the two principal safeguards concerns at an NUCP as: "1) diversion of pure materials for further processing or use elsewhere and 2) processing of undeclared feed to produce undeclared pure products (e.g., UO_2, UF_6)." Additionally, the paper listed the following as the most important diversion and undeclared processing scenarios:

- "Diversion of uranium from the declared material balance;
- Processing of undeclared UOC through production of UF_6;
- Processing of undeclared impure uranium feed materials (e.g., UOC or uranyl nitrate) through the solvent-extraction purification process and the production of purified uranyl nitrate; and
- Processing of undeclared pure uranium feed materials (e.g., uranyl nitrate, uranium precipitant, UO_2, or UF_4) through the UF_6 production step" (Boyer et al. 2004).

The second INMM paper was authored by Faulkner et al. 2004 and discussed the Oak Ridge National Laboratory (ORNL) efforts to enhance conversion plant safeguards. The ORNL work was focused on

defining generic conversion facilities as well as reviewing various natural uranium conversion plants and process flowsheets in order to create a technical basis for selecting an effective safeguard program. Additionally, Oak Ridge used the most appropriate process configurations to constitute a set of process models that were used to determine logical locations for mass balance evaluations. ORNL also completed in-depth analyses of diversion scenarios which will be summarized below.

According to Faulkner et al. 2004, "a clear understanding of the chemical conversion process is essential in selecting an appropriate set of safeguard controls." However, traditional IAEA inventory controls do not begin until the last step of an NUCP when the UF_6 product is certified for use as feed to an enrichment facility. Faulkner et al. 2004 states the reasoning behind safeguarding NUCPs: "Each NUCP processing step increases the nuclear material attractiveness for diversion as the uranium is purified and as the chemical form is converted to one that is more suitable for use in a nuclear weapon[s] program. The quantity of uranium available, the ease of removal from the process, and the ability to obfuscate diversion were special considerations in the diversion analysis. Safeguard controls must include defense-in-depth approaches to achieve a reasonable level of detection capability."

Faulkner et al. 2004 performed a diversion analysis by analyzing the generic conversion process to determine potential diversion routes for intermediate products. After the uranium is in the form of a purified uranyl nitrate solution, it becomes attractive for use in a weapons program and therefore in need of safeguarding. The purified uranyl nitrate solution can be denitrated to form UO_3 or UO_2. Either of which is well suited for production of UCl_4 by chlorination, which is the preferred chemical form for an electromagnetic isotope separation (EMIS) enrichment process or for a chemical/ion exchange enrichment process. In addition, UO_2 can be hydrofluorinated to produce UF_4, which can be metallothermically reduced to uranium metal for use in an AVLIS enrichment process or in plutonium production. Moreover, uncertified UF_6 is not currently monitored by IAEA safeguards and could be shipped to a clandestine site for fractional distillation prior to feeding to a gas centrifuge or gaseous diffusion enrichment plant. Figure 2.1 provides a pictorial view of the potential diversion paths for intermediate products from an NUCP.

Diversion scenarios also include other options such as,

1. Material substitution (substitution of feed materials that have higher uranium content than declared or the clandestine removal of uranium-bearing material in exchange for materials of similar characteristics but with less or no uranium content) (Faulty Cases 2 and 6),
2. Equipment alterations (addition of bypass piping, valves, or other equipment used to divert or introduce materials clandestinely; or modification to equipment (e.g., heating), resulting in incomplete conversions or inefficient operation with excess uranium in the waste or tails) (Faulty Cases 5, 8, 9, and 11),
3. Modified operations (intentionally operating processes inefficiently so that more uranium is contained in recycle, sample, or waste streams), (Faulty Cases 3, 4, 7, and 10) and
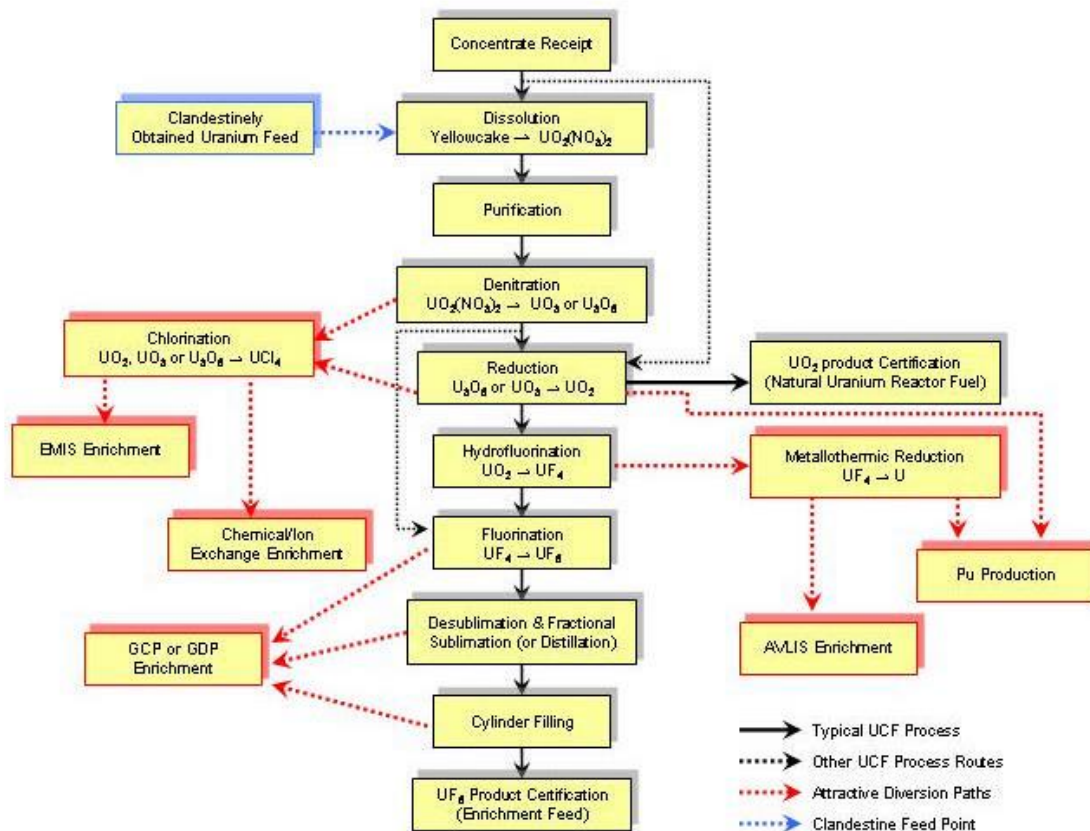
Figure 2.1. Pictorial View of the Potential Diversion Pathways for Intermediate Products from an NUCP. Note that the solid black arrows follow the steps in a typical uranium conversion process. The dashed black arrows denote alternate routes in the conversion process. The dashed red lines show attractive diversion paths. The dashed blue line shows the feed point for clandestinely obtained uranium. (Source: R. L. Faulkner, J. M. Begovich, J. J. Ferrada, R. D. Spence, J. M. Whitaker, W. J. Bicha, and L. G. Loden. 2004. "Oak Ridge Efforts to Enhance Conversion Plant Safeguards." *Proceedings 45th Annual Meeting of Institute of Nuclear Materials Management (INMM)*, July 18–22, 2004, Orlando.)

4. Data tampering (keeping two records of operation with one showing less throughput than actually processed; declaration of understated records to inspectors) (Faulkner et al. 2004).

A safeguards system that uses a combination of accountability principles with unattended monitors to verify data would significantly enhance a diversion detection system. Faulkner et al. 2004 proposed that "the optimum system would include verifiable accountability data for feed and the withdrawal streams plus several inline detection systems." Eight points in an overall uranium conversion process were identified by Faulkner et al. 2004 for possible monitoring or accountability (Figure 2.2). The first monitoring point is the accountability data for the declared yellowcake receipt at the plant inlet (Figure 2.2, Point 1). A comparison of the record of the rate and amount of uranium mass exiting the plant in the UF$_6$ product (Figure 2.2, Point 8) against that of a record of the uranium mass entering the plant in the feed provides the means for an overall plant uranium mass balance, minus the uranium leaving as waste. The yellowcake exiting the feed hopper into the dissolver (Figure 2.2, Point 2) is the first opportunity in the process to verify the uranium mass recorded in the accountability data for the yellowcake received at the NUCP. One possible location for inline monitoring is at the point just after dissolution, downstream of the uranyl nitrate tank (Figure 2.2, Point 3). This would be the first point where uranium is in solution. Both the aqueous stripping solution loaded with uranium (Figure 2.2, Point 4) and the organic solution stripped of uranium exiting the strip column (Figure 2.2, Point 5) should be monitored. These points help to prevent inefficient stripping by the operator and provide a mass check after the purification of the uranium. The concentrated solution from the evaporator can be measured at one of two locations: (1) just out of the evaporator before the pump (Figure 2.2, Point 6a) or (2) downstream of the reflux lines and valves but before the cooler (Figure 2.2, Point 6b). Point 7 (Figure 2.2), the last in-line process monitor, would be located at the end of the precipitation or denitration step. Point 7 (Figure 2.2) also helps to verify the uranium dissolved and purified. With two accountability points and six in-line monitors in place, it is possible that this defense-in-depth safeguards approach could detect a significant quantity of uranium diversion with a reasonably high probability of detection for the small-scale plant. A minimum case for the small-scale (100-MTU/yr) plant is probably one in-line monitor, preferably at Point 4 (Figure 2.2), plus the accountability data at Points 1 and 8 (Figure 2.2) (Faulkner et al. 2004).

Ferrada 2004 provided the following information on possible monitors that could be used at the points shown in Figure 2.2. These monitoring points are mainly driven by mass balance principles. Therefore, the monitoring points should be supported by instrumentation that can verify mass balances. Flowmeters, to measure flow of material, and instruments that measure concentration of uranium are ultimately required for this analysis. Real-time, inline monitoring may be practical for a uranium solution, after the uranium is extracted from the yellowcake and before the uranium is changed into a solid form (Figure 2.2, Points 3–6). This type of monitoring requires the liquid flow rate (typically volume per unit time) and uranium concentration (mass per unit volume). Volumetric flowmeters are readily available from commercial suppliers. Mass flowmeters are also available, many of which also measure density. Monitoring of liquid density can help verify the uranium concentration since density is a
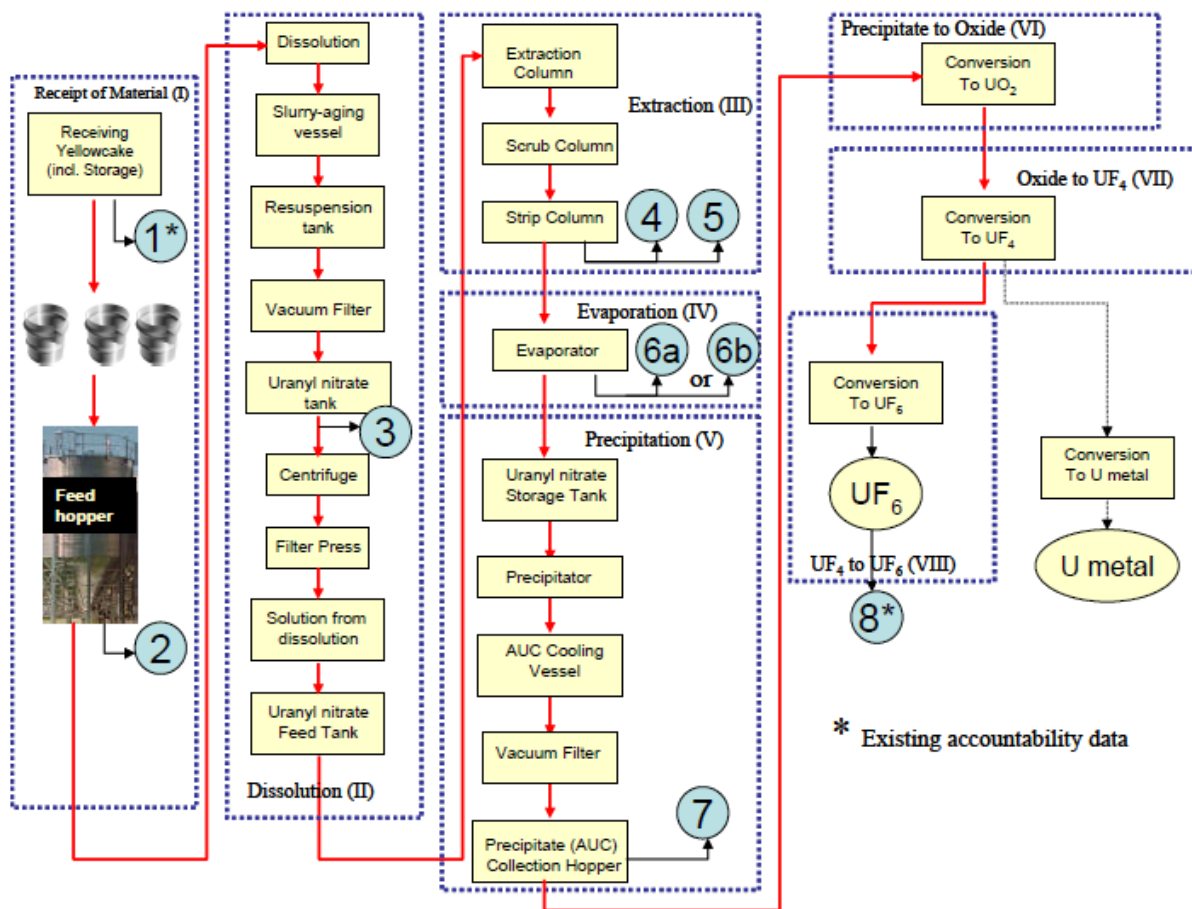
Figure 2.2. Uranium Conversion Process for a Small Size Plant with Proposed Safeguards Monitoring Points Identified. Note: Points 1 and 8 are existing accountability data; Point 8 is also the traditional start of IAEA safeguards. The remaining points are proposed in-line process monitoring points; values at all 8 points are correlated through material balance constraints and process operating conditions. (Source: R. L. Faulkner, J. M. Begovich, J. J. Ferrada, R. D. Spence, J. M. Whitaker, W. J. Bicha, and L. G. Loden. 2004. "Oak Ridge Efforts to Enhance Conversion Plant Safeguards." *Proceedings 45th Annual Meeting of Institute of Nuclear Materials Management (INMM)*, July 18–22, 2004, Orlando.)

function of the uranium concentration. According to Ferrada 2004, the primary monitoring should be a direct measurement of the uranium concentration and flow rate and monitoring of density should be secondary to verify that the primary monitoring is working properly. Inline meters for measurement of uranium concentration directly are more problematic. Low uranium concentrations result in impractical count times for the low-energy gamma from radio decay daughters. Photometric meters for inline measurement of uranium concentration exist, but matching safeguard needs with instrument capabilities has not been done. Picking monitoring points where higher concentrations are expected (e.g., after evaporators) would help. For a solid material stream, inline monitoring of uranium is impractical. Gravimetric feeding of solids accompanied by real-time recording of the mass fed per unit time is possible. However, it is necessary to know the uranium assay of the yellowcake being fed into the dissolver in order to obtain the uranium mass fed per unit time into the dissolver. In order to determine the uranium assay, grab samples would have to be taken at regular intervals followed by destructive analysis of the uranium concentration. Gamma spectroscopy of the low-energy gamma from the uranium decay daughters is being used with good success for qualitative, semi-quantitative, and even quantitative analysis, especially with regard to the relative ratio of ^{235}U and ^{238}U. However, it is questionable whether this technique or others will provide practical real-time monitoring of the uranium concentration in a process flow of a solid material with the precision and accuracy required for detecting undeclared production. A gravimetric feed and monitoring system may provide the total mass per unit time, but grab sampling and analysis would still be required to obtain the uranium mass per unit time. In addition, the facilities accountability records (e.g., number of drums and their weights with the date and time filled) can be verified using onsite monitoring (e.g., cameras), random checking of drum weight, and a sampling program for the uranium concentration. No matter the location in the plant, real-time process monitors that can compare NUCP accountability data with actual process data can be very useful, especially if the software can indicate trends in the relationship of accountability and actual data using statistical control charts to document anomalies (Ferrada 2004).

The third INMM paper was authored by Elayat, Lambert, and O'Connell 2004 and covered systems analysis. As part of the multi-laboratory effort covered in the four companion INMM papers, Lawrence Livermore National Laboratory provided systems modeling and analysis of facility and safeguards operations, diversion path generation, and safeguards system effectiveness using directed graphs (digraphs) and fault trees. The purpose of the digraph-fault tree methodology was to systematically generate and analyze diversion scenarios. The final INMM paper is authored by Miller et al. 2004 and discussed nuclear source terms (neutron and gamma-ray) in support of the other papers. The fourth paper was not applicable to this effort and was not reviewed but is mentioned here for completeness.

The work by Faulkner et al. 2004 was used as a starting point for defining the ideal plant modeled in this effort. The faulty cases that were used to test the detection framework were based on the diversion scenario analyses by Faulkner et al. 2004. In relation to the proposed approach by Boyer et al. 2004, the decision framework developed in this research could be expanded to provide the following for safeguarding conversion plants:

- An unattended system that could monitor key process parameters at specific locations within the plant and provide an alarm if a parameter varies outside a specified range;
- Provide verification that the declared uranium balance is concurrent with monitored process parameters; and
- Provide verification that operator declarations are reasonable based on monitored parameters.

2.3 PRINCIPAL COMPONENT ANALYSIS

The core of the research method applied in this study is the use of a multivariate statistical approach to analyze data to develop a reduced dimensional framework that would be able to detect the diversion of intermediate products in an NUCP. One of the multivariate statistical methodology's workhorses is the PCA approach in analyzing data, establishing the base model, and monitoring future operations. The implementation of PCA will be through the use of singular value decomposition (SVD) of the base case data matrix, X (Wang 2006). The data matrix is $m \times n$ with $m \gg n$ where each row represents an observation and each column represents a state variable.

$$X = \begin{bmatrix} x_{1,1} & \cdots & x_{n,1} \\ \vdots & \ddots & \vdots \\ x_{m,1} & \cdots & x_{m,n} \end{bmatrix}$$

Each row of the data matrix, X, has n elements and can be viewed as a point in an n-dimensional space. The m rows of X can be depicted as 'm' points in this n-dimensional space. Even though the points are in an n-dimensional space, the span of the points is such that they occupy a much reduced dimensional space. This is similar in notion as points in a 2-D space scattered mostly along one dominant line if the x and y coordinates for the sample points are correlated.

Principal component analysis is a data analysis method used to reduce a correlated data set which consists of a large number of interrelated process variables by reducing the dimensionality while retaining as much of the variations present as possible (Jolliffe 1986). The discarded dimensionality corresponds to the last $(n - r)$ outer products of the SVD of X, where r is deemed the 'true' dimensionality of the process data matrix and n is the total number of original process variables. Sources for more information on PCA include Jolliffe 1986; Jackson 2003; Martin, Morris, and Lane 2002; and Martin, Morris, and Zhang 1996. PCA is used to reduce the dimensionality of a system by creating orthogonal latent variables (i.e., principal components) which correspond to the V vectors of the SVD of the process data matrix, X. Each of these principal components is a weighted, linear combination of the original process variables. PCA was first introduced in 1901 by Pearson and later independently developed by Hotelling in 1933. As mentioned in the Introduction, some recent applications of PCA include process monitoring, fault diagnostics, gross error detection, multivariate statistical process control, data rectification, disturbance detection and isolation, gene expression analysis, facial recognition, signal processing, factor analysis, chemometrics, and chemical processes data analysis

(Brauner and Shacham 2000; Valle, Li, and Qin 1999; Bakshi, 1998). In chemical engineering, PCA is used to monitor batch and continuous processes, monitor product quality control, missing value replacement, identify and reconstruct sensor and/or process faults, and detect disturbances (Valle, Li, and Qin 1999). PCA is also being applied to nuclear processes (Hines, Upadhyaya, and Henkel 2008) and to nuclear forensics (Robel, Kristo, and Heller 2009).

Some relevant mathematical concepts will now be presented. A basis for a linear vector space, S, of dimension n is a set of n independent vectors $w_1, \ldots, w_n$ with the property that every vector, x, in the space, S, can be expressed uniquely as a linear combination of these basis vectors, i.e., for every x, there exists a unique set of $\{\alpha_i\}$ $\alpha_i \in \mathbb{R}$ such that $x = \sum_{i=1}^{n} \alpha_i w_i$ for all $x \in S$. One property of linear algebra of fundamental importance is the ability to transform the representation of a vector from one basis to another. This is called a change of basis. Change of basis to a particularly convenient basis allows one to detect the relatively weak dimensions of a data set; thus allowing one to reduce the dimension of a data matrix without losing much meaningful information. One can do a change of basis for a data matrix, X, from one set of basis vectors, W, to that of another, for instance V, where all the vectors of V will come from the right singular vectors of the SVD of X (all the V_i vectors chosen are already orthogonal to each other). Each row of the data matrix represents a measurement vector of the various process variables at a particular time point. If there is a strong correlation between the X variables, then the sum of the squares of the projection of X along the first singular vector of V (V_1) will be much greater than X along the second singular vector and any subsequent basis of V ($V_2, \ldots, V_r$). Therefore, V_1 is the vector of all possible chosen vectors that maximizes the sum of squares of the projections of the original data sample points. For instance, for a 2-dimensional X data matrix when the two x variables are highly correlated, $\left\| X_{V_2} \right\|_2$ will be much less than $\left\| X_{V_1} \right\|_2$, where $\| \ \|_2$ denotes the 2-norm of a vector. The components of X along V_2 can be considered to come from noise in nature and the system can be reduced from a 2-dimensional representation to a 1-dimensional representation of the original data without losing any meaningful information contained in the original data matrix. Therefore, a reduction of rank of the data matrix has occurred. The key to this approach is determining how many of the new basis vectors to transform X to and which vectors to project onto. Singular Value Decomposition (SVD) provides guidance.

SVD is used to determine the orthogonal basis vectors which best represent the original data where the sum of squares of the projections of the original data onto each successive orthogonal basis vector in V becomes less and less. According to the theory of SVD, every matrix, X (of dimension $m \times n$), can be decomposed into the product of three special matrices, U, Σ, and V, according to Eq. (2.3.1) (Strang 2006)

$$X = U\Sigma V'$$
(2.3.1)

where U and V have orthonormal columns and Σ is a diagonal matrix with positive elements (i.e., the singular values) arranged in a descending order. After singular value decomposition of X, the right

singular vectors, i.e., the n columns of the V matrix, are unit length and orthogonal to one another. The columns of the V matrix provide a new set of basis vectors. The first V vector, V_1, or the first principal component (PC), is such that it is the direction vector upon which the sum of squares of the projections of all the m row vectors of X is the maximum of all possible direction vectors that can be chosen in the n-dimensional space. The second V vector, V_2, or the second principal component, being orthogonal to V_1, is one such that the sum of squares of the projections of the residual of the m points (after projection onto V_1 is subtracted) is maximum. It is likewise for the subsequent V vectors. Therefore, the sum of squares of the projections onto the last few vectors of V are the least. And if the last few vectors of V capture less variation than that of the first few, then projections along these basis vectors are considered as to have come from noise and uncertainty associated with the measurement of the process variables represented in X. The vector of projections of the rows of X along a particular basis vector, V_i, are called the scores and are given by Eq. (2.3.2).

$$X_{V_i} = X * V_i \tag{2.3.2}$$

The scores (unnormalized) of a sample point refer to the magnitude of the projections of the sample point (or a row of the original data matrix) onto each of the principal component vectors. This projection process can be viewed as a change of basis from that of the original to a new set of mutually orthogonal basis vectors given by the 'n' V vectors. The scores of a sample point can be viewed as the new coordinate of the sample point along V_1, along V_2, etc. The scores for a sample point, for example, the first row of X (X_{r1}), are calculated by finding the inner product (dot product) of X_{r1} with each of the 'n' vectors in V to give a vector with n components (or scores) for the first sample point. The inner product of X_{r1} with V_1 gives a number that is equal to the magnitude of the projection of X_{r1}, or the first sample point, onto V_1, which is referred to as the score along V_1, or the score along PC1 for sample 1 from the data matrix, X. The inner product of X_{r1} with V_2 gives a number that is equal to the magnitude of the projection of the first sample, onto V_2, of PC2, which is referred to as the score along V_2 or PC2. It is likewise for the inner product of X_{r1} with the subsequent V vectors. Through the use of SVD, a data matrix can be decomposed into mutually orthogonal outer product components of decreasing significance as shown below Eq. (2.3.3);

$$X = U\Sigma V' = \begin{bmatrix} \vdots & \vdots & & \vdots \\ U_1 & U_2 & \cdots & U_n \\ \vdots & \vdots & & \vdots \\ \vdots & \vdots & & \vdots \end{bmatrix} \begin{bmatrix} \sigma_1 & & \\ & \ddots & \\ & & \sigma_n \end{bmatrix} \begin{bmatrix} \vdots & \vdots & & \vdots \\ V_1 & V_2 & \cdots & V_n \\ \vdots & \vdots & & \vdots \end{bmatrix}'$$

$$= \sigma_1 \begin{bmatrix} U_1 \end{bmatrix} \begin{bmatrix} & V_1' & \end{bmatrix} + \cdots + \sigma_n \begin{bmatrix} U_n \end{bmatrix} \begin{bmatrix} & V_n' & \end{bmatrix}$$

$$= \sigma_1 U_1 V_1' + \sigma_2 U_2 V_2' + \cdots + \sigma_n U_n V_n' = \sum_i \sigma_i U_i V_i' \tag{2.3.3}$$

The first outer product, $\sigma_1 U_1 V_1'$, through the associated σ_1, which being the largest of all singular values, captures the most variation in one dimension represented by the original data matrix; meaning $\sigma_1 U_1 V_1'$

is the best rank-1 approximation of the X data matrix. Each subsequent outer product makes progressively less and less contribution to X. Therefore, the first term of the outer products of the SVD of X contributes to the most original information captured in X, while the second term contributes the next most, and the last term contributes the least information. Each term of the outer products of the SVD of the data matrix, X, will be an $m \times n$ matrix if X is $m \times n$, and each outer product matrix is independent of all other outer products because all of the U_i's are mutually orthonormal and all of the V_i's are mutually orthonormal.

The following basic approach to PCA was adapted from Wang 2006; Martin, Morris, and Lane 2002; and Kourti 2002. The overall approach for this work is located in Chapter 3. PCA can be performed in two ways: with or without normalizing the data matrix to have unit or weighted standard deviation in each variable. Normalization must be used when the data set contains variables with different physical units. Therefore it is common to standardize all the data (columns of X) to have zero mean and unit standard deviation. Weighted scaling is used when certain process variables need to be brought out as more important than other variables, such as the uranium-bearing product streams in this work. Therefore, the first step in applying PCA is to standardize the data matrix, X, which contains m samples of n variables with $m \gg n$. The data matrix is standardized by mean centering each column to give a zero mean and dividing each centered column by its standard deviation, see Eq. (2.3.4)

$$X_{s,i} = \frac{x_i - \bar{x}_i}{s_i} \qquad\qquad i = 1, 2, \dots, n \qquad\qquad (2.3.4)$$

where $X_{s,i}$ for process variable i denotes the i-th standardized x variable; x_i is the i-th original process variable vector; $\bar{x}_i$ is the mean of the x_i column vector; and s_i is the standard deviation for the i-th mean-centered x_i. Therefore, the resultant data matrix has a mean of zero and a standard deviation of one for each column. In weighted scaling, the standard deviation is divided by a scaling factor before normalization such that the resultant data matrix has a mean of zero and a standard deviation of the value of the scaling factor for each column. After the variables have been normalized, SVD is performed according to Eq. (2.3.5) (Wang 2006)

$$X_s / \sqrt{m-1} = U\Sigma V' \qquad\qquad (2.3.5)$$

where X_s is the standardized data matrix. A key consideration in developing a PCA model is to choose an appropriate number of principal components to represent the original data in an optimal way; if too few PCs are selected, a poor model will be obtained and an incomplete representation of the process results; if more PCs than necessary are selected, the model will be over-parameterized and will include a modeling component for noise (Valle, Li, and Qin 1999). The diagonal values of the Σ matrix can be used to determine the effective rank of the X_s data matrix by doing a Scree test. In the Scree test, the cumulative singular values, σ^2, are plotted in a simple curve against the index count. The point at which the slope changes and appears to level off to the right of the plot suggests the break point to discard additional principal components. The discarded principal components are assumed to represent the

process noise and reflect redundancy of the process variables. Using this method, PCA can effectively separate the signal from the noise in a process (Martin, Morris, and Lane 2002).

The original observations (i.e., rows of X) are then projected onto the smaller principal component subspace spanned by the chosen set of reduced number PCs or the 'a' number of retained mutually orthogonal principal component vectors to give principal component scores (T). The T matrix, as shown in Eq. (2.3.6), is the product of X with V_a where 'a' refers to the number of PCs selected to be retained to build the PC model to represent the original data.

$$T = X_s * V_a \qquad (2.3.6)$$

Usually, 'a' is much smaller than 'n', because 'a' represents the 'true' degree of freedom exhibited by the sample points, even though they reside in a much larger n-dimensional space. The 'n' process variables represented in X, are all correlated through conservation of mass equations. The underlying degree of freedom is a function of the number of physically independent input variables that the process is operated under. The response of the process variables to their variations under normal operations with anticipated variation in the various input variables are what are captured in the data matrix, X. Therefore the 'true' degree of freedom reflects the number of 'independent' acting inputs to the process which bring about the responses in the dependent process variables whose values are measured and go into the data matrix, X. The residuals matrix, E, is to be computed using Eq. (2.6.7).

$$E = (X_s - X_s * V_a * V_a') \qquad (2.3.7)$$

The i-th Mahalanobis distance of T^2 which is the i-th diagonal element of the T^2 matrix shown below, and the i-th diagonal element Q-statistic are to be calculated using Eq. (2.3.8) and (2.3.9), respectively,

$$T^2 = (T * \Sigma_a^{-1}) * (T * \Sigma_a^{-1})' = U_a U_a' \qquad (2.3.8)$$

$$Q_i = \|E_i\|_2^2 \qquad (2.3.9)$$

where $\|E_i\|_2$ denotes the 2-norm (or Euclidean norm) of the i-th residual vector (row) in E. The normalized scores of a sample data point refer to the scores along the 'a' principal components after normalization with the respective singular value for the PC. Since the singular value gives the square root of the sum of squares of the projections of all sample points onto a given principal component, the scores of a sample point along the various PCs are scaled differently by their respective singular value. In order to bring the scores to equal scale, the score along a PC is normalized by its respective associated singular value. This normalization is achieved by multiplying the individual score in a scores vector by the inverse of the respective singular value. Equation (2.3.8) shows this operation. Normalization of the scores can be thought of as rescaling the coordinate axis by the inverse of the respective singular value. The relative positions of the scores points of the original sample points are not changed by the process of normalization. The various diagnostic plots presented in this dissertation used to detect possible faults utilize normalized scores. Qualitatively, these diagnostic plots would look exactly the same if

'unnormalized' scores are used instead. In this case, the actual scale labeling along PC1, PC2, and PC3 will be different from that of the normalized case, but the relative positions of the scores points on the plot would not appear any differently.

The 95% confidence threshold for $\{T_i^2\}$ and $\{Q_i\}$ are established as shown in Eq. (2.3.10) and (2.3.11), respectively,

$$T_\alpha^2 = \frac{a(m-1)(m+1)}{m(m-a)} * F_\alpha(a, m-a) \tag{2.3.10}$$

where m is the number of samples, a is the number of PCs retained for the model, and F_α is the critical value for the F-distribution that leaves $\alpha\%$ area to the right for $[a, m-a]$ degrees of freedom.

$$Q_\alpha = \theta_1 \left[\frac{h_o * c_\alpha * \sqrt{2\theta_2}}{\theta_1} + 1 + \frac{\theta_2 * h_o * (h_o - 1)}{\theta_1^2}\right]^{\frac{1}{h_o}} \tag{2.3.11}$$

The θ terms are defined as

$$\theta_i = \sum_{j=a+1}^{n} \sigma_j^{2i} \tag{2.3.12}$$

for $i = 1,2,3$ and h_o is defined as

$$h_o = 1 - \frac{2\theta_1 \theta_3}{3\theta_2^2} \tag{2.3.13}$$

where c_α is the critical value for a normal distribution that leaves $\alpha\%$ area to the right and σ_j is the j-th singular value of the $X_s/\sqrt{m-1}$ matrix.

As mentioned previously, one common way of presenting the information obtained from PCA models is through two-dimensional plots of the scores of the principal components or through plots of the scores, T^2, and the SPE or Q-statistic. In monitoring, a time series of the T^2 and the SPE can be plotted against time to show trending behavior. The SPE is the sum of the squared difference between the observed values and the predicted values from the base case PCA model, and reflects the residuals after fitting with the PCA model. If a change among the relative relationship between the process variables has occurred, the PCA model constructed from historical operating data is not expected to fit as well, thus leading to increased residuals. The T^2 statistic is a measure of the Mahalanobis distance in the reduced scores space between the position of a sample and the origin that defines those samples exhibiting minimal variation (i.e., average behavior of the process) derived from the historical data set. The SPE plot allows one to identify the onset of a new event not previously captured in the data. However, if the process change is caused by a larger than normal shift in one or more of the process variables, but the basic relationship between the quality and/or process variables remains unchanged, then a translation in the scores plane will result, with the SPE remaining under an acceptable level. In this instance, an 'out-of-control' signal will be seen in the T^2 plot, but not in the Q-statistic plot.

3. METHODOLOGY

The methodology that was used for the development of the diversion detection framework is outlined below. This methodology starts with an overview of the overall approach followed by the material balances of the processes in the conversion plant. A description of the sensitivity analysis is followed by descriptions of the normal and faulty cases including the application of PCA to the problem.

As a reminder, this study was developed for a 100 MTU/yr NUCP using the wet solvent extraction method for the purification of uranium ore concentrate in the form of U_3O_8. It was assumed that the process was operating continuously and was at steady-state.

3.1 OVERALL APPROACH

The overall approach used to develop the monitoring framework is shown in the flow diagram in Figure 3.1.

The first major step in the overall approach was to define the base case and generate the 'normal' data set. First, the process equations that describe the steady-state system were defined. These equations are based on concentration of mass of the various chemical species and are a function of the state variables and the input variables of interest, where x and u denote the full state variables of interest ($n \times 1$) and full input variables ($m \times 1$), and 'f' denotes the nonlinear algebraic equations. The change in the system, $\dot{X}$, is zero when the system is at steady-state.

$$\dot{X} = f(x, u)$$

For this work, the system of equations was based on the material balances, and the component molar flow rates of the various streams were the state variables. A total of 273 process variables were chosen to be monitored. All of the parameters and input variables were then defined. The input variables were the operational variables whose values can be set to drive the system operation, e.g., flow rate and concentration in the inlet stream to a reactor, etc. A total of seven input variables were chosen. For the input variables, the normal range profile for each variable was established, i.e., 'normal' flow rate of elemental uranium into the plant was specified as 50 kg/h. Next, the steady-state solution to all the material balance equations at the specified nominal input operating profile was obtained. The 'fsolve' function in MATLAB® was used to determine the steady-state solution. According to the MATLAB® 2013a Documentation, 'fsolve' is used to find a root or zero of a system of n nonlinear functions in n variables by the trust-region-dogleg algorithm (MATLAB® 2013). The algorithm is a variant of the Powell dogleg method, a numerical method for solving nonlinear equations. The steady-state solution was substituted back into the equations to check that the solution to the system of equations was indeed

Base Case

- Define the process equations used to describe the system based on material balances
- Identify all parameters associated with the process operation
- Identify overall input variables of interest and establish input variable's normal range profile
- Obtain the initial, nominal steady-state solution for the initial set of input variables
- Generate base case data

Principal Component Model

- Add random Gaussian noise to base case data set
- Pre-process data (normalize, mean-center, and scale)
- Extract PC model using SVD
- Determine effective rank
- Establish statistical bounds

Faulty Cases

- Simulate several 'faulty' or 'off-normal' operations
- Regress faulty data against base case model
- Evaluate ability to detect 'fault'
- Conclusion

Figure 3.1. Flow Diagram of the Overall Approach Method for Developing a Modeling Framework.

essentially zero. Once the nominal state-steady values were determined, it was possible to generate a set of 'base case' operating values from which the PCA model was built. The set of chosen input variables were varied around the nominal operational point to simulate 'normal' variation of these variables in actual operation. The reasonable range on either side of the nominal values was established, e.g., ±10% for flow rates. Thousands of data points were needed to build the base case PCA model. This was accomplished through the use of nested loops that cycle through all possible combinations of the levels of input variables. For example, assume that three input variables have been chosen to vary over 20 different values in the range of each variable; the simulation would generate 20^3 = 8000 data points. Therefore, the base case data matrix was generated by determining the steady-state intermediate variable measurements in response to normal variation in the input variables based on material balances. Each newly calculated steady-state solution (x) and the corresponding input variable values (u) are stored as a row vector of the large base case data matrix (X_{ss}). Each row represents a process response to a different combination of input variable values. There are a total of 273 state variables and seven input variables. The input variable values were placed as the last seven variables in the data matrix [Xss(274)–Xss(280)].

The next major step in the overall approach was to determine the reduced-dimension base case model following the procedure discussed in Chapter 2. The base case or 'normal' principal component model using the PCA approach was established based on normal operating profiles and expected normal variations. Before PCA could be applied to the base case data, random Gaussian white noise was added to all the measurement variables to simulate measurement noise. The data set was then pre-processed, i.e., standardized by mean centering each column to give a zero mean and normalized each column to have unit or weighted variance by dividing each centered column by its standard deviation. Singular value decomposition (SVD) was used to extract the principal components. The effective rank was determined in order to select the appropriate number of principal components to retain to represent the normal state of operation. The statistical bounds of T^2 and Q of the PCA model were established from the reduced-dimensional principal component framework.

The next step in the approach was to test the monitoring framework using faulty operational cases. Several faulty scenarios were simulated by introducing 'faults' into the operation. The faulty data sets were analyzed using the base case principal component model and the established statistical bounds. The ability of the model to detect each fault was evaluated.

3.2 MATERIAL BALANCES

A flowsheet of the overall NUCP is shown in Figure 3.2. Component mole balances were used to model each of the process units in the NUCP. The general form quoted for a mass balance is "the mass that enters a system must, by conservation of mass, either leave the system or accumulate within the system" (Himmelblau 1967). The general equation for material balances is shown in Eq. (3.2.0.1).
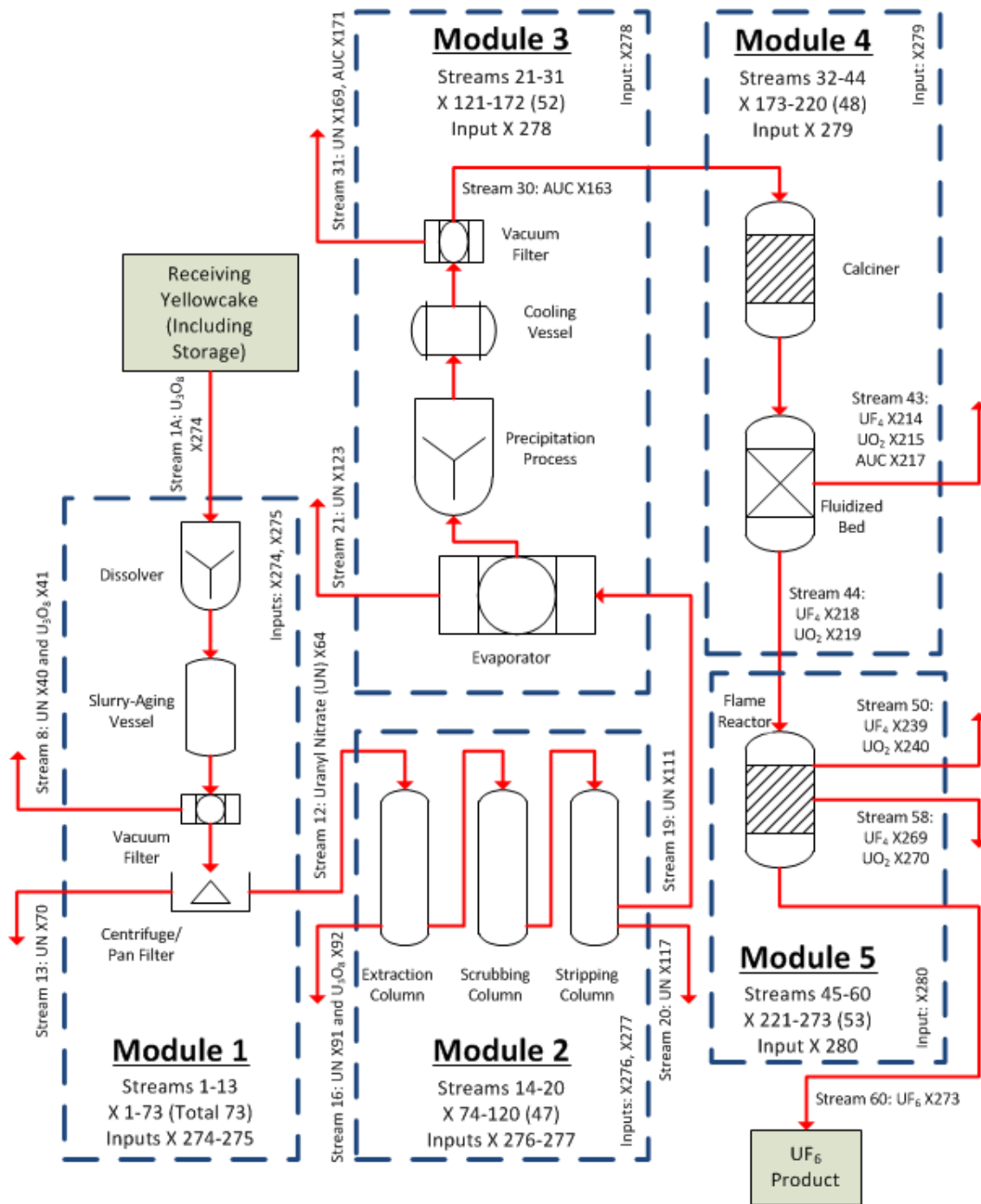
Figure 3.2. Block Diagram of a Natural Uranium Conversion Plant (NUCP). This diagram represents a small-size plant that processes 100 MTU/yr using the wet solvent extraction method. The primary input, product, and waste streams are labeled. The state variable numbers associated with each Module are listed along with the variable numbers for the input variables. The state variable numbers for the components in each stream are given as well.

$$Input + Generation = Output + \ Accumulation + Consumption \qquad (3.2.0.1)$$

At steady state, the accumulation is zero and Eq. (3.2.0.1) can be rewritten as shown in Eq. (3.2.0.2).

$$Input + Generation - Output - Consumption = 0 \qquad (3.2.0.2)$$

A material balance can be done around the entire NUCP (see Figure 3.2), around any given section of the plant (blue dashed boxes in Figure 3.2), or around each unit and/or piece of equipment within the plant. Any diversion of an intermediate will distort the expected relative proportions of the components at steady state leading to a deviation from the 'normal' pattern of relative proportions of components based on material balances.

In order to simplify model construction and debugging, the flowsheet for a natural uranium conversion plant (Figure 3.2) was divided into five modules to represent the major processing units within the plant, which are shown in Figure 3.2 as blue dashed boxes. Each module was further subdivided as needed to facilitate material balance calculations. The five modules were 1) Dissolution, 2) Solvent Extraction, 3) Evaporation and Precipitation, 4) Conversion to UO_2 and UF_4, and 5) Conversion of UF_4 to UF_6.

Additionally, each chemical component used in the model was assigned a component number which was used in the model instead of the chemical formula. Table 3.1 lists each component number, chemical name, chemical formula, molecular weight, and which modules the chemical components were used.

For the material balances discussed below, the component molar flow rate is represented by $F_{i,j}$, where i denotes the stream number and j denotes the chemical component number as defined in Table 3.1. These $F_{i,j}$ are the state variables, also denoted by X_{ss}. Tables 3.2–3.6 list the state variable numbers, stream numbers, and chemical component numbers associated with each module. The values in Tables 3.2–3.6 provide a map of which $F_{i,j}$ corresponds to each Xss. For example, the $F_{i,j}$ for water in Stream 1 is $F_{1,1}$ which is also Xss(1). Another example is that Xss(73) is $F_{13,21}$ which is the molar flow rate of the soluble component (#21) in Stream 13. Table 3.7 provides a summary of the modules including streams and the associated state variable numbers.

Table 3.8 lists the primary state variables for each module. Each state variable was a component molar flow rate for a stream within that module. Additionally, each of the primary state variables was a uranium-bearing component molar flow rate. The type of stream in the table refers to whether the stream was an intermediate stream within the specified module, a waste stream that exited the process completely, a module-specific product which became a feed stream to the subsequent module, or in the case of the final stream, the overall product. The primary state variables are the most important state variables to track throughout the system. Some streams did not have a uranium component or the uranium component was so small that it was unreasonable to track.

Table 3.1. List of Chemical Components

Component Number	Chemical Name	Chemical Formula	Molecular Weight (g/mol)	Module
1	water	H_2O	18.0153	1, 2, 3, 4
2	nitrogen	N_2	28.0134	4, 5
3	ammonia	NH_3	17.0305	3, 4
4	nitrogen dioxide	NO_2	46.0055	1
5	hydrogen	H_2	2.0159	4
6	hydrogen fluoride	HF	20.0063	4
7	fluorine	F_2	37.9968	5
8	carbon dioxide	CO_2	43.9987	3, 4
9	nitric acid	HNO_3	63.0128	1, 2, 3
10	methanol	CH_3OH	32.0365	3
11	tributyl phosphate (TBP)	$(CH_3CH_2CH_2CH_2O)_3PO$	228.0000	2
12	ammonium nitrate	NH_4NO_3	80.0434	3
13	ammonium carbonate	$(NH_4)_2CO_3.H_2O$	114.1011	3
14	uranyl nitrate (UN)	$UO_2(NO_3)_2$	394.0375	1, 2, 3
15	uranium hexafluoride	UF_6	352.0193	5
16	uranium tetrafluoride	UF_4	314.0225	4, 5
17	uranium dioxide	UO_2	270.0277	4
18	triuranium octoxide	U_3O_8	842.0819	1, 2, 3, 4, 5
19	ammonium uranyl carbonate (AUC)	$(NH_4)_4UO_2(CO_3)_3$	522.1489	3, 4
20	impurities in U_3O_8	insoluble	500 (assumption)	1, 2
21	impurities in U_3O_8	soluble	500 (assumption)	1, 2, 3

Table 3.2. State Variable Numbers for Module 1 [Xss(1–73)]

Chemical Component	Component Number	1	2	3	4	5	6	7	8	9	10	11	12	13
		\multicolumn Xss Number												
H_2O	1	1	--	8	14	20	26	32	38	44	50	56	62	68
NO_2	4	--	7	--	--	--	--	--	--	--	--	--	--	--
HNO_3	9	2	--	9	15	21	27	33	39	45	51	57	63	69
$UO_2(NO_3)_2$	14	3	--	10	16	22	28	34	40	46	52	58	64	70
U_3O_8	18	4	--	11	17	23	29	35	41	47	53	59	65	71
Insoluble	20	5	--	12	18	24	30	36	42	48	54	60	66	72
Soluble	21	6	--	13	19	25	31	37	43	49	55	61	67	73

The header spans "Stream Number" over columns 1–13, and "Xss Number" subtitle below it.

Table 3.3. State Variable Numbers for Module 2 [Xss(74–120)]

Chemical Component	Component Number	Stream Number						
		14	15	16	17	18	19	20
		Xss Number						
H_2O	1	74	81	88	95	102	109	114
HNO_3	9	75	82	89	96	103	110	115
TBP	11	76	83	90	97	104	--	116
$UO_2(NO_3)_2$	14	77	84	91	98	105	111	117
U_3O_8	18	78	85	92	99	106	112	118
Insoluble	20	79	86	93	100	107	--	119
Soluble	21	80	87	94	101	108	113	120

Table 3.4. State Variable Numbers for Module 3 [Xss(121–172)]

Chemical Component	Component Number	Stream Number										
		21	22	23	24	25	26	27	28	29	30	31
		Xss Number										
H_2O	1	121	126	131	--	--	134	141	--	152	161	164
NH_3	3	--	--	--	132	--	135	142	150	--	--	--
CO_2	8	--	--	--	--	133	136	143	151	--	--	--
HNO_3	9	122	127	--	--	--	137	144	--	153	--	165
CH_3OH	10	--	--	--	--	--	--	--	--	154	--	166
NH_4NO_3	12	--	--	--	--	--	--	145	--	155	--	167
$(NH_4)_2CO_3.H_2O$	13	--	--	--	--	--	--	--	--	156	--	168
$UO_2(NO_3)_2$	14	123	128	--	--	--	138	146	--	157	--	169
U_3O_8	18	124	129	--	--	--	139	147	--	158	162	170
$(NH_4)_4UO_2(CO_3)_3$	19	--	--	--	--	--	--	148	--	159	163	171
soluble	21	125	130	--	--	--	140	149	--	160	--	172

Table 3.5. State Variable Numbers for Module 4 [Xss(173–220)]

Chemical Component	Component Number	Stream Number						
		32	33	34	35	36	37	38
		Xss Number						
H_2O	1	--	--	176	--	187	--	193
N_2	2	--	174	177	--	188	192	194
NH_3	3	173	--	178	--	189	--	195
H_2	5	--	175	179	--	190	--	196
HF	6	--	--	--	--	--	--	--
CO_2	8	--	--	180	--	191	--	197
UF_4	16	--	--	--	--	--	--	--
UO_2	17	--	--	181	184	--	--	--
U_3O_8	18	--	--	182	185	--	--	--
$(NH_4)_4UO_2(CO_3)_3$	19	--	--	183	186	--	--	--

Chemical Component	Component Number	Stream Number					
		39	40	41	42	43	44
		Xss Number					
H_2O	1	--	--	--	204	211	--
N_2	2	--	--	202	205	212	--
NH_3	3	--	--	--	--	--	--
H_2	5	--	--	--	--	--	--
HF	6	--	201	203	206	213	--
CO_2	8	--	--	--	--	--	--
UF_4	16	--	--	--	207	214	218
UO_2	17	198	--	--	208	215	219
U_3O_8	18	199	--	--	209	216	220
$(NH_4)_4UO_2(CO_3)_3$	19	200	--	--	210	217	--

Table 3.6. State Variable Numbers for Module 5 [Xss(221–273)]

Chemical Component	Component Number	Stream Number							
		45	46	47	48	49	50	51	52
		Xss Number							
N_2	2	--	--	--	228	233	--	242	--
F_2	7	--	--	227	229	234	--	243	--
UF_6	15	--	--	--	--	235	--	244	246
UF_4	16	221	224	--	230	236	239	245	--
UO_2	17	222	225	--	231	237	240	--	--
U_3O_8	18	223	226	--	232	238	241	--	--

Chemical Component	Component Number	Stream Number							
		53	54	55	56	57	58	59	60
		Xss Number							
N_2	2	247	251	257	263	--	--	--	--
F_2	7	248	252	258	264	--	--	--	--
UF_6	15	249	253	259	--	265	--	272	273
UF_4	16	250	254	260	--	266	269	--	--
UO_2	17	--	255	261	--	267	270	--	--
U_3O_8	18	--	256	262	--	268	271	--	--

Table 3.7. Summary of the Modules

Module	Number of External Inputs	Number of Intermodular Inputs	Number of Output Streams	Number of Streams
1	4	0	4	13
2	5	1	3	7
3	1	1	4	11
4	2	1	3	13
5	1	1	4	16

Module	Stream Numbers	Number of Chemical Components	Number of State Variables	State Variable Numbers
1	1–13	7	73	1–73
2	14–20	7	47	74–120
3	21–31	11	52	121–172
4	32–44	10	48	173–220
5	45–60	6	53	221–273

Table 3.8. Primary Uranium Bearing State Variables within Each Module

State Variable	Stream	Component Formula	Number	Type of Stream
		Module 1		
Xss(3)	1	UN	14	Intermediate
Xss(10)	3	UN	14	Intermediate
Xss(16)	4	UN	14	Intermediate
Xss(40)	8	UN	14	Waste
Xss(41)	8	U_3O_8	18	Waste
Xss(64)	12	UN	14	Product
Xss(70)	13	UN	14	Waste
		Module 2		
Xss(77)	14	UN	14	Intermediate
Xss(84)	15	UN	14	Intermediate
Xss(91)	16	UN	14	Waste
Xss(92)	16	U_3O_8	18	Waste
Xss(98)	17	UN	14	Intermediate
Xss(111)	19	UN	14	Product
Xss(117)	20	UN	14	Waste
		Module 3		
Xss(123)	21	UN	14	Waste
Xss(128)	22	UN	14	Intermediate
Xss(138)	26	UN	14	Intermediate
Xss(148)	27	AUC	19	Intermediate
Xss(159)	29	AUC	19	Intermediate
Xss(163)	30	AUC	19	Product
Xss(169)	31	UN	14	Waste
Xss(171)	31	AUC	19	Waste
		Module 4		
Xss(181)	34	UO_2	17	Intermediate
Xss(184)	35	UO_2	17	Intermediate
Xss(198)	39	UO_2	17	Intermediate
Xss(207)	42	UF_4	16	Intermediate
Xss(208)	42	UO_2	17	Intermediate
Xss(214)	43	UF_4	16	Waste
Xss(215)	43	UO_2	17	Waste
Xss(217)	43	AUC	19	Waste
Xss(218)	44	UF_4	16	Product
Xss(219)	44	UO_2	17	Product

Table 3.8. Primary Uranium Bearing State Variables within Each Module (continued)

State Variable	Stream	Component Formula	Number	Type of Stream
		Module 5		
Xss(221)	45	UF_4	16	Intermediate
Xss(222)	45	UO_2	17	Intermediate
Xss(224)	46	UF_4	16	Intermediate
Xss(225)	46	UO_2	17	Intermediate
Xss(230)	48	UF_4	16	Intermediate
Xss(235)	49	UF_6	15	Intermediate
Xss(239)	**50**	**UF_4**	**16**	**Waste**
Xss(240)	**50**	**UO_2**	**17**	**Waste**
Xss(244)	51	UF_6	15	Intermediate
Xss(246)	52	UF_6	15	Intermediate
Xss(249)	53	UF_6	15	Intermediate
Xss(253)	54	UF_6	15	Intermediate
Xss(254)	54	UF_4	16	Intermediate
Xss(259)	55	UF_6	15	Intermediate
Xss(265)	57	UF_6	15	Intermediate
Xss(269)	**58**	**UF_4**	**16**	**Waste**
Xss(270)	**58**	**UO_2**	**17**	**Waste**
Xss(272)	59	UF_6	15	Intermediate
Xss(273)	**60**	**UF_6**	**15**	**Product**

3.2.1 Module 1: Dissolution

Yellowcake (also known as, uranium ore concentrate) contains impurities at a level such that it cannot be used directly as feed for producing uranium compounds or metal for a nuclear program and must be purified. Purification of yellowcake generally starts with a dissolution process. The dissolution process was used as the start of the ideal natural uranium conversion plant that was the focus of this effort.

Module 1, Dissolution, encompassed the receipt of yellowcake at the facility to the transfer of uranyl nitrate to the solvent extraction process. Module 1 has been further subdivided into five sub-modules. The flowsheet for Module 1 is shown in Figure 3.3.

Yellowcake dissolution is typically performed using nitric acid in some type of stirred, heated vessel. The uranium concentration in the dissolver product solution is varied, depending upon the downstream process requirements (typically ranging between 200–400 g U/L of solution). Both batch and continuous modes of operation can be used in the dissolution process. The equipment utilized must be constructed of materials that are resistant to nitric acid corrosion (e.g., stainless steels). This effort has been limited to only consider a conversion plant that processes 100 MTU/yr. Although the model assumes continuous operation at steady state, the input flow rate of uranium was based on operation of 8 h/day, 5 days/week, and 50 weeks/yr. This resulted in an input flow rate of 50 kg U/h.
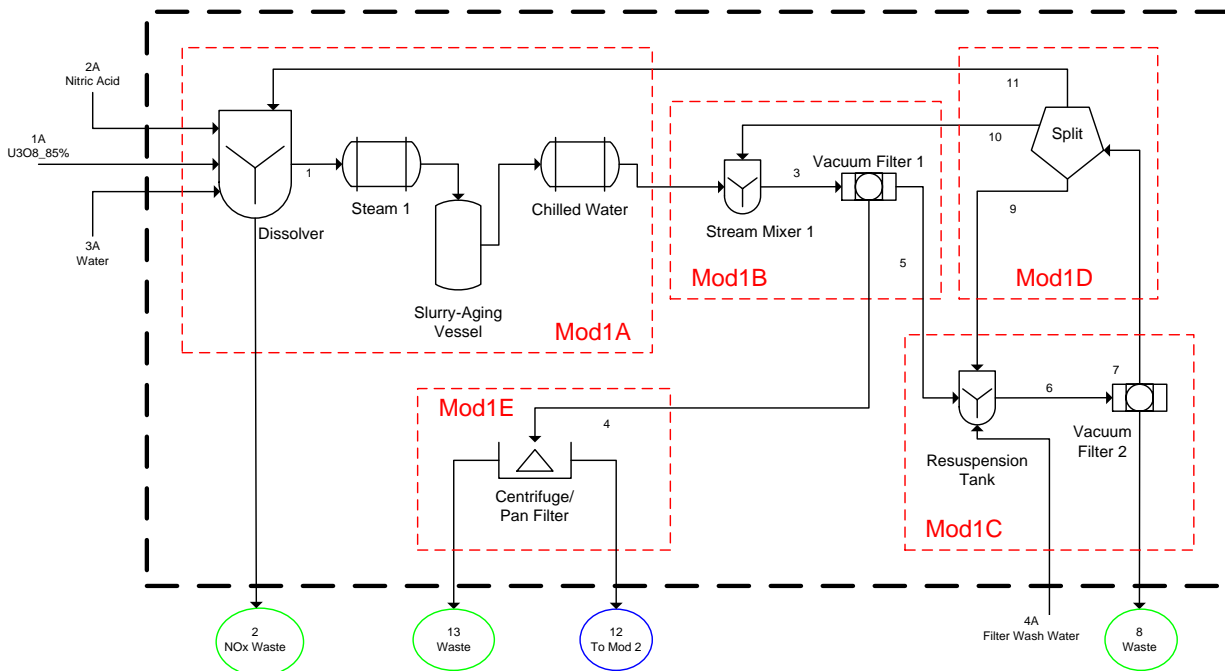
Figure 3.3. Module 1: The Dissolution Process of a Natural Uranium Conversion Plant. In this figure, the plant is processing 100 MTU/yr and utilizing uranium recovery to reduce uranium losses to waste.

Module 1 (Figure 3.3) started with the dissolution of yellowcake in nitric acid to produce uranyl nitrate [$UO_2(NO_3)_2$]. Yellowcake, as impure U_3O_8, was fed into a material feed hopper that feeds a dissolver tank by means of a screw conveyor. The dissolution process was carried out at 80°C. Heat was provided indirectly through a steam jacket surrounding the dissolver tank. After dissolution, the material was sent to a slurry-aging vessel; this is especially necessary if silicas were present in the incoming yellowcake. The slurry-aging vessel was also heated at 90–95°C indirectly by means of a steam jacket. The final concentration of uranium was expected within the range of 400–450 g U/L with a 2.5 N free HNO_3. The slurry was then cooled with chilled water and sent to a vacuum filter system. The liquids from the vacuum filter were pumped to a centrifuge that separates the last solid particles from the liquid. The retained solid particles were part of the solid waste, and the liquid was then sent to the solvent extraction purification system. This liquid was sent to a uranyl nitrate holding tank. The concentration in this tank reached 350–400 g U/L with a concentration of HNO_3 ranging from 1.5 N to 2 N free acid. Uranium losses in the waste stream from the centrifuge can range from less than 0.2% with uranium recovery to 2% for a low efficiency case in a small plant. Module 1 included uranium recovery. The solids from the vacuum filter were transferred to a resuspension tank. This tank was agitated at 25–50 rpm, and water was added. The suspended slurry was sent to a secondary vacuum filter where the filtrate was sent back to the dissolver unit, and the wet solids constituted solid waste.

3.2.1.1 Module 1A

The inputs to the dissolver were the uranium ore concentrate which was assumed to be 85-wt% U_3O_8 and 15-wt% impurities (7.5-wt% soluble impurities and 7.5-wt% insoluble impurities), nitric acid, water, and a recycle stream from Module 1D (internal to Module 1). There were two outputs from the dissolver: 1) the liquid product stream and 2) NO_2 which was vented as waste. The reaction that occurred in the dissolver is shown in Eq. (3.2.1.1).

$$U_3O_8 + 8HNO_3 \rightarrow 3UO_2(NO_3)_2 + 2NO_2 + 4H_2O \qquad (3.2.1.1)$$
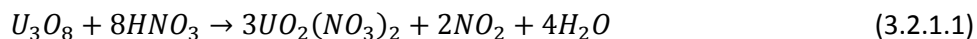
Equation (3.2.1.1) is the idealized form of the reaction. In reality, various forms of NO_x are formed. Additionally, the reaction does not go to completion; the extent of reaction is 0.9799, meaning that 97.99% of the uranium in the U_3O_8 is converted to uranyl nitrate [$UO_2(NO_3)_2$]. Figure 3.4 shows a block diagram of Module 1A with the input and output streams labeled.

Stream 1A was the uranium-bearing input stream which was assumed to be 85 wt-% U_3O_8 and 15 wt-% impurities (7.5 wt-% soluble impurities and 7.5 wt-% insoluble impurities). The molecular weight of U_3O_8 is 842.1 g/mol. Also, U_3O_8 is insoluble in water but soluble in nitric acid. The flow rate of elemental uranium to the dissolver was specified at 50 kg/h. Additionally, the soluble and insoluble impurities do not participate in the reaction. The molecular weight for each impurity was assumed to be 500 g/mol. These impurities are the other metal oxides that would be present following the mining and milling
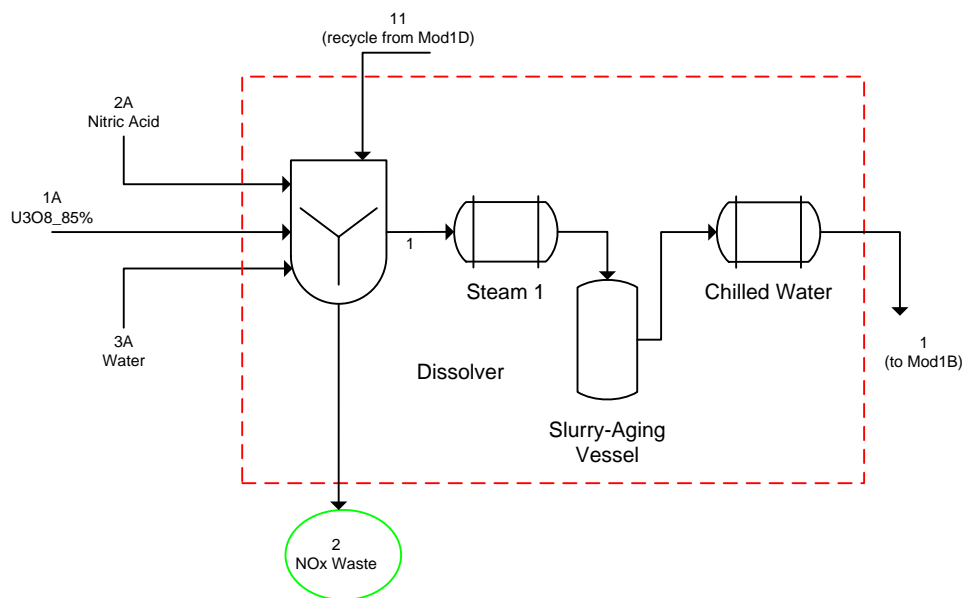
Figure 3.4. Block Diagram of the Module 1A Showing Input and Output Streams.

operations that are performed prior to the conversion process. The mass flow rate of U_3O_8 in Stream 1A based on the assumptions above was 69.37 kg/h.

Stream 2A was the nitric acid input stream to the dissolver. It was assumed that the nitric acid feed stream was commercially available nitric acid which was 70 wt% HNO_3 (15.698 M) with a density of 1.413 g/mL and a molecular weight of 63.01 g/mol. Using the flow rate of uranium into the dissolver and the stoichiometric coefficients from the reaction, the volumetric flow rate of nitric acid needed for the reaction was calculated to be 35.68 L/h. Stream 2A was fed in 20% excess, so the actual flow rate of nitric acid was 42.82 L/h. Nitric acid recycle is not considered as part of this work but it is expected that a plant of this size, especially feeding nitric acid in excess, would use a nitric acid recovery system for cost savings.

Stream 3A was the water input stream. This stream was used to adjust the nitric acid concentration in the dissolver to 6 *N*, which was the specified concentration. The volume of water needed was calculated using the dilution equation, $C_1V_1 = C_2V_2$. Based on the flow rate of nitric acid, the flow rate of water was 69.21 L/h. Stream 11 was a recycle stream from Module 1D and was calculated simultaneously when Module 1 was simulated.

A reaction rate for the dissolution of U_3O_8 in nitric acid based on concentration was not found. However, the dissolution rate based on particle surface area was available. Both Inoue and Tsujino 1984 and Yasuike, Ikeda, and Takashima 1995 provide dissolution rate information for U_3O_8 powders in nitric acid.

The flux, ϕ (mol/cm^2/min), was defined as the dissolution rate per unit surface area of U_3O_8 powder. In order to determine the dissolution rate, the following assumptions were made: the U_3O_8 powders were spherical particles and dissolved homogeneously from their external surface. The dissolution rate from Yasuike, Ikeda, and Takashima 1995 is shown in Eq. (3.2.1.2)

$$\phi = A_1\exp(-5.58 \times 10^4/RT)[HNO_3] + A_2\exp(-6.60 \times 10^4/RT)[HNO_2] \cdot [HNO_3]^2 \qquad (3.2.1.2)$$

where A_1, A_2, R, and T are 35 cm/min, 2.0×10^4 cm^7/mol^2·min, the gas constant (8.314 J/mol·K), and the absolute temperature (K), respectively. The units of the concentration are mol/cm^3. In order to use the rate equation in the development of state equations, it would have been necessary to make many assumptions. Due to this and since the extent of reaction was known, it was determined to be reasonable to use the extent of reaction instead of the dissolution rate especially since this process was being modeled at steady-state.

The component mole balance equations used to model the dissolver are shown below. There are seven chemical components present in Module 1: U_3O_8, HNO_3, H_2O, $UO_2(NO_3)_2$, NO_2, insoluble and soluble impurities. Equation (3.2.1.3) is the conversion of the input mass flow rate of U_3O_8 to moles, where F_{iA} is the mass flow rate of input stream iA (kg/h), $x_{i,j}$ is the mass fraction of component j in stream i (wt-%), MW_j is the molecular weight of component j (g/mol), and $F_{i,j}$ is the molar flow rate of component j in stream i (mol/h). Equations (3.2.1.4) and (3.2.1.5) is the conversion of the input mass flow rate of water to moles in Streams 2A and 3A, respectively.

$$F_{1A} * x_{1A,18} * \frac{1000}{MW_{18}} = F_{1A,18} \qquad (3.2.1.3)$$

$$F_{2A} * x_{2A,1} * \frac{1000}{MW_1} = F_{2A,1} \qquad (3.2.1.4)$$

$$F_{3A} * x_{3A,1} * \frac{1000}{MW_1} = F_{3A,1} \qquad (3.2.1.5)$$

Water entered the reactor from input streams 2A and 3A as well as the recycle stream, Stream 11. Additional water was produced in the dissolver during the reaction of U_3O_8 with nitric acid. Equation (3.2.1.6) is the mole balance for water, where $n_{Mod1,i}$ is the stoichiometric coefficient of the i-th component of the dissolution reaction and X_{Mod1} is the extent of reaction for the dissolution reaction. The stoichiometric coefficients are positive for products and negative for reactants.

$$F_{2A,1} + F_{3A,1} + F_{11,1} - F_{1,1} + n_{Mod1,1} * X_{Mod1} * (F_{1A,18} + F_{11,18}) = 0 \quad (3.2.1.6)$$

Nitric acid entered the reactor from input stream 2A as well as the recycle stream, Stream 11. Nitric acid was consumed in the dissolver during the reaction of U_3O_8 with nitric acid. Since nitric acid was fed in excess and the reaction does not go to completion, it was expected that there would be nitric acid present in the product stream. Equation (3.2.1.7) is the mole balance for nitric acid.

$$F_{2A} * x_{2A,9} * \frac{1000}{MW_9} + F_{11,9} - F_{1,9} + n_{Mod1,9} * X_{Mod1} * \left(F_{1A,18} + F_{11,18}\right) = 0 \qquad (3.2.1.7)$$

Equation (3.2.1.8) is the mole balance for uranyl nitrate. It entered the reactor from the recycle stream (Stream 11) and was produced in the dissolver during the reaction of U_3O_8 with nitric acid.

$$F_{11,14} - F_{1,14} + n_{Mod1,14} * X_{Mod1} * \left(F_{1A,18} + F_{11,18}\right) = 0 \qquad (3.2.1.8)$$

Equation (3.2.1.9) is the mole balance for U_3O_8, which entered the reactor from input stream 1A as well as the recycle stream and was partially consumed in the reaction.

$$F_{1A,18} + F_{11,18} - F_{1,18} + n_{Mod1,18} * X_{Mod1} * \left(F_{1A,18} + F_{11,18}\right) = 0 \qquad (3.2.1.9)$$

Equations (3.2.1.10) and (3.2.1.11) are the mole balances for the insoluble and soluble impurities, respectively. Both impurities entered the reactor from input stream 1A as well as the recycle stream, but did not participate in the reaction.

$$F_{1A} * x_{1A,20} * \frac{1000}{MW_{20}} + F_{11,20} - F_{1,20} = 0 \qquad (3.2.1.10)$$

$$F_{1A} * x_{1A,21} * \frac{1000}{MW_{21}} + F_{11,21} - F_{1,21} = 0 \qquad (3.2.1.11)$$

Equation (3.2.1.12) is the mole balance for NO_2 which was the waste stream, Stream 2. It was produced during the reaction but did not enter as an input or from the recycle stream. For this ideal case, it was assumed that no other NO_x compounds were produced and that all NO_2 exited in Stream 2 and that only NO_2 was present in Stream 2.

$$-F_{2,4} + n_{Mod1,4} * X_{Mod1} * \left(F_{1A,18} + F_{11,18}\right) = 0 \qquad (3.2.1.12)$$

The remainder of Module 1A included the heat exchangers and a slurry-aging vessel. The heat exchangers and vessel do not change the composition and were not included in the model.

3.2.1.2 Module 1B

Module 1B included a stream mixer and the primary vacuum filter. The stream mixer was used to mix the output of the dissolver with a recycle stream from Module 1D. The vacuum filter separated the liquid product from any undissolved solids. The liquid was sent to Module 1E, and the solids were sent to Module 1C to be recycled through the process. Figure 3.5 shows a block diagram of Module 1B with the input and output streams labeled.

44
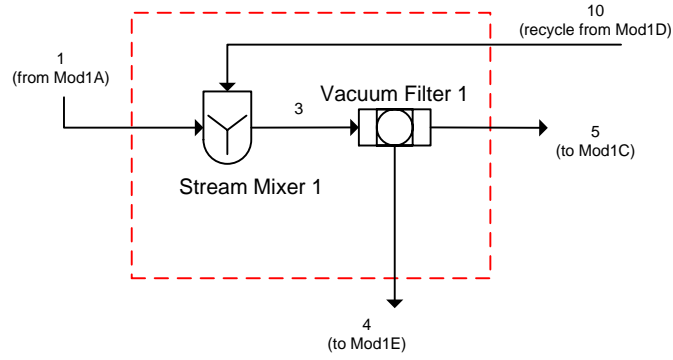
Figure 3.5. Block Diagram of the Module 1B Showing Input and Output Streams.

The component mole balances for the stream mixer are shown below in Eqs. (3.2.1.13)–(3.2.1.18).

$$F_{1,1} + F_{10,1} - F_{3,1} = 0 \qquad (3.2.1.13)$$

$$F_{1,9} + F_{10,9} - F_{3,9} = 0 \qquad (3.2.1.14)$$

$$F_{1,14} + F_{10,14} - F_{3,14} = 0 \qquad (3.2.1.15)$$

$$F_{1,18} + F_{10,18} - F_{3,18} = 0 \qquad (3.2.1.16)$$

$$F_{1,20} + F_{10,20} - F_{3,20} = 0 \qquad (3.2.1.17)$$

$$F_{1,21} + F_{10,21} - F_{3,21} = 0 \qquad (3.2.1.18)$$

The vacuum filter separated Stream 3 into two streams. The separation was defined as the fraction that went to the liquid stream from the input stream by parameter, $K_{Mod1B,i}$, where each component, i, had a different fractionation. Equations (3.2.1.19)–(3.2.1.24) define the separation of Stream 3 into Stream 4.

$$K_{Mod1B,1} * F_{3,1} - F_{4,1} = 0 \qquad (3.2.1.19)$$

$$K_{Mod1B,9} * F_{3,9} - F_{4,9} = 0 \qquad (3.2.1.20)$$

$$K_{Mod1B,14} * F_{3,14} - F_{4,14} = 0 \qquad (3.2.1.21)$$

$$K_{Mod1B,18} * F_{3,18} - F_{4,18} = 0 \qquad (3.2.1.22)$$

$$K_{Mod1B,20} * F_{3,20} - F_{4,20} = 0 \qquad (3.2.1.23)$$

$$K_{Mod1B,21} * F_{3,21} - F_{4,21} = 0 \qquad (3.2.1.24)$$

45

Equations (3.2.1.25)–(3.2.1.30) calculate the mole balances for Stream 5.

$$F_{3,1} - F_{4,1} - F_{5,1} = 0 \tag{3.2.1.25}$$

$$F_{3,9} - F_{4,9} - F_{5,9} = 0 \tag{3.2.1.26}$$

$$F_{3,14} - F_{4,14} - F_{5,14} = 0 \tag{3.2.1.27}$$

$$F_{3,18} - F_{4,18} - F_{5,18} = 0 \tag{3.2.1.28}$$

$$F_{3,20} - F_{4,20} - F_{5,20} = 0 \tag{3.2.1.29}$$

$$F_{3,21} - F_{4,21} - F_{5,21} = 0 \tag{3.2.1.30}$$

3.2.1.3 Module 1C

Module 1C encompassed the resuspension tank and the secondary vacuum filter. The resuspension tank had inputs of the solid stream exiting the primary vacuum filter, a recycle stream from Module 1D, and a new input stream of water which was used to resuspend the solids. There was only one output from the resuspension tank which was fed to the secondary vacuum filter. Figure 3.6 shows a block diagram of Module 1C with the input and output streams labeled.
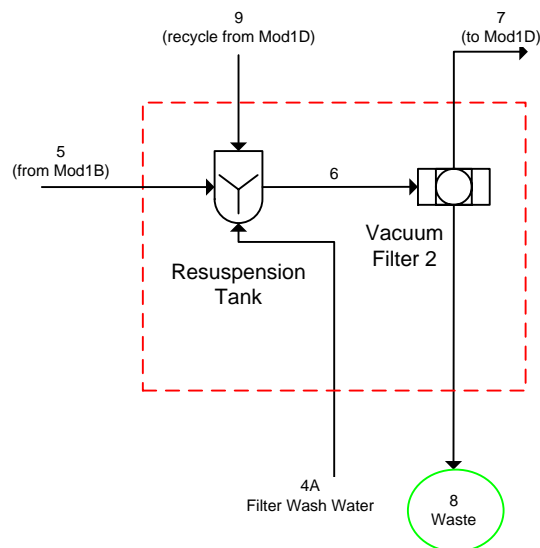
Figure 3.6. Block Diagram of the Module 1C Showing Input and Output Streams.

Equations (3.2.1.31)–(3.2.1.36) are the component mole balances for the resuspension tank.

$$F_{5,1} + F_{9,1} + F_{4A} * \frac{1000}{MW_1} - F_{6,1} = 0 \qquad (3.2.1.31)$$

$$F_{5,9} + F_{9,9} - F_{6,9} = 0 \qquad (3.2.1.32)$$

$$F_{5,14} + F_{9,14} - F_{6,14} = 0 \qquad (3.2.1.33)$$

$$F_{5,18} + F_{9,18} - F_{6,18} = 0 \qquad (3.2.1.34)$$

$$F_{5,20} + F_{9,20} - F_{6,20} = 0 \qquad (3.2.1.35)$$

$$F_{5,21} + F_{9,21} - F_{6,21} = 0 \qquad (3.2.1.36)$$

The secondary vacuum filter separated the remaining solid waste from the liquid which was sent to a splitter to be recycled upstream in the process. The separation was defined as the fraction that was sent to the liquid stream from the input stream by parameter, $K_{Mod1C,i}$, where each component, i, had a different fractionation. Equations (3.2.1.37)–(3.2.1.42) define the separation of Stream 6 into Stream 7.

$$K_{Mod1C,1} * F_{6,1} - F_{7,1} = 0 \qquad (3.2.1.37)$$

$$K_{Mod1C,9} * F_{6,9} - F_{7,9} = 0 \qquad (3.2.1.38)$$

$$K_{Mod1C,14} * F_{6,14} - F_{7,14} = 0 \qquad (3.2.1.39)$$

$$K_{Mod1C,18} * F_{6,18} - F_{7,18} = 0 \qquad (3.2.1.40)$$

$$K_{Mod1C,20} * F_{6,20} - F_{7,20} = 0 \qquad (3.2.1.41)$$

$$K_{Mod1C,21} * F_{6,21} - F_{7,21} = 0 \qquad (3.2.1.42)$$

Equations (3.2.1.43)–(3.2.1.48) calculate the mole balance for Stream 8, which was a waste stream that completely exits Module 1 and the process.

$$F_{6,1} - F_{7,1} - F_{8,1} = 0 \qquad (3.2.1.43)$$

$$F_{6,9} - F_{7,9} - F_{8,9} = 0 \qquad (3.2.1.44)$$

$$F_{6,14} - F_{7,14} - F_{8,14} = 0 \qquad (3.2.1.45)$$

$$F_{6,18} - F_{7,18} - F_{8,18} = 0 \qquad (3.2.1.46)$$

$$F_{6,20} - F_{7,20} - F_{8,20} = 0 \qquad (3.2.1.47)$$

$$F_{6,21} - F_{7,21} - F_{8,21} = 0 \qquad (3.2.1.48)$$

3.2.1.4 Module 1D

Module 1D was the splitter which creates the recycle streams for the previous sub-modules. This recycle reduced the amount of uranium that was lost to waste. The input stream was evenly split into three output streams, as shown in Eqs. (3.2.1.49)–(3.2.1.66). Figure 3.7 shows a block diagram of Module 1D with the input and output streams labeled.

$$F_{7,1} * \left(\frac{1}{3}\right) - F_{9,1} = 0 \qquad (3.2.1.49)$$

$$F_{7,9} * \left(\frac{1}{3}\right) - F_{9,9} = 0 \qquad (3.2.1.50)$$

$$F_{7,14} * \left(\frac{1}{3}\right) - F_{9,14} = 0 \qquad (3.2.1.51)$$

$$F_{7,18} * \left(\frac{1}{3}\right) - F_{9,18} = 0 \qquad (3.2.1.52)$$

$$F_{7,20} * \left(\frac{1}{3}\right) - F_{9,20} = 0 \qquad (3.2.1.53)$$

$$F_{7,21} * \left(\frac{1}{3}\right) - F_{9,21} = 0 \qquad (3.2.1.54)$$

$$F_{7,1} * \left(\frac{1}{3}\right) - F_{10,1} = 0 \qquad (3.2.1.55)$$

$$F_{7,9} * \left(\frac{1}{3}\right) - F_{10,9} = 0 \qquad (3.2.1.56)$$

$$F_{7,14} * \left(\frac{1}{3}\right) - F_{10,14} = 0 \qquad (3.2.1.57)$$

$$F_{7,18} * \left(\frac{1}{3}\right) - F_{10,18} = 0 \qquad (3.2.1.58)$$

$$F_{7,20} * \left(\frac{1}{3}\right) - F_{10,20} = 0 \qquad (3.2.1.59)$$
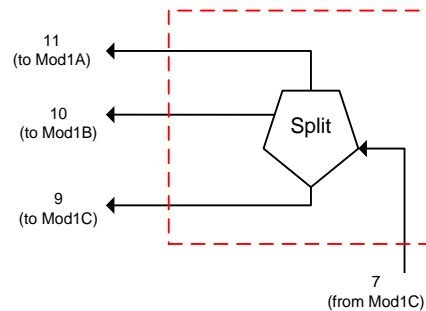
Figure 3.7. Block Diagram of the Module 1D Showing Input and Output Streams.

48

$$F_{7,21} * \left(\frac{1}{3}\right) - F_{10,21} = 0 \tag{3.2.1.60}$$

$$F_{7,1} - F_{9,1} - F_{10,1} - F_{11,1} = 0 \tag{3.2.1.61}$$

$$F_{7,9} - F_{9,9} - F_{10,9} - F_{11,9} = 0 \tag{3.2.1.62}$$

$$F_{7,14} - F_{9,14} - F_{10,14} - F_{11,14} = 0 \tag{3.2.1.63}$$

$$F_{7,18} - F_{9,18} - F_{10,18} - F_{11,18} = 0 \tag{3.2.1.64}$$

$$F_{7,20} - F_{9,20} - F_{10,20} - F_{11,20} = 0 \tag{3.2.1.65}$$

$$F_{7,21} - F_{9,21} - F_{10,21} - F_{11,21} = 0 \tag{3.2.1.66}$$

3.2.1.5 Module 1E

Module 1E was the final sub-module in Module 1. In this module, the liquid from the primary vacuum filter was centrifuged to remove additional solid particulates. There were two outputs from the centrifuge: 1) the impure liquid uranyl nitrate stream which was sent to solvent extraction for purification and 2) the solid waste. The separation was defined as the fraction that was sent to the liquid stream from the input stream by parameter, $K_{Mod1E,i}$, where each component, i, had a different fractionation value. Figure 3.8 shows a block diagram of Module 1E with the input and output streams labeled.
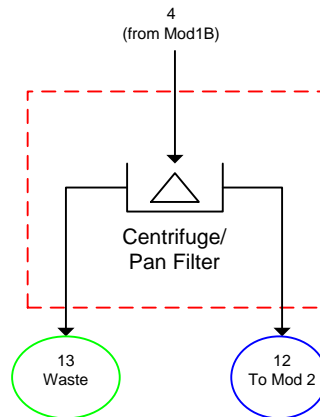
Figure 3.8. Block Diagram of the Module 1E Showing Input and Output Streams.

Equations (3.2.1.67)–(3.2.1.72) define the separation of Stream 4 into Stream 12. Stream 12 exits Module 1 and was one of the feed streams to Module 2.

$$K_{Mod1E,1} * F_{4,1} - F_{12,1} = 0 \tag{3.2.1.67}$$

$$K_{Mod1E,9} * F_{4,9} - F_{12,9} = 0 \tag{3.2.1.68}$$

$$K_{Mod1E,14} * F_{4,14} - F_{12,14} = 0 \tag{3.2.1.69}$$

$$K_{Mod1E,18} * F_{4,18} - F_{12,18} = 0 \tag{3.2.1.70}$$

$$K_{Mod1E,20} * F_{4,20} - F_{12,20} = 0 \tag{3.2.1.71}$$

$$K_{Mod1E,21} * F_{4,21} - F_{12,21} = 0 \tag{3.2.1.72}$$

Equations (3.2.1.73)–(3.2.1.78) calculate the mole balances for Stream 13, the waste stream. Stream 13 completely exited Module 1 and the process.

$$F_{4,1} - F_{12,1} - F_{13,1} = 0 \tag{3.2.1.73}$$

$$F_{4,9} - F_{12,9} - F_{13,9} = 0 \tag{3.2.1.74}$$

$$F_{4,14} - F_{12,14} - F_{13,14} = 0 \tag{3.2.1.75}$$

$$F_{4,18} - F_{12,18} - F_{13,18} = 0 \tag{3.2.1.76}$$

$$F_{4,20} - F_{12,20} - F_{13,20} = 0 \tag{3.2.1.77}$$

$$F_{4,21} - F_{12,21} - F_{13,21} = 0 \tag{3.2.1.78}$$

3.2.1.6 Module 1: Overall Material Balance

The overall material balances served as an internal check that the calculations of the sub-module component balances were correct. Component mole balances were used to model each of the process units in all of the modules, but the same method was applied to the overall module as well.

The streams used for the overall material balances were those that cross the dark dashed boundary that enclosed all of Module 1. There were four input streams and four output streams for Module 1. Additionally, there was one reaction in Module 1 that occurred in the dissolver and was described by Eq. (3.2.1.1).

$$U_3O_8 + 8HNO_3 \rightarrow 3UO_2(NO_3)_2 + 2NO_2 + 4H_2O \qquad (3.2.1.1)$$
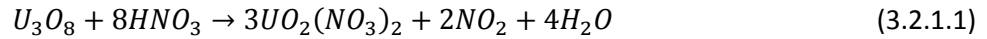
The overall component material balances are Module 1 are shown in Eqs. (3.2.1.79)–(3.2.1.85).

$$F_{2A,1} + F_{3A,1} + F_{4A,1} + \left(n_{Mod1A,1} * X_{Mod1A} * \left(F_{1A,18} + F_{11,18}\right)\right) - F_{8,1} - F_{12,1} - F_{13,1} = 0$$
$$(3.2.1.79)$$

$$\left(n_{Mod1A,4} * X_{Mod1A} * \left(F_{1A,18} + F_{11,18}\right)\right) - F_{2,4} = 0 \qquad (3.2.1.80)$$

$$F_{2A} * x_{2A,9} * \frac{1000}{MW_9} + \left(n_{Mod1A,9} * X_{Mod1A} * \left(F_{1A,18} + F_{11,18}\right)\right) - F_{8,9} - F_{12,9} - F_{13,9} = 0 \quad (3.2.1.81)$$

$$\left(n_{Mod1A,14} * X_{Mod1A} * \left(F_{1A,18} + F_{11,18}\right)\right) - F_{8,14} - F_{12,14} - F_{13,14} = 0 \qquad (3.2.1.82)$$

$$F_{1A} * x_{1A,18} * \frac{1000}{MW_{18}} + \left(n_{Mod1A,18} * X_{Mod1A} * \left(F_{1A,18} + F_{11,18}\right)\right) - F_{8,18} - F_{12,18} - F_{13,18} = 0$$
$$(3.2.1.83)$$

$$F_{1A} * x_{1A,20} * \frac{1000}{MW_{20}} - F_{8,20} - F_{12,20} - F_{13,20} = 0 \qquad (3.2.1.84)$$

$$F_{1A} * x_{1A,21} * \frac{1000}{MW_{21}} - F_{8,21} - F_{12,21} - F_{13,21} = 0 \qquad (3.2.1.85)$$

3.2.2 Module 2: Solvent Extraction

The uranyl nitrate solution obtained from dissolution is typically purified using liquid-liquid solvent extraction. The organic solvent that is most commonly used for the extraction of uranium from uranyl nitrate solutions is tributyl phosphate (TBP) diluted in kerosene.

Module 2, Solvent Extraction, encompassed the purification of the dissolved uranium ore concentrate using TBP. Module 2 was further subdivided into four sub-modules. The flowsheet for Module 2 is shown in Figure 3.9.

The uranyl nitrate from the dissolution process was sent to a feed-adjustment tank where the concentration was expected to be in the range of 350–400 g U/L, and the concentration of free acid was expected to be 1.5–2 N. Water and HNO_3 were used to adjust the feed to the desired values (typically 250–350 g U/L and 1–4 N free acid).

The purification process typically consists of three parts, where each of the parts performs a different function in the purification process. The first part extracts the uranium from the aqueous solution into the organic phase, referred to as extraction. The second part removes impurities from the uranium-bearing organic stream, referred to as the scrubbing section. In the third part, uranium is
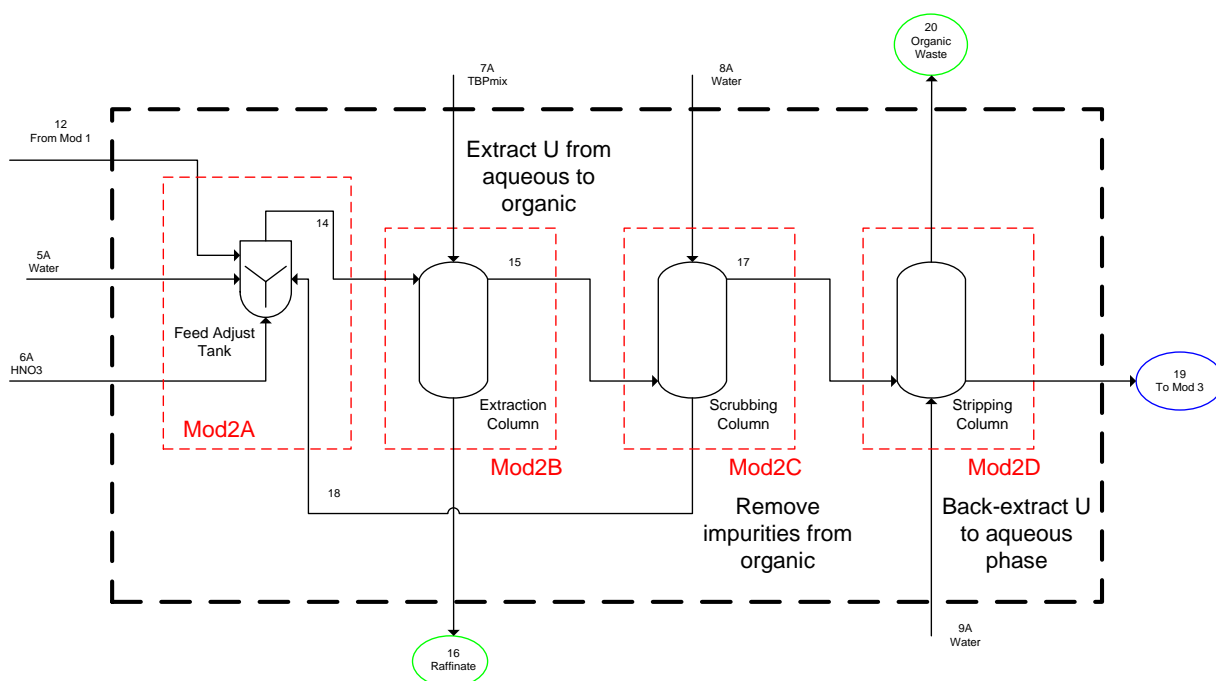
Figure 3.9. Module 2: The Solvent Extraction Process of a Natural Uranium Conversion Plant.

stripped (back-extracted) from the scrubbed uranium-bearing organic stream back into an aqueous stream, referred to as the stripping or re-extraction section.

The organic phase leaves the extraction column at the top, and the raffinate was collected at the bottom. Raffinate constituted another waste stream of the process. The organic phase was pumped to the bottom of the scrubbing column, where impurities contained in the organic phase were washed into demineralized water in a counter current mode. The bottom aqueous liquid was sent back to the adjustment tank to be returned to the extraction column, and the top organic stream was sent to the stripping column. The uranium was stripped from the scrubbed uranium-bearing organic stream back into an aqueous stream. The top product was organic material that was sent to the solvent storage or to the organic cleanup facility. The bottom product was the purified uranyl nitrate that was sent to a storage tank. The expected concentration of this liquid was 80–100 gU/L with very little contaminants. In an actual conversion plant, solvent extraction takes approximately 6 hours with a 2 hour equilibrium period. The uranium losses to the raffinate and organic waste streams are 0.6–1.0% due to limited separation capability as well as phase carryover.

Various types of extraction equipment (e.g., mixer-settlers, pulsed columns, packed columns, mixer-agitated columns, and centrifugal contactors) are used in conversion facilities. Because the

aqueous stream containing uranium is nitric acid, the equipment utilized in purification must be constructed of materials that are resistant to nitric acid corrosion (i.e., stainless steels). The extraction process in this study, for example, utilized pulse columns.

The solvent, TBP, tends to degrade over time, especially in the presence of acids. The presence of the degradation products, such as the dibutyl phosphate (DBP), mono-butyl phosphate (MBP), and phosphoric acid, can have a detrimental effect on the extraction process. Some of the problems encountered include poor phase separation in the extraction equipment, extraction of other elements in addition to uranium, loss of uranium caused by the formation of stable complexes in the organic phase, and the formation of precipitates. Thus, the degradation products are periodically removed from the organic stream in order to maintain purification of the uranyl nitrate solutions to the desired level. Typically, the organic stream leaving the extraction strip column is periodically cleaned by mixing with a dilute sodium carbonate solution (~5-wt% Na_2CO_3). The degradation products readily dissolve in the solution forming soluble sodium salts. The organic, after treatment, is washed with water and dilute nitric acid to remove emulsions and to neutralize any residual alkalinity prior to returning it to the extraction process. The cleaned organic, which contains residual uranium, is returned to the extraction process for reuse. The organic recovery process is outside the scope of this work but is important to note for potential diversion scenarios. The formation of DBP, MBP, and phosphoric acid are not considered in the material balance calculations for this ideal case.

3.2.2.1 Module 2A

Module 2A encompassed the feed adjustment tank. In the feed adjustment tank, the concentration of the uranyl nitrate and the amount of acid were adjusted to the desired levels by the addition of water and nitric acid. The solution was typically adjusted to 250–350 g U/L and 1–4 N free acid. The inputs to the feed adjustment tank included the uranyl nitrate stream from Module 1, water, nitric acid, and a recycle stream from Module 2C (internal to Module 2). There was one output from Module 2A which was the adjusted uranyl nitrate solution. Figure 3.10 shows a block diagram of Module 2A with the input and output streams labeled.

Component mole balances were used to model each of the process units in Module 2. The component mole balances for the feed adjustment tank are shown below in Eqs. (3.2.2.1)–(3.2.2.7). Streams 5A and 6A are pure water and pure nitric acid, respectively. Tributyl phosphate enters with the recycle stream. The amount of TBP in the recycle stream is based on a set level of solvent carryover.

$$F_{12,1} + F_{5A} * \frac{1000}{MW_1} + F_{18,1} - F_{14,1} = 0 \qquad (3.2.2.1)$$

$$F_{12,9} + F_{6A} * \frac{1000}{MW_9} + F_{18,9} - F_{14,9} = 0 \qquad (3.2.2.2)$$

53
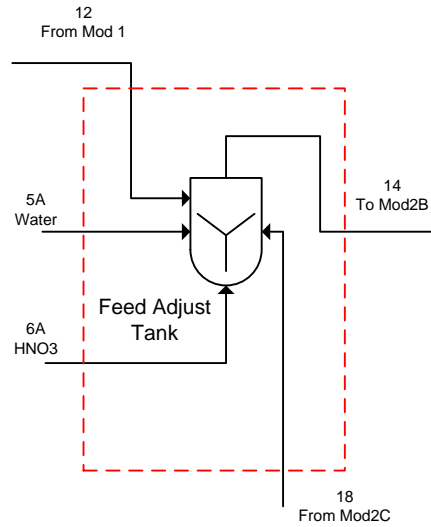
Figure 3.10. Block Diagram of the Module 2A Showing Input and Output Streams.

$$F_{18,11} - F_{14,11} = 0 \tag{3.2.2.3}$$

$$F_{12,14} + F_{18,14} - F_{14,14} = 0 \tag{3.2.2.4}$$

$$F_{12,18} + F_{18,18} - F_{14,18} = 0 \tag{3.2.2.5}$$

$$F_{12,20} + F_{18,20} - F_{14,20} = 0 \tag{3.2.2.6}$$

$$F_{12,21} + F_{18,21} - F_{14,21} = 0 \tag{3.2.2.7}$$

3.2.2.2 Module 2B

Module 2B encompassed the extraction column, where uranium was extracted from the aqueous uranyl nitrate solution into the organic phase using TBP. The stripping of uranium from the aqueous phase to the organic phase is explained by Eq. (3.2.2.8).

$$UO_2(NO_3)_2 \cdot 6H_2O(aq) + 2TBP(or) \leftrightarrow UO_2(NO_3)_2 \cdot 2TBP(or) + 6H_2O(aq) \tag{3.2.2.8}$$
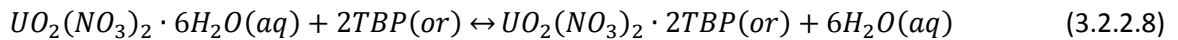
The inputs to Module 2B were the output of Module 2A and the TBP/diluent mixture. There were two outputs from Module 2B: (1) the raffinate to waste and (2) the uranium-bearing organic stream to scrubbing. Figure 3.11 shows a block diagram of Module 2B with the input and output streams labeled.
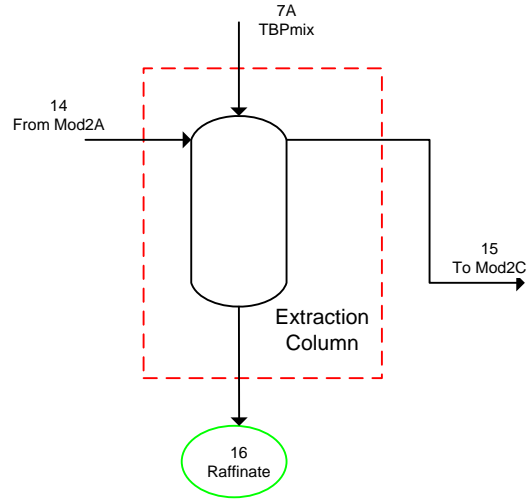
Figure 3.11. Block Diagram of the Module 2B Showing Input and Output Streams.

The extraction column separated Stream 14 along with Stream 7A into two streams. Stream 7A was defined as pure TBP, where TBP here actually represented the TBP/diluent mixture. The separation was defined as the fraction that was sent to the organic stream from the input stream by parameter, $K_{Mod2B,i}$, where each component, i, had a different fractionation. Equations (3.2.2.9)–(3.2.2.15) define the separation of Stream 14 and Stream 7A into Stream 15.

$$K_{Mod2B,1} * F_{14,1} - F_{15,1} = 0 \tag{3.2.2.9}$$

$$K_{Mod2B,9} * F_{14,9} - F_{15,9} = 0 \tag{3.2.2.10}$$

$$K_{Mod2B,11} * \left(F_{14,11} + F_{7A} * \frac{1000}{MW_{11}} \right) - F_{15,11} = 0 \tag{3.2.2.11}$$

$$K_{Mod2B,14} * F_{14,14} - F_{15,14} = 0 \tag{3.2.2.12}$$

$$K_{Mod2B,18} * F_{14,18} - F_{15,18} = 0 \tag{3.2.2.13}$$

$$K_{Mod2B,20} * F_{14,20} - F_{15,20} = 0 \tag{3.2.2.14}$$

$$K_{Mod2B,21} * F_{14,21} - F_{15,21} = 0 \tag{3.2.2.15}$$

Equations (3.2.2.16)–(3.2.2.22) calculate the mole balances for Stream 16.

$$F_{14,1} - F_{15,1} - F_{16,1} = 0 \tag{3.2.2.16}$$

$$F_{14,9} - F_{15,9} - F_{16,9} = 0 \tag{3.2.2.17}$$

$$\left(F_{14,11} + F_{7A} * \frac{1000}{MW_{11}} \right) - F_{15,11} - F_{16,11} = 0 \qquad (3.2.2.18)$$

$$F_{14,14} - F_{15,14} - F_{16,14} = 0 \qquad (3.2.2.19)$$

$$F_{14,18} - F_{15,18} - F_{16,18} = 0 \qquad (3.2.2.20)$$

$$F_{14,20} - F_{15,20} - F_{16,20} = 0 \qquad (3.2.2.21)$$

$$F_{14,21} - F_{15,21} - F_{16,21} = 0 \qquad (3.2.2.22)$$

3.2.2.3 Module 2C

Module 2C encompassed the scrubbing column, which removed impurities from the uranium-bearing organic phase. The inputs to Module 2C were the output of Module 2B and water. There were two outputs from Module 2C: (1) the recycle which was returned to Module 2A and (2) the uranium-bearing organic stream to stripping. Figure 3.12 shows a block diagram of Module 2C with the input and output streams labeled.

The scrubbing column separated Stream 15 along with Stream 8A into two streams. Stream 8A was pure water. The separation was defined as the fraction that was sent to the organic stream from the input stream by parameter, $K_{Mod2C,i}$, where each component, i, had a different fractionation. Equations (3.2.2.23)–(3.2.2.29) define the separation of Stream 15 and Stream 8A into Stream 17.
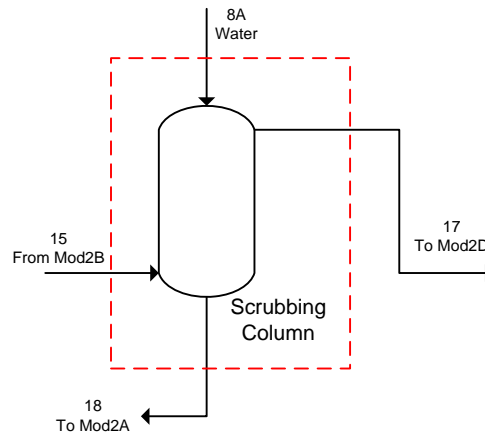
Figure 3.12. Block Diagram of the Module 2C Showing Input and Output Streams.

$$K_{Mod2C,1} * \left(F_{15,1} + F_{8A} * \frac{1000}{MW_1} \right) - F_{17,1} = 0 \qquad (3.2.2.23)$$

$$K_{Mod2C,9} * F_{15,9} - F_{17,9} = 0 \qquad (3.2.2.24)$$

$$K_{Mod2C,11} * F_{15,11} - F_{17,11} = 0 \qquad (3.2.2.25)$$

$$K_{Mod2C,14} * F_{15,14} - F_{17,14} = 0 \qquad (3.2.2.26)$$

$$K_{Mod2C,18} * F_{15,18} - F_{17,18} = 0 \qquad (3.2.2.27)$$

$$K_{Mod2C,20} * F_{15,20} - F_{17,20} = 0 \qquad (3.2.2.28)$$

$$K_{Mod2C,21} * F_{15,21} - F_{17,21} = 0 \qquad (3.2.2.29)$$

Equations (3.2.2.30)–(3.2.2.36) calculate the mole balances for Stream 18.

$$\left(F_{15,1} + F_{8A} * \frac{1000}{MW_1} \right) - F_{17,1} - F_{18,1} = 0 \qquad (3.2.2.30)$$

$$F_{15,9} - F_{17,9} - F_{18,9} = 0 \qquad (3.2.2.31)$$

$$F_{15,11} - F_{17,11} - F_{18,11} = 0 \qquad (3.2.2.32)$$

$$F_{15,14} - F_{17,14} - F_{18,14} = 0 \qquad (3.2.2.33)$$

$$F_{15,18} - F_{17,18} - F_{18,18} = 0 \qquad (3.2.2.34)$$

$$F_{15,20} - F_{17,20} - F_{18,20} = 0 \qquad (3.2.2.35)$$

$$F_{15,21} - F_{17,21} - F_{18,21} = 0 \qquad (3.2.2.36)$$

3.2.2.4 Module 2D

Module 2D encompassed the stripping column, which back extracted the purified uranium out of the organic phase into the aqueous phase. The inputs to Module 2D were the output of Module 2C and water. There were two outputs from Module 2D: (1) the organic waste stream and (2) the uranium-bearing aqueous stream to Module 3. Figure 3.13 shows a block diagram of Module 2D with the input and output streams labeled.

The stripping column separates Stream 17 along with Stream 9A into two streams. Stream 9A was pure water. The separation was defined as the fraction that was sent to the aqueous stream from the input stream by parameter, $K_{Mod2D,i}$, where each component, i, had a different fractionation. Equations
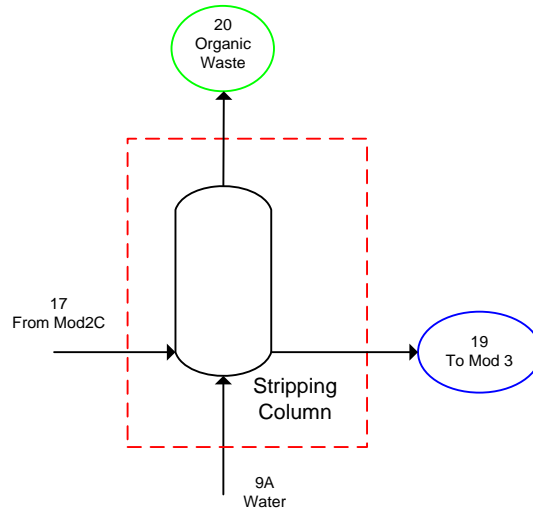
Figure 3.13. Block Diagram of the Module 2D Showing Input and Output Streams.

(3.2.2.37)–(3.2.2.41) define the separation of Stream 17 and Stream 9A into Stream 19. All of the TBP and the insoluble impurities were sent to the organic waste stream.

$$K_{Mod2D,1} * \left(F_{17,1} + F_{9A} * \frac{1000}{MW_1}\right) - F_{19,1} = 0 \qquad (3.2.2.37)$$

$$K_{Mod2D,9} * F_{17,9} - F_{19,9} = 0 \qquad (3.2.2.38)$$

$$K_{Mod2D,14} * F_{17,14} - F_{19,14} = 0 \qquad (3.2.2.39)$$

$$K_{Mod2D,18} * F_{17,18} - F_{19,18} = 0 \qquad (3.2.2.40)$$

$$K_{Mod2D,21} * F_{17,21} - F_{19,21} = 0 \qquad (3.2.2.41)$$

Equations (3.2.2.42)–(3.2.2.48) calculate the mole balances for Stream 20.

$$\left(F_{17,1} + F_{9A} * \frac{1000}{MW_1}\right) - F_{19,1} - F_{20,1} = 0 \qquad (3.2.2.42)$$

$$F_{17,9} - F_{19,9} - F_{20,9} = 0 \qquad (3.2.2.43)$$

$$F_{17,11} - F_{20,11} = 0 \qquad (3.2.2.44)$$

$$F_{17,14} - F_{19,14} - F_{20,14} = 0 \qquad (3.2.2.45)$$

$$F_{17,18} - F_{19,18} - F_{20,18} = 0 \qquad (3.2.2.46)$$

$$F_{17,20} - F_{20,20} = 0 \qquad\qquad (3.2.2.47)$$

$$F_{17,21} - F_{19,21} - F_{20,21} = 0 \qquad\qquad (3.2.2.48)$$

3.2.2.5 Module 2: Overall Material Balance

The streams used for the overall material balances were those that cross the dark dashed boundary that enclosed all of Module 2. There were six input streams and three output streams for Module 2. One of the input streams was an output of Module 1. There was no reaction in Module 2. The overall component material balances for Module 2 are shown in Eqs. (3.2.2.49)–(3.2.2.55).

$$F_{5A,1} + F_{8A,1} + F_{9A,1} + F_{12,1} - F_{16,1} - F_{19,1} - F_{20,1} = 0 \qquad\qquad (3.2.2.49)$$

$$F_{6A} * \frac{1000}{MW_9} + F_{12,9} - F_{16,9} - F_{19,9} - F_{20,9} = 0 \qquad\qquad (3.2.2.50)$$

$$F_{7A} * \frac{1000}{MW_{11}} - F_{16,11} - F_{20,11} = 0 \qquad\qquad (3.2.2.51)$$

$$F_{12,14} - F_{16,14} - F_{19,14} - F_{20,14} = 0 \qquad\qquad (3.2.2.52)$$

$$F_{12,18} - F_{16,18} - F_{19,18} - F_{20,18} = 0 \qquad\qquad (3.2.2.53)$$

$$F_{12,20} - F_{16,20} - F_{20,20} = 0 \qquad\qquad (3.2.2.54)$$

$$F_{12,21} - F_{16,21} - F_{19,21} - F_{20,21} = 0 \qquad\qquad (3.2.2.55)$$

3.2.2.6 The Kremser Equation

The Kremser Equation provides an algebraic solution for analyzing N ideal equilibrium stages connected with countercurrent flow. The Kremser Equation, also known as the Kremser Group Method, was originally designed for countercurrent gas absorption. It is a group method because it is an approximate calculation method to relate compositions of streams entering and exiting cascades to the number of equilibrium stages required but does not consider detailed changes in temperature, flow rates, and composition in the individual stages. The Kremser equation can be applied to liquid-liquid separations such as the solvent extraction process in a natural uranium conversion plant. It assumes dilute solutions, so that solvent density is solution density.

The following explanation of the Kremser equation was taken from Benedict, Pigford, and Levi 1981. A full derivation is provided in Appendix A. When the distribution coefficients are independent of stage number, an equation can be derived for analytical calculation of the number of stages. A material

balance on one extractable component can be written as Eq. (3.2.2.56), where y_{n-1} is the concentration of the $n-1$ stage for component y, y_0 is the initial concentration of component y in the solvent, x_n is the concentration of component x in the n-th stage, x_1 is the concentration of component x in the raffinate, E is the flow rate of the extractant, and F is the flow rate of the feed.

$$y_{n-1} - y_0 = \frac{F}{E}(x_n - x_1) \tag{3.2.2.56}$$

Concentrations in the organic and aqueous phases leaving a stage are related by the equilibrium relation in Eq. (3.2.2.57), where D_n is the distribution coefficient at the conditions of the n-th stage.

$$y_n = D_n x_n \tag{3.2.2.57}$$

For any extractable component with a constant distribution coefficient, Eqs. (3.2.2.56) and (3.2.2.57) can be rewritten in terms of the constant extraction factor, β, as shown in Eq. (3.2.2.58).

$$y_n = \beta(y_{n-1} - y_0) + Dx_1 \tag{3.2.2.58}$$

The extraction factor, β, is defined in Eq. (3.2.2.59).

$$\beta \equiv \frac{DE}{F} \tag{3.2.2.59}$$

Then, Eq. (3.2.2.56) can be written as

$$y_n = Dx_n \tag{3.2.2.60}$$

For $n = 1$, Eq. (3.2.2.60) becomes

$$y_1 = Dx_1 \tag{3.2.2.61}$$

For $n = 2$, Eq. (3.2.2.60) becomes

$$y_2 = (\beta + 1)Dx_1 - \beta y_0 \tag{3.2.2.62}$$

Proceeding this way to stage N, Eq. (3.2.2.60) becomes

$$y_N = (1 + \beta + \cdots + \beta^{N-1})Dx_1 - (\beta + \cdots + \beta^{N-1})y_0 \tag{3.2.2.63}$$

Which is identical to

$$y_N = \frac{\beta^N - 1}{\beta - 1}(Dx_1 - y_0) + y_0 \tag{3.2.2.64}$$

Equation (3.2.2.64) is a form of the Kremser equation.

Additional information about the Kremser Equation can be found in McCabe, Smith, and Harriott 1993; Benedict, Pigford, and Levi 1981; and Seader and Henley (1998). This discussion was included for completeness as the Kremser Equation was considered as a means to describe the process in Module 2 for the base case model. It was decided to treat each pulsed column as a "black box" and to treat each one as separators as done in the other modules for filters, separators, etc. This allows for greater flexibility to test sensitivity and diversions within Module 2. No reaction rate information was found for the solvent extraction process.

3.2.3 Module 3: Evaporation and Precipitation

The purified uranyl nitrate solution from the solvent extraction process is converted into a solid substance, such as UO_3, U_3O_8, ammonium diuranate (ADU), ammonium uranyl carbonate (AUC), or uranyl peroxide (UO_4). The uranyl nitrate solution is converted to solid forms using either a thermal denitration or precipitation process. The thermal denitration process is used to produce a uranium oxide (i.e., UO_3 or U_3O_8) and is the preferred process for larger NUCPs. The precipitation process produces an intermediate material (i.e., ADU, AUC, UO_4) that is subsequently converted to UO_2 or other oxides and appears to be the preferred process for smaller NUCPs.

The uranyl nitrate solution may also be used to produce UO_2 that is suitable for use in nuclear fuel. Production of UO_2 for this purpose is typically done in a precipitation type process where ammonium diuranate [$(NH_4)_2U_2O_7$], generally referred to as ADU, or ammonium uranyl carbonate [$(NH_4)_4UO_2(CO_3)_3$], known as AUC, are formed. Uranyl peroxide is another precipitation product that can be used in the production of UO_2, but has not typically been utilized in conversion facilities.

ADU is precipitated from uranyl nitrate solution with ammonium hydroxide according to Eq. (3.2.3.1).

$$2UO_2(NO_3)_2 + 6NH_4OH \rightarrow (NH_4)_2U_2O_7 + 4NH_4NO_3 + 3H_2O \qquad (3.2.3.1)$$
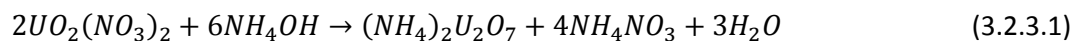
AUC is precipitated from uranyl nitrate solution with ammonia (NH_3) and carbon dioxide (CO_2) or ammonium bicarbonate [$(NH_4)HCO_3$], according to Eq. (3.2.3.2).

$$UO_2(NO_3)_2 + 6NH_3 + 3CO_2 + 3H_2O \rightarrow (NH_4)_4UO_2(CO_3)_3 + 2NH_4NO_3 \qquad (3.2.3.2)$$

In the case of the research presented here, the scope of the work was limited to small NUCPs and was further limited to the precipitation process used to produce AUC.

Module 3, Evaporation and Precipitation, encompassed the processes to concentrate the purified liquid uranyl nitrate stream from solvent extraction and then convert the concentrated product to a solid. Module 3 was further subdivided into four sub-modules. The flowsheet for Module 3 is shown in Figure 3.14.
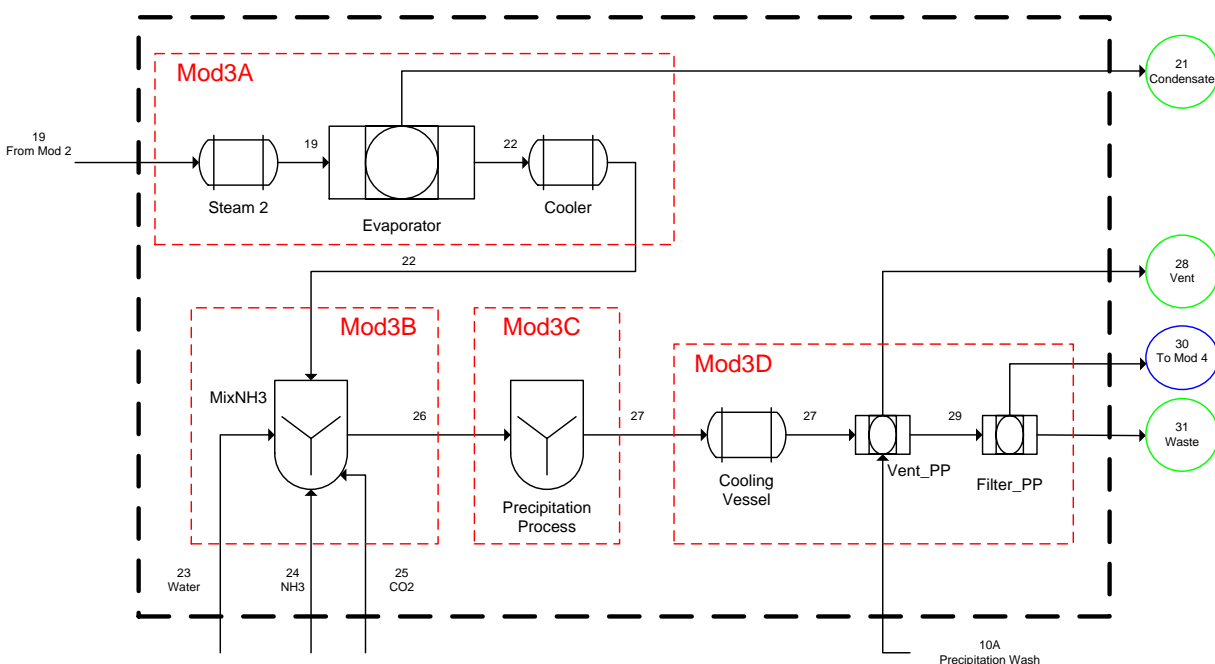
Figure 3.14. Module 3: The Evaporation and Precipitation Processes of a Natural Uranium Conversion Plant.

The purified uranyl nitrate from the solvent extraction process was pumped to an evaporator for further concentration of the uranium constituent. The concentrated solution of uranyl nitrate was cooled and pumped to a uranyl nitrate storage tank. The concentration at this point was to 350–400 g U/L. The concentrated solution was sent to a mixer-reactor where the solution was mixed with CO_2 and NH_3 to form a solid precipitate of AUC. The slurry was pumped to an agitated AUC cooling vessel. The vessel was cooled with a chilled water jacket. The agitation was between 50 and 100 rpm. The cooled suspended AUC slurry was pumped to a rotary vacuum filter and washed with methanol, water, and ammonium carbonate. The filtrate was sent to various waste streams, and the solid AUC was sent to a collection hopper where the AUC may be dried with heated air.

Some uranium could have been in the condensate stream from the evaporator, but how much depends on how the evaporator was operated. The vent from the precipitation stage could also contain residual uranium material. The filtration process after the precipitation stage produced a solid product and a liquid stream that was considered a waste. Solid from the precipitation system was sent to a collection vessel from which it was sent to the next processes (calcining and hydrofluorination).

3.2.3.1 Module 3A

Module 3A encompassed the evaporation process. The evaporation process was used to remove some of the water from the purified uranyl nitrate stream from the solvent extraction process prior to precipitation. The input to the evaporation process was the uranyl nitrate stream from Module 2. There were two output streams from Module 3A; one output was the condensate which was sent to waste. Figure 3.15 shows a block diagram of Module 3A with the input and output streams labeled.

Component mole balances were used to model each of the process units in Module 3. The evaporator separated Stream 19 into two streams. The separation was defined as the fraction that was sent to the condensate stream from the input stream by parameter, $K_{Mod3A,i}$, where each component, i, had a different fractionation. Equations (3.2.3.3)–(3.2.3.7) define the separation of Stream 19 into Stream 21.

$$K_{Mod3A,1} * F_{19,1} - F_{21,1} = 0 \tag{3.2.3.3}$$

$$K_{Mod3A,9} * F_{19,9} - F_{21,9} = 0 \tag{3.2.3.4}$$

$$K_{Mod3A,14} * F_{19,14} - F_{21,14} = 0 \tag{3.2.3.5}$$

$$K_{Mod3A,18} * F_{19,18} - F_{21,18} = 0 \tag{3.2.3.6}$$

$$K_{Mod3A,21} * F_{19,21} - F_{21,21} = 0 \tag{3.2.3.7}$$

Equations (3.2.3.8)–(3.2.3.12) calculate the component mole balances for Stream 22.

$$F_{19,1} - F_{21,1} - F_{22,1} = 0 \tag{3.2.3.8}$$

$$F_{19,9} - F_{21,9} - F_{22,9} = 0 \tag{3.2.3.9}$$
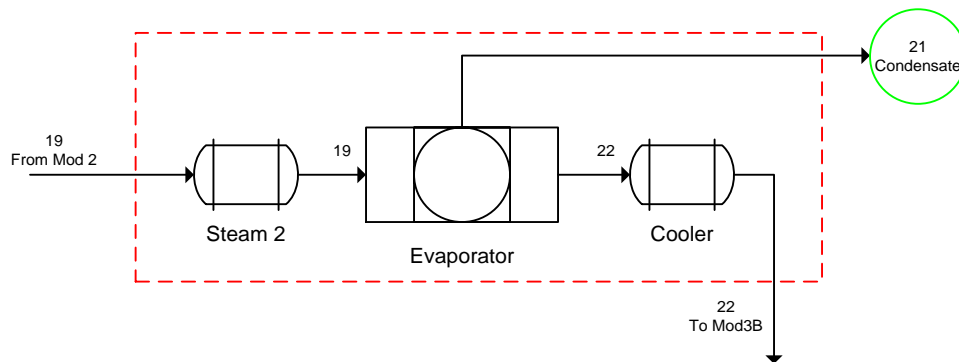
Figure 3.15. Block Diagram of the Module 3A Showing Input and Output Streams.

63

$$F_{19,14} - F_{21,14} - F_{22,14} = 0 \qquad (3.2.3.10)$$

$$F_{19,18} - F_{21,18} - F_{22,18} = 0 \qquad (3.2.3.11)$$

$$F_{19,21} - F_{21,21} - F_{22,21} = 0 \qquad (3.2.3.12)$$

3.2.3.2 Module 3B

Module 3B represented the mixer that was used to mix the reactants prior to the precipitation process. The inputs to Module 3B were the output of Module 3A along with water, ammonia, and carbon dioxide. There was one output from Module 3B. Figure 3.16 shows a block diagram of Module 3B with the input and output streams labeled.

The reactants (Streams 23–25) were fed into the process in excess based on the amount of uranyl nitrate in Stream 22 according to parameter, α_{Mod3B}, as shown in Eqs. (3.2.3.13)–(3.2.3.15) for water, ammonia, and carbon dioxide, respectively, where $n_{Mod3C,i}$ was the stoichiometric coefficient of the i-th component.

$$F_{23,1} - \alpha_{Mod3B} * \left| n_{Mod3C,1} \right| * F_{22,14} = 0 \qquad (3.2.3.13)$$

$$F_{24,3} - \alpha_{Mod3B} * \left| n_{Mod3C,3} \right| * F_{22,14} = 0 \qquad (3.2.3.14)$$

$$F_{25,8} - \alpha_{Mod3B} * \left| n_{Mod3C,8} \right| * F_{22,14} = 0 \qquad (3.2.3.15)$$
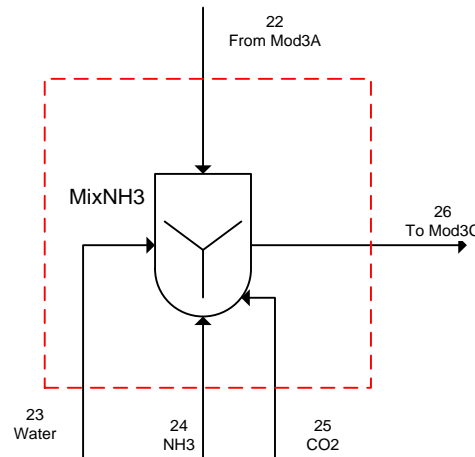
Figure 3.16. Block Diagram of the Module 3B Showing Input and Output Streams.

Equations (3.2.3.16)–(3.2.3.22) calculate the component mole balances for Stream 26.

$$F_{22,1} + F_{23,1} - F_{26,1} = 0 \tag{3.2.3.16}$$

$$F_{24,3} - F_{26,3} = 0 \tag{3.2.3.17}$$

$$F_{25,8} - F_{26,8} = 0 \tag{3.2.3.18}$$

$$F_{22,9} - F_{26,9} = 0 \tag{3.2.3.19}$$

$$F_{22,14} - F_{26,14} = 0 \tag{3.2.3.20}$$

$$F_{22,18} - F_{26,18} = 0 \tag{3.2.3.21}$$

$$F_{22,21} - F_{26,21} = 0 \tag{3.2.3.22}$$

3.2.3.3 Module 3C

Module 3C encompassed the precipitation process. The input to Module 3C was the output of Module 3B, and there was one output from Module 3C which was the solid AUC and ammonium nitrate along with the unreacted water, ammonia, and carbon dioxide. Module 3C was the only sub-module in Module 3 in which reaction occurred. The reaction that occurred in Module 3C is shown in Eq. (3.2.3.2).

$$UO_2(NO_3)_2 + 6NH_3 + 3CO_2 + 3H_2O \rightarrow (NH_4)_4UO_2(CO_3)_3 + 2NH_4NO_3 \tag{3.2.3.2}$$

The reaction was actually a composite of three reactions which were equivalent to Eq. (3.2.3.2), as shown in Eqs. (3.2.3.23a–c). The three simultaneous reactions take place immediately and go 100% to completion.

$$UO_2(NO_3)_2 + 6NH_3 \rightarrow UO_2(NO_3)_2(NH_3)_6 \tag{3.2.3.23a}$$

$$UO_2(NO_3)_2(NH_3)_6 + 3CO_2 \rightarrow UO_2(NO_3)_2(NH_3)_6(CO_2)_3 \tag{3.2.3.23b}$$

$$UO_2(NO_3)_2(NH_3)_6(CO_2)_3 + 3H_2O \rightarrow (NH_4)_4UO_2(CO_3)_3 + 2NH_4NO_3 \tag{3.2.3.23c}$$
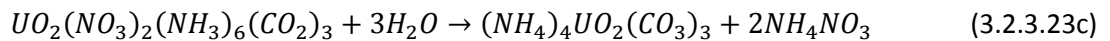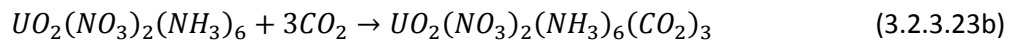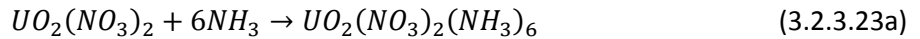
Figure 3.17 shows a block diagram of Module 3C with the input and output streams labeled. Equations (3.2.3.24)–(3.2.3.32) describe to the precipitation reaction, where X_{Mod3C} was the extent of reaction for the precipitation process. The stoichiometric coefficients are positive for products and negative for reactants.

$$F_{26,1} + \left(n_{Mod3C,1} * X_{Mod3C} * F_{26,14} \right) - F_{27,1} = 0 \tag{3.2.3.24}$$
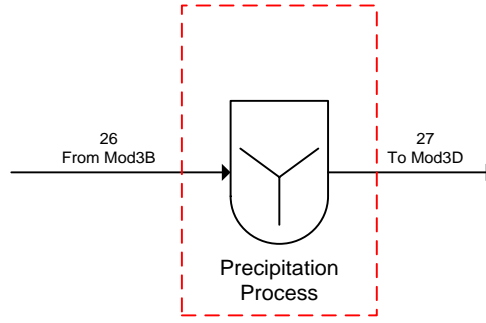
Figure 3.17. Block Diagram of the Module 3C Showing Input and Output Streams.

$$F_{26,3} + \left(n_{Mod3C,3} * X_{Mod3C} * F_{26,14}\right) - F_{27,3} = 0 \qquad (3.2.3.25)$$

$$F_{26,8} + \left(n_{Mod3C,8} * X_{Mod3C} * F_{26,14}\right) - F_{27,8} = 0 \qquad (3.2.3.26)$$

$$F_{26,9} - F_{27,9} = 0 \qquad (3.2.3.27)$$

$$\left(n_{Mod3C,12} * X_{Mod3C} * F_{26,14}\right) - F_{27,12} = 0 \qquad (3.2.3.28)$$

$$F_{26,14} + \left(n_{Mod3C,14} * X_{Mod3C} * F_{26,14}\right) - F_{27,14} = 0 \qquad (3.2.3.29)$$

$$F_{26,18} - F_{27,18} = 0 \qquad (3.2.3.30)$$

$$\left(n_{Mod3C,19} * X_{Mod3C} * F_{26,14}\right) - F_{27,19} = 0 \qquad (3.2.3.31)$$

$$F_{26,21} - F_{27,21} = 0 \qquad (3.2.3.32)$$

Mellah, Chegrouche, and Barkat 2007 describes the kinetics of the precipitation of AUC using ammonia and carbon dioxide. Mellah, Chegrouche, and Barkat 2007 states that "the predominant chemical reaction of AUC precipitation was
$UO_2(NO_3)_2 \cdot 6H_2O(aq) + 6NH_3(g) + 3CO_2(g) \rightarrow (NH_4)_4UO_2(CO_3)_3(s) + 2NH_4NO_3(aq) + 3H_2O(l)$." It is unclear from the article what was meant by "predominant" reaction. The kinetics of the above reaction was the only one given. However, the reaction used in the model [Eq. (3.2.3.2)] was discussed in the article. According to Mellah, Chegrouche, and Barkat 2007 and in reference to the above reaction, the reaction best fits a second order rate equation. The rate constants, k_2, were 0.310 L/mol/min at T=313.15 K and 0.437 L/mol/min at T=330.15 K, and the activation energy, E_a, determined using the Arrehenius equation was found as 17.4 kJ/mol. This information was provided for completeness, but the reaction rate information was not used in the model.

3.2.3.4 Module 3D

Module 3D was the post-precipitation processing of the solid product before transfer to the calciner for conversion to UO_2. This processing included a cooling vessel, a vent, and a filter. The inputs to Module 3D were the output of Module 3C and a filter wash stream. There were three outputs from Module 3D, one from the vent and two from the filter. Figure 3.18 shows a block diagram of Module 3D with the input and output streams labeled.

The precipitation process vent (Vent_PP) separated Stream 27 into two streams. It was assumed that only gaseous components exited in the vent and that all of the gaseous components exited to the vent. Equations (3.2.3.33) and (3.2.3.34) are the component mole balances for the vent waste stream.

$$F_{27,3} - F_{28,3} = 0 \tag{3.2.3.33}$$

$$F_{27,8} - F_{28,8} = 0 \tag{3.2.3.34}$$

Equations (3.2.3.35)–(3.2.3.43) calculate the component mole balances for Stream 29.

$$F_{27,1} + \left(F_{10A} * x_{10A,1} * \frac{1000}{MW_1}\right) - F_{29,1} = 0 \tag{3.2.3.35}$$

$$F_{27,9} - F_{29,9} = 0 \tag{3.2.3.36}$$

$$\left(F_{10A} * x_{10A,10} * \frac{1000}{MW_{10}}\right) - F_{29,10} = 0 \tag{3.2.3.37}$$

$$F_{27,12} - F_{29,12} = 0 \tag{3.2.3.38}$$
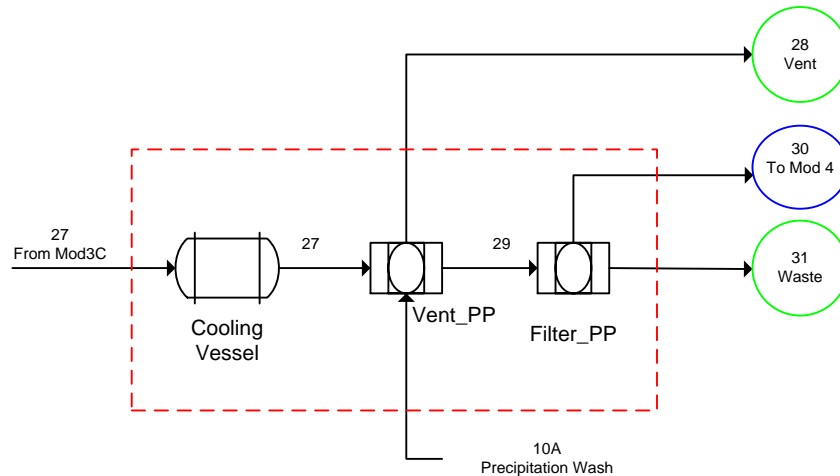
Figure 3.18. Block Diagram of the Module 3D Showing Input and Output Streams.

$$\left(F_{10A} * x_{10A,13} * \frac{1000}{MW_{13}}\right) - F_{29,13} = 0 \tag{3.2.3.39}$$

$$F_{27,14} - F_{29,14} = 0 \tag{3.2.3.40}$$

$$F_{27,18} - F_{29,18} = 0 \tag{3.2.3.41}$$

$$F_{27,19} - F_{29,19} = 0 \tag{3.2.3.42}$$

$$F_{27,21} - F_{29,21} = 0 \tag{3.2.3.43}$$

The precipitation process filter (Filter_PP) separated Stream 29 into two streams. The separation was defined as the fraction that was sent to the product stream from the input stream by parameter, $K_{Mod3D,i}$, where each component, i, had a different fractionation. Equations (3.2.3.44)–(3.2.3.46) define the separation of Stream 29 into Stream 30.

$$K_{Mod3D,1} * F_{29,1} - F_{30,1} = 0 \tag{3.2.3.44}$$

$$K_{Mod3D,18} * F_{29,18} - F_{30,18} = 0 \tag{3.2.3.45}$$

$$K_{Mod3D,19} * F_{29,19} - F_{30,19} = 0 \tag{3.2.3.46}$$

Equations (3.2.3.47)–(3.2.3.55) calculate the component mole balances for Stream 31.

$$F_{29,1} - F_{30,1} - F_{31,1} = 0 \tag{3.2.3.47}$$

$$F_{29,9} - F_{31,9} = 0 \tag{3.2.3.48}$$

$$F_{29,10} - F_{31,10} = 0 \tag{3.2.3.49}$$

$$F_{29,12} - F_{31,12} = 0 \tag{3.2.3.50}$$

$$F_{29,13} - F_{31,13} = 0 \tag{3.2.3.51}$$

$$F_{29,14} - F_{31,14} = 0 \tag{3.2.3.52}$$

$$F_{29,18} - F_{30,18} - F_{31,18} = 0 \tag{3.2.3.53}$$

$$F_{29,19} - F_{30,19} - F_{31,19} = 0 \tag{3.2.3.54}$$

$$F_{29,21} - F_{31,21} = 0 \tag{3.2.3.55}$$

3.2.3.5 Module 3: Overall Material Balance

The streams used for the overall material balances were those that cross the dark dashed boundary that enclosed all of Module 3. There were five input streams and four output streams for Module 3. One of the input streams was the output of Module 2, and three of the input streams were dependent. Additionally, there was one reaction in Module 3 that occurs in the precipitation process and is described by Eq. (3.2.3.2).

$$UO_2(NO_3)_2 + 6NH_3 + 3CO_2 + 3H_2O \rightarrow (NH_4)_4UO_2(CO_3)_3 + 2NH_4NO_3 \qquad (3.2.3.2)$$

The overall component material balances for Module 3 are shown in Eqs. (3.2.3.56)–(3.2.3.66).

$$F_{10A,1} + F_{19,1} + F_{23,1} + \left(n_{Mod3C,1} * X_{Mod3C} * F_{26,14}\right) - F_{21,1} - F_{30,1} - F_{31,1} = 0 \qquad (3.2.3.56)$$

$$F_{24,3} + \left(n_{Mod3C,3} * X_{Mod3C} * F_{26,14}\right) - F_{28,3} = 0 \qquad (3.2.3.57)$$

$$F_{25,8} + \left(n_{Mod3C,8} * X_{Mod3C} * F_{26,14}\right) - F_{28,8} = 0 \qquad (3.2.3.58)$$

$$F_{19,9} + \left(n_{Mod3C,9} * X_{Mod3C} * F_{26,14}\right) - F_{21,9} - F_{31,9} = 0 \qquad (3.2.3.59)$$

$$F_{10A} * x_{10A,10} * \frac{1000}{MW_{10}} - F_{31,10} = 0 \qquad (3.2.3.60)$$

$$\left(n_{Mod3C,12} * X_{Mod3C} * F_{26,14}\right) - F_{31,12} = 0 \qquad (3.2.3.61)$$

$$F_{10A} * x_{10A,13} * \frac{1000}{MW_{13}} - F_{31,13} = 0 \qquad (3.2.3.62)$$

$$F_{19,14} + \left(n_{Mod3C,14} * X_{Mod3C} * F_{26,14}\right) - F_{21,14} - F_{31,14} = 0 \qquad (3.2.3.63)$$

$$F_{19,18} + \left(n_{Mod3C,18} * X_{Mod3C} * F_{26,14}\right) - F_{21,18} - F_{30,18} - F_{31,18} = 0 \qquad (3.2.3.64)$$

$$\left(n_{Mod3C,19} * X_{Mod3C} * F_{26,14}\right) - F_{30,19} - F_{31,19} = 0 \qquad (3.2.3.65)$$

$$F_{19,21} - F_{21,21} - F_{31,21} = 0 \qquad (3.2.3.66)$$

3.2.4 Module 4: Conversion to Uranium Dioxide then Uranium Tetrafluoride

Uranium Dioxide Production

One of the primary products of an NUCP is UO_2 that can be used in reactor fuel. Uranium dioxide is also generated as an intermediate material in the NUCP in the conversion of yellowcake to uranium tetrafluoride (UF_4). Uranium dioxide may be produced via calcination and reduction of precipitates (ADU or AUC) or the reduction of UO_3 with hydrogen.

If the precipitation process is used, the ADU and AUC powders are readily converted to UO_2 by heating (calcining) in a reducing environment that has a hydrogen atmosphere. ADU generally consists of agglomerates of small irregularly shaped crystals (1 to 20 micron) and is usually converted to UO_2 in a calciner (rotary furnace) or a fixed-bed type of furnace. The use of fluidized beds for conversion of ADU to uranium oxides is generally not considered practical because of the poor flowability of ADU and the large amount of particles lost to the fluid bed off-gas stream. The following reaction [Eq. (3.2.4.1)] takes place when ADU is contacted with hydrogen in a heated vessel.

$$(NH_4)_2U_2O_7 + 2H_2 \rightarrow 2UO_2 + 3H_2O + 2NH_3 \qquad (3.2.4.1)$$
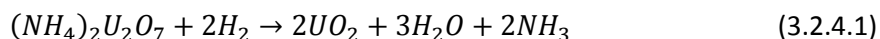
Ammonium uranyl carbonate is a coarser, more free-flowing powder as compared to ADU. Ammonium uranyl carbonate can be calcined/reduced in a fluidized bed, as well as a rotary calciner or a fixed-bed type of furnace. The following reaction [Eq. (3.2.4.2)] takes place when AUC is contacted with hydrogen in a heated vessel.

$$(NH_4)_4UO_2(CO_3)_3 + H_2 \rightarrow UO_2 + 3H_2O + 4NH_3 + 3CO_2 \qquad (3.2.4.2)$$
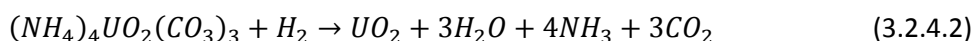
Uranium oxides [i.e., yellowcake in the form of uranium oxide (U_3O_8 or UO_3) from the denitration process] can be directly reduced using H_2 to produce UO_2. Typically, this UO_2 is an intermediate compound produced in an NUCP that is subsequently reduced to UF_4. Direct reduction of the yellowcake (that has been converted to either UO_3 or U_3O_8) takes place when the yellowcake is fairly pure, thus the need for dissolution and solvent extraction of the yellowcake is not warranted. UO_3 and U_3O_8 are readily reduced to UO_2 by heating the oxides in a hydrogen atmosphere. The reactions involved in the reduction of these oxides are shown in Eqs. (3.2.4.3) and (3.2.4.4).

$$UO_3 + H_2 \xrightarrow{heat} UO_2 + H_2O \qquad (3.2.4.3)$$

$$U_3O_8 + H_2 \xrightarrow{heat} 3UO_2 + 2H_2O \qquad (3.2.4.4)$$
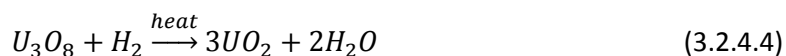
This discussion is limited to the conversion of AUC to UO_2.

Different types of heated vessels, such as a fixed bed, rotary calciners, stirred bed, fluidized bed, or vibrating-tray type reactors are used in the reduction of UO_3 or U_3O_8 to UO_2. The material of construction for this equipment is typically stainless steel. The hydrogen used is typically generated on-site at an NUCP via dissociation of ammonia.

Uranium Tetrafluoride Production

Uranium tetrafluoride is an intermediate compound that is generated in an NUCP that is utilized in the production of UF_6 or uranium metal. Uranium tetrafluoride is typically produced by reacting UO_2 with anhydrous hydrogen fluoride (AHF) in what is known as a hydrofluorination process. The chemical reaction that takes place in hydrofluorination is shown in Eq. (3.2.4.5).

70

$$UO_2 + 4HF \leftrightarrow UF_4 + 2H_2O \qquad\qquad (3.2.4.5)$$

Different types of heated vessels, such as screw reactors, rotary calciners, fluidized beds, stirred beds, or vibrating-tray type beds are used in the hydrofluorination process. Because hydrogen fluoride (HF), which is extremely corrosive, is used in this reaction, the equipment involved in hydrofluorination must be fabricated from materials resistant to HF (e.g., Hastelloy®, Monel®, and Inconel®).

Module 4, Conversion to UO_2 and UF_4, encompassed the processes to convert the solid AUC to solid UO_2 and then convert the UO_2 to UF_4. Module 4 was subdivided into six sub-modules. The flowsheet for Module 4 is shown in Figure 3.19.

Nitrogen and hydrogen were preheated to 500–1000°C and fed countercurrently to the calciner. The washed and dried AUC was introduced via a feed hopper to the rotary calciner by means of a screw conveyor. The rotary calciner operates at 550–650°C. Uranium dioxide was produced in the calciner and subsequently cooled to less than 100°C in a UO_2 screw conveyor with a cooling jacket. The UO_2 was collected in a UO_2 collection hopper where it was eventually transferred to storage containers (i.e., drums).
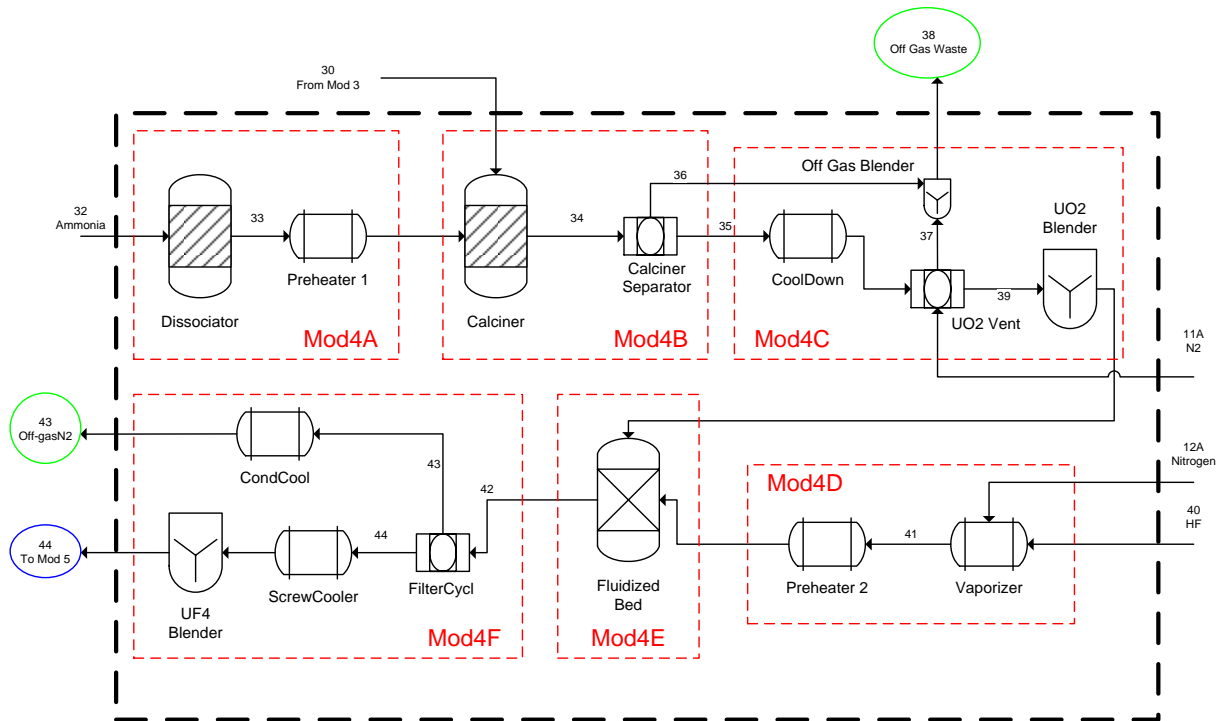
Figure 3.19. Module 4: The Hydrofluorination Process of a Natural Uranium Conversion Plant.

The hopper fed UO_2 into the fluidized bed reactor where it was reacted with anhydrous HF (AHF) in the presence of N_2 to produce UF_4. The reactor operates between 300 and 550°C. The AHF was superheated to approximately 150°C. Nitrogen was added to the system and the mixture was preheated to approximately 250°C before entering the fluidized bed reactor. The UF_4 was withdrawn from the bottom of the reactor into a UF_4 hopper that fed a screw conveyor where the solid was cooled indirectly by a cooling jacket. The UF_4 left the conveyor at a temperature below 100°C and was collected in a UF_4 collection hopper. The hopper was used to feed the UF_4 blender. The gaseous stream, which contained unreacted HF, left the reactor through the top. The HF could be condensed into liquid HF in a storage tank. Anhydrous HF could also be recovered and stored in a liquid AHF storage tank for reuse. Residual HF remaining in the off-gas stream was removed using a packed bed scrubber with potassium hydroxide (KOH) solution. The scrubbed off-gas was discharged from the top of the scrubber, and the bottom liquid was part of the waste streams.

Complete recovery of UO_2 and UF_4 from the fluidized bed was assumed. However in actual operation, filtration and recycle would be required to recover the product powders that would be entrained in the reactor. Waste streams could contain from 0.2% to 2.0% uranium depending on recovery systems.

3.2.4.1 Module 4A

Module 4A was the ammonia cracking process which was used to produce hydrogen for the conversion of AUC to UO_2. In industrial processes, it is safer and more economical to crack ammonia in order to obtain hydrogen rather than supplying hydrogen directly. The input to the cracking process was pure ammonia. The output stream from Module 4A was hydrogen and nitrogen. The ammonia cracking chemical reaction is shown in Eq. (3.2.4.6).

$$2NH_3 \rightarrow N_2 + 3H_2 \qquad (3.2.4.6)$$

Figure 3.20 shows a block diagram of Module 4A with the input and output streams labeled.

Component mole balances were used to model each of the process units in Module 4. Ammonia (Stream 32) was fed into the process in excess based the amount of AUC in Stream 30 that was fed to the calciner according to parameter, α_{Mod4A}, as shown in Eq. (3.2.4.7), where $n_{Mod4A,i}$ was the stoichiometric coefficient of the i-th component of the dissociation reaction and $n_{Mod4B,i}$ was the stoichiometric coefficient of the i-th component of the conversion of AUC to UO_2. The stoichiometric coefficients are positive for products and negative for reactants.

$$F_{32,3} - \alpha_{Mod4A} * \left| \frac{n_{Mod4B,5}}{n_{Mod4B,19}} \right| * \left| \frac{n_{Mod4A,3}}{n_{Mod4A,5}} \right| * F_{30,19} = 0 \qquad (3.2.4.7)$$
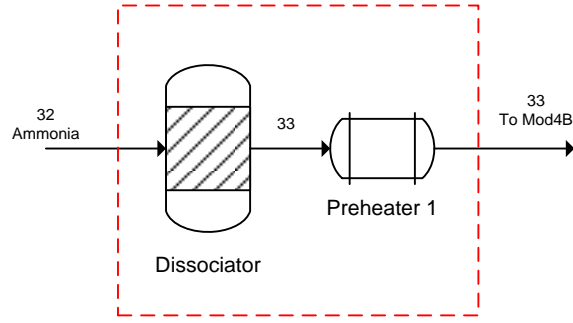
Figure 3.20. Block Diagram of the Module 4A Showing Input and Output Streams.

The dissociator separated the incoming ammonia into nitrogen and hydrogen, as shown in Eqs. (3.2.4.8) and (3.2.4.9), where X_{Mod4A} was the extent of reaction for the dissociation of ammonia. These equations assumed complete conversion of ammonia so that no ammonia was in the stream feeding the calciner.

$$\left(n_{Mod4A,2} * X_{Mod4A} * F_{32,3}\right) - F_{33,2} = 0 \tag{3.2.4.8}$$

$$\left(n_{Mod4A,5} * X_{Mod4A} * F_{32,3}\right) - F_{33,5} = 0 \tag{3.2.4.9}$$

3.2.4.2 Module 4B

Module 4B encompassed the calciner and associated separator. The inputs to Module 4B were the output of Module 3 and the output of Module 4A. There were two outputs from Module 4B, (1) the UO_2 solid product and (2) the off-gas which was sent to waste after mixing with additional off-gas in Module 4C. The reaction that occurs in Module 4B is shown in Eq. (3.2.4.2). Figure 3.21 shows a block diagram of Module 4B with the input and output streams labeled.

$$(NH_4)_4 UO_2(CO_3)_3 + H_2 \rightarrow UO_2 + 3H_2O + 4NH_3 + 3CO_2 \tag{3.2.4.2}$$
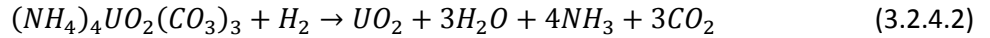
Equations (3.2.4.10)–(3.2.4.17) describe to the conversion of AUC to UO_2 using hydrogen, where X_{Mod4B} was the extent of reaction for the conversion of AUC to UO_2.

$$F_{30,1} + \left(n_{Mod4B,1} * X_{Mod4B} * F_{30,19}\right) - F_{34,1} = 0 \tag{3.2.4.10}$$

$$F_{33,2} + \left(n_{Mod4B,2} * X_{Mod4B} * F_{30,19}\right) - F_{34,2} = 0 \tag{3.2.4.11}$$

$$\left(n_{Mod4B,3} * X_{Mod4B} * F_{30,19}\right) - F_{34,3} = 0 \tag{3.2.4.12}$$
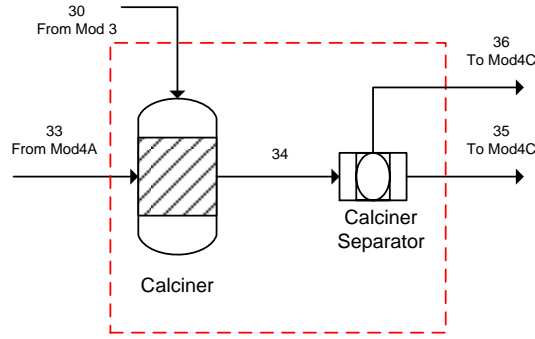
Figure 3.21. Block Diagram of the Module 4B Showing Input and Output Streams.

$$F_{33,5} + \left(n_{Mod4B,5} * X_{Mod4B} * F_{30,19}\right) - F_{34,5} = 0 \qquad (3.2.4.13)$$

$$\left(n_{Mod4B,8} * X_{Mod4B} * F_{30,19}\right) - F_{34,8} = 0 \qquad (3.2.4.14)$$

$$\left(n_{Mod4B,17} * X_{Mod4B} * F_{30,19}\right) - F_{34,17} = 0 \qquad (3.2.4.15)$$

$$F_{30,18} + \left(n_{Mod4B,18} * X_{Mod4B} * F_{30,19}\right) - F_{34,18} = 0 \qquad (3.2.4.16)$$

$$F_{30,19} + \left(n_{Mod4B,19} * X_{Mod4B} * F_{30,19}\right) - F_{34,19} = 0 \qquad (3.2.4.17)$$

It was assumed that all solid components were sent to Stream 35 and that all other components left this sub-module as waste according to Eqs. (3.2.4.18)–(3.2.4.25).

$$F_{34,17} - F_{35,17} = 0 \qquad (3.2.4.18)$$

$$F_{34,18} - F_{35,18} = 0 \qquad (3.2.4.19)$$

$$F_{34,19} - F_{35,19} = 0 \qquad (3.2.4.20)$$

$$F_{34,1} - F_{36,1} = 0 \qquad (3.2.4.21)$$

$$F_{34,2} - F_{36,2} = 0 \qquad (3.2.4.22)$$

$$F_{34,3} - F_{36,3} = 0 \qquad (3.2.4.23)$$

$$F_{34,5} - F_{36,5} = 0 \qquad (3.2.4.24)$$

$$F_{34,8} - F_{36,8} = 0 \qquad (3.2.4.25)$$

Reaction rate data for the conversion of AUC to UO_2 using hydrogen was not available.

3.2.4.3 Module 4C

Module 4C included the UO_2 post-processing equipment and the off-gas from the calciner. Module 4C included the following equipment: a cooler, UO_2 vent, gaseous waste blender, and UO_2 blender. The inputs to Module 4C were both outputs from Module 4B and nitrogen to the UO_2 vent. There were two outputs from Module 4C, the gaseous waste stream and the blended UO_2 product. Figure 3.22 shows a block diagram of Module 4C with the input and output streams labeled.

It was assumed that the stream leaving the UO_2 vent was pure nitrogen according to Eq. (3.2.4.26).

$$\left(F_{11A} * x_{11A,2} * \frac{1000}{MW_2}\right) - F_{37,2} = 0 \tag{3.2.4.26}$$

The off-gas blender was used to blend the nitrogen exiting the UO_2 vent and the gaseous waste stream from Module 3B as shown in Eqs. (3.2.4.27)–(3.2.4.31).

$$F_{36,1} - F_{38,1} = 0 \tag{3.2.4.27}$$

$$F_{36,2} + F_{37,2} - F_{38,2} = 0 \tag{3.2.4.28}$$

$$F_{36,3} - F_{38,3} = 0 \tag{3.2.4.29}$$

$$F_{36,5} - F_{38,5} = 0 \tag{3.2.4.30}$$

$$F_{36,8} - F_{38,8} = 0 \tag{3.2.4.31}$$
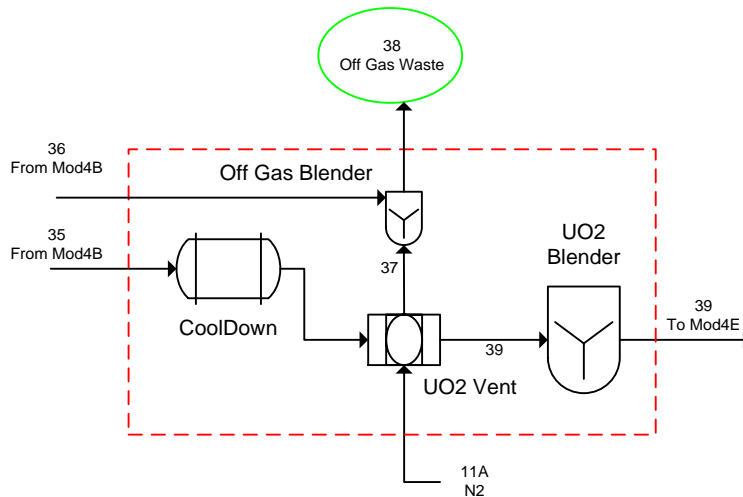
Figure 3.22. Block Diagram of the Module 4C Showing Input and Output Streams.

The solid product from the calciner passed through the UO_2 vent to the UO_2 blender according to Eqs. (3.2.4.32)–(3.2.4.34).

$$F_{35,17} - F_{39,17} = 0 \tag{3.2.4.32}$$

$$F_{35,18} - F_{39,18} = 0 \tag{3.2.4.33}$$

$$F_{35,19} - F_{39,19} = 0 \tag{3.2.4.34}$$

3.2.4.4 Module 4D

Module 4D was the HF feeding process for the hydrofluorination process. The input and output of Module 4D were HF and nitrogen. Figure 3.23 shows a block diagram of Module 4D with the input and output streams labeled.

The HF input stream was assumed to be pure. Additionally, the feed of hydrogen fluorine must always be sufficient for the conversion in Module 4E based on parameter, α_{Mod4D}, as shown in Eq. (3.2.4.35). However, HF was never fed in excess so as there was little to no residual HF after the reaction.

$$F_{40,6} - \alpha_{Mod4D} * \left| \frac{n_{Mod4E,6}}{n_{Mod4E,17}} \right| * F_{39,17} = 0 \tag{3.2.4.35}$$

Nitrogen was mixed with the HF and pre-heated prior to being fed to the fluidized bed reactor [Eqs. (3.2.4.36) and (3.2.4.37)].

$$\left(F_{12A} * x_{12A,2} * \frac{1000}{MW_2} \right) - F_{41,2} = 0 \tag{3.2.4.36}$$

$$F_{40,6} - F_{41,6} = 0 \tag{3.2.4.37}$$
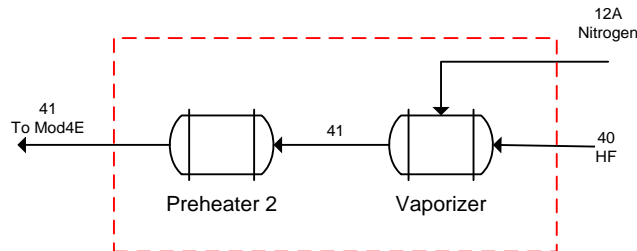
Figure 3.23. Block Diagram of the Module 4D Showing Input and Output Streams.

3.2.4.5 Module 4E

Module 4E was the fluidized bed reactor where UO_2 was hydrofluorinated in HF to produce UF_4 [Eq. (3.2.4.5)]. The inputs to Module 4E were the output of Module 4C and 4D. There was one output from Module 4E which was the solid UF_4. In an actual plant, approximately 117 kg AUC/h is processed with 0.2–2.0% uranium lost to waste streams.

$$UO_2 + 4HF \leftrightarrow UF_4 + 2H_2O \tag{3.2.4.5}$$

Figure 3.24 shows a block diagram of Module 4E with the input and output streams labeled. Equations (3.2.4.38)–(3.2.4.44) describe the conversion of UO_2 to UF_4 using HF, where $n_{Mod4E,i}$ was the stoichiometric coefficient of the i-th component of the hydrofluorination reaction and X_{Mod4E} was the extent of reaction for the hydrofluorination reaction in terms of hydrogen fluoride. The stoichiometric coefficients are positive for products and negative for reactants.

$$\left(n_{Mod4E,1} * X_{Mod4E} * F_{41,6}\right) - F_{42,1} = 0 \tag{3.2.4.38}$$

$$F_{41,2} + \left(n_{Mod4E,2} * X_{Mod4E} * F_{41,6}\right) - F_{42,2} = 0 \tag{3.2.4.39}$$

$$F_{41,6} + \left(n_{Mod4E,6} * X_{Mod4E} * F_{41,6}\right) - F_{42,6} = 0 \tag{3.2.4.40}$$

$$\left(n_{Mod4E,16} * X_{Mod4E} * F_{41,6}\right) - F_{42,16} = 0 \tag{3.2.4.41}$$

$$F_{39,17} + \left(n_{Mod4E,17} * X_{Mod4E} * F_{41,6}\right) - F_{42,17} = 0 \tag{3.2.4.42}$$

$$F_{39,18} + \left(n_{Mod4E,18} * X_{Mod4E} * F_{41,6}\right) - F_{42,18} = 0 \tag{3.2.4.43}$$

$$F_{39,19} + \left(n_{Mod4E,19} * X_{Mod4E} * F_{41,6}\right) - F_{42,19} = 0 \tag{3.2.4.44}$$
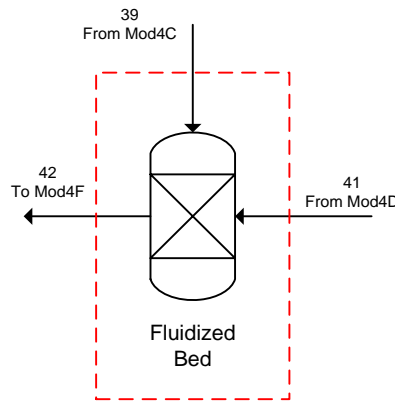
Figure 3.24. Block Diagram of the Module 4E Showing Input and Output Streams.

According to Nicole et al. 1996, "the kinetics of the transformation of uranium dioxide to uranium tetrafluoride by hydrofluorination have been studied with the aid of thermogravimetric experiments performed at temperatures from 220 to 450°C in a nitrogen-diluted hydrogen fluoride atmosphere." The Grainy Pellet Model coupled with an optimization program was used to determine the reaction rate. The reaction rate was determined to be first order with respect to hydrogen fluoride. The reaction rate constant varies with temperature in the range 220–450°C according to an Arrhenius law, with an activation energy of 25 kJ/mol, and a frequency factor of 5.88 x 10^{-3} m/s. Additionally, it follows a chemical or intermediate regime, depending on the pellet diameter. Diffusion in the bulk of the small grains comprising the pellets is not rate-controlling. It was also shown that the ideal pellet size in the industrial process is of the order of 1 mm in diameter.

The following discussion was taken from Nicole et al. 1996. The Grainy Pellet Model assumes the pellets to be composed of initially non-porous grains of identical shape and size. The shrinking core model is applied locally to each grain within the pellet. As the reaction progresses, a layer of solid product forms around the shrinking core of reactant. Mass transport involves several mechanisms: transfer from the bulk of the gas to the pellet surface, followed by diffusion between the grains composing the pellet (intergranular diffusion) and diffusion from the grain surface to the reaction front (intragranular diffusion), and the chemical reaction itself at the interface between the layer of reaction product and the shrinking core of solid reactant. The overall reaction kinetics are determined by the slowest of these steps, known as the rate-controlling mechanism(s).

Nicole et al. 1996 makes the following simplifying assumptions:

a) Pseudo-steady-state approximation is appropriate for describing the concentration of the gaseous species within the pellet. This assumption is valid whenever the ratio C_A/C_B between the concentrations of the gaseous reactant C_A and the solid reactant C_B remains small, which is verified in most gas-solid systems.

b) The resistance to external transfer is negligible.

c) The system is isothermal. In spite of the exothermic nature of the reaction, this assumption is justified by the experimental conditions, which involved a small mass of pellets, dilution of the gaseous reactant and a high total gas flowrate.

d) The convective flux resulting from non-equimolar reaction is negligible since reactant and product gases were strongly diluted.

e) The reaction is irreversible. Although the reaction is normally reversible, under the conditions employed, involving a reaction temperature below 500°C and a gaseous reactant concentration small but well above the equilibrium level, the reverse reaction was negligible.

f) The chemical reaction has first-order kinetics with respect to gaseous reactant.

g) Pellet and grains are spherical.

The information was provided for completeness but was not used in the model.

3.2.4.6 Module 4F

Module 4F included the UF_4 post-processing equipment which was a filter, two coolers, and a UF_4 blender. The input to Module 4F was the output of Module 4E. There were two outputs from Module 4F, one from a cooler and one from the UF_4 blender. Figure 3.25 shows a block diagram of Module 4F with the input and output streams labeled.

The filter separates Stream 42 into two streams. The separation was defined as the fraction that was sent to the waste stream (Stream 43) by parameter, $K_{Mod4F,i}$, where each component, i, had a different fractionation. Equations (3.2.4.45)–(3.2.4.51) define the separation of Stream 42 into Stream 43.

$$K_{Mod4F,1} * F_{42,1} - F_{43,1} = 0 \tag{3.2.4.45}$$

$$K_{Mod4F,2} * F_{42,2} - F_{43,2} = 0 \tag{3.2.4.46}$$

$$K_{Mod4F,6} * F_{42,6} - F_{43,6} = 0 \tag{3.2.4.47}$$

$$K_{Mod4F,16} * F_{42,16} - F_{43,16} = 0 \tag{3.2.4.48}$$

$$K_{Mod4F,17} * F_{42,17} - F_{43,17} = 0 \tag{3.2.4.49}$$

$$K_{Mod4F,18} * F_{42,18} - F_{43,18} = 0 \tag{3.2.4.50}$$

$$K_{Mod4F,19} * F_{42,19} - F_{43,19} = 0 \tag{3.2.4.51}$$
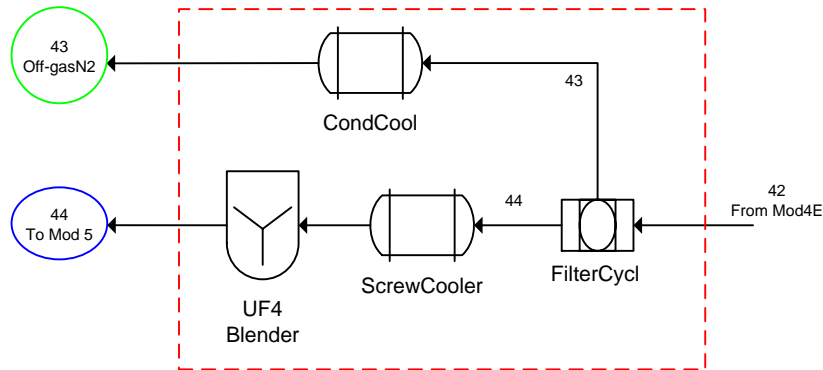
Figure 3.25. Block Diagram of the Module 4F Showing Input and Output Streams.

79

Equations (3.2.4.52)–(3.2.4.54) calculate the component mole balances for Stream 44.

$$F_{42,16} - F_{43,16} - F_{44,16} = 0 \qquad (3.2.4.52)$$

$$F_{42,17} - F_{43,17} - F_{44,17} = 0 \qquad (3.2.4.53)$$

$$F_{42,18} - F_{43,18} - F_{44,18} = 0 \qquad (3.2.4.54)$$

3.2.4.7 Module 4: Overall Material Balance

The streams used for the overall material balances were those that cross the dark dashed boundary that enclosed all of Module 4. There were five input streams and three output streams for Module 4. One of the input streams was the output of Module 3 and two of the input streams were dependent. Additionally, there were three reactions in Module 4. The first occurred in the dissociator and was described by Eq. (3.2.4.6). The second occurred in the calciner and was described by Eq. (3.2.4.2). The third occurred in the fluidized bed reactor and was described by Eq. (3.2.4.5).

$$2NH_3 \rightarrow N_2 + 3H_2 \qquad (3.2.4.6)$$

$$(NH_4)_4UO_2(CO_3)_3 + H_2 \rightarrow UO_2 + 3H_2O + 4NH_3 + 3CO_2 \qquad (3.2.4.2)$$

$$UO_2 + 4HF \leftrightarrow UF_4 + 2H_2O \qquad (3.2.4.5)$$
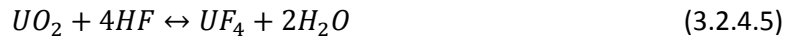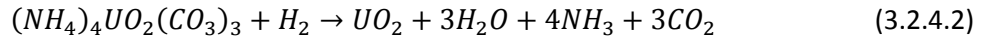
The overall component material balances for Module 4 are shown in Eqs. (3.2.4.55)–(3.2.4.64).

$$F_{30,1} + \left(n_{Mod4B,1} * X_{Mod4B} * F_{30,19}\right) + \left(n_{Mod4E,1} * X_{Mod4E} * F_{41,6}\right) - F_{38,1} - F_{43,1} = 0 \qquad (3.2.4.55)$$

$$F_{11A,2} + F_{12A,2} + \left(n_{Mod4A,2} * X_{Mod4A} * F_{32,3}\right) - F_{38,2} - F_{43,2} = 0 \qquad (3.2.4.56)$$

$$F_{32,3} + \left(n_{Mod4A,3} * X_{Mod4A} * F_{32,3}\right) + \left(n_{Mod4B,3} * X_{Mod4B} * F_{30,19}\right) - F_{38,3} = 0 \qquad (3.2.4.57)$$

$$\left(n_{Mod4A,5} * X_{Mod4A} * F_{32,3}\right) + \left(n_{Mod4B,5} * X_{Mod4B} * F_{30,19}\right) - F_{38,5} = 0 \qquad (3.2.4.58)$$

$$F_{40,6} + \left(n_{Mod4E,6} * X_{Mod4E} * F_{41,6}\right) - F_{43,6} = 0 \qquad (3.2.4.59)$$

$$\left(n_{Mod4B,8} * X_{Mod4B} * F_{30,19}\right) - F_{38,8} = 0 \qquad (3.2.4.60)$$

$$\left(n_{Mod4E,16} * X_{Mod4E} * F_{41,6}\right) - F_{43,16} - F_{44,16} = 0 \qquad (3.2.4.61)$$

$$\left(n_{Mod4B,17} * X_{Mod4B} * F_{30,19}\right) + \left(n_{Mod4E,17} * X_{Mod4E} * F_{41,6}\right) - F_{43,17} - F_{44,16} = 0 \qquad (3.2.4.62)$$

$$F_{30,18} + \left(n_{Mod4B,18} * X_{Mod4B} * F_{30,19}\right) - F_{43,18} - F_{44,18} = 0 \qquad (3.2.4.63)$$

$$F_{30,19} + \left(n_{Mod4B,19} * X_{Mod4B} * F_{30,19}\right) - F_{43,19} = 0 \qquad (3.2.4.64)$$

3.2.5 Module 5: Conversion of Uranium Tetrafluoride to Uranium Hexafluoride

Uranium hexafluoride is one of the main products of an NUCP. The process that is primarily utilized throughout the world in the production of UF_6 is the reaction of UF_4 with fluorine gas. Uranium tetrafluoride reacts rapidly with fluorine in a highly exothermic reaction to form UF_6 according to Eq. (3.2.5.1).

$$UF_4 + F_2 \rightarrow UF_6 + heat \qquad (3.2.5.1)$$

Different types of vessels, such as a tube furnace, a vertical open-pipe reactor (known as a flame tower), or a fluidized bed can be used in the conversion of UF_4 to UF_6. Fluorine is an extremely corrosive gas, thus the equipment utilized must be fabricated from materials resistant to F_2 (e.g., Monel®, Hastelloy®, and Inconel®).

If fairly pure U_3O_8 and UO_3 are available, then one may choose direct fluorination of the oxides for the production of UF_6. Note that direct fluorination of oxides requires significantly more fluorine for conversion than does that required for UF_4. The oxide fluorination reactions are shown in Eqs. (3.2.5.2) and (3.2.5.3).

$$UO_3 + 3F_2 \rightarrow UF_6 + 1.5O_2 + heat \qquad (3.2.5.2)$$

$$U_3O_8 + 9F_2 \rightarrow 3UF_6 + 4O_2 + heat \qquad (3.2.5.3)$$
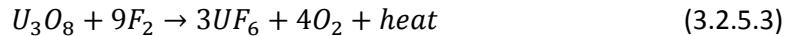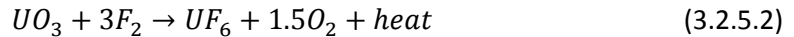
Different types of vessels such as a fixed bed reactor or a fluidized bed containing inert materials (such as calcium fluoride) are used in the conversion of uranium oxides to UF_6. As with UF_4 fluorination, the equipment utilized must be fabricated from materials resistant to F_2 (e.g., Monel®, Hastelloy®, and Inconel®). This work was limited to the fluorination of UF_4 and did not cover oxides.

Module 5, Conversion of UF_4 to UF_6, encompassed the processes necessary to convert the solid uranium tetrafluoride to gaseous uranium hexafluoride. Module 5 was further subdivided into six sub-modules. The flowsheet for Module 5 is shown in Figure 3.26. Figure 3.26 illustrates the process of fluorination of UF_4 utilizing a flame tower. From the UF_4 feed hopper (not modeled), UF_4 was fed into the flame tower reactor where it reacted with the F_2 that was produced from local electrolytic cells or supplied from F_2 bottle storage. The fluorine gas was preheated in the presence of nitrogen to a temperature between 300 and 400°C. Gaseous UF_6 was condensed to a solid in a cold trap. Unreacted solids, known as ash, were collected at the bottom of the flame tower reactor. The vent stream from the flame reactor could contain some uranium material. There was a secondary flame reactor that was used to remove the excess fluorine contained in the primary flame reactor's off-gas stream via reaction with UF_4.
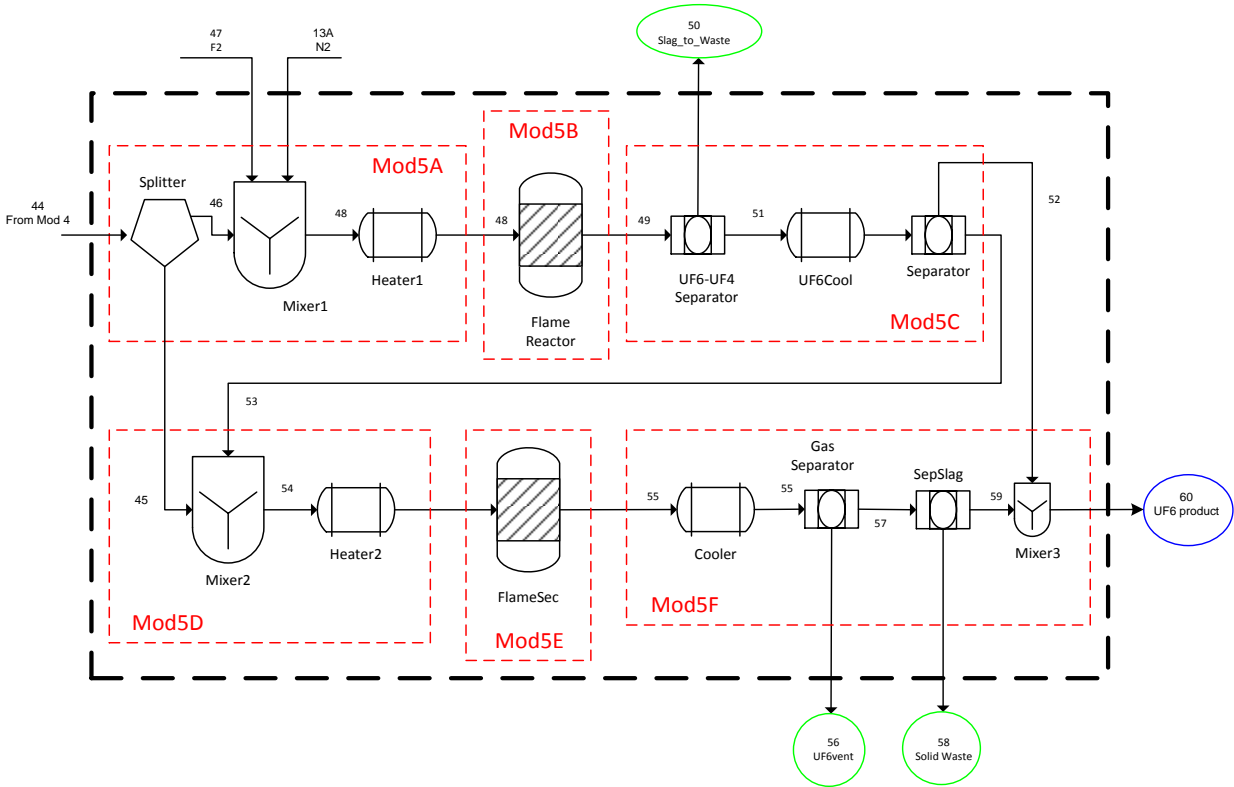
Figure 3.26. Module 5: The Fluorination Process of a Natural Uranium Conversion Plant.

Uranium hexafluoride collected in the cold traps was heated to increase the UF_6 temperature above the triple point, and the liquid UF_6 was gravity drained into UF_6 cylinders. After the cylinders were filled to the appropriate level, the cylinders were disconnected from the process and moved to a storage pad for the liquid UF_6 to cool to a solid before shipment. The waste streams were relatively low, 0.1% to 0.2%.

3.2.5.1 Module 5A

Module 5A included the stream splitter, a mixer, and the gas pre-heater. The stream splitter was used to send a fraction of the incoming UF_4 further down the process for secondary reaction that removed excess fluorine from the process. The inputs to Module 5A were the UF_4 product stream from Module 4, fluorine, and nitrogen. There were two output streams from Module 5A. Figure 3.27 shows a block diagram of Module 5A with the input and output streams labeled.

The splitter separation was defined as the fraction that was sent to the secondary reactor from the input stream by parameter, S_{Mod5A}. Equations (3.2.5.4)–(3.2.5.6) define the separation of Stream 44 into Stream 45.
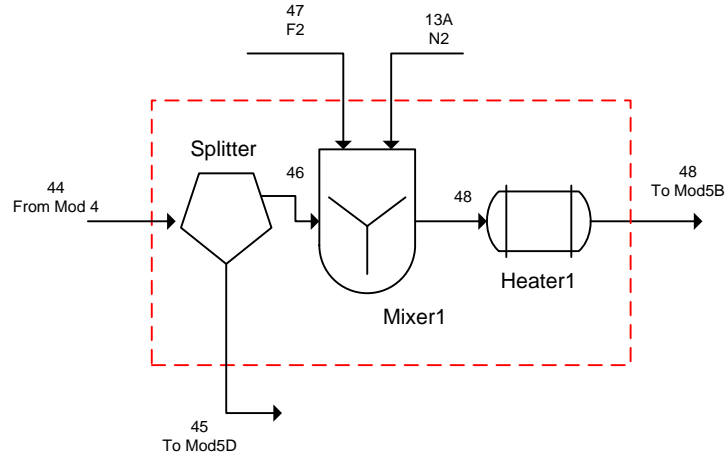
Figure 3.27. Block Diagram of the Module 5A Showing Input and Output Streams.

$$S_{Mod5A} * F_{44,16} - F_{45,16} = 0 \tag{3.2.5.4}$$

$$S_{Mod5A} * F_{44,17} - F_{45,17} = 0 \tag{3.2.5.5}$$

$$S_{Mod5A} * F_{44,18} - F_{45,18} = 0 \tag{3.2.5.6}$$

Equations (3.2.5.7)–(3.2.5.9) calculate the mole balances for Stream 46.

$$F_{44,16} - F_{45,16} - F_{46,16} = 0 \tag{3.2.5.7}$$

$$F_{44,17} - F_{45,17} - F_{46,17} = 0 \tag{3.2.5.8}$$

$$F_{44,18} - F_{45,18} - F_{46,18} = 0 \tag{3.2.5.9}$$

Pure fluorine (Stream 47) was fed into the process in excess based the amount of UF_4 in Stream 44 that was fed to the reactor according to parameter, α_{Mod5A}, as shown in Eq. (3.2.5.10), where $n_{Mod5B,i}$ was the stoichiometric coefficient of the i-th component of the fluorination reaction. The stoichiometric coefficients are positive for products and negative for reactants.

$$F_{47,7} - \alpha_{Mod5A} * \left| \frac{n_{Mod5B,7}}{n_{Mod5B,16}} \right| * F_{44,16} = 0 \tag{3.2.5.10}$$

Equations (3.2.5.11)–(3.2.5.15) define Stream 48.

$$\left(F_{13A} * x_{13A,2} * \frac{1000}{MW_2} \right) - F_{48,2} = 0 \tag{3.2.5.11}$$

$$F_{47,7} - F_{48,7} = 0 \tag{3.2.5.12}$$

$$F_{46,16} - F_{48,16} = 0 \tag{3.2.5.13}$$

$$F_{46,17} - F_{48,17} = 0 \tag{3.2.5.14}$$

$$F_{46,18} - F_{48,18} = 0 \tag{3.2.5.15}$$

3.2.5.2 Module 5B

Module 5B was the flame reactor where UF_4 was converted to UF_6 using fluorine gas Eq. (3.2.5.1). The input to Module 5B was the output of Module 5A. There was only one output from Module 5B which was predominately gaseous UF_6 product with the remainder being N_2, F_2, UF_4, UO_2, and U_3O_8. Figure 3.28 shows a block diagram of Module 5B with the input and output streams labeled.

Equations (3.2.5.16)–(3.2.5.21) describe to the fluorination of UF_4 to UF_6, where X_{Mod5B} was the extent of reaction in terms of UF_4.

$$F_{48,2} + \left(n_{Mod5B,2} * X_{Mod5B} * F_{48,16}\right) - F_{49,2} = 0 \tag{3.2.5.16}$$

$$F_{48,7} + \left(n_{Mod5B,7} * X_{Mod5B} * F_{48,16}\right) - F_{49,7} = 0 \tag{3.2.5.17}$$

$$\left(n_{Mod5B,15} * X_{Mod5B} * F_{48,16}\right) - F_{49,15} = 0 \tag{3.2.5.18}$$

$$F_{48,16} + \left(n_{Mod5B,16} * X_{Mod5B} * F_{48,16}\right) - F_{49,16} = 0 \tag{3.2.5.19}$$

$$F_{48,17} + \left(n_{Mod5B,17} * X_{Mod5B} * F_{48,16}\right) - F_{49,17} = 0 \tag{3.2.5.20}$$

$$F_{48,18} + \left(n_{Mod5B,18} * X_{Mod5B} * F_{48,16}\right) - F_{49,18} = 0 \tag{3.2.5.21}$$
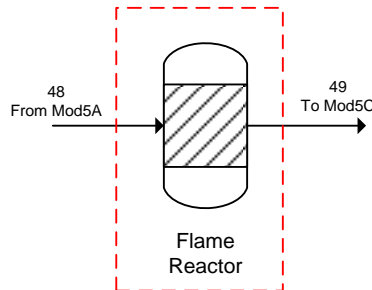
Figure 3.28. Block Diagram of the Module 5B Showing Input and Output Streams.

The following discussion of the kinetics of the fluorination of UF_4 to form UF_6 was adapted from Labaton and Johnson 1959. It was deduced from the reaction studied that the reaction is first order with respect to fluorine pressure. The UF_6 production rate is in agreement with the kinetics expected for reaction between a gas and a solid at a spherical interface which is continuously diminishing due to reaction with the gas. The rate of reaction depends on the temperature, and no reaction is detectable below 220°C. The activation energy for UF_4 that was produced by hydrofluorination was determined to be 19.1 kcal/mol. A linear relationship is shown to exist between the reaction rate and partial pressure of fluorine, but within the range examined the reaction rate is not affected by the velocity of gaseous reactant past the solid. The rate of UF_6 production is dependent on an "effective" surface area of UF_4, rather than the surface area determined by gaseous adsorption. The information was provided for completeness, but was not used in the final model.

3.2.5.3 Module 5C

Module 5C encompassed the separations following the primary flame reactor which included two separators and a cooling vessel. The output from Module 5B was the input to Module 5C. There were three outputs from Module 5C, one from the first separator to the waste and two from the second separator. Figure 3.29 shows a block diagram of Module 5C with the input and output streams labeled.

The first separator removed any unreacted uranium to the waste. The separation was defined as the fraction that was sent to the waste by parameter, $K1_{Mod5C,i}$, where each component, i, had a different fractionation. Equations (3.2.5.22)–(3.2.5.24) define the separation of Stream 49 into Stream 50. It is assumed at any residual UO_2 and U_3O_8 exited in this waste stream.
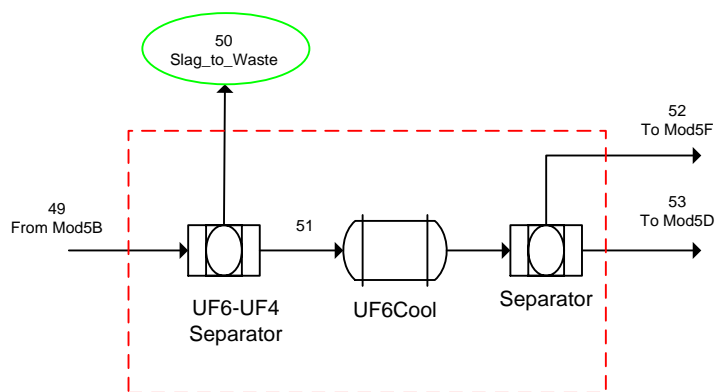
Figure 3.29. Block Diagram of the Module 5C Showing Input and Output Streams.

$$K1_{Mod5C,16} * F_{49,16} - F_{50,16} = 0 \qquad (3.2.5.22)$$

$$K1_{Mod5C,17} * F_{49,17} - F_{50,17} = 0 \qquad (3.2.5.23)$$

$$K1_{Mod5C,18} * F_{49,18} - F_{50,18} = 0 \qquad (3.2.5.24)$$

Equations (3.2.5.25)–(3.2.5.28) define Stream 51.

$$F_{49,2} - F_{51,2} = 0 \qquad (3.2.5.25)$$

$$F_{49,7} - F_{51,7} = 0 \qquad (3.2.5.26)$$

$$F_{49,15} - F_{51,15} = 0 \qquad (3.2.5.27)$$

$$F_{49,16} - F_{50,16} - F_{51,16} = 0 \qquad (3.2.5.28)$$

The second separator separated most of the UF_6 product from any remaining UF_4 and all of the F_2. Stream 52 was assumed to be pure UF_6 at this point and was sent to Module 5F where it was blended with the product from the secondary reactor. Stream 53 contained any unreacted UF_4 and the excess unreacted F_2 that was consumed in the secondary reactor. The separation was defined as the fraction that was sent to the UF_6 product by parameter, $K2_{Mod5C}$. Equation (3.2.5.29) defines the separation of Stream 51 into Stream 52.

$$K2_{Mod5C} * F_{51,15} - F_{52,15} = 0 \qquad (3.2.5.29)$$

Equations (3.2.5.30)–(3.2.5.33) define Stream 53.

$$F_{51,2} - F_{53,2} = 0 \qquad (3.2.5.30)$$

$$F_{51,7} - F_{53,7} = 0 \qquad (3.2.5.31)$$

$$F_{51,15} - F_{52,15} - F_{53,15} = 0 \qquad (3.2.5.32)$$

$$F_{51,16} - F_{53,16} = 0 \qquad (3.2.5.33)$$

3.2.5.4 Module 5D

Module 5D included the mixer and heater for the secondary reactor. The inputs to Module 5D included the UF_4 from the splitter in Module 5A and the unreacted compounds from the second separator in Module 5C. There was one output from Module 5D. Figure 3.30 shows a block diagram of Module 5D with the input and output streams labeled.
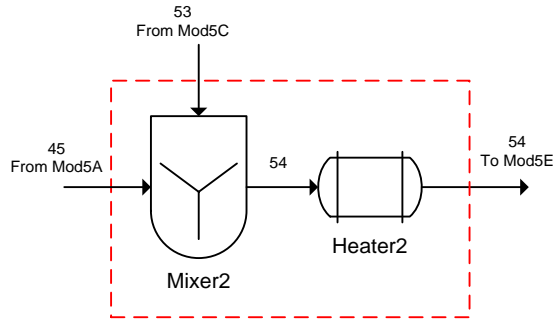
Figure 3.30. Block Diagram of the Module 5D Showing Input and Output Streams.

The component mole balances for Stream 54 are shown in Eqs. (3.2.5.34)–(3.2.5.39).

$$F_{53,2} - F_{54,2} = 0 \tag{3.2.5.34}$$

$$F_{53,7} - F_{54,7} = 0 \tag{3.2.5.35}$$

$$F_{53,15} - F_{54,15} = 0 \tag{3.2.5.36}$$

$$F_{45,16} + F_{53,16} - F_{54,16} = 0 \tag{3.2.5.37}$$

$$F_{53,17} - F_{54,17} = 0 \tag{3.2.5.38}$$

$$F_{53,18} - F_{54,18} = 0 \tag{3.2.5.39}$$

3.2.5.5 Module 5E

Module 5E was the secondary flame reactor. The secondary flame reactor was used to remove excess fluorine from the system for safety and equipment preservation based on Eq. (3.2.5.1). There was a small fraction of UF$_4$ split off in Module 5A to provide sufficient UF$_4$ to react the excess fluorine. The other input to Module 5E was the output of Module 5D. There was one output from Module 5D. Figure 3.31 shows a block diagram of Module 5E with the input and output streams labeled.

Equations (3.2.5.40)–(3.2.5.45) describe to the fluorination of UF$_4$ to UF$_6$ in the secondary flame reactor, where X_{Mod5E} was the extent of reaction in terms of UF$_4$.

$$F_{54,2} + \left(n_{Mod5E,2} * X_{Mod5E} * F_{54,16} \right) - F_{55,2} = 0 \tag{3.2.5.40}$$

$$F_{54,7} + \left(n_{Mod5E,7} * X_{Mod5E} * F_{54,16} \right) - F_{55,7} = 0 \tag{3.2.5.41}$$
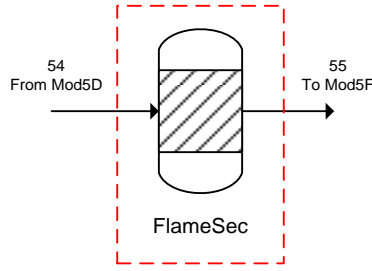
Figure 3.31. Block Diagram of the Module 5E Showing Input and Output Streams.

$$F_{54,15} + \left(n_{Mod5E,15} * X_{Mod5E} * F_{54,16}\right) - F_{55,15} = 0 \qquad (3.2.5.42)$$

$$F_{54,16} + \left(n_{Mod5E,16} * X_{Mod5E} * F_{54,16}\right) - F_{55,16} = 0 \qquad (3.2.5.43)$$

$$F_{54,17} + \left(n_{Mod5E,17} * X_{Mod5E} * F_{54,16}\right) - F_{55,17} = 0 \qquad (3.2.5.44)$$

$$F_{54,18} + \left(n_{Mod5E,18} * X_{Mod5E} * F_{54,16}\right) - F_{55,18} = 0 \qquad (3.2.5.45)$$

3.2.5.6 Module 5F

Module 5F encompassed the final separations of the UF_6 product. The equipment included in Module 5F was a cooler, two separators, and a mixer. The inputs to Module 5F included the output of Module 5E and the UF_6 product from the second separator in Module 5C. There were three outputs from Module 5E, a gaseous waste stream, a solid waste stream, and the UF_6 product line. Figure 3.32 shows a block diagram of Module 5F with the input and output streams labeled.

The first separator removed all of the gaseous components except the UF_6 product, as shown as in Eqs. (3.2.5.46) and (3.2.5.47).

$$F_{55,2} - F_{56,2} = 0 \qquad (3.2.5.46)$$

$$F_{55,7} - F_{56,7} = 0 \qquad (3.2.5.47)$$

The component mole balances for Stream 57 are shown in Eqs. (3.2.5.48)–(3.2.5.51).

$$F_{55,15} - F_{57,15} = 0 \qquad (3.2.5.48)$$

$$F_{55,16} - F_{57,16} = 0 \qquad (3.2.5.49)$$

$$F_{55,17} - F_{57,17} = 0 \qquad (3.2.5.50)$$
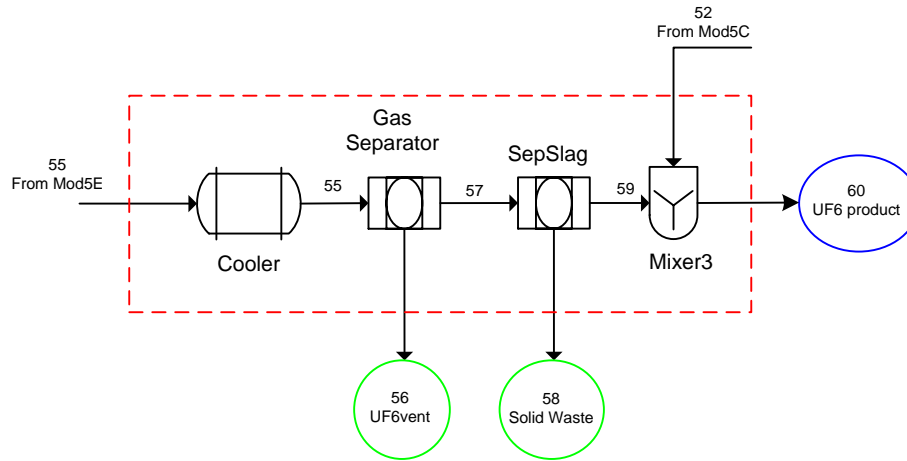
Figure 3.32. Block Diagram of the Module 5F Showing Input and Output Streams.

$$F_{55,18} - F_{57,18} = 0 \qquad (3.2.5.51)$$

The second separator removed any remaining solid components to the waste. Stream 59 was assumed to be pure UF$_6$ and was blended with the UF$_6$ from Module 5C. Equations (3.2.5.52)–(3.2.5.54) define Stream 58 and Eq. (3.2.5.55) defines Stream 59.

$$F_{57,16} - F_{58,16} = 0 \qquad (3.2.5.52)$$

$$F_{57,17} - F_{58,17} = 0 \qquad (3.2.5.53)$$

$$F_{57,18} - F_{58,18} = 0 \qquad (3.2.5.54)$$

$$F_{57,15} - F_{59,15} = 0 \qquad (3.2.5.55)$$

The pure UF$_6$ from both Module 5C and 5F were blended before exiting the facility as the final product, according to Eq. (3.2.5.56).

$$F_{52,15} + F_{59,15} - F_{60,15} = 0 \qquad (3.2.5.56)$$

3.2.5.7 Module 5: Overall Material Balance

The streams used for the overall material balances were those that cross the dark dashed boundary that enclosed all of Module 5. There were three input streams and four output streams for Module 5. One of the input streams was the output of Module 4 and one of the input streams was dependent.

Additionally, there was one reaction in Module 5 that occurred in both of the flame reactors and is described by Eq. (3.2.5.1).

$$UF_4 + F_2 \rightarrow UF_6 + heat \qquad (3.2.5.1)$$

The overall component material balances for Module 5 are shown in Eqs. (3.2.5.57)–(3.2.5.62).

$$F_{13A} * x_{13A,2} * \frac{1000}{MW_2} - F_{56,2} = 0 \qquad (3.2.5.57)$$

$$F_{47,7} + \left(n_{Mod5B,7} * X_{Mod5B} * F_{48,16}\right) + \left(n_{Mod5E,7} * X_{Mod5E} * F_{54,16}\right) - F_{56,7} = 0 \qquad (3.2.5.58)$$

$$\left(n_{Mod5B,15} * X_{Mod5B} * F_{48,16}\right) + \left(n_{Mod5E,15} * X_{Mod5E} * F_{54,16}\right) - F_{60,15} = 0 \qquad (3.2.5.59)$$

$$F_{44,16} + \left(n_{Mod5B,16} * X_{Mod5B} * F_{48,16}\right) + \left(n_{Mod5E,16} * X_{Mod5E} * F_{54,16}\right) - F_{50,16} - F_{58,16} = 0$$
$$\qquad (3.2.5.60)$$

$$F_{44,17} + \left(n_{Mod5B,17} * X_{Mod5B} * F_{48,16}\right) + \left(n_{Mod5E,17} * X_{Mod5E} * F_{54,16}\right) - F_{50,17} - F_{58,17} = 0$$
$$\qquad (3.2.5.61)$$

$$F_{44,18} + \left(n_{Mod5B,18} * X_{Mod5B} * F_{48,16}\right) + \left(n_{Mod5E,18} * X_{Mod5E} * F_{54,16}\right) - F_{50,18} - F_{58,18} = 0$$
$$\qquad (3.2.5.62)$$

3.3 SENSITIVITY ANALYSIS

Sensitivity analysis is the development of the degree of sensitivity of a process state or output variable to a change in a process input variable or process parameter. Sensitivity analysis served several purposes in this study, including:

- Testing the robustness of the results of the model with regard to uncertainty, i.e., which parameters the model was most sensitive to.
- Increasing understanding of the relationships between the input and output variables.
- Model simplification (fixing parameters such as incoming flow rates that had no effect on the output and ignoring changes in input variables).
- Selection of parameters to change for faulty operations testing (testing both highly sensitive and less sensitive parameters without testing parameters that had no effect on the output).
- Identification of optimum sensor placement or locations that require more frequent monitoring.

There were a total of 82 parameters tested for the sensitivity analysis. These parameters included items that may be controlled by an operator in the facility or would vary naturally due to equipment fouling or other equipment modifications. The parameters were input flow rates, flow parameters used to control dependent input streams, extent of reactions, and fractionation factors for separators. All of the flow rates of the incoming streams (Table 3.9) and all of the module-specific parameters (Table 3.10) were tested.

For the sensitivity analysis, each of the parameters was varied by ±10% using a one-at-a-time approach to determine a new steady-state solution for all of the state variables. The one-at-a-time approach involved changing one parameter while keeping all of the others at their nominal values and determining the output, then returning that parameter to its nominal value and repeating for each of the other parameters in the same way. This approach was logical since any change observed in the output was unambiguously due to the single variable changed. Since this approach does not take into account the simultaneous variation of parameters, it was incomplete and cannot detect the presence of interactions between parameters or any nonlinear effect of the input variables. Additionally, it shows cases were the process is nonlinear when the response is not the same for both ±10%. However, the sensitivity analysis utilized in this study was an initial effort and additional study would be required to fully understand this detection framework in a facility. For parameters that could not vary by +10% such as an extent of reaction with a value of one, the parameter was only varied by -10%.

For the sensitivity analysis, the sensitivity factor for each parameter and each steady-state state variable was determined. The sensitivity factor is unit-less and defined as shown in Eq. (3.3.0.1), where $\gamma_{i,j}$ is the sensitivity factor for the percent change of the i-th state variable (y) to the percent change in the j-th parameter (u) at steady state. For example, a γ value of 1 means that a 10% change in the parameter resulted in a 10% change in the state variable.

$$\gamma_{i,j} \triangleq \frac{\Delta y_i / y_{i,0}}{\Delta u_j / u_{j,0}} \qquad (3.3.0.1)$$

Table 3.9. Base Case Flow Rates (kg/h) for Input Streams for Each Module

Identifier	Stream	Value	Chemical Component
$F_{1A,U}$	1A	50.00	Uranium
F_{4A}	4A	8.00	Water
F_{5A}	5A	4.00	Water
F_{6A}	6A	0.80	Nitric Acid
F_{7A}	7A	60.00	TBP
F_{8A}	8A	42.00	Water
F_{9A}	9A	95.00	Water
F_{10A}	10A	14.00	Wash Solution
F_{11A}	11A	14.00	Nitrogen
F_{12A}	12A	42.00	Nitrogen
F_{13A}	13A	14.00	Nitrogen

Table 3.10. Base Case Parameters for Each Module

Identifier	Value	Description
Module 1		
α_{Mod1A}	1.2	Flow parameter that insures sufficient HNO_3, Mod1A
X_{Mod1A}	0.9799	Extent of Reaction (moles U_3O_8 reacted/moles U_3O_8 fed), Mod1A
$K_{Mod1B,1}$	0.9	
$K_{Mod1B,9}$	0.97	
$K_{Mod1B,14}$	0.98	Component Filter Fractionation Factors (mol-%), Mod1B
$K_{Mod1B,18}$	0.02	
$K_{Mod1B,20}$	0.01	
$K_{Mod1B,21}$	0.97	
$K_{Mod1C,1}$	0.75	
$K_{Mod1C,9}$	0.9	
$K_{Mod1C,14}$	0.8	Component Filter Fractionation Factors (mol-%), Mod1C
$K_{Mod1C,18}$	0.7	
$K_{Mod1C,20}$	0.01	
$K_{Mod1C,21}$	0.99	
$S1_{Mod1D}$	0.333	Splitter, fraction of flow from Stream 7 to Stream 9, Mod1D
$S2_{Mod1D}$	0.333	Splitter, fraction of flow from Stream 7 to Stream 10, Mod1D
$K_{Mod1E,1}$	0.999	
$K_{Mod1E,9}$	0.9999	
$K_{Mod1E,14}$	0.9999	Component Filter Fractionation Factors (mol-%), Mod1E
$K_{Mod1E,18}$	0.9999	
$K_{Mod1E,20}$	0.2	
$K_{Mod1E,21}$	0.9999	
Module 2		
$K_{Mod2B,1}$	0.001	
$K_{Mod2B,9}$	0.001	
$K_{Mod2B,11}$	0.999	
$K_{Mod2B,14}$	0.995	Column component mole fraction fractionation (mol-%), Mod2B
$K_{Mod2B,18}$	0.001	
$K_{Mod2B,20}$	0.001	
$K_{Mod2B,21}$	0.1	
$K_{Mod2C,1}$	0.001	
$K_{Mod2C,9}$	0.005	
$K_{Mod2C,11}$	0.999	
$K_{Mod2C,14}$	0.999	Column component mole fraction fractionation (mol-%), Mod2C
$K_{Mod2C,18}$	0.001	
$K_{Mod2C,20}$	0.001	
$K_{Mod2C,21}$	0.05	

Table 3.10. Base Case Parameters for Each Module (continued)

Identifier	Value	Description
Module 2 (continued)		
$K_{Mod2D,1}$	0.9999	
$K_{Mod2D,9}$	0.995	
$K_{Mod2D,14}$	0.999	Column component mole fraction fractionation (mol-%), Mod2D
$K_{Mod2D,18}$	0.001	
$K_{Mod2D,21}$	0.995	
Module 3		
$K_{Mod3A,1}$	0.6	
$K_{Mod3A,9}$	0.6	
$K_{Mod3A,14}$	0.0001	Evaporator component mole fraction fractionation (mol-%), Mod3A
$K_{Mod3A,18}$	0.0001	
$K_{Mod3A,21}$	0.0001	
α_{Mod3B}	1.5	Flow parameter that insures sufficient reactants (H_2O, NH_3, and CO_2), Mod3B
X_{Mod3C}	0.9999	Extent of Reaction (moles uranyl nitrate reacted/moles uranyl nitrate fed), Mod3C
$K_{Mod3D,1}$	0.06	
$K_{Mod3D,18}$	0.995	Filter component mole fraction fractionation (mol-%), Mod3D
$K_{Mod3D,19}$	0.995	
Module 4		
α_{Mod4A}	1.25	Flow parameter that insures sufficient NH_3 is fed for conversion, Mod4A
X_{Mod4A}	1	Extent of reaction (moles NH_3 reacted/moles NH_3 fed), Mod4A
X_{Mod4B}	0.9999	Extent of reaction (moles AUC reacted/moles AUC fed), Mod4B
α_{Mod4D}	0.95	Flow parameter that insures sufficient HF is fed for conversion, Mod4D
X_{Mod4E}	0.9999	Extent of reaction (moles HF reacted/moles HF fed), Mod4E
$K_{Mod4F,1}$	1	
$K_{Mod4F,2}$	1	
$K_{Mod4F,6}$	1	
$K_{Mod4F,16}$	1E-05	Filter component mole fraction fractionation (mol-%), Mod4F
$K_{Mod4F,17}$	0.001	
$K_{Mod4F,18}$	0.001	
$K_{Mod4F,19}$	1	
Module 5		
α_{Mod5A}	1.1	Flow parameter that insures sufficient F_2 is fed for conversion, Mod5A
X_{Mod5B}	0.999	Extent of reaction (moles UF_4 reacted/moles UF_4 fed), Mod5B
S_{Mod5A}	0.1	Splitter fractionation (mol-%), Mod5A

Table 3.10. Base Case Parameters for Each Module (continued)

Identifier	Value	Description
		Module 5 (continued)
$K1_{Mod5C,16}$	0.99	
$K1_{Mod5C,17}$	1	Filter component mole fraction fractionation (mol-%), Mod5C (UF$_6$-UF$_4$ Separator)
$K1_{Mod5C,18}$	1	
$K2_{Mod5C,15}$	0.99	Filter component mole fraction fractionation(mol-%), Mod5C (Separator)
X_{Mod5E}	0.999	Extent of reaction (moles UF$_4$ reacted/moles UF$_4$ fed), Mod5E

3.4 BASE "NORMAL" CASE

Following the overall approach outlined in Figure 3.1, this section explains how the base case data set was obtained. The first step was to define the process equations used to describe the system. These were the material balance equations provided in Section 3.2. Next, all of the parameters were identified. In this work, parameters are constants and do not vary in the base case model. The parameters are listed in the tables in Section 3.3. Based on the sensitivity analysis (results of which are discussed in Chapter 4), seven parameters were selected as input variables. For the input variables, the normal range profile for each variable was established, i.e., 'normal' flow rate of uranium into the plant was 50 kg/h and varied by ±10%. The input variables with variations are summarized in Table 3.11 with more description for each below.

The first and most important input variable selected was the flow rate of uranium to the facility [Xss(274)]. This was the impure uranium ore or yellowcake that was the feedstock to the facility from the mining and milling operation. This effort assumed that the incoming yellowcake was 85% U$_3$O$_8$ and 15% impurities (7.5% soluble and 7.5% insoluble). The feed rate of uranium was 50 kg U/h, based on the assumption that this model represented a small-sized conversion plant that processed 100 MTU/yr with an operating schedule of 8 h/day, 5 days/week, and 50 weeks/yr. This rate was elemental uranium, not U$_3$O$_8$, and it was expected to vary some since the operators would be loading drums into a feed hopper to supply the dissolver. The model included a variation of ±10% of the 50 kg U/h nominal flow rate.

The second input variable selected was the uranyl nitrate filter fractionation parameter in Module 1B [Xss(275)]. That was the amount of uranyl nitrate that was separated from Stream 3 to Stream 4. Stream 3 was the exit of the stream mixer in Module 1B which included the dissolver output and the recycle for the splitter in Module 1D. Stream 4 was the input stream to Module 1E where the Module 1 product was separated from any remaining solids that were not dissolved. This parameter was selected due to the sensitivity analysis which showed that 42% of the state variables were sensitive to this parameter. Additionally, 62% of those sensitive state variables were uranium-bearing components.

Table 3.11. List of Input Variables

Module	Input Variable Name	Variable Number	Nominal Value	Units	Variation for Base Case	Description
1	$F_{1A,U}$	Xss(274)	50.00	kg/h	±10%	Flow rate of uranium in stream 1A, Mod1A
1	$K_{Mod1B,14}$	Xss(275)	0.98	mol-%	-5%	Uranyl Nitrate Filter Fractionation, Mod1B
2	$K_{Mod2B,14}$	Xss(276)	0.995	mol-%	-5%	Uranyl Nitrate Filter Fractionation, Mod2B
2	$K_{Mod2D,14}$	Xss(277)	0.999	mol-%	-5%	Uranyl Nitrate Filter Fractionation, Mod2D
3	$K_{Mod3D,19}$	Xss(278)	0.995	mol-%	-5%	Ammonium Uranyl Carbonate Filter Fractionation, Mod3D
4	α_{Mod4D}	Xss(279)	0.95		±5%	Flow parameter, insures sufficient HF is fed for conversion, Mod4D
5	S_{Mod5A}	Xss(280)	0.1	mol-%	±10%	Splitter fractionation, Mod5A

The third and fourth variables selected as inputs were the uranyl nitrate filter fractionation parameters in Module 2 [Xss(276) and Xss(277)]. These parameters were from the extraction column (Module 2B) and the stripping column (Module 2D). The uranyl nitrate component was selected because uranium was the species of interest throughout this process. Additionally, over 35% of the state variables were sensitive to changes in these parameters with over 50% of those sensitive state variables being uranium-bearing components. The initial value given was the maximum so the variation was a reduction in the fractionation.

The fifth input variable selected was the AUC filter fractionation parameter in Module 3D [Xss(278)]. That was the amount of AUC that was separated from Stream 29 and sent to Stream 30. This determined how much of the solid AUC became the Module 3 product and how much was waste. Depending on the filter media, amount of washing, and particle size, it was reasonable that there would be some variation in the amount of AUC in the Module 3 product. Again, the initial value given was the maximum so the variation was a reduction in the fractionation. Additionally, 28% of the state variables, 58% of which contained uranium, were sensitive to this parameter.

The sixth input variable selected was the flow parameter that was used to ensure sufficient hydrogen fluoride was fed for the hydrofluorination reaction in Module 4D [Xss(279)]. This parameter was used to define the amount of HF that was fed to the system; the incoming HF stream was a dependent input stream and therefore an unknown since it was based on the amount of UO_2 that was fed to the fluidized bed reactor. Hydrogen fluoride was the rate controlling reactant in the hydrofluorination reaction. The

amount of HF was fed in less than stoichiometric amounts so that minimal HF remained after the reaction. This parameter affected the uranium components from Module 4D downstream which was expected since it affected the amount of UF_4 produced and the amount of UO_2 consumed. Almost 18% of the state variables, 71% of which contained uranium, were sensitive to this parameter.

The final input variable selected was the splitter fractionation in Module 5A [Xss(280)]. A splitter was different from the other separators since it split the stream into multiple streams but retained the same component ratios of the initial stream. The stream splitter was used to send a fraction of the incoming UF_4 further down the process for secondary reaction used to remove excess fluorine from the process. A change in this parameter affected most of the unknowns in Module 5. Over 77% of the state variables in Module 5 were sensitive to this parameter; 68% of the sensitive state variables contained uranium. It was also reasonable from an operations standpoint to expect this split to vary slightly.

Once all of the equations, parameters, and input variables were defined, the 'fsolve' function in MATLAB® was used to determine the initial steady-state solution at the nominal parameter and input variable settings. This was the solution for the material balance equations solved simultaneously using the nominal values from Table 3.11. The base case data set was generated by systematically calculating the steady-state solution for each combination of values of the input variables using the range of variation provided in Table 3.11. Each row of the data matrix represented one steady-state solution.

Figure 3.33 lists the MATLAB® files used to generate the base case data. A description of each file is also provided in the figure.

3.5 PRINCIPAL COMPONENT MODEL

Once the base case data set was generated, the principal component model could be obtained. It was necessary to do some pre-processing of the data before application of SVD. First, random Gaussian white noise was added. The addition of white noise simulates measurement and instrumentation error. After adding white noise at 1% of the respected nominal value, each data column was mean-centered to move the origin to the mean of each column.

Scaling is very important in PCA. If there are large differences between the variances of the data, those variables whose variances are large will tend to dominate the first few principal components even if those variables are not actually important in indicating process malfunctions (Martin, Morris, and Zhang 1996). The data matrix consisted of state variables of all the same type (molar flow rates) but with very large variances. Therefore, the mean-centered noisy data matrix was scaled so that the standard deviation of each column was one. Weighted scaling was used for all of the input variables and the primary uranium-bearing output of each module. For those state variables that weighted scaling was used, the standard deviation was the scaling factor as opposed to one as stated above. Singular Value

fsolve_BC.m
- Solves the system of nonlinear equations that describe the operation of the conversion plant
- Calls the function file Xss_BC.m
- Outputs the steady-state state variable solution (Xss) at the stated input variable values

parameters_BC.m
- Loads the base case parameters for the subsequent files
- Must match the parameters in Xss_BC.m
- Also loads the steady-state input variables

Xdot_BC.m
- Checks the steady-state solution to give Xdot=0
- The system of equations must match those in Xss_BC.m
- Output is Xdot and should be equal to evaluated from fsolve_BC.m
- The solution of Xdot should be zero

OMB_BC.m
- Checks the overall material balance for each module
- The solution of OMB should be zero

BC_data.m
- Calls NUCP_BC.m
- The system of equations must match those in Xss_BC.m
- Generates the base case data matrix by varying the input variables using nested loops

Figure 3.33. List and Description of the MATLAB® files used to Generate the Base Case Data.

Decomposition (SVD) was used to extract the principal component model as described in Chapter 2. The effective rank was determined using a Scree plot. The effective rank determines the most likely degree of freedom the data matrix exhibits and suggests the number of principal components that should be retained to represent the overall model. The scores and residuals were calculated as described previously. The Mahalanobis distance and the Q-statistic along with the 95%-confidence threshold for the scores in the principal component space were calculated. Loadings plots were generated to determine which state variables contribute the most weight to each principal component and therefore which group of state variables dominates each degree of freedom that was represented by each principal component. The scores plots were generated for the base case for future comparison with faulty cases. Additionally, plots of the Mahalanobis distance and the Q-statistic were generated for the base case to serve as the reference for the detection of 'faults' in the faulty cases. Figure 3.34 lists the MATLAB® files used to generate the base case principal component model and initial plots. A description of each file is also provided in the figure.

The base case PCA model was verified by means of a control case. For the control case, all of the parameters and input variables were set within the set of base case values. Table 3.12 lists the input variables with both the base case and control case variations. Once the control case data were generated, the data matrix was pre-processed in the same manner (Gaussian noise added, mean-centered, and scaled) as the base case data. However, the original base case mean and standard deviation were used to mean-center and scale the control case. The associated scores, the Mahalanobis distance, and the Q-statistic were computed. The diagnostic plots [scores (2-D and 3-D), T^2, Q-statistic, and 2-D scores vs. SPE] were plotted with the base case confidence boundaries superimposed onto the plots to detect presence of a fault. Since all of the control case data should be within the base case data, it was expected that all of the control case data would lie within the base case confidence boundaries.

Table 3.12. List of Control Case Variable Variations

Variable	Base Case Variation	Control Case Variation
$F_{1A,U}$	±10%	±8%
$K_{Mod1B,14}$	-5%	-4%
$K_{Mod2B,14}$	-5%	-4%
$K_{Mod2D,14}$	-5%	-4%
$K_{Mod3D,19}$	-5%	-4%
α_{Mod4D}	±5%	±4%
S_{Mod5A}	±10%	±8%

PCA_nonoise.m
- Pre-processes the data (normalize, mean-center, and scale)
- Determines the effective rank using the singular values from SVD

Add_noise.m
- Adds Gaussian white noise to the base case data matrix
- Checks that noise is properly scaled

PCA_noise.m
- Pre-processes the noisy data (normalize, mean-center, and scale)
- Extracts the principal component model from SVD
- Determines the effective rank using the singular values from SVD

PCA_BCmodel.m
- Determines the number of factors to keep based on the effective rank
- Plots the loadings vectors
- Computes the scores
- Computes the Mahalanobis distance and 95% confidence interval
- Computes the Q-statistic and 95% confidence interval

PCA_BCfigures.m
- Draws the 2-D and 3-D scores plots and 95% confidence boundary
- Plots the Mahalanobis distance and 95% confidence boundary
- Plots the Q-statistic and 95% confidence boundary
- Draws the 3-D plot of PC1 scores, PC2 scores, and SPE

Figure 3.34. List and Description of the MATLAB® files used to Generate the Principal Component Model.

3.6 FAULTY "OFF-NORMAL" CASES

This section discusses the potential diversion scenarios in a conversion plant along with which faulty cases were selected for testing. Figure 3.35 lists the MATLAB® files used to generate the faulty case data and the diagnostic plots. A description of each file is also provided in the figure.

3.6.1 Potential Diversion Scenarios in Conversion Plants

This section covers the potential diversion scenarios that could occur in the operation of a conversion plant and the scenarios that were selected for testing the detection framework of this research. For each potential diversion scenario, a description of each case is provided along with an explanation of why it is of interest. Potential diversion scenarios are listed for each of the modules. The faulty cases should test the model's response using both the Mahalanobis distance and the Q-statistic. The Mahalanobis distance is used to measure the variation in the scores space and to determine if the variations fall outside the 95% confidence boundary (i.e., are the input values outside the accepted normal range?). The Q-statistic is used to determine if the process is operating normally as defined by the model (i.e., does the model still fit?).

3.6.1.1 Module 1

Potential diversion scenarios that involve alterations to Module 1 include:

1. Additional uranium added to dissolver;
2. Different purity of uranium fed to the dissolver;
3. Uranium not completely dissolved (inefficient operations); or
4. Withdrawal of uranyl nitrate stream downstream of the dissolver but still within the same module.

Addition of uranium could be accomplished through an additional port or existing sample line, instrument line, or observation port (temporary hook-up) to the dissolver or through other process input lines (nitric acid or water supply). The result would be that more uranium is processed in the plant than declared with excess uranium being diverted prior to downstream sampling points. It is not likely that diversion would occur until after the purification step. Modeling of this scenario would involve adding an additional input stream to the dissolver. For scenario 2 of Module 1, it is expected that the purity of the incoming uranium ore would vary slightly. However, a much higher purity fed could result in more uranium being processed than declared by the plant. Modeling this would require changing the mass fractions of the incoming uranium ore. Inefficient operations (scenario 3) would result in uranium that could be diverted from the process in filter cake solids. However, diversion at this point in the

fsolve_case#.m
- Solves the system of nonlinear algebraic equations describing the faulty operation of the conversion plant for the specified case
- Calls the function file Xss_case#.m
- Outputs the steady-state state variable solution (Xss) at the stated faulty input variable and/or parameter values

parameters_c#.m
- Loads the specified faulty case parameters for the subsequent files
- Must match the parameters in Xss_case#.m
- Also loads the steady-state input variables

Xdot_case#.m
- Checks the steady-state solution for the specified faulty case
- The system of equations must match those in Xss_case#.m
- Output is Xdot and is equal to that evaluated from fsolve_case#.m
- The solution for Xdot should be zero

OMB_case#.m
- Checks the overall material balance for each module
- The solution for the overall mass balance should be zero

C#_data.m
- Calls NUCP_case#.m
- The system of equations must match those in Xss_case#.m
- Generates the faulty case data matrix by varying the input variables using nested loops

PCA_model_#.m
- Adds Gaussian white noise to the faulty case data matrix and checks that noise is properly scaled
- Pre-processes the noisy data (normalize, mean-center, and scale) using the base case mean and standard deviation(s)
- Computes the scores, the Mahalanobis distance, and the Q-statistic using the base case reduced scores and singular values
- Draws the diagnostic plots as done with PCA_BCfigures.m using the base case confidence boundaries and including the base case data for comparison

Figure 3.35. List and Description of the MATLAB® files used to Generate the Faulty "Off-Normal" Cases and Diagnostic Plots.

process would require a duplicate clandestine NUCP facility somewhere else to process the diverted solids. Modeling of this scenario would involve changing the extent of reaction for the dissolution reaction. Finally, withdrawal of uranyl nitrate could be accomplished through an additional port or existing sample or instrument line (with a temporary hook-up) downstream of the dissolver (between the dissolver and the uranyl nitrate storage tank) and the water or filter wash solution could be increased to ensure flow rates to the tank remain as expected for declared input. Diversion at this point in the process would require a duplicate clandestine facility somewhere else to process the diverted solution. Modeling of this scenario can be accomplished either by changing the fractions so that more uranyl nitrate would go to waste or by adding an additional output stream at the appropriate point.

3.6.1.2 Module 2

Potential diversion scenarios that involve alterations to Module 2 include:

1. Additional uranium added to extraction column;
2. Inefficient extraction of uranium from aqueous stream;
3. Withdrawal of uranyl nitrate downstream of the scrub or stripping columns; or
4. Inefficient re-extraction of uranium from organic stream.

The addition of uranium could be accomplished through an additional port or existing sample line, instrument line (temporary hook-up) to dissolver or through other process input lines (nitric acid or water supply). The result is that more uranium is processed in the plant than declared with excess uranium being diverted prior to downstream sampling points. Modeling of this scenario would involve adding an additional input stream to the extraction column. Inefficient extraction of uranium from the aqueous stream would result in diversion of uranium in the raffinate stream from extraction column. Withdrawal of uranyl nitrate could be done through an additional port or existing sample or instrument line (with a temporary hook-up) downstream of the scrub or re-extraction columns and the purified uranyl nitrate storage tank along with an increase in strip solution to ensure flow rates to product tank remains as expected for declared input. Inefficient re-extraction of uranium from the organic stream would result in diversion of uranium in the organic waste stream from re-extraction (stripping) column. For scenarios 2–4 in Module 2, diversion would require a duplicate clandestine facility (from purification on) somewhere else to process the diverted material. Modeling scenarios 2–4 of Module 2 would require altering the fractionation parameters for each of the columns to direct uranium into the waste streams.

3.6.1.3 Module 3

Potential diversion scenarios that involve alterations to the evaporation process in Module 3 include:

1. Additional uranium, in the form of uranyl nitrate, added to evaporator;
2. Evaporator reflux is operated such that more condensate is produced; or
3. Withdrawal of concentrated uranyl nitrate stream downstream of evaporator.

The addition of uranium to the evaporator feed could be accomplished through an additional port or existing sample line, instrument line (temporary hook-up) or through other process input lines (water supply). The result is that more uranium is processed in the plant than declared with excess uranium being diverted prior to downstream sampling points. Modeling of this scenario would involve adding an additional input stream to the evaporator. The evaporator reflux could be operated such that more condensate is produced resulting in more uranium being diverted in the condensate stream. Withdrawal of concentrated uranyl nitrate could be done through an additional port or existing sample or instrument line (with a temporary hook-up) downstream of the evaporator. For scenarios 2 and 3 in the evaporation process of Module 3, diversion would require a duplicate clandestine facility (downstream of purification) somewhere else to process the diverted material. Modeling these scenarios would require altering the fractionation parameters for the evaporator to direct uranium into the waste streams. For scenario 3, modeling could also be accomplished by adding an additional output stream at the appropriate point.

Potential diversion scenarios that involve alterations to the precipitation process in Module 3 include:

1. Additional uranium added to the precipitation process;
2. Inefficient precipitation operations; or
3. Withdrawal of uranium powder through the exhaust system.

The addition of uranium to the precipitation process feed could be accomplished through an additional port or existing sample line, instrument line or recirculation (temporary hook-up) to the precipitator or through other process liquid input lines. The result is that more uranium is processed in the plant than declared with excess uranium being diverted prior to downstream sampling points. Modeling of this scenario would involve adding an additional input stream to the precipitator. Inefficient precipitation operations would result in uranium that could be diverted in the waste stream from the precipitator product filter. Uranium diverted through the filtrate stream could easily be retrieved in a separate process. Modeling of this scenario would involve changing the extent of reaction for the precipitation reaction. In order for additional uranium to be withdrawn, a vacuum would need to be applied to the powder collection point so that more powder is entrained in the exhaust system. Modeling of this scenario would be accomplished by changing the fractions so that more uranium would go to exhaust.

3.6.1.4 Module 4

Potential diversion scenarios that involve alterations to Module 4 include:

1. Additional uranium added to the calciner; or
2. Withdrawal of uranium powder through the exhaust system in either Module 4C or 4F.

The addition of uranium to the calciner could be accomplished through an additional port. The result is that more uranium is processed in the plant than declared with excess uranium being diverted prior to downstream sampling points. Modeling of this scenario would involve adding an additional input stream to the calciner. In order for additional uranium to be withdrawn, a vacuum would need to be applied to the powder collection point so that more powder is entrained in the exhaust system. Modeling of this scenario can be accomplished by changing the filter fractionations so that more uranium would go to exhaust streams in either Module 4C or 4F.

3.6.1.5 Module 5

Potential diversion scenarios that involve alterations to Module 5 include:

1. Withdrawal of uranium powder through the exhaust system of the secondary fluorination system;
2. Withdrawal of UF_6 upstream of the cold traps;
3. Inefficient operation of the fluorination unit; or
4. Inefficient operation of the UF_6 collection units.

In order for additional uranium to be withdrawn through the exhaust system, a vacuum would need to be applied to the powder collection point on the secondary fluorination system so that more powder is entrained in the exhaust system. Modeling of this scenario would be accomplished by changing the filter fractionations so that more uranium would go to exhaust stream in Module 5F. Uranium hexafluoride could also be diverted from the process and collected in separate cold traps or a chemical trap. Modeling this scenario would also involve changing the filter fractionations at the appropriate point. Inefficient fluorination operations would result in additional UF_4 that collects in the ash and could be sent to another facility for recovery. Modeling of this scenario would involve changing the extent of reaction for the fluorination reaction for either the primary or secondary reactions. Inefficient operation of the UF_6 collection units would result in additional UF_6 that exits the vent system and is collected on chemical traps that are diverted to another facility. Modeling this would involve adding an additional output to the last unit operation in Module 5F.

3.6.1.6 Multiple Modules

Potential diversion scenarios that involve alterations to more than one Module include:

1. Adjusting the flow parameters that ensure sufficient reactants;
2. Data spoofing; or
3. Changing two parameters that may cancel each other's effects.

Adjusting the flow parameters would affect how much uranium is converted and also how much reactant is left after the reaction. These parameters exist in all of the modules except Module 2, so more than one scenario could be tested. Data spoofing is a concern for actual operations. It would be possible to test the data spoofing by generating a random set of data where each of the unknowns varies within the acceptable range. However, the relationship between the unknowns of one sample may not fit the model. Finally, it is possible that two parameters could cancel one another's effects. This is mostly the scenario for the flow parameters and extents of reaction.

3.6.2 Selected Faulty "Off-Normal" Cases

This section discusses the actual faulty "off-normal" cases that were selected for study. Table 3.13 provides a summary of each of the cases. Following Table 3.13, each case is described along with a brief analysis of why the case is important. The first three cases test processes included in Module 1. The fourth case applies to Module 2. Cases 5–7 are specific to Module 3. Case 8 applies to Module 4. Cases 9–11 are specific to Module 5. Cases 12–14 test the effect of changing multiple parameters or inputs which could result in cancellation of the fault detection or an additive effect to the fault.

3.6.2.1 Case 1

The first faulty case that was investigated was an increase in the total throughput of the facility. In this case, all incoming flow rates (Streams 1A, 4A–13A) were increased with no other changes in the model. The initial test was to increase the throughput by 50% to determine the model's response. This was done by multiplying all eleven incoming base case flow rates (see Table 3.9) by 1.5. Since up to 10% change was built into the base case model for the incoming uranium flow rate, an increase in total throughput of 10% was also tested. In this case, the Q-statistic was expected to be outside of the accepted range since most of these flow rates were parameters and therefore the relative relationships between the parameters and the state variables would change. The Mahalanobis distance was expected to show that the values are outside of the accepted range. Additionally, only the incoming uranium flow rate was increased leaving all other parameters and inputs unchanged from the base case.

Table 3.13. Summary of Faulty Cases

Case #	Safeguards Priority	Module	Fault Variable	Base Case Value	Fault Value	Description
1A	High	1	All F values	Varies	+50%	Increase total plant throughput by 50%
1B	High	1	All F values	Varies	+10%	Increase total plant throughput by 10%
1C	High	1	$F_{1A,U}$	50 kg/h	57.5 kg/h	Increase uranium throughput by 15%
1D	High	1	$F_{1A,U}$	50 kg/h	62.5 kg/h	Increase uranium throughput by 25%
2	Low	1	$x_{1A,18}$	0.85	0.90	Increase the incoming uranium purity by 5.9%
3	Medium	1	X_{Mod1A}	0.9799	0.95	Inefficient dissolver operations, reduce extent of reaction by 3%
4	High	2	$K_{Mod2D,14}$	0.999	0.9	Inefficient re-extraction operations, reduce uranyl nitrate extraction by 9.9%
5	High	3	S_{Mod3A}	N/A	0.0025	Diversion of 0.25% of the uranium from the evaporator
6	High	3	F_{14A}	N/A	10 kg/h	Addition of uranyl nitrate to the precipitation process
7	Low	3	X_{Mod3C}	0.9999	0.9	Inefficient precipitation process operations, reduce extent of reaction by 10%
8	Medium	4	$K_{Mod4F,16}$; $K_{Mod4F,17}$	0.00001; 0.001	0.0001; 0.01	Inefficient separation downstream of the hydrofluorination reaction
9	Medium	5	$S_{Mod5F,1}$	N/A	0.75	Diversion of 75% of the UF_6 from the secondary fluorination process
10	High	5	X_{Mod5B}; X_{Mod5E}	0.999	0.95	Inefficient operations of the fluorination processes, reduce extent of reaction by 4.9%
11	High	5	$S_{Mod5F,2}$	N/A	0.2	Diversion of 20% of the purified UF_6
12	High	1 and 5	$F_{1A,U}$; $S_{Mod5F,2}$	50 kg/h; N/A	62.5 kg/h; 0.2	multiple parameters
13	High	3 and 5	X_{Mod3C}; X_{Mod5B}; X_{Mod5E}	0.9999; 0.999	0.9; 0.95	multiple parameters
14	Low	1	$x_{1A,18}$; X_{Mod1A}	0.85; 0.9799	0.90; 0.95	multiple parameters

An increase in throughput of a facility was a highly likely scenario. It was expected that a plant would have some variation in throughput. This expected variation was built into the model by varying the incoming uranium flow rate by ±10% as part of the base case. Since most plants have a design capacity that is greater than normal operating conditions, detection of an increase above the accepted range is of great importance to safeguards since additional material could be processed and diverted before safeguards declarations.

3.6.2.2 Case 2

The second faulty case that was selected for testing was to change the purity of the uranium fed to the dissolver in Module 1. It is possible that higher purity uranium could arrive in drums and be fed to the plant. Conversion plants operate with a very narrow band of purity. The amount of uranium and impurities drive the amount of reactants needed and it is desired that there not be much variability in uranium purity. No variation in uranium purity was built into the model due to this. However, higher purity uranium could result in additional uranium being processed in a plant than is declared. This is of low priority for safeguards since it is expected that material substitution of this manner would not occur until later in the process. For this case, the uranium input stream was changed from 85 wt-% U_3O_8 and 15 wt-% impurities (7.5 wt-% soluble impurities and 7.5 wt-% insoluble impurities) to 90 wt-% U_3O_8 and 10 wt-% impurities (5 wt-% soluble impurities and 5 wt-% insoluble impurities). It was expected that the Q-statistic would produce a fault since this was a change in a parameter and therefore a change in the relative relationships between the state variables.

3.6.2.3 Case 3

The third test case investigated inefficient dissolver operations in Module 1. Inefficient operations would result in the uranium not being completely dissolved. This would cause uranium to be diverted to waste where it could be recovered and further processed elsewhere. Inefficient operations could be a result of equipment malfunction such as the heated jacket not reaching the necessary temperature due to a faulty thermocouple or it could be an operator purposely operating inefficiently to divert material. This is a medium priority case for safeguards. This case was modeled by changing the extent of reaction for the dissolution reaction, X_{Mod1A}, from 0.9799 to 0.95. It was expected that all of the diagnostic plots would produce a fault since this was outside normal conditions and changed the relative relationships between the state variables. This was outside normal operating conditions since it changed the amount of uranium that proceeded through the process downstream of the dissolver.

3.6.2.4 Case 4

The fourth test case investigated inefficient operations in Module 2, specifically the re-extraction of uranium from the organic phase. Inefficient re-extraction results in additional uranium being diverted to the organic waste stream. The waste stream could be processed at an undeclared facility to recover purified uranium that could be further converted to desirable forms. This scenario is of high priority for safeguards. As with Case 3, this fault could be due to faulty equipment or intentional diversion. This case was modeled by changing the column fractionation parameter for the uranyl nitrate in Module 2D, $K_{Mod2D,14}$. This parameter was one of the input variables and was varied in the computation of the base case. For this case, the initial value of this input was reduced from 0.999 to 0.9. It was expected that all of the diagnostic plots would produce a fault since this was outside normal conditions and changed the relative relationship between the state variables.

3.6.2.5 Case 5

Case five tested the model's ability to detect the diversion of a fraction of the stream exiting the evaporator in Module 3A. The faulty case block diagram of Module 3A is shown in Figure 3.36. A new stream (Stream 61) was added to represent the diversion stream. The condensate stream (Stream 21) remained unchanged in the model. The new stream was modeled as a split of Stream 22 and therefore had the same composition as Stream 22. A new parameter, S_{Mod3A}, which was the fraction of Stream 22 that was split to Stream 61 was created. Diversion of intermediate products such as the uranyl nitrate that was diverted for this case becomes of greater concern as the material becomes more purified. The material is considered to be highly purified anywhere downstream of the solvent extraction process that is represented by Module 2. Therefore, this diversion is a high priority for safeguards. It was expected that all of the diagnostic plots would produce a fault since this was outside normal conditions and changes the relative relationship between the state variables. This was a change in the normal operating conditions because it reduced the amount of uranium available for conversion downstream of the evaporator.

3.6.2.6 Case 6

Case six tested the model's ability to detect the addition of uranium to the system prior to precipitation in Module 3B. The faulty case block diagram of Module 3B is shown in Figure 3.37. A new stream was added as an additional input stream (Stream 14A). This new stream was assumed to be pure uranyl nitrate. The flow rate of the stream was assumed to be 10 kg/h which corresponds to an additional 12.4% based on the amount of uranyl nitrate in Stream 22 which also feeds the precipitator. It was an additional 12% based on the nominal flow rate of the uranium fed to the plant in Module 1. No other
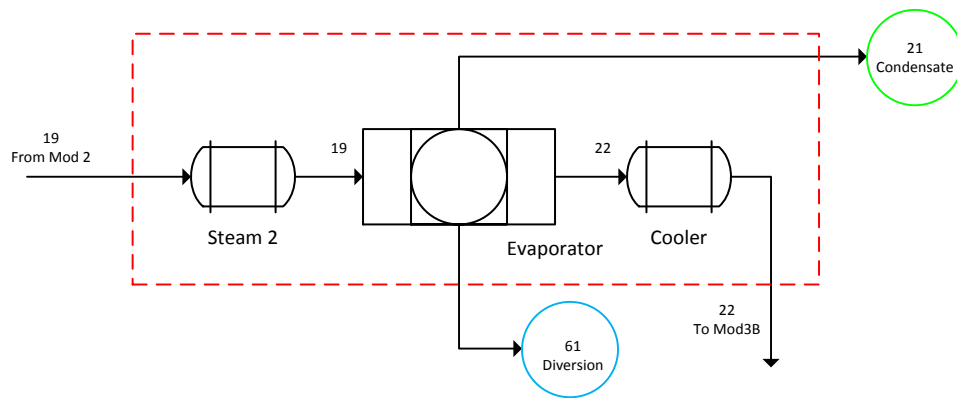
Figure 3.36. Block Diagram of the Module 3A Showing Input and Output Streams According to Faulty Case 5.
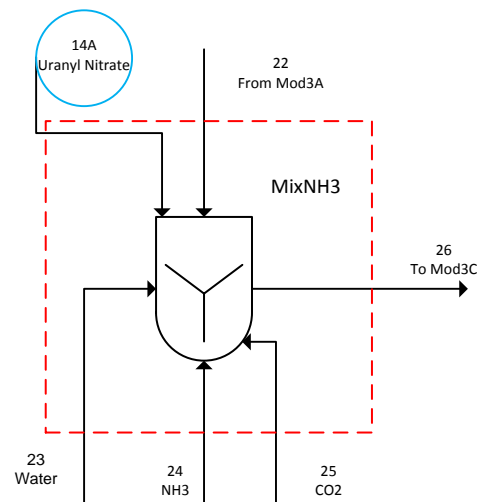
Figure 3.37. Block Diagram of the Module 3B Showing Input and Output Streams According to Faulty Case 6.

parameters or inputs were changed from the base case. The processing of undeclared uranium is of high concern for safeguards. The addition of undeclared material was suggested in Figure 1.2. It was expected that all of the diagnostic plots would produce a fault since this was outside normal conditions and changes the relative relationship between the state variables.

3.6.2.7 Case 7

The seventh test case investigated inefficient precipitation process operations in Module 3. Inefficient operations would result in incomplete conversion of the uranyl nitrate to ammonium uranyl carbonate. This would cause uranium to be diverted to waste where it could be recovered and further processed elsewhere. Inefficient operations could be a result of equipment malfunction, or it could be an operator purposely operating inefficiently to divert material. This is a low priority case for safeguards since the reaction goes to 100% completion immediately but could simulate a diversion of AUC to waste which is a high priority safeguards concern. This case was modeled by changing the extent of reaction for the precipitation reaction, X_{Mod3C}, from 0.9999 to 0.9, which was a 10% reduction. It was expected that all of the diagnostic plots would produce a fault since this was outside normal conditions and changes the relative relationship between the state variables. Again, this was outside normal operating conditions since it affected the amount of uranium available for conversion later in the plant and increased the uranium in the waste.

3.6.2.8 Case 8

The eighth test case investigated inefficient separation in Module 4, specifically the filtration system downstream of the hydrofluorination reaction. Inefficient filtration results in additional uranium being diverted to the off-gas waste stream. The waste stream could be processed at an undeclared facility to recover the uranium that could be further converted as desired. Any diversion of uranium to a waste stream is of great concern for safeguards. This case was considered medium priority for safeguards because the likelihood of it occurring is lower than other cases and the fractionation was so low. This case was modeled by changing the filter fractionation parameters for the UF_4 and UO_2 in Module 4F, $K_{Mod4F,16}$ and $K_{Mod4F,17}$, respectively. For both, the base case value was increased ten times. Therefore, the value of $K_{Mod4F,16}$ was increased from 0.00001 to 0.0001, and the value of $K_{Mod4F,17}$ was increased from 0.001 to 0.01. It was expected that all of the diagnostic plots would produce a fault since this was outside normal conditions and changes the relative relationship between the state variables. This was outside normal operating conditions because it changed the amount of uranium that proceeded through the remainder of the process and increased the uranium in the waste. The detectability of a fault in the scores and Mahalanobis distance would depend on how far outside of normal operating conditions this was. Even though the increase was large, the fractions were very small

even after the increase. The fault in the Q-statistic was expected to be large since this was a large change in two parameters which should result in a detectable change in the relative relationship between the state variables.

3.6.2.9 Case 9

The ninth faulty case tested the ability of the model to detect the diversion of UF_6 from the secondary fluorination process in Module 5. In this case, the model was modified to allow for UF_6 to exit the process at the gas separator in Module 5F. In the base case, only F_2 and N_2 were assumed to exit at that point. It was necessary to add a UF_6 component stream to Stream 56. Then the UF_6 exiting in the vent was defined as the percentage of the incoming UF_6 in Stream 55 that exited in Stream 56. The remaining UF_6 proceeded to the slag separator. Several percentages were tested; only the 75% results are presented in Chapter 4. This appears to be a very large diversion but since only 10% of the incoming uranium to Module 5 was diverted to the secondary reactor this diversion was not significant. Again, any diversion of uranium to a waste stream is of great concern for safeguards, especially purified UF_6. However, since this is from the secondary fluorination process, it was considered medium priority for safeguards. Since this was the secondary fluorination section and only a small fraction of the material was included in this process, it was expected that the Q-statistic would detect the fault due to the change in the relative relationship between the state variables. No faults were expected in the scores or the Mahalanobis distance plots since this corresponds to an overall diversion of 7.5% which would be within normal operating conditions even though the diversion itself was outside normal operating conditions.

3.6.2.10 Case 10

The tenth faulty case tested the ability of the model to detect inefficient operations of the fluorination processes in Module 5. In this case, the extents of reaction for both the primary and secondary fluorination reactions were changed from 0.999 to 0.95. In real operations, this would result in less UF_4 being converted to UF_6 and would cause an increase in the amount of UF_4 in the waste streams which could be recovered and processed elsewhere. As with the other diversion scenarios, any diversion of uranium to a waste stream is high priority for safeguards, especially later in the process. It was expected that all diagnostic plots may produce a fault since this was outside normal conditions and the relative relationship between the state variables. Reduction in the amount of uranium converted was a change in the normal operating conditions since it changed the amount of final product outside the normal levels. However, since this was only approximately a 5% reduction and ±10% change in the incoming uranium was built into the base case model, there may not be a detectable fault in the scores or

Mahalanobis distance. A fault in the Q-statistic was expected since this was a change in the relative relationship between the state variables.

3.6.2.11 Case 11

Case eleven tested the model's ability to detect the diversion of purified UF_6 from Module 5. The scenarios assumed that the UF_6 collection system was operated inefficiently either due to equipment failure or for the purposes of diversion of material. The faulty case block diagram of Module 5F is shown in Figure 3.38. A new stream (Stream 61) was added to represent the diversion stream. Streams 52 and 59 were pure UF_6 that were mixed to form the final product of the process. In this case, the new stream was formed by diverting a percentage of the streams that were inputs to the mixer. Several percentages were tested, but only the results of the 20% diversion case are presented in Chapter 4. This case is of extremely high concern for safeguards. At this point the material is completely purified and can be used for enrichment to support a weapons program. Since current safeguards policy is not applied until the product is declared it is feasible that material could be diverted before declaration. It was expected that only the Q-statistic would detect this fault since this stream was exiting the model and there was no longer any interaction with the model and since a new parameter was introduced which would change the relative relationship between the state variables.
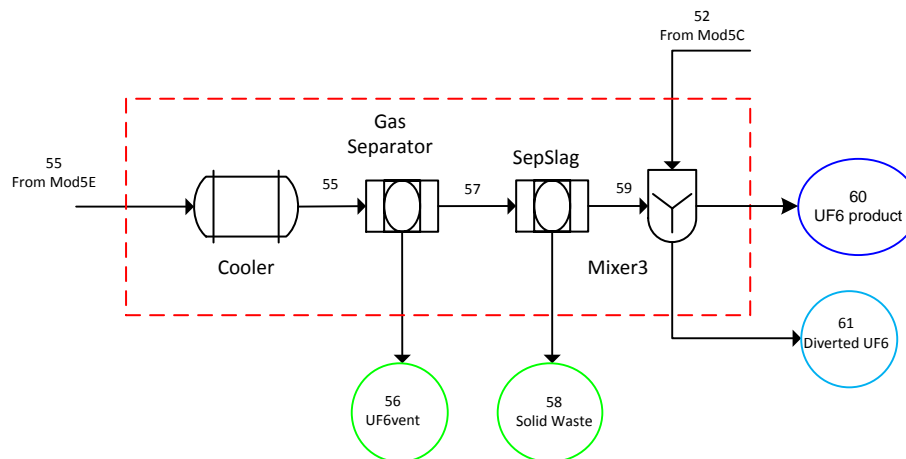
Figure 3.38. Block Diagram of the Module 5F Showing Input and Output Streams According to Faulty Case 11.

3.6.2.12 Case 12

Faulty Case 12 was the first case used to test the effect of changes to multiple parameters or inputs. This case was a combination of Case 1D and Case 11. In Case 1D, the uranium input flow rate was increased by 25% in Module 1. In Case 11, 20% of the UF_6 product was diverted through a new output stream in Module 5. This test was investigated since it is a likely scenario of concern for safeguards. This case models the scenario where additional uranium is fed to the process and then additional purified uranium is diverted before declaration at the end of the process. It was expected that this case would produce faults in all of the diagnostic plots since this was outside normal conditions and changes the relative relationship between the state variables.

3.6.2.13 Case 13

Faulty Case 13 was the second case used to test the effect of changes to multiple parameters or inputs. This case was a combination of Case 7 and Case 10. In Case 7, inefficient precipitation process operations were investigated by changing the extent of reaction for the precipitation reaction, X_{Mod3C}, from 0.9999 to 0.9 in Module 3. In Case 10, inefficient operations of the fluorination processes in Module 5 were investigated by changing the extents of reaction for both the primary and secondary fluorination reactions from 0.999 to 0.95. Inefficient operations results in additional uranium in the waste streams which can be recovered and further purified as needed at an undeclared location. As with the other diversion scenarios, any diversion of uranium to a waste stream is of great concern for safeguards, especially later in the process. Since this was diversion of material in two locations, it was considered high priority. It was expected that all diagnostic plots would produce a fault since this was outside normal conditions and changes the relative relationship between the state variables. Since this case was a combination of inefficient operations, it was also expected that the faults could be larger due to additive effects of the faults which was one of the reasons this case was selected for testing.

3.6.2.14 Case 14

Faulty Case 14 was the third case used to test the effect of changes to multiple parameters or inputs. This case was a combination of Case 2 and Case 3. In Case 2, the effect of changing the purity of the uranium feed was investigated by changing the uranium input stream from 85 wt-% U_3O_8 and 15 wt-% impurities (7.5 wt-% soluble impurities and 7.5 wt-% insoluble impurities) to 90 wt-% U_3O_8 and 10 wt-% impurities (5 wt-% soluble impurities and 5 wt-% insoluble impurities) in Module 1. In Case 3, inefficient dissolver operations in Module 1 were investigated by changing the extent of reaction for the dissolution reaction, X_{Mod1}, from 0.9799 to 0.95. This case was selected as one possible case in which two faults could cancel each other out and result in no detection of the fault. This case was low priority for safeguards.

114

4. RESULTS AND DISCUSSION

The results of the sensitivity analysis, modeling of the base case model, the control case, and the numerous faulty test cases are detailed in this chapter.

4.1 SENSITIVITY ANALYSIS

As stated in the Chapter 3 discussion of the approach for the sensitivity analysis, each of the parameters was varied by ±10% using a one-at-a-time approach to determine a new steady-state solution for all of the state variables. For parameters that could not vary by +10%, such as an extent of reaction with a value of one, the parameter was only tested at -10%.

Also discussed in Chapter 3, the sensitivity analysis involved the derivation of a sensitivity factor for each parameter and steady-state state variable solution combination. The sensitivity factor is unit-less and calculated using Eq. (3.3.0.1), where $\gamma_{i,j}$ is the sensitivity factor for the i-th state variable (y) of the j-th parameter (u) at steady state.

$$\gamma_{i,j} \triangleq \frac{\Delta y_i / y_{i,0}}{\Delta u_j / u_{j,0}} \tag{3.3.0.1}$$

For the sensitivity analysis, only the primary uranium-bearing streams (as listed in Table 3.8) were considered. For simplification of the sensitivity matrices shown below and since all of the parameters tested did not result in a response in the primary streams, Table 4.1 lists the parameters that are part of the sensitivity factor matrix.

For the sensitivity factor matrix, the bold numbers across the top correspond to the parameter (u) numbers listed in Table 4.1 and the bold numbers listed in the first column correspond to the state variable (y) number. The y numbers are also the same as the Xss numbers (refer to Table 3.8 for primary state variables). The numbers within the table are the sensitivity factor (γ) for the specific combination of parameter and state variable. Any empty cells mean that the value of that sensitivity factor was below the selected threshold value of ±0.10. Values equal to one mean that a 10% change in the specific parameter resulted in a 10% change in the corresponding state variable. For values less than one, a 10% change in the specific parameter resulted in less than a 10% change in the corresponding state variable. The reverse of that was also true for values greater than one where a 10% change in the specific parameter resulted in more than 10% in the corresponding state variable. In the case of negative values, a 10% increase in a specific parameter resulted in a decrease in the corresponding state variable or a 10% decrease in a specific parameter resulted in an increase in the corresponding state variable.

Table 4.1. Parameters for the Sensitivity Analysis

Parameter Number	Parameter Name	Nominal Value	Description
1	$F_{1A,U}$	50	Flow rate of uranium in stream 1A, Mod1A
2	X_{Mod1A}	0.9799	Extent of Reaction (moles U_3O_8 reacted/moles U_3O_8 fed), Mod1A
3	$K_{Mod1B,14}$	0.98	Uranyl Nitrate Filter Fractionation Factor (mol-%), Mod1B
4	$K_{Mod1B,18}$	0.02	U_3O_8 Filter Fractionation Factor (mol-%), Mod1B
5	$K_{Mod1C,14}$	0.8	Uranyl Nitrate Filter Fractionation Factor (mol-%), Mod1C
6	$K_{Mod1C,18}$	0.7	U_3O_8 Filter Fractionation Factor (mol-%), Mod1C
7	$S1_{Mod1D}$	0.333	Splitter, fraction of flow from Stream 7 to Stream 9, Mod1D
8	$S2_{Mod1D}$	0.333	Splitter, fraction of flow from Stream 7 to Stream 10, Mod1D
9	$K_{Mod1E,14}$	0.9999	Uranyl Nitrate Filter Fractionation Factor (mol-%), Mod1E
10	$K_{Mod1E,18}$	0.9999	U_3O_8 Filter Fractionation Factor (mol-%), Mod1E
11	$K_{Mod2B,14}$	0.995	Uranyl Nitrate Column Fractionation Factor (mol-%), Mod2B
12	$K_{Mod2C,14}$	0.999	Uranyl Nitrate Column Fractionation Factor (mol-%), Mod2C
13	$K_{Mod2D,14}$	0.999	Uranyl Nitrate Column Fractionation Factor (mol-%), Mod2D
14	$K_{Mod3A,14}$	0.0001	Uranyl Nitrate Filter Fractionation Factor (mol-%), Mod3A
15	X_{Mod3C}	0.9999	Extent of Reaction (moles uranyl nitrate reacted/moles uranyl nitrate fed), Mod3C
16	$K_{Mod3D,19}$	0.995	AUC Filter Fractionation Factor (mol-%), Mod3D
17	X_{Mod4B}	0.9999	Extent of reaction (moles AUC reacted/moles AUC fed), Mod4B
18	α_{Mod4D}	0.95	Flow parameter that insures sufficient HF is fed for conversion, Mod4D
19	X_{Mod4E}	0.9999	Extent of reaction (moles HF reacted/moles HF fed), Mod4E
20	$K_{Mod4F,16}$	1×10^{-5}	UF_4 Filter Fractionation Factor (mol-%), Mod4F
21	$K_{Mod4F,17}$	0.001	UO_2 Filter Fractionation Factor (mol-%), Mod4F
22	$K_{Mod4F,19}$	1	AUC Filter Fractionation Factor (mol-%), Mod4F
23	S_{Mod5A}	1.1	Splitter, fraction of flow from Stream 44 to Stream 45, Mod5A
24	X_{Mod5B}	0.999	Extent of reaction (moles UF_4 reacted/moles UF_4 fed), Mod5B
25	$K1_{Mod5C,16}$	0.99	UF_4 Mole Fraction Fractionation (mol-%), Mod5C (UF_6-UF_4 Separator)
26	$K1_{Mod5C,17}$	1	UO_2 Mole Fraction Fractionation (mol-%), Mod5C (UF_6-UF_4 Separator)
27	$K2_{Mod5C,15}$	0.99	UF_6 Mole Fraction Fractionation(mol-%), Mod5C (Separator)
28	X_{Mod5E}	0.999	Extent of Reaction (moles UF_4 reacted/moles UF_4 fed), Mod5E

Table 4.2 is the sensitivity factor matrix for all of the modules for a 10% increase of the parameters included in the matrix. There are only a few parameters listed since many of the parameters could not be increased by 10%. Only ten of the 82 parameters tested resulted in a sensitivity factor above the threshold value for the 51 primary state variables for a 10% increase in nominal value of the parameter. All of the primary state variables (see Table 3.8) were sensitive to changes in the incoming flow rate of elemental uranium in the U_3O_8 fed to the plant, $F_{1A,U}$. This was expected since uranium was the species of interest for this work and participated in nearly all of the reactions throughout the process. Additionally, the sensitivity factor for each of the primary state variables/incoming elemental uranium flow rate was one. This was also expected due to the stoichiometry of the reactions. For all of the reactions involving uranium, the stoichiometric coefficient for the uranium compound was one.

For most of the other parameters, only a few of the state variables had a sensitivity factor above the threshold. For $K_{Mod1C,14}$ (parameter 5) only one state variable had a sensitivity factor above the threshold. Sensitivity factor $\gamma_{40,5}$ was -3.8. This state variable was the uranyl nitrate in Stream 8 which was a waste stream in Module 1. This state variable was very sensitive to changes in this parameter. The negative response was expected because increasing the parameter increased the amount of uranyl nitrate in Stream 7 and therefore reduced the amount of uranyl nitrate in Stream 8. The high sensitivity was also expected because Stream 7 was part of the recycle that was internal to Module 1 so that at steady state multiple recycle passes have occurred and the amount of uranyl nitrate in Stream 8 would have decreased with each recycle. Therefore, it is recommended that this stream be monitored frequently to detect the presence of excess uranium in the waste.

For S_{Mod5A} (parameter 23), several state variables had sensitivity factors above the threshold. Sensitivity factors $\gamma_{221,23}$, $\gamma_{222,23}$, and $\gamma_{254,23}$ were one. These state variables were the UF_4 and UO_2 in Stream 45 and UF_4 in Stream 54 which were intermediate streams in Module 5. Stream 45 was directly related to the parameter since it was the stream directly downstream of the splitter. Stream 54 was immediately downstream of Stream 45 following the mixer that mixed Stream 45 with Stream 53. The sensitivity factors for ten of the state variables with respect to parameter 23 were -0.11. These state variables were the primary uranium components in the primary fluorination section of Module 5. The negative response was expected as well as the sensitivity factor value being the same of all of the state variables because the parameter determined the amount of Module 5 feed that was directed to the secondary fluorination process and therefore reduced the amount available for the primary fluorination process. Sensitivity factors $\gamma_{269,23}$ and $\gamma_{270,23}$ were one. These state variables were the UF_4 and UO_2 in Stream 58 which was a waste stream in Module 5. Sensitivity factors $\gamma_{259,23}$, $\gamma_{265,23}$, and $\gamma_{272,23}$ were 0.91. These state variables were the UF_6 in Streams 55, 57, and 59 which were an intermediate streams in Module 5 in the secondary fluorination process. These streams were impacted by the amount of material that was directed to the secondary process as well as the amount of material that was recycled from the primary process.

Table 4.2. Sensitivity Factors for the Primary State Variables for 10% Increase in Each Parameter (All Modules)

u / y	1	4	5	6	7	8	14	20	21	23
Module 1										
3	1.0									
10	1.0									
16	1.0									
40	1.0		-3.8		0.37					
41	1.0			-1.6	0.45	0.44				
64	1.0									
70	1.0									
Module 2										
77	1.0									
84	1.0									
91	1.0									
92	1.0	1.0		0.63	0.13	0.44				
98	1.0									
111	1.0									
117	1.0									
Module 3										
123	1.0						1.0			
128	1.0									
138	1.0									
148	1.0									
159	1.0									
163	1.0									
169	1.0									
171	1.0									
Module 4										
181	1.0									
184	1.0									
198	1.0									
207	1.0									
208	1.0									
214	1.0							1.0		
215	1.0								1.0	
217	1.0									
218	1.0									
219	1.0									

Table 4.2. Sensitivity Factors for the Primary State Variables for 10% Increase in Each Parameter (All Modules) (continued)

u / y	1	4	5	6	7	8	14	20	21	23
Module 5										
221	1.0									1.0
222	1.0									1.0
224	1.0									-0.11
225	1.0									-0.11
230	1.0									-0.11
235	1.0									-0.11
239	1.0									-0.11
240	1.0									-0.11
244	1.0									-0.11
246	1.0									-0.11
249	1.0									-0.11
253	1.0									-0.11
254	1.0									1.0
259	1.0									0.91
265	1.0									0.91
269	1.0									1.0
270	1.0									1.0
272	1.0									0.91
273	1.0									

Table 4.3 is the sensitivity factor matrix for all modules for a 10% decrease of the parameters included in the matrix. Twenty-eight of the 82 parameters tested at a 10% decrease resulted in a sensitivity factor above the threshold value for the 51 primary state variables. A decrease in some of the parameters such as fractionation factors resulted in very large negative sensitivity factors (e.g., -999). One would expect that a change in these fractionations would be very small unlike the 10% that was tested for sensitivity. Therefore, in some cases, the state variables that were extremely sensitive were excluded from the faulty case analysis so as to not bias the results. The matrices also have a lower triangular form because a state variable cannot be sensitive to a parameter that was changed in a module downstream of that state variable since there was no recycle between modules. This provided an additional check to the model.

As with a 10% increase, all of the primary state variables were sensitive to changes in the incoming flow rate of elemental uranium in the U_3O_8, $F_{1A,U}$. For X_{Mod1A} (parameter 2), all of the sensitivity factors were above the threshold, and all of the sensitivity factors were 0.61 except for two. Sensitivity factor $\gamma_{41,2}$ and $\gamma_{92,2}$ were -51.3. These state variables were the U_3O_8 in Streams 8 and 16 which were waste streams in Modules 1 and 2, respectively. This high sensitivity factor indicates that these streams need to be monitored frequently for the presence of excess uranium. The parameter was extent of reaction based on U_3O_8 for the dissolver in Module 1. A decrease in extent of reaction resulted in additional U_3O_8 that was unreacted which increased the amount of U_3O_8 in the waste streams.

For $K_{Mod1B,14}$ (parameter 3), all of the sensitivity factors were above the threshold, and all of the sensitivity factors were 0.30 except for three. Sensitivity factors $\gamma_{3,3}$, $\gamma_{10,3}$, and $\gamma_{40,3}$ were -0.39, -0.78, and -53.6, respectively. The first two state variables were the uranyl nitrate in Streams 1 and 3 which were intermediate streams in Module 1, and the third state variable was the uranyl nitrate in Stream 8. This parameter was the filter fractionation for the vacuum filter in Module 1B. It determined the amount of uranyl nitrate that was sent from Stream 3 to Stream 4. A decrease in this fractionation would increase the amount of uranyl nitrate that was sent to the recycle section of Module 1. Therefore, the uranyl nitrate in the intermediate and waste streams was increased. Additionally, the uranyl nitrate in Stream 8 should be monitored frequently due to its high sensitivity.

For $K_{Mod1C,14}$ (parameter 5), only one state variable had a sensitivity factor above the threshold. Sensitivity factor $\gamma_{40,5}$ was -3.5. For a 10% increase, the sensitivity factor was -3.8. There was a slight nonlinear response from the model to this parameter. Nonlinearity is discussed below. For $K_{Mod1E,14}$ (parameter 9), nearly all of the primary state variables downstream of this parameter had a sensitivity factor above the threshold. Sensitivity factor $\gamma_{i,9}$ was one. This parameter determined the amount of uranyl nitrate that would be sent to waste in Module 1E. The other uranium components were sensitive because uranyl nitrate was the major component exiting Module 1 and was the uranium component in the first downstream reaction. A decrease in this component resulted in a decrease in all of the downstream state variables except Stream 16 which was waste and exited the process prior to the first downstream reaction from this parameter. The values were all one due to stoichiometry.

Table 4.3. Sensitivity Factors for the Primary State Variables for 10% Decrease in Each Parameter (All Modules)

u / y	1	2	3	4	5	6	7	8	9	10	11	12	13
Module 1													
3	1.0	0.61	-0.39										
10	1.0	0.61	-0.78										
16	1.0	0.61	0.30										
40	1.0	0.61	-53.6		-3.5		0.34						
41	1.0	-51.3				-1.3	0.41	0.40					
64	1.0	0.61	0.30						1.0				
70	1.0	0.61	0.30						-9999				
Module 2													
77	1.0	0.61	0.30						1.0			-1.1	
84	1.0	0.61	0.30						1.0		1.0	-1.1	
91	1.0	0.61	0.30						1.0		-199	-1.1	
92	1.0	-51.3		1.0		0.52	0.12	0.40		1.0			
98	1.0	0.61	0.30						1.0		1.0		
111	1.0	0.61	0.30						1.0		1.0		1.0
117	1.0	0.61	0.30						1.0		1.0		-999
Module 3													
123	1.0	0.61	0.30						1.0		1.0		1.0
128	1.0	0.61	0.30						1.0		1.0		1.0
138	1.0	0.61	0.30						1.0		1.0		1.0
148	1.0	0.61	0.30						1.0		1.0		1.0
159	1.0	0.61	0.30						1.0		1.0		1.0
163	1.0	0.61	0.30						1.0		1.0		1.0
169	1.0	0.61	0.30						1.0		1.0		1.0
171	1.0	0.61	0.30						1.0		1.0		1.0
Module 4													
181	1.0	0.61	0.30						1.0		1.0		1.0
184	1.0	0.61	0.30						1.0		1.0		1.0
198	1.0	0.61	0.30						1.0		1.0		1.0
207	1.0	0.61	0.30						1.0		1.0		1.0
208	1.0	0.61	0.30						1.0		1.0		1.0
214	1.0	0.61	0.30						1.0		1.0		1.0
215	1.0	0.61	0.30						1.0		1.0		1.0
217	1.0	0.61	0.30						1.0		1.0		1.0
218	1.0	0.61	0.30						1.0		1.0		1.0
219	1.0	0.61	0.30						1.0		1.0		1.0

Table 4.3. Sensitivity Factors for the Primary State Variables for 10% Decrease in Each Parameter (All Modules) (continued)

u⟍y	1	2	3	4	5	6	7	8	9	10	11	12	13
Module 5													
221	1.0	0.61	0.30						1.0		1.0		1.0
222	1.0	0.61	0.30						1.0		1.0		1.0
224	1.0	0.61	0.30						1.0		1.0		1.0
225	1.0	0.61	0.30						1.0		1.0		1.0
230	1.0	0.61	0.30						1.0		1.0		1.0
235	1.0	0.61	0.30						1.0		1.0		1.0
239	1.0	0.61	0.30						1.0		1.0		1.0
240	1.0	0.61	0.30						1.0		1.0		1.0
244	1.0	0.61	0.30						1.0		1.0		1.0
246	1.0	0.61	0.30						1.0		1.0		1.0
249	1.0	0.61	0.30						1.0		1.0		1.0
253	1.0	0.61	0.30						1.0		1.0		1.0
254	1.0	0.61	0.30						1.0		1.0		1.0
259	1.0	0.61	0.30						1.0		1.0		1.0
265	1.0	0.61	0.30						1.0		1.0		1.0
269	1.0	0.61	0.30						1.0		1.0		1.0
270	1.0	0.61	0.30						1.0		1.0		1.0
272	1.0	0.61	0.30						1.0		1.0		1.0
273	1.0	0.61	0.30						1.0		1.0		1.0

Table 4.4 is the sensitivity factor matrix for Modules 3–5 for a 10% decrease of the parameters included in the matrix. Table 4.3 and 4.4 were divided this way for readability.

For α_{Mod4D} (parameter 18) and X_{Mod4E} (parameter 19), all of the sensitivity factors were above the threshold, and most of the sensitivity factors were one downstream of this parameter. Additionally, the sensitivity factors for parameters 18 and 19 were the same for all of the primary state variables. Seven of the sensitivity factors were -19. These state variables were all UO_2 streams in Modules 4 and 5. Due to the high sensitivity of these state variables, the product and waste streams in Modules 4 and 5 should be frequently monitored for uranium content. Parameter 18 was a flow parameter that was used to insure sufficient HF was fed for conversion Module 4D, and parameter 19 was the extent of reaction for the hydrofluorination reaction that used HF to convert UO_2 to UF_4. If less HF was fed to the process or if less UO_2 was converted to UF_4 due to a change in the extent of reaction, then additional UO_2 would be present downstream. Additionally, four times the number of moles of HF is required to convert each mole of UO_2. Therefore, it is reasonable for these seven state variables to be very sensitive to changes in parameters 18 and 19.

For X_{Mod5B} (parameter 24), six of the sensitivity factors were above the threshold, and five of the sensitivity factors were one. The sixth sensitivity factor, $\gamma_{273,24}$, was 0.89. The other state variables were Xss(235), Xss(244), Xss(246), Xss(249), and Xss(253). These were all downstream of the primary fluorination but upstream of the secondary fluorination except Xss(273) which was the final product. The parameter was the extent of reaction based on UF_4 for the primary fluorination process in Module 5. A decrease in extent of reaction resulted in a decrease in the amount in all of the uranium streams downstream of the process until it reached the secondary fluorination process. All of the values are one based on stoichiometry. The sixth sensitivity factor, $\gamma_{273,24}$, which was less than one did not follow the stoichiometry since that state variable included the additional material from the secondary fluorination process.

For $K2_{Mod5C,15}$ (parameter 27), four state variables had sensitivity factors above the threshold. Sensitivity factors $\gamma_{259,27}$, $\gamma_{265,27}$, and $\gamma_{272,27}$ were -8.2. These state variables were the UF_6 in Streams 55, 57, and 59 which were intermediate streams in Module 5. These streams should be monitored frequently for uranium content due to the high sensitivity factor values. This parameter determined the amount of UF_6 that was directed to Module 5D or Module 5F. For X_{Mod5E} (parameter 28), four of the sensitivity factors were above the threshold. The parameter was the extent of reaction based on UF_4 for the secondary fluorination process in Module 5. Sensitivity factor $\gamma_{273,28}$ was 0.1, and sensitivity factors $\gamma_{259,28}$, $\gamma_{265,28}$, and $\gamma_{272,28}$ were 0.92. These were all UF_6 streams downstream of the secondary fluorination process. A decrease in extent of reaction resulted in a decrease in the amount in all of the UF_6 streams downstream of the process. These were not one as would have been expected based on stoichiometry because there was already some UF_6 in the streams from the primary fluorination process.

Table 4.4. Sensitivity Factors for the Primary State Variables for 10% Decrease in Each Parameter (Modules 3-5)

u \ y	14	15	16	17	18	19	20	21	22	23	24	25	26	27	28
Module 3															
123	1.0														
128															
138															
148		1.0													
159		1.0													
163		1.0	1.0												
169		-9999													
171		1.0	-199												
Module 4															
181		1.0	1.0	1.0											
184		1.0	1.0	1.0											
198		1.0	1.0	1.0											
207		1.0	1.0	1.0	1.0	1.0									
208		1.0	1.0	1.0	-19	-19									
214		1.0	1.0	1.0	1.0	1.0	1.0								
215		1.0	1.0	1.0	-19	-19		1.0							
217		1.0	1.0	-9999					1.0						
218		1.0	1.0	1.0	1.0	1.0									
219		1.0	1.0	1.0	-19	-19									
Module 5															
221		1.0	1.0	1.0	1.0	1.0				1.0					
222		1.0	1.0	1.0	-19	-19				1.0					
224		1.0	1.0	1.0	1.0	1.0				-0.11					
225		1.0	1.0	1.0	-19	-19				-0.11					
230		1.0	1.0	1.0	1.0	1.0				-0.11					
235		1.0	1.0	1.0	1.0	1.0				-0.11	1.0				
239		1.0	1.0	1.0	1.0	1.0				-0.11	-999	1.0			
240		1.0	1.0	1.0	-19	-19				-0.11			1.0		
244		1.0	1.0	1.0	1.0	1.0				-0.11	1.0				
246		1.0	1.0	1.0	1.0	1.0				-0.11	1.0			1.0	
249		1.0	1.0	1.0	1.0	1.0				-0.11	1.0			-99	
253		1.0	1.0	1.0	1.0	1.0				-0.11	1.0			-99	
254		1.0	1.0	1.0	1.0	1.0				1.0					
259		1.0	1.0	1.0	1.0	1.0				0.91				-8.2	0.92
265		1.0	1.0	1.0	1.0	1.0				0.91				-8.2	0.92
269		1.0	1.0	1.0	1.0	1.0				1.0					-999
270		1.0	1.0	1.0	-19	-19				1.0					
272		1.0	1.0	1.0	1.0	1.0				0.91				-8.2	0.92
273		1.0	1.0	1.0	1.0	1.0					0.89				0.1

It was determined during the sensitivity analysis that the system was not linear. If the system was linear then both +10% and -10% would have the same value for sensitivity factor. Table 4.5 summarizes the cases where nonlinearity was observed. Four of the parameters resulted in nonlinear responses from three of the state variables. All four parameters were from Module 1 and the state variables were waste streams in Modules 1 and 2.

4.2 BASE "NORMAL" CASE

This section discusses the results of the base case model. This section includes the steady-state solution obtained using the 'fsolve' function in MATLAB®, the results for the overall material balances, and the generation of the base case data set and PCA model. This section also includes the results of the control case that was used to verify the base case data.

4.2.1 Base Case

The steady-state solution (the molar flow rate of each component in each of the streams) was obtained from MATLAB® using 'fsolve' and the nominal values of the input variables shown in Table 3.11. The steady-state solutions for Module 1–5 are shown in Tables 4.6–4.10, respectively. Table 4.11 shows the steady-state solution for the primary streams. Remember that as defined in Chapter 3, the primary state variables are the most important state variables to track throughout the system. Additionally, each of the primary state variables was a uranium-bearing component molar flow rate.

Table 4.5. Comparison of Sensitivity Factors for the Primary State Variables for ±10% Changes in Selected Parameters (All Modules)

u	5			6			7			8		
y	+10%	-10%	%Diff	+10%	-10%	%Diff	+10%	-10%	%Diff	+10%	-10%	%Diff
40	-3.8	-3.5	7.7				0.37	0.34	7.1			
41				-1.6	-1.3	17.5	0.45	0.41	8.6	0.44	0.40	8.4
92				0.63	0.52	17.5	0.13	0.12	8.6	0.44	0.40	8.4

Table 4.6. Steady-State Component Molar Flow Rate (mol/h) for Module 1

Component Formula	#	Stream Number (Stream Type)					
		1A (Input)	2A (Input)	3A (Input)	1 (Intermed.)	2 (Waste)	3 (Intermed.)
H_2O	1	0	1.01×10^3	3.84×10^3	5.47×10^3	0	5.81×10^3
NO_2	4	0	0	0	0	138	0
HNO_3	9	0	672	0	120	0	122
$UO_2(NO_3)_2$	14	0	0	0	209	0	211
U_3O_8	18	70.0	0	0	1.42	0	2.02
Insoluble	20	10.4	0	0	10.4	0	10.5
Soluble	21	10.4	0	0	10.6	0	10.7

Component Formula	#	Stream Number (Stream Type)					
		4 (Intermed.)	5 (Recycle)	4A (Input)	6 (Recycle)	7 (Recycle)	8 (Waste)
H_2O	1	5.23×10^3	581	444	1.37×10^3	1.03×10^3	342
NO_2	4	0	0	0	0	0	0
HNO_3	9	118	3.65	0	5.22	4.69	0.522
$UO_2(NO_3)_2$	14	206	4.21	0	5.75	4.60	1.15
U_3O_8	18	4.05×10^{-2}	1.98	0	2.59	1.81	0.776
Insoluble	20	0.105	10.4	0	10.4	0.104	10.3
Soluble	21	10.4	0.322	0	0.480	0.475	4.80×10^{-3}

Component Formula	#	Stream Number (Stream Type)				
		9 (Recycle)	10 (Recycle)	11 (Recycle)	12 (Product)	13 (Waste)
H_2O	1	342	342	342	5.22×10^3	5.23
NO_2	4	0	0	0	0	0
HNO_3	9	1.56	1.56	1.56	118	1.18×10^{-2}
$UO_2(NO_3)_2$	14	1.53	1.53	1.53	206	2.06×10^{-2}
U_3O_8	18	0.603	0.603	0.603	4.05×10^{-2}	4.05×10^{-6}
Insoluble	20	3.47×10^{-2}	3.47×10^{-2}	3.47×10^{-2}	2.09×10^{-2}	8.38×10^{-2}
Soluble	21	0.158	0.158	0.158	10.4	1.04×10^{-3}

Table 4.7. Steady-State Component Molar Flow Rate (mol/h) for Module 2

Component Formula	#	12 (Input)	5A (Input)	6A (Input)	14 (Intermed.)	7A (Input)
		Stream Number (Stream Type)				
H_2O	1	5.22×10^3	222	0	7.78×10^3	0
HNO_3	9	0	0	12.7	131	0
TBP	11	118	0	0	0.263	263
$UO_2(NO_3)_2$	14	206	0	0	207	0
U_3O_8	18	4.05×10^{-2}	0	0	4.05×10^{-2}	0
Insoluble	20	2.09×10^{-2}	0	0	2.10×10^{-2}	0
Soluble	21	10.4	0	0	11.5	0

Component Formula	#	15 (Intermed.)	16 (Waste)	8A (Input)	17 (Intermed.)
		Stream Number (Stream Type)			
H_2O	1	7.78	7.77×10^3	2.33×10^3	2.34
HNO_3	9	0.131	131	0	6.54×10^{-4}
TBP	11	263	0.263	0	263
$UO_2(NO_3)_2$	14	206	1.03	0	205
U_3O_8	18	4.05×10^{-2}	4.05×10^{-2}	0	4.05×10^{-8}
Insoluble	20	2.10×10^{-2}	2.09×10^{-2}	0	2.10×10^{-8}
Soluble	21	1.15	10.3	0	5.75×10^{-2}

Component Formula	#	18 (Recycle)	9A (Input)	19 (Product)	20 (Waste)
		Stream Number (Stream Type)			
H_2O	1	2.34×10^3	5.27×10^3	5.28×10^3	0.528
HNO_3	9	0.130	0	6.51×10^{-4}	3.27×10^{-6}
TBP	11	0.263	0	0	263
$UO_2(NO_3)_2$	14	0.206	0	205	0.205
U_3O_8	18	4.05×10^{-5}	0	4.05×10^{-11}	4.05×10^{-8}
Insoluble	20	2.09×10^{-5}	0	0	2.10×10^{-8}
Soluble	21	1.09	0	5.72×10^{-2}	2.87×10^{-4}

Table 4.8. Steady-State Component Molar Flow Rate (mol/h) for Module 3

Component Formula	#	Stream Number (Stream Type) 19 (Input)	21 (Waste)	22 (Intermed.)	23 (Dep. Input)	24 (Dep. Input)
H_2O	1	5.28×10^3	3.17×10^3	2.11×10^3	923	0
NH_3	3	0	0	0	0	1.85×10^3
HNO_3	9	6.51×10^{-4}	3.91×10^{-4}	2.60×10^{-4}	0	0
$UO_2(NO_3)_2$	14	205	2.05×10^{-2}	205	0	0
U_3O_8	18	4.05×10^{-11}	4.05×10^{-15}	4.05×10^{-11}	0	0
soluble	21	5.72×10^{-2}	5.72×10^{-6}	5.72×10^{-2}	0	0

Component Formula	#	Stream Number (Stream Type) 25 (Dep. Input)	26 (Intermed.)	27 (Intermed.)	10A (Input)
H_2O	1	0	3.03×10^3	2.42×10^3	311
NH_3	3	0	1.85×10^3	616	0
CO_2	8	923	923	308	0
HNO_3	9	0	2.60×10^{-4}	2.60×10^{-4}	0
CH_3OH	10	0	0	0	87.4
NH_4NO_3	12	0	0	410	0
$(NH_4)_2CO_3.H_2O$	13	0	0	0	49.1
$UO_2(NO_3)_2$	14	0	205	2.05×10^{-2}	0
U_3O_8	18	0	4.05×10^{-11}	4.05×10^{-11}	0
$(NH_4)_4UO_2(CO_3)_3$	19	0	0	205	0
soluble	21	0	5.72×10^{-2}	5.72×10^{-2}	0

Component Formula	#	Stream Number (Stream Type) 28 (Waste)	29 (Intermed.)	30 (Product)	31 (Waste)
H_2O	1	0	2.73×10^3	164	2.56×10^3
NH_3	3	616	0	0	0
CO_2	8	308	0	0	0
HNO_3	9	0	2.60×10^{-4}	0	2.60×10^{-4}
CH_3OH	10	0	87.4	0	87.4
NH_4NO_3	12	0	410	0	410
$(NH_4)_2CO_3.H_2O$	13	0	49.1	0	49.1
$UO_2(NO_3)_2$	14	0	2.05×10^{-2}	0	2.05×10^{-2}
U_3O_8	18	0	4.05×10^{-11}	4.03×10^{-11}	2.02×10^{-13}
$(NH_4)_4UO_2(CO_3)_3$	19	0	205	204	1.03
soluble	21	0	5.72×10^{-2}	0	5.72×10^{-2}

Table 4.9. Steady-State Component Molar Flow Rate (mol/h) for Module 4

Component Formula	#	30 (Input)	32 (Dep. Input)	33 (Intermed.)	34 (Intermed.)	35 (Intermed.)	36 (Intermed.)
H_2O	1	164	0	0	776	0	776
N_2	2	0	0	85.1	85.1	0	85.1
NH_3	3	0	170	0	816	0	816
H_2	5	0	0	255	51.1	0	51.1
HF	6	0	0	0	0	0	0
CO_2	8	0	0	0	612	0	612
UF_4	16	0	0	0	0	0	0
UO_2	17	0	0	0	204	204	0
U_3O_8	18	4.03×10^{-11}	0	0	4.03×10^{-11}	4.03×10^{-11}	0
$(NH_4)_4UO_2(CO_3)_3$	19	204	0	0	2.04×10^{-2}	2.04×10^{-2}	0

Component Formula	#	11A (Input)	37 (Intermed.)	38 (Waste)	39 (Intermed.)	12A (Input)
H_2O	1	0	0	776	0	0
N_2	2	500	500	585	0	1.50×10^3
NH_3	3	0	0	816	0	0
H_2	5	0	0	51.1	0	0
HF	6	0	0	0	0	0
CO_2	8	0	0	612	0	0
UF_4	16	0	0	0	0	0
UO_2	17	0	0	0	204	0
U_3O_8	18	0	0	0	4.03×10^{-11}	0
$(NH_4)_4UO_2(CO_3)_3$	19	0	0	0	2.04×10^{-2}	0

Component Formula	#	40 (Dep. Input)	41 (Intermed.)	42 (Intermed.)	43 (Waste)	44 (Product)
H_2O	1	0	0	388	388	0
N_2	2	0	1.50×10^3	1.50×10^3	1.50×10^3	0
NH_3	3	0	0	0	0	0
H_2	5	0	0	0	0	0
HF	6	776	776	7.76×10^{-2}	7.76×10^{-2}	0
CO_2	8	0	0	0	0	0
UF_4	16	0	0	194	1.94×10^{-3}	194
UO_2	17	0	0	10.2	1.02×10^{-2}	10.2
U_3O_8	18	0	0	4.03×10^{-11}	4.03×10^{-14}	4.02×10^{-11}
$(NH_4)_4UO_2(CO_3)_3$	19	0	0	2.04×10^{-2}	2.04×10^{-2}	0

Table 4.10. Steady-State Component Molar Flow Rate (mol/h) for Module 5

Component Formula	#	Stream Number (Stream Type)					
		44 (Input)	45 (Intermed.)	46 (Intermed.)	13A (Input)	47 (Dep. Input)	48 (Intermed.)
N_2	2	0	0	0	500	0	500
F_2	7	0	0	0	0	213	213
UF_6	15	0	0	0	0	0	0
UF_4	16	194	19.4	174	0	0	174
UO_2	17	10.2	1.02	9.19	0	0	9.19
U_3O_8	18	4.02×10^{-11}	4.02×10^{-12}	3.62×10^{-11}	0	0	3.62×10^{-11}

Component Formula	#	Stream Number (Stream Type)					
		49 (Intermed.)	50 (Waste)	51 (Intermed.)	52 (Intermed.)	53 (Intermed.)	54 (Intermed.)
N_2	2	500	0	500	0	500	500
F_2	7	39.0	0	39.0	0	39.0	39.0
UF_6	15	174	0	174	173	1.74	1.74
UF_4	16	0.174	0.173	1.74×10^{-3}	0	1.74×10^{-3}	19.4
UO_2	17	9.19	9.19	0	0	0	1.02
U_3O_8	18	3.62×10^{-11}	3.62×10^{-11}	0	0	0	4.02×10^{-12}

Component Formula	#	Stream Number (Stream Type)					
		55 (Intermed.)	56 (Waste)	57 (Intermed.)	58 (Waste)	59 (Intermed.)	60 (Product)
N_2	2	500	500	0	0	0	0
F_2	7	19.6	19.6	0	0	0	0
UF_6	15	21.1	0	21.1	0	21.1	194
UF_4	16	1.94×10^{-2}	0	1.94×10^{-2}	1.94×10^{-2}	0	0
UO_2	17	1.02	0	1.02	1.02	0	0
U_3O_8	18	4.02×10^{-12}	0	4.02×10^{-12}	4.02×10^{-12}	0	0

Table 4.11. Primary State Variables Steady-State Solution

State Variable	Stream	Component Formula	Component Number	Type of Stream	Molar Flow Rate (mol/h)
Module 1					
Xss(274)	1A	U_3O_8	18	Input	70.0
Xss(3)	1	UN	14	Intermediate	209
Xss(10)	3	UN	14	Intermediate	211
Xss(16)	4	UN	14	Intermediate	206
Xss(40)	8	UN	14	Waste	1.15
Xss(41)	8	U_3O_8	18	Waste	0.776
Xss(64)	12	UN	14	Product	206
Xss(70)	13	UN	14	Waste	2.06×10^{-2}
Module 2					
Xss(77)	14	UN	14	Intermediate	207
Xss(84)	15	UN	14	Intermediate	206
Xss(91)	16	UN	14	Waste	1.03
Xss(92)	16	U_3O_8	18	Waste	4.05×10^{-2}
Xss(98)	17	UN	14	Intermediate	205
Xss(111)	19	UN	14	Product	205
Xss(117)	20	UN	14	Waste	0.205
Module 3					
Xss(123)	21	UN	14	Waste	2.05×10^{-2}
Xss(128)	22	UN	14	Intermediate	205
Xss(138)	26	UN	14	Intermediate	205
Xss(148)	27	AUC	19	Intermediate	205
Xss(159)	29	AUC	19	Intermediate	205
Xss(163)	30	AUC	19	Product	204
Xss(169)	31	UN	14	Waste	2.05×10^{-2}
Xss(171)	31	AUC	19	Waste	1.03
Module 4					
Xss(181)	34	UO_2	17	Intermediate	204
Xss(184)	35	UO_2	17	Intermediate	204
Xss(198)	39	UO_2	17	Intermediate	204
Xss(207)	42	UF_4	16	Intermediate	194
Xss(208)	42	UO_2	17	Intermediate	10.2
Xss(214)	43	UF_4	16	Waste	1.94×10^{-3}
Xss(215)	43	UO_2	17	Waste	1.02×10^{-2}
Xss(217)	43	AUC	19	Waste	2.04×10^{-2}
Xss(218)	44	UF_4	16	Product	194
Xss(219)	44	UO_2	17	Product	10.2

Table 4.11. Primary State Variables Steady-State Solution (Con't.)

State Variable	Stream	Component Formula	Number	Type of Stream	Molar Flow Rate (mol/h)
			Module 5		
Xss(221)	45	UF_4	16	Intermediate	19.4
Xss(222)	45	UO_2	17	Intermediate	1.02
Xss(224)	46	UF_4	16	Intermediate	174
Xss(225)	46	UO_2	17	Intermediate	9.19
Xss(230)	48	UF_4	16	Intermediate	174
Xss(235)	49	UF_6	15	Intermediate	174
Xss(239)	**50**	**UF_4**	**16**	**Waste**	**0.173**
Xss(240)	**50**	**UO_2**	**17**	**Waste**	**9.19**
Xss(244)	51	UF_6	15	Intermediate	174
Xss(246)	52	UF_6	15	Intermediate	173
Xss(249)	53	UF_6	15	Intermediate	1.74
Xss(253)	54	UF_6	15	Intermediate	1.74
Xss(254)	54	UF_4	16	Intermediate	19.4
Xss(259)	55	UF_6	15	Intermediate	21.1
Xss(265)	57	UF_6	15	Intermediate	21.1
Xss(269)	**58**	**UF_4**	**16**	**Waste**	**1.94×10^{-2}**
Xss(270)	**58**	**UO_2**	**17**	**Waste**	**1.02**
Xss(272)	59	UF_6	15	Intermediate	21.1
Xss(273)	**60**	**UF_6**	**15**	**Product**	**194**

The MATLAB® 'fsolve' function provides the steady-state solution to the set of simultaneous algebraic equations that represent the mass balance in the NUCP. Additionally, the steady-state solution was checked by substituting the values of the steady-state solution back into the set of simultaneous equations and determining the result. As expected, the equations all resulted in '0' for the rate of change values using both 'fsolve' and for substitution to check the 'fsolve' solution. The rate of change of the overall material balances served as an internal check that the calculations were correct. Table 4.12 lists the rate of change of the overall material balances for each Module. As expected, each was approximately zero.

There were 273 state variables and seven input variables. In order to generate the base case data, the input variables were varied within the range given in Table 3.11. To generate a reasonable amount of data, each input variable was used at five evenly spaced intervals over the range provided in Table 3.11 including the initial value. Such that for an input variable that was varied over a range of ±10%, the input variable was used at the initial value and 90%, 95%, 105%, and 110% of that value. This resulted in a base case data matrix of 78,125×280, where the 280 included the 273 state variables and the seven input variables. The variable index numbers for the input variables were 274–280 (see Table 3.11).

Continuing to follow the overall approach for the development of the detection framework laid out in Figure 3.1, Gaussian white noise was added to the base case data set. A matrix of normally distributed random numbers with mean of zero and standard deviation of one was generated. The random numbers of each column was scaled by the nominal steady-state values of the respective variable times the percent of noise desired. In this case, 1% noise was added. One percent is small but not unreasonably so with current advances in electronic equipment. Additionally, the primary state variables that represented the uranium-bearing component(s) of the product stream in each module and the input variables were scaled to give a heavier standard deviation, using the values shown in Table 4.13. Weighted scaling was accomplished by dividing the standard deviation of the appropriate state variable by the desired scaling factor. This resulted in a new standard deviation, which was equal to the scaling factor, for the mean-centered and weighted-scale state variables since the mean-centered columns were divided by the new scaled standard deviation. Since there are just a few product variables and seven input variables out of the 280 total state variables, the variations in these few variables would be overwhelmed by the variations in the more than two hundred intermediate state variables. Therefore, the product and input variables were weighted more heavily during the normalization stage. This weighted scaling was done because all of the intermediate and waste streams contain uranium and it was important to ensure that the product streams were not masked by the other streams. The final scaling factors were chosen after some trial and error testing to see what scaling factor would bring forth these state variables to be heavily contributing components in the first principal component.

Table 4.12. Rate of Change of the Overall Material Balances

Module	Solution
1	1×10^{-11}
2	1×10^{-10}
3	1×10^{-12}
4	1×10^{-12}
5	1×10^{-13}

Table 4.13. Scaling Factors for Selected State Variables in the Base Case

Variable Number	Scaling Factor	Type of Variable
Xss(64)	**5**	
Xss(111)	**5**	
Xss(163)	**5**	Primary State Variables/
Xss(218)	**5**	Product Streams
Xss(219)	**5**	
Xss(273)	**5**	
Xss(274)	5	
Xss(275)	1.1	
Xss(276)	2	
Xss(277)	2	Input Variable
Xss(278)	2	
Xss(279)	5	
Xss(280)	1	

In order to ensure that there was not too much noise added to the data, it was necessary to determine the effective rank of the base case data. The effective rank was determined by performing SVD on the data prior to the addition of noise. The Scree plot for the base case data without added noise is shown in Figure 4.1.

As shown in Figure 4.1, there is a strong elbow at two which retains 90.2% percent of the original information. However, keeping only two principal components does not fully model the system. There is another elbow at three which retains 94% of the original information. Four principal components were needed to retain at least 95% of the original data. Therefore, the effective rank without noise was determined to be four. The first ten singular values (S) from SVD of the base case data with and without noise and the cumulative sum ($S_i^2 / \sum_{j=1} S_j^2$) are listed in Table 4.14.

During the data processing, it became expedient to remove some of the variables from the data matrix. The variables that were removed are listed in Table 4.15. These variables turned out to be completely extraneous and did not add any useful information to the model. Additionally, these variables did not vary at all with the changes in the input variables, resulting in a standard deviation of zero. All of these state variables represented components that did not participate in any reactions in the process. A total of twenty-five state variables were removed from the base case.

The Scree plot for the base case data with noise is shown in Figure 4.2. As seen, there is a strong elbow at two which retains 87.4% percent of the original information. However, keeping only two principal components does not appear to fully model the system. As shown in the top plot of Figure 4.2, there is another elbow at three which retains 91.1% of the original information. Six principal components were needed to retain at least 95% of the original data. Based on this analysis, the effective rank after the addition of noise was determined to be five where 94.4% of the original data was retained. Further analysis of the loadings vectors, it was determined that five principal components would be retained for the model. Retaining too many principal components results in noise being retained as part of the base case model. A bar chart of the loadings vectors for all the variables of the base case model is shown in Figure 4.3.
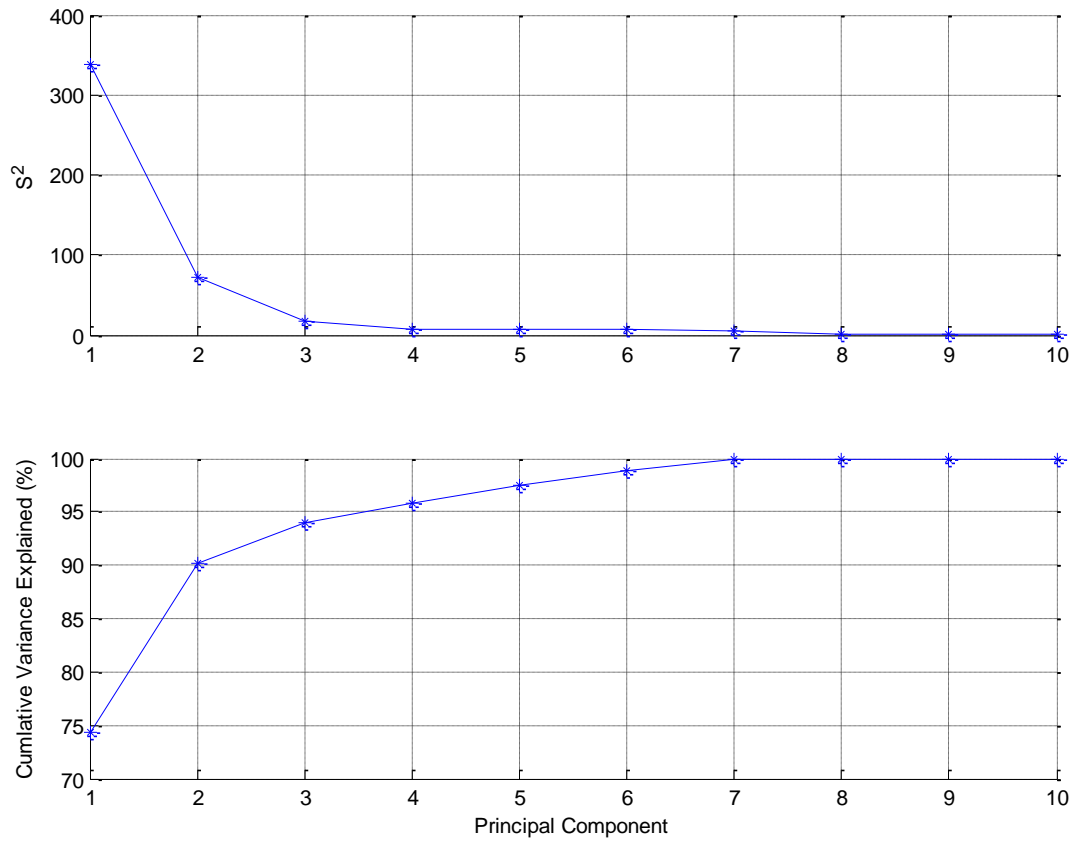
Figure 4.1. Scree Plot of the Base Case Data before the Addition of Gaussian White Noise.

Table 4.14. First Ten Singular Values for the Base Case

Index	Without Noise		With Noise	
	Singular Value	Cumulative Sum	Singular Value	Cumulative Sum
1	18.4070	74.2676	18.0998	71.8095
2	8.5192	90.1764	8.4354	87.4068
3	4.1977	94.0388	4.0830	91.0611
4	2.8477	95.8164	2.8002	92.7798
5	2.7068	97.4223	2.6896	94.3655
6	2.5482	98.8457	2.4719	95.7048
7	2.2583	99.9636	2.2094	96.7748
8	0.3127	99.9851	1.1535	97.0664
9	0.1584	99.9906	1.0005	97.2858
10	0.1298	99.9943	0.9995	97.5048

Table 4.15. State Variables (25 Total) Removed from the Base Case Model

State Variable	Stream	Chemical Component	Component Number	Reason for Removal
Module 2				
Xss(76)	14	TBP	11	
Xss(83)	15	TBP	11	
Xss(90)	16	TBP	11	TBP acts as a diluent and does not participate in
Xss(97)	17	TBP	11	any of the reactions
Xss(104)	18	TBP	11	
Xss(116)	20	TBP	11	
Xss(109)	19	H_2O	1	Water acts as a wash solution in this case and
Xss(114)	20	H_2O	1	does not participate in any of the reactions
Module 3				
Xss(121)	21	H_2O	1	Water acts as a wash solution in this case and
Xss(126)	22	H_2O	1	does not participate in any of the reactions
Xss(154)	29	CH_3OH	10	
Xss(166)	31	CH_3OH	10	Both methanol and ammonium carbonate are a
Xss(156)	29	$(NH_4)_2CO_3.H_2O$	13	wash solution and do not participate in any of the reactions
Xss(168)	31	$(NH_4)_2CO_3.H_2O$	13	
Module 4				
Xss(192)	37	N_2	2	
Xss(202)	41	N_2	2	Nitrogen is a carrier gas and does not participate
Xss(205)	42	N_2	2	in any of the reactions
Xss(212)	43	N_2	2	
Module 5				
Xss(228)	48	N_2	2	
Xss(233)	49	N_2	2	
Xss(242)	51	N_2	2	
Xss(247)	53	N_2	2	Nitrogen is a carrier gas and does not participate in any of the reactions
Xss(251)	54	N_2	2	
Xss(257)	55	N_2	2	
Xss(263)	56	N_2	2	
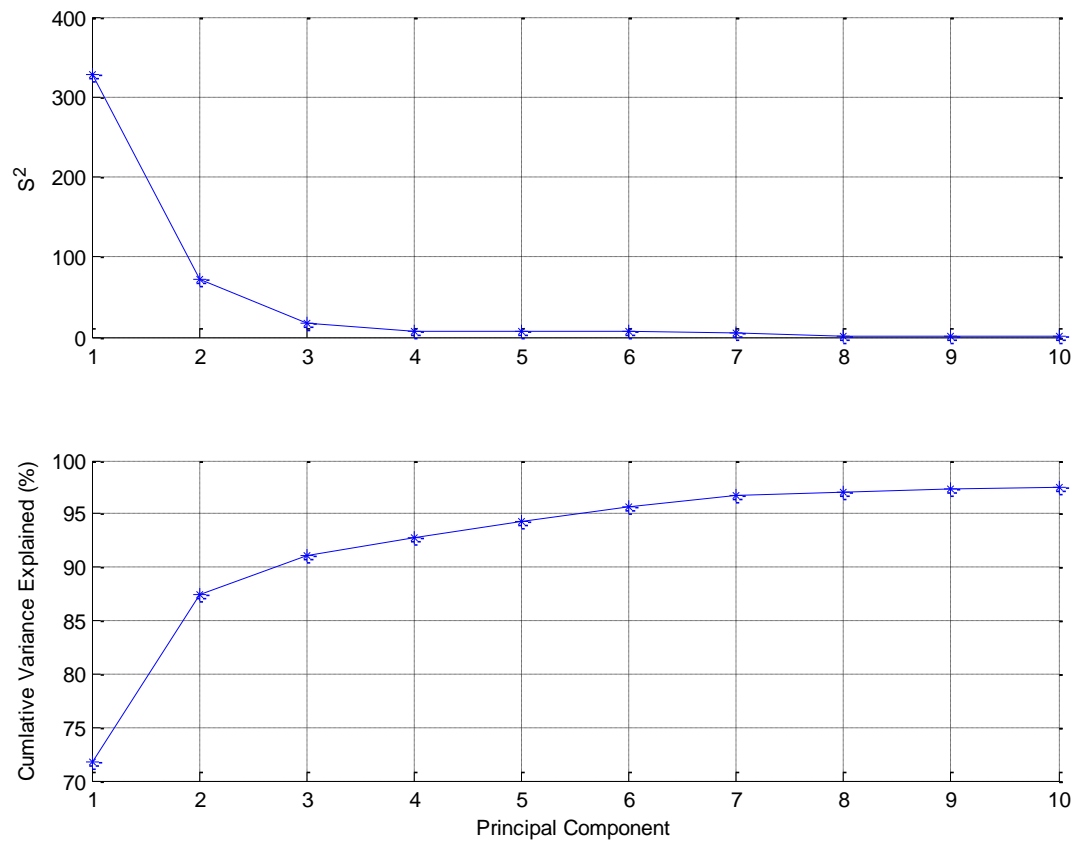
Figure 4.2. Scree Plot of the Base Case Data after the Addition of Gaussian White Noise.
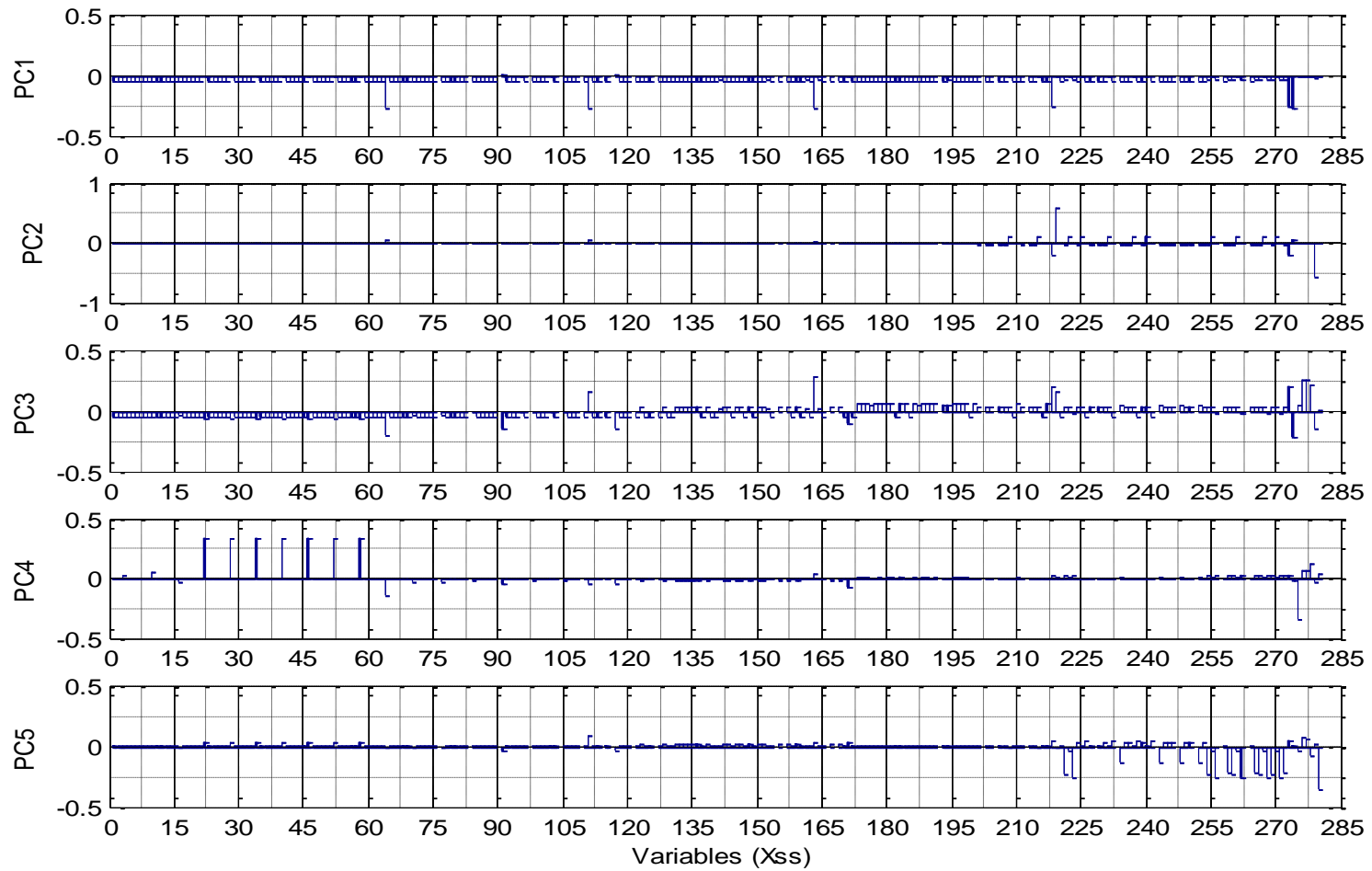
Figure 4.3. Base Case Loadings Vectors for All State Variables.

The variable index was preserved when the state variables listed in Table 4.15 were removed. A plot of each principal component loadings vector is separately shown below. Figure 4.4 shows the bar chart of the first principal component loadings vector for all the state variables of the base case model. The heaviest contributors to PC1 are shown in Figure 4.4 in red, and the heaviest contributors correspond to the main input and product variables out of the modules, the ones that have been scaled differentially with a heavier normalization factor. Table 4.16 provides a summary of how the primary state variables contributed to the first principal component.

Heavy contributors to PC1 are the input uranium feed flow rate [Xss(274)] to Module 1 and the output uranium-bearing product flow rates from each of the five modules [Xss(64), Xss(111), Xss(163), Xss(218), and Xss(273)], thus showing the effect of the uranium feed flow rate on the molar flow rates of uranium out of each of the five modules. (Please refer to Figure 3.2 for a flowsheet of the process). This correlation pattern is highly anticipated, since the molar flow rates of the uranium-bearing output streams should all be highly correlated to the main feed flow rate. This correlation pattern only became apparent after these state variable data column values were differentially weighted (as shown in Table 4.13) to exert their influence on the subsequent singular value decomposition. The internal state variables of all the modules representing the intermediate uranium-bearing flow rates contributed moderately to PC1, also as expected since these are all correlated to the product flow rates out of the modules. Since they are not differentially weighted, their contributions to PC1 are nominally lower than those representing the primary uranium-bearing product flow rates.

Figure 4.5 shows the bar chart of the second principal component loadings vector for all the state variables of the base case model. The heaviest contributors to PC2 are shown in Figure 4.5 in red, displaying the effect of α_{Mod4D} [Xss(279)] on the UO_2 flow rate out of Module 4. Table 4.17 provides a summary of how the primary state variables contributed to the second principal component.

Figure 4.5 shows that PC2 mainly captures the variation of two state variables; that of the UO_2 product flow rate [Xss(219)] from Module 4, correlated with the input variable α_{Mod4D} [Xss(279)]. The input variable α_{Mod4D} is a flow parameter that insures sufficient HF is fed to the hydrofluorination reaction for the conversion of UO_2 to UF_4. The UO_2 product flow rate [Xss(219)] from Module 4 is negatively correlated with the input variable α_{Mod4D} [Xss(279)] because increasing that input variable causes more HF to be available for reaction which results in more UO_2 being converted to UF_4 therefore reducing the UO_2 in the Module 4 output.
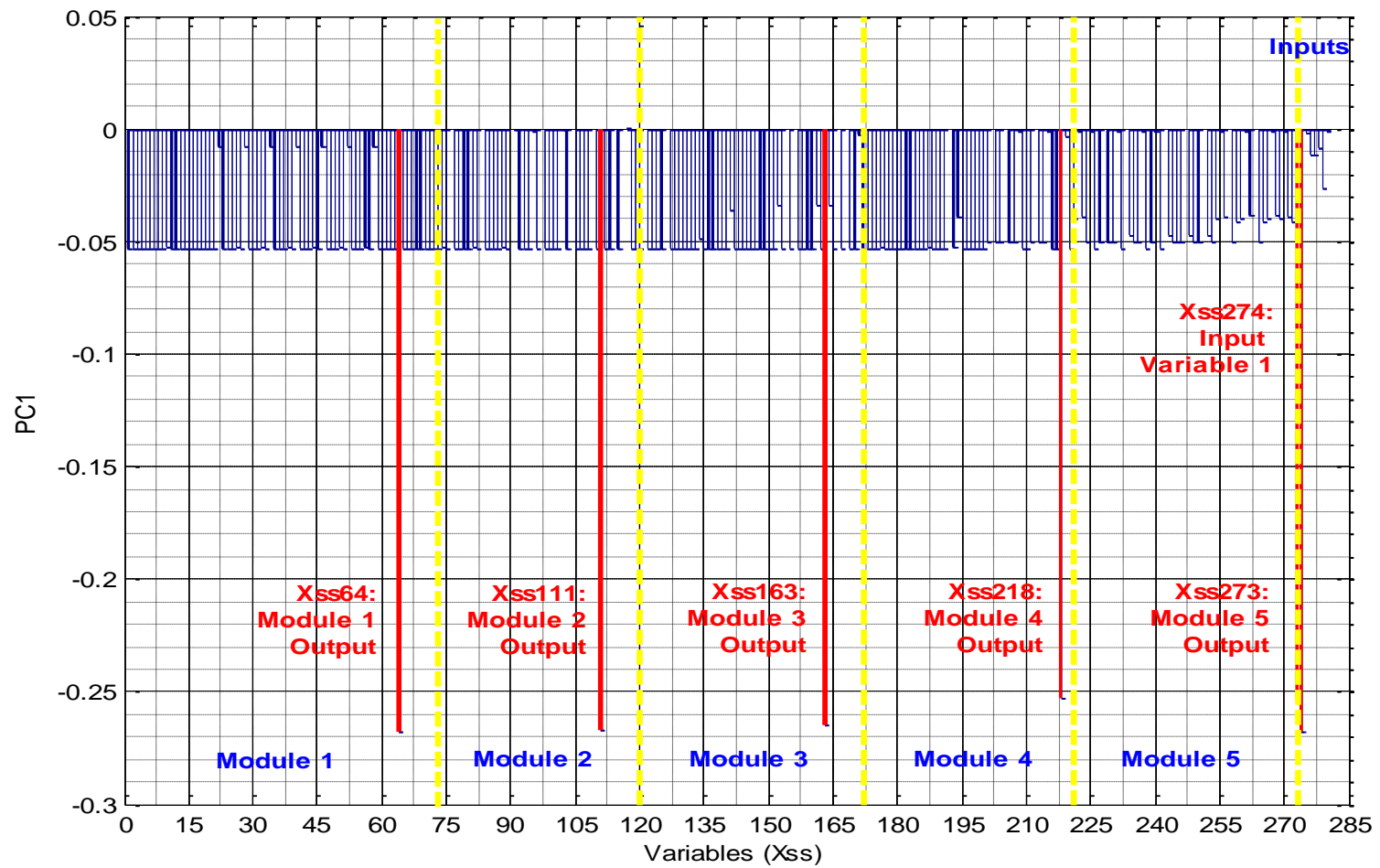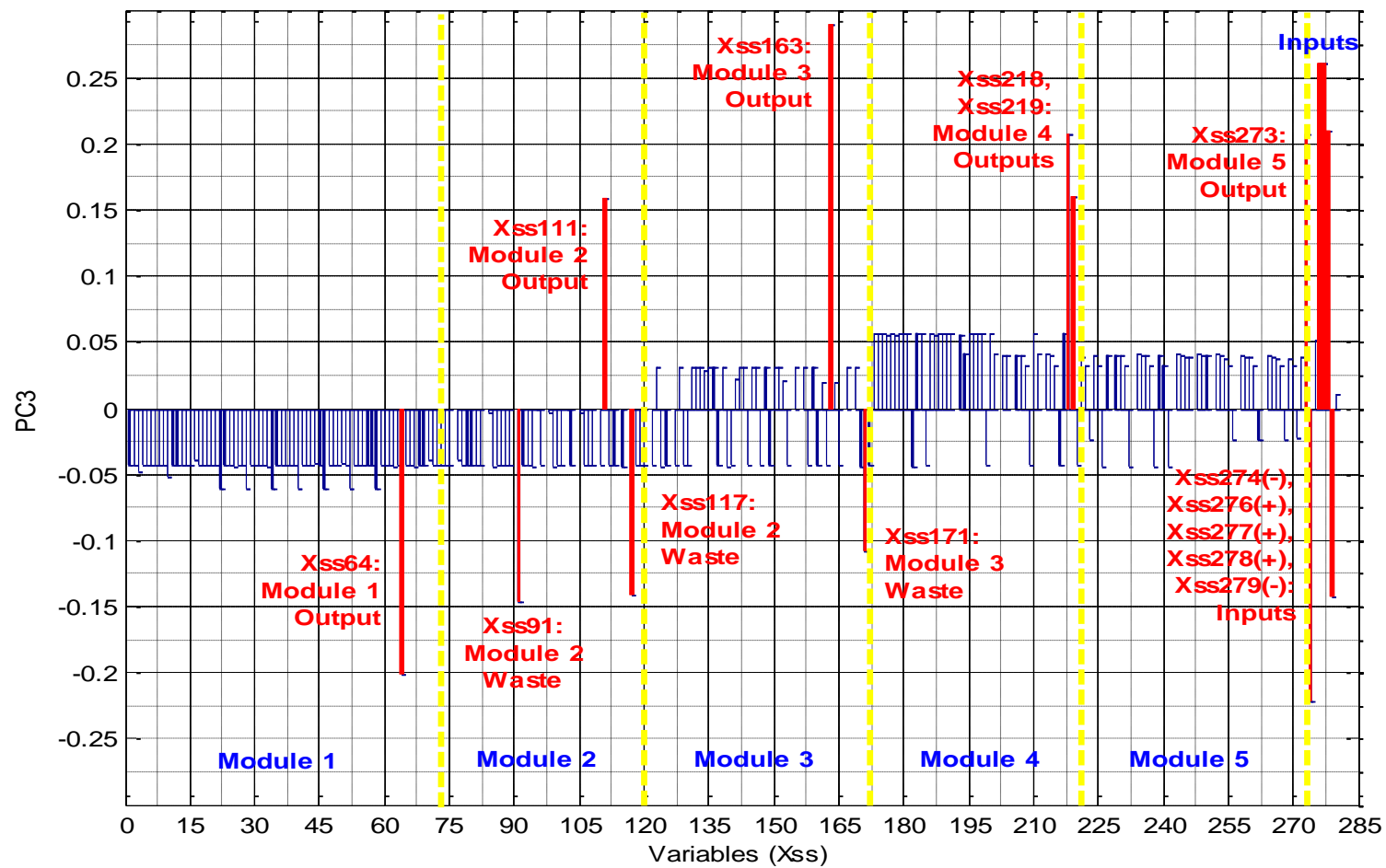
Figure 4.4. Base Case Principal Component 1 Loadings Vector.

Table 4.16. Primary State Variable Contributions to the First Principal Component

Contribution							
Heavy				**Moderate**			
Xss	**Module**	**Stream**	**Chemical**	**Xss**	**Module**	**Stream**	**Chemical**
64	1	12	UN	3	1	1	UN
111	2	19	UN	10	1	3	UN
163	3	30	AUC	16	1	4	UN
218	4	44	UF_4	41	1	8	U_3O_8
273	5	60	UF_6	70	1	13	UN
274	Input 1	1A	U	77	2	14	UN
Slight				84	2	15	UN
Xss	**Module**	**Stream**	**Chemical**	92	2	16	U_3O_8
221	5	45	UF_4	98	2	17	UN
254	5	54	UF_4	123	3	21	UN
259	5	55	UF_6	128	3	22	UN
265	5	57	UF_6	138	3	26	UN
269	5	58	UF_4	148	3	27	AUC
272	5	59	UF_6	159	3	29	AUC
None				169	3	31	UN
Xss	**Module**	**Stream**	**Chemical**	181	4	34	UO_2
40	1	8	UN	184	4	35	UO_2
91	2	16	UN	198	4	39	UO_2
117	2	20	UN	207	4	42	UF_4
171	3	31	AUC	214	4	43	UF_4
208	4	42	UO_2	217	4	43	AUC
215	4	43	UO_2	224	5	46	UF_4
219	4	44	UO_2	230	5	48	UF_4
222	5	45	UO_2	235	5	49	UF_6
225	5	46	UO_2	239	5	50	UF_4
240	5	50	UO_2	244	5	51	UF_6
270	5	58	UO_2	246	5	52	UF_6
275	Input 2	4 & 5	UN	249	5	53	UF_6
276	Input 3	15 & 16	UN	253	5	54	UF_6
277	Input 4	19 & 20	UN				
278	Input 5	30 & 31	AUC				
279	Input 6	40	HF				
280	Input 7	45	UF_4				
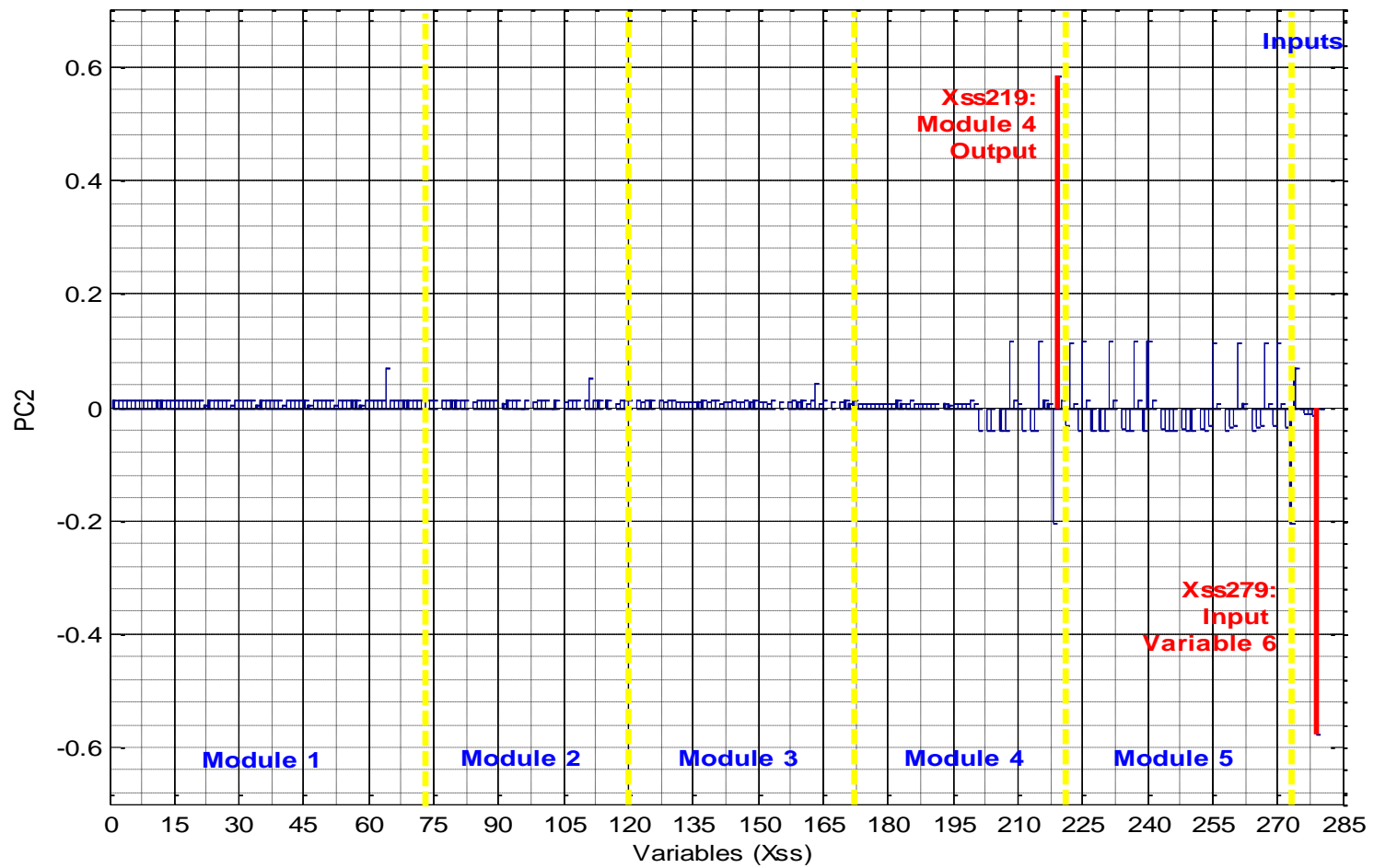
Figure 4.5. Base Case Principal Component 2 Loadings Vector.

Table 4.17. Primary State Variable Contributions to the Second Principal Component

Xss	Module	Stream	Chemical	Xss	Module	Stream	Chemical
Heavy				**None**			
219	4	44	UO_2	3	1	1	UN
279	Input 6	40	HF	10	1	3	UN
Moderate				16	1	4	UN
64	1	12	UN	40	1	8	UN
208	4	42	UO_2	41	1	8	U_3O_8
215	4	43	UO_2	70	1	13	UN
218	4	44	UF_4	77	2	14	UN
222	5	45	UO_2	84	2	15	UN
225	5	46	UO_2	91	2	16	UN
240	5	50	UO_2	92	2	16	U_3O_8
270	5	58	UO_2	98	2	17	UN
273	5	60	UF_6	117	2	20	UN
274	Input 1	1A	U	123	3	21	UN
Slight				128	3	22	UN
111	2	19	UN	138	3	26	UN
163	3	30	AUC	148	3	27	AUC
207	4	42	UF_4	159	3	29	AUC
214	4	43	UF_4	169	3	31	UN
221	5	45	UF_4	171	3	31	AUC
224	5	46	UF_4	181	4	34	UO_2
230	5	48	UF_4	184	4	35	UO_2
235	5	49	UF_6	198	4	39	UO_2
239	5	50	UF_4	217	4	43	AUC
244	5	51	UF_6	275	Input 2	4 & 5	UN
246	5	52	UF_6	276	Input 3	15 & 16	UN
249	5	53	UF_6	277	Input 4	19 & 20	UN
253	5	54	UF_6	278	Input 5	30 & 31	AUC
254	5	54	UF_4	280	Input 7	45	UF_4
259	5	55	UF_6				
265	5	57	UF_6				
269	5	58	UF_4				
272	5	59	UF_6				

Figure 4.6 shows the bar chart of the third principal component loadings vector for all the state variables of the base case model. The heaviest contributors to PC3 are shown in Figure 4.6 in red. Table 4.18 provides a summary of how the primary state variables contributed to the third principal component.

Figure 4.6 shows that PC3 captures the relationships between five of the seven input variables to all of the uranium-bearing product flow rates from the five modules and uranium-bearing waste streams from Modules 2 and 3.

The uranyl nitrate flow rate [Xss(91)] in the waste stream from Module 2B was negatively correlated with the input variable $K_{Mod2B,14}$ [Xss(276)] as expected since input variable $K_{Mod2B,14}$ controls how much of the uranyl nitrate in Stream 14 goes to Stream 15. Therefore, if $K_{Mod2B,14}$ increases then the uranyl nitrate in Stream 15 increases and the uranyl nitrate in Stream 16 [Xss(91)] must decrease. The uranyl nitrate output flow rate [Xss(111)] is positively correlated with the input variable $K_{Mod2B,14}$ [Xss(276)] as expected for the same reason as above. Additionally, Xss(111) is negatively correlated with Xss(91) because more uranyl nitrate in the product results in less uranyl nitrate in the waste.

The uranyl nitrate flow rate [Xss(117)] in the waste stream from Module 2D was negatively correlated with the input variable $K_{Mod2D,14}$ [Xss(277)] as expected since input variable $K_{Mod2D,14}$ controls how much of the uranyl nitrate in Stream 17 goes to Stream 19. Therefore, if $K_{Mod2D,14}$ increases then the uranyl nitrate in Stream 19 increases and the uranyl nitrate in Stream 20 [Xss(117)] must decrease. The uranyl nitrate output flow rate [Xss(111)] is positively correlated with the input variable $K_{Mod2D,14}$ [Xss(277)] as expected for the same reason as above. Additionally, Xss(111) is negatively correlated with Xss(117) because more uranyl nitrate in the product results in less uranyl nitrate in the waste.

The AUC flow rate [Xss(171)] in the waste stream from Module 3D was negatively correlated with the input variable $K_{Mod3D,19}$ [Xss(278)] as expected since input variable $K_{Mod3D,19}$ controls how much of the AUC in Stream 29 goes to Stream 30. Therefore, if $K_{Mod3D,19}$ increases then the AUC in Stream 30 increases and the AUC in Stream 31 [Xss(171)] must decrease. The AUC output flow rate [Xss(163)] is positively correlated with the input variable $K_{Mod3D,19}$ [Xss(278)] as expected for the same reason as above. Additionally, Xss(163) is negatively correlated with Xss(171) because more AUC in the product results in less AUC in the waste.

Figure 4.6. Base Case Principal Component 3 Loadings Vector.

146

Table 4.18. Primary State Variable Contributions to the Third Principal Component

Contribution

Heavy

Xss	Module	Stream	Chemical
64	1	12	UN
91	2	16	UN
111	2	19	UN
117	2	20	UN
163	3	30	AUC
171	3	31	AUC
218	4	44	UF_4
219	4	44	UO_2
273	5	60	UF_6
274	Input 1	1A	U
276	Input 3	15 & 16	UN
277	Input 4	19 & 20	UN
278	Input 5	30 & 31	AUC
279	Input 6	40	HF

Moderate

Xss	Module	Stream	Chemical
3	1	1	UN
10	1	3	UN
40	1	8	UN
181	4	34	UO_2
184	4	35	UO_2
198	4	39	UO_2
217	4	43	AUC
275	Input 2	4 & 5	UN

None

Xss	Module	Stream	Chemical
84	2	15	UN
98	2	17	UN
280	Input 7	45	UF_4

Slight

Xss	Module	Stream	Chemical
16	1	4	UN
41	1	8	U_3O_8
70	1	13	UN
77	2	14	UN
92	2	16	U_3O_8
123	3	21	UN
128	3	22	UN
138	3	26	UN
148	3	27	AUC
159	3	29	AUC
169	3	31	UN
207	4	42	UF_4
208	4	42	UO_2
214	4	43	UF_4
215	4	43	UO_2
221	5	45	UF_4
222	5	45	UO_2
224	5	46	UF_4
225	5	46	UO_2
230	5	48	UF_4
235	5	49	UF_6
239	5	50	UF_4
240	5	50	UO_2
244	5	51	UF_6
246	5	52	UF_6
249	5	53	UF_6
253	5	54	UF_6
254	5	54	UF_4
259	5	55	UF_6
265	5	57	UF_6
269	5	58	UF_4
270	5	58	UO_2
272	5	59	UF_6

Since the contributions made by PC4 and PC5 were so small, the detailed correlation patterns cannot realistically be interpreted meaningfully. Therefore, those figures are not included here. Table 4.19 summarizes how the primary state variables loaded each of the principal components including PC4 and PC5. The state variables that represent the uranium component in the product stream from each module are highlighted in red.

According to Table 4.19, PC4 captured variation in input variable $K_{Mod1B,14}$ and the uranyl nitrate flow rate [Xss(40)] in the waste from Stream 8 in Module 1. These were negatively correlated which was expected since $K_{Mod1B,14}$ controls how much of the uranyl nitrate in Stream 3 goes to Stream 4. An increase in $K_{Mod1B,14}$ would increase the uranyl nitrate in Stream 4 and reduce the uranyl nitrate in Stream 5 thereby reducing the uranyl nitrate in Stream 8.

Also according to Table 4.19, PC5 captured variation in input variable S_{Mod5A} and several of the molar flow rate of the uranium-bearing streams in Module 5, most of which were in the secondary fluorination section of Module 5. All of these variables were positively correlated. This correlation pattern was expected since S_{Mod5A} controls how much of the feed stream to Module 5 is split to the secondary process. An increase in S_{Mod5A} would result in increases in molar flow rate of the uranium-bearing streams in this section of Module 5.

Table 4.20 lists the first five loadings vectors for the input variables. This shows that the first input variable was the heaviest contributor to the first principal component while the other input variables did not contribute at all. For the second principal component, only the sixth input variable contributed heavily. Input variables 1, 3–6 contributed heavily to the third principal component. Additionally in PC3, input variables 2–5 and 7 are positively correlated to one another and negatively correlated to input variables 1 and 6. For the fourth principal component, input variable 2 contributed heavily. Input variable 7 contributed heavily to the fifth principal component. Table 4.20 also shows that it is necessary to retain the first five principal components in order to capture variation in all of the input variables.

Table 4.19. Summary of How the Primary State Variables within Each Module Load Each Principal Component

State Variable	PC1	PC2	PC3	PC4	PC5	Type of Stream
Module 1						
Xss(274)	Heavy	Moderate	Heavy	None	None	Input
Xss(275)	None	None	Moderate	Heavy	Slight	Input
Xss(3)	Moderate	None	Moderate	Slight	None	Intermediate
Xss(10)	Moderate	None	Moderate	Moderate	None	Intermediate
Xss(16)	Moderate	None	None	Slight	None	Intermediate
Xss(40)	None	None	Moderate	Heavy	None	Waste
Xss(41)	Moderate	None	None	None	Slight	Waste
Xss(64)	Heavy	Moderate	Heavy	Moderate	None	Product
Xss(70)	Moderate	None	None	Slight	None	Waste
Module 2						
Xss(276)	None	None	Heavy	Moderate	Slight	Input
Xss(277)	None	None	Heavy	Moderate	Slight	Input
Xss(77)	Moderate	None	None	Slight	None	Intermediate
Xss(84)	Moderate	None	None	Slight	None	Intermediate
Xss(91)	None	None	Heavy	Slight	Slight	Waste
Xss(92)	Moderate	None	None	None	None	Waste
Xss(98)	Moderate	None	None	Slight	None	Intermediate
Xss(111)	Heavy	Slight	Heavy	Slight	Slight	Product
Xss(117)	None	None	Heavy	Slight	Slight	Waste
Module 3						
Xss(278)	None	None	Heavy	Moderate	Slight	Input
Xss(123)	Moderate	None	None	None	None	Waste
Xss(128)	Moderate	None	None	None	None	Intermediate
Xss(138)	Moderate	None	None	None	None	Intermediate
Xss(148)	Moderate	None	None	None	None	Intermediate
Xss(159)	Moderate	None	None	None	None	Intermediate
Xss(163)	Heavy	Slight	Heavy	Slight	Slight	Product
Xss(169)	Moderate	None	None	None	None	Waste
Xss(171)	None	None	Heavy	Moderate	Slight	Waste
Module 4						
Xss(279)	None	Heavy	Heavy	Slight	Slight	Input
Xss(181)	Moderate	None	Moderate	None	None	Intermediate
Xss(184)	Moderate	None	Moderate	None	None	Intermediate
Xss(198)	Moderate	None	Moderate	None	None	Intermediate
Xss(207)	Moderate	Slight	None	None	None	Intermediate
Xss(208)	None	Moderate	None	None	None	Intermediate
Xss(214)	Moderate	Slight	None	None	None	Waste
Xss(215)	None	Moderate	None	None	None	Waste
Xss(217)	Moderate	None	Moderate	None	None	Waste
Xss(218)	Heavy	Moderate	Heavy	Slight	Slight	Product
Xss(219)	None	Heavy	Heavy	Slight	None	Product

Table 4.19. Summary of How the Primary State Variables within Each Module Load Each Principal Component (continued)

State Variable	PC1	PC2	PC3	PC4	PC5	Type of Stream
			Module 5			
Xss(280)	None	None	None	Slight	Heavy	Input
Xss(221)	Slight	Slight	None	Slight	Heavy	Intermediate
Xss(222)	None	Moderate	None	None	Slight	Intermediate
Xss(224)	Moderate	Slight	None	None	Slight	Intermediate
Xss(225)	None	Moderate	None	None	None	Intermediate
Xss(230)	Moderate	Slight	None	None	Slight	Intermediate
Xss(235)	Moderate	Slight	None	None	Slight	Intermediate
Xss(239)	Moderate	Slight	None	None	Slight	Waste
Xss(240)	None	Moderate	None	None	None	Waste
Xss(244)	Moderate	Slight	None	None	Slight	Intermediate
Xss(246)	Moderate	Slight	None	None	Slight	Intermediate
Xss(249)	Moderate	Slight	None	None	Slight	Intermediate
Xss(253)	Moderate	Slight	None	None	Slight	Intermediate
Xss(254)	Slight	Slight	None	Slight	Heavy	Intermediate
Xss(259)	Slight	Slight	None	Slight	Heavy	Intermediate
Xss(265)	Slight	Slight	None	Slight	Heavy	Intermediate
Xss(269)	Slight	Slight	None	Slight	Heavy	Waste
Xss(270)	None	Moderate	None	None	Slight	Waste
Xss(272)	Slight	Slight	None	Slight	Heavy	Intermediate
Xss(273)	Heavy	Moderate	Heavy	Slight	Slight	Product

Table 4.20. The First Five Loadings Vectors for the Input Variables

State Variable	Input Variables	Loadings Vectors				
		V_1	V_2	V_3	V_4	V_5
Xss(274)	u_1	-0.2674	0.0698	-0.2220	-0.0088	0.0123
Xss(275)	u_2	-0.0019	-0.0011	0.0521	-0.3414	-0.0408
Xss(276)	u_3	-0.0111	-0.0094	0.2615	0.0691	0.0740
Xss(277)	u_4	-0.0115	-0.0096	0.2613	0.0709	0.0682
Xss(278)	u_5	-0.0082	-0.0125	0.2096	0.1269	-0.0697
Xss(279)	u_6	-0.0265	-0.5755	-0.1417	-0.0238	0.0265
Xss(280)	u_7	-0.0010	-0.0014	0.0106	0.0390	-0.3602

The scores, T, were calculated using the noisy, mean-centered, scaled base case data matrix, X_s, and the reduced set of loadings vectors, V_a, as discussed earlier. Additionally, the residuals, the Mahalanobis distance (T^2), and the Q-statistic were calculated for the base case. The scores plot can be used later on to monitor if the input values are outside the accepted normal operating range resulting in a larger than normal responses in the key state variables. In monitoring future operations, the Mahalanobis distance would be used to measure the variation in the scores space and to determine if the variations fall outside the 95% confidence boundary. The 95% confidence level on T^2 was determined to be ~11. Figures 4.7–4.9 show the scores plots for PC1 versus PC2, PC1 versus PC3, and PC2 versus PC3, respectively. Figures 4.10 shows a 3D plot of the scores for PC1, PC2, and PC3 where the 95% boundary is a transparent ellipsoid. For each of these plots, only a few points lie outside the bounding ellipse as expected. Figure 4.11 shows the Mahalanobis distance and its 95% confidence level. Again most points are within the 95% confidence level. When monitoring future operations, the Q-statistic would be used to determine if the process is operating normally as defined by the base case PCA model (i.e., does the model still fit). The 95% confidence level on Q was ~62. Figure 4.12 shows the Q-statistic and its 95% confidence level. Figure 4.13 shows a 3D plot of Q vs. PC1 and PC2 scores. The patterns in the data were an artifact of how the data were generated and were not significant to the model. The data were generated in a stepwise fashion by systemically changing each input variable and calculating the result.

The nominal steady-state solution showed a 92% recovery of the uranium in the system from feed to the plant to conversion to the final UF_6 product. This means that 92% of the uranium feed to the plant was converted to UF_6 for the nominal steady-state solution. Therefore, 8% of the uranium feed was lost to waste streams throughout the plant. Additionally, the variation of the UF_6 product in comparison to the nominal base case solution was -27.8% to +15.5%.
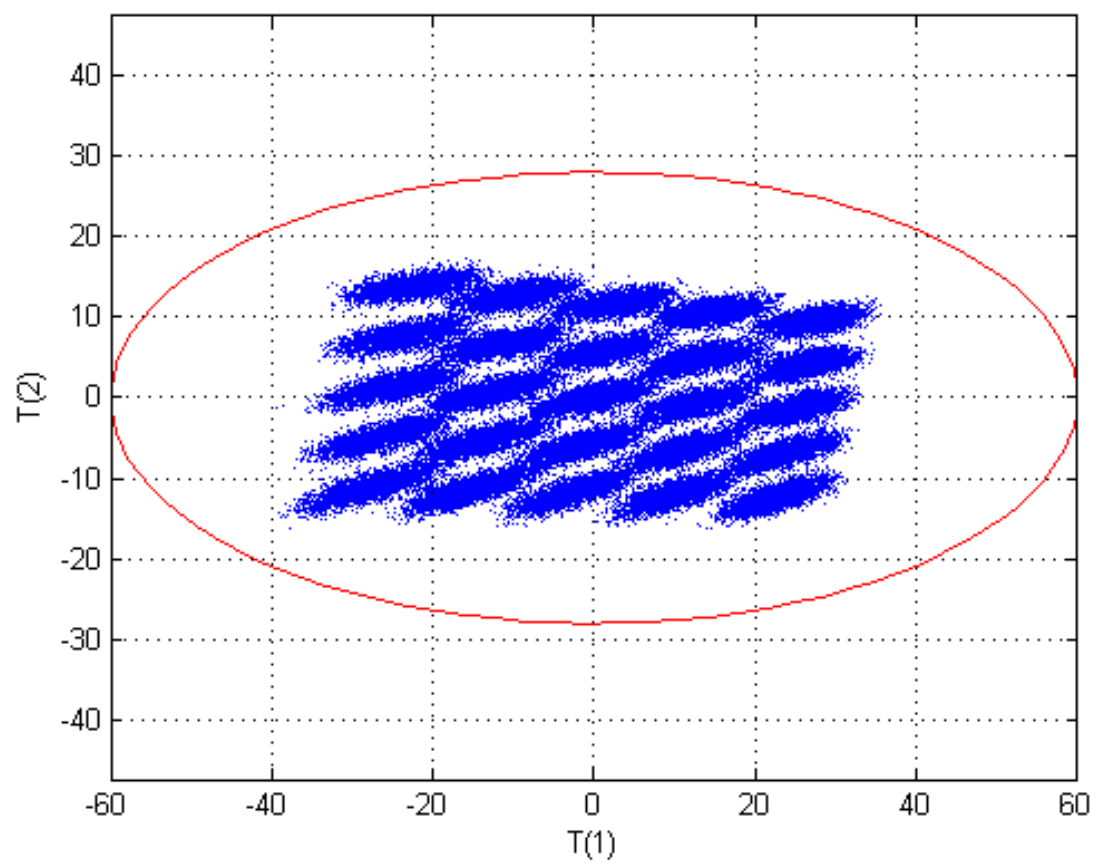
Figure 4.7. Base Case Scores Plot for PC1 and PC2.
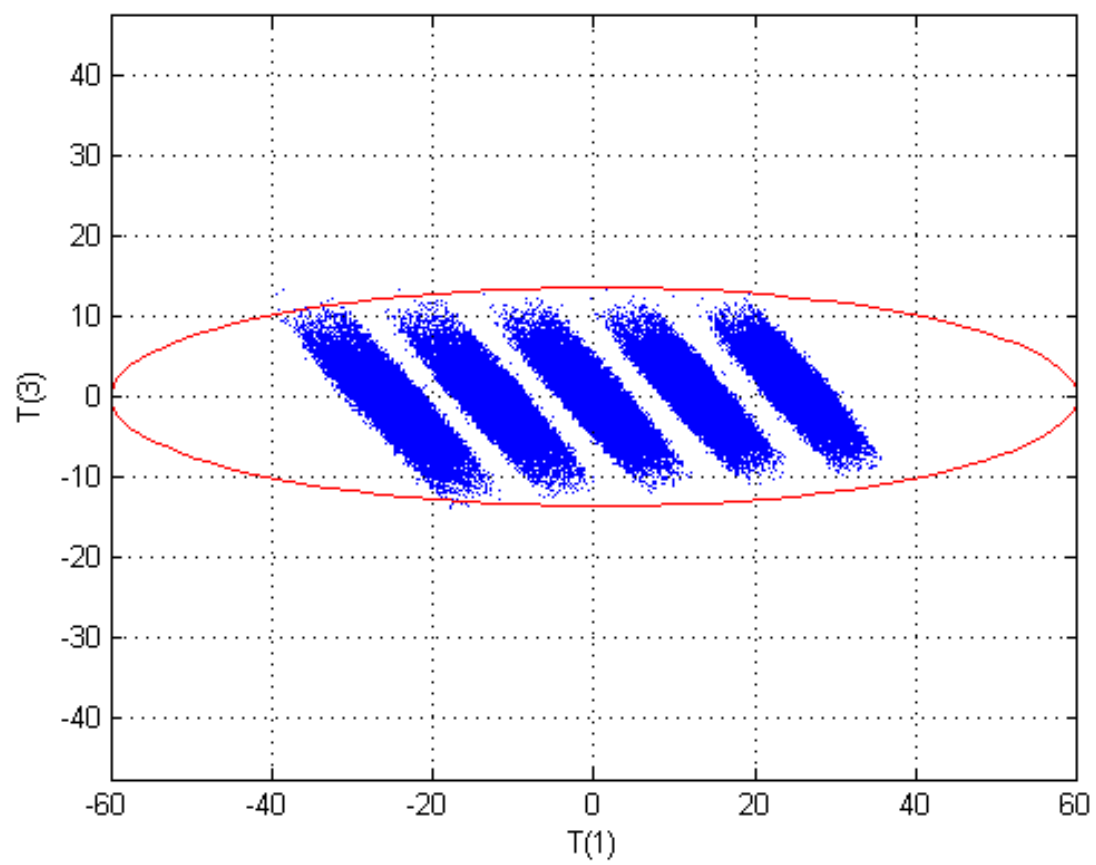
Figure 4.8. Base Case Scores Plot for PC1 and PC3.
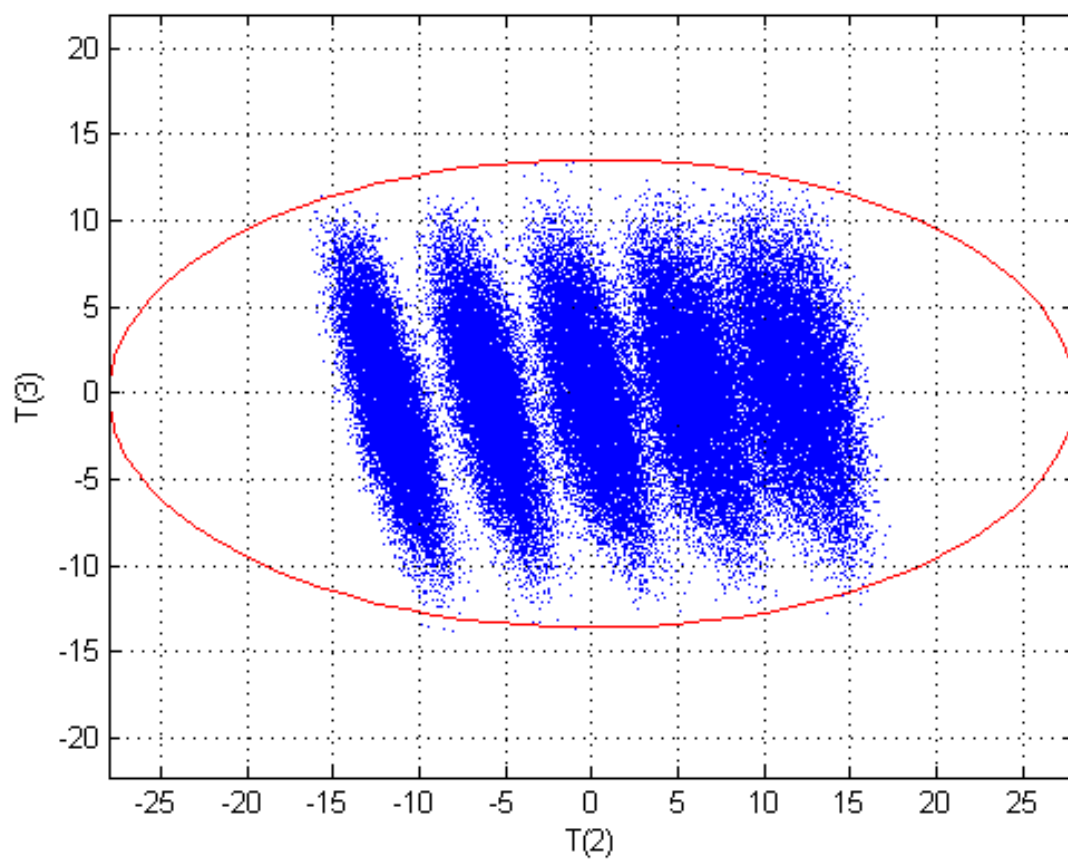
Figure 4.9. Base Case Scores Plot for PC2 and PC3.
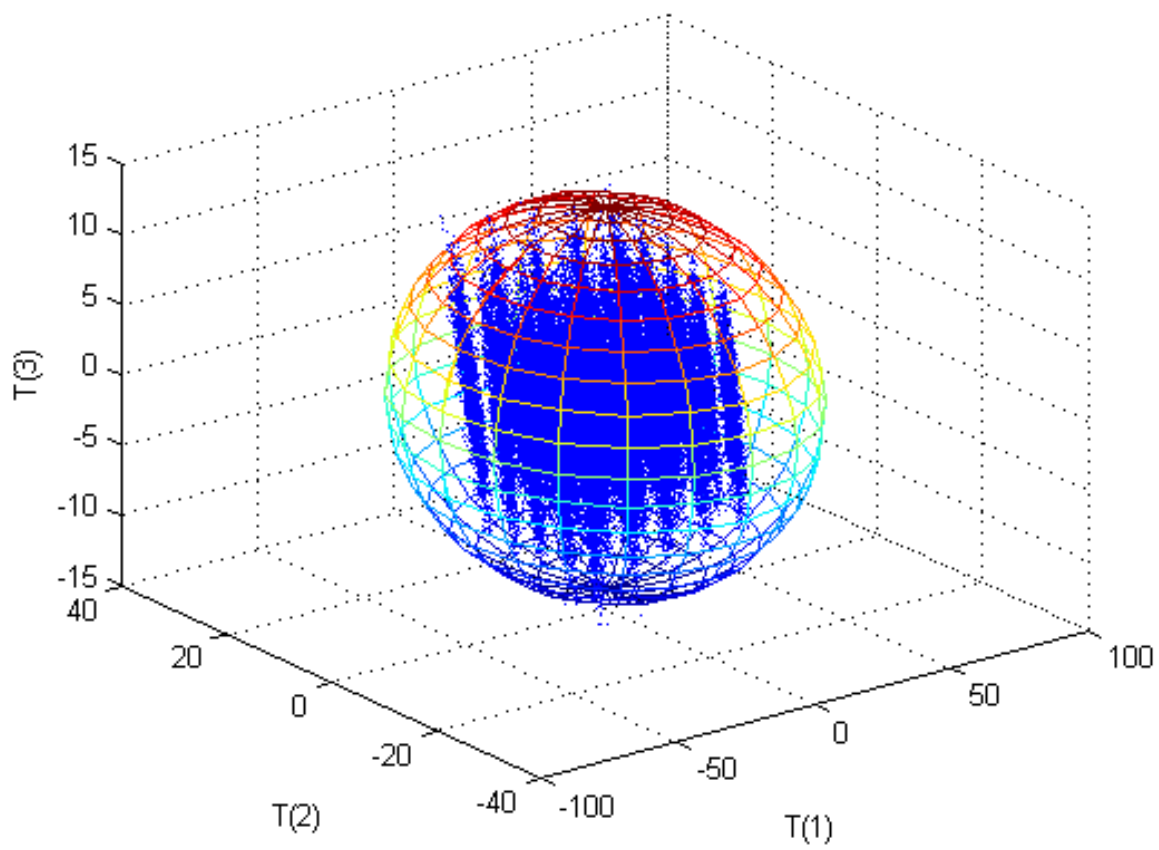
Figure 4.10. Base Case 3D Scores Plot for PC1, PC2, and PC3.
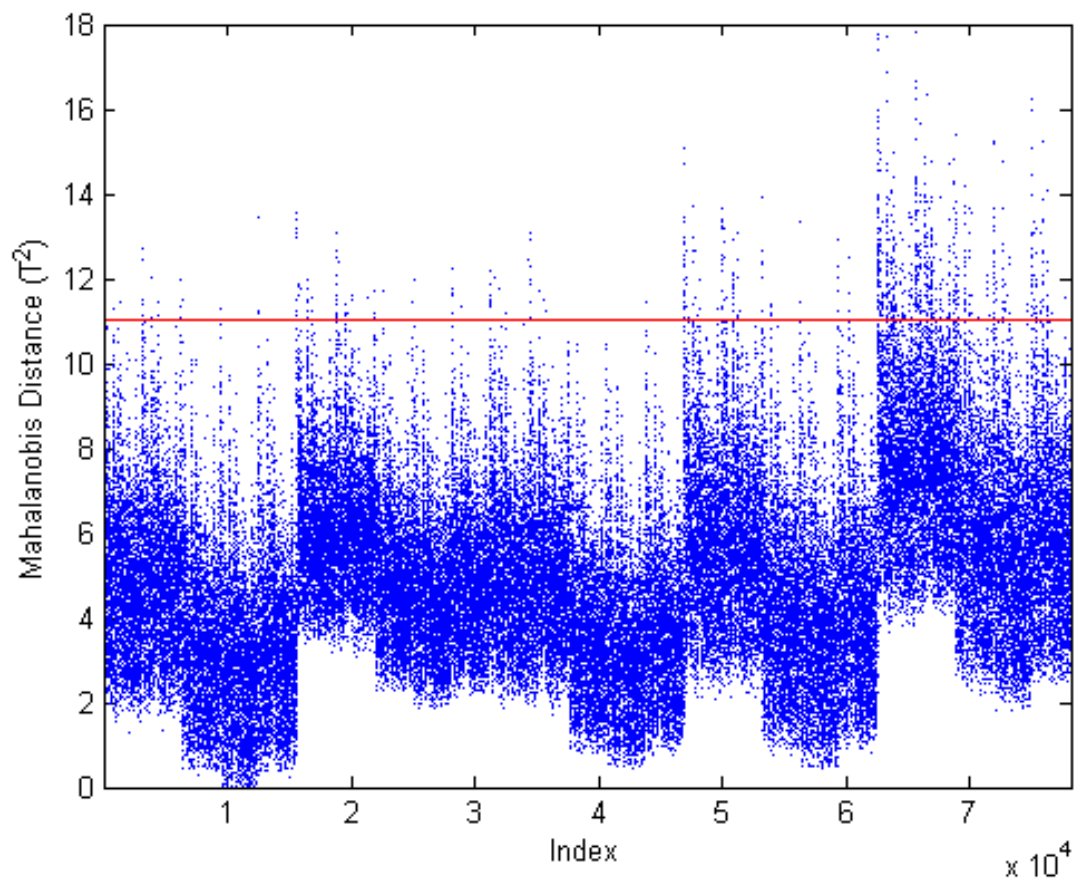
Figure 4.11. Base Case Mahalanobis Distance and 95% Confidence Boundary.
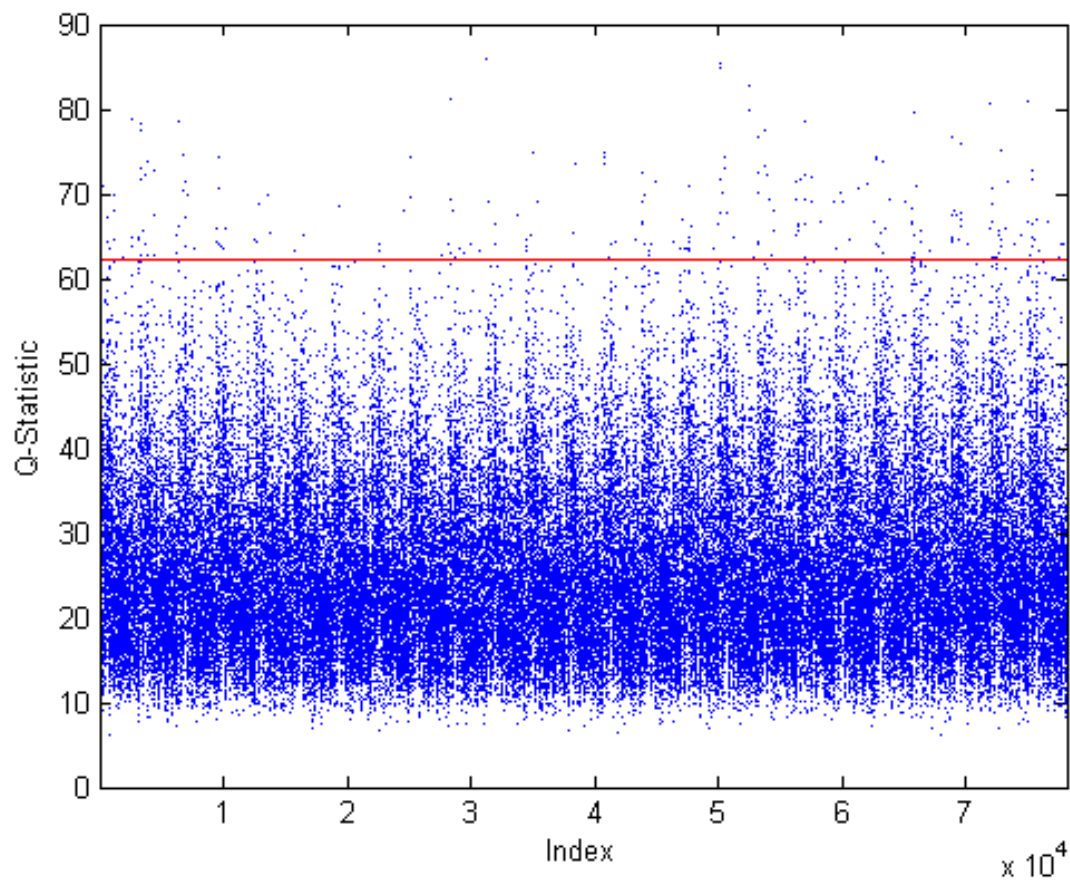
Figure 4.12. Base Case Q-Statistic and 95% Confidence Boundary.
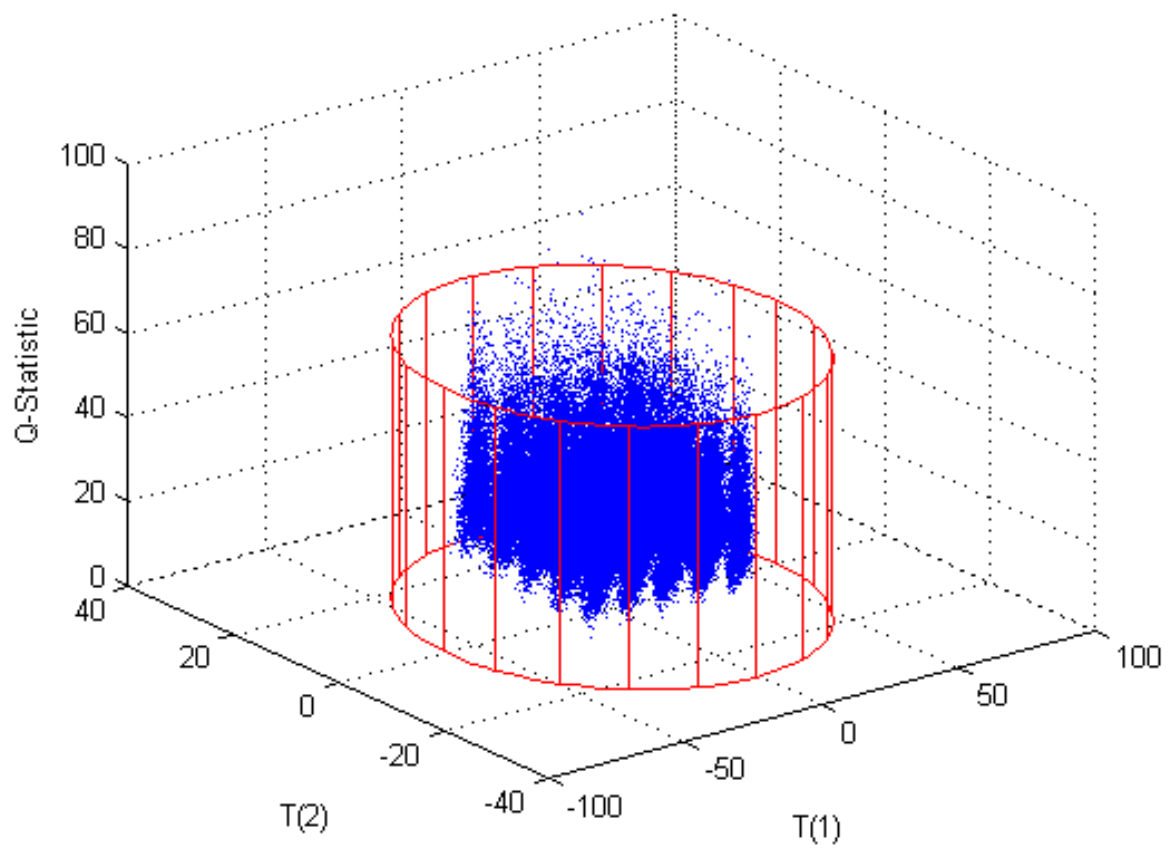
Figure 4.13. Base Case PC1, PC2, and Q-Statistic with 95% Confidence Boundary.

4.2.2 Control Case

The control case was used to partially validate the base case PCA model. For the control case, all of the parameters and input variables were set at the base case values. The variations of the input variables were made such that the variations were still within the ranges of the base case variations (see Table 3.12). Once the control case data were generated, the data matrix was pre-processed in the same manner (Gaussian noise added, mean-centered, and scaled) as the base case data using the base case means and standard deviations. The same number of data points were generated for the control case as the base case. Figures 4.14–4.16 show the scores plots for PC1 versus PC2, PC1 versus PC3, and PC2 versus PC3, respectively. Figures 4.17 shows a 3D plot of the scores for PC1, PC2, and PC3 where the 95% boundary is a transparent ellipsoid. Figure 4.18 shows the Mahalanobis distance and its 95% confidence level. Figure 4.19 shows the Q-statistic and its 95% confidence level. Figure 4.20 shows a 3D plot of Q vs. PC1 and PC2 scores. Since all of the control case variation was contained within the variation of the base case data, all of the control case data points were also within the base case confidence boundaries as expected.
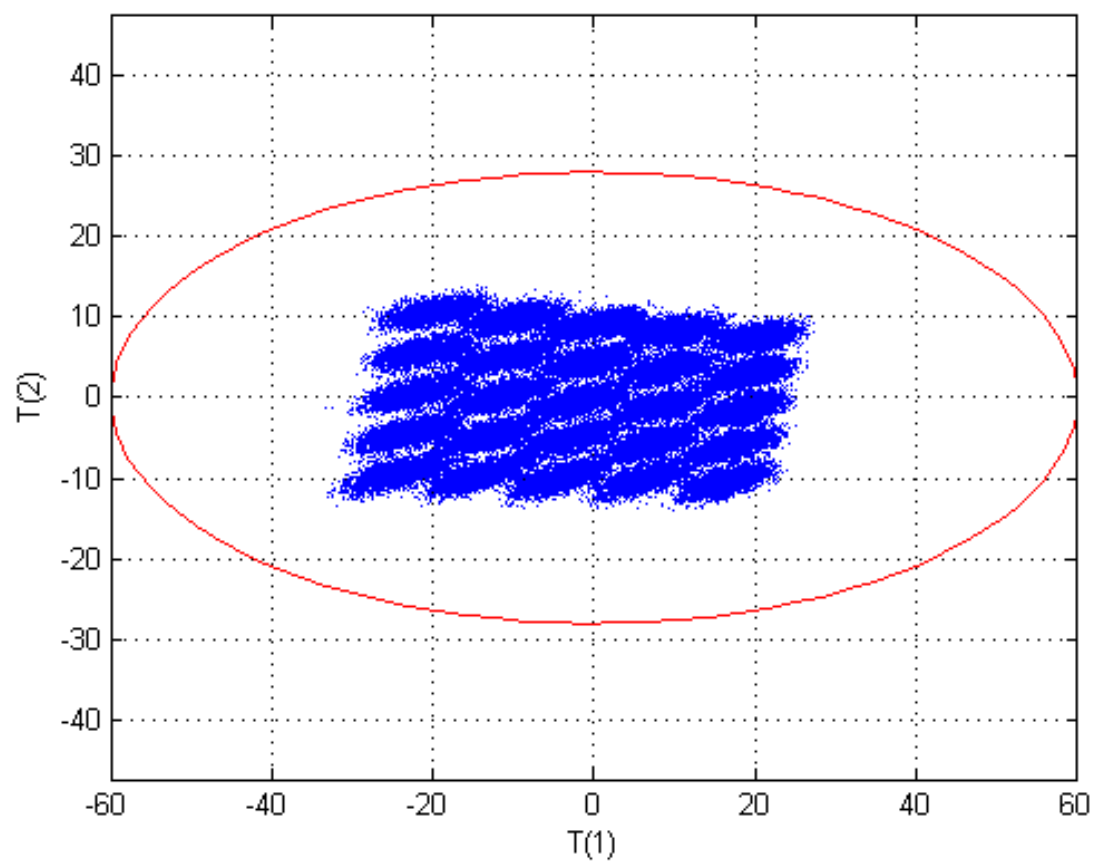
Figure 4.14. Control Case Scores Plot for PC1 and PC2.
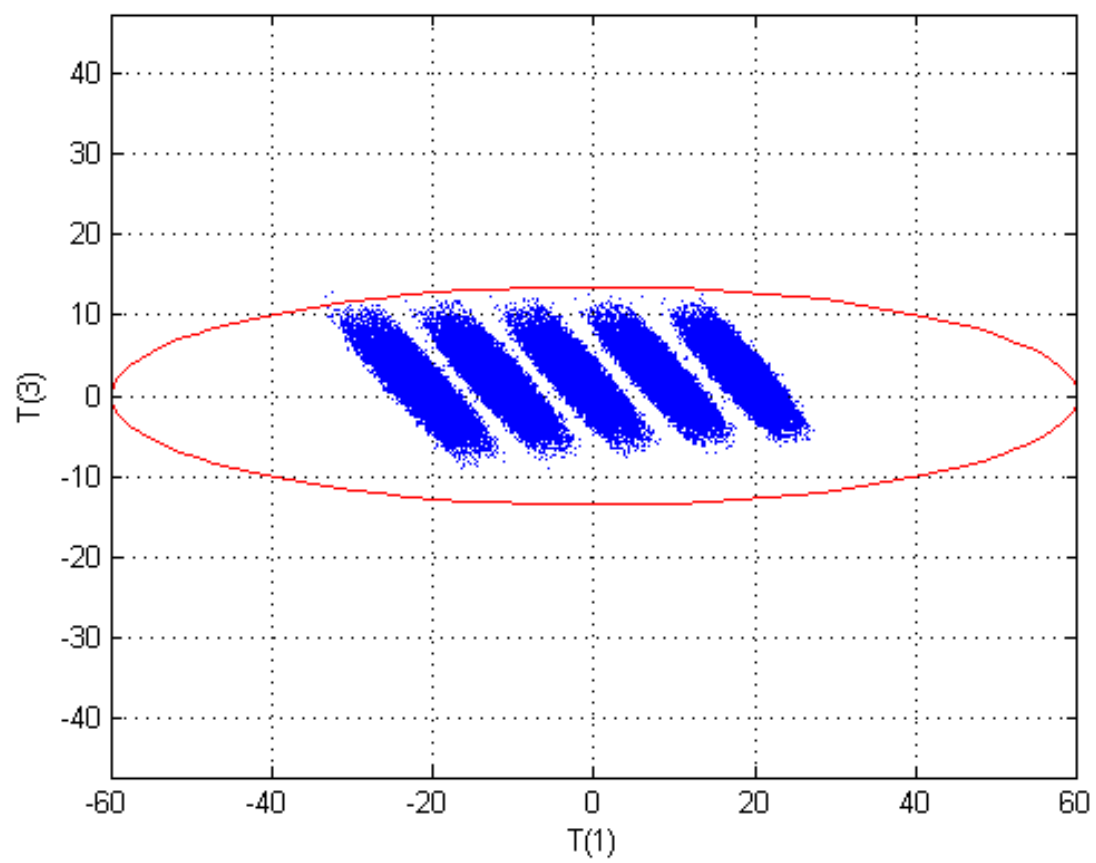
Figure 4.15. Control Case Scores Plot for PC1 and PC3.
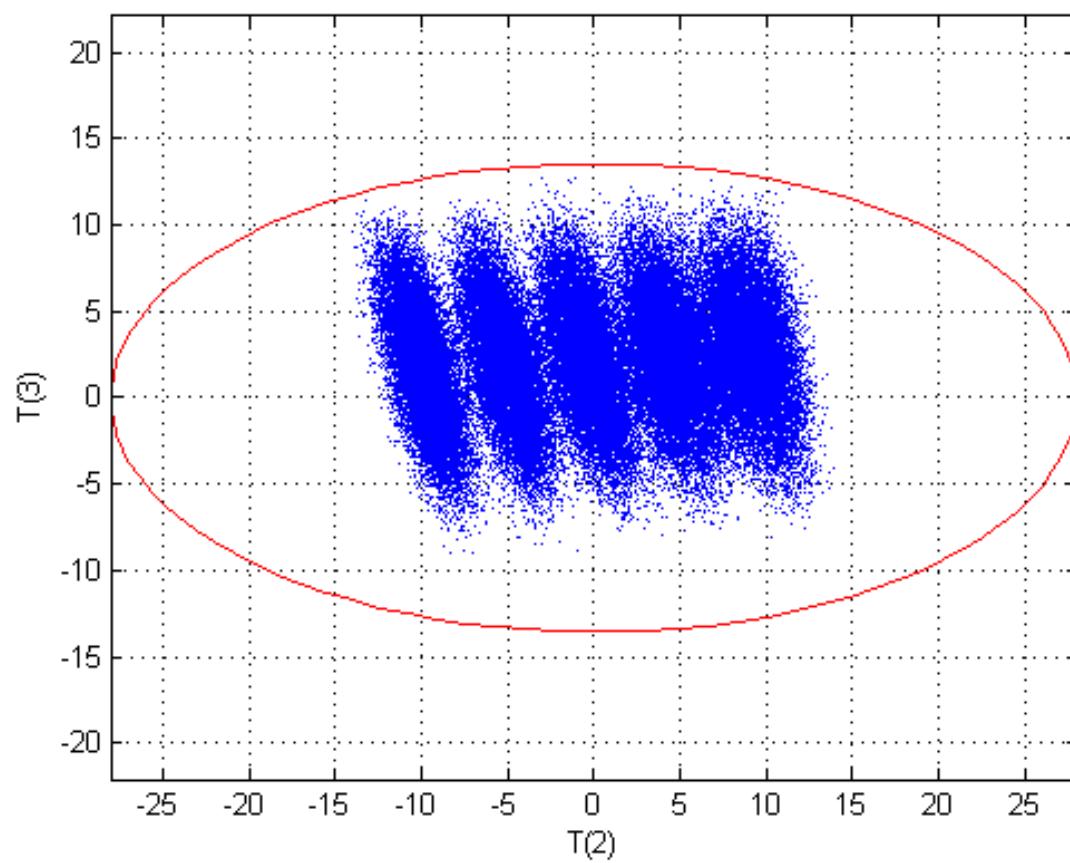
Figure 4.16. Control Case Scores Plot for PC2 and PC3.
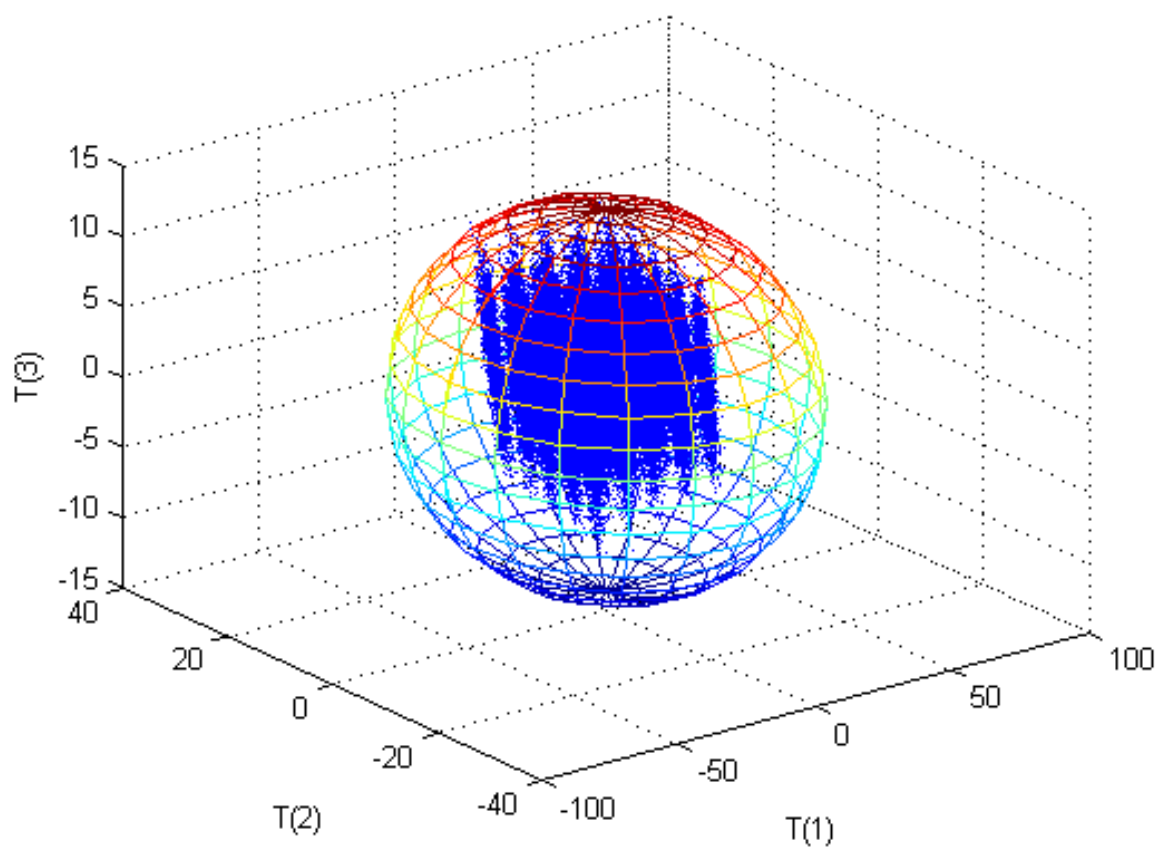
Figure 4.17. Control Case 3D Scores Plot for PC1, PC2, and PC3.
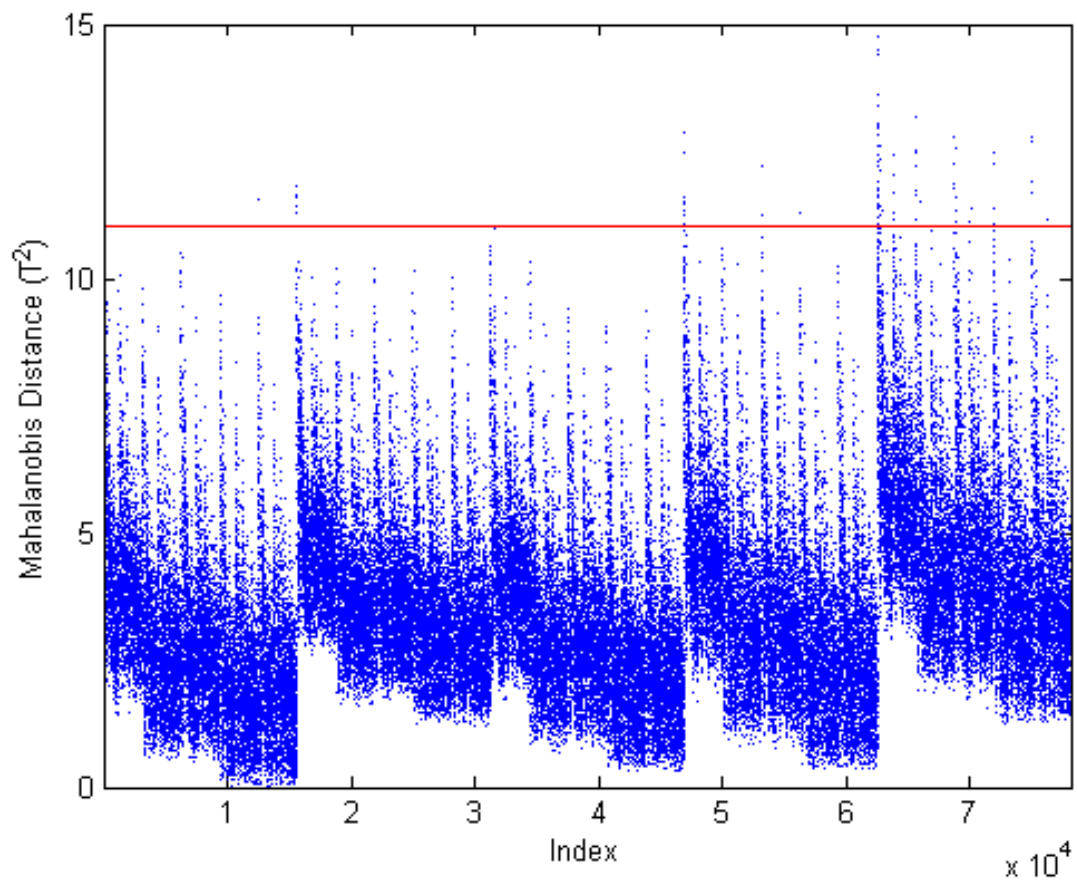
Figure 4.18. Control Case Mahalanobis Distance and 95% Confidence Boundary.
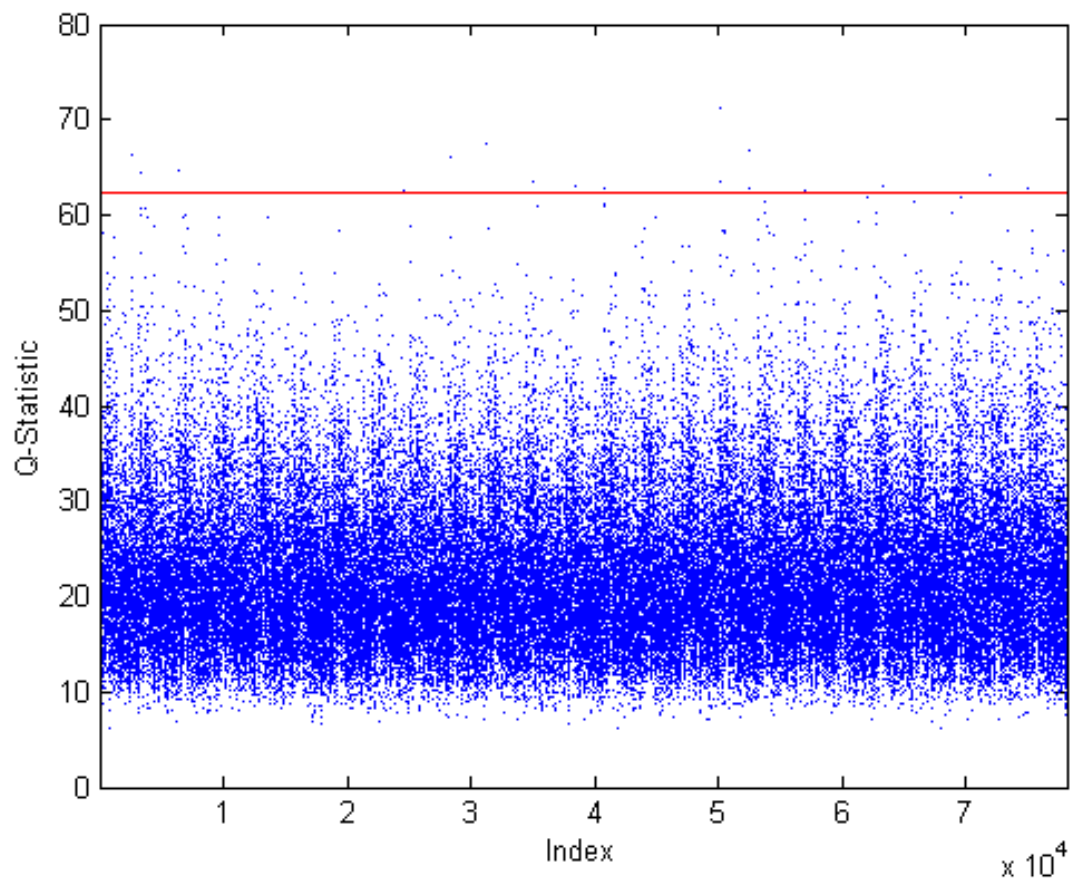
Figure 4.19. Control Case Q-Statistic and 95% Confidence Boundary.
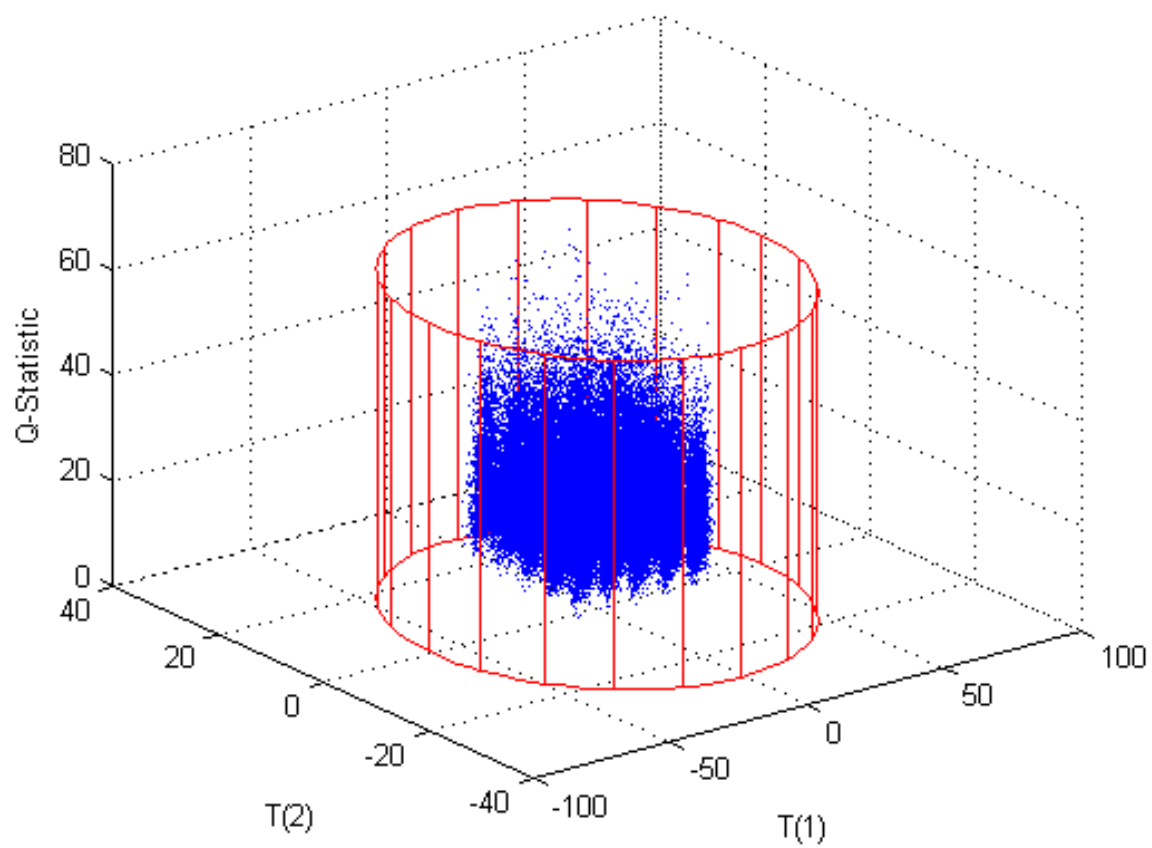
Figure 4.20. Control Case PC1, PC2, and Q-Statistic with 95% Confidence Boundary.

4.3 FAULTY "OFF-NORMAL" CASES

For each faulty case, both the steady-state solution and the overall material balances were checked to verify that the model was correctly simulated. As with the base case, the steady-state state variable solution was substituted back into the set of simultaneous equations to verify that the right side of the result for the material balance equations was the same as that provided by 'fsolve' and also that the result was approximately zero to be within round-off error of the computer. The overall material balances were also checked especially in the cases where additional streams were added. The overall rate of change was approximately zero (at least 1×10^{-10}) in all cases. For all of the plots below, only the faulty case data points are displayed with the 95% confidence boundaries from the base case PCA model superimposed. In all cases, the same number of data points as the base case were generated.

Within each faulty case, recommendations are made for which streams should be monitored in order to detect the particular fault. These recommendations are to provide data for the monitoring framework and a never meant to be recommendations for considering individual measurements separately. One of the benefits of the multivariate statistic approach is that the system is considered as a whole and the individual measurements need not be considered separately. The multivariate approach reveals correlations with the data which may not be noticeable in the individual measurements.

Also for each faulty case, the detectability of the specific fault using the diagnostic plots is reference in two ways: clearly detectable or detectable in trending monitoring. A clearly detectable fault is one where all of the simulated faulty data is outside the 95% confidence boundary. This means that the fault is detectable under all possible operations conditions that were considered in this model. A fault that is not clearly detectable may still be detectable using trend monitoring. In these cases, the data points are shifted by may still be partially or completely within the 95% confidence boundary. Monitoring for a continuous trend in the data may reveal this shift in the operating conditions before the process is completely out of bounds.

4.3.1 Case 1

For the first faulty case, the total throughput of the facility was increased. Initially, all incoming flow rates (Streams 1A, 4A–13A) were increased by 50% with no other changes in the model. Refer to Table 3.9 for the nominal values of these incoming flow rates. This initial test was used to determine the extent of the model response. The results show that the change in the PC1 scores and the Mahalanobis distance was significant as expected. There was also a significant increase in the Q-statistic. The flow rate of one of the incoming streams (1A) was also an input variable [Xss(274)] while the other incoming flow rates appear as model parameters. This result implies that the base case model no longer fits the current process operation when a change in total flow rates to the plant was introduced, which was expected since most of the incoming flow rates appear as model parameters. It was also expected that a

167

fault would occur in the scores on the first principal component since the incoming uranium flow rate was a heavy contributor. Results for both a 50% and 10% increase in all incoming flow rates are presented below. In an additional faulty case, only the incoming uranium flow rate was increased leaving all other parameters and inputs unchanged from the base case. Results for both 15% and 25% increases in only the incoming uranium flow rate are also presented below. A summary of the Faulty Case 1 simulation is provided in Table 4.21.

Based on the sensitivity analysis, only a few state variables would be sensitive to changes in the incoming flow rates except the incoming uranium flow rate. None of the primary state variables were sensitive to any changes in the incoming flow rates except for the incoming uranium flow rate, which all of the primary state variables were sensitive to with a sensitivity factor value of one.

In order to detect these types of faults, it is recommended that the uranium feed to the plant be monitored for both flow rate and uranium content. Additionally, it is recommended that the streams exiting each major process (e.g., dissolution, solvent extraction, fluorination) as product or waste be monitored for flow rate and uranium content.

Table 4.21. Summary of Faulty Case 1

Case	Priority	Module	Faulty Variable	Base Case Value	Faulty Value	Physical Description
			Summary of Faulty Case			
1A	High	1	All F values	Varies	+50%	Increase total plant throughput by 50%
1B	High	1	All F values	Varies	+10%	Increase total plant throughput by 10%
1C	High	1	$F_{1A,U}$	50 kg/h	57.5 kg/h	Increase uranium throughput by 15%
1D	High	1	$F_{1A,U}$	50 kg/h	62.5 kg/h	Increase uranium throughput by 25%

		PC1 Scores	PC2 Scores	PC3 Scores	T2	Q
		Summary of Results				
1A	**Direction**	---	+	0	++	++++
	Detectability	Yes	No	No	Yes	Yes
1B	**Direction**	0	0	0	~+	++
	Detectability	No	No	No	No	Yes
1C	**Direction**	-	0	0	~+	0
	Detectability	No	No	No	Not likely	No
1D	**Direction**	-	0	0	+	0
	Detectability	Possibly	No	No	Yes	No

4.3.1.1 Case 1A – Fifty Percent Increase in Total Flow Rate

For this case, the incoming flow rate of uranium [$F_{1A,U}$ also Xss(274)] was increased by 50% along with the other incoming flow rates (Streams 4A–13A). The results show that this fault was clearly detected in PC1 scores, the Mahalanobis distance, and the Q-statistic.

There was a significant fault in PC1 scores which was expected since Xss(274) was a heavy contributor to PC1 (Figures 4.21–4.22). There was a very slight shift in PC2 scores (Figure 4.23). However, the shift in PC2 scores was not detectable since many of the data points are within the confidence boundary of the base case model. The 3D plot of the scores for PC1, PC2, and PC3 also shows the fault in PC1 scores (Figure 4.24). As expected since increasing the total flow rate by 50% was outside of normal operating conditions and resulted in a fault in the PC1 scores, there was a significant increase in the Mahalanobis distance (Figure 4.25). There was also a significant increase in the Q-statistic (Figure 4.26) as expected since increasing total throughput changed the relative relationship between the state variables since all of the incoming flow rates except the incoming uranium flow rate appear as model parameters. The faults in both PC1 scores and the Q-statistic are visible in the 3D plot of Q vs. PC1 and PC2 scores (Figure 4.27).
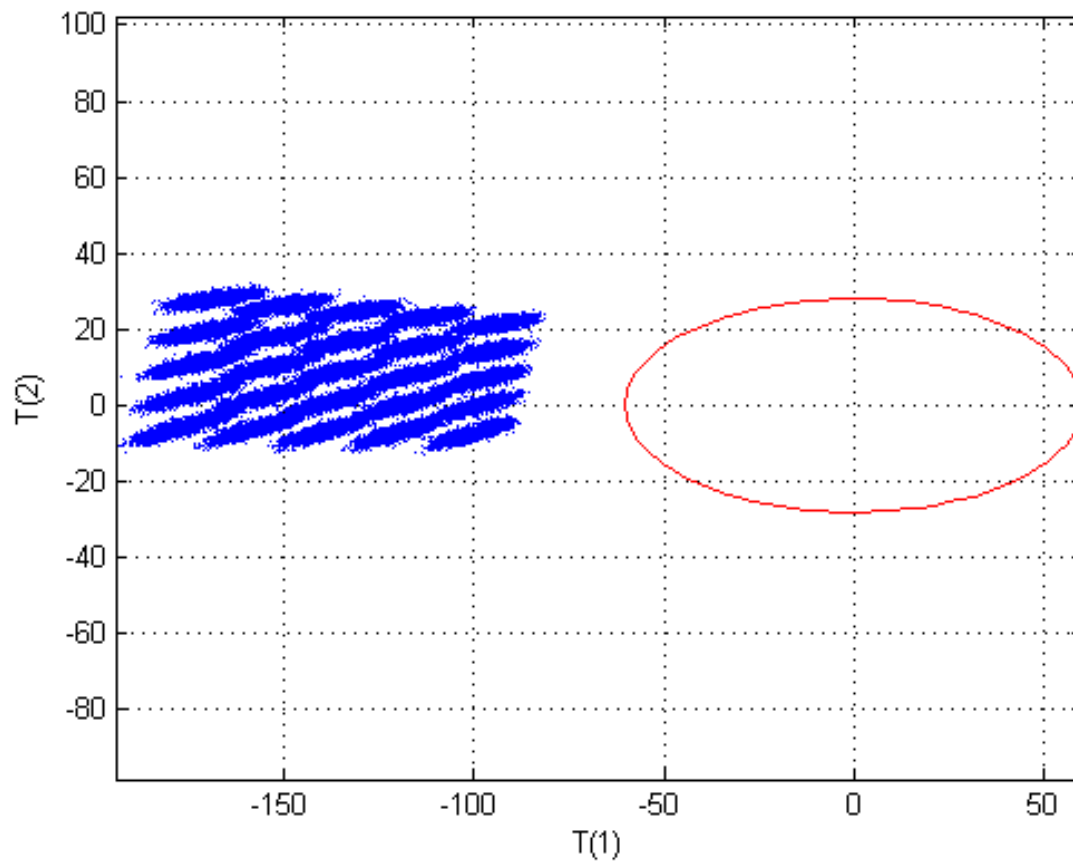
Figure 4.21. Faulty Case 1A Scores Plot for PC1 and PC2. *Note: Only the faulty data are shown with the base case 95% confidence boundary displayed in red. There was a fault in PC1 scores.*
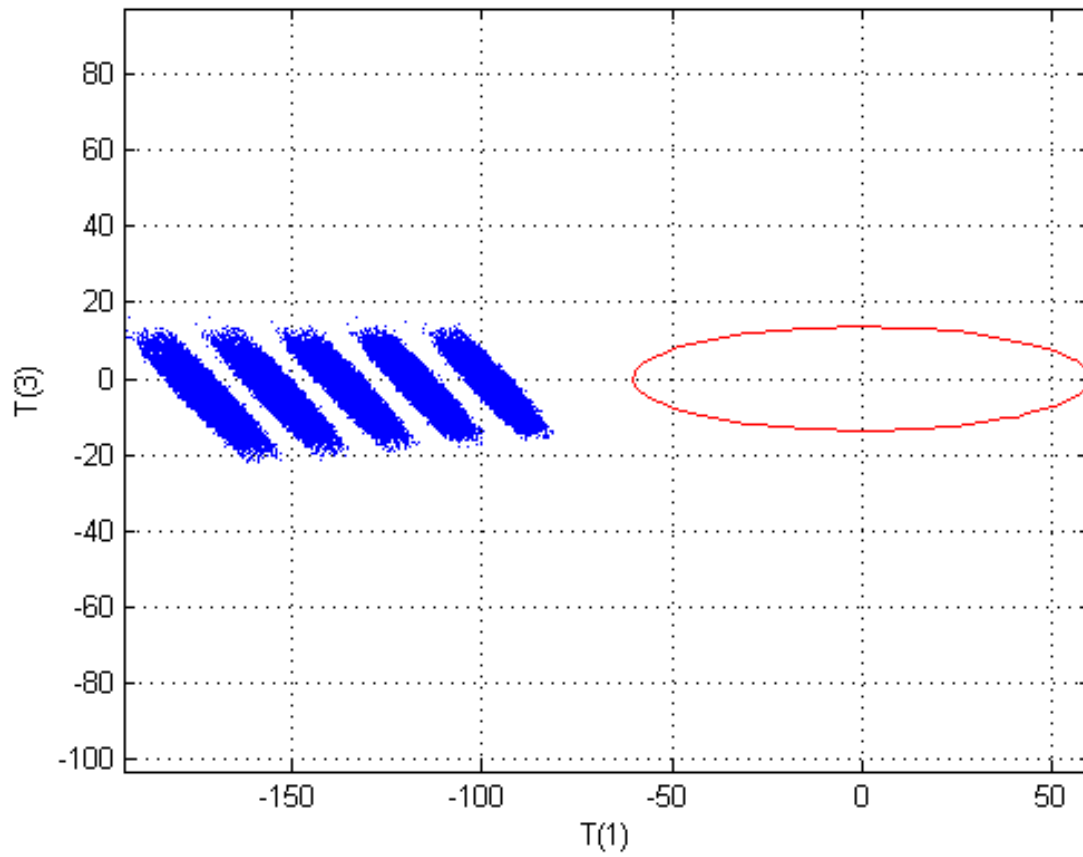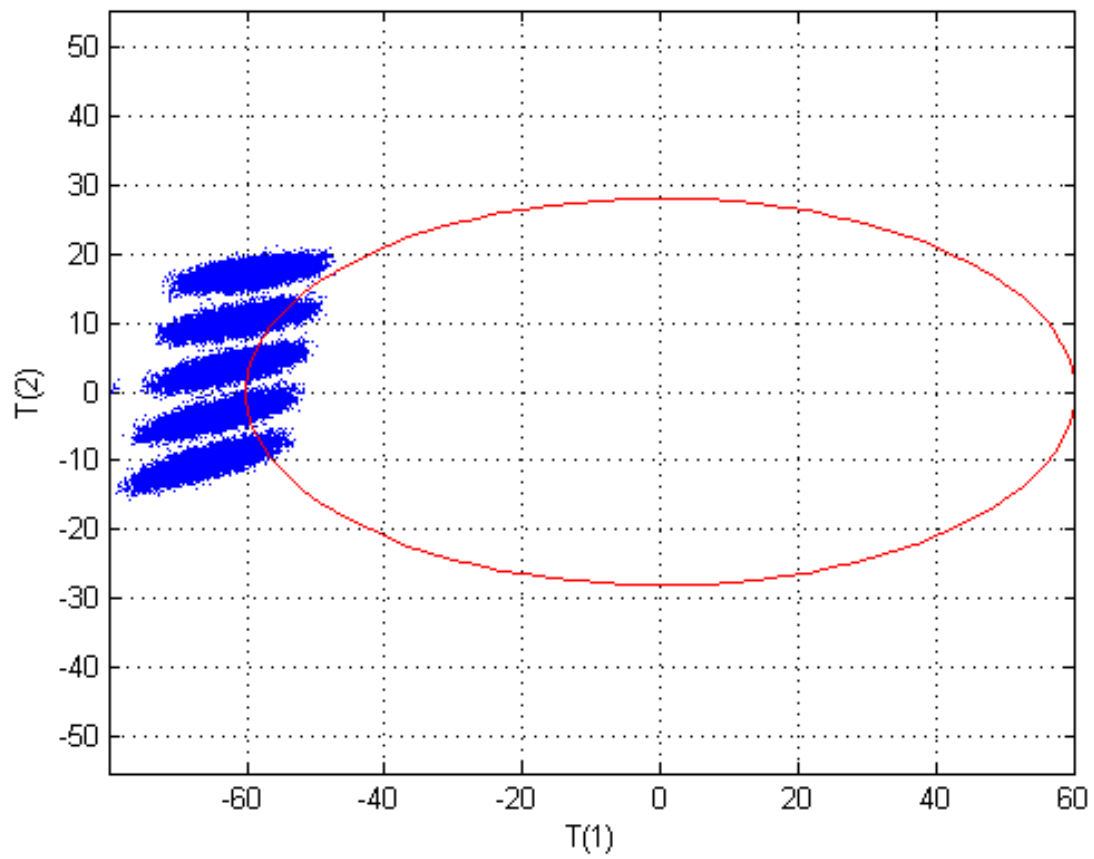
Figure 4.22. Faulty Case 1A Scores Plot for PC1 and PC3. *Note: Only the faulty data are shown with the base case 95% confidence boundary displayed in red. There was a fault in PC1 scores.*
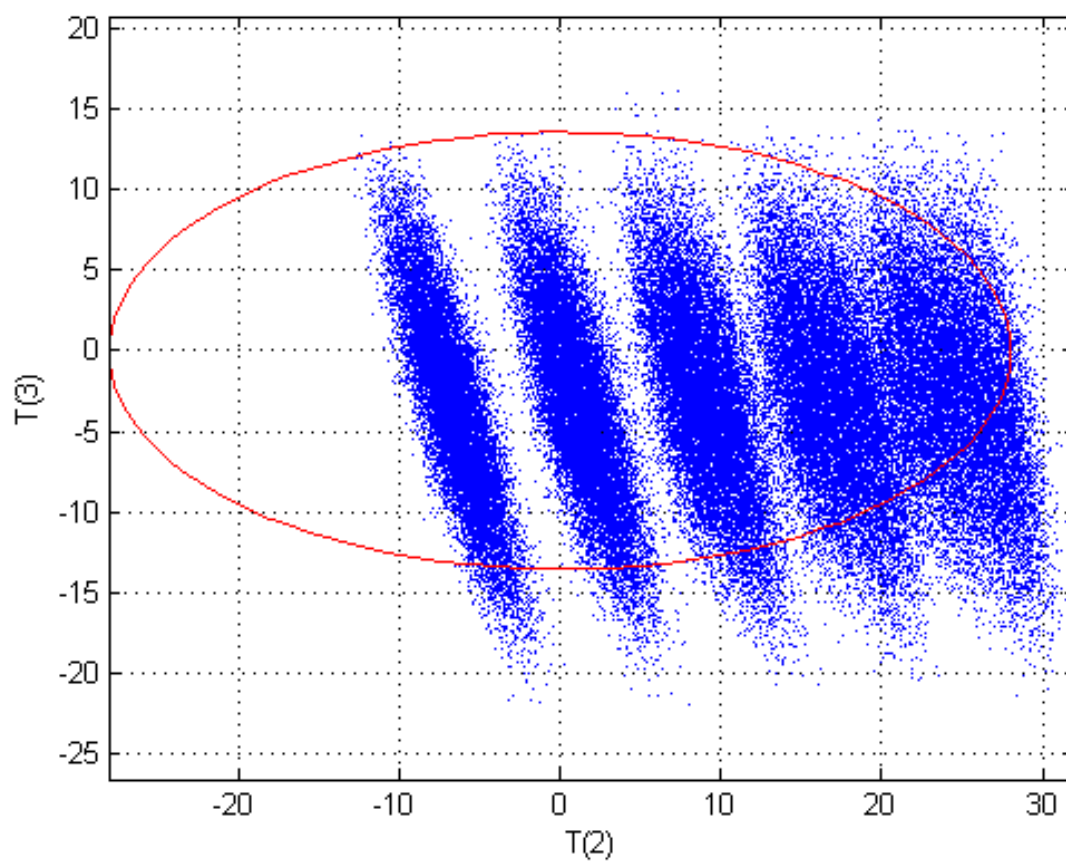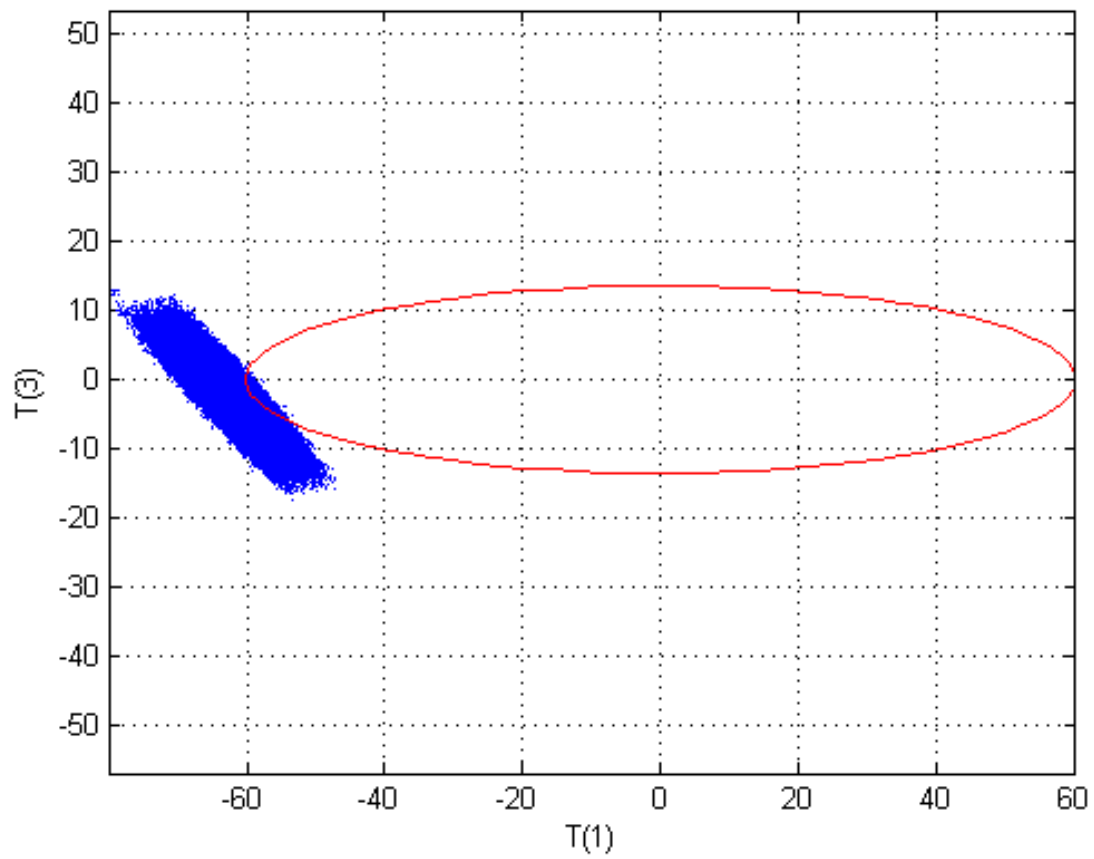
Figure 4.23. Faulty Case 1A Scores Plot for PC2 and PC3. *Note: Only the faulty data are shown with the base case 95% confidence boundary displayed in red. There was a slight shift in PC2 scores but the fault was not detectable.*
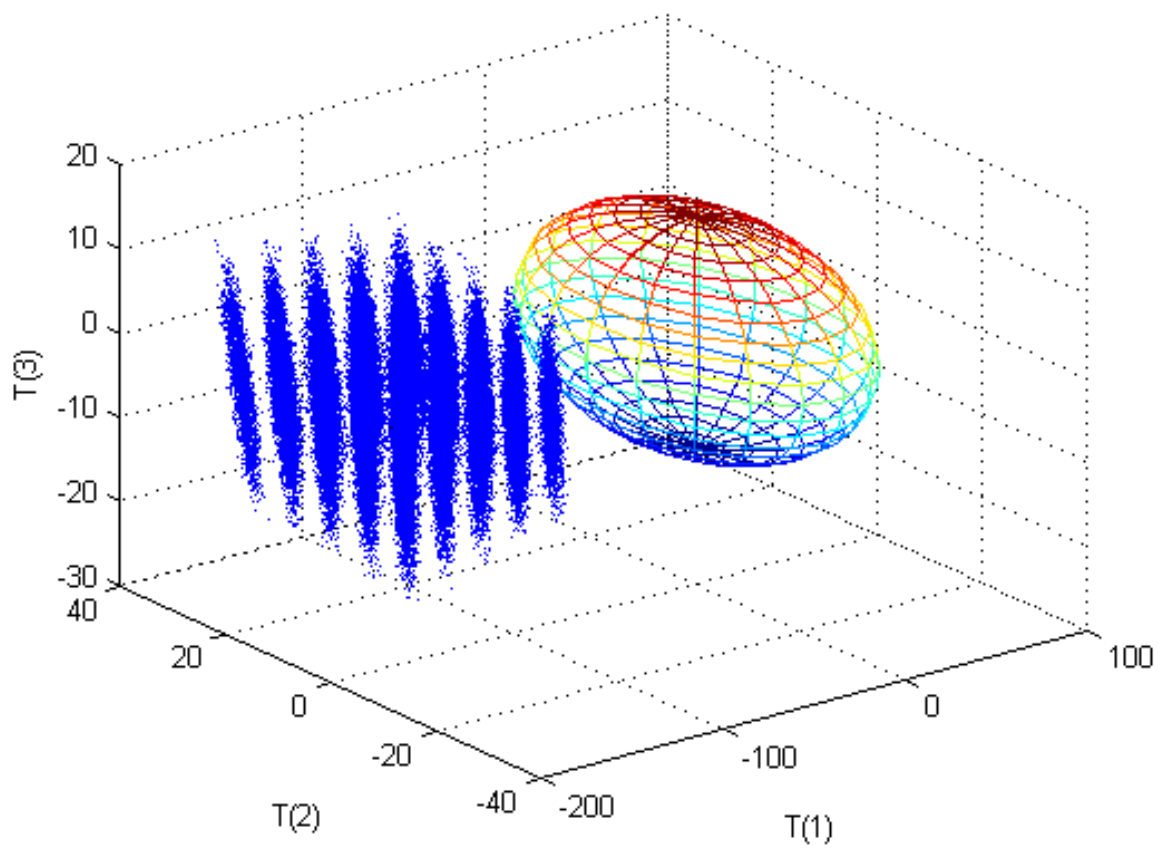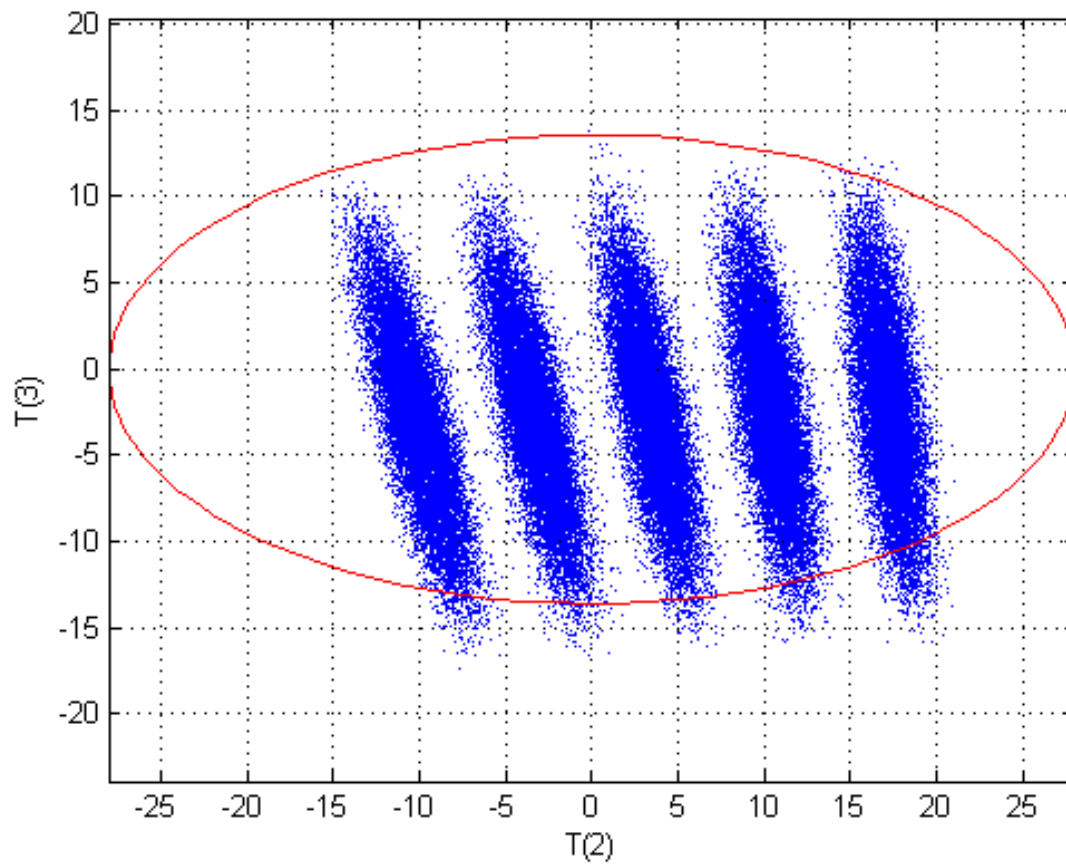
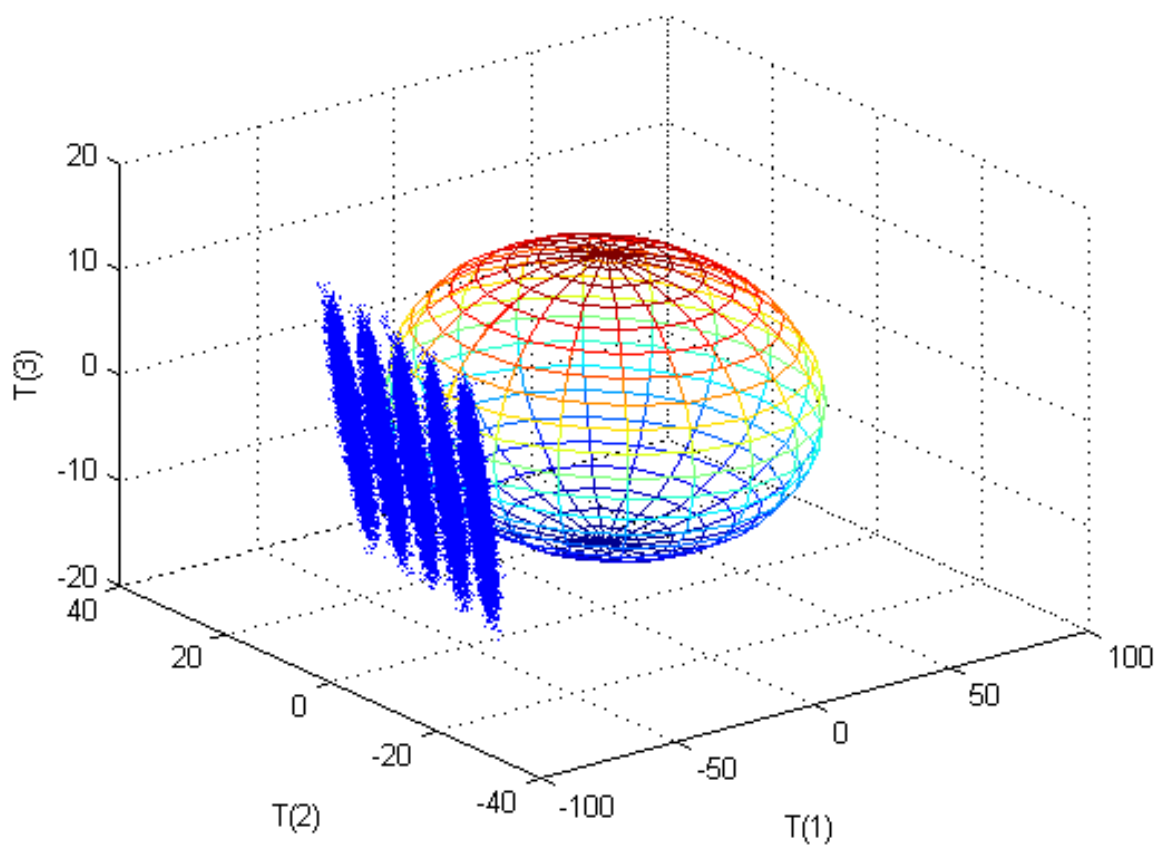**Figure 4.24. Faulty Case 1A 3D Scores Plot for PC1, PC2, and PC3.** *Note: Only the faulty data are shown with the base case 95% confidence boundary displayed as an ellipsoid. There was a detectable fault in PC1 scores.*
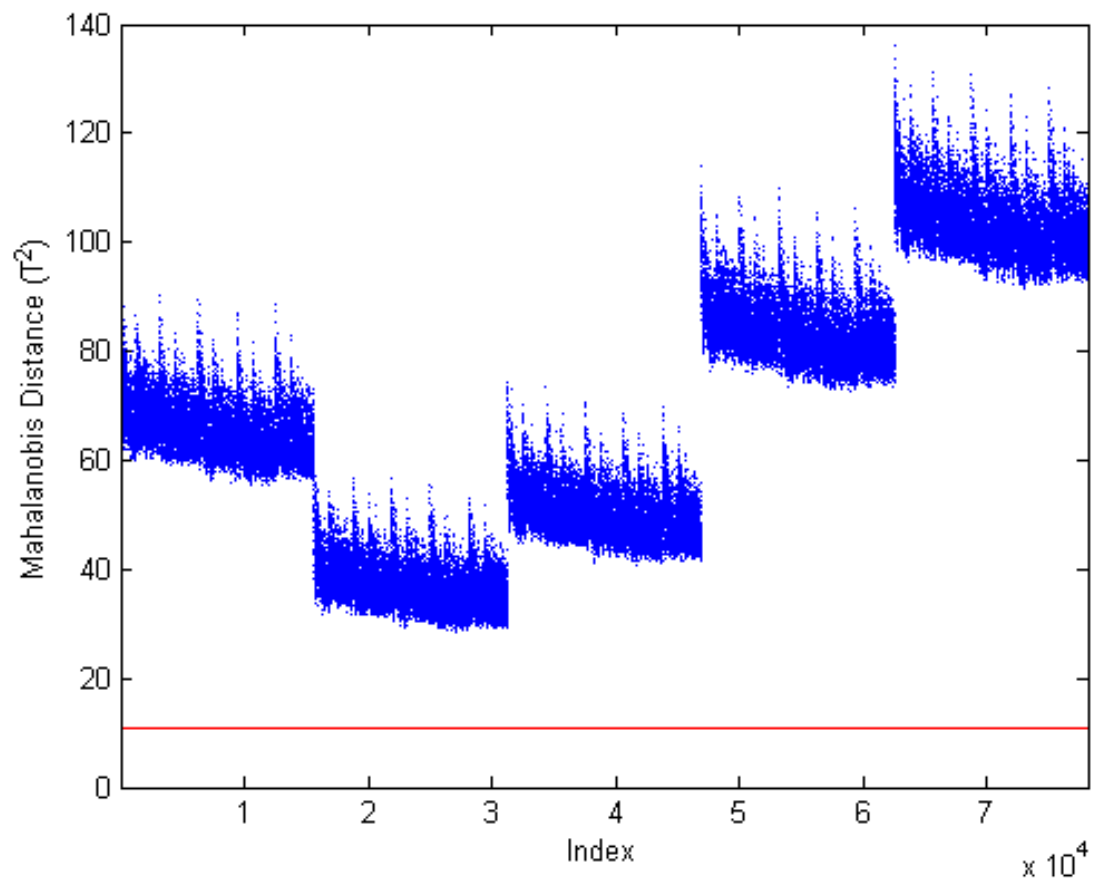
Figure 4.25. Faulty Case 1A Mahalanobis Distance Plot. *Note: Only the faulty data are shown with the base case 95% confidence boundary displayed in red. There was a detectable fault.*
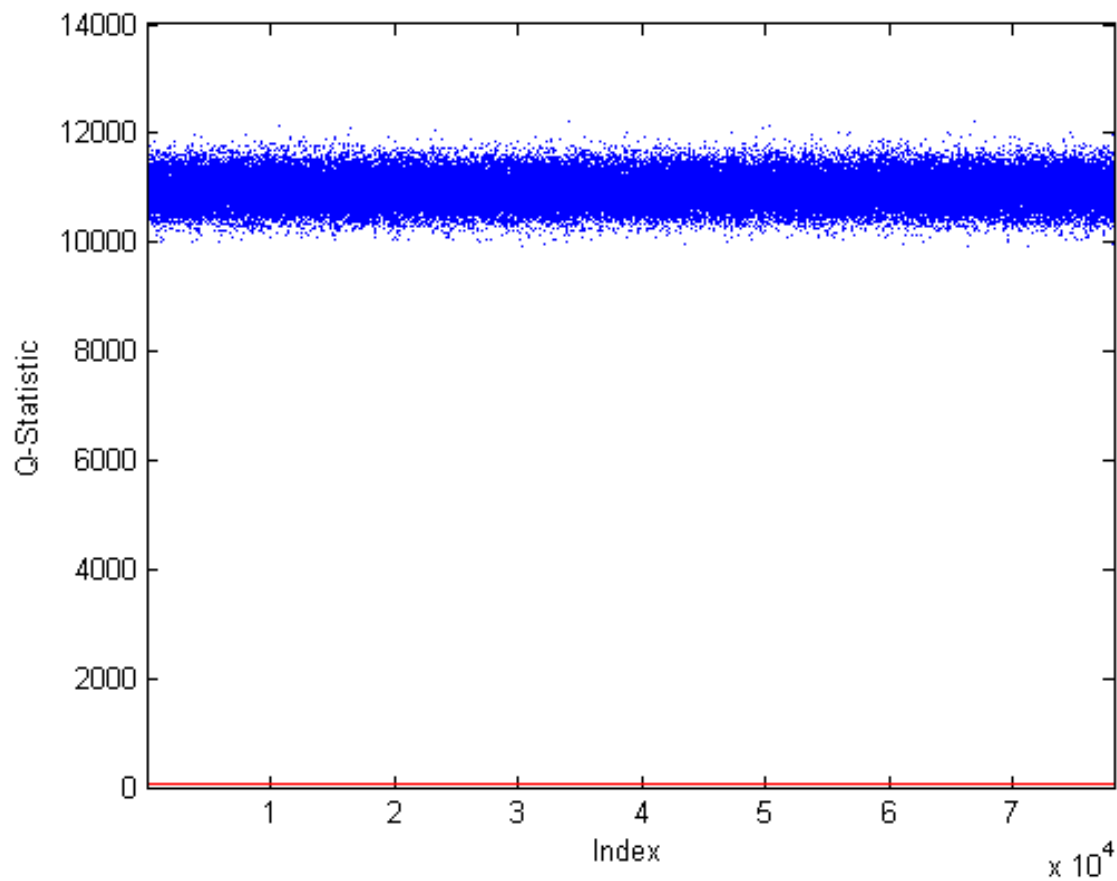
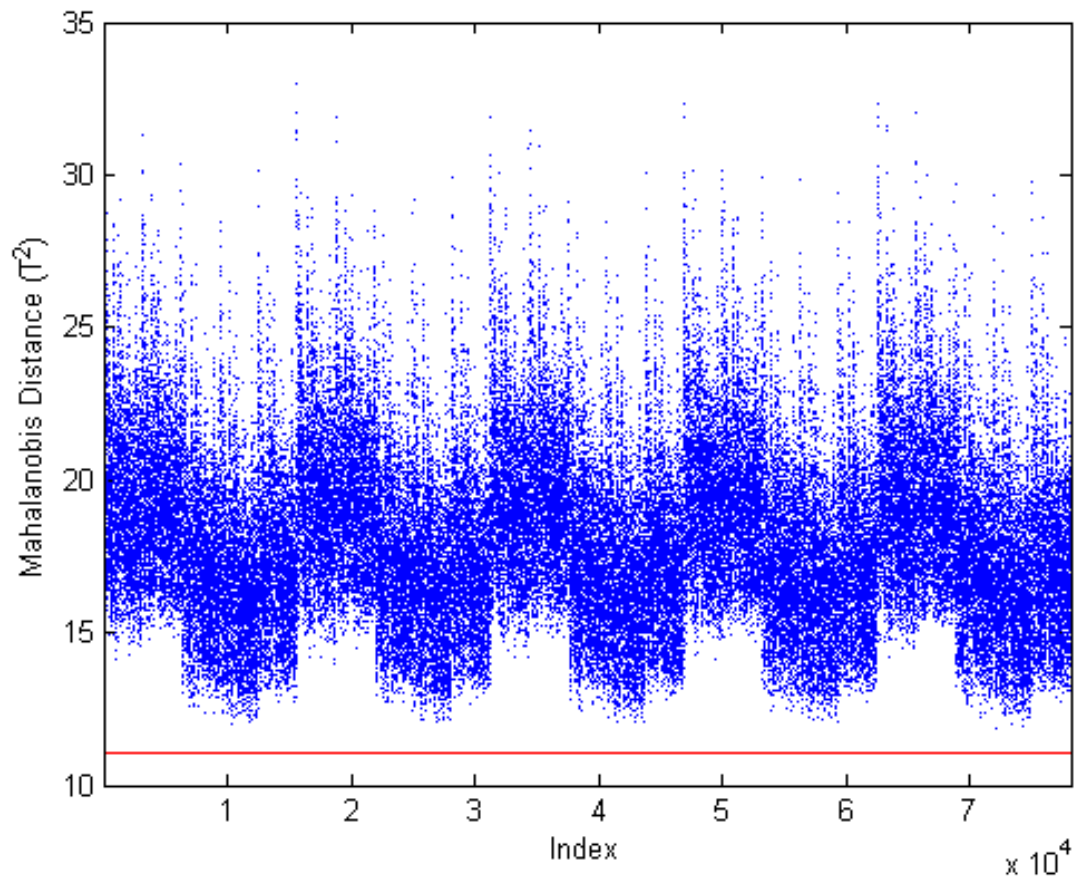**Figure 4.26. Faulty Case 1A** *Q***-Statistic Plot.** *Note: Only the faulty data are shown with the base case 95% confidence boundary displayed in red. There was a detectable fault.*
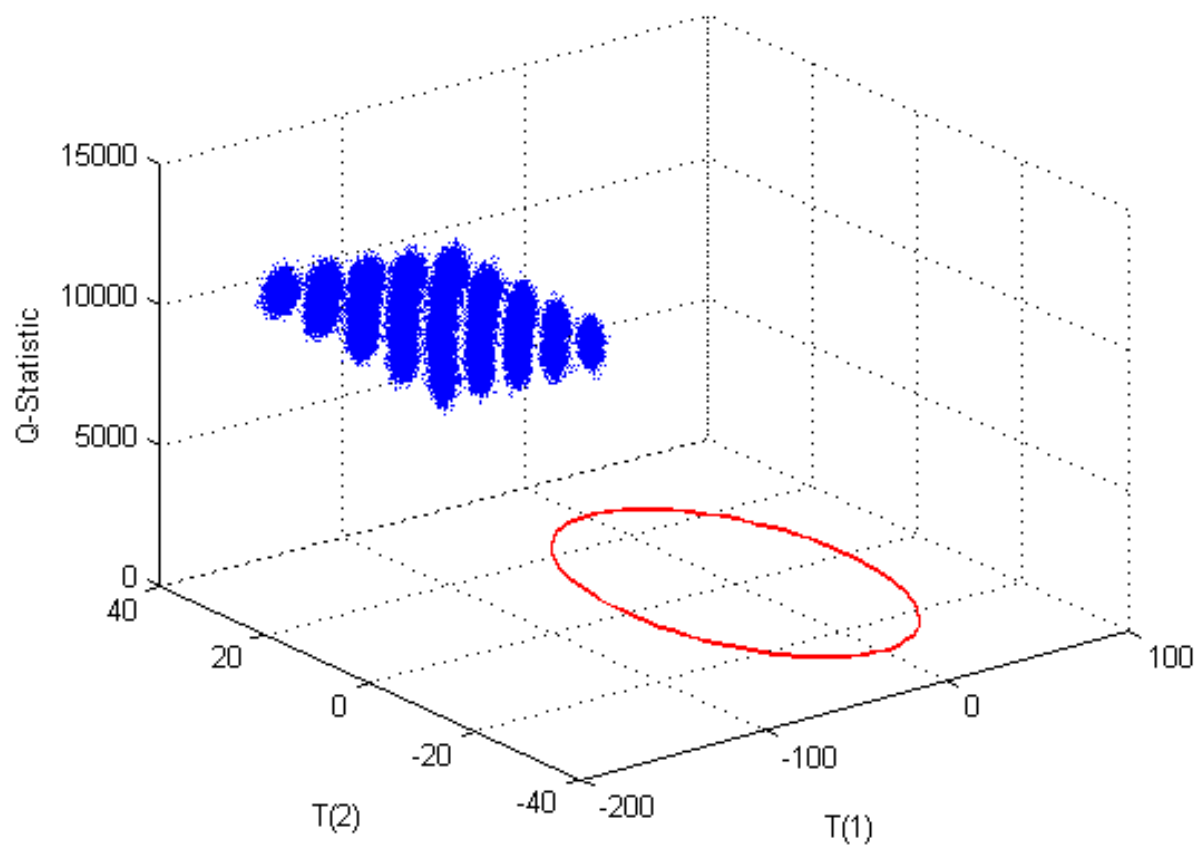
Figure 4.27. Faulty Case 1A PC1, PC2, and Q-Statistic Plot. *Note: Only the faulty data are shown with the base case 95% confidence boundary displayed in red. There was a detectable fault.*

### 4.3.1.2 Case 1B – Ten Percent Increase in Total Flow Rate

Since the base case model included a ±10% variation in the incoming uranium flow rate, this faulty case provided a new incoming flow rate that was 10% over the nominal base case value with no variation allowed. Therefore, $F_{1A,U}$ [Xss(274)] was set at 55 kg/h for this case. The other incoming flow rates (for which variations were not included in the base case) were also increased by 10% for this case. The results show that the fault in this case was only detectable in the Q-statistic (Figures 4.28–4.29). An increase in the Q-statistic was expected since the flow rates other than $F_{1A,U}$ appear as model parameters and this change resulted in a change in the relative relationship between the state variables. The Mahalanobis distance was not expected to exhibit a fault since the change in $F_{1A,U}$ was within the normal range of the base case. There was a slight increase in the number of data points above the 95% confidence boundary (Figure 4.30), but the fault was not detectable. There were no detectable changes in the scores plots.
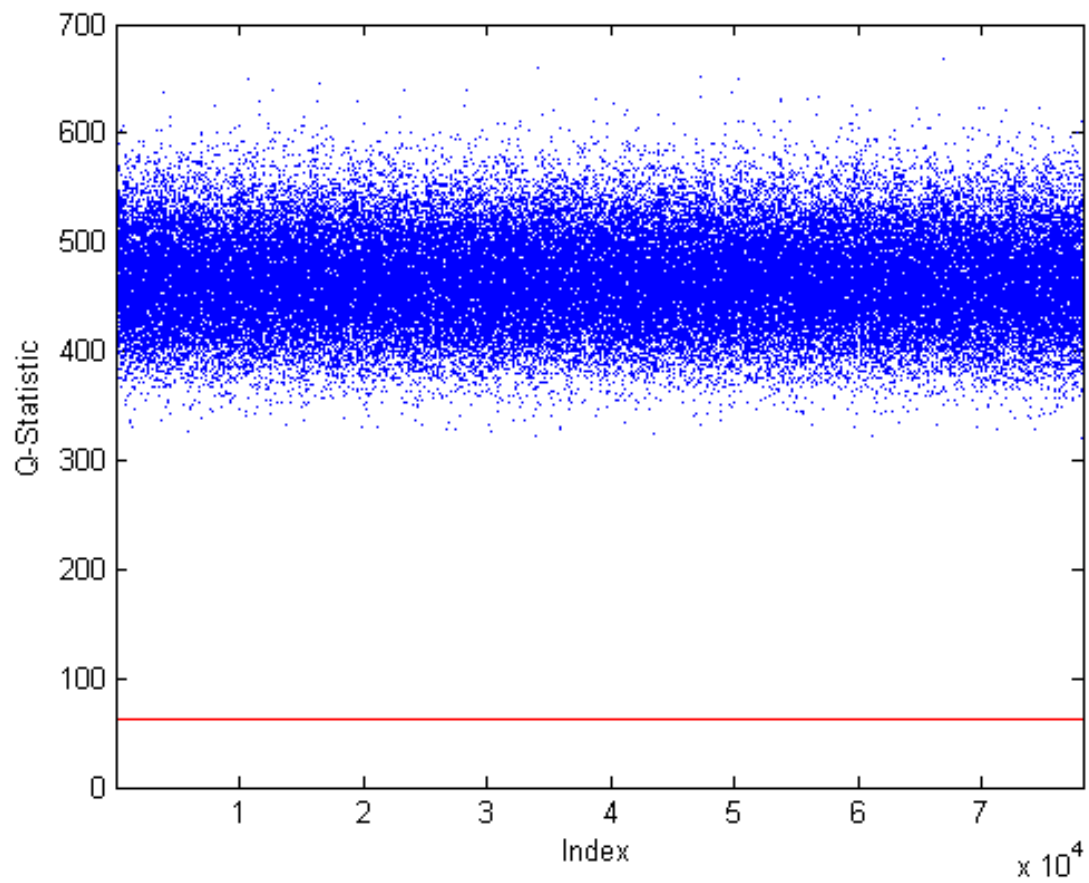
Figure 4.28. Faulty Case 1B *Q*-Statistic Plot. *Note: Only the faulty data are shown with the base case 95% confidence boundary displayed in red. There was a detectable fault.*
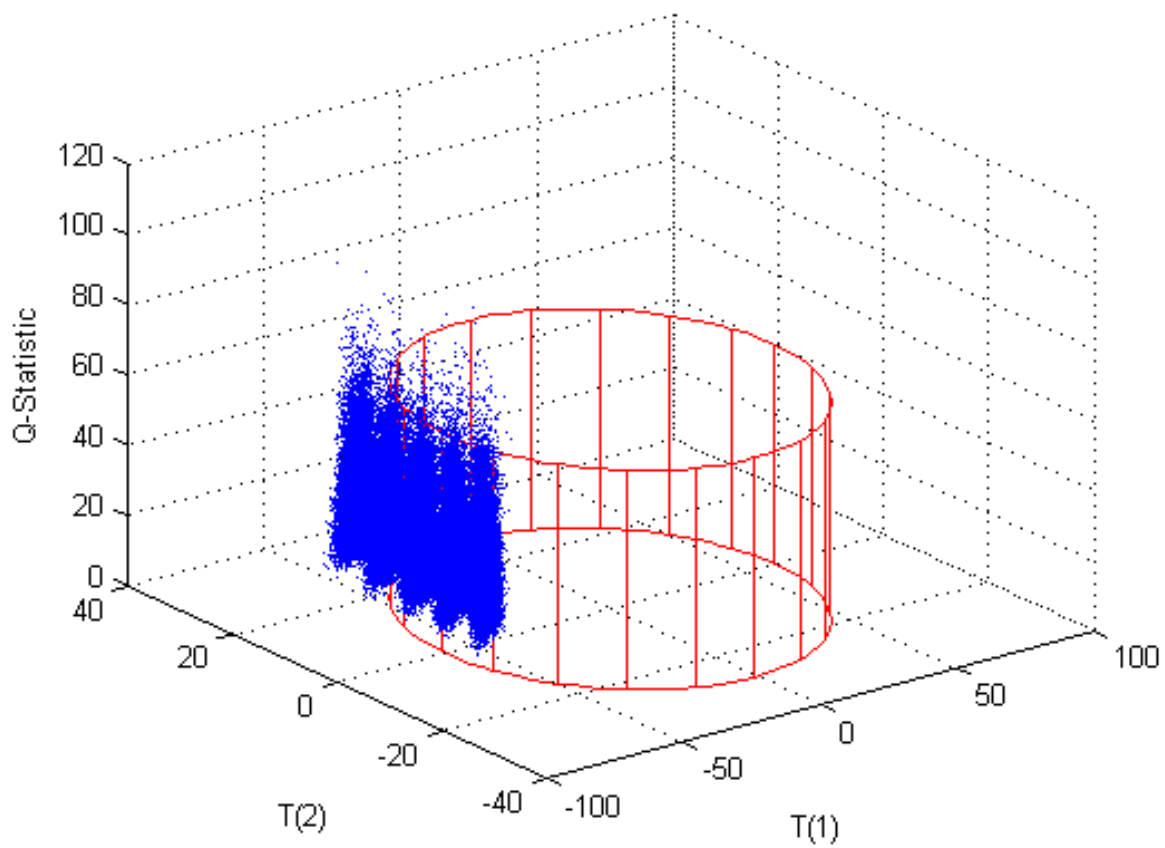
179
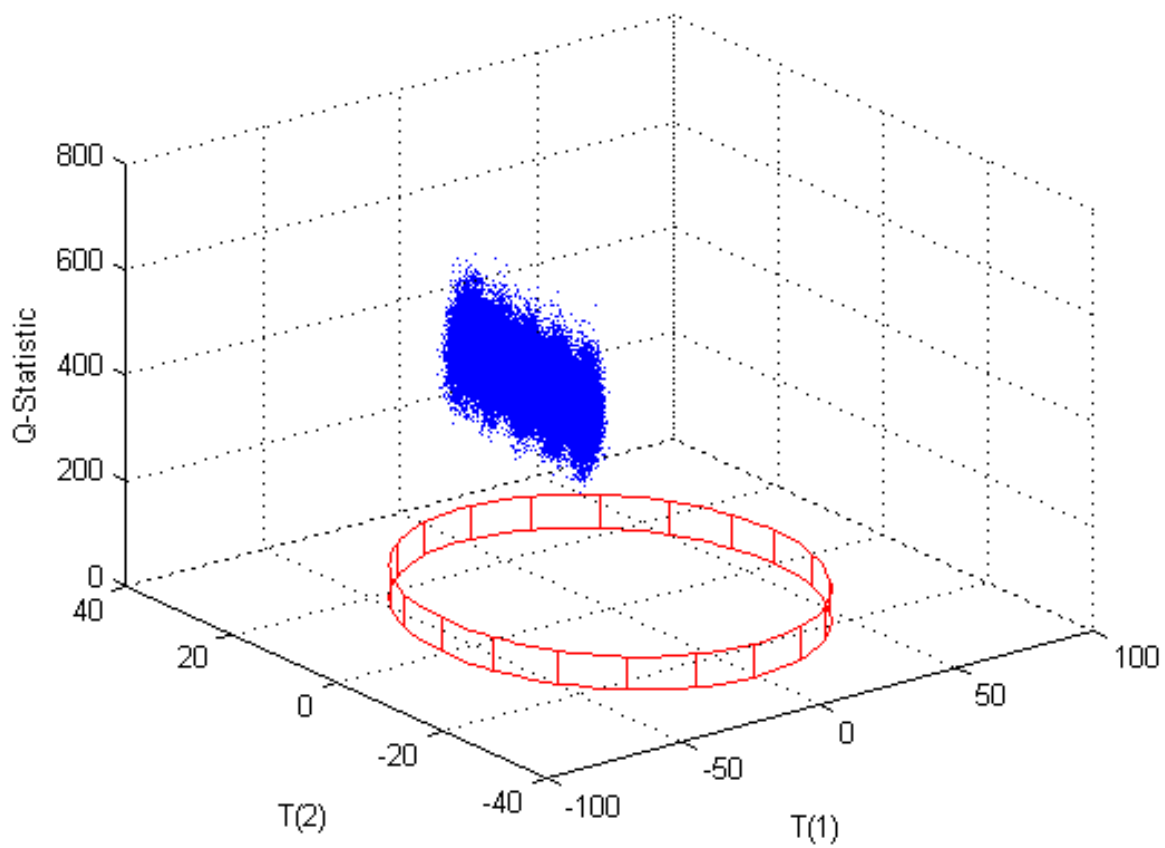
Figure 4.29. Faulty Case 1B PC1, PC2, and _Q_-Statistic Plot. _Note: Only the faulty data are shown with the base case 95% confidence boundary displayed in red. There was a detectable fault in the Q-statistic._
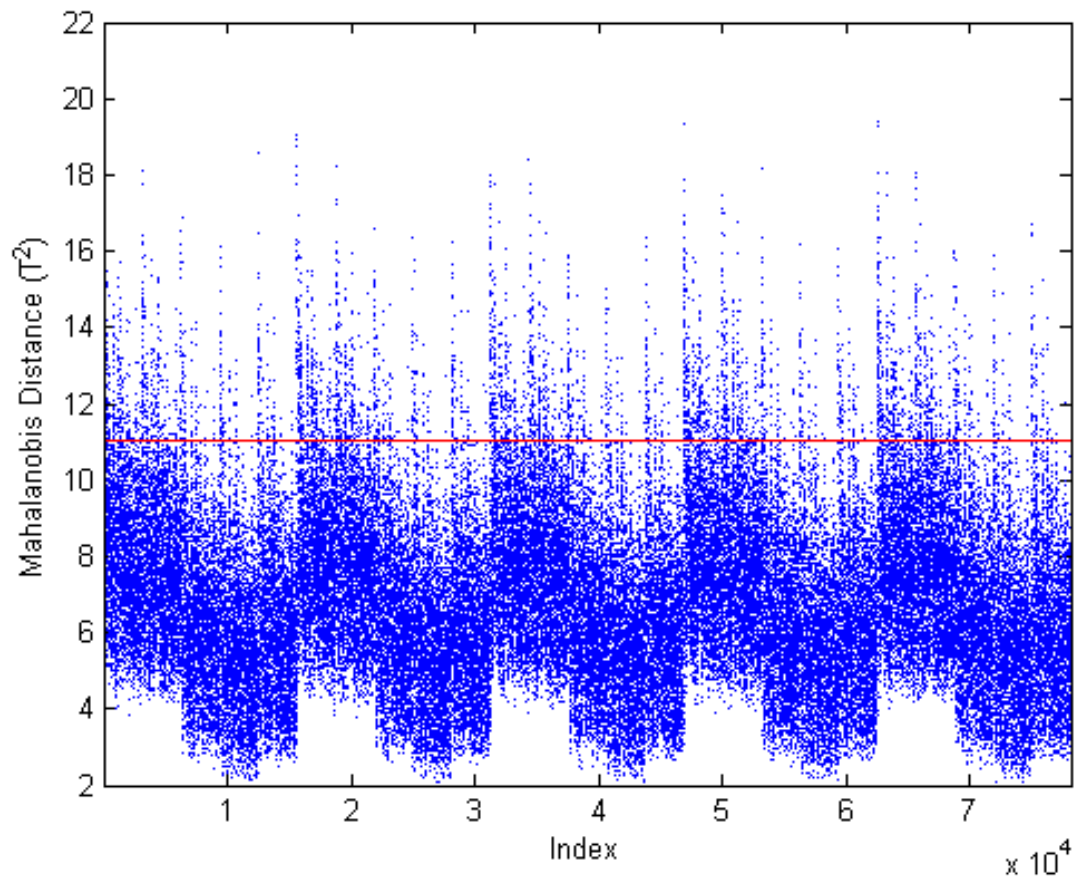
Figure 4.30. Faulty Case 1B Mahalanobis Distance Plot. *Note: Only the faulty data are shown with the base case 95% confidence boundary displayed in red. There was no detectable fault.*

4.3.1.3 Case 1C – Fifteen Percent Increase in Uranium Flow Rate

For the case of a 15% increase in the incoming uranium flow rate only, $F_{1A,U}$ [Xss(274)] was set at 57.5 kg/h with no variation in this input variable during data generation. The other input variables were allowed to vary as specified in the base case and all parameters were set at the nominal base case values. The results show that the fault in this case would most likely not be detectable in a clean since the only change occurred in the Mahalanobis distance and most of the data points were still within the 95% confidence boundary (Figure 4.31). This was only 5% over the allowed maximum for the model and the goal for detection was 10% diversion.

In this case, the model was expected to fit based on the Q-statistic, but it was expected that the Mahalanobis distance would show that the values would be somewhat outside of the accepted range which turned out to be the case. However, since this was only 5% above the maximum allowed flow rate of uranium in the base case, there was only a slight increase in the Mahalanobis distance which may not be detectable depending on operating conditions. There were no detectable faults in the scores or the Q-statistic. These results showed that the model still fits well enough based on the Q-statistic and therefore all of the relative relationships between the state variables were as expected but the range was slightly above what was expected based on the Mahalanobis distance. There was only slight increase in the Mahalanobis distance which may not be detectable and there was a slightly negative shift in the PC1 scores that was within the confidence boundary. This shift in PC1 scores was enough to increase the number of points above the 95% confidence boundary in the Mahalanobis distance.
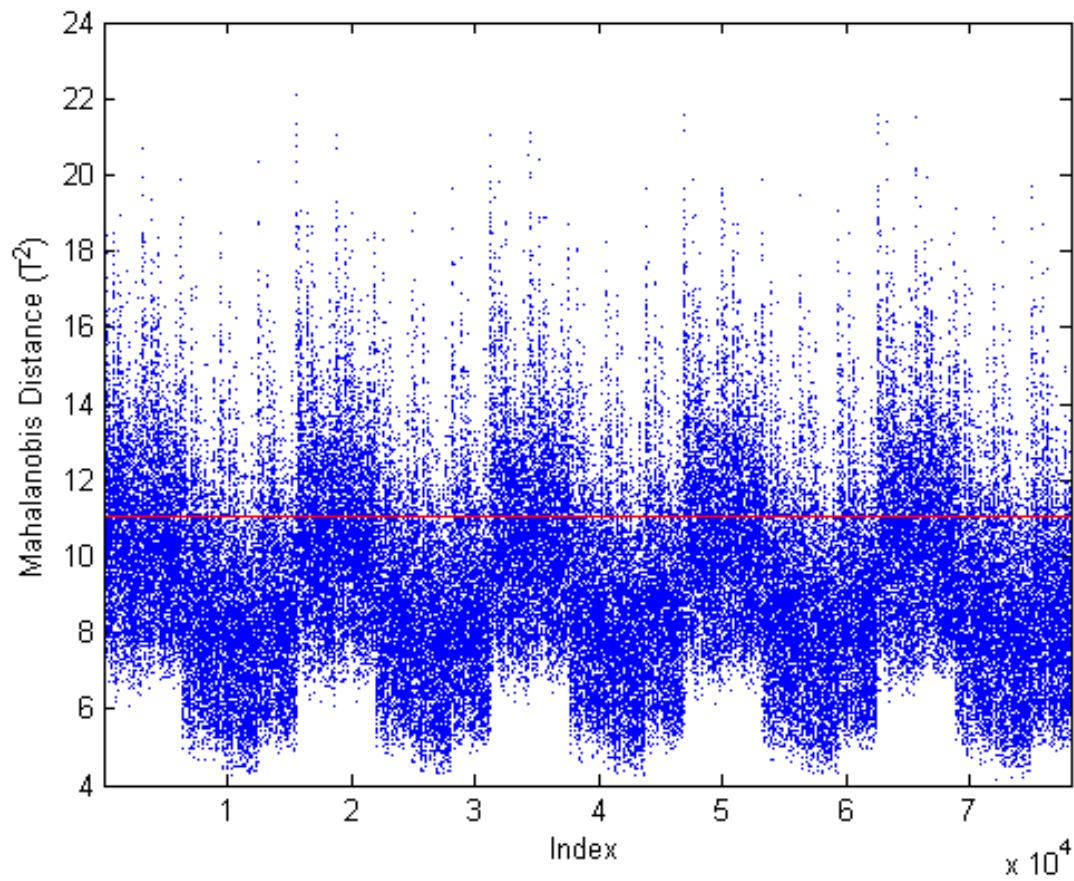
Figure 4.31. Faulty Case 1C Mahalanobis Distance Plot. *Note: Only the faulty data are shown with the base case 95% confidence boundary displayed in red. There was a slight increase but it may not be a detectable fault.*

183

4.3.1.4 Case 1D – Twenty-Five Percent Increase in Uranium Flow Rate

Since the Case 1C fault was not detectable unambiguously, higher flow rates of incoming uranium were tested. Twenty percent increase over the base case nominal value was still likely not clearly detectable since many of the data points were still within the 95% confidence boundary. The 20% increase corresponded to 10% over the maximum allowed variation in that input variable and the detection goal stated for this framework. The results of the 25% increase are shown below. As shown, this faulty case was notably detectable in the Mahalanobis distance.

This case was modeled in the same manner as Case 1C with $F_{1A,U}$ [Xss(274)] set to a constant 62.5 kg/h. There was a fault in PC1 scores which was expected since Xss(274) was a heavy contributor to PC1. However, some of the data points were still within the 95% confidence boundary meaning that there are some operating conditions under which that fault would not be detectable using just PC1 scores monitoring. There were no detectable changes in PC2 or PC3 scores. The scores plots are shown in Figures 4.32–4.35. There was a significant increase in the Mahalanobis distance (Figure 4.36) which was expected since this case was outside the normal operating conditions and an overall shift in the PC1 scores. There were no detectable faults in the Q-statistic which was also expected since no parameters were changed (Figures 4.37–4.38). The results for a 25% increase were expected to be the same as for the 15% increase but with larger and more clearly detectable faults which was the case. Based on these results, a 25% increase in uranium feed rate is deemed detectable.

Figure 4.32. Faulty Case 1D Scores Plot for PC1 and PC2. *Note: Only the faulty data are shown with the base case 95% confidence boundary displayed in red. There was a fault in PC1 scores.*

Figure 4.33. Faulty Case 1D Scores Plot for PC1 and PC3. *Note: Only the faulty data are shown with the base case 95% confidence boundary displayed in red. There was a fault in PC1 scores.*

186

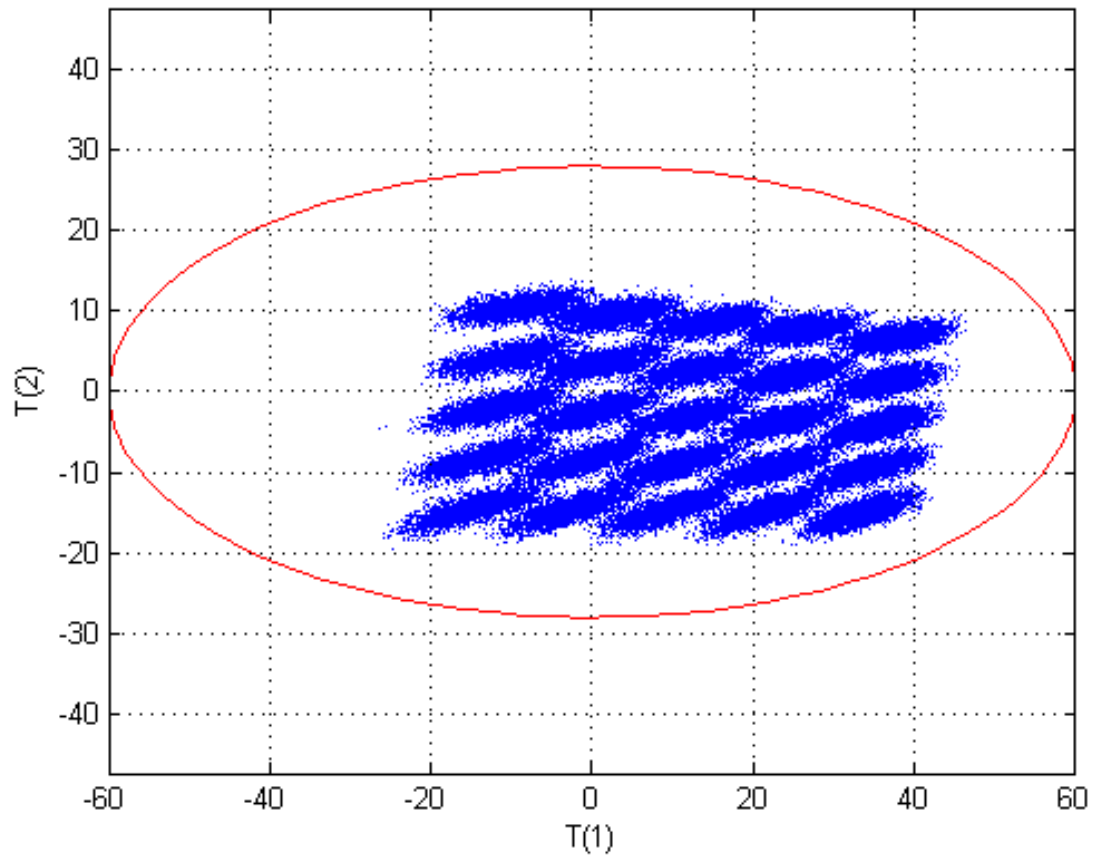**Figure 4.34. Faulty Case 1D Scores Plot for PC2 and PC3.** *Note: Only the faulty data are shown with the base case 95% confidence boundary displayed in red. There was no detectable fault.*
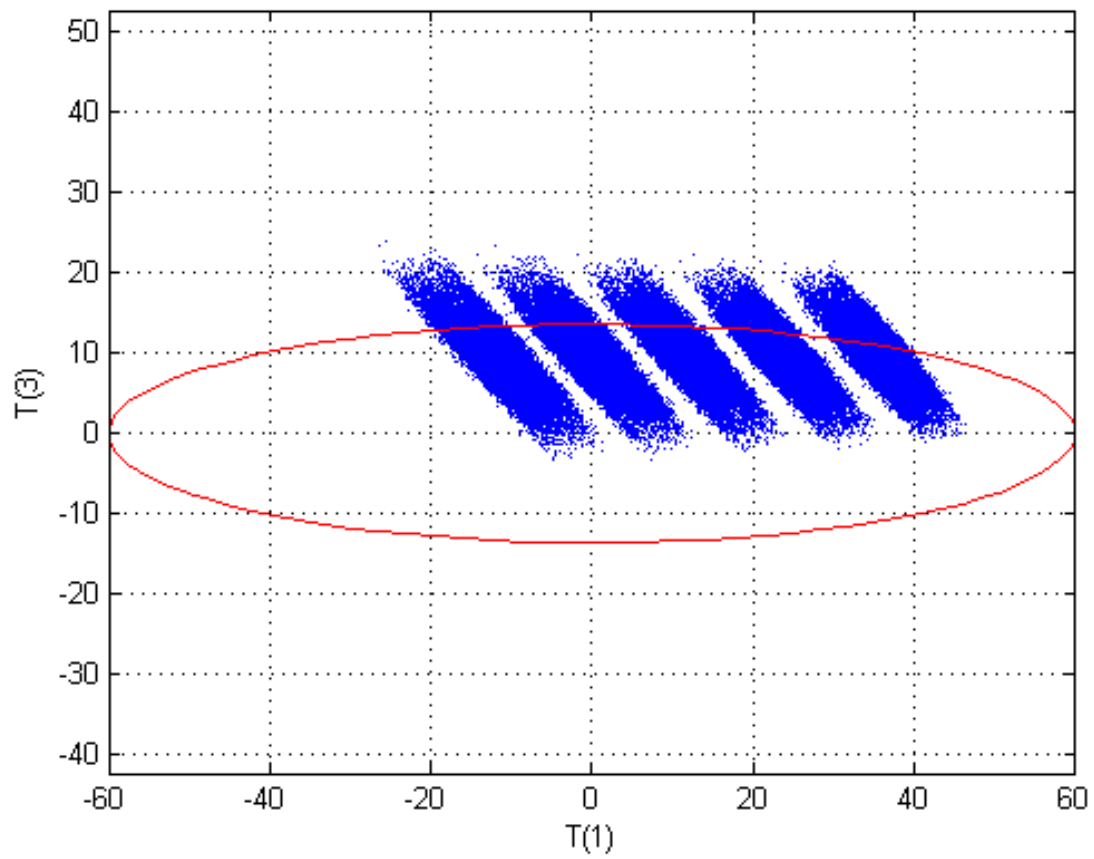
Figure 4.35. Faulty Case 1D 3D Scores Plot for PC1, PC2, and PC3. *Note: Only the faulty data are shown with the base case 95% confidence boundary displayed in red. There was a fault in PC1 scores.*

Figure 4.36. Faulty Case 1D Mahalanobis Distance Plot. *Note: Only the faulty data are shown with the base case 95% confidence boundary displayed in red. There was a detectable fault.*
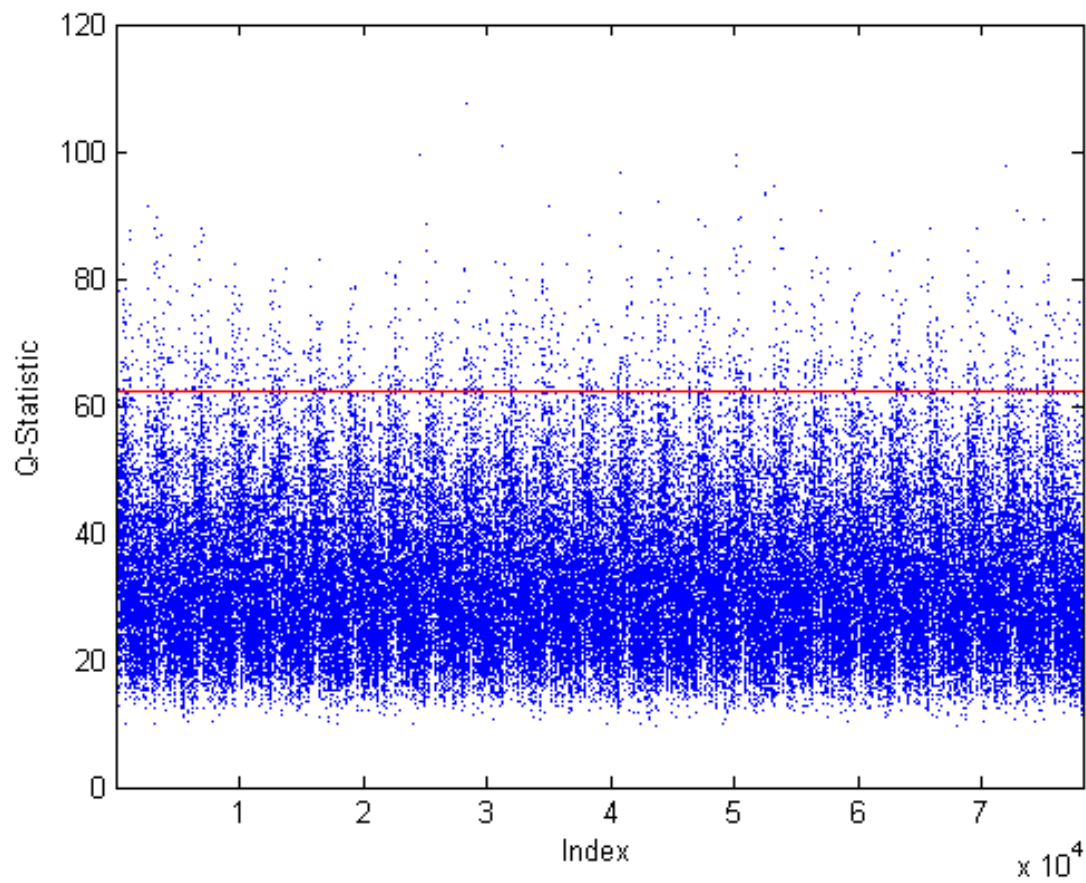
Figure 4.37. Faulty Case 1D *Q*-Statistic Plot. *Note: Only the faulty data are shown with the base case 95% confidence boundary displayed in red. There was no detectable fault.*

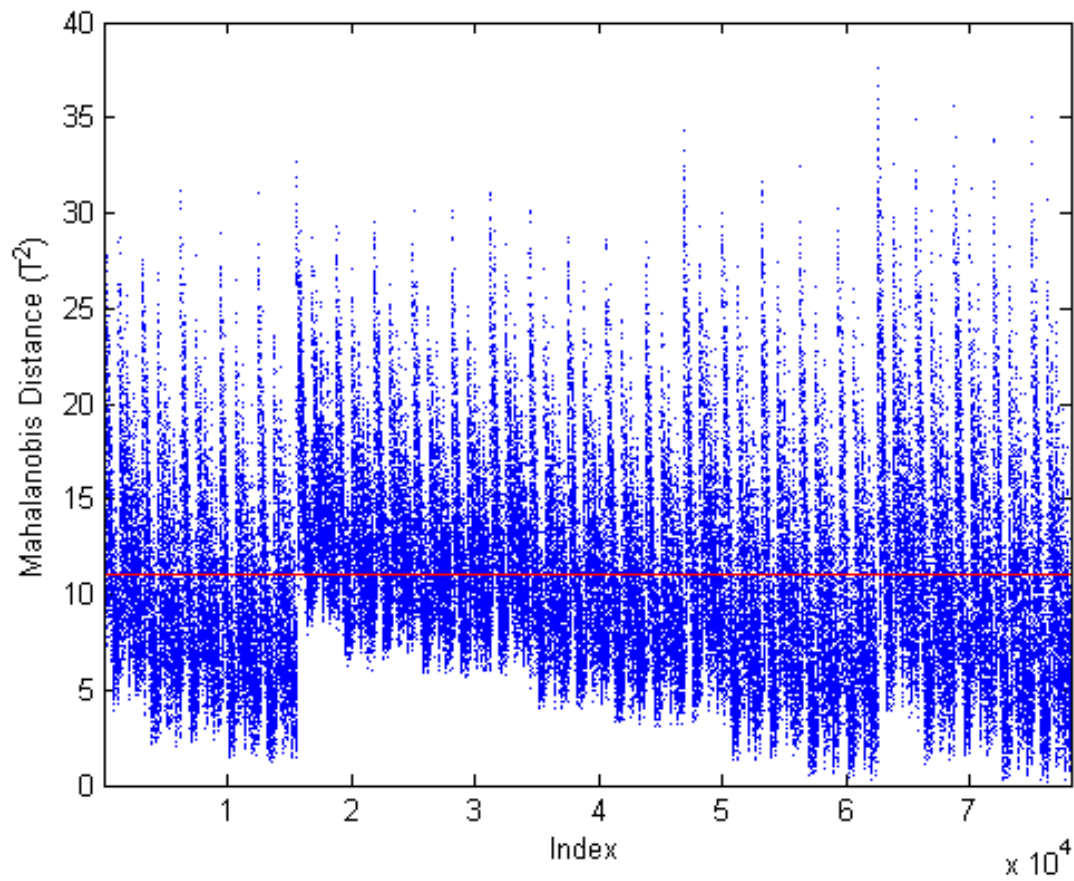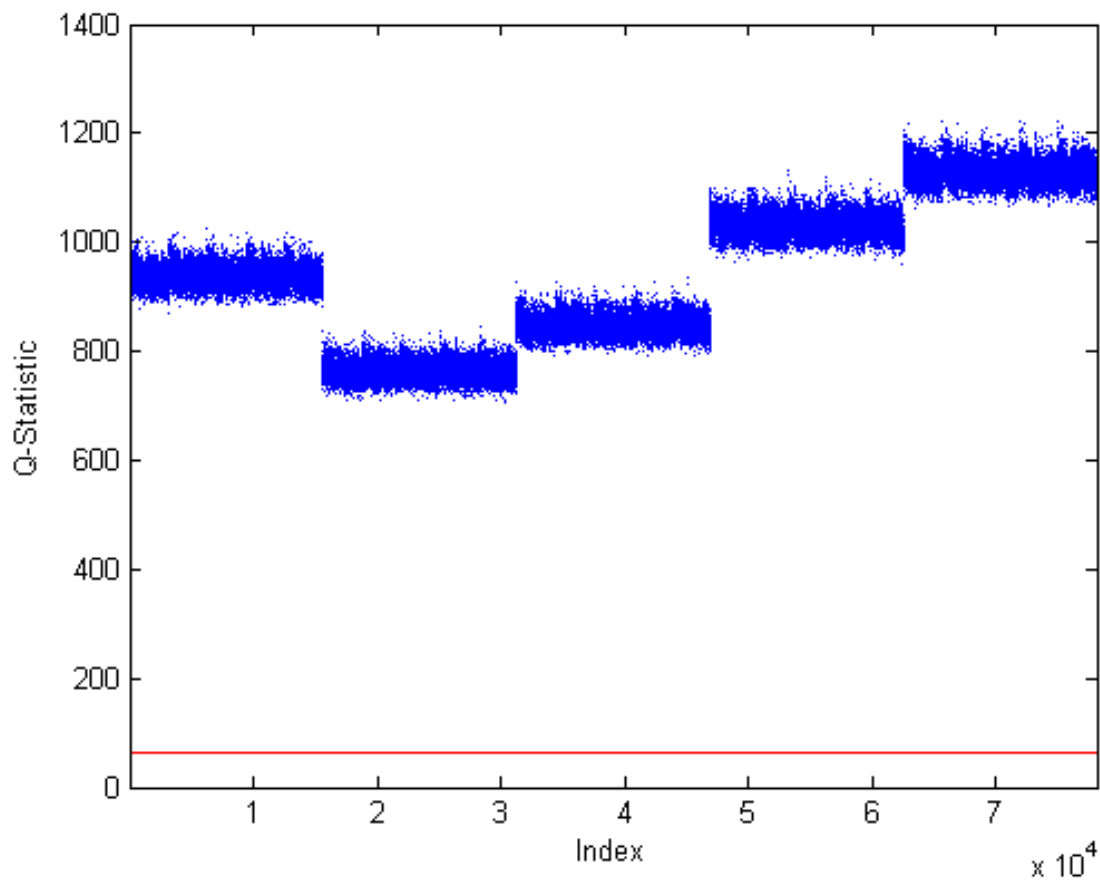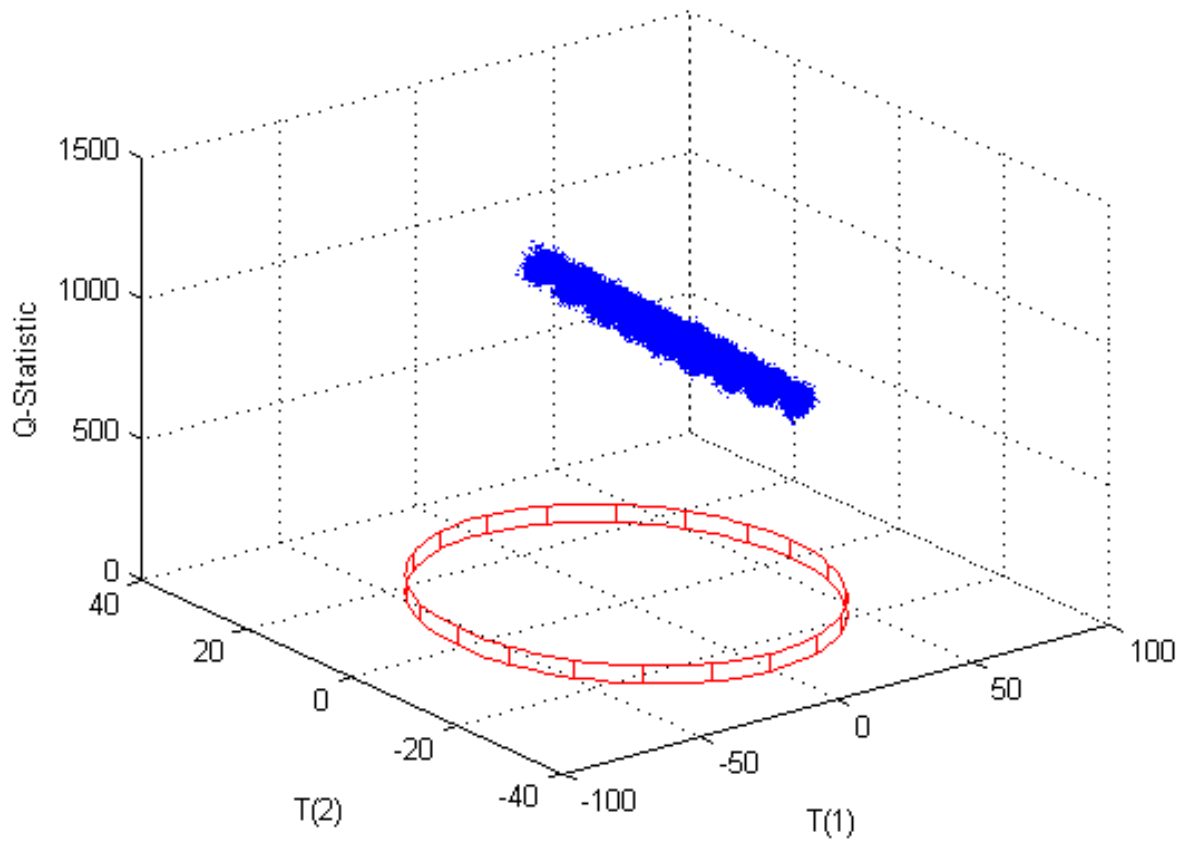**Figure 4.38. Faulty Case 1D PC1, PC2, and Q-Statistic Plot.** *Note: Only the faulty data are shown with the base case 95% confidence boundary displayed in red. There was a fault in PC1 scores.*

4.3.2 Case 2

For the second faulty case, the purity of the uranium fed to the dissolver was changed by changing the uranium input stream composition from 85 wt-% U_3O_8 and 15 wt-% impurities (7.5 wt-% soluble impurities and 7.5 wt-% insoluble impurities) to 90 wt-% U_3O_8 and 10 wt-% impurities (5 wt-% soluble impurities and 5 wt-% insoluble impurities). No variation in uranium purity was built into the base case PCA model. The results show that the fault in this case was clearly detectable in the Q-statistic and may also be detectable in PC3 scores and the Mahalanobis distance depending on operating conditions.

Since this parameter was not tested in the original sensitivity analysis, a quick sensitivity analysis was completed for the uranium purity. The sensitivity of all of the state variables to this parameter was developed by changing the purity of the incoming uranium by ±10%. The uranium purity was changed by changing the mass fractions in Stream 1A. The mass fractions of the impurities were also changed so that the mass fractions totaled one. Additionally, the soluble and insoluble impurities were assumed to be equal fractions as in the base case. The results show that none of the uranium-bearing streams were sensitive to changes in the purity of the incoming uranium because the feed to the plant was specified based on mass of elemental uranium not concentration, therefore changing the purity did not change the incoming amount of uranium. The 43 state variables that were sensitive to changes in mass fractions of Stream 1A were the insoluble and soluble components in Modules 1–3. The sensitivity factor was -6.1 for a +10% change in purity and -7.4 for a -10% change in purity. Therefore, the response to changes in uranium purity was nonlinear.

Based on the fact that the incoming uranium flow rate is specified based on the mass elemental uranium, the total flow rate of Stream 1A (F_{1A}) was calculated as discussed in Section 3.2.1.1 and shown in Eq. (4.3.2.1) in terms of Xss(274). Therefore, F_{1A} changes with changes in purity but Xss(274) does not.

$$F_{1A} = \frac{Xss(274)}{3*MW_U} * \frac{MW_{18}}{x_{1A,18}} \tag{4.3.2.1}$$

Therefore, the equations where the changes in uranium purity appear in the model are in Eqs. (3.2.1.10) and (3.2.1.11) which are restated here in terms of the state variables. These are the material balances for the insoluble and soluble impurities in Stream 1 of Module 1.

$$F_{1A} * x_{1A,20} * \frac{1000}{MW_{20}} + Xss(60) - Xss(5) = 0 \tag{3.2.1.10}$$

$$F_{1A} * x_{1A,21} * \frac{1000}{MW_{21}} + Xss(61) - Xss(6) = 0 \tag{3.2.1.11}$$

The 43 state variables that were sensitive to changes in mass fractions of Stream 1A moderately loaded PC1 and slightly loaded PC3. Those same 43 state variables result in a nominal reduction of approximately 37% in comparison with the nominal base case solution. There was a slight shift in both

PC1 and PC2 scores but no detectable fault was observed since all of the data points were within the 95% confidence boundary for normal operation (Figure 4.39). There was also a shift in PC3 scores (Figures 4.40–4.42). However, this fault would only be detectable in PC3 scores under certain operating conditions since approximately 50% of the data points were still within the 95% confidence boundary. There was also an increase in the Mahalanobis distance (Figure 4.43), but this shift may not result in a detectable fault because many of the data points were within the 95% confidence boundary. This increase was not initially expected since this fault did not change the operating ranges. However, increasing the uranium purity decreases the impurities and therefore changes the molar flow rates of the waste streams that contain the impurities. Therefore, this case does change the operating conditions for non-uranium components. There was a significant increase in the Q-statistic (Figures 4.44–4.45). An increase was expected in the Q-statistic since changing the purity changes some of the parameter values and therefore the relative relationship between the state variables would be different. A relatively small (~6%) increase in the purity of the uranium feed produced a highly detectable fault in the Q-statistic as well as potentially detectable faults in PC3 scores and the Mahalanobis distance.

Monitoring the uranium feed for both flow rate and uranium content would be the recommended approach for detecting this type of fault. However, monitoring the streams exiting each major process (e.g., dissolution, solvent extraction, fluorination) as product or waste for flow rate and uranium content would also detect this fault. A summary of Case 2 results is provided in Table 4.22.

Table 4.22. Summary of Faulty Case 2

Summary of Faulty Case					
Priority	**Module**	**Faulty Variable**	**Base Case Value**	**Faulty Value**	**Physical Description**
Low	1	$x_{1A,18}$	0.85	0.90	Increase the incoming uranium purity by 5.9% and decrease the impurities

Summary of Results				
	PC1 Scores	**PC2 Scores**	**PC3 Scores**	**T2**	**Q**
Direction	+	-	+	~+	+++
Detectability	No	No	Possibly	Possibly	Yes

Figure 4.39. Faulty Case 2 Scores Plot for PC1 and PC2. *Note: Only the faulty data are shown with the base case 95% confidence boundary displayed in red. There was a slight shift in both PC1 and PC2 scores but no fault was detectable.*

Figure 4.40. Faulty Case 2 Scores Plot for PC1 and PC3. *Note: Only the faulty data are shown with the base case 95% confidence boundary displayed in red. There was a shift in PC3 scores but the fault may not be detectable depending on operating conditions.*
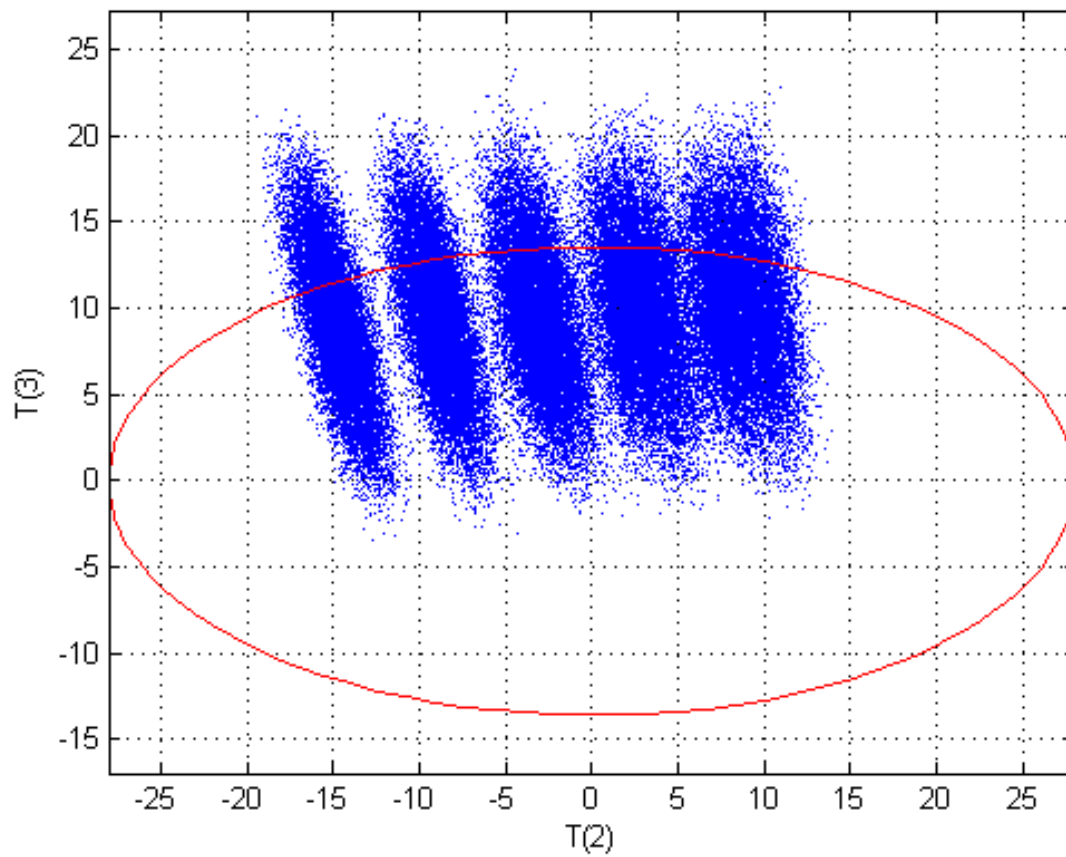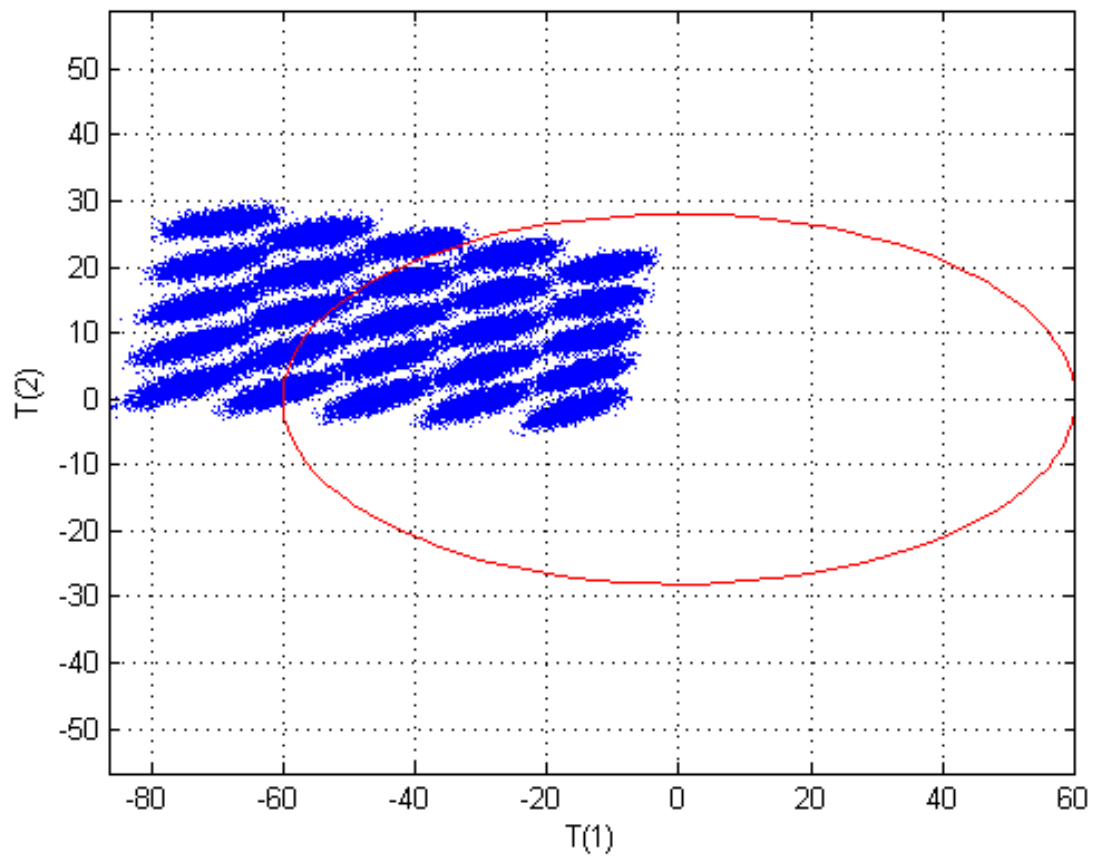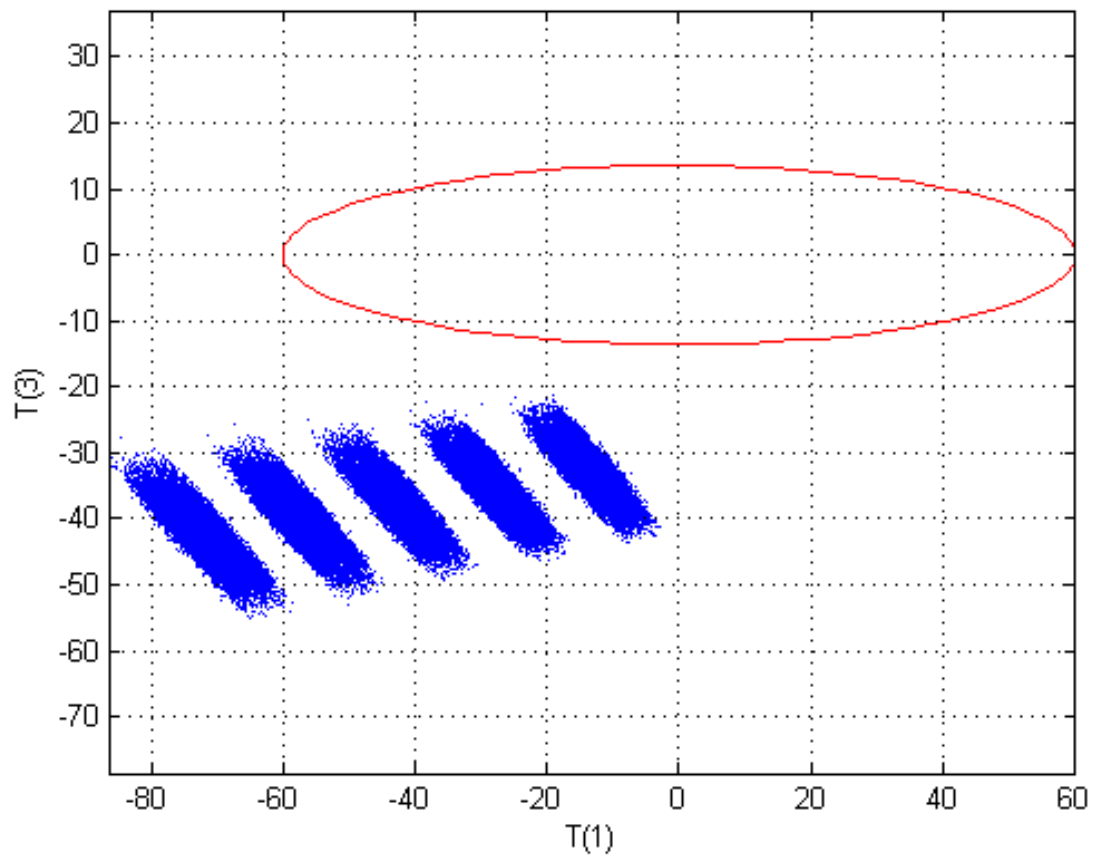
Figure 4.41. Faulty Case 2 Scores Plot for PC2 and PC3. *Note: Only the faulty data are shown with the base case 95% confidence boundary displayed in red. There was a shift in PC3 scores but the fault may not be detectable depending on operating conditions.*
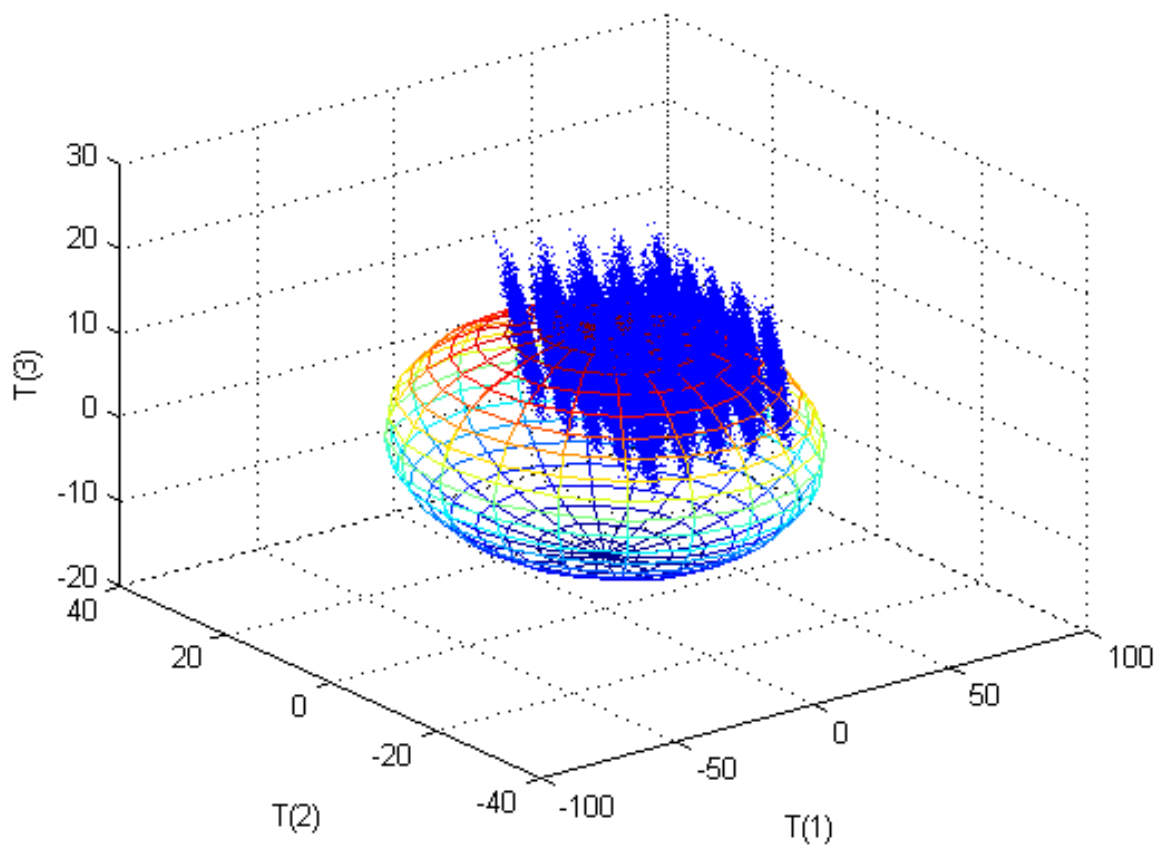
Figure 4.42. Faulty Case 2 3D Scores Plot for PC1, PC2, and PC3. *Note: Only the faulty data are shown with the base case 95% confidence boundary displayed as an ellipsoid. There was a shift in all PC scores with the most noticeable shift being in PC3 scores but the fault may not be detectable depending on operating conditions.*

197

Figure 4.43. Faulty Case 2 Mahalanobis Distance Plot. *Note: Only the faulty data are shown with the base case 95% confidence boundary displayed in red. There was a shift but the fault may not be detectable depending on operating conditions.*

Figure 4.44. Faulty Case 2 *Q***-Statistic Plot.** *Note: Only the faulty data are shown with the base case 95% confidence boundary displayed in red. There was a detectable fault.*

Figure 4.45. Faulty Case 2 PC1, PC2, and *Q*-Statistic Plot. *Note: Only the faulty data are shown with the base case 95% confidence boundary displayed in red. There was a detectable fault in the Q-statistic.*

4.3.3 Case 3

For the third faulty case, the effect of inefficient dissolver operations in Module 1 was investigated. Inefficient operations would result in the uranium not being completely dissolved and therefore additional uranium would leave the process as waste. This case was modeled by changing the extent of reaction for the dissolution reaction, X_{Mod1A}, from 0.9799 to 0.95. Based on the sensitivity analysis, all of the primary state variables were sensitive ($\gamma = 0.61$) to a decrease in X_{Mod1A}. Two of the primary state variables [Xss(41) and Xss(92)], which were the U_3O_8 in waste Streams 8 and 16, were extremely sensitive to a decrease in X_{Mod1A} and resulted in a sensitivity factor of -51.3. An additional 39 non-primary state variables also had a sensitivity factor of -51.3. These state variables were the U_3O_8 throughout the process; these were not considered primary because the molar flow rate value was very small. The results show that this fault was clearly detectable in PC3 scores, the Mahalanobis distance, and the Q-statistic.

This parameter appears in the Module 1A component mole balances [Eqs. (3.2.1.6)–(3.2.1.9)] which are restated here in terms of state variable numbers.

$$F_{2A,1} + F_{3A,1} + \text{Xss}(56) - \text{Xss}(1) + n_{Mod1,1} * X_{Mod1A} * \left(F_{1A,18} + \text{Xss}(59)\right) = 0 \qquad (4.3.3.1)$$

$$F_{2A} * x_{2A,9} * \frac{1000}{MW_9} + \text{Xss}(57) - \text{Xss}(2) + n_{Mod1,9} * X_{Mod1A} * \left(F_{1A,18} + \text{Xss}(59)\right) = 0 \qquad (4.3.3.2)$$

$$\text{Xss}(58) - \text{Xss}(3) + n_{Mod1,14} * X_{Mod1A} * \left(F_{1A,18} + \text{Xss}(59)\right) = 0 \qquad (4.3.3.3)$$

$$F_{1A,18} + \text{Xss}(59) - \text{Xss}(4) + n_{Mod1,18} * X_{Mod1A} * \left(F_{1A,18} + \text{Xss}(59)\right) = 0 \qquad (4.3.3.4)$$

The 41 state variables that were most sensitive to changes in this parameter increased 152% due to this fault. These state variables were mostly moderate contributors to PC1 and slight contributors to PC3. There was a slight overall shift in both PC1 and PC2 scores which would result in a detectable fault using trend monitoring (Figure 4.46). There was a significant shift in PC3 scores(Figures 4.47–4.49) which would result in a clearly detectable fault under all operating conditions since all of the data points were outside the 95% confidence boundaries. The fault in PC3 scores was expected because PC3 was heavily loaded by state variables that represented the uranium components in both the product and waste streams of Modules 1–3 and the product streams in Modules 4–5. These state variables would be directly affected by this change. This change resulted in a significant increase in the Mahalanobis distance (Figure 4.50). This fault was expected since a change in the extent of reaction would affect the amount of material in the streams downstream of that parameter. There was also a significant increase in the Q-statistic (Figures 4.51–4.52). Additionally, a fault was expected in the Q-statistic since changing the extent of reaction constitutes a change in the parameters and therefore the relative relationship between the state variables would be different. A relatively small (~3%) reduction in the extent of reaction produced a significant and clearly detectable faults in PC3 scores, the Mahalanobis distance, and the Q-statistic diagnostic plots. Such drastic deviations from that of the base case profile reflect the

201

higher sensitivity of the process operation to the incomplete dissolution of U_3O_8. Due to this, it is recommended that the waste streams from both the dissolution and solvent extraction processes be monitored for both flow rate and uranium content. Table 4.23 summarizes this faulty case.

Table 4.23. Summary of Faulty Case 3

Summary of Faulty Case					
Priority	Module	Faulty Variable	Base Case Value	Faulty Value	Physical Description
Medium	1	X_{Mod1A}	0.9799	0.95	Inefficient dissolver operations resulted in less U_3O_8 converted to UN and more U in waste streams
Summary of Results					
	PC1 Scores	PC2 Scores	PC3 Scores	T2	Q
Direction	-	+	--	+++	++++
Detectability	Possibly	Possibly	Yes	Yes	Yes

Figure 4.46. Faulty Case 3 Scores Plot for PC1 and PC2. *Note: Only the faulty data are shown with the base case 95% confidence boundary displayed in red. There was a shift in both PC1 and PC2 scores but the fault may not be detectable.*

Figure 4.47. Faulty Case 3 Scores Plot for PC1 and PC3. *Note: Only the faulty data are shown with the base case 95% confidence boundary displayed in red. There was a fault in both PC1 and PC3 scores.*
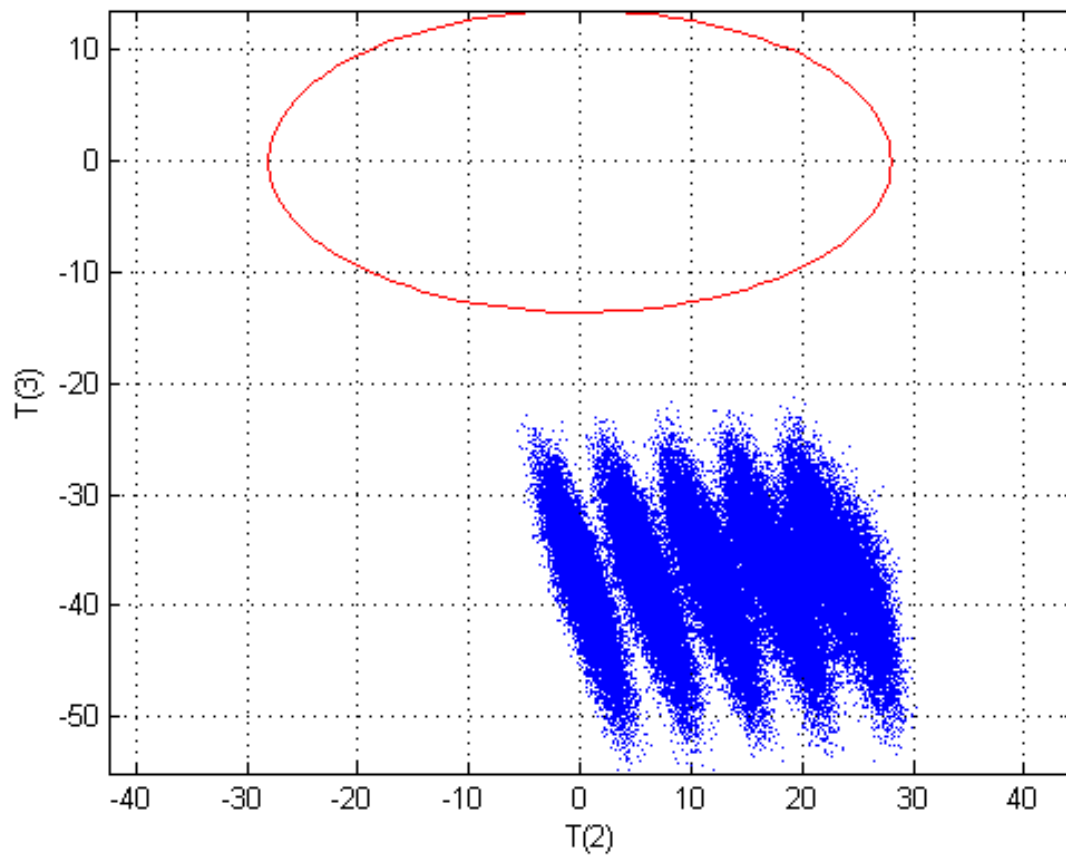
Figure 4.48. Faulty Case 3 Scores Plot for PC2 and PC3. *Note: Only the faulty data are shown with the base case 95% confidence boundary displayed in red. There was a fault in both PC2 and PC3 scores.*
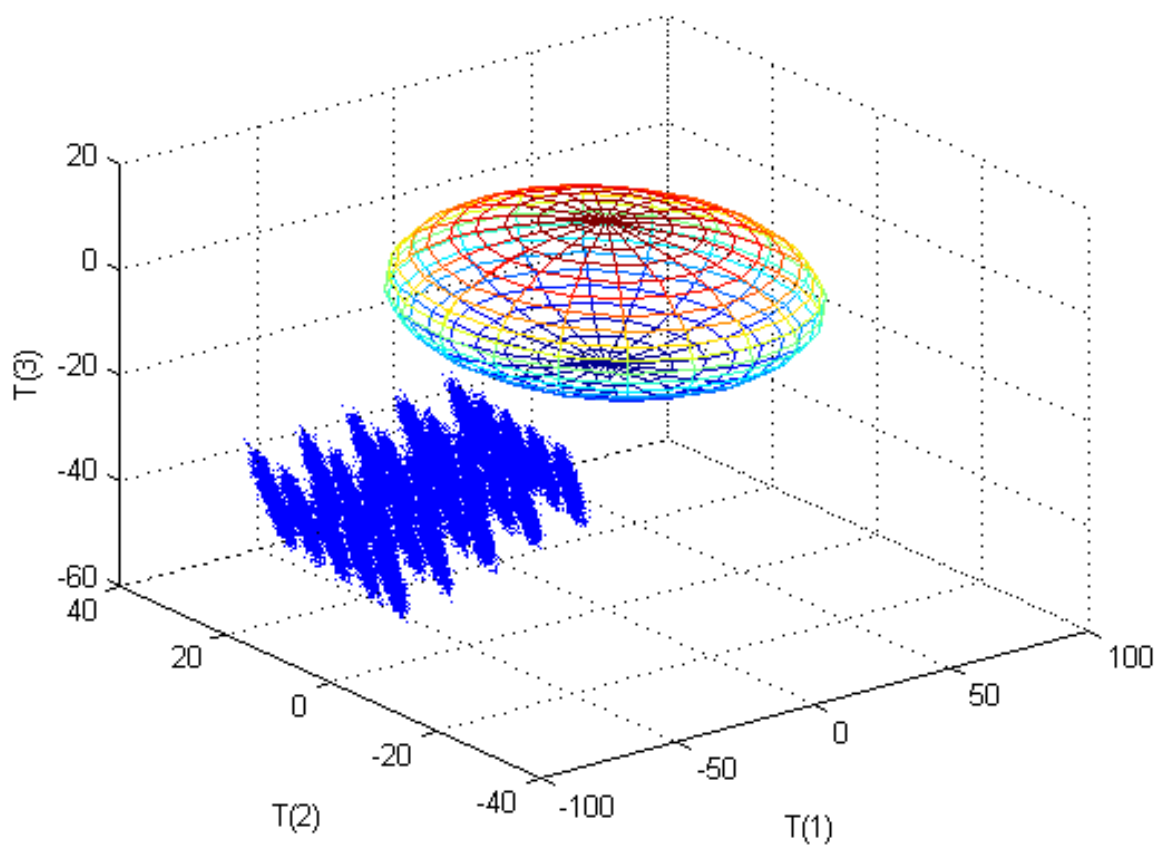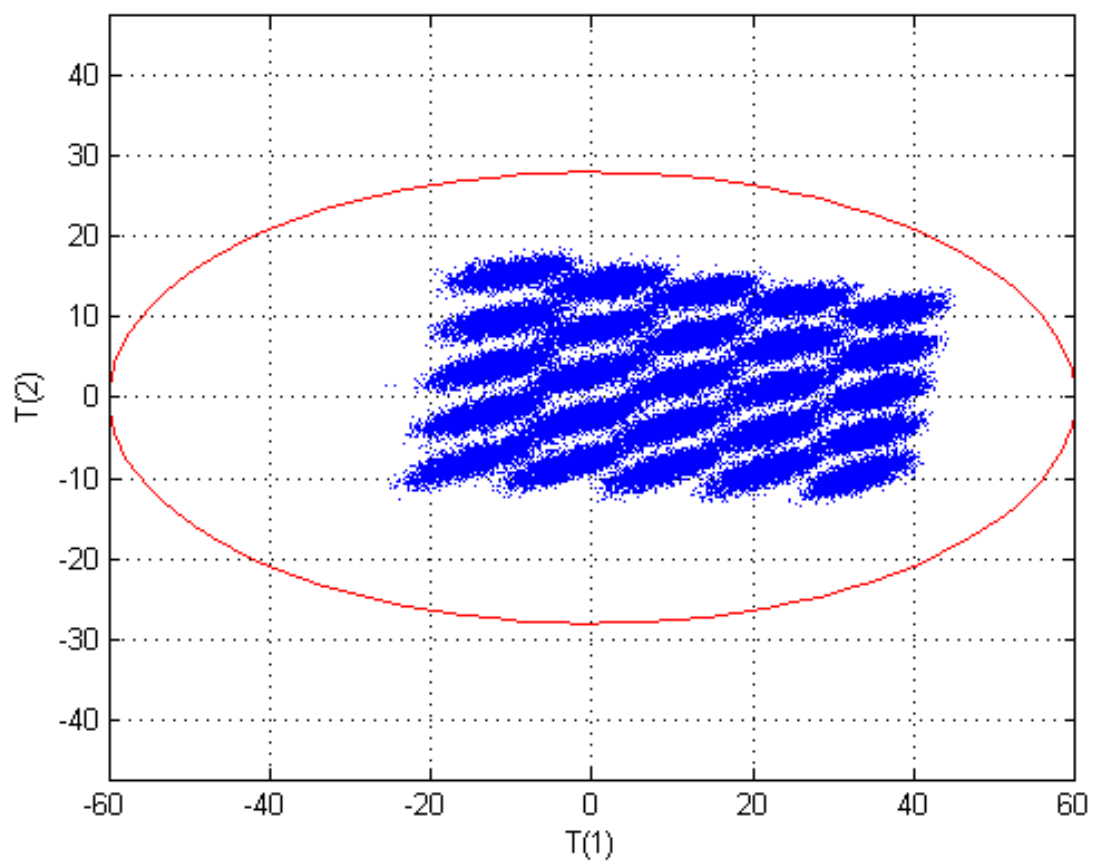
Figure 4.49. Faulty Case 3 3D Scores Plot for PC1, PC2, and PC3. *Note: Only the faulty data are shown with the base case 95% confidence boundary displayed as an ellipsoid. There was a detectable fault in all three scores.*
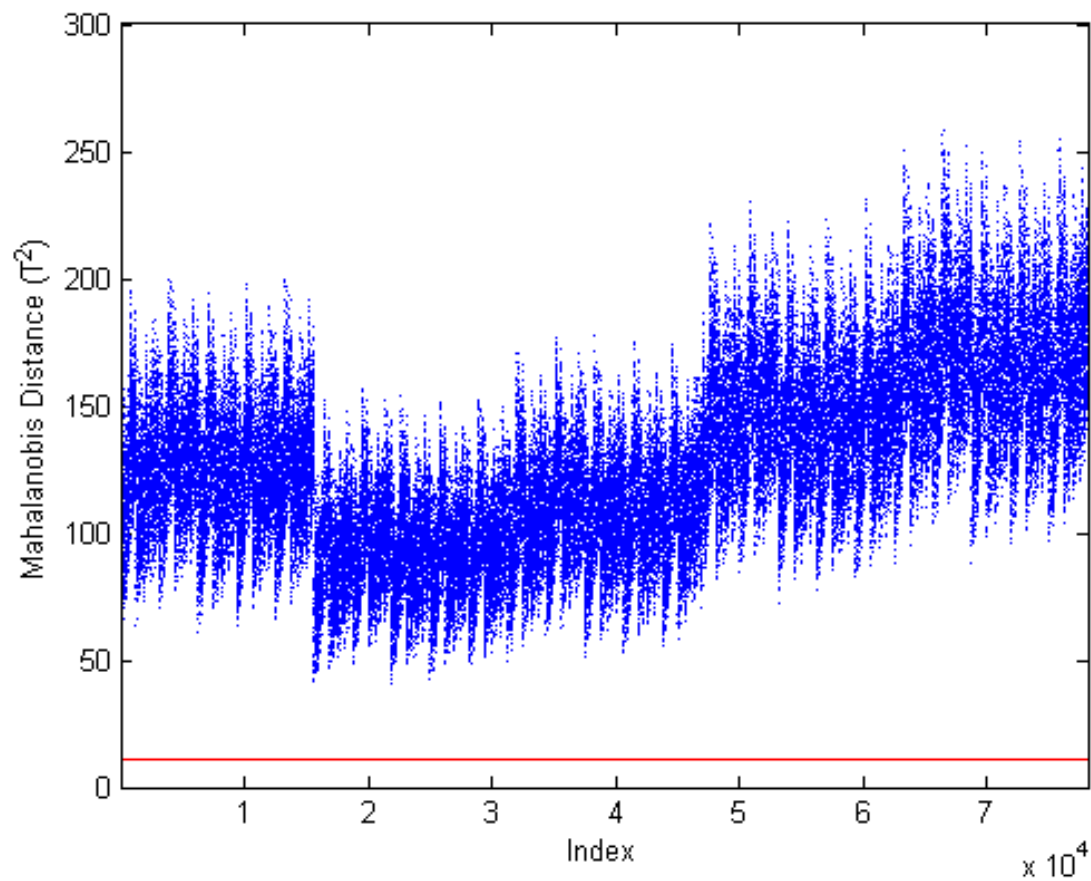
Figure 4.50. Faulty Case 3 Mahalanobis Distance Plot. *Note: Only the faulty data are shown with the base case 95% confidence boundary displayed in red. There was a detectable fault.*
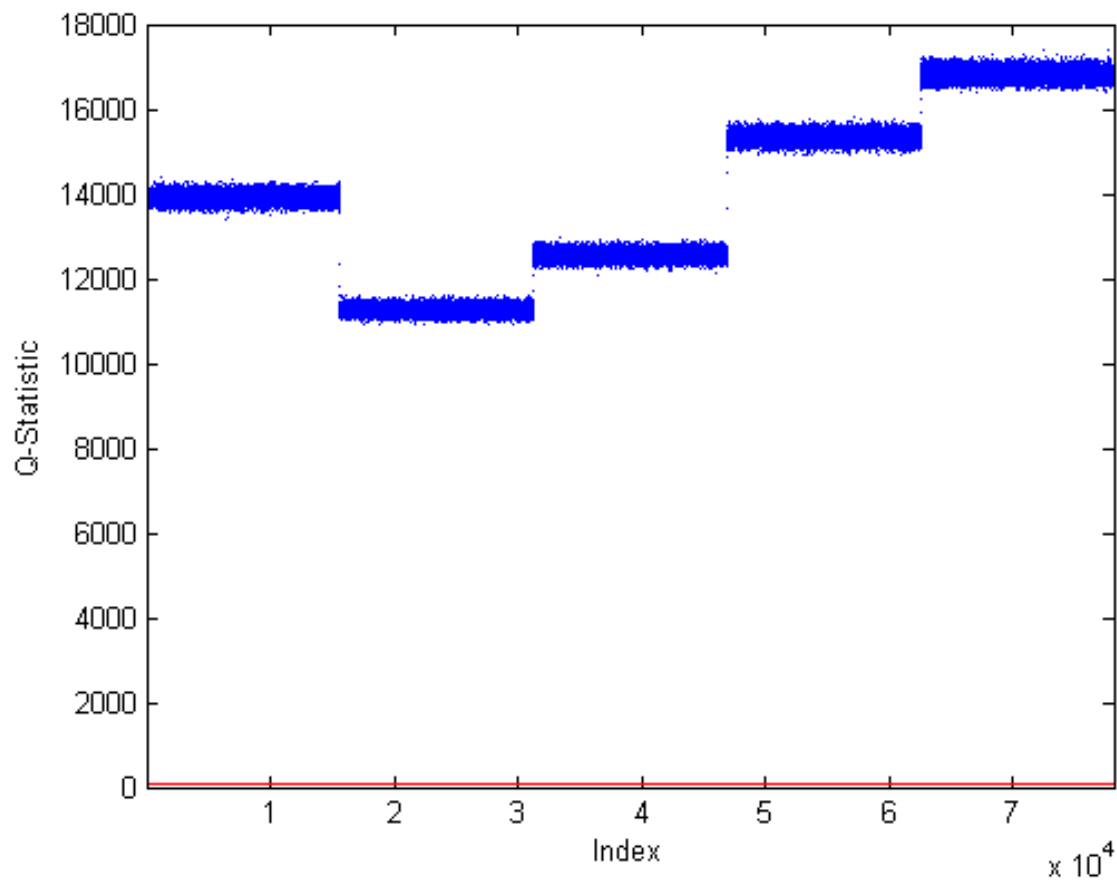
Figure 4.51. Faulty Case 3 *Q-Statistic Plot. Note: Only the faulty data are shown with the base case 95% confidence boundary displayed in red. There was a detectable fault.*
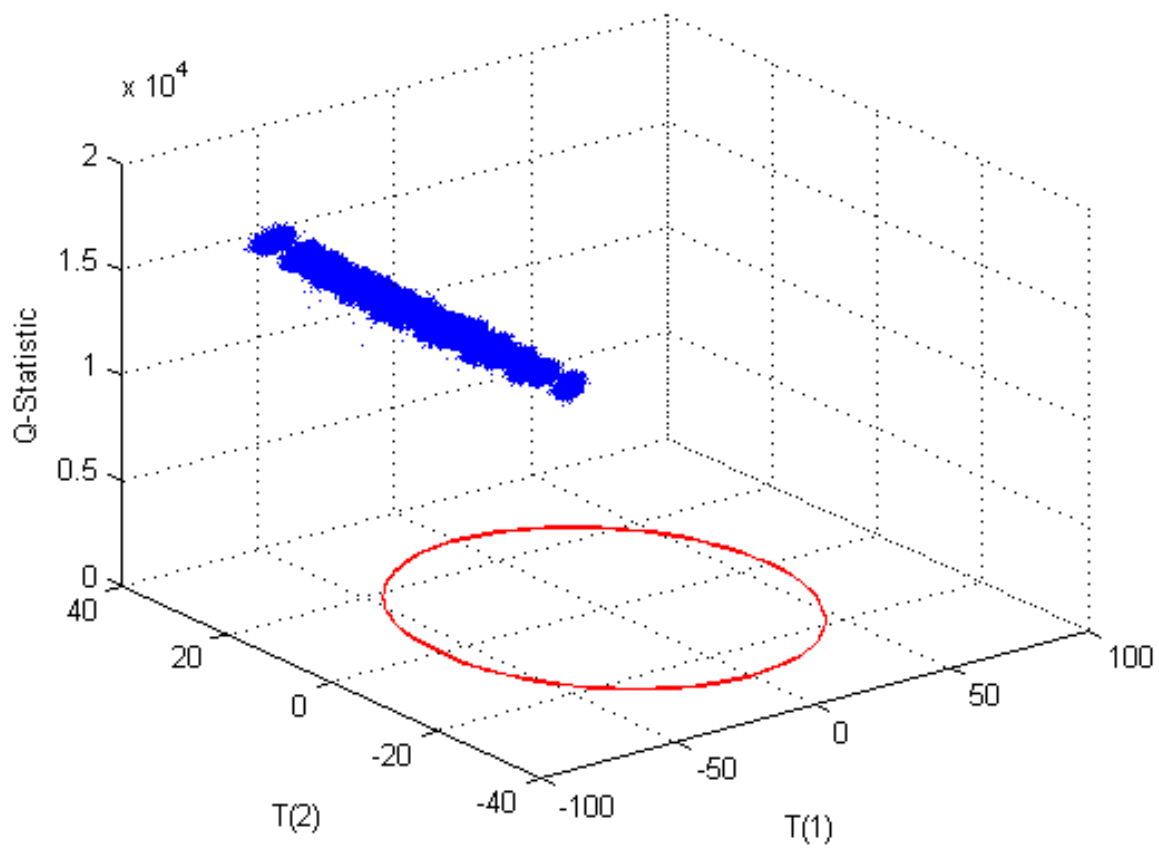
Figure 4.52. Faulty Case 3 PC1, PC2, and *Q*-Statistic Plot. *Note: Only the faulty data are shown with the base case 95% confidence boundary displayed in red. There was a detectable fault.*

4.3.4 Case 4

For the fourth faulty case, inefficient operations of the re-extraction of uranium from the organic phase in Module 2 were investigated. Inefficient re-extraction would result in additional uranium being diverted to the organic waste stream. This case was modeled by changing the initial value of the column fractionation parameter for the uranyl nitrate in Module 2D, $K_{Mod2D,14}$, which corresponds to the fourth input variable [Xss(277)], from 0.999 to 0.9. The results show that this reasonably sized (~10%) reduction in the filter fractionation may be detectable in the PC3 scores, the Mahalanobis distance, and the Q-statistic but it would only be detectable under certain operating conditions, or would be detectable as a trending shift when the data points are still be within the 95% confidence boundary.

This parameter appears in only one place in the model as shown in Eq. (3.2.2.39) and restated here in terms of state variable numbers. The state variables in Eq. (4.3.4.1) also appear in Eq. (3.2.2.45) which is also restated here as Eq. (4.3.4.2) in terms of state variable numbers.

$$Xss(277) * Xss(98) - Xss(111) = 0 \qquad (4.3.4.1)$$

$$Xss(98) - Xss(111) - Xss(117) = 0 \qquad (4.3.4.2)$$

State variable Xss(117) was extremely sensitive to a change in this parameter resulting in a sensitivity factor of -999. Since this was a change at the end of Module 2, only variables from state variables downstream of the change should be affected. The first three principal components had heavy contributors downstream of the point this parameter controls. Therefore, it was expected that there would be shifts in all three scores. It turns out that there was a slight shift in both PC1 and PC2 scores in the positive direction, but the fault would not necessarily be detectable since all of the data points were still within the 95% confidence boundary for normal operation (Figure 4.53) but may be detectable in a trending shift. There was a slightly negative shift in PC3 scores (Figures 4.54–4.56), but the fault may not be detectable depending on operating conditions since many of the data points were inside the 95% confidence boundaries, again,a shift in the trend of PC3 scores may be detectable to indicate a possible fault. The fault in PC3 scores was expected because Xss(277) heavily loaded PC3 along with Xss(117). This resulted in an increase in the Mahalanobis distance (Figure 4.57), but the fault may not be detectable depending on operating conditions since many of the data points were inside the 95% confidence boundary, although a shift in the trend of T^2 may be detectable. An increase in the Mahalanobis distance was expected since this was one of the input variables and the change was greater than the allowed variation of the base case. There was a shift in the Q-statistic (Figures 4.58–4.59). However, this fault may also not be detectable depending on operating conditions since some of the data points were within the 95% confidence boundary. A fault was expected in the Q-statistic since changing the filter fractionation changes the parameters and therefore the relative relationship between the state variables would be different. This fault, though reasonably sized at approximately 10%, was not significant enough to be detectable by any of the diagnostic plots except at certain operating conditions or in trend monitoring. Due to this and since this is a high priority for safeguards, it

is very strongly recommended that the product and waste streams from the solvent extraction process be monitored for both flow rate and uranium content. A summary of this case is shown in Table 4.24.

Table 4.24. Summary of Faulty Case 4

Summary of Faulty Case					
Priority	**Module**	**Faulty Variable**	**Base Case Value**	**Faulty Value**	**Physical Description**
High	2	$K_{Mod2D,14}$, $Xss(277)$	0.999	0.9	Inefficient re-extraction operations, reduce uranyl nitrate extraction in Module 2 resulting in more U in Module 2 waste
Summary of Results					
	PC1 Scores	**PC2 Scores**	**PC3 Scores**	**T2**	**Q**
Direction	+	+	-	~+	++
Detectability	No	No	Possibly	Possibly	Possibly

Figure 4.53. Faulty Case 4 Scores Plot for PC1 and PC2. *Note: Only the faulty data are shown with the base case 95% confidence boundary displayed in red. There was no detectable fault.*
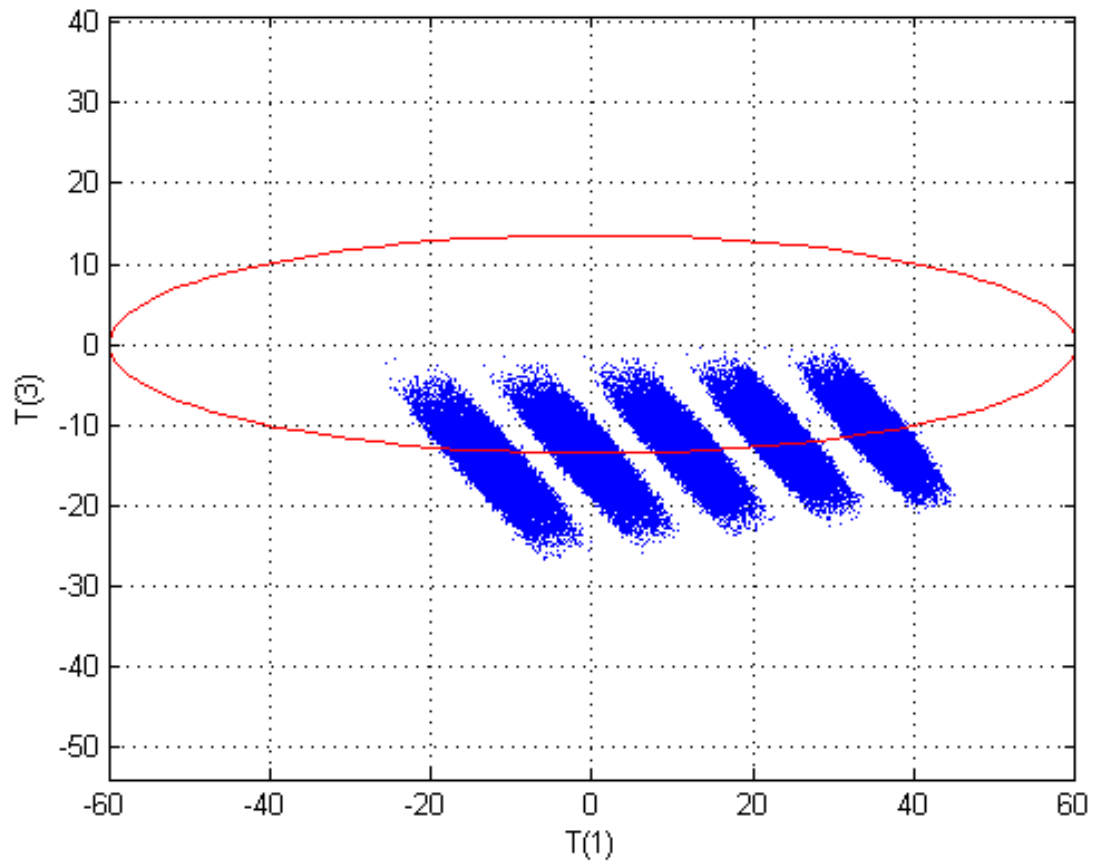
Figure 4.54. Faulty Case 4 Scores Plot for PC1 and PC3. *Note: Only the faulty data are shown with the base case 95% confidence boundary displayed in red. There was a shift in PC3 scores but the fault may not be detectable.*
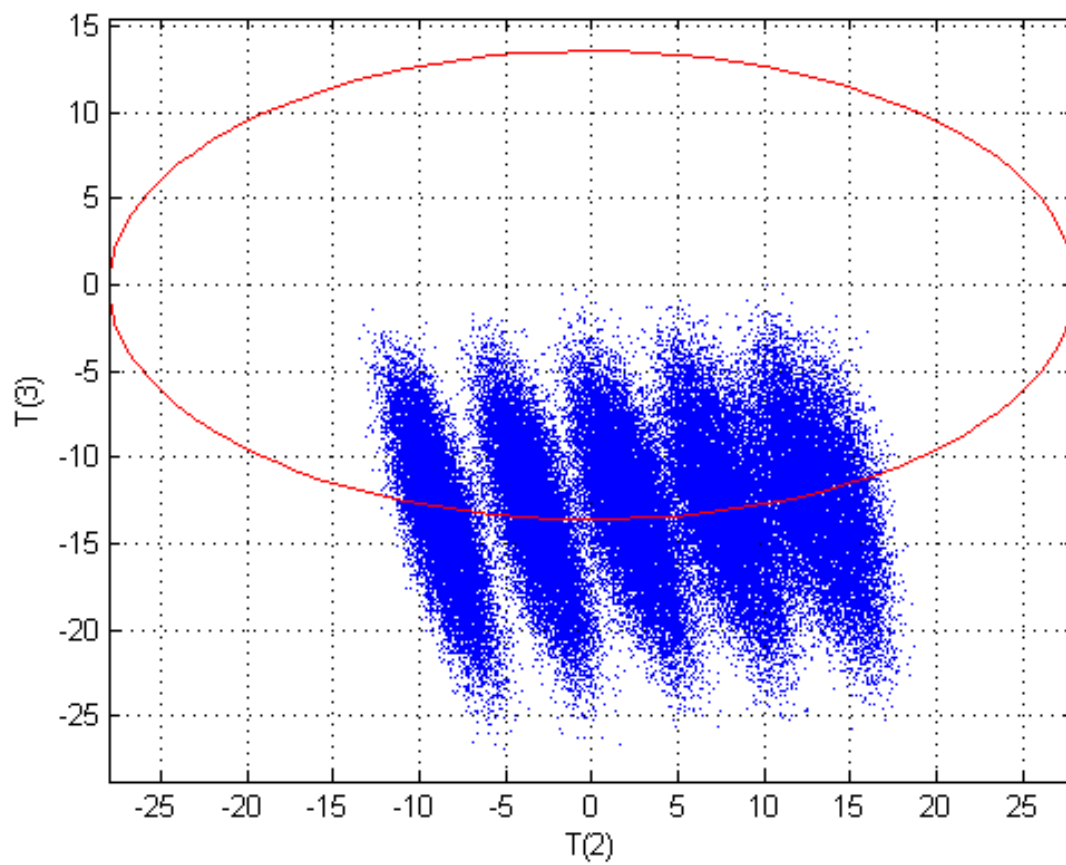
Figure 4.55. Faulty Case 4 Scores Plot for PC2 and PC3. *Note: Only the faulty data are shown with the base case 95% confidence boundary displayed in red. There was a shift in PC3 scores but the fault may not be detectable.*
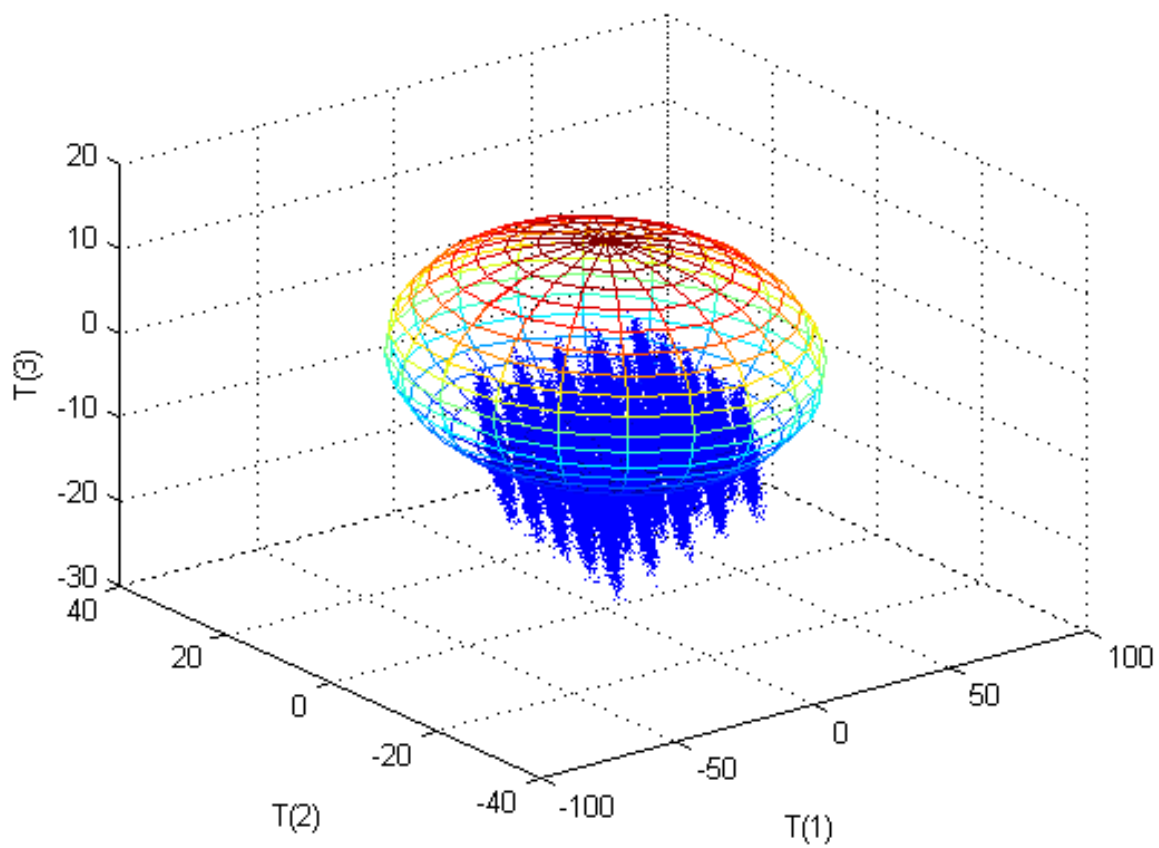
Figure 4.56. Faulty Case 4 3D Scores Plot for PC1, PC2, and PC3. *Note: Only the faulty data are shown with the base case 95% confidence boundary displayed as an ellipsoid. There was a shift in PC3 scores but the fault may not be detectable.*
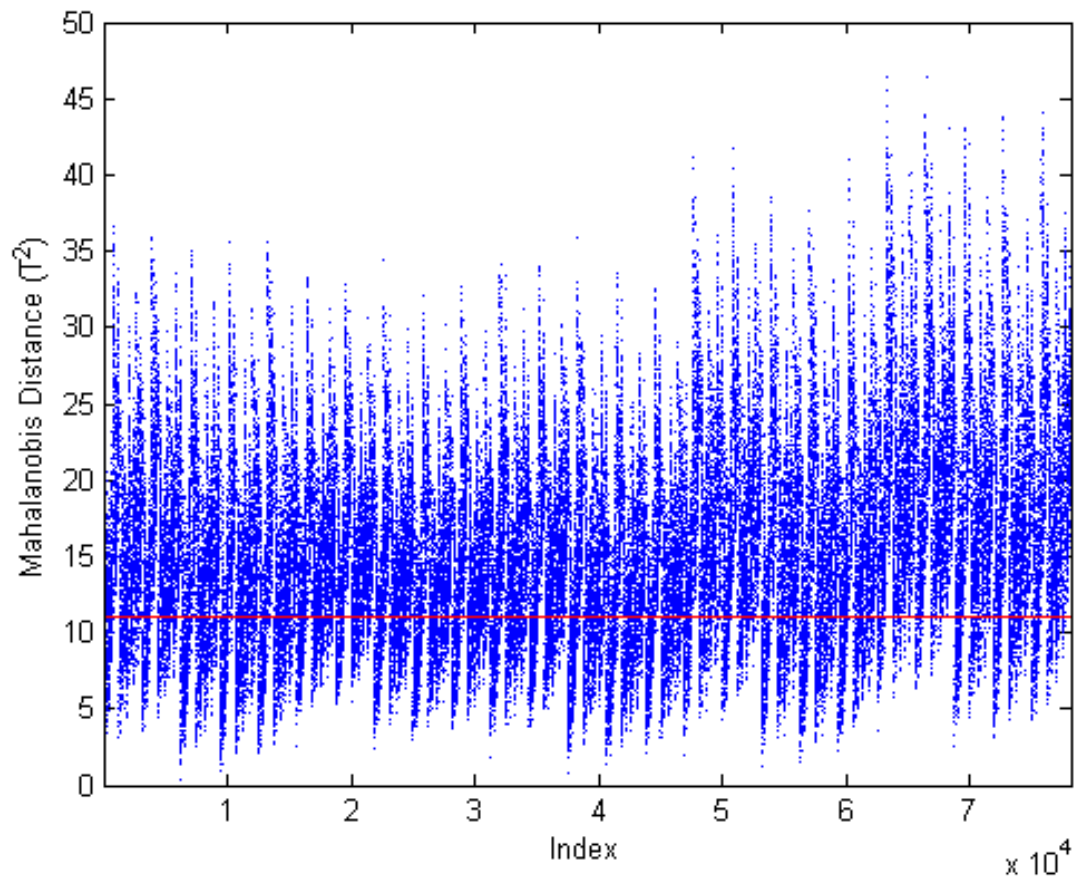
Figure 4.57. Faulty Case 4 Mahalanobis Distance Plot. *Note: Only the faulty data are shown with the base case 95% confidence boundary displayed in red. There was a shift but the fault may not be detectable.*
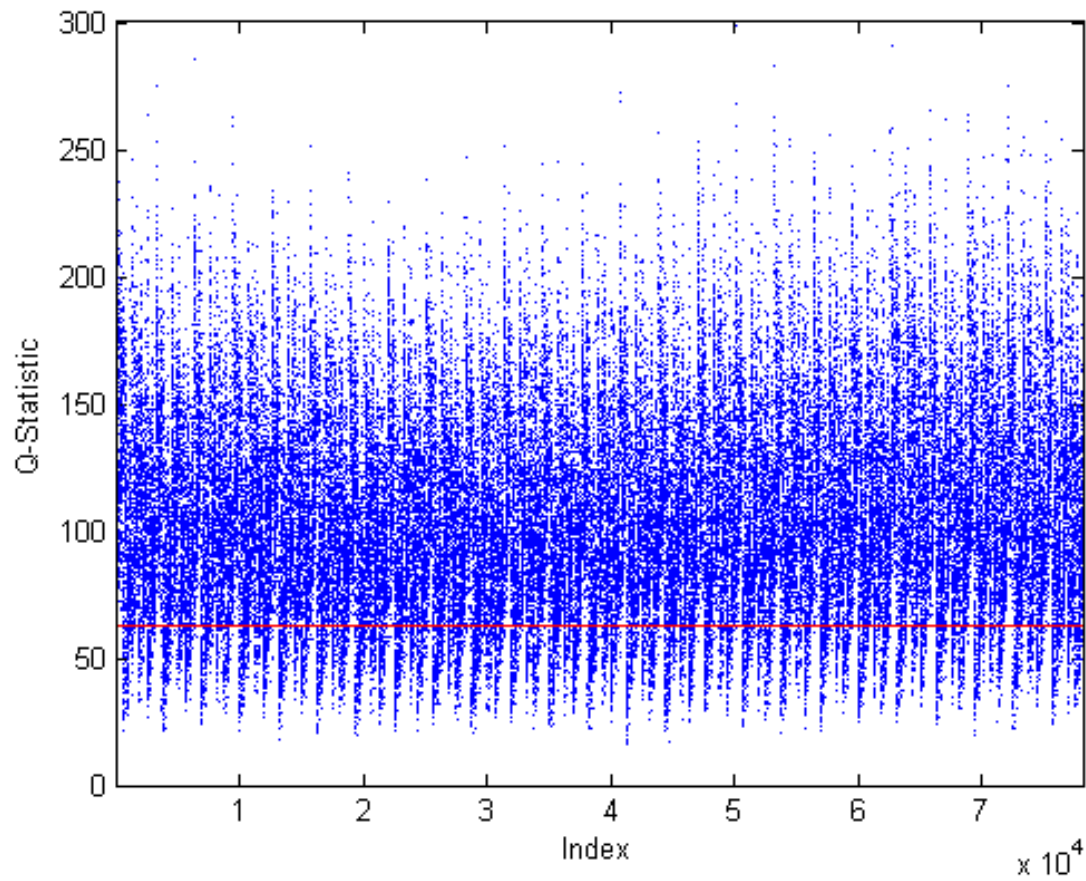
Figure 4.58. Faulty Case 4 *Q*-Statistic Plot. *Note: Only the faulty data are shown with the base case 95% confidence boundary displayed in red. There was a shift but the fault may not be detectable.*
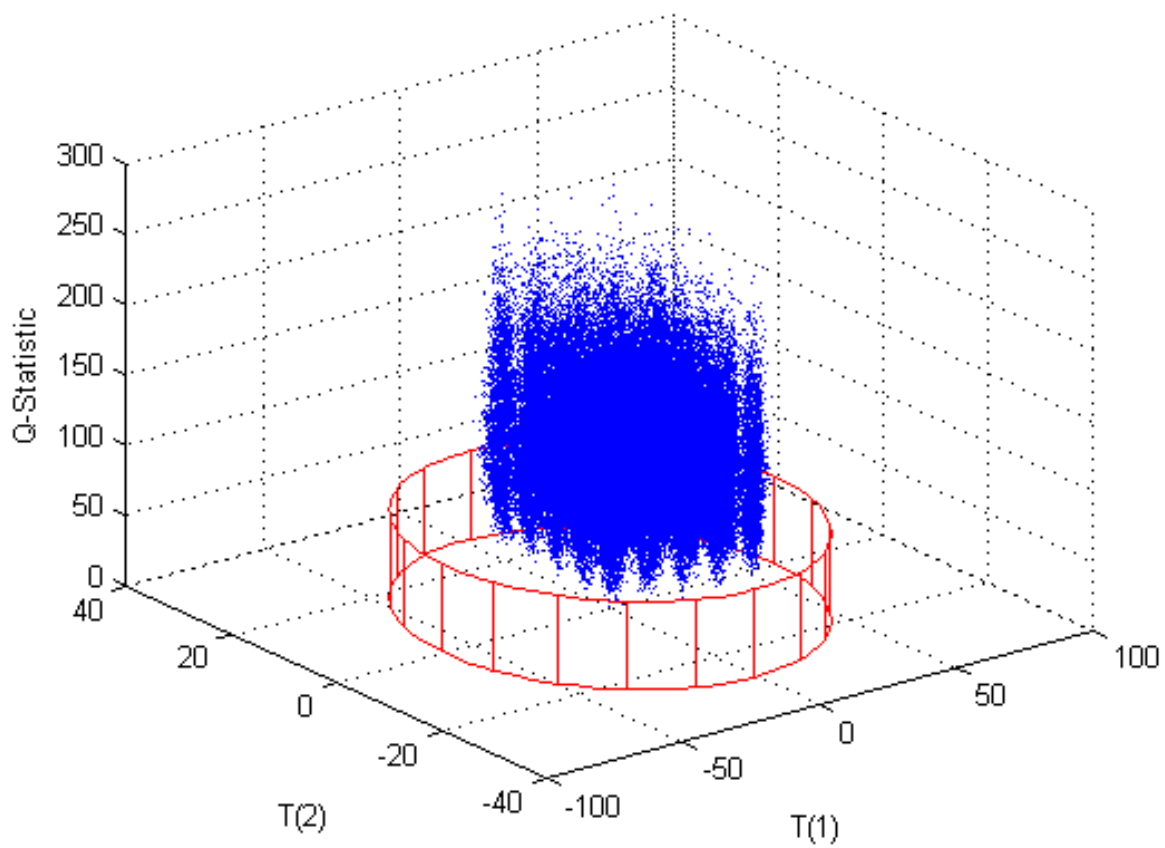
Figure 4.59. Faulty Case 4 PC1, PC2, and Q-Statistic Plot. *Note: Only the faulty data are shown with the base case 95% confidence boundary displayed in red. There was a shift in the Q-statistic but the fault may not be detectable.*

218

4.3.5 Case 5

For the fifth faulty case, a small amount of uranium was diverted from the evaporator in Module 3A. Stream 21, the condensate, was left unchanged from the base case and was still treated as a waste stream. A new parameter, S_{Mod3A}, was created. This parameter was used to specify how much of the material in the evaporator was diverted. Since the condensate stream was not changed, this parameter basically specified how much of the other evaporator output stream (Stream 22) was diverted. Additionally, the new stream and Stream 22 are to have the same composition. Initially, S_{Mod3A} was set at 0.1 such that 10% of the evaporator output was diverted. This produced an enormous fault to which the base case 95% confidence boundary was not visible on the same diagnostic plots. The final value of S_{Mod3A} was set at 0.0025 such that only 0.25% was diverted. This still produced enormous faults as discussed below. The model was extremely sensitive to that new parameter because diverting material at this point in the process reduces the amount of material available downstream and therefore affects other very sensitive parameters based on the sensitivity analysis. The results show that this fault was clearly detectable on all of the diagnostic plots.

The equations used to determine the component molar flow rates in the new output stream are shown below in terms of state variable numbers, where Xss(281)–Xss(285) represent the components of the new stream.

$$S_{Mod3A} * Xss(126) - Xss(281) = 0 \qquad (4.3.5.1)$$

$$S_{Mod3A} * Xss(127) - Xss(282) = 0 \qquad (4.3.5.2)$$

$$S_{Mod3A} * Xss(128) - Xss(283) = 0 \qquad (4.3.5.3)$$

$$S_{Mod3A} * Xss(129) - Xss(284) = 0 \qquad (4.3.5.4)$$

$$S_{Mod3A} * Xss(130) - Xss(285) = 0 \qquad (4.3.5.5)$$

This change resulted in all of the uranyl nitrate, U_3O_8, and soluble components [Xss(123), Xss(124), and Xss(125), respectively] of Stream 21 to go to zero meaning that there was none of these compounds in Stream 21 under this fault. The results show that there was a detectable fault in all of the scores plots (Figures 4.60–4.63). A fault in the scores was expected since the model is highly sensitive to changes in the uranium bearing streams throughout the process. The largest scores shift occurred in the positive direction for PC1 scores. There was a significant shift in the PC3 scores in the positive direction. There were some operating conditions where this fault would not be detectable in PC1 and PC2 scores plot only. This change only affected Stream 21 and those downstream. The first principal component was heavily loaded by the product streams from each module including those in Modules 3–5 which would be affected by this diversion of material. The first principal component was also moderately loaded by most of the primary state variables in Modules 3–5 which were also impacted by this diversion. These loadings explain why this diversion resulted in the largest shift being in PC1 scores. The second principal

component was loaded heavily by one of the products from Module 4 which would be affected by this change as well but less so thus resulting in the smallest shift in the scores plots being in PC2 scores. The third principal component was also heavily loaded by the product streams from Modules 3–5 and the waste stream in Module 3 which were all affected by this diversion, and therefore resulted in the shift in PC3 scores.

The faults in the scores also resulted in a detectable fault in the Mahalanobis distance (Figure 4.64). This fault was expected since an additional output stream was outside normal operating conditions. Additionally, this diversion would result in less uranium downstream which is also outside normal operating conditions. There was also a significant increase in the Q-statistic (Figures 4.65–4.66). A fault was expected in the Q-statistic since diverting material changes the relative relationships between state variables downstream of the diversion. The Q-statistic increase was significant while the Mahalanobis distance was within the same order of magnitude as the base case. Therefore, a very small diversion of material from the evaporator was clearly detectable.

From a safeguards perspective, it would be expected that a diversion of this nature would be very small so as not to be detected. It is recommended that the stream leaving the evaporator to feed the precipitation process be monitored for both flow rate and uranium content. This area of the plant should also be inspected for additional piping which may be diverting material to another location. Additionally, the waste stream from the evaporator should be monitored for flow rate and uranium content as well in case material is being diverted to the waste directly. Table 4.25 provides a summary of this case.

Table 4.25. Summary of Faulty Case 5

Summary of Faulty Case					
Priority	Module	Faulty Variable	Base Case Value	Faulty Value	Physical Description
High	3	S_{Mod3A}	N/A	0.0025	Diversion of 0.25% of the uranium from the evaporator
Summary of Results					
	PC1 Scores	PC2 Scores	PC3 Scores	T2	Q
Direction	+	-	+	+	+++++
Detectability	Possibly	Possibly	Yes	Yes	Yes
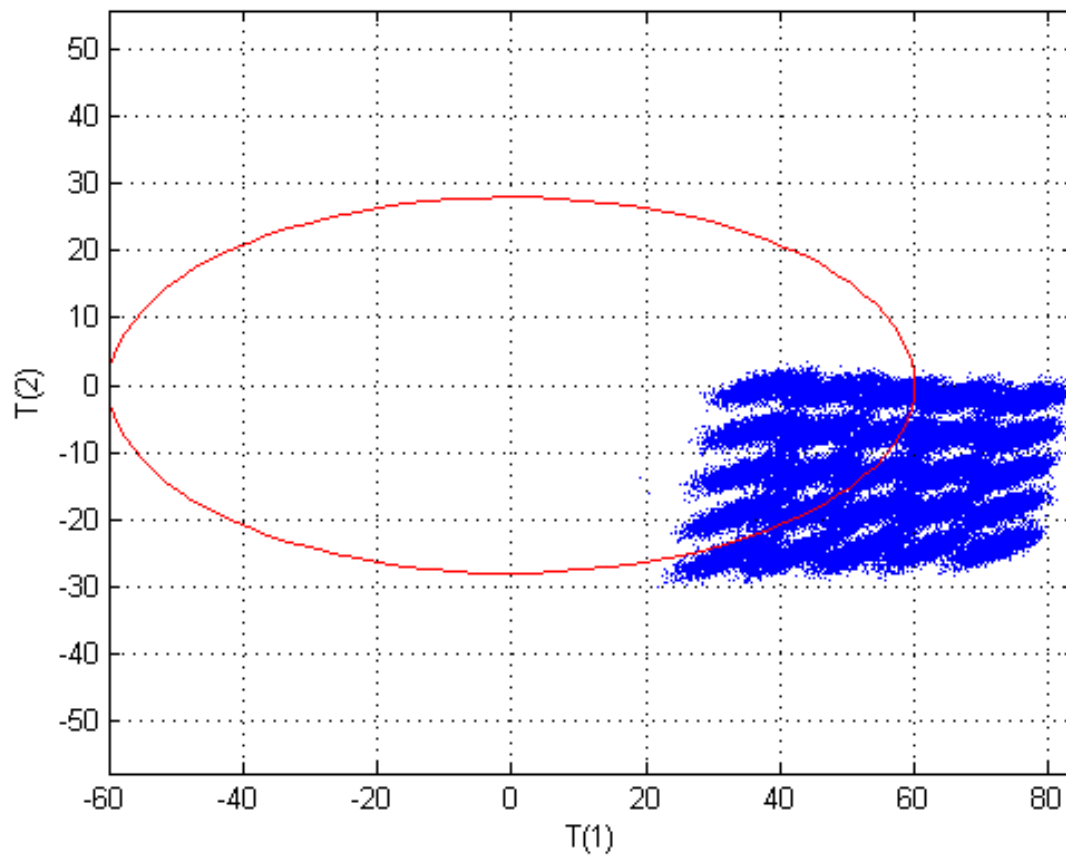
Figure 4.60. Faulty Case 5 Scores Plot for PC1 and PC2. *Note: Only the faulty data are shown with the base case 95% confid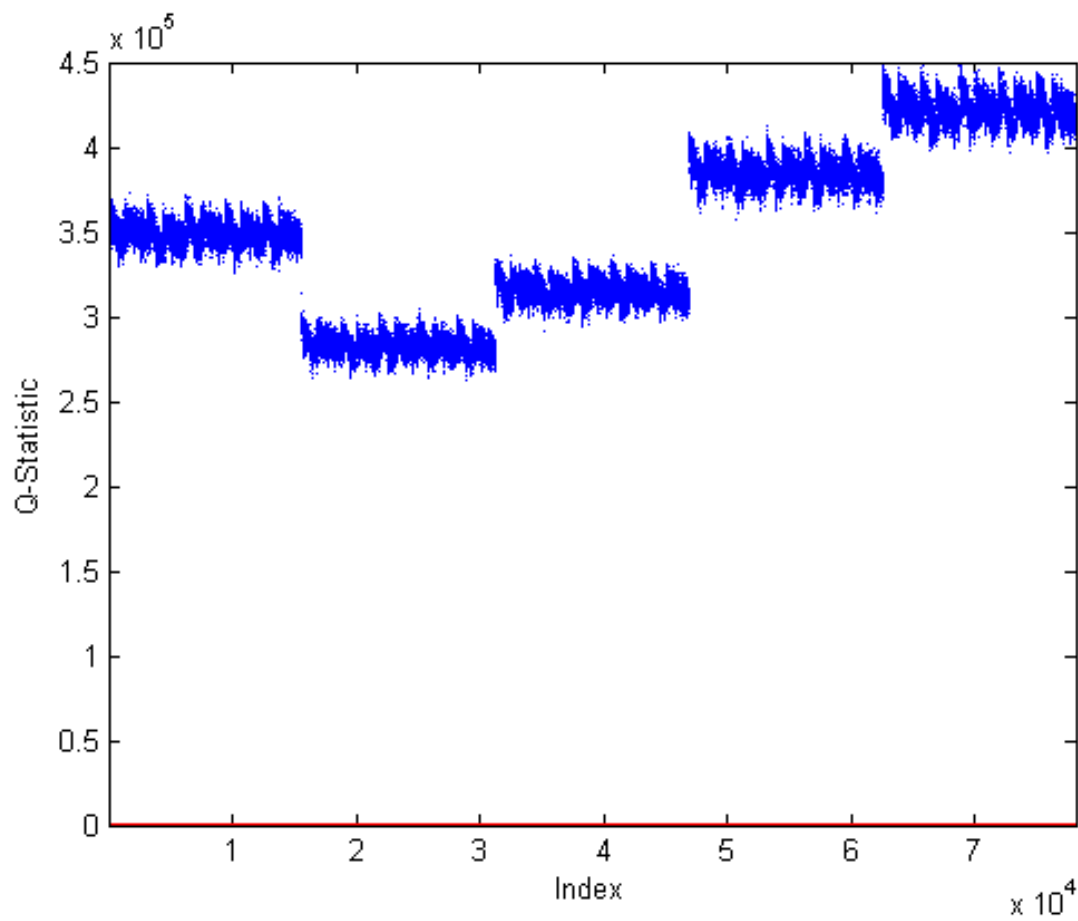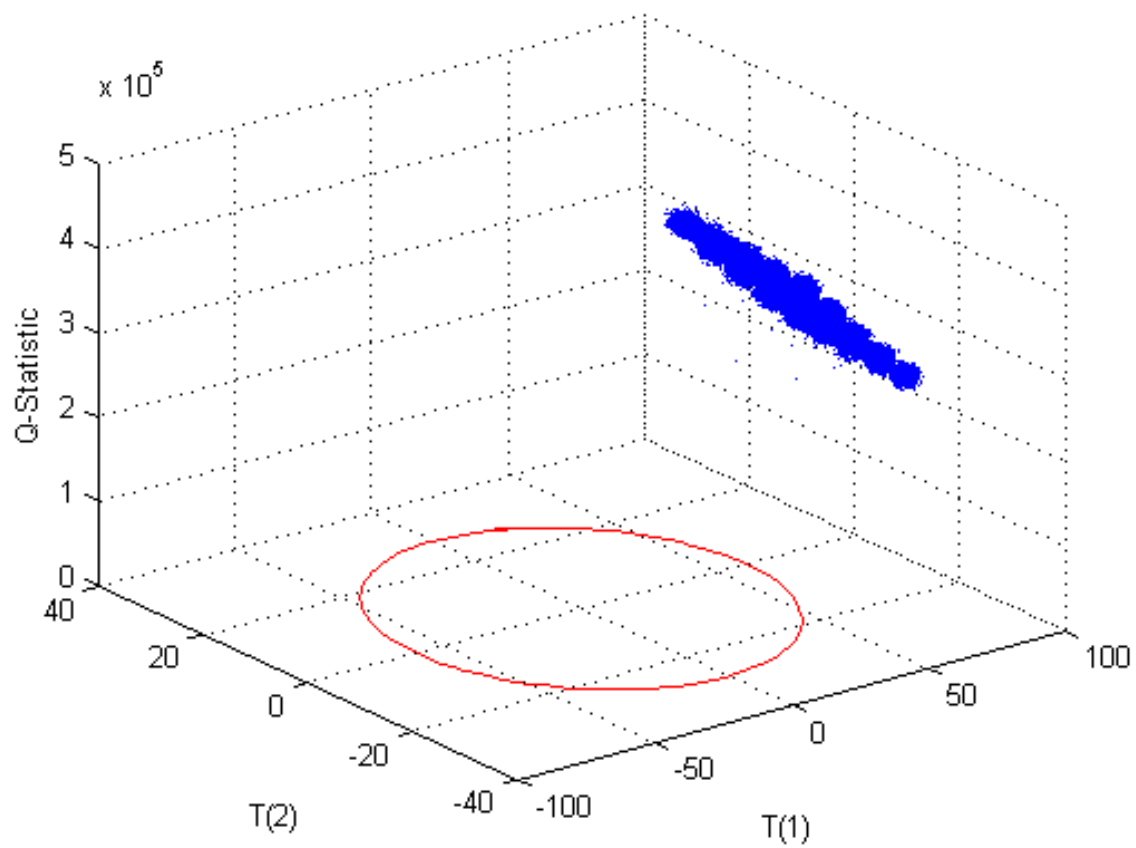ence boundary displayed in red. There was a detectable fault in PC1 and PC2 scores. There were some operating conditions where this fault would not be detectable in PC1 and PC2 scores only.*
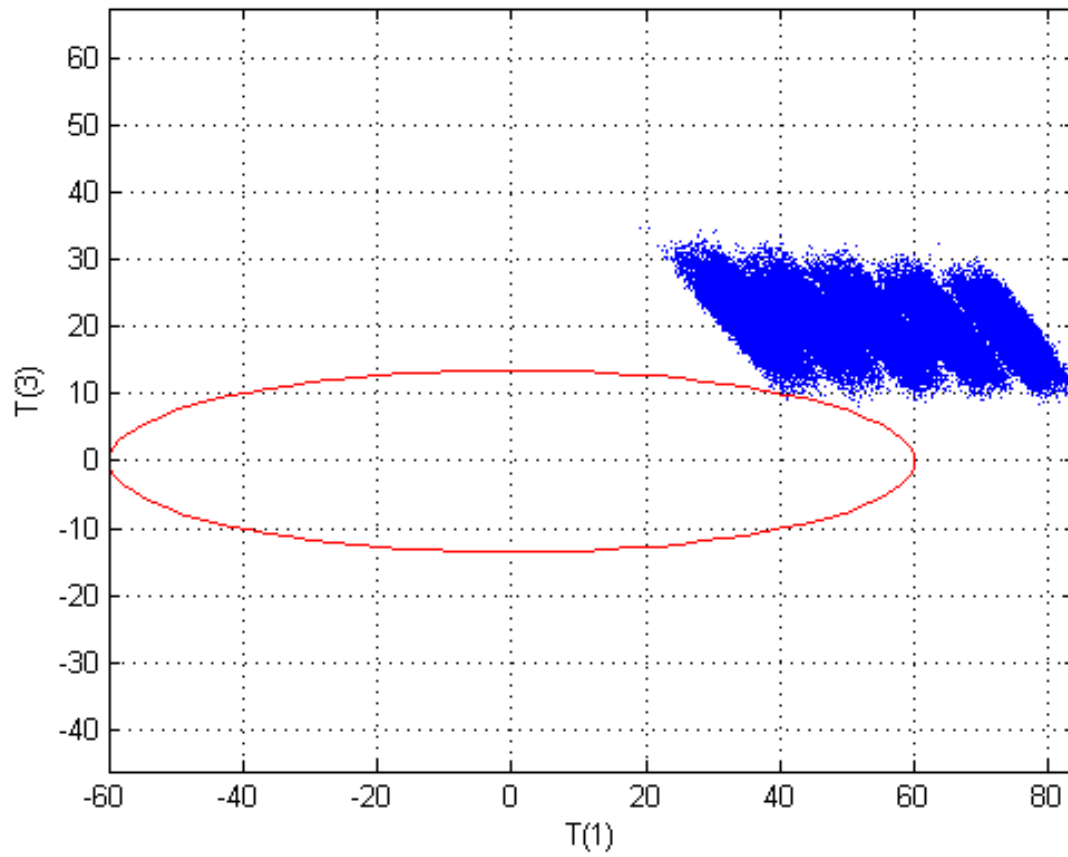
Figure 4.61. Faulty Case 5 Scores Plot for PC1 and PC3. *Note: Only the faulty data are shown with the base case 95% confidence boundary displayed in red. There was a detectable fault in PC1 and PC3 scores.*
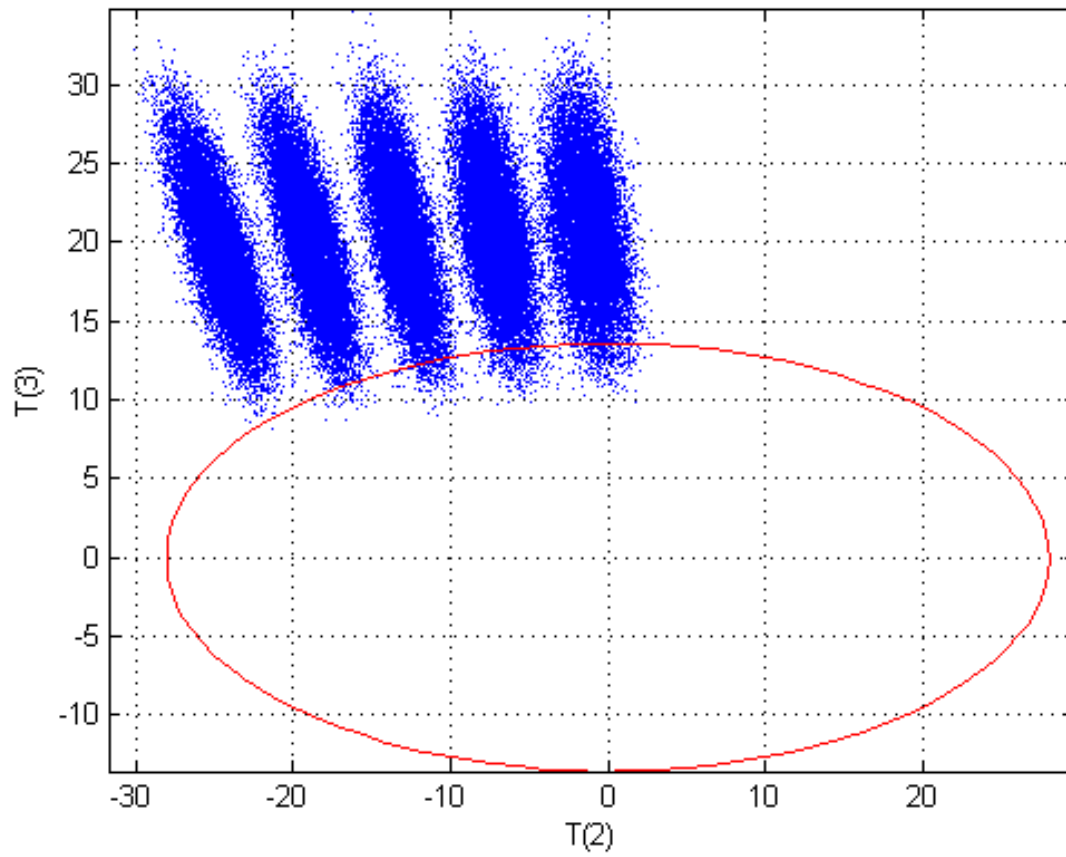
Figure 4.62. Faulty Case 5 Scores Plot for PC2 and PC3. *Note: Only the faulty data are shown with the base case 95% confidence boundary displayed in red. There was a detectable fault in PC2 and PC3 scores.*
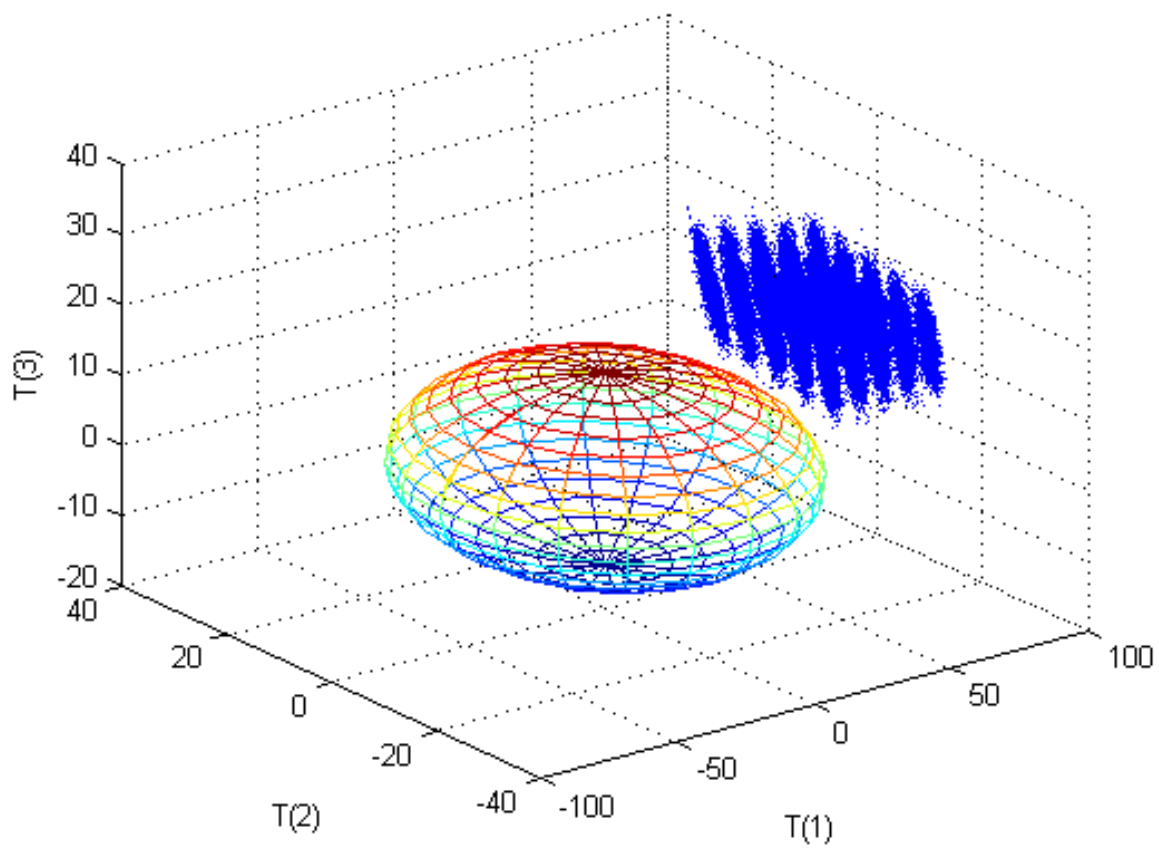
Figure 4.63. Faulty Case 5 3D Scores Plot for PC1, PC2, and PC3. *Note: Only the faulty data are shown with the base case 95% confidence boundary displayed as an ellipsoid. There was a detectable fault in all three scores.*
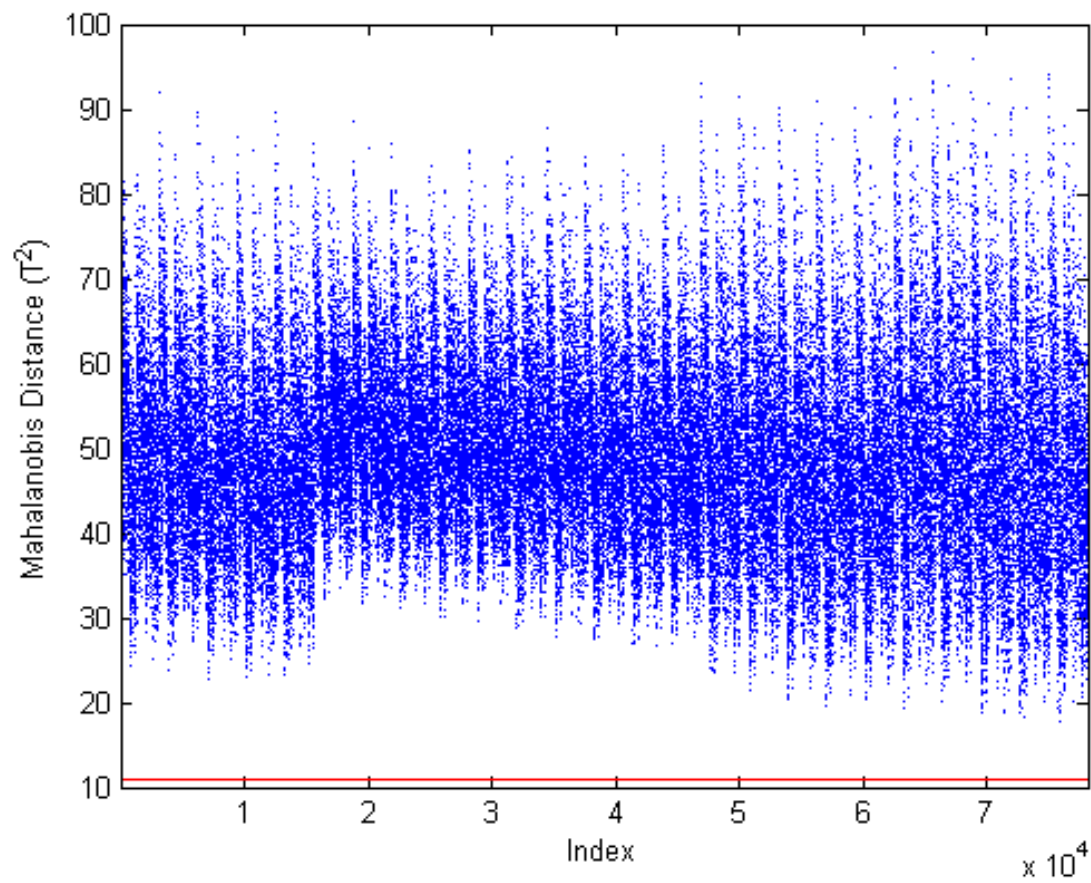
Figure 4.64. Faulty Case 5 Mahalanobis Distance Plot. *Note: Only the faulty data are shown with the base case 95% confidence boundary displayed in red. There was a detectable fault.*

Figure 4.65. Faulty Case 5 *Q*-**Statistic Plot.** *Note: Only the faulty data are shown with the base case 95% confidence boundary displayed in red. There was a detectable fault.*

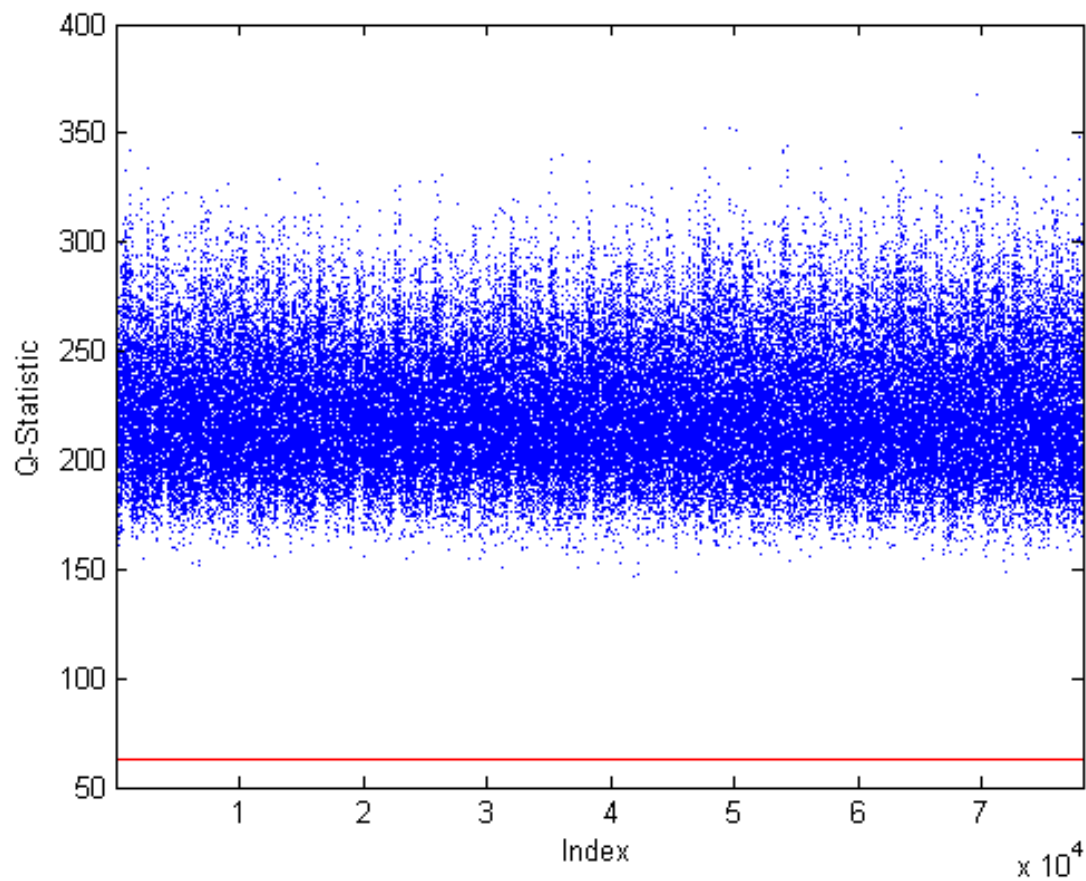**Figure 4.66. Faulty Case 5 PC1, PC2, and** *Q*-**Statistic Plot.** *Note: Only the faulty data are shown with the base case 95% confidence boundary displayed in red. There was a detectable fault in the scores and the Q-statistic.*

4.3.6 Case 6

For the sixth faulty case, a small amount of uranium was added to the precipitation process in Module 3B. This simulated the processing of undeclared uranium which is of great concern of safeguards. The flow rate of the new stream (14A) was set at 10 kg/h and was assumed to be pure uranyl nitrate. The results show that the fault in this case was clearly detectable using the Q-statistic.

Equation (4.3.6.1) shows the calculation of the uranyl nitrate balance for Stream 26 where Stream 14A has been added to Stream 22.

$$Xss(128) - Xss(138) + F_{14A} * x_{14A,14} * \frac{1000}{MW_{14}} = 0 \qquad (4.3.6.1)$$

Both Xss(128) and Xss(138) moderately loaded PC1. State variable Xss(142), Xss(143), Xss(150), and Xss(151) decreased by 25% in comparison with the base case nominal solution with the addition of this stream. These were the ammonia and CO_2 in Streams 27 and 28. The addition of this new stream caused an additional 82 state variables to increase by 12% when compared to the base case nominal solution. These 82 state variables included state variables that were heavy contributors to PC1, PC2, or PC3.

There was a slight shift in both PC1 and PC2 scores (Figure 4.67), but the fault was not detectable since nearly all of the data points were still within the 95% confidence boundary. There was a slightly larger shift in PC3 scores (Figures 4.68–4.70), but the fault may not be detectable depending on operating conditions since approximately 50% of the data points were within the normal operation confidence boundaries, but the fault may be detectable using trend monitoring. These shifts in the scores were expected since the model was highly sensitive to changes in the uranium bearing streams throughout the process and based on the loadings discussed above.

The shifts in the scores resulted in an increase in the Mahalanobis distance (Figure 4.71) which may be detectable depending on operating conditions and by using trend monitoring. An increase in the Mahalanobis distance was expected since the addition of material would increase the amount of uranium downstream of the addition which would be outside of normal operating conditions. There was a significant increase in the Q-statistic (Figures 4.72–4.73), as expected. A fault in the Q-statistic was expected since material addition changes the relative relationships of the state variables downstream of the new input. Therefore, an addition of material was detectable but only in the Q-statistic. Since the base case incoming uranium was allowed to vary by ±10%, it was reasonable that the scores and Mahalanobis distance plots did not produce a clearly detectable fault since this was only slightly more than a 10% addition of uranium material. Therefore, this was mostly within the normal operating conditions but the relative relationship between the state variables was no longer as modeled. For this case, it is recommended that the uranium feed to the plant be monitored for both flow rate and uranium content. It is also recommended that the streams exiting each major process (e.g., dissolution, solvent extraction, fluorination) as product or waste be monitored for flow rate and uranium content.

Additionally, this area of the plant should be inspected to determine that there is not additional uranium being fed to the process. Table 4.26 summarizes this faulty case.

Table 4.26. Summary of Faulty Case 6

Summary of Faulty Case					
Priority	**Module**	**Faulty Variable**	**Base Case Value**	**Faulty Value**	**Physical Description**
High	3	F_{14A}	N/A	10 kg/h	Addition of uranyl nitrate to the precipitation process
Summary of Results					
	PC1 Scores	**PC2 Scores**	**PC3 Scores**	**T2**	**Q**
Direction	-	-	+	~+	++
Detectability	No	No	Possibly	Possibly	Yes
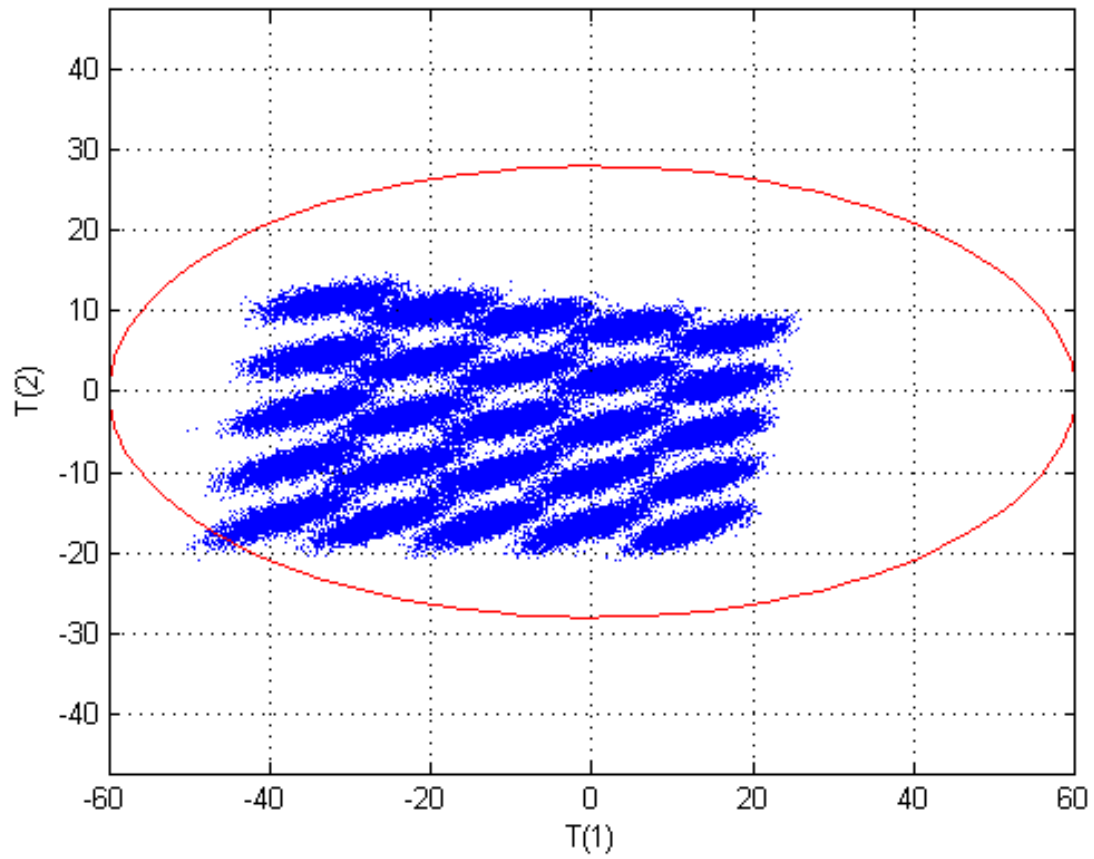
Figure 4.67. Faulty Case 6 Scores Plot for PC1 and PC2. *Note: Only the faulty data are shown with the base case 95% confidence boundary displayed in red. There was a slight change in PC1 and PC2 scores, but there was no detectable fault.*
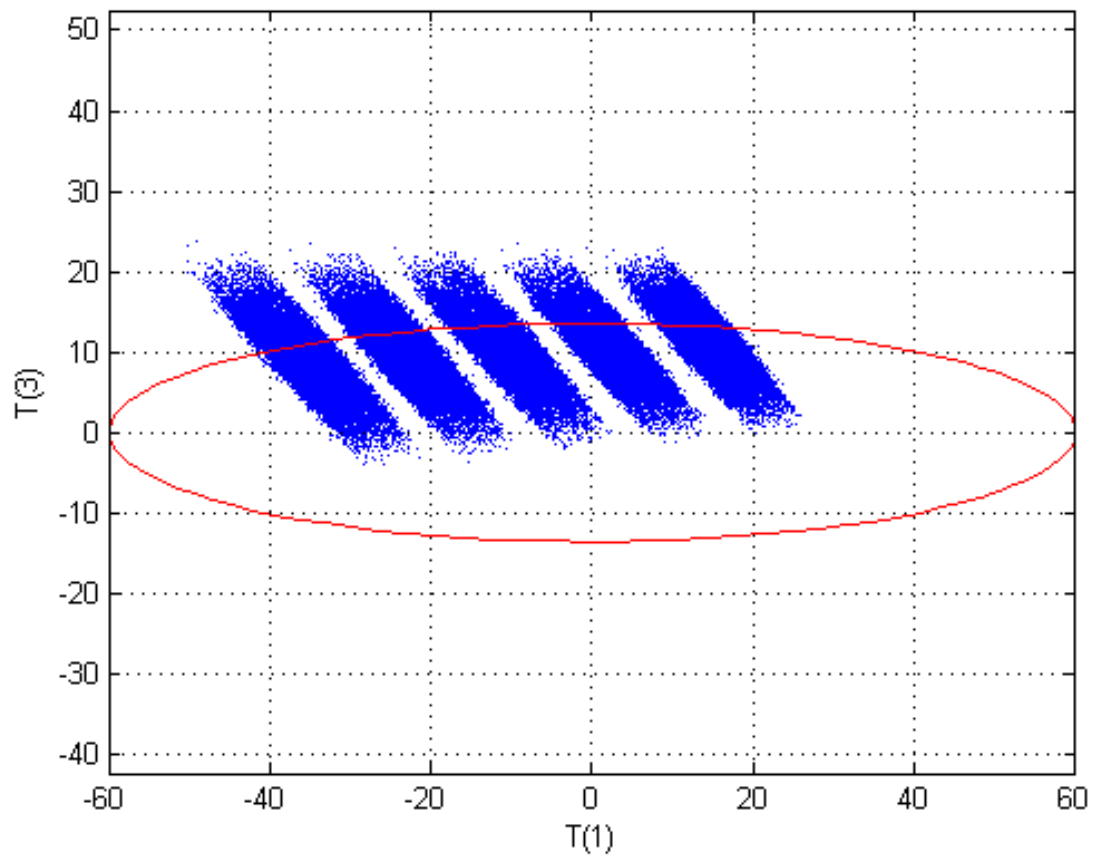
Figure 4.68. Faulty Case 6 Scores Plot for PC1 and PC3. *Note: Only the faulty data are shown with the base case 95% confidence boundary displayed in red. There was a slight change in PC1 and PC3 scores, but the fault was only detectable under certain operating conditions.*
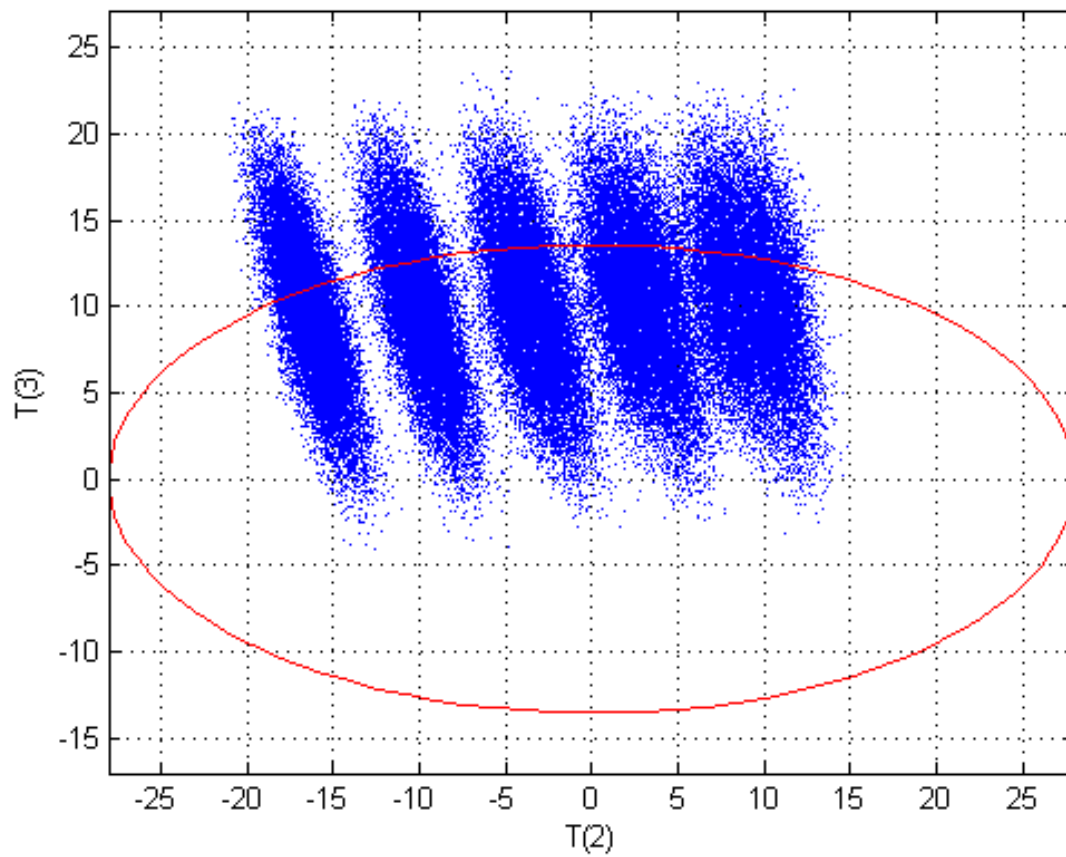
Figure 4.69. Faulty Case 6 Scores Plot for PC2 and PC3. *Note: Only the faulty data are shown with the base case 95% confidence boundary displayed in red. There was a slight change in PC2 and PC3 scores, but the fault was only detectable under certain operating conditions.*
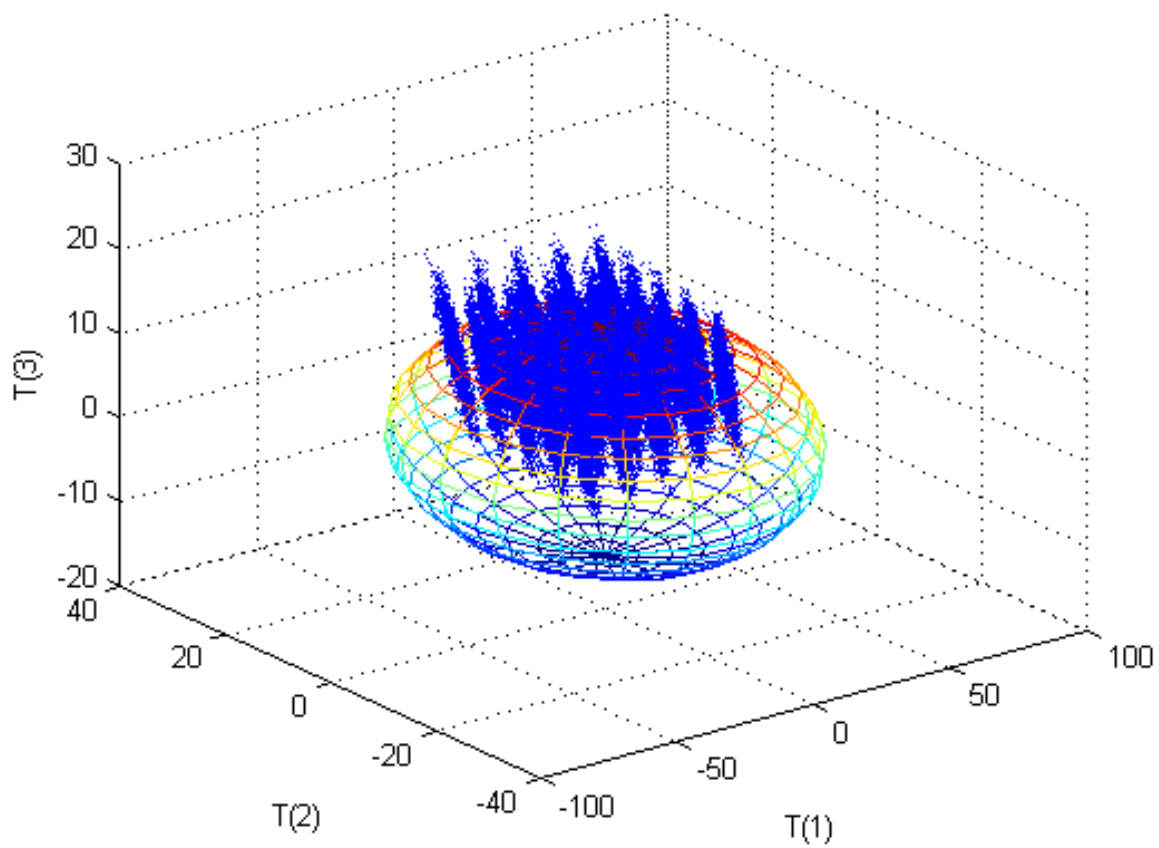
Figure 4.70. Faulty Case 6 3D Scores Plot for PC1, PC2, and PC3. *Note: Only the faulty data are shown with the base case 95% confidence boundary displayed as an ellipsoid. There was a slight change in all scores, but the fault is likely undetectable at most operating conditions.*
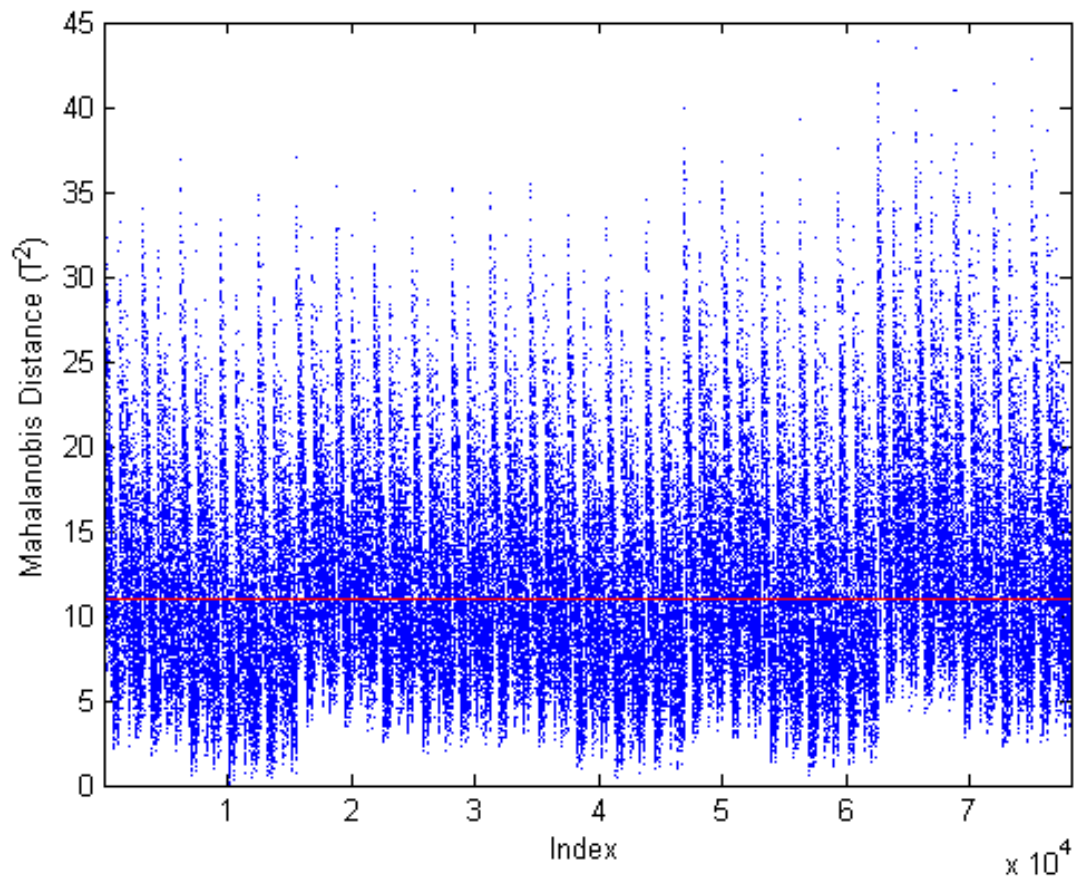
Figure 4.71. Faulty Case 6 Mahalanobis Distance Plot. *Note: Only the faulty data are shown with the base case 95% confidence boundary displayed in red. There was a slight change in the Mahalanobis distance, but the fault is likely undetectable at most operating conditions.*

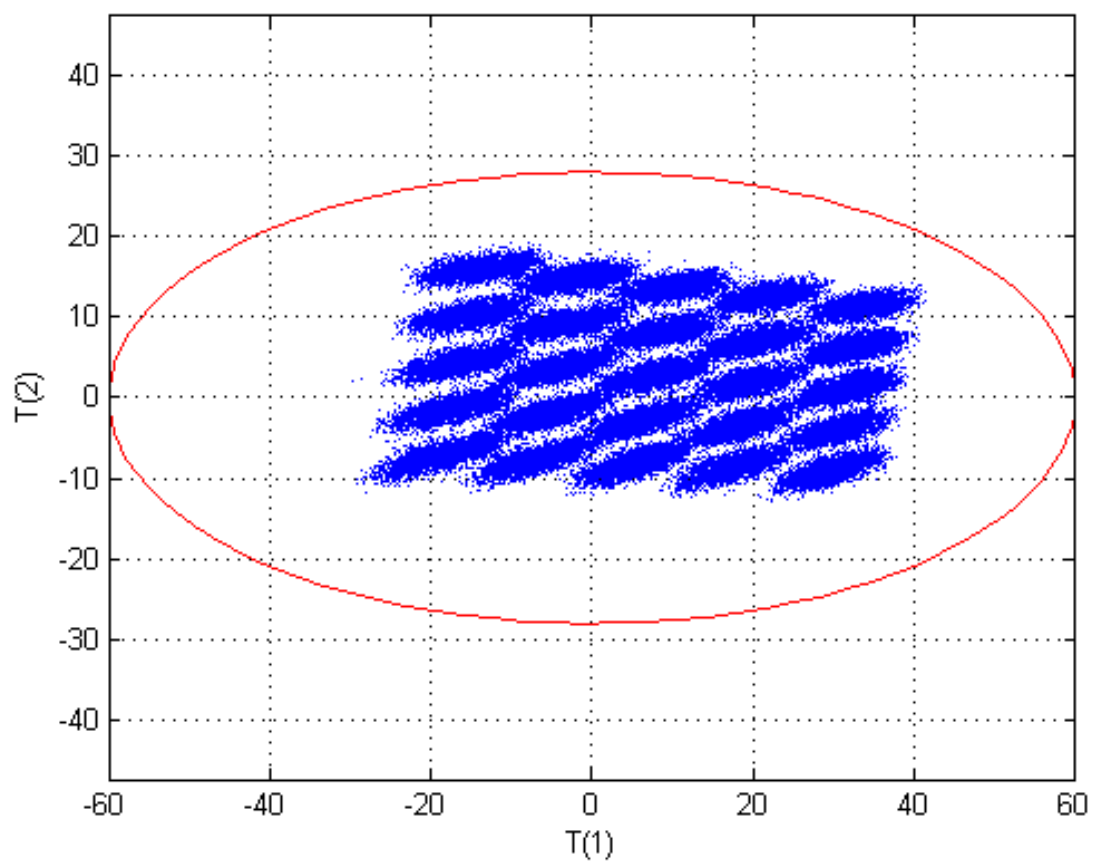**Figure 4.72. Faulty Case 6** *Q*-**Statistic Plot.** *Note: Only the faulty data are shown with the base case 95% confidence boundary displayed in red. There was a detectable fault.*
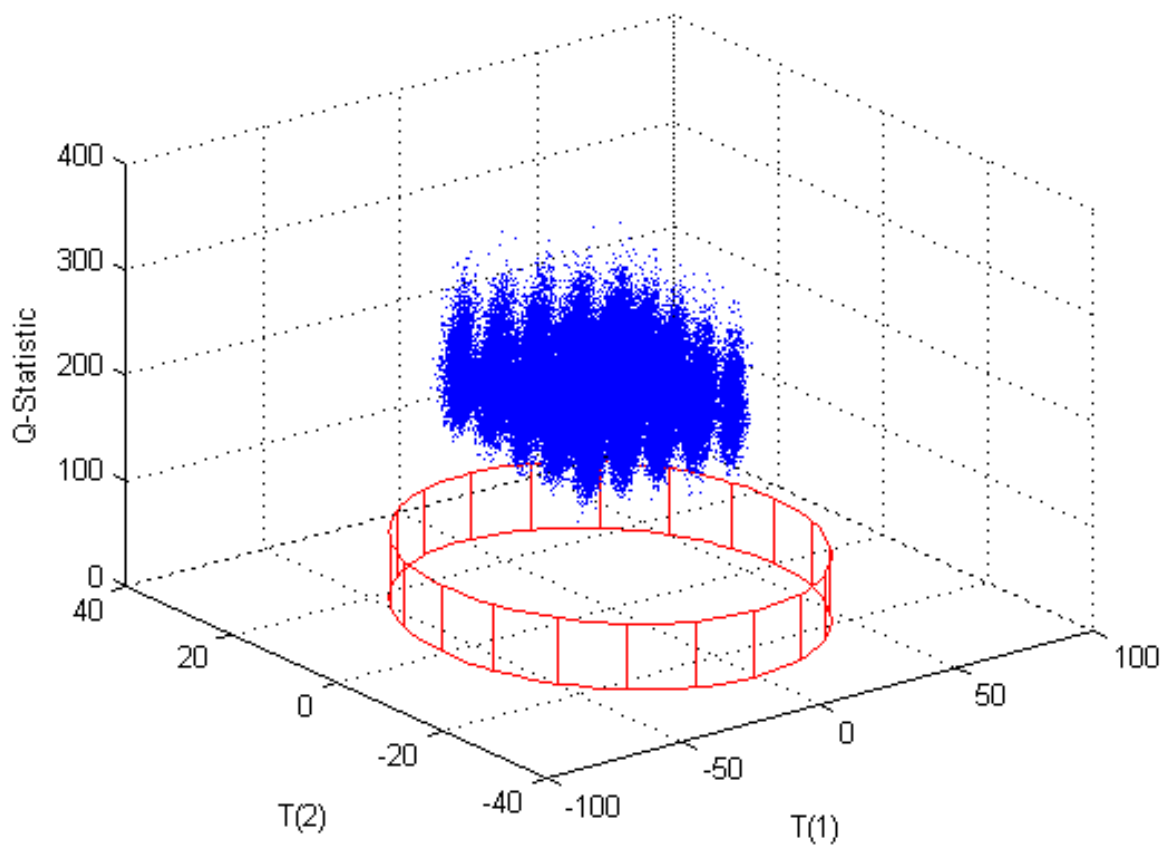
Figure 4.73. Faulty Case 6 PC1, PC2, and Q-Statistic Plot. *Note: Only the faulty data are shown with the base case 95% confidence boundary displayed in red. There was a detectable fault in the Q-statistic.*

4.3.7 Case 7

For case seven, the effect of inefficient precipitation process operations in Module 3 was investigated. Inefficient operations results in uranyl nitrate not being completely converted to AUC and therefore additional uranium would leave the process as waste. This case was modeled by changing the extent of reaction for the precipitation reaction, X_{Mod3C}, from 0.9999 to 0.9. During the sensitivity analysis, three state variables were identified as being extremely sensitive to changes in this parameter, such that the sensitivity factor was -9999. Those state variables were Xss(146), Xss(157), and Xss(169) which correspond to the uranyl nitrate in Streams 27, 29, and 31, respectively. In order to get a realistic response from the PCA model, these state variables were excluded from the faulty case analysis so as to not bias the scores of the new sample runs. Additionally, the molar flow rates of these components were very small, so excluding them from analysis was reasonable. The results show that the fault in this case was clearly detectable using the Q-statistic.

The extent of reaction for the precipitation reaction, X_{Mod3C}, appears in the model as shown in Eqs. (3.2.3.24)–(3.2.3.32) which are restated here in terms of state variable numbers.

$$Xss(134) + \left(n_{Mod3C,1} * X_{Mod3C} * \text{Xss}(138)\right) - \text{Xss}(141) = 0 \qquad (4.3.7.1)$$

$$\text{Xss}(135) + \left(n_{Mod3C,3} * X_{Mod3C} * \text{Xss}(138)\right) - \text{Xss}(142) = 0 \qquad (4.3.7.2)$$

$$Xss(136) + \left(n_{Mod3C,8} * X_{Mod3C} * \text{Xss}(138)\right) - \text{Xss}(143) = 0 \qquad (4.3.7.3)$$

$$\left(n_{Mod3C,12} * X_{Mod3C} * \text{Xss}(138)\right) - \text{Xss}(145) = 0 \qquad (4.3.7.4)$$

$$Xss(138) + \left(n_{Mod3C,14} * X_{Mod3C} * \text{Xss}(138)\right) - \text{Xss}(146) = 0 \qquad (4.3.7.5)$$

$$\left(n_{Mod3C,19} * X_{Mod3C} * \text{Xss}(138)\right) - \text{Xss}(148) = 0 \qquad (4.3.7.6)$$

State variables Xss(142), Xss(143), Xss(150), and Xss(151) increased by 20% in comparison with the base case nominal solution with the addition of this stream. These were the ammonia and CO_2 in Streams 27 and 28. An additional 78 state variables decreased by 10% when compared to the base case nominal solution. These 78 state variables included state variables that were heavy contributors to PC1, PC2, or PC3.

There was a slight shift in all of the scores (Figures 4.74–4.77). However, the fault was not clearly detectable in the scores plots because most of the data points were within the 95% confidence boundaries, but the fault may be detectable using trend monitoring. A fault in the scores was expected since the model is highly sensitive to changes in the uranium bearing streams throughout the process, but the fault was not large enough to be detectable in the scores based on all state variables except

Xss(146), Xss(157), and Xss(169) which were found to be highly sensitive to changes in this parameter. The largest increase was in the third principal component which was heavily loaded by both the product and waste streams at the end of Module 3 which were directly affected by this fault. There was also a shift in the Mahalanobis distance (Figure 4.78), but some of the data points were within the confidence boundary making the fault only detectable under certain operating conditions or by using trend monitoring. An increase in the Mahalanobis distance was expected since additional uranium leaving as waste was the outside normal operating conditions. Since the fault was not large enough to be clearly detectable it showed that this fault was not large enough to be outside of normal operating conditions. There was a significant increase in the Q-statistic (Figures 4.79–4.80). The Q-statistic fault was expected since changing the extent of reaction changes the model parameters and therefore the relative relationship between the state variables would be different. A 10% reduction in the extent of reaction produced a clearly detectable fault only in the Q-statistic.

It is recommended that the product and waste streams in the evaporation and precipitation process areas of the facility be monitored for both flow rate and uranium content. For this fault specifically, it is recommended that the outlet stream from the precipitation process be monitored for flow rate and uranium content as well as type of uranium compound. Table 4.27 summarizes the Case 7 results.

Table 4.27. Summary of Faulty Case 7

Summary of Faulty Case					
Priority	**Module**	**Faulty Variable**	**Base Case Value**	**Faulty Value**	**Physical Description**
Low	3	X_{Mod3C}	0.9999	0.9	Inefficient precipitation process operations resulted in less UN converted AUC and more U in waste streams
Summary of Results					
	PC1 Scores	**PC2 Scores**	**PC3 Scores**	**T2**	**Q**
Direction	+	+	-	~+	++
Detectability	No	No	Not likely	Possibly	Yes

Figure 4.74. Faulty Case 7 Scores Plot for PC1 and PC2. *Note: Only the faulty data are shown with the base case 95% confidence boundary displayed in red. There was no detectable fault.*
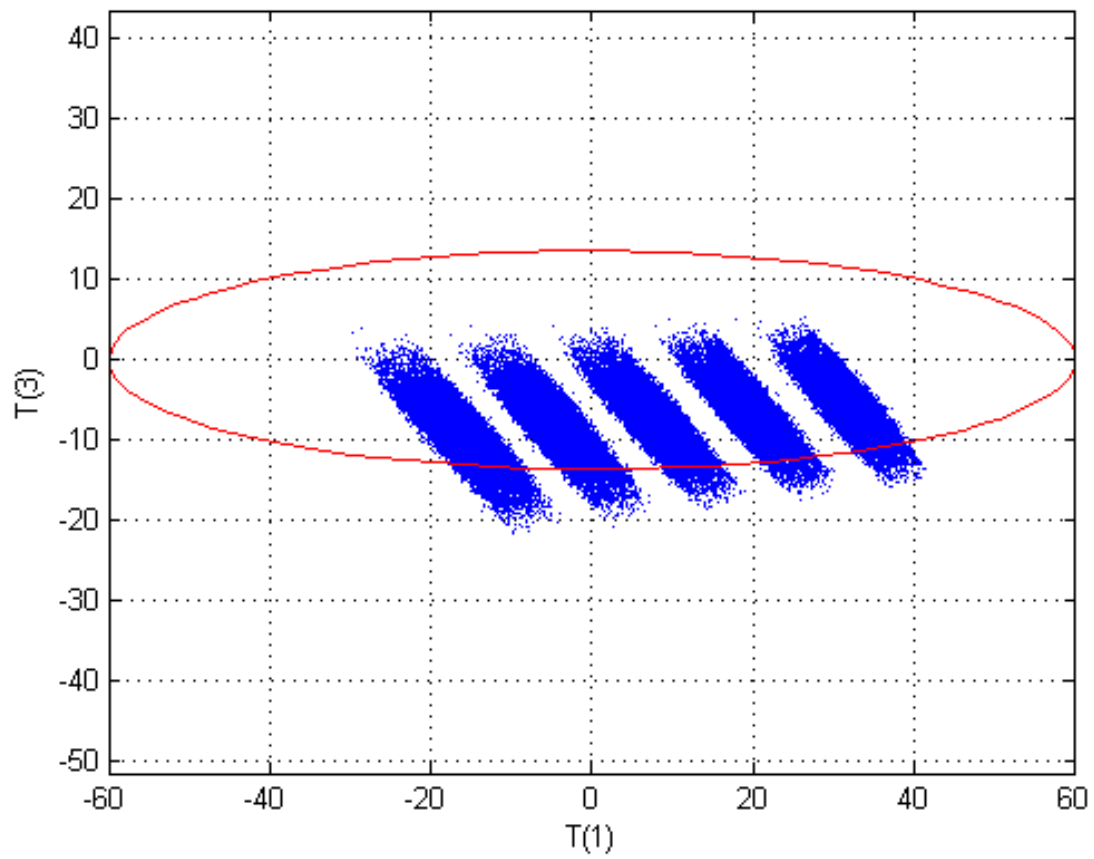
Figure 4.75. Faulty Case 7 Scores Plot for PC1 and PC3. *Note: Only the faulty data are shown with the base case 95% confidence boundary displayed in red. There was a slight change in PC3 scores but no detectable fault.*
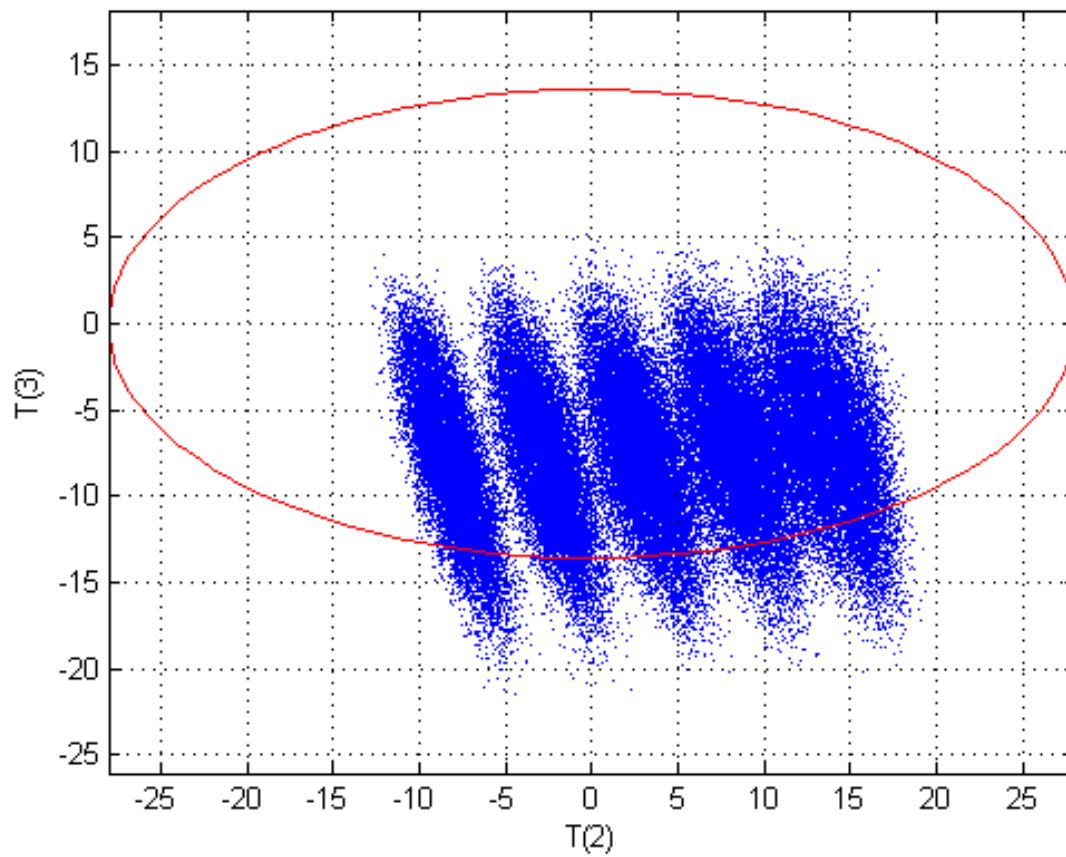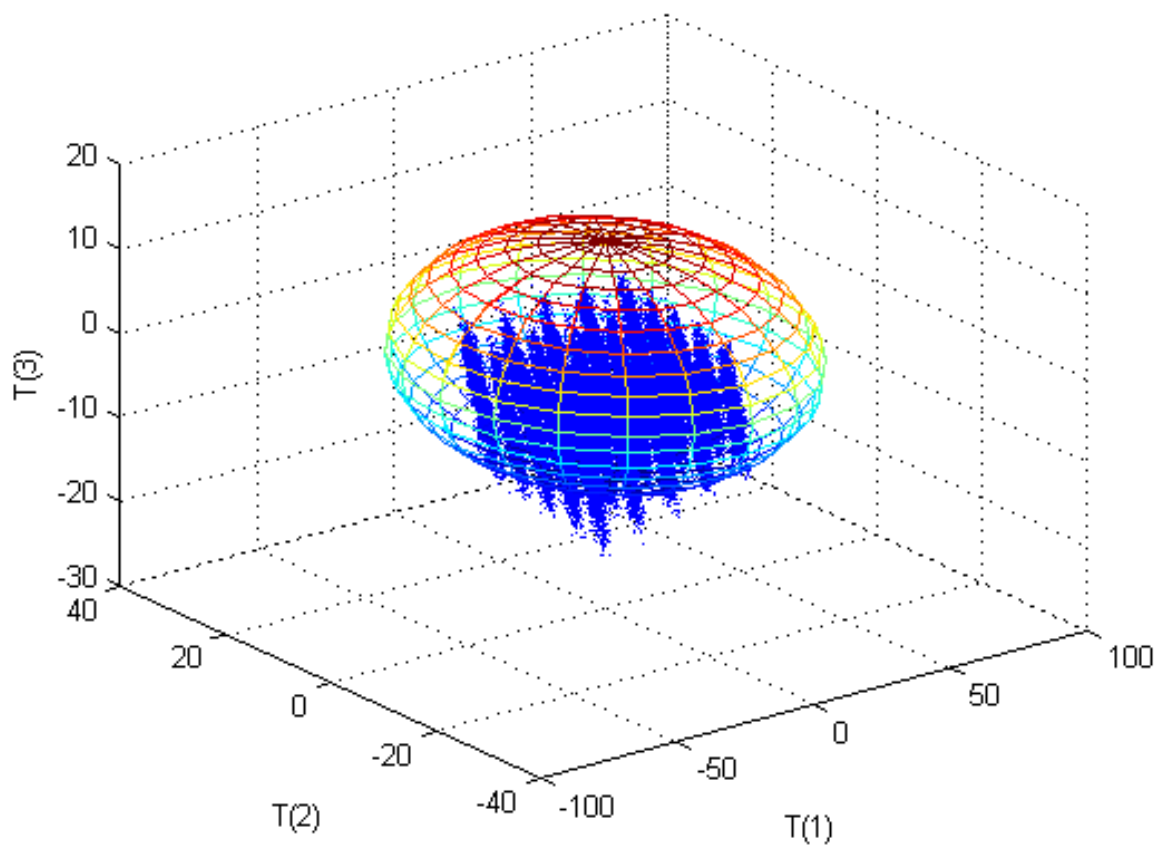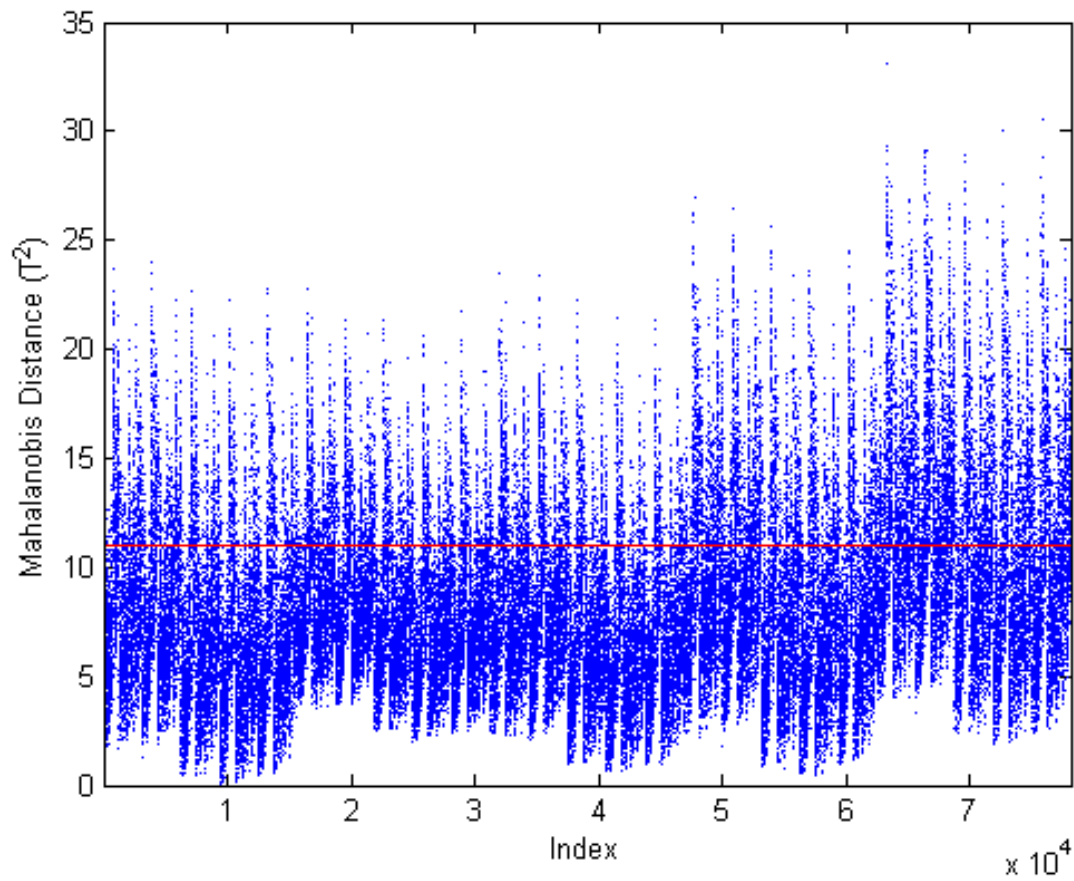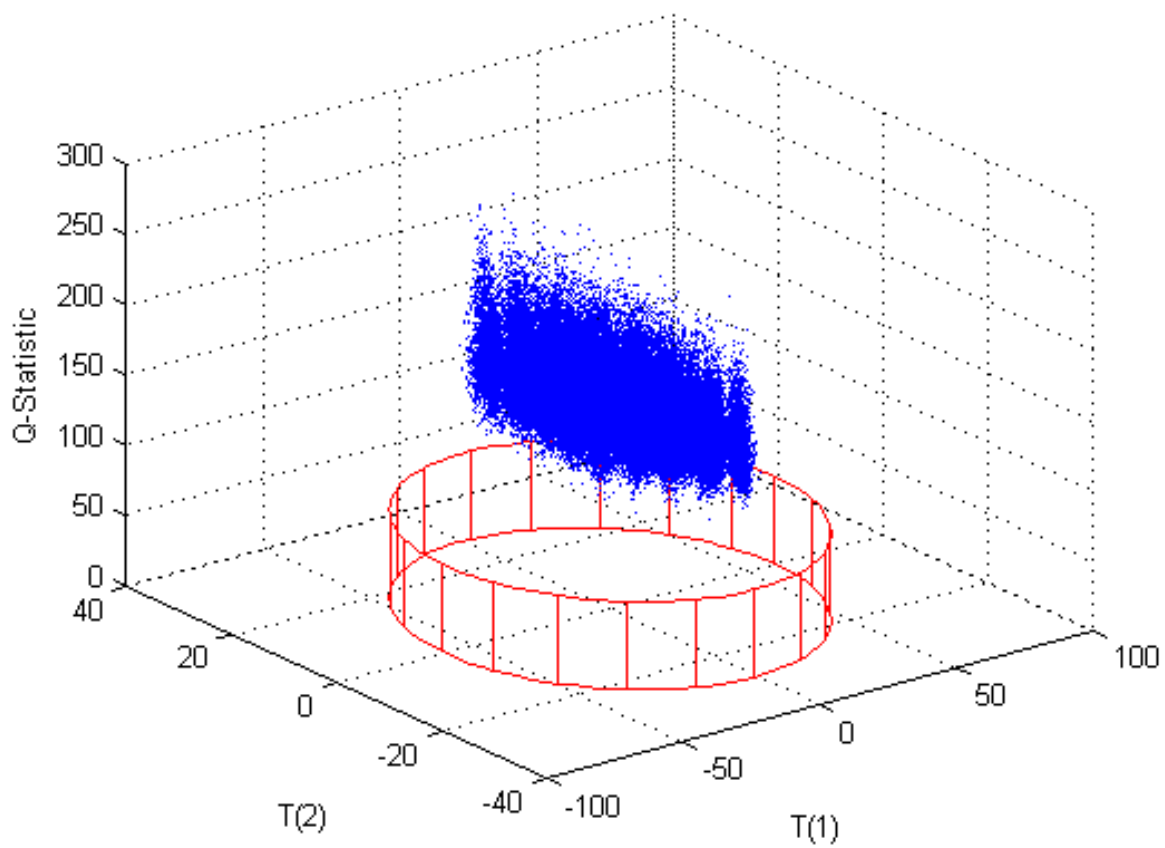
Figure 4.76. Faulty Case 7 Scores Plot for PC2 and PC3. *Note: Only the faulty data are shown with the base case 95% confidence boundary displayed in red. There was a slight change in both PC2 and PC3 scores but no detectable fault.*

Figure 4.77. Faulty Case 7 3D Scores Plot for PC1, PC2, and PC3. *Note: Only the faulty data are shown with the base case 95% confidence boundary displayed as an ellipsoid. There was a slight change in both PC2 and PC3 scores but no detectable fault.*

Figure 4.78. Faulty Case 7 Mahalanobis Distance Plot. *Note: Only the faulty data are shown with the base case 95% confidence boundary displayed in red. There was shift but the fault may not be detectable depending on operating conditions.*
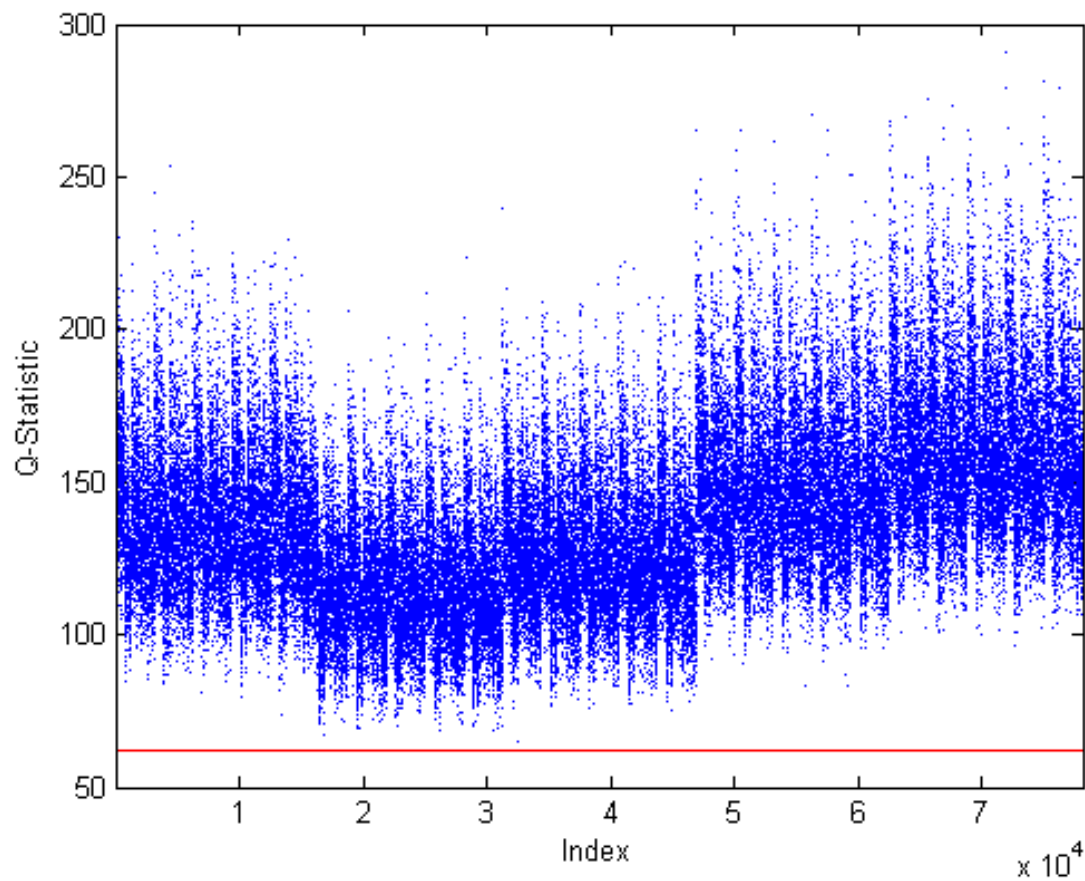
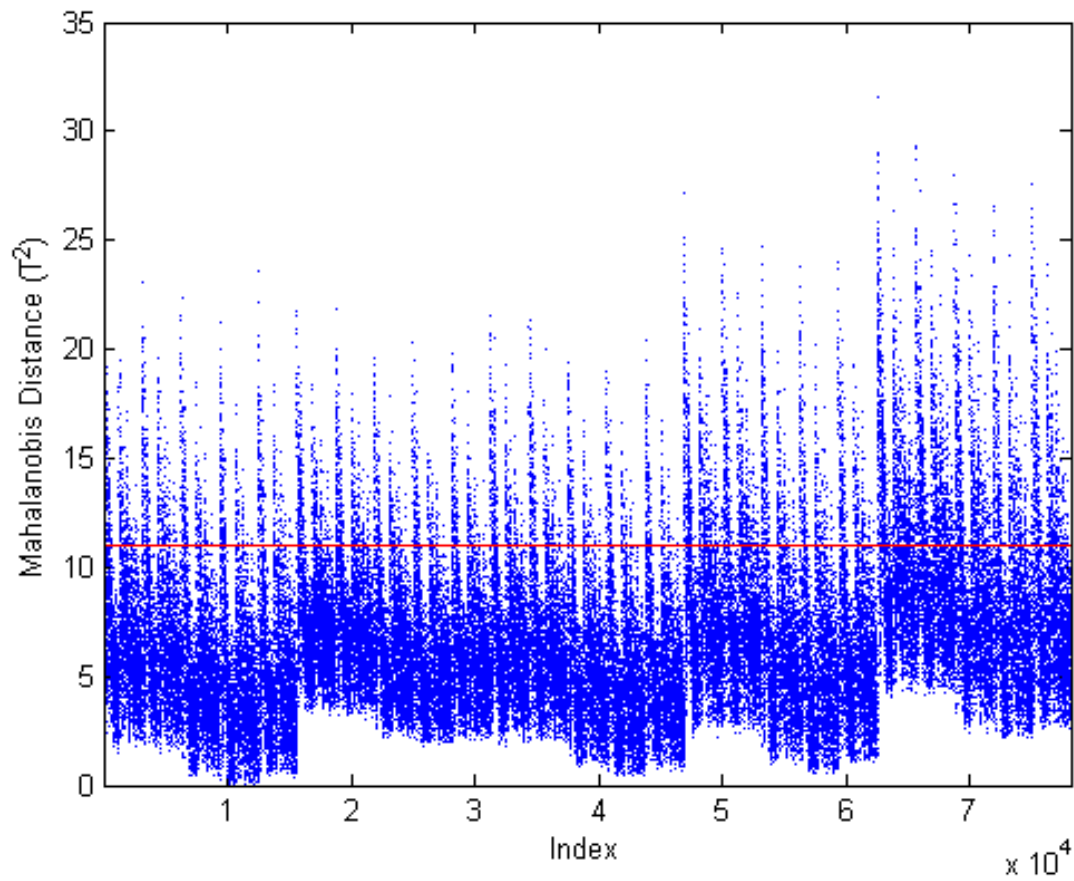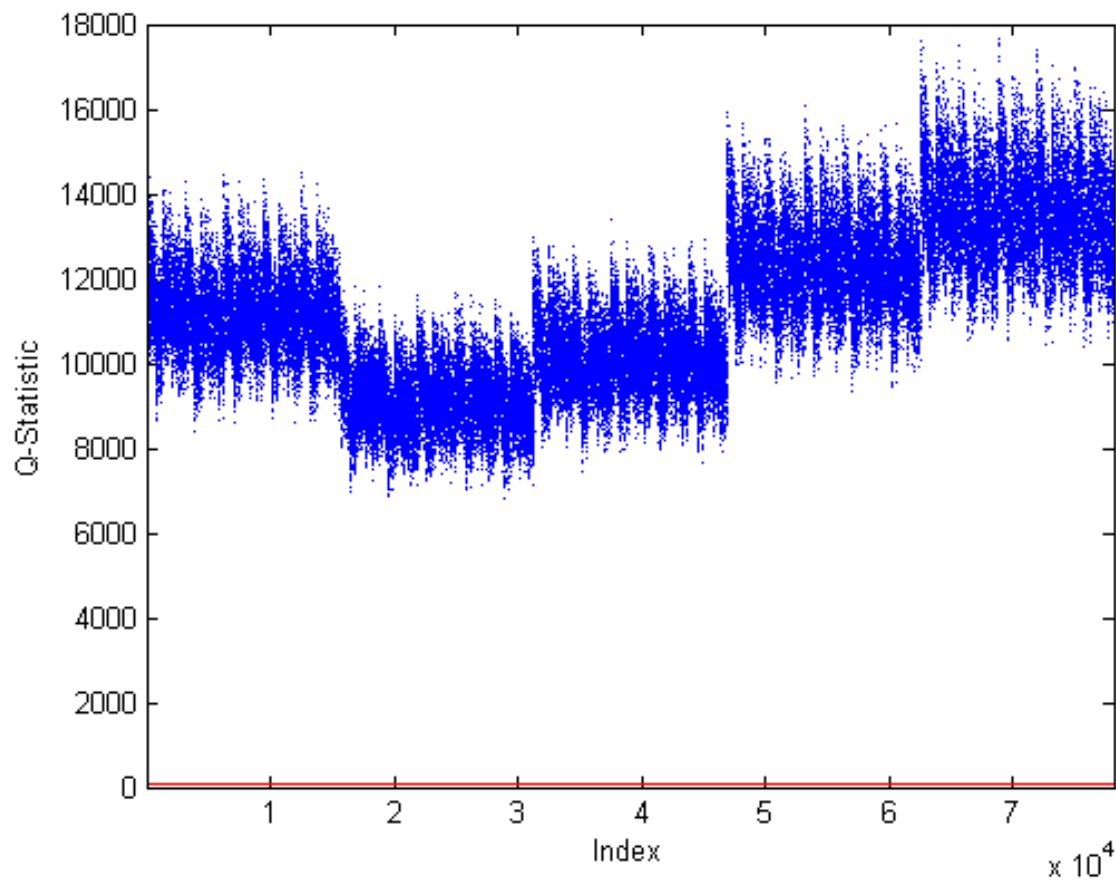**Figure 4.79. Faulty Case 7** *Q*-**Statistic Plot.** *Note: Only the faulty data are shown with the base case 95% confidence boundary displayed in red. There was a detectable fault.*

Figure 4.80. Faulty Case 7 PC1, PC2, and *Q*-Statistic Plot. *Note: Only the faulty data are shown with the base case 95% confidence boundary displayed in red. There was a detectable fault in the Q-statistic.*

4.3.8 Case 8

For the eighth faulty case, inefficient separation operations of the filtration system downstream of the hydrofluorination reaction in Module 4 were investigated. Inefficient filtration resulted in additional uranium being diverted to the off-gas waste stream. This case was modeled by changing the filter fractionation parameters $K_{Mod4F,16}$ and $K_{Mod4F,17}$ for the UF_4 and UO_2 in Module 4F, respectively. For both, the base case value was increased ten times. Therefore, the value of $K_{Mod4F,16}$ was increased from 0.00001 to 0.0001, and the value of $K_{Mod4F,17}$ was increased from 0.001 to 0.01. The results show that this fault was only detectable in the Q-statistic.

These parameters appear in the model as shown in Eqs. (3.2.4.48) and (3.2.4.49) which are restated here in terms of state variable numbers.

$$K_{Mod4F,16} * \text{Xss}(207) - \text{Xss}(214) = 0 \qquad (4.3.8.1)$$

$$K_{Mod4F,17} * \text{Xss}(208) - \text{Xss}(215) = 0 \qquad (4.3.8.2)$$

The base case nominal value for Xss(214) was 0.002 while the faulty case 8 value was 0.02. The base case nominal value for Xss(215) was 0.01 while the faulty case 8 value was 0.1. This is an increase of ten times in both cases. Based on the sensitivity analysis, Xss(214) was the only state variable sensitive to changes in $K_{Mod4F,16}$ and Xss(215) was the only state variable sensitive to changes in $K_{Mod4F,17}$. The sensitivity factors for each of these were one, which was corroborated by the results. Xss(207) and Xss(214) moderately loaded PC1 while Xss(208) and Xss(215) moderately loaded PC2.

There was no detectable fault in any of the scores plots even though there were slight shifts in the scores. There was a slight increase in the Mahalanobis distance (Figure 4.81), but most of the data points were still within the 95% confidence boundary so the fault was not likely to be detectable. An increase in the Mahalanobis distance was expected since additional material in the waste is outside normal operating conditions. However, since this was such a small change, it was not significant enough to be outside of normal conditions. Even though the increase was large, the actual amounts from the fractionations were still very small even after the increase. A significant increase occurred in the Q-statistic (Figures 4.82–4.83). This fault was expected in the Q-statistic since changing the filter fractionation changes the parameters and therefore the relative relationship between the state variables would be different. The fault in the Q-statistic was expected to be large since this was a large change in two parameters which should result in a detectable change in the relationships between the parameters and state variables. If a fault of this nature needs to be detectable, then the state variables Xss(214) and Xss(215) need to be weighted much more during the scaling stage in the data pre-processing since they are the only two state variables affected by a change in $K_{Mod4F,16}$ and $K_{Mod4F,17}$ according to the results of the sensitivity analysis. These parameters were increased significantly (approximately 900% over the nominal base case values) even though the values were very small so that there was not a significant change in the amount of uranium diverted to waste. The diversion was

clearly detectable in the Q-statistic. It is recommended that the off-gas stream from the hydrofluorination process be monitored for uranium content. This case is summarized in Table 4.28.

Table 4.28. Summary of Faulty Case 8

Summary of Faulty Case					
Priority	Module	Faulty Variable	Base Case Value	Faulty Value	Physical Description
Medium	4	$K_{Mod4F,16}$ and $K_{Mod4F,17}$	0.00001; 0.001	0.0001; 0.01	Inefficient separation downstream of the hydrofluorination reaction results in more U in Module 4 waste
Summary of Results					
	PC1 Scores	PC2 Scores	PC3 Scores	T2	Q
Direction	-	-	+	~+	++++
Detectability	No	No	No	Not Likely	Yes

Figure 4.81. Faulty Case 8 Mahalanobis Distance Plot. *Note: Only the faulty data are shown with the base case 95% confidence boundary displayed in red. There was shift, but the fault may not be detectable under most operating conditions.*

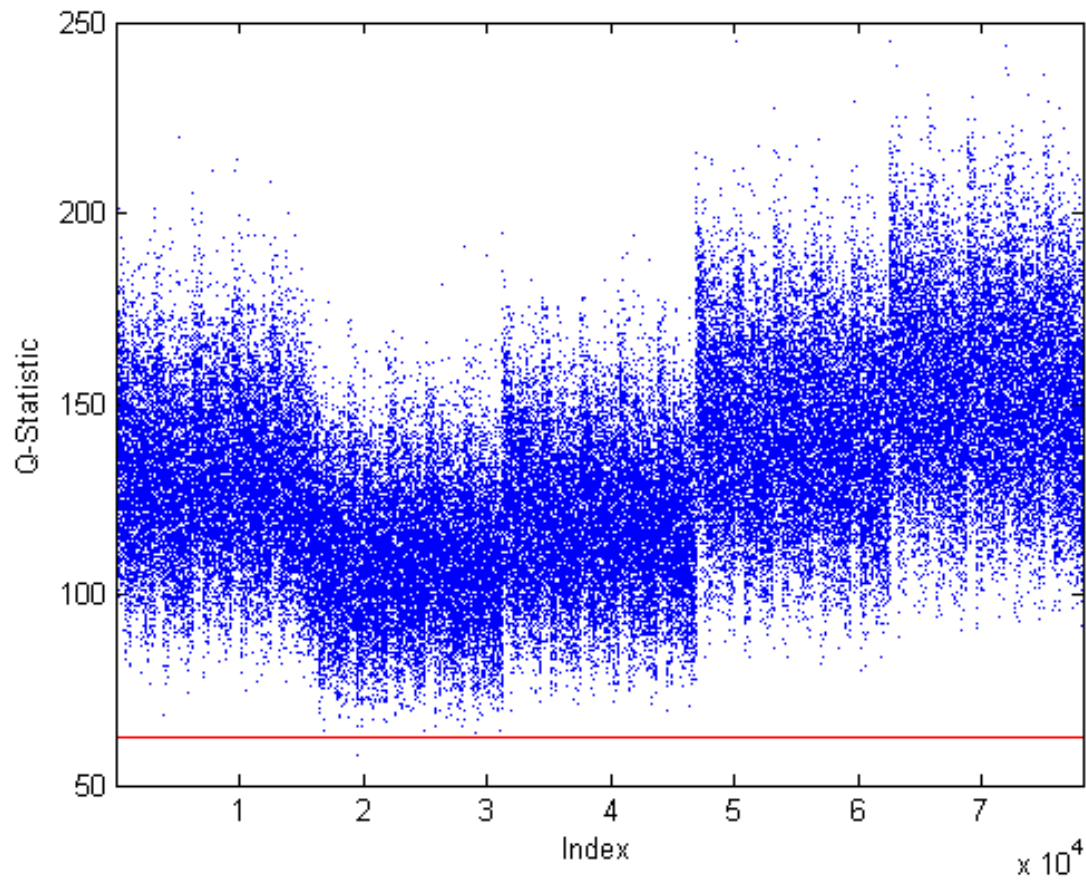**Figure 4.82. Faulty Case 8 *Q*-Statistic Plot.** *Note: Only the faulty data are shown with the base case 95% confidence boundary displayed in red. There was a detectable fault.*

249
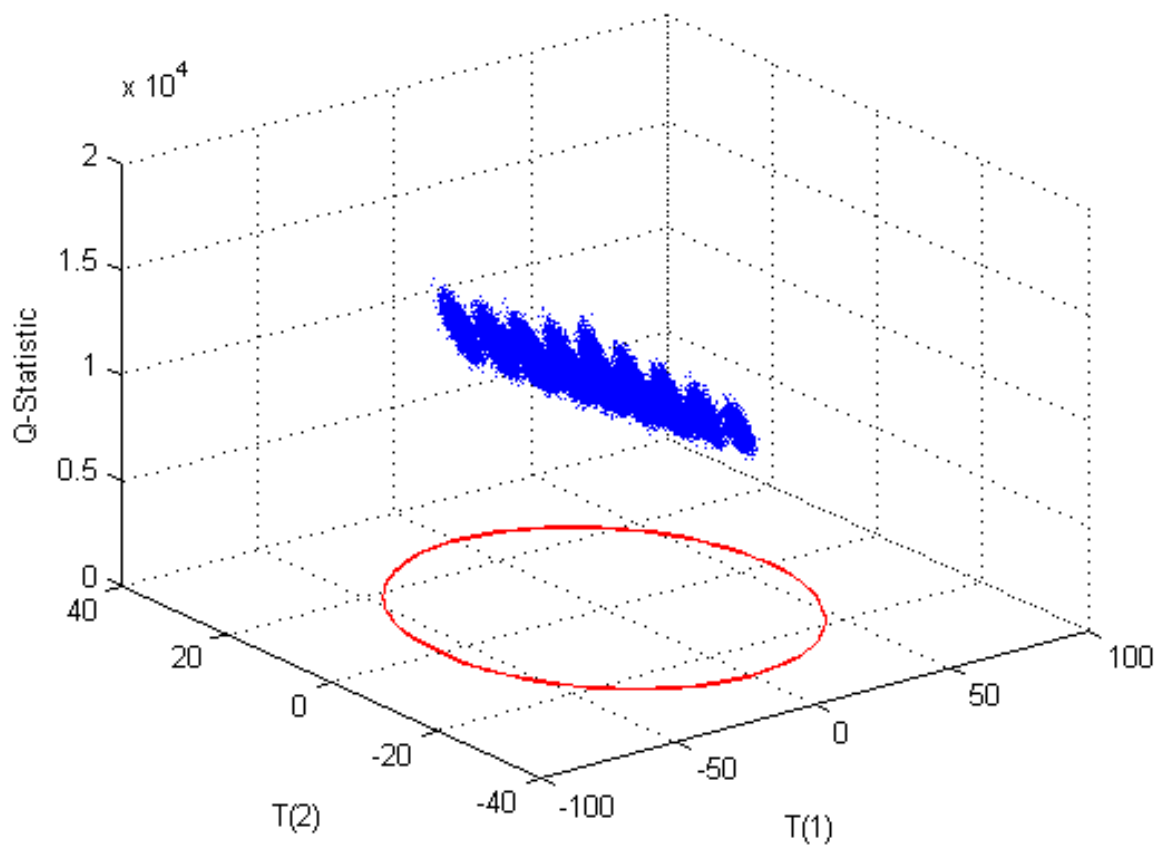
Figure 4.83. Faulty Case 8 PC1, PC2, and *Q*-Statistic Plot. *Note: Only the faulty data are shown with the base case 95% confidence boundary displayed in red. There was a detectable fault in the Q-statistic.*
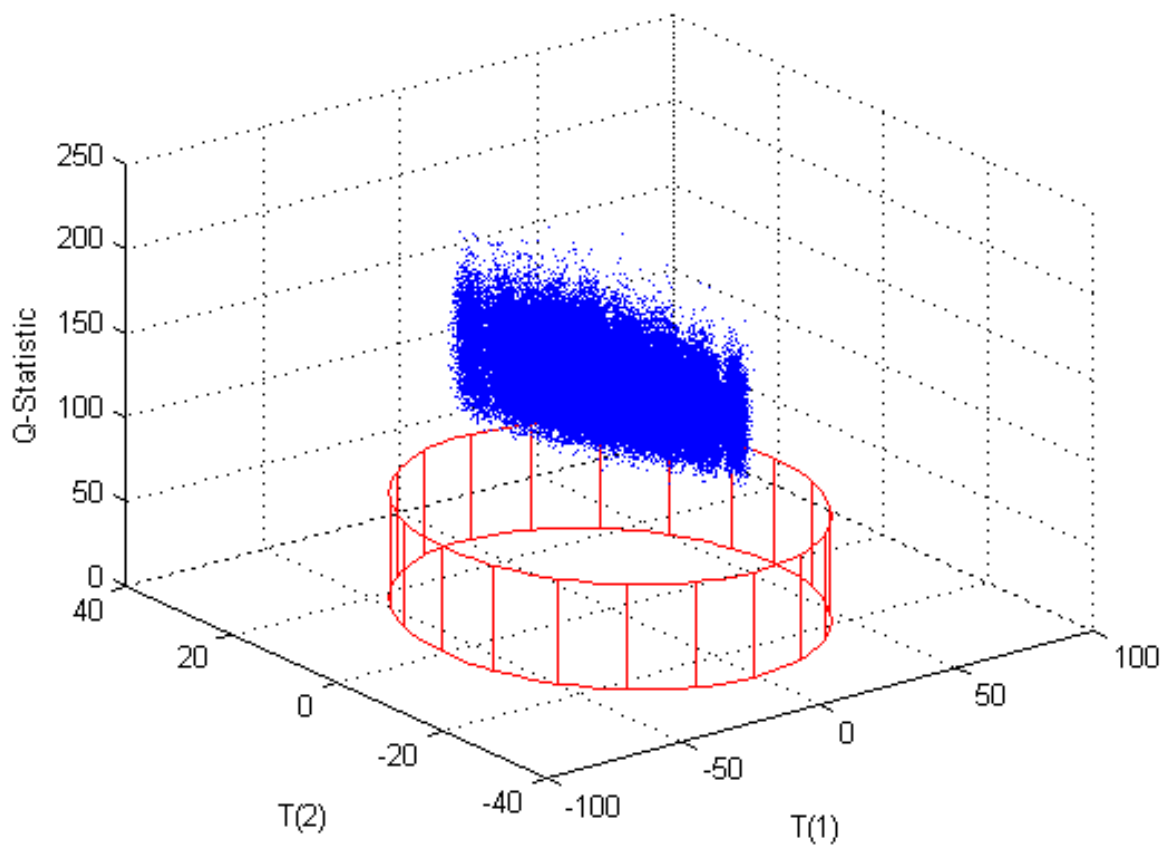
4.3.9 Case 9

The ninth faulty case tested the ability of the model to detect the diversion of UF_6 from the secondary fluorination process in Module 5. In this case, the model was modified to allow for UF_6 to exit the process at the gas separator in Module 5F. Several percentages of diversion were tested to reach a detectable scenario; only the 75% diversion results are presented below. This appears to be a very large diversion but since only 10% of the incoming uranium to Module 5 was diverted to the secondary reactor this diversion was not significant. Therefore, this corresponded to an overall diversion of approximately 8%. The results show that this fault was only detectable in the Q-statistic.

Equation (4.3.9.1) shows the UF_6 balance for the gas separator, where Xss(281) represents the UF_6 in Stream 56.

$$S_{Mod5F,1} * Xss(259) - Xss(281) = 0 \qquad (4.3.9.1)$$

$$Xss(259) - Xss(265) - Xss(281) = 0 \qquad (4.3.9.2)$$

$$Xss(265) - Xss(272) = 0 \qquad (4.3.9.3)$$

In this faulty case, both Xss(265) and Xss(272) result in a reduction of 75% in comparison to the base case nominal values as expected. The final product [Xss(273)] results in an 8% reduction in comparison to the base case nominal values which would be within the range of normal operation.

There was no detectable fault in any of the scores plots. It was expected that there would be no fault in the scores because the primary state variables [Xss(265), Xss(269), Xss(270), and Xss(272)] that were most directly affected by this fault contributed only slightly if at all to the first four principal components because they were not differentially weighted. There was also no detectable change in the Mahalanobis distance. It was expected that there would not be a fault in the Mahalanobis distance since this reduced the final uranium product by only 8% which should be within the allowed ±10% variation of the base case model. There was an increase in the Q-statistic (Figures 4.84–4.85). The Q-statistic fault was expected since this changed a parameter and therefore the relative relationship between the state variables. The fault in the Q-statistic was detectable at this percentage of diversion but may not be detectable at lower percentages of diversion. It is highly recommended that the final product from the NUCP be monitored and correlated to the uranium feed to the plant. Table 4.29 summarizes this faulty case.

Table 4.29. Summary of Faulty Case 9

Summary of Faulty Case					
Priority	**Module**	**Faulty Variable**	**Base Case Value**	**Faulty Value**	**Physical Description**
Medium	5	$S_{Mod5F,1}$	N/A	0.75	Diversion of UF_6 through the off-gas of the secondary fluorination process in Module 5

Summary of Results					
	PC1 Scores	**PC2 Scores**	**PC3 Scores**	**T2**	**Q**
Direction	0	0	0	0	++
Detectability	No	No	No	No	Yes

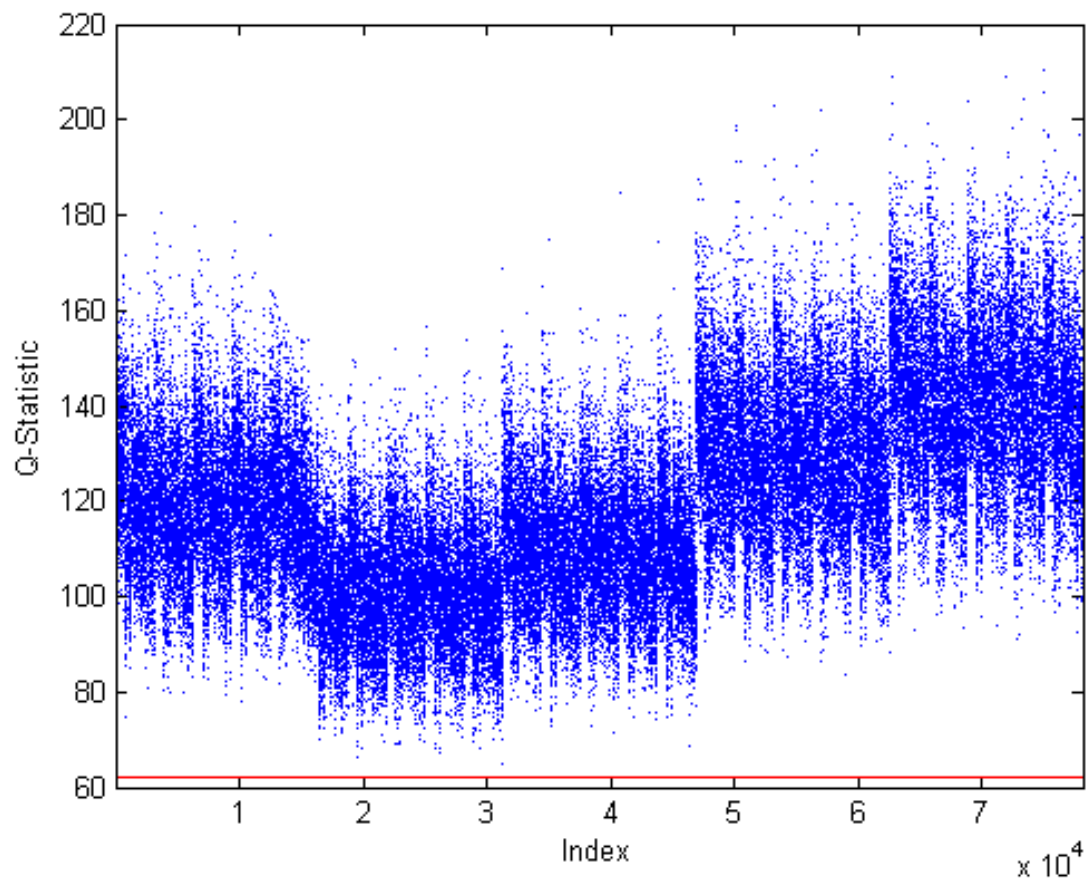**Figure 4.84. Faulty Case 9 *Q*-Statistic Plot.** *Note: Only the faulty data are shown with the base case 95% confidence boundary displayed in red. There was a detectable fault.*

253

Figure 4.85. Faulty Case 9 PC1, PC2, and *Q*-Statistic Plot. *Note: Only the faulty data are shown with the base case 95% confidence boundary displayed in red. There was a detectable fault in the Q-statistic.*

4.3.10 Case 10

The tenth faulty case tested the ability of the model to detect inefficient operations of the fluorination processes in Module 5. In this case, the extents of reaction for both the primary and secondary fluorination reactions were changed from 0.999 to 0.95. During the sensitivity analysis, seven variables were identified as being extremely sensitive to changes in these parameters. Those state variables were Xss(236), Xss(239), Xss(245), Xss(250), Xss(260), Xss(266), and Xss(269) which correspond to the UF_4 in Streams 49, 50, 51, 53, 55, 57, and 58, respectively. The results show that this fault was only detectable in the Q-statistic.

The extents of reaction for both the primary and secondary fluorination reactions appear in the model as shown in Eqs. (3.2.5.17)–(3.2.5.19) and Eqs. (3.2.5.41)–(3.2.5.43) which are restated here in terms of state variable numbers.

$$Xss(229) + \left(n_{Mod5B,7} * X_{Mod5B} * Xss(230)\right) - Xss(234) = 0 \qquad (4.3.10.1)$$

$$\left(n_{Mod5B,15} * X_{Mod5B} * Xss(230)\right) - Xss(235) = 0 \qquad (4.3.10.2)$$

$$Xss(230) + \left(n_{Mod5B,16} * X_{Mod5B} * Xss(230)\right) - Xss(236) = 0 \qquad (4.3.10.3)$$

$$Xss(252) + \left(n_{Mod5E,7} * X_{Mod5E} * Xss(254)\right) - Xss(258) = 0 \qquad (4.3.10.4)$$

$$Xss(253) + \left(n_{Mod5E,15} * X_{Mod5E} * Xss(254)\right) - Xss(259) = 0 \qquad (4.3.10.5)$$

$$Xss(254) + \left(n_{Mod5E,16} * X_{Mod5E} * Xss(254)\right) - Xss(260) = 0 \qquad (4.3.10.6)$$

Both Xss(258) and Xss(264) which correspond to the fluorine in Streams 55 and 56, respectively, increased by 48% over the base case nominal value due to this change in the extent of reaction. Another nine state variables decreased between 4.5% and 4.9% in comparison to the base case nominal values as well. These were the UF_6 in Streams 49, 51–55, 57, 59, and 60.

There was no detectable fault in any of the scores plots. It was expected that there would be no fault in the scores because the primary state variables in Module 5 with the exception of Xss(273) contributed at most moderately and in most cases only slightly if at all to the first four principal components. There was also no detectable change in the Mahalanobis distance. It was expected that there would not be a fault in the Mahalanobis distance since this was only approximately a 5% reduction in the final uranium product which may be within the normal variation of the base case model. There was an increase in the Q-statistic (Figures 4.86–4.87). The Q-statistic fault was expected since this changed parameters and therefore the relative relationship between the state variables. The fault in the Q-statistic was clearly

detectable. It is recommended that the feed, product, and waste streams in the fluorination process area be monitored for flow rate and uranium content. Table 4.30 summarizes this faulty case.

Table 4.30. Summary of Faulty Case 10

			Summary of Faulty Case		
Priority	**Module**	**Faulty Variable**	**Base Case Value**	**Faulty Value**	**Physical Description**
High	5	X_{Mod5B} and X_{Mod5E}	0.999	0.95	Inefficient operations of the fluorination processes in Module 5 results in less UF_4 converted to UF_6 and more U in the waste streams

		Summary of Results			
	PC1 Scores	**PC2 Scores**	**PC3 Scores**	**T2**	**Q**
Direction	0	0	0	0	++
Detectability	No	No	No	No	Yes

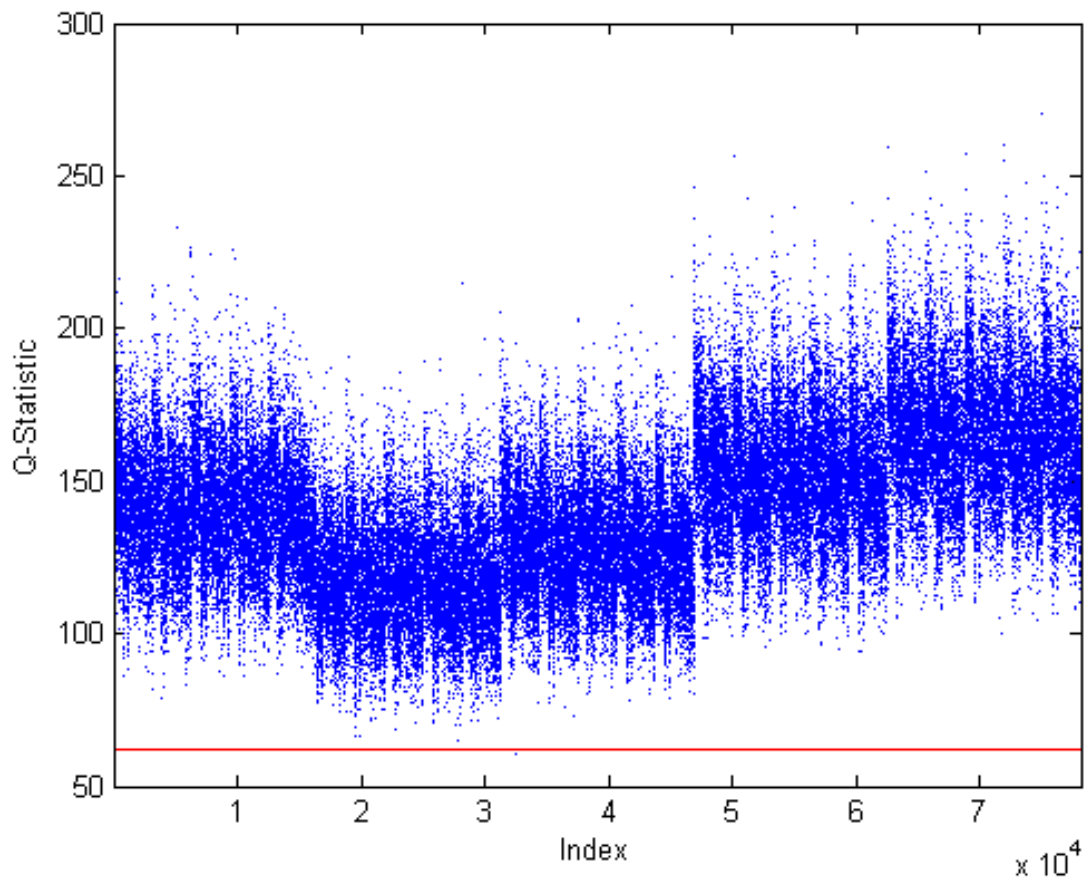**Figure 4.86. Faulty Case 10** *Q*-**Statistic Plot.** *Note: Only the faulty data are shown with the base case 95% confidence boundary displayed in red. There was a detectable fault.*

257
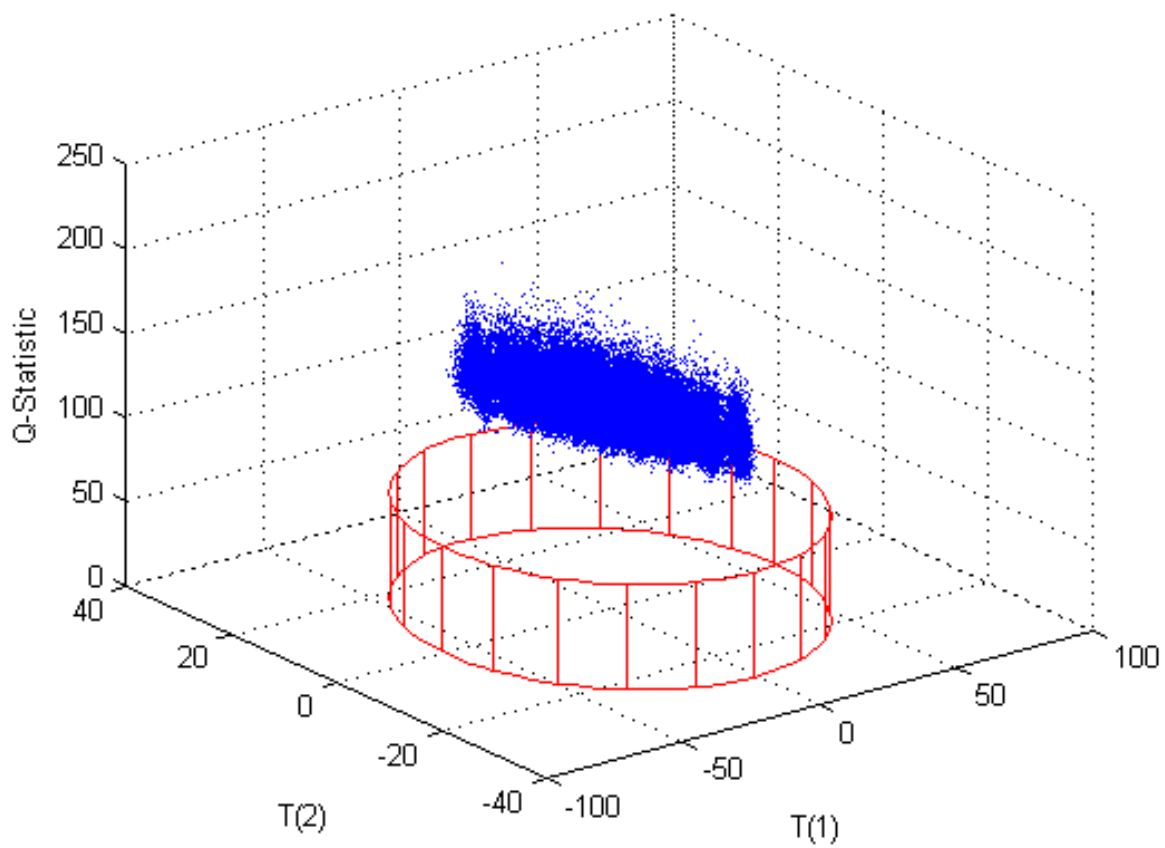
Figure 4.87. Faulty Case 10 PC1, PC2, and *Q*-Statistic Plot. *Note: Only the faulty data are shown with the base case 95% confidence boundary displayed in red. There was a detectable fault in the Q-statistic.*

4.3.11 Case 11

For the eleventh faulty case, a percentage of the UF$_6$ product was diverted from the final mixer in Module 5. Streams 52 and 59 were pure UF$_6$ that were mixed to form the final product of the process. In this case, a new stream (61) was formed by diverting a percentage of Streams 52 and 59. Several percentages were tested; the diversion of 20% is presented below. The results show that this fault was only detectable in the Q-statistic.

Equations (4.3.11.1) and (4.3.11.2) show the material balance for the UF$_6$ in Streams 60 and 61, where Xss(281) represents the UF$_6$ in Stream 61.

$$Xss(246) + Xss(272) - Xss(273) - Xss(281) = 0 \qquad (4.3.11.1)$$

$$S_{Mod5F,2} * [Xss(246) + Xss(272)] - Xss(281) = 0 \qquad (4.3.11.2)$$

There was no detectable fault in any of the scores plots. It was expected that there would be no fault in the scores because the diversion stream and the final product [Xss(273)] both exit the plant and have no additional interaction with the model. Even though Xss(273) was a heavy contributor to both PC1 and PC3, it was the only primary state variable affected by this diversion and the diversion was not significant enough to result in a detectable fault in the scores plots. There was also no detectable change in the Mahalanobis distance. It was expected that there would not be a detectable fault in the Mahalanobis distance since only one primary state variable was affected even though the diversion was above the 10% allowed variation. There was an increase in the Q-statistic (Figures 4.88–4.89). The Q-statistic fault was expected since this changed the relative relationship between the state variables. This case is of extremely high concern for safeguards and the goal of this detection framework was to be able to detect 10% diversion. However, since the final product in the base case data matrix varied from -27.8% to +15.5% based on the nominal steady-state solution for Xss(273), this diversion of UF$_6$ could be within the normal variation of the base case. It is highly recommended that the final product from the NUCP be monitored and correlated to the uranium feed to the plant. Table 4.31 summarizes this faulty case.

Table 4.31. Summary of Faulty Case 11

		Summary of Faulty Case			
Priority	**Module**	**Faulty Variable**	**Base Case Value**	**Faulty Value**	**Physical Description**
High	5	$S_{Mod5F,2}$	N/A	0.2	Diversion of 20% of the purified UF_6
		Summary of Results			
	PC1 Scores	**PC2 Scores**	**PC3 Scores**	**T2**	**Q**
Direction	0	0	0	0	++
Detectability	No	No	No	No	Yes

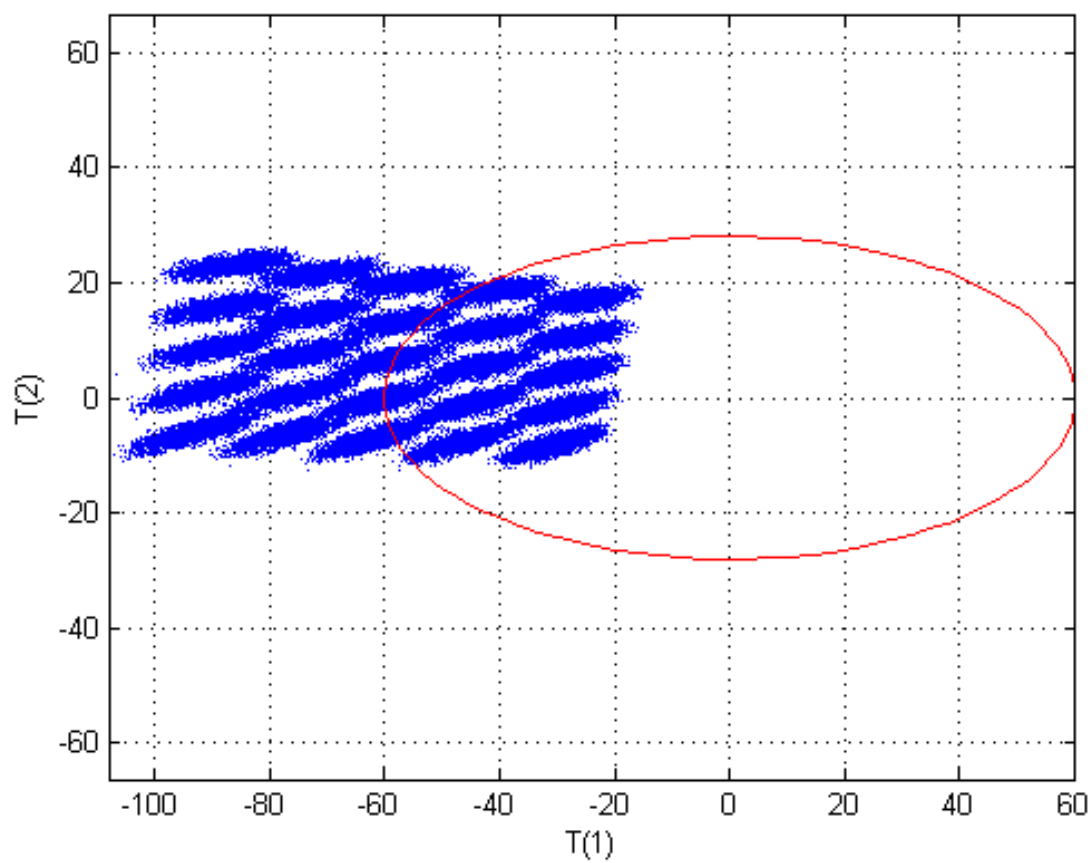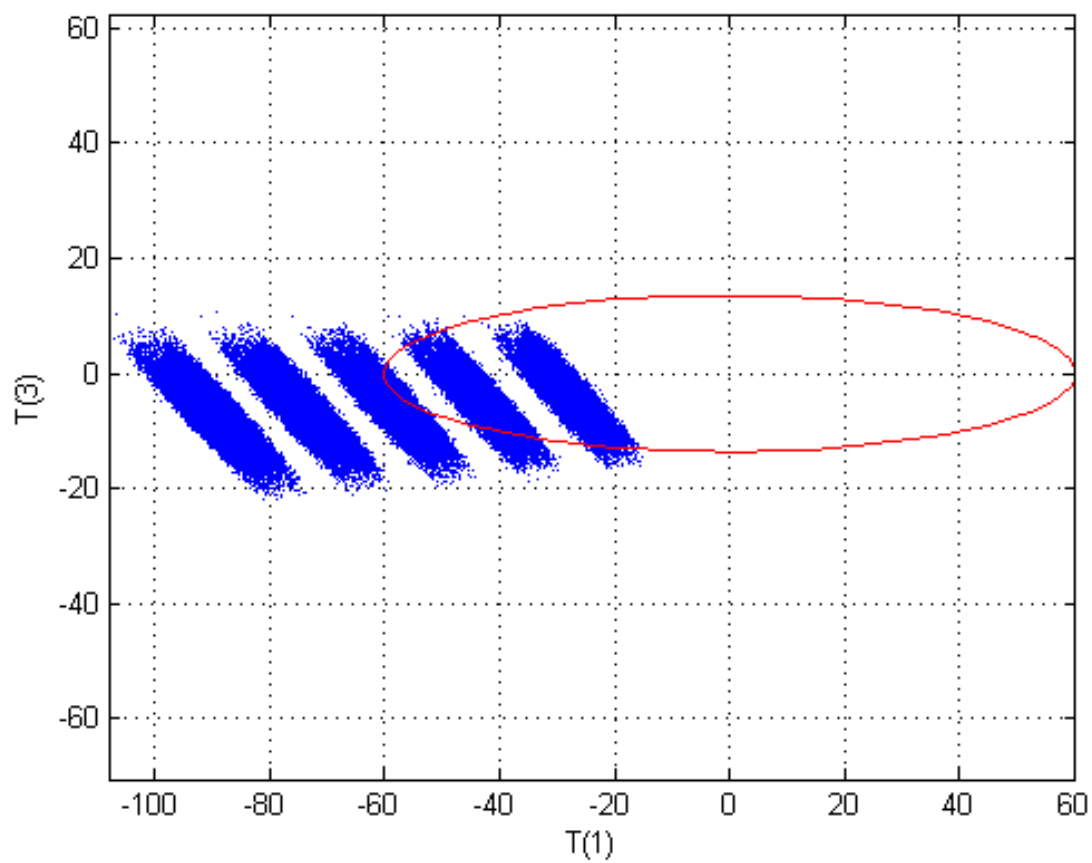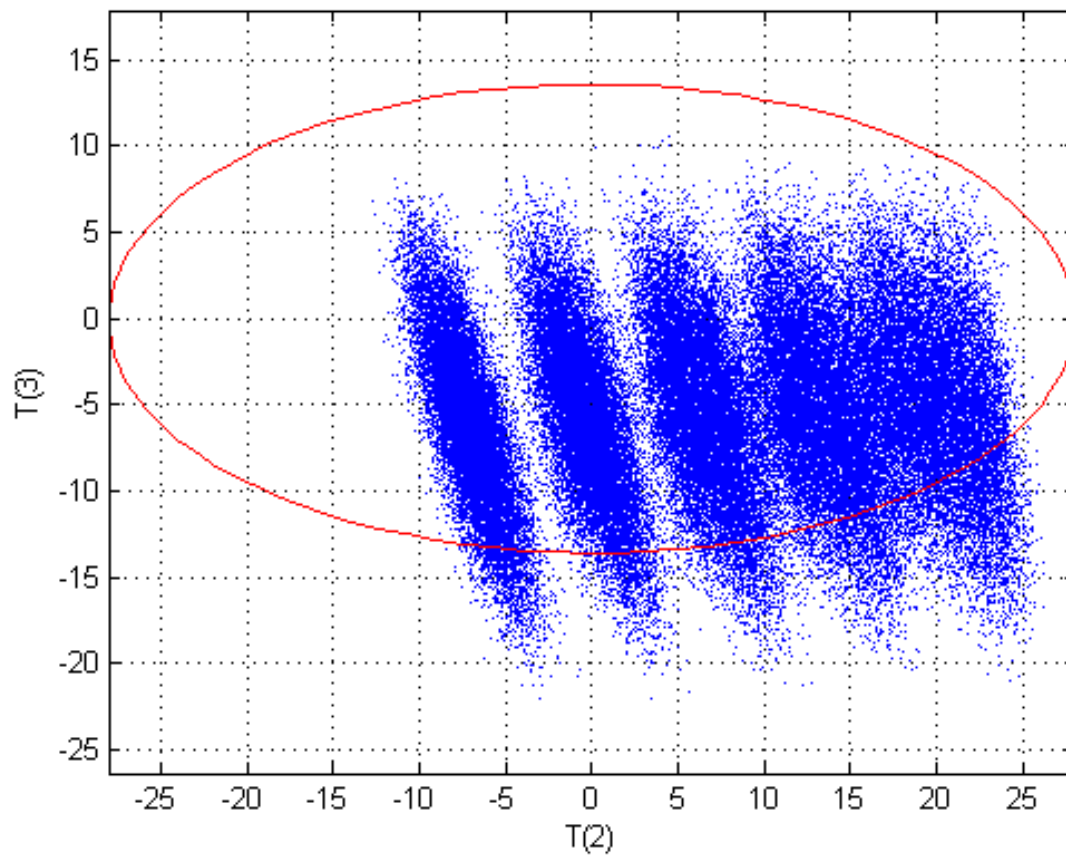**Figure 4.88. Faulty Case 11 Q-Statistic Plot.** *Note: Only the faulty data are shown with the base case 95% confidence boundary displayed in red. There was a detectable fault.*
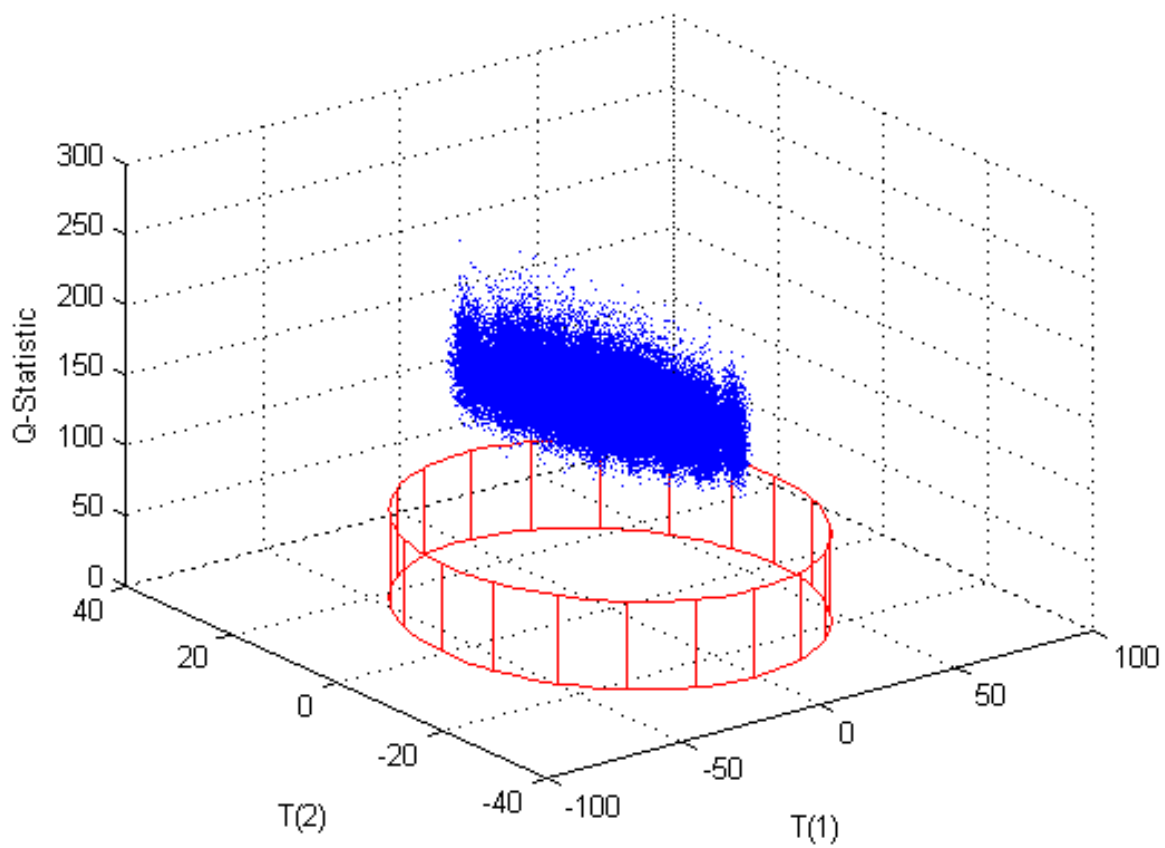
Figure 4.89. Faulty Case 11 PC1, PC2, and *Q*-Statistic Plot. *Note: Only the faulty data are shown with the base case 95% confidence boundary displayed in red. There was a detectable fault in the Q-statistic.*

4.3.12 Case 12

Faulty Case 12 was the first case used to test the effect of changes in multiple parameters or inputs. It combined changes in two previous faulty cases: Case 1D and Case 11. The uranium input flow rate was increased by 25% in Module 1 for Case 1D and 20% of the UF$_6$ product was diverted through a new output stream in Module 5 for Case 11. This case models the scenario where additional uranium is fed to the process and then additional purified uranium is diverted before declaration at the end of the process. In Case 1D, the uranium input flow rate was not allowed to vary for data generation however in this case variation was set at ±10% as in the base case. The results show that this combination of faults was clearly detectable under all conditions using the Q-statistic. Additionally, under some conditions, this fault was detectable using PC1 scores and the Mahalanobis distance.

There was a shift in PC1 scores as expected based on Case 1D because the incoming uranium flow rate [Xss(274)] was a heavy contributor to PC1. However, the fault in PC1 scores was not clearly detectable under all conditions since approximately 50% of the data points were still within the 95% confidence boundary. However, since the shift was rather significant, a shift in the trend of the PC1 scores may be easily detectable when monitored. There were also slight shift in PC2 and PC3 scores but these were not clearly detectable under nearly all conditions. The scores plots are shown in Figures 4.90–4.93. There was an increase in the Mahalanobis distance as well (Figure 4.94). However, there are some conditions under which this fault would not be detectable using the Mahalanobis distance since some of the data points were within the 95% confidence boundary, but a shift in the trend in T^2 may be more detectable. The shift in the Mahalanobis distance was expected based on Case 1D and because an increase in the throughput by 25% is outside the normal operating conditions of ±10% variation in incoming uranium flow rate. There was a significant increase in the Q-statistic (Figures 4.95–4.96) to well outside the 95% confidence boundary. The fault was clearly detectable under all operating conditions using the Q-statistic. The fault in the Q-statistic was expected based on Case 11 and because the diversion was based on a parameter change which changes the relative relationship between the state variables. It is recommended that the uranium feed to the plant be monitored for both flow rate and uranium content. Additionally, it is recommended that the streams exiting each major process (e.g., dissolution, solvent extraction, fluorination) as product or waste be monitored for flow rate and uranium content. It is highly recommended that the final product from the NUCP be monitored and correlated to the uranium feed to the plant. This faulty case along with a comparison of the Case 1D and Case 11 results are provided in Table 4.32.

Table 4.32. Summary of Faulty Case 12

		Summary of Faulty Case			
Priority	Modules	Faulty Variable	Base Case Value	Faulty Value	Physical Description
High	1 and 5	$F_{1A,U}$ and $S_{Mod5F,2}$	50 kg/h; N/A	62.5 kg/h; 0.2	Increase uranium throughput by 25% then divert 20% of the purified UF_6
		Summary of Results			
	PC1 Scores	PC2 Scores	PC3 Scores	T2	Q
Direction	-	+	-	+	++
Detectability	Possibly	No	No	Possibly	Yes
		Comparison to Individual Faulty Case Results			
	PC1 Scores	PC2 Scores	PC3 Scores	T2	Q
		Case 1D			
Direction	-	0	0	+	0
Detectability	Possibly	No	No	Yes	No
		Case 11			
Direction	0	0	0	0	++
Detectability	No	No	No	No	Yes

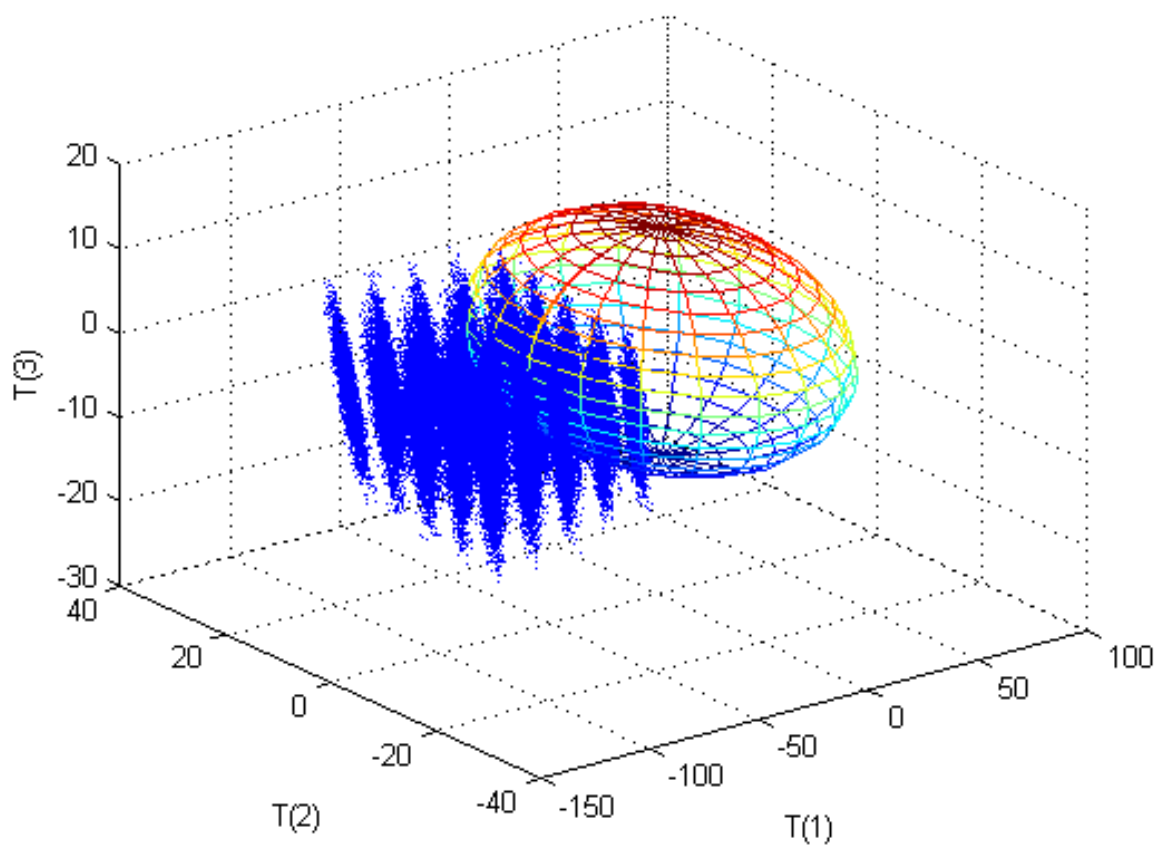**Figure 4.90. Faulty Case 12 Scores Plot for PC1 and PC2.** *Note: Only the faulty data are shown with the base case 95% confidence boundary displayed in red. There was a shift in PC1 scores which may not be detectable depending on operating conditions.*

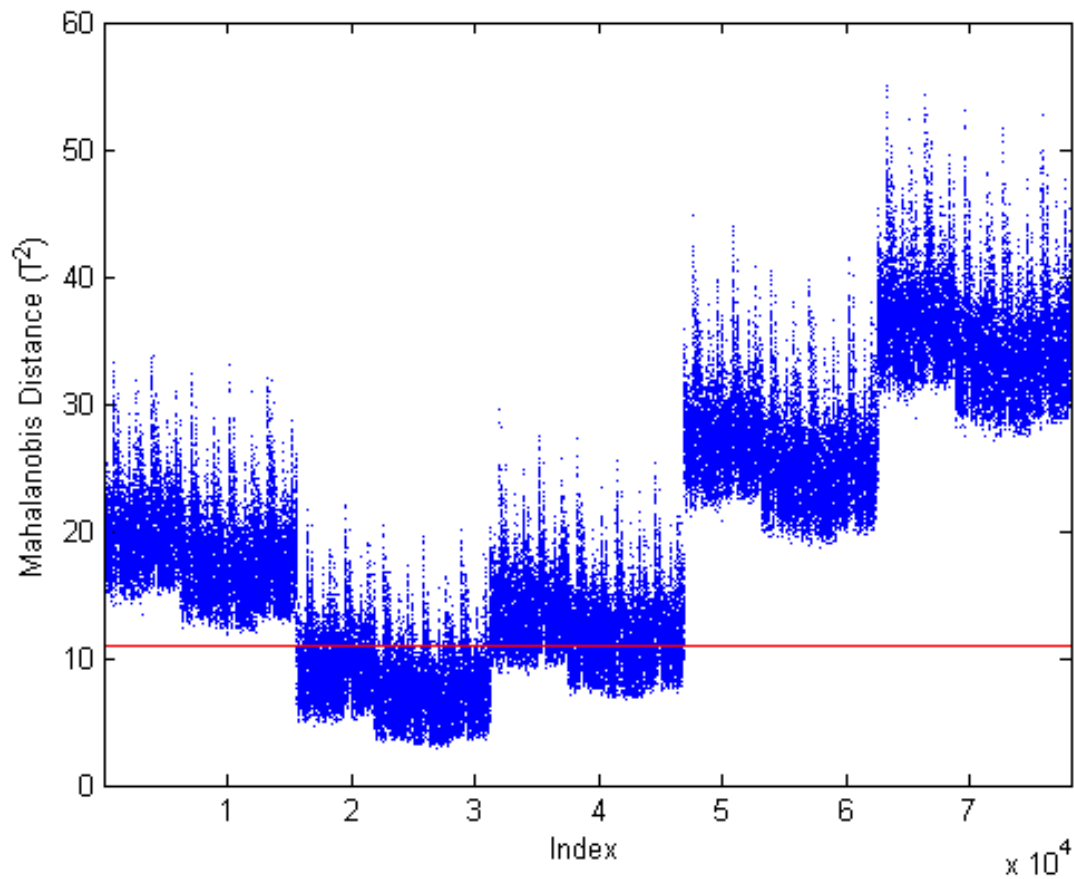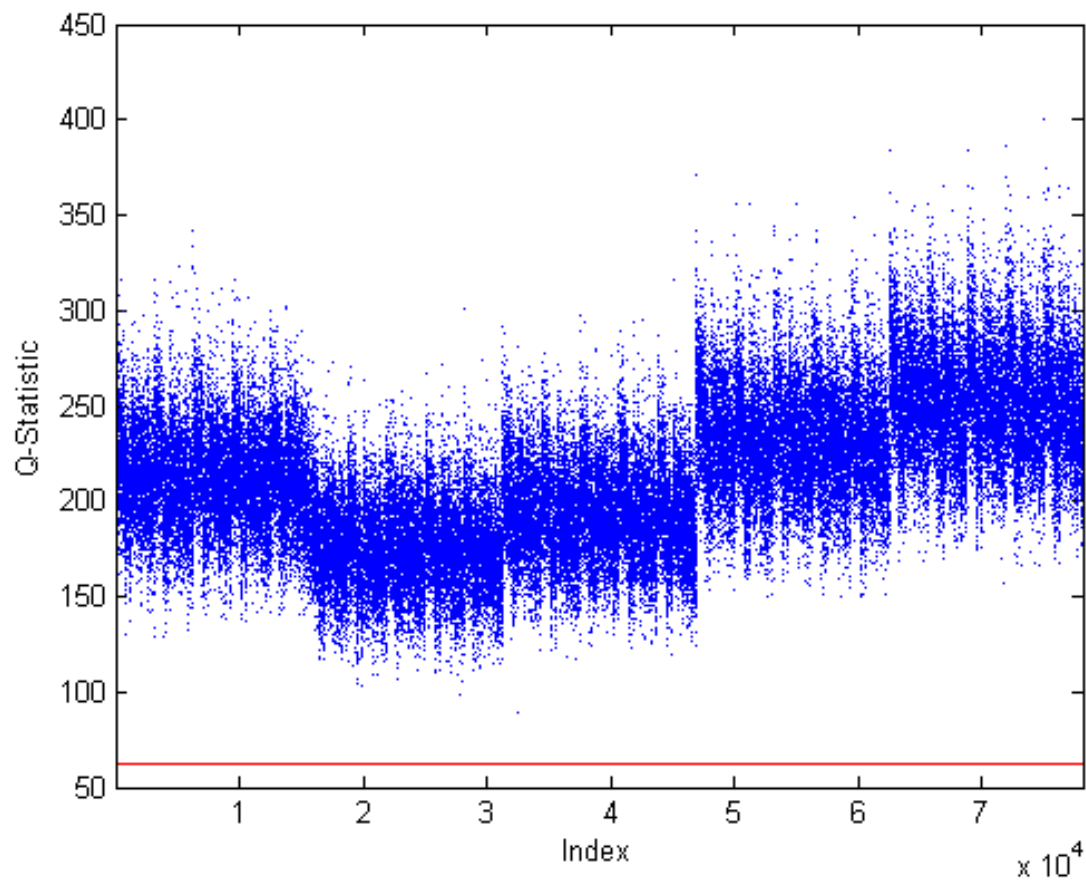**Figure 4.91. Faulty Case 12 Scores Plot for PC1 and PC3.** *Note: Only the faulty data are shown with the base case 95% confidence boundary displayed in red. There was a shift in PC1 scores which may not be detectable depending on operating conditions.*

Figure 4.92. Faulty Case 12 Scores Plot for PC2 and PC3. *Note: Only the faulty data are shown with the base case 95% confidence boundary displayed in red. There was no detectable fault.*

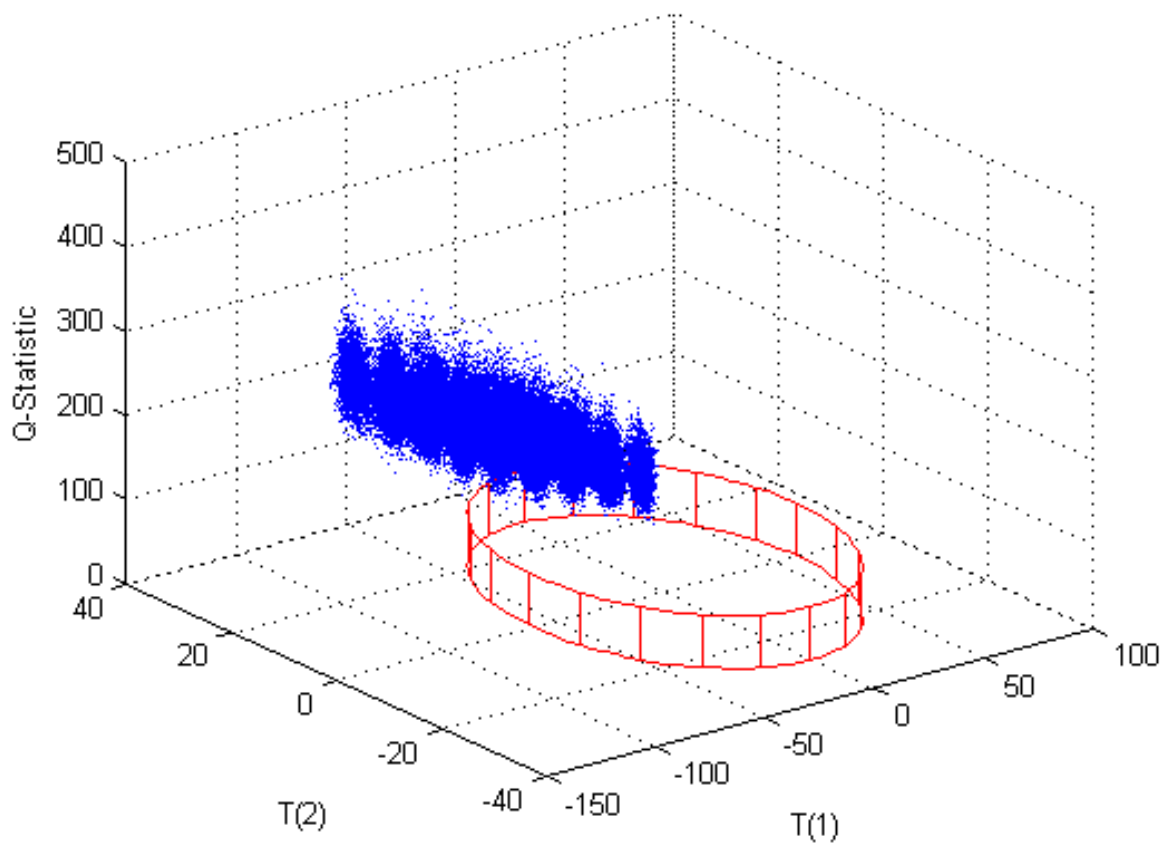**Figure 4.93. Faulty Case 12 3D Scores Plot for PC1, PC2, and PC3.** *Note: Only the faulty data are shown with the base case 95% confidence boundary displayed as an ellipsoid. There was a shift in PC1 scores which may not be detectable depending on operating conditions.*

267

Figure 4.94. Faulty Case 12 Mahalanobis Distance Plot. *Note: Only the faulty data are shown with the base case 95% confidence boundary displayed in red. There was a shift, but it may not be detectable depending on operating conditions.*

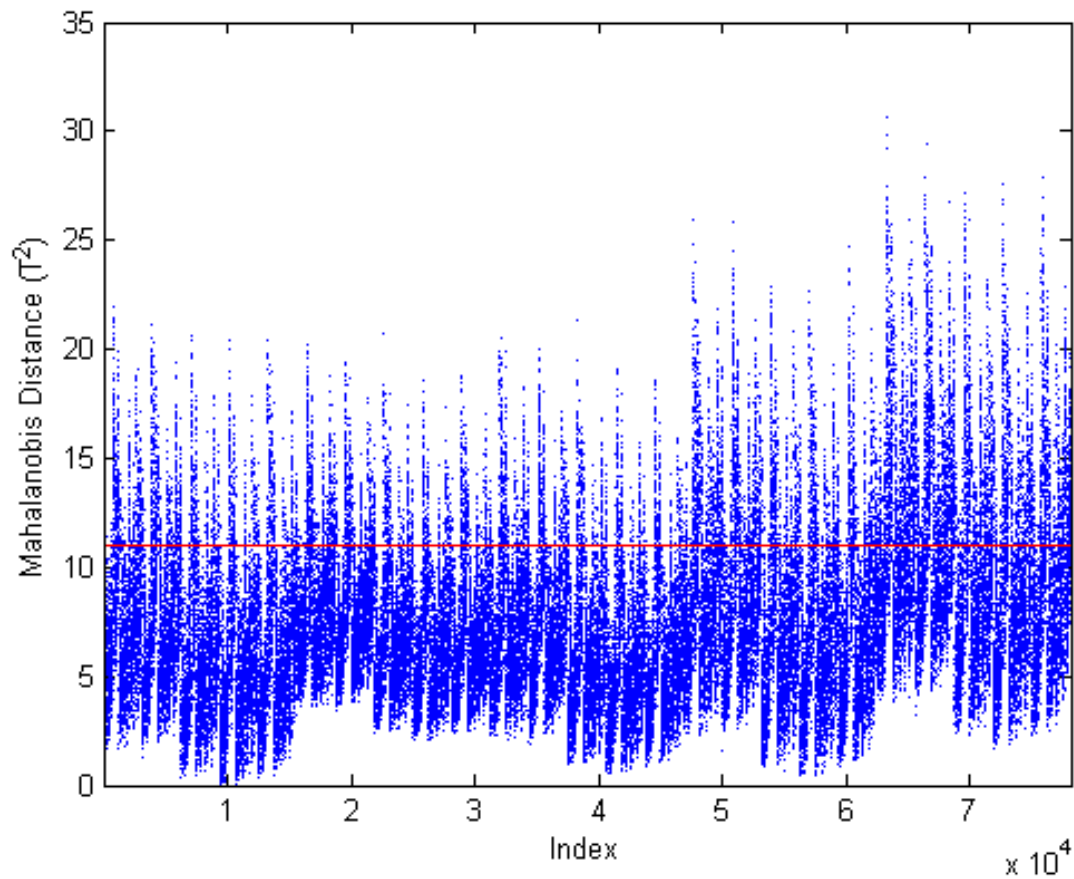**Figure 4.95. Faulty Case 12** *Q*-**Statistic Plot.** *Note: Only the faulty data are shown with the base case 95% confidence boundary displayed in red. There was a detectable fault.*

Figure 4.96. Faulty Case 12 PC1, PC2, and *Q*-Statistic Plot. *Note: Only the faulty data are shown with the base case 95% confidence boundary displayed in red. There was a detectable fault in the Q-statistic.*

4.3.13 Case 13

Faulty Case 13 was the second case used to test the effect of changes in multiple parameters or inputs. It combined changes in two previous faulty cases: Case 7 and Case 10. Both of the previous cases investigated inefficient operations. In Case 7, inefficient precipitation process operations were investigated by changing the extent of reaction for the precipitation reaction, X_{Mod3C}, from 0.9999 to 0.9 in Module 3. In Case 10, inefficient operations of the fluorination processes in Module 5 were investigated by changing the extents of reaction for both the primary and secondary fluorination reactions from 0.999 to 0.95. The results show that this combination of faults was clearly detectable using the Q-statistic.

There was a slight shift in PC1, PC2, and PC3 scores with PC3 scores having the greatest shift. However, there were no clearly detectable faults in the scores plots. The responses in the scores were very similar to those from Case 7. There was also an increase in the Mahalanobis distance (Figure 4.97) which was similar to Case 7. The fault would only be detectable under certain conditions since many of the data points were still within the 95% confidence boundary or detectable in trend monitoring. There was an increase in the Q-statistic (Figures 4.98–4.99) which was larger than that from both Case 7 and Case 10. Since this case was a combination of inefficient operations, it was also expected that the effects of the faults would be larger due to an additive effects of the faults which was the case for the Q-statistic, since it was the only diagnostic plot that resulted in a clearly detectable fault for both individual cases. It is recommended that the outlet stream from the precipitation process be monitored for flow rate and uranium content as well as type of uranium compound. It is also recommended that the feed, product, and waste streams in the fluorination process area be monitored for flow rate and uranium content. This faulty case along with a comparison of the Case 7 and Case 10 results are provided in Table 4.33.

Table 4.33. Summary of Faulty Case 13

Summary of Faulty Case					
Priority	**Modules**	**Faulty Variable**	**Base Case Value**	**Faulty Value**	**Physical Description**
High	3 and 5	X_{Mod3C}, X_{Mod5B}, and X_{Mod5E}	0.9999; 0.999	0.9; 0.95	Inefficient operations in Module 3 and 5 resulted in less U converted to desired products and more U in waste streams
Summary of Results					
	PC1 Scores	**PC2 Scores**	**PC3 Scores**	**T2**	**Q**
Direction	+	+	-	~+	++
Detectability	No	No	Not likely	Possibly	Yes
Comparison to Individual Faulty Case Results					
	PC1 Scores	**PC2 Scores**	**PC3 Scores**	**T2**	**Q**
Case 7					
Direction	+	+	-	~+	++
Detectability	No	No	Not likely	Possibly	Yes
Case 10					
Direction	0	0	0	0	++
Detectability	No	No	No	No	Yes

Figure 4.97. Faulty Case 13 Mahalanobis Distance Plot. *Note: Only the faulty data are shown with the base case 95% confidence boundary displayed in red. There was a shift but the fault may not be detectable depending on operating conditions.*
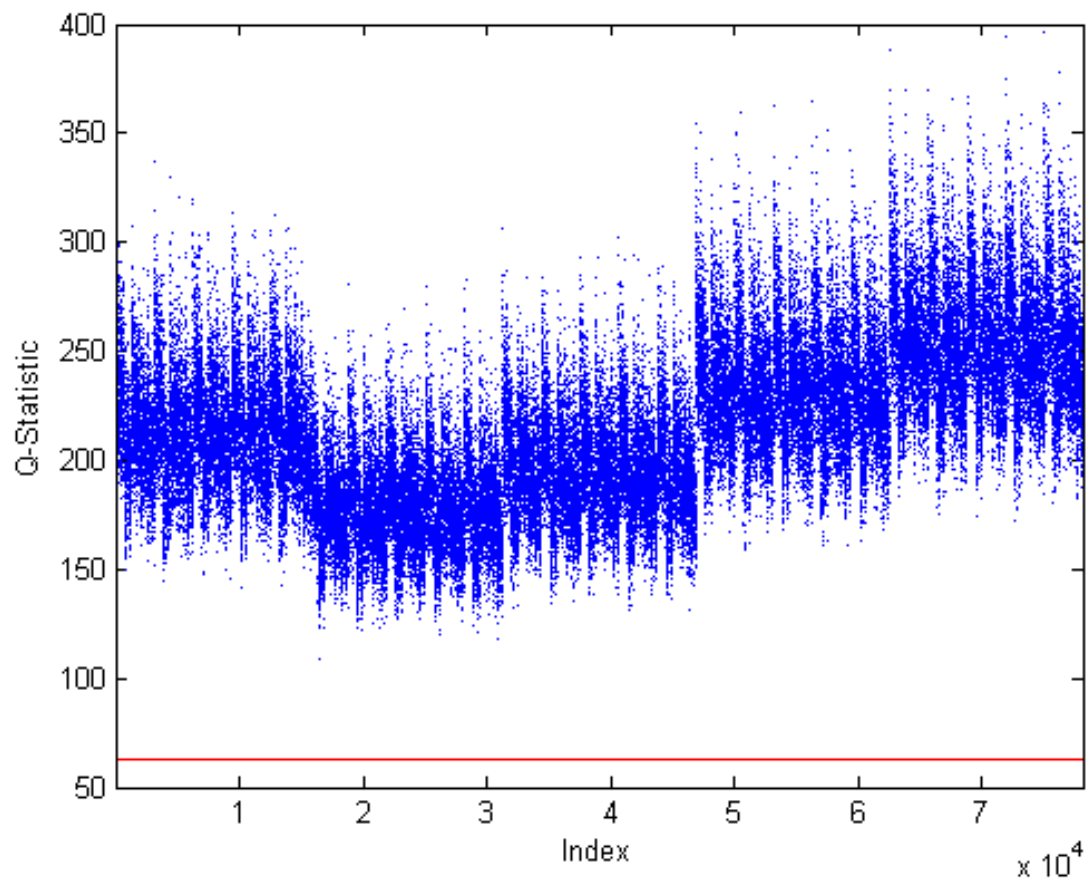
Figure 4.98. Faulty Case 13 *Q*-**Statistic Plot.** *Note: Only the faulty data are shown with the base case 95% confidence boundary displayed in red. There was a detectable fault.*
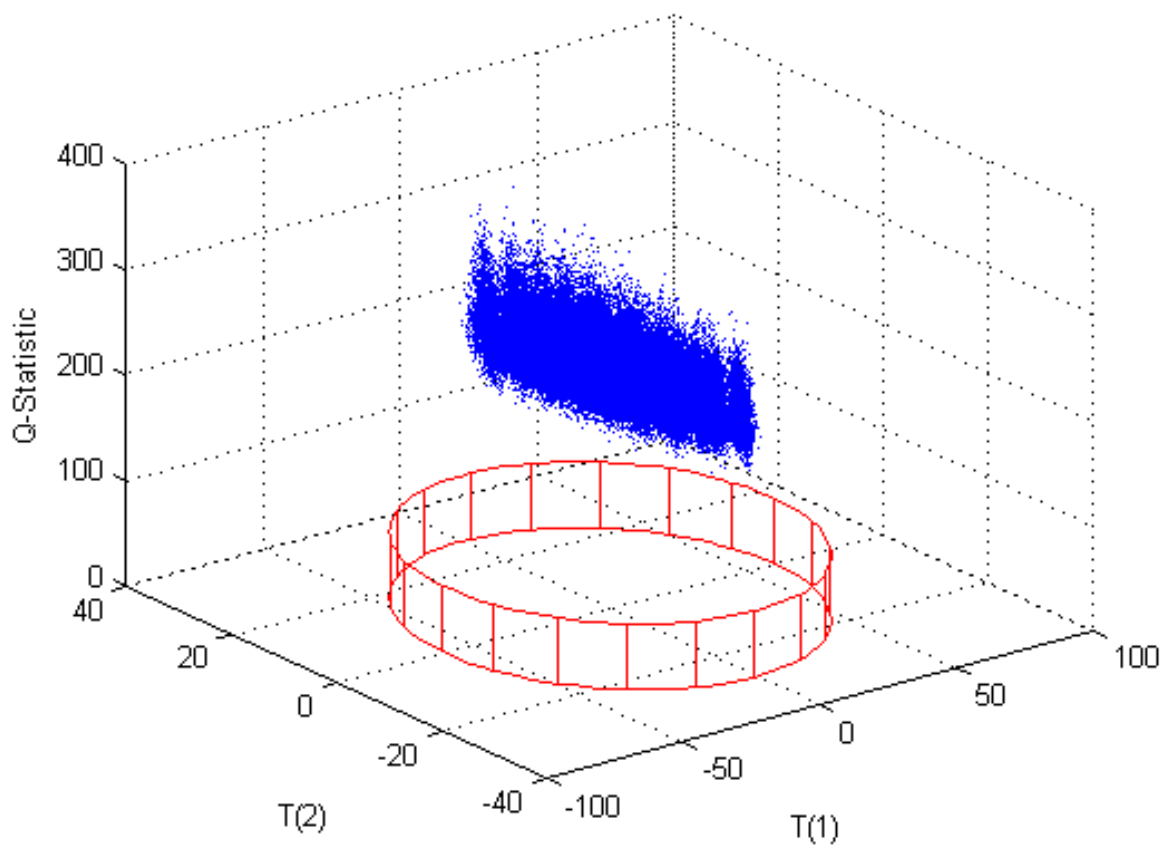
Figure 4.99. Faulty Case 13 PC1, PC2, and Q**-Statistic Plot.** *Note: Only the faulty data are shown with the base case 95% confidence boundary displayed in red. There was detectable fault in the Q-statistic.*

4.3.14 Case 14

Faulty Case 14 was the third case used to test the effect of changes in multiple parameters or inputs. It combined changes in two previous faulty cases: Case 2 and Case 3. In Case 2, the effect of changing the purity of the uranium feed was investigated by changing the uranium input stream from 85 wt-% U_3O_8 and 15 wt-% impurities (7.5 wt-% soluble impurities and 7.5 wt-% insoluble impurities) to 90 wt-% U_3O_8 and 10 wt-% impurities (5 wt-% soluble impurities and 5 wt-% insoluble impurities) in Module 1. In Case 3, inefficient dissolver operations in Module 1 were investigated by changing the extent of reaction for the dissolution reaction, X_{Mod1}, from 0.9799 to 0.95. The results show that the combination of faults was clearly detectable in all of the diagnostic plots.

There was a shift in all of the scores plots (Figures 4.100–103) with the largest fault being in PC3 scores. There was a detectable increase in the Mahalanobis distance (Figure 4.104). There was also a significant increase in the Q-statistic (Figures 4.105–106). The results from Case 2 produced shifts in all of the scores but no detectable faults, a shift in the Mahalanobis distance which may not be detectable depending on operating conditions, and a large increase in the Q-statistic (see Figures 4.39–4.45). The results from Case 3 produced faults in all of the scores plots, along with a large increase in the Mahalanobis distance, and a significant increase in the Q-statistic (see Figure 4.46–4.52). For Case 14, it was hypothesized that based on the direction of the faults in the scores of Cases 2 and 3 that it was possible for these faults to cancel one another out. However, the faults caused by Case 3 were so large that the overall faults were not canceled but the fault magnitude was reduced slightly in both the scores and the Mahalanobis distance. For the Q-statistic the combined fault was larger than the individual cases showing an additive effect such as that in Case 13. It is recommended that the streams exiting each major process (e.g., dissolution, solvent extraction, fluorination) as product or waste be monitored for flow rate and uranium content would also detect this fault. It is possible that there is a combination of faults that could cancel out one another's effects such that the fault is not detectable. This faulty case along with a comparison of the Case 2 and Case 3 results are provided in Table 4.34.

Table 4.34. Summary of Faulty Case 14

Priority	Module	Faulty Variable	Base Case Value	Faulty Value	Physical Description
Summary of Faulty Case					
Low	1	$x_{1A,18}$ and X_{Mod1A}	0.85; 0.9799	0.90; 0.95	Decrease the impurities in the uranium feed and reduce the amount of U_3O_8 converted to UN resulting in more U in waste streams

	PC1 Scores	PC2 Scores	PC3 Scores	T2	Q
Summary of Results					
Direction	-	+	--	++	++++
Detectability	Possibly	Possibly	Yes	Yes	Yes

	PC1 Scores	PC2 Scores	PC3 Scores	T2	Q
Comparison to Individual Faulty Case Results					
Case 2					
Direction	+	-	+	~+	+++
Detectability	No	No	Possibly	Possibly	Yes
Case 3					
Direction	-	+	--	+++	++++
Detectability	Possibly	Possibly	Yes	Yes	Yes

Figure 4.100. Faulty Case 14 Scores Plot for PC1 and PC2. *Note: Only the faulty data are shown with the base case 95% confidence boundary displayed in red. There was shift in both PC1 and PC2 scores, but the fault may not be detectable depending on operating conditions.*
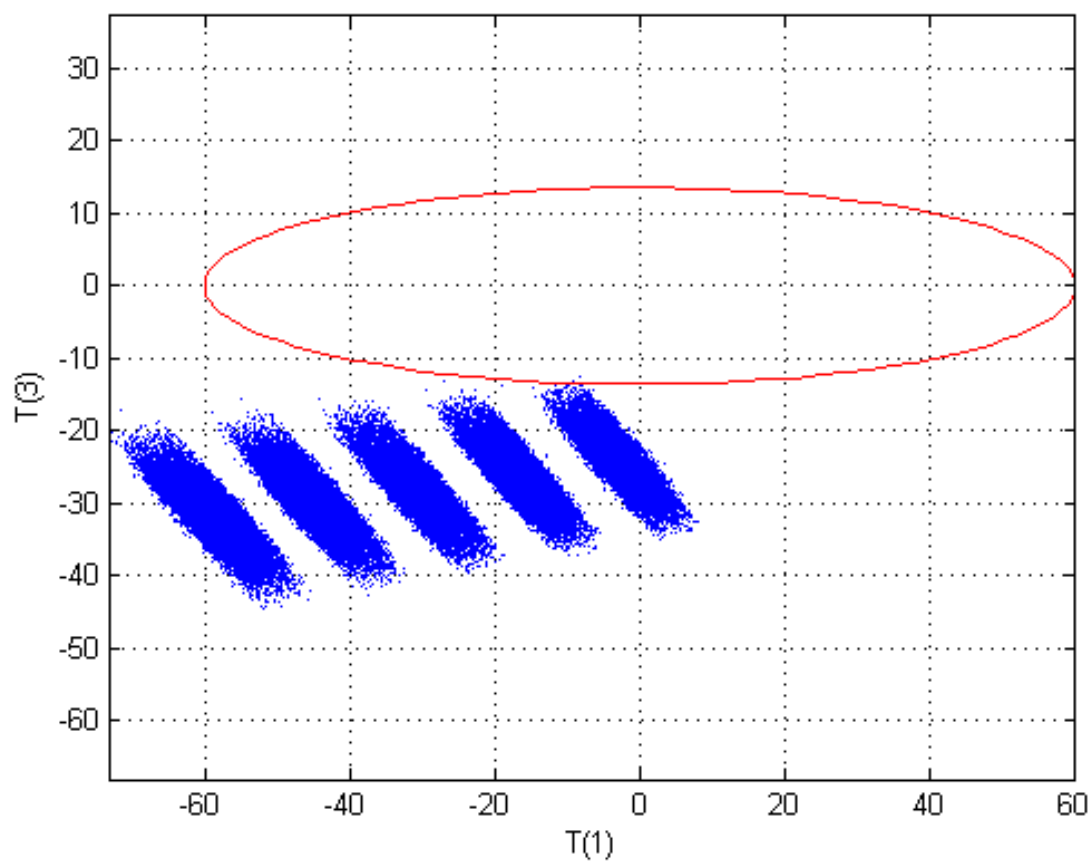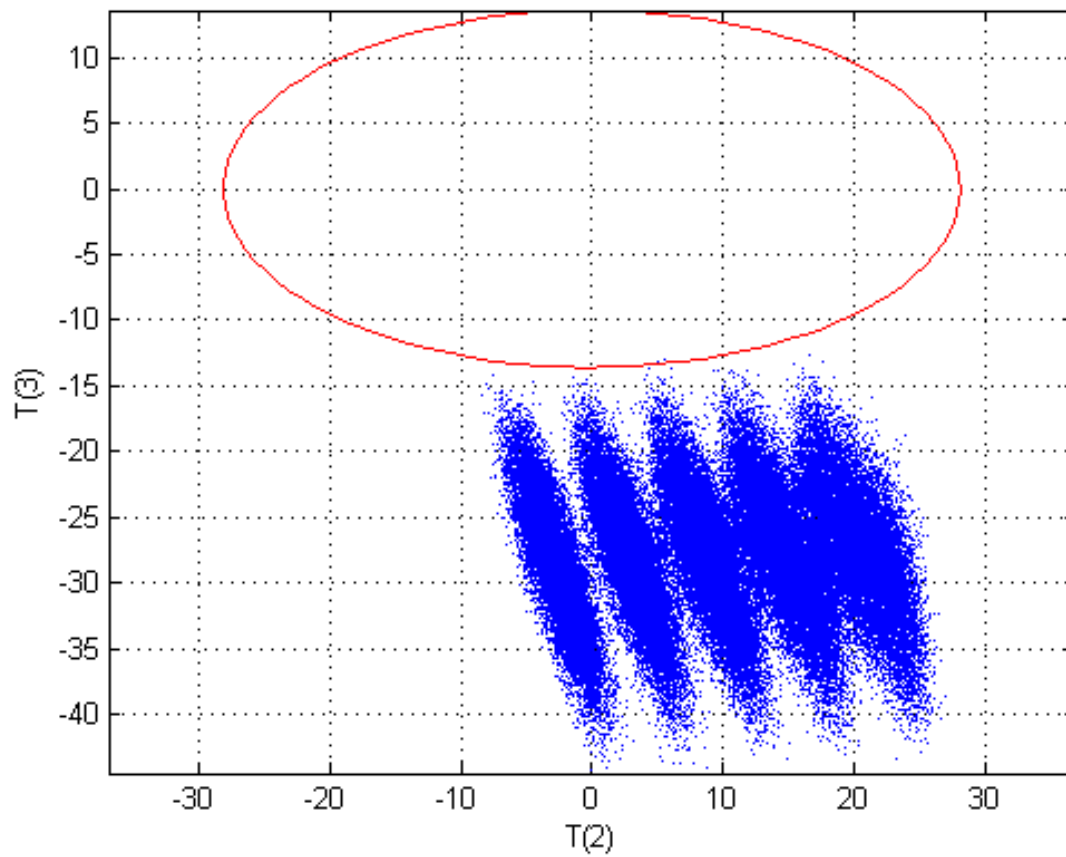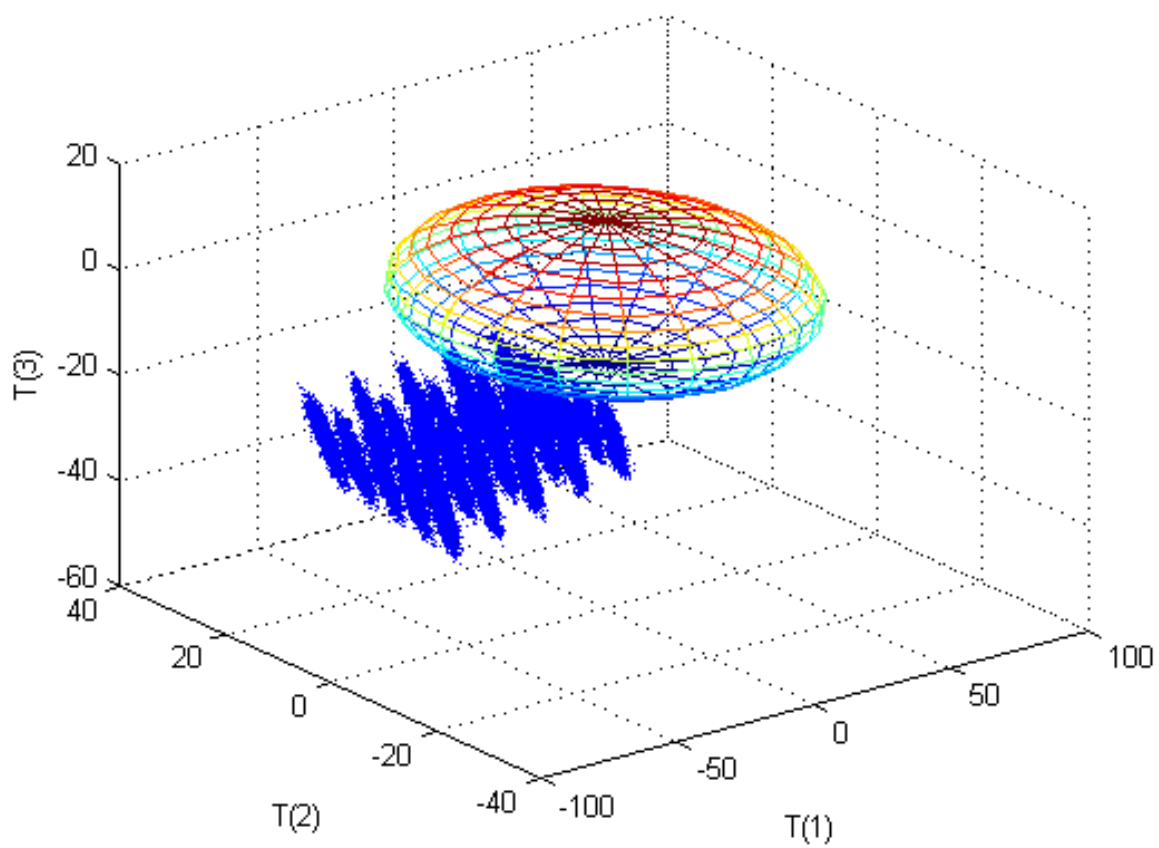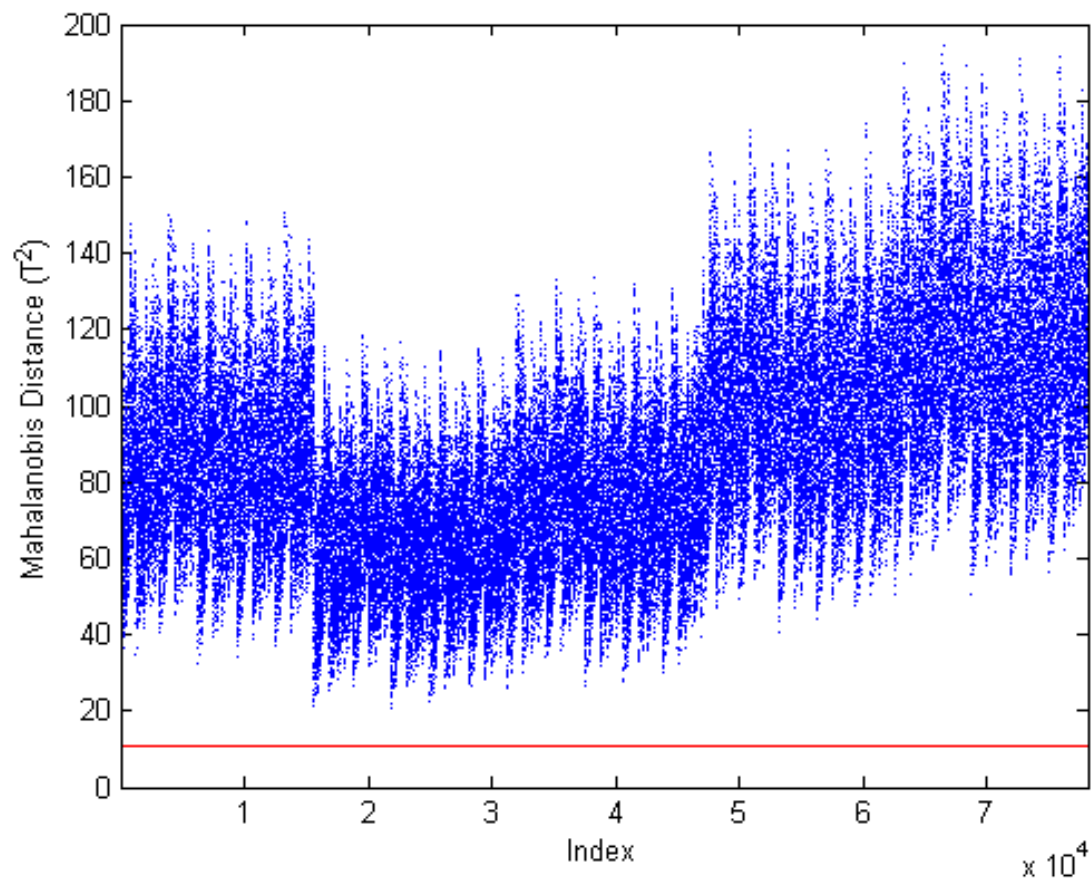
Figure 4.101. Faulty Case 14 Scores Plot for PC1 and PC3. *Note: Only the faulty data are shown with the base case 95% confidence boundary displayed in red. There was shift in both PC1 and PC3 scores, and the fault was detectable.*

Figure 4.102. Faulty Case 14 Scores Plot for PC2 and PC3. *Note: Only the faulty data are shown with the base case 95% confidence boundary displayed in red. There was shift in both PC2 and PC3 scores, and the fault was detectable.*

Figure 4.103. Faulty Case 14 3D Scores Plot for PC1, PC2, and PC3. *Note: Only the faulty data are shown with the base case 95% confidence boundary displayed as an ellipsoid. There was a detectable fault.*

Figure 4.104. Faulty Case 14 Mahalanobis Distance Plot. *Note: Only the faulty data are shown with the base case 95% confidence boundary displayed in red. There was detectable fault.*
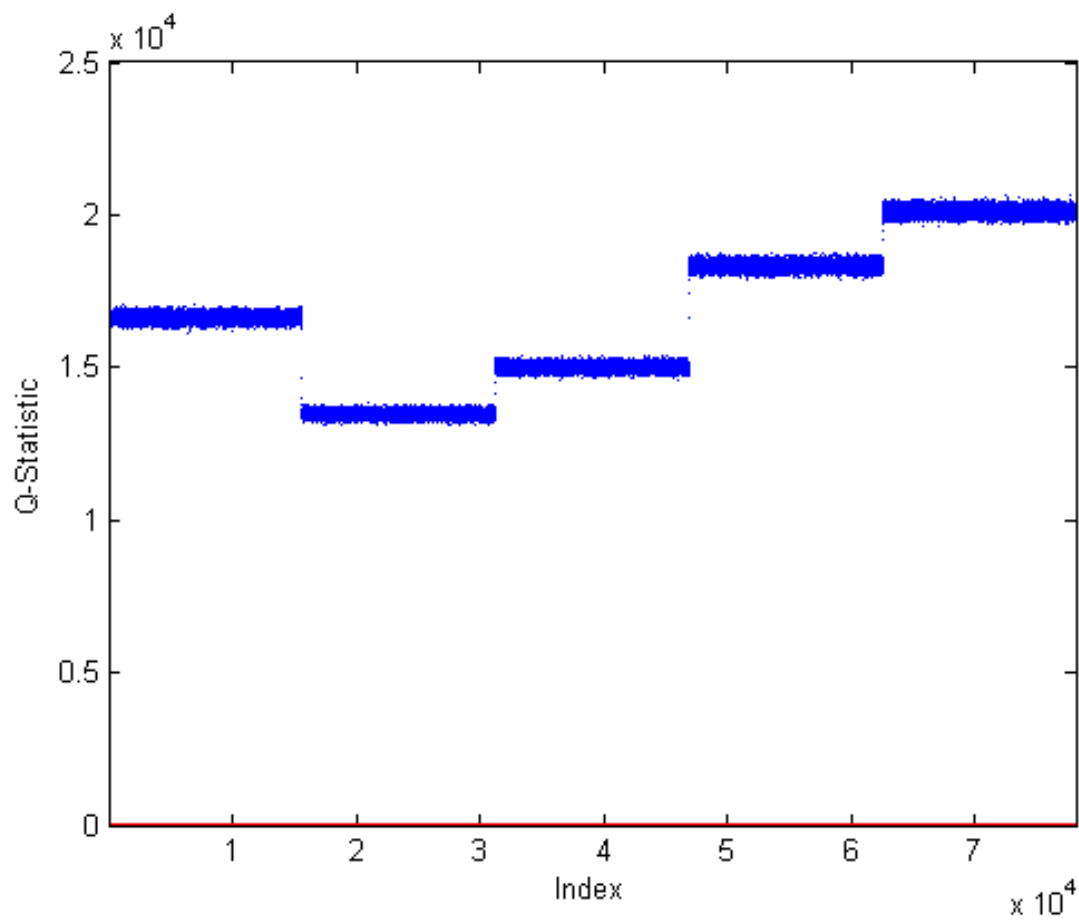
Figure 4.105. Faulty Case 14 *Q*-Statistic Plot. *Note: Only the faulty data are shown with the base case 95% confidence boundary displayed in red. There was detectable fault.*
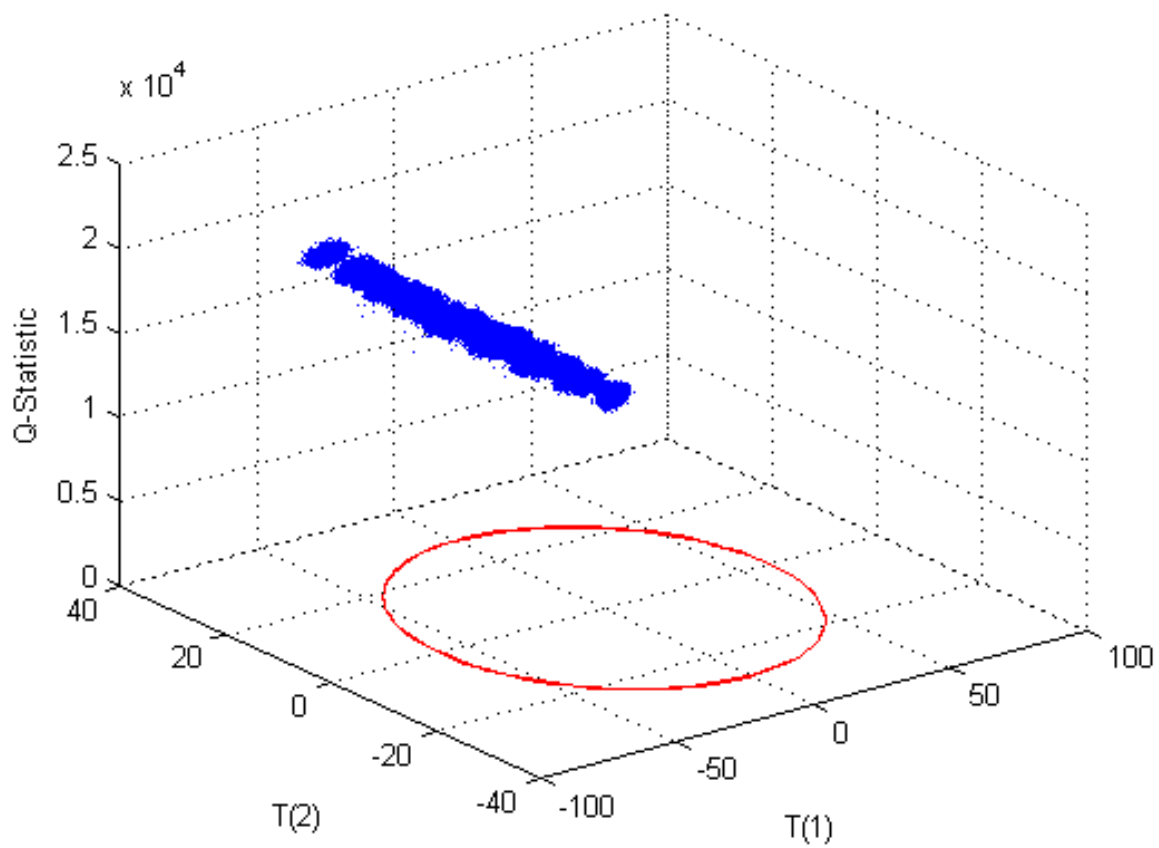
Figure 4.106. Faulty Case 14 PC1, PC2, and *Q***-Statistic Plot.** *Note: Only the faulty data are shown with the base case 95% confidence boundary displayed in red. There was detectable fault in the Q-statistic.*

4.3.15 Summary of Faulty Case Results

Table 4.35 summarizes which diagnostic plots detected the fault represented by each case. The goal of detectability was to detect the diversion of 10% of the uranium throughput on this size conversion plant which was satisfied in the case of total plant throughput. Faulty Case 1 tested increasing the total throughput (10% and 50%) and the uranium throughput (15% and 25%). Increasing the total throughput resulted in a fault in PC1 scores, the Mahalanobis distance, and the Q-statistic. For a 10% increase in total throughput, the Q-statistic fault was the only detectable fault while the 50% increase caused both the fault in PC1 scores, the Mahalanobis distance, and the Q-statistic to be detectable. Based on these results and the magnitude of the fault in the Q-statistic, a 10% increase in all incoming flow rates was still clearly detectable which indicates that a smaller increase in total throughput may be detectable as well. Increasing the uranium throughput by 25% resulted in a fault in PC1 scores, a detectable increase in the Mahalanobis distance, and no obvious change in the Q-statistic. The fault in PC1 scores was expected since the loadings vector for PC1 was dominated by the incoming uranium flow rate and the model was very sensitive to changes in the incoming uranium. The 15% increase in uranium throughput was not detectable in any of the diagnostic plots. However, this was still reasonable since ±10% variation was built into the base case for the incoming uranium. Therefore, the minimum detectable level was between 5–15% and the goal was 10% which means that the goal was also met for the case of increasing uranium throughput only. Additional scaling may improve the detectability of this fault. It is recommended that the uranium feed to the plant be monitored for both flow rate and uranium content. Additionally, it is recommended that the streams exiting each major process (e.g., dissolution, solvent extraction, fluorination) as product or waste be monitored for flow rate and uranium content.

Increasing the purity of the uranium feed by approximately 6% (Case 2) was clearly detectable in the Q-statistic and may also be detectable in PC3 scores and the Mahalanobis distance depending on operating conditions. Since the model was developed based on the feed to the plant being specified as the mass of elemental uranium not concentration, this case physically represented a reduction in the impurities that were also fed to the plant along with the uranium. Monitoring the uranium feed for both flow rate and uranium content would be the recommended approach for detecting this type of fault. However, monitoring the streams exiting each major process (e.g., dissolution, solvent extraction, fluorination) as product or waste for flow rate and uranium content would also detect this fault.

Even a relatively small (~3%) reduction in the efficiency of the dissolver operation (Case 3) was clearly detectable in PC3 scores, the Mahalanobis distance, and the Q-statistic. Inefficient operations would result in the uranium not being completely dissolved and therefore additional uranium would leave the process as waste. The U_3O_8 component in the waste from both the dissolution and solvent extraction processes was extremely sensitive to a decrease the extent of the dissolution reaction. Due to this, it is recommended that the waste streams from both the dissolution and solvent extraction processes be monitored for both flow rate and uranium content.

Table 4.35. Summary of Faulty Case Results

Case #	Safeguards Priority	Description	Detectable Faults
1A	High	Increase total plant throughput by 50%	PC1 scores, T2, Q
1B	High	Increase total plant throughput by 10%	Q
1C	High	Increase uranium throughput by 15%	None, maybe T2
1D	High	Increase uranium throughput by 25%	T2, maybe PC1 scores
2	Low	Increase the incoming uranium purity by 5.9%	Q, maybe PC3 scores and T2
3	Medium	Inefficient dissolver operations, reduce extent of reaction by 3%	PC3 scores, T2, Q, maybe PC1 scores and PC2 scores
4	High	Inefficient re-extraction operations, reduce uranyl nitrate extraction by 9.9%	PC3 scores, T2, Q but only under certain conditions
5	High	Diversion of 0.25% of the uranium from the evaporator	All diagnostic plots
6	High	Addition of uranyl nitrate to the precipitation process	Q, maybe PC3 scores and T2
7	Low	Inefficient precipitation process operations, reduce extent of reaction by 10%	Q
8	Medium	Inefficient separation downstream of the hydrofluorination reaction	Q
9	Medium	Diversion of 75% of the UF_6 from the secondary fluorination process	Q
10	High	Inefficient operations of the fluorination processes, reduce extent of reaction by 4.9%	Q
11	High	Diversion of 20% of the purified UF_6	Q
12	High	multiple parameters	Q, maybe PC1 scores and T2
13	High	multiple parameters	Q, maybe T2
14	Low	multiple parameters	All diagnostic plots

A reduction of approximately 10% in the efficiency of the re-extraction of uranium from the organic phase (Case 4) may be detectable in the PC3 scores, the Mahalanobis distance, and the Q-statistic but only under certain operating conditions. Additional scaling may improve the detectability of this fault. Inefficient re-extraction results in additional uranium being diverted to the organic waste stream where it could be recovered and purified at an undeclared location. Due to this and since this is a high priority for safeguards, it is very strongly recommended that the product and waste streams from the solvent extraction process be monitored for both flow rate and uranium content.

Diverting only 0.25% of the material in the evaporator in Module 3A to waste (Case 5) produced large faults in all of the diagnostic plots (scores, Mahalanobis distance, and Q-statistic). From a safeguards perspective, it would be expected that a diversion of this nature would be very small so as not to be detected. The model was extremely sensitive to diversion of material within the evaporation and precipitation portion of the process. It is recommended that the stream leaving the evaporator to feed the precipitation process be monitored for both flow rate and uranium content. This area of the plant should also be inspected for additional piping which may be diverting material to another location. Additionally, the waste stream from the evaporator should be monitored for flow rate and uranium content as well in case material is being diverted to the waste directly.

Case 6 determined that adding a small amount (~12% of the original incoming uranium) of pure uranyl nitrate to the precipitation process was clearly detectable in the Q-statistic. This fault may also be detectable in PC3 scores and the Mahalanobis distance depending on operating conditions. Since the base case incoming uranium was allowed to vary by ±10%, it was reasonable that the scores and Mahalanobis distance plots did not produce a detectable fault under all conditions since this was only slightly more than the normal operating conditions. For this case, it is recommended that the uranium feed to the plant be monitored for both flow rate and uranium content. It is also recommended that the streams exiting each major process (e.g., dissolution, solvent extraction, fluorination) as product or waste be monitored for flow rate and uranium content. Additionally, this area of the plant should be inspected to determine that there is not additional uranium being fed to the process.

A 10% reduction in the efficiency of the precipitation process in Module 3 (Case 7) produced a clearly detectable fault in the Q-statistic. Inefficient operations results in uranyl nitrate not being completely converted AUC and therefore additional uranium would leave the process as waste. It is recommended that the product and waste streams in the evaporation and precipitation process areas of the facility be monitored for both flow rate and uranium content. For this fault specifically, it is recommended that the outlet stream from the precipitation process be monitored for flow rate and uranium content as well as type of uranium compound.

Inefficient separation operations of the filtration system downstream of the hydrofluorination reaction Module 4 (Case 8) resulted in additional uranium being diverted to the off-gas waste stream. This fault was only detectable in the Q-statistic. These parameters were increased significantly even though the

values were very small so that there was not a significant change in the amount of uranium diverted to waste. It is recommended that the off-gas stream from the hydrofluorination process be monitored for uranium content.

Case 9 tested the ability of the model to detect the diversion of UF_6 from the secondary fluorination process in Module 5; several diversion scenarios were tested but 75% was determined to be the minimum detectable limit and the fault was only detectable in the Q-statistic. This appeared to be a very large diversion but since only 10% of the incoming uranium to Module 5 was sent to the secondary reactor this diversion was not significant (~7.5% overall diversion). Additionally, this was within the detection goal for the monitoring framework. Additional scaling may improve the detection limits of this fault. It is highly recommended that the final product from the NUCP be monitored. The final product should also be related back to the uranium feed to the plant.

A small reduction (~5%) in the efficiency of both of the fluorination processes in Module 5 (Case 10) produced a detectable fault the Q-statistic. In real operations, this would result in less UF_4 being converted to UF_6 and would cause an increase in the amount of UF_4 in the waste streams which could be recovered and processed elsewhere. It is recommended that the feed, product, and waste streams in the fluorination process area be monitored for flow rate and uranium content.

A diversion of 20% of the UF_6 product from the final mixer in Module 5 to an undeclared product stream (Case 11) was detectable in the Q-statistic plot only. This case is of extremely high concern for safeguards and the goal of this detection framework was to be able to detect 10% diversion which was possible since this case represents 10% over the maximum of the base case allowed variation in uranium of ±10%. It is highly recommended that the final product from the NUCP be monitored and correlated to the uranium feed to the plant.

Case 12 combined two previous cases: Case 1D (uranium input flow rate increased by 25%) and Case 11 (20% of the UF_6 product diverted through a new output stream). This case models the scenario where additional uranium is fed to the process and then additional purified uranium is diverted before declaration at the end of the process. This fault was detectable under all conditions using the Q-statistic. Additionally, under some conditions, this fault was detectable using PC1 scores and the Mahalanobis distance. It is recommended that the uranium feed to the plant be monitored for both flow rate and uranium content. Additionally, it is recommended that the streams exiting each major process (e.g., dissolution, solvent extraction, fluorination) as product or waste be monitored for flow rate and uranium content. It is highly recommended that the final product from the NUCP be monitored and correlated to the uranium feed to the plant.

Case 13 also combined two previous cases that both investigated inefficient operations: Case 7 (precipitation process) and Case 10 (fluorination processes). There was a large fault in the Q-statistic which was larger than that of the individual cases showing that multiple faults can have an additive effect on the diagnostic plot results. Case 13 had similar results to Case 7 in the scores and Mahalanobis

distance. There were no detectable faults in the scores or Mahalanobis distance in Case 10 to impact the results of Case 13. However, the faults in Case 13 would only be detectable under certain conditions using the scores or Mahalanobis distance since many of the data points were still within the 95% confidence boundary. Since this case was a combination of inefficient operations, it was also expected that the faults would be larger due to an additive effects of the faults which was the case for the Q-statistic since it was the only diagnostic plot that resulted in a fault for both individual cases. It is recommended that the outlet stream from the precipitation process be monitored for flow rate and uranium content as well as type of uranium compound. It is also recommended that the feed, product, and waste streams in the fluorination process area be monitored for flow rate and uranium content.

Case 14 combined two previous cases: Case 2 (increased purity of uranium feed) and Case 3 (inefficient dissolver operations). The results show that the fault in this case was detectable in all of the diagnostic plots. For Case 14, it was hypothesized that based on the direction of the faults in the scores of Cases 2 and 3 that it was possible for these faults to cancel one another out. However, the faults caused by Case 3 were so large that the overall faults were not canceled but the fault magnitude was reduced slightly in both the scores and the Mahalanobis distance. For the Q-statistic the combined fault was larger than the individual cases showing an additive effect such as that in Case 13. It is recommended that the streams exiting each major process (e.g., dissolution, solvent extraction, fluorination) as product or waste be monitored for flow rate and uranium content to detect this fault. It is possible that there is a combination of faults that could cancel out one another's effects such that the fault is not detectable.

4.3.16 Recommendations for Safeguards Monitoring

Based on the results of this work, the following recommendations are made for monitoring an NUCP for safeguards. At a minimum, the uranium feed to the plant must be monitored both for feed rate and uranium content as well as the final product from the plant. These need to be correlated such that it can be determined that all of the uranium feed was converted and exited the plant in the final UF_6 product with the exception of acceptable losses to waste (total loss of up to 10%). The loss to waste in the ideal plant model was nominally 8%. If the uranium losses are greater than expected, then it must be determined where the uranium was lost/diverted. Since the IAEA safeguards goal for a small NUCP (100 MTU/yr) is to detect the diversion of 10 MT of natural uranium with a timeliness period of one year and a detection probability of 50%, a loss of 10% to waste may not be too much to achieve the detection goal. Therefore, it is also recommended that all of the waste streams be monitored to detect excess uranium. Since the process operates serially where the product of one process becomes the feed to the next process, monitoring the feed, final product, and all waste streams provides the minimum monitoring necessary to close the material balance and offer any certainty that uranium has not been diverted or additional uranium has not been fed to the plant. If it is not reasonable to monitor all wastes then the waste streams that are most likely to contain diverted uranium must be monitored. These

would be Module 1 Stream 8, Module 2 Stream 20, Module 3 Stream 31, Module 4 Stream 43, and Module 5 Stream 50.

The second option for monitoring that is recommended would be to add monitoring of the intermediate products throughout the process to the recommendation above. These are the products from each module that becomes the feed to the next module: Module 1 Stream 12, Module 2 Stream 19, Module 3 Stream 30, and Module 4 Stream 44. Since there is normally some time lag between processes in actual plants, these would need to be monitored as the product of one process and then the feed to the next process. Monitoring both the flow rate and the uranium content would be necessary to determine that diversion of uranium had not occurred.

The third option for monitoring that could confirm that diversion had not occurred would be the monitoring of select intermediate streams. These streams could be correlated with the feed, product, and waste streams in that process area to determine that uranium was not diverted or added to the process. These streams are Module 1 Streams 1 and 4; Module 2 Stream 14; Module 3 Streams 22 and 27; Module 4 Streams 34, 39, and 42; and Module 5 Streams 46, 49, 52, 55, and 59. Based on this research, it is unnecessary to monitor this number of streams in the plant.

The final level of monitoring that would be able to completely close the material balance and ensure that no additional uranium is fed to the process and that no uranium is diverted from the process would require monitoring all of the streams throughout the plant for both flow rate and uranium content. However, this would be too challenging to implement both from the perspective of the plant and the costs required to purchase and install that number of monitoring points. Additionally, based on this research, it is extremely unnecessary to monitor all of the streams in the plant.

Therefore, if not cost prohibitive, the second option would be the best safeguards monitoring system to be applied with this detection framework. Since all of the intermediate and product stream content are highly correlated, monitoring of selected subset of stream flow rates and uranium content would be adequate. This framework could also be applied to the less intrusive option 1 as well. However, the likelihood of detection is reduced as the number of monitoring points is reduced.

4.3.17 Reduced State Variable Monitoring Framework Test Case

As recommended above, the second option would be the best safeguards monitoring system to be applied with this detection framework. However, this framework could also be applied to the less intrusive option 1 as well. Due to this, a cursory test of the monitoring framework was completed to determine whether or not option 2 would be a viable option for fault detection.

4.3.17.1 Reduced Base Case

For this reduced case monitoring framework, the original base case system was reduced from 273 state variables to 23 state variables. The state variables retained for the reduced base case along with the nominal steady-state solution is shown in Table 4.36. The only state variables retained for the reduced case were the uranium-bearing components in the product stream of each module and the uranium-bearing components in the waste streams from each module. A total of fourteen streams not including input streams are represented in the reduced case as opposed to sixty streams in the original case.

The reduced case data matrix was generated in the same manner as the original base case data matrix. The parameters were set at the same values and the same input variables and variation ranges were used in the reduced case. The data matrix was pre-processed in the same manner except that differential weighted scaling was not used in the reduced case; the data matrix was scaled to unit standard deviation. One percent Gaussian white noise was also added to the reduced case. For the reduced case, the columns of the data matrix which represented the state variables that were retained (Table 4.36) were extracted to form the new reduced case data matrix. Singular value decomposition was applied to this new reduced case data matrix to extract the principal component model. Based on the Scree plot (Figure 4.107), six principal components were retained for the reduced case PC model. This retains approximately 92% of the original information. The 95% confidence boundaries were established for the new PC model.

The first principal component is an average of the behavior of the system where most of the state variables are equal contributors including the first input variable [Xss(274)]. The second principal component represents variables within Module 4. The third principal component represents correlations between the input variables and state variables within Modules 1–3.

Three of the faulty cases were used to test the new reduced PC model for the detection of diversion of uranium in an NUCP. The cases were 1D, 4, and 11. In each case, the fault was clearly detectable in at least one of the diagnostic plots. The faulty case data matrices were generated in the same manner as before. Noise was added and the data matrices were also pre-processed in the same manner as before but without differential weighted scaling. As with the reduced base case, the columns of the data matrix which represented the state variables that were retained (Table 4.36) were extracted to form the new reduced faulty case data matrix which was then regressed against the PC model to determine the detectability of the fault. Each faulty case is briefly discussed below. Based on these initial results, it is possible to detect diversion in an NUCP by monitoring only the uranium input, the final UF_6 product, the intermediate uranium-bearing products from each module, and the uranium-bearing waste streams. Therefore, option 2 is sufficient as a safeguards monitoring system to be applied with this detection framework.

Table 4.36. Reduced Case Steady-State Solution

State Variable	Stream	Component Formula	Number	Type of Stream	Molar Flow Rate (mol/h)
Module 1					
Xss(40)	8	UN	14	Waste	1.15
Xss(41)	8	U_3O_8	18	Waste	0.776
Xss(64)	**12**	**UN**	**14**	**Product**	**206**
Xss(65)	**12**	**U_3O_8**	**18**	**Product**	**4.05×10^{-2}**
Xss(70)	13	UN	14	Waste	2.06×10^{-2}
Module 2					
Xss(91)	16	UN	14	Waste	1.03
Xss(92)	16	U_3O_8	18	Waste	4.05×10^{-2}
Xss(111)	**19**	**UN**	**14**	**Product**	**205**
Xss(117)	20	UN	14	Waste	0.205
Module 3					
Xss(123)	21	UN	14	Waste	2.05×10^{-2}
Xss(163)	**30**	**AUC**	**19**	**Product**	**204**
Xss(169)	31	UN	14	Waste	2.05×10^{-2}
Xss(171)	31	AUC	19	Waste	1.03
Module 4					
Xss(214)	43	UF_4	16	Waste	1.94×10^{-3}
Xss(215)	43	UO_2	17	Waste	1.02×10^{-2}
Xss(217)	43	AUC	19	Waste	2.04×10^{-2}
Xss(218)	**44**	**UF_4**	**16**	**Product**	**194**
Xss(219)	**44**	**UO_2**	**17**	**Product**	**10.2**
Module 5					
Xss(239)	50	UF_4	16	Waste	0.173
Xss(240)	50	UO_2	17	Waste	9.19
Xss(269)	58	UF_4	16	Waste	1.94×10^{-2}
Xss(270)	58	UO_2	17	Waste	1.02
Xss(273)	**60**	**UF_6**	**15**	**Product**	**194**
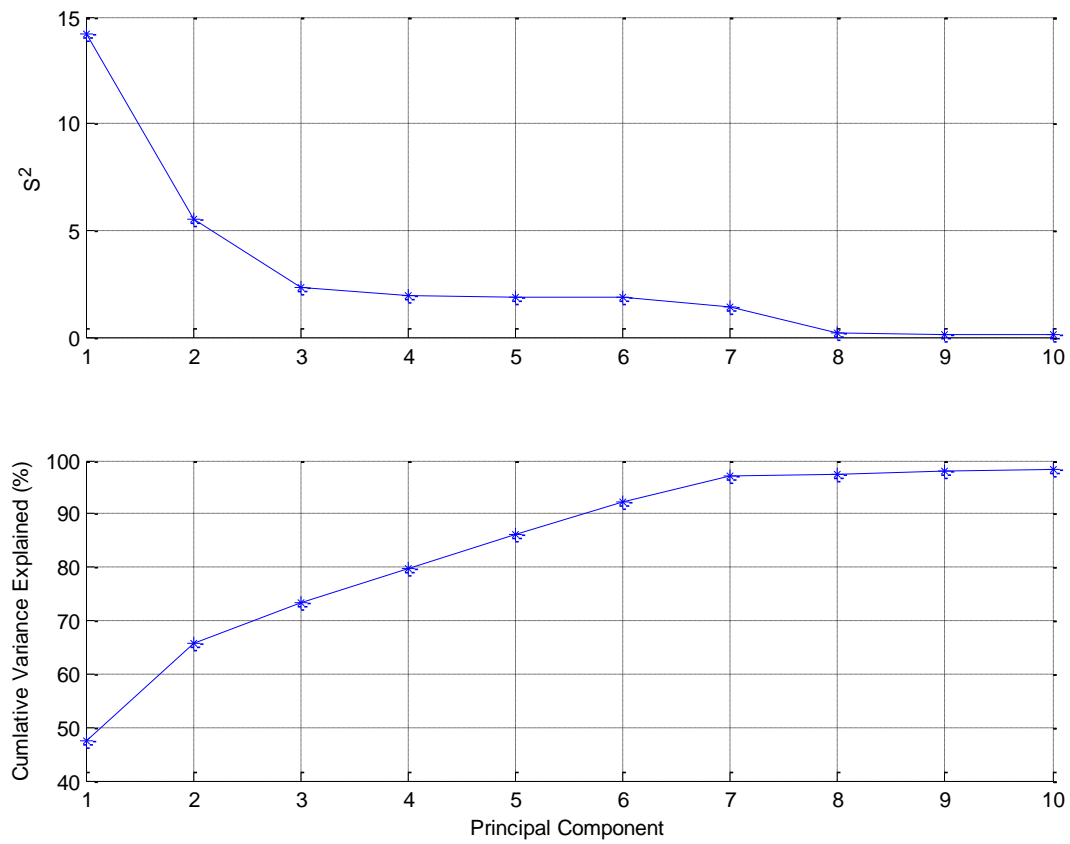
Figure 4.107. Scree Plot of the Reduced Case Data after the Addition of Gaussian White Noise.

4.3.17.2 Reduced Case 1D

Case 1D tested the detectability of a 25% increase in the uranium flow rate to the process. The results showed that this faulty case was clearly detectable in PC1 scores and the Mahalanobis distance using the reduced case PC model.

This case was modeled in the same manner as the original Case 1D with $F_{1A,U}$ [Xss(274)] set to a constant 62.5 kg/h. There was a fault in PC1 scores which was expected since Xss(274) was a heavy contributor to PC1. However, some of the data points were still within the 95% confidence boundary meaning that there are some operating conditions under which that fault would not be detectable using only PC1 scores monitoring but may be detectable using trend monitoring as was the case with the original Case 1D. There were only slight changes in PC2 or PC3 scores. The scores plots are shown in Figures 4.108–4.111. There was a significant increase in the Mahalanobis distance (Figure 4.112) which was expected since this case was outside the normal operating conditions. There were no detectable faults in the Q-statistic which was also expected since no parameters were changed (Figures 4.113–4.114). Based on these results, a 25% increase in uranium feed rate is deemed detectable using the reduced case PC model.
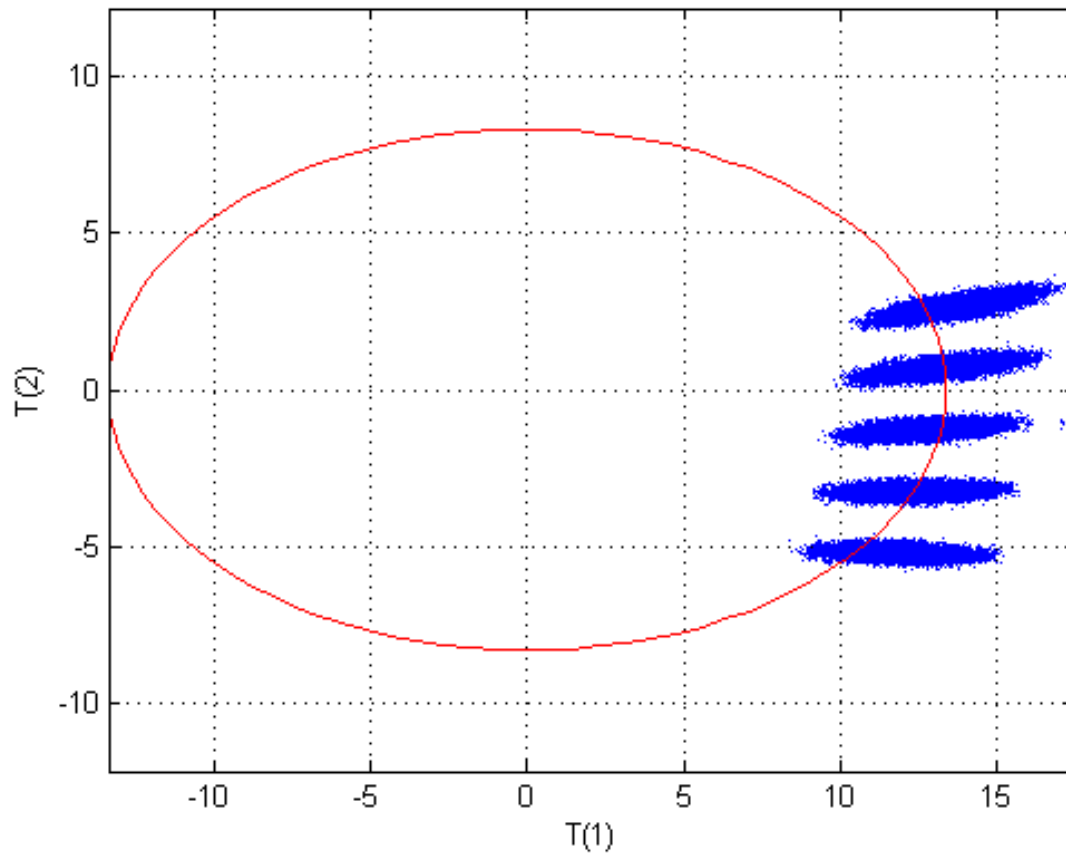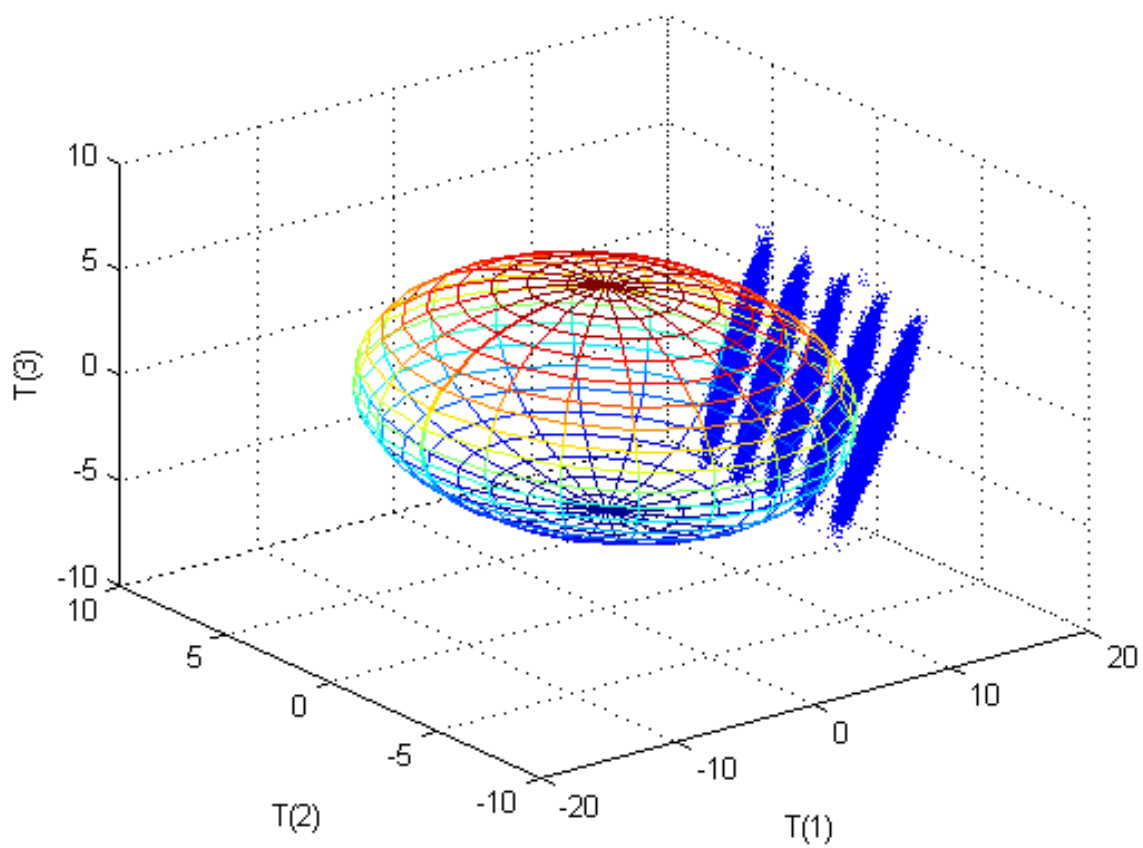
Figure 4.108. Reduced Faulty Case 1D Scores Plot for PC1 and PC2. *Note: Only the faulty data are shown with the base case 95% confidence boundary displayed in red. There was a fault in PC1 scores.*
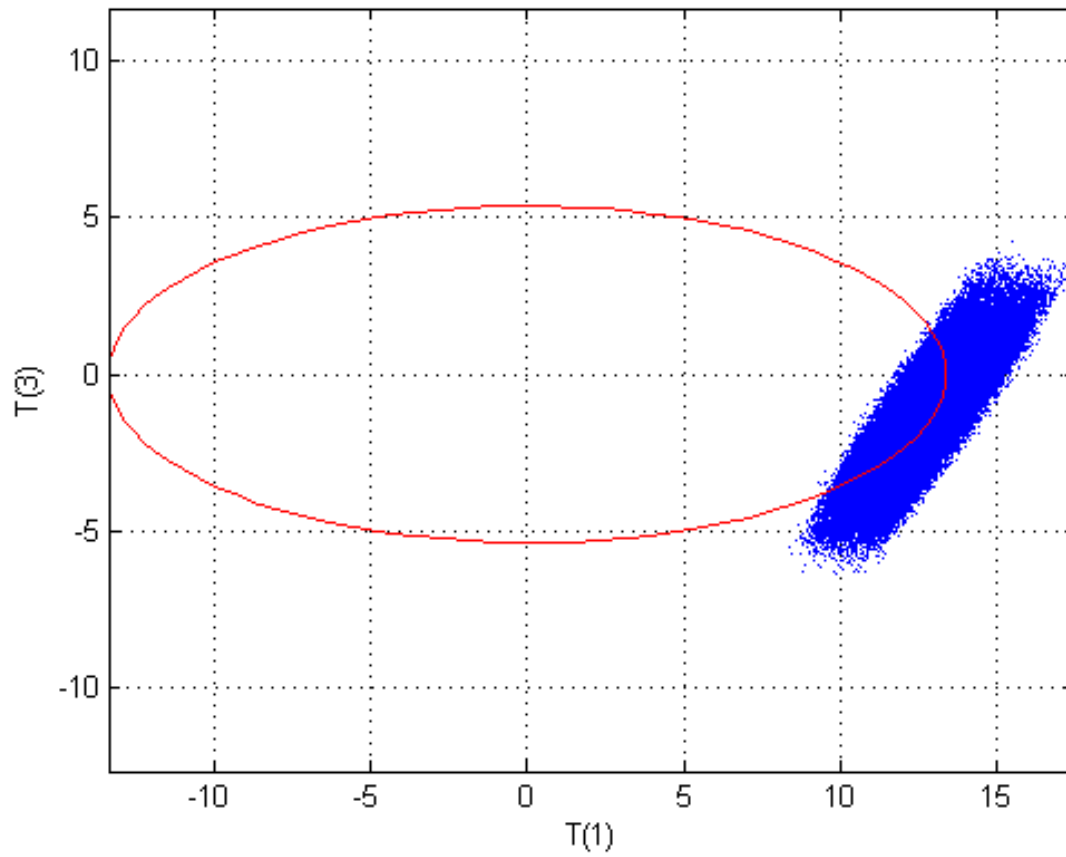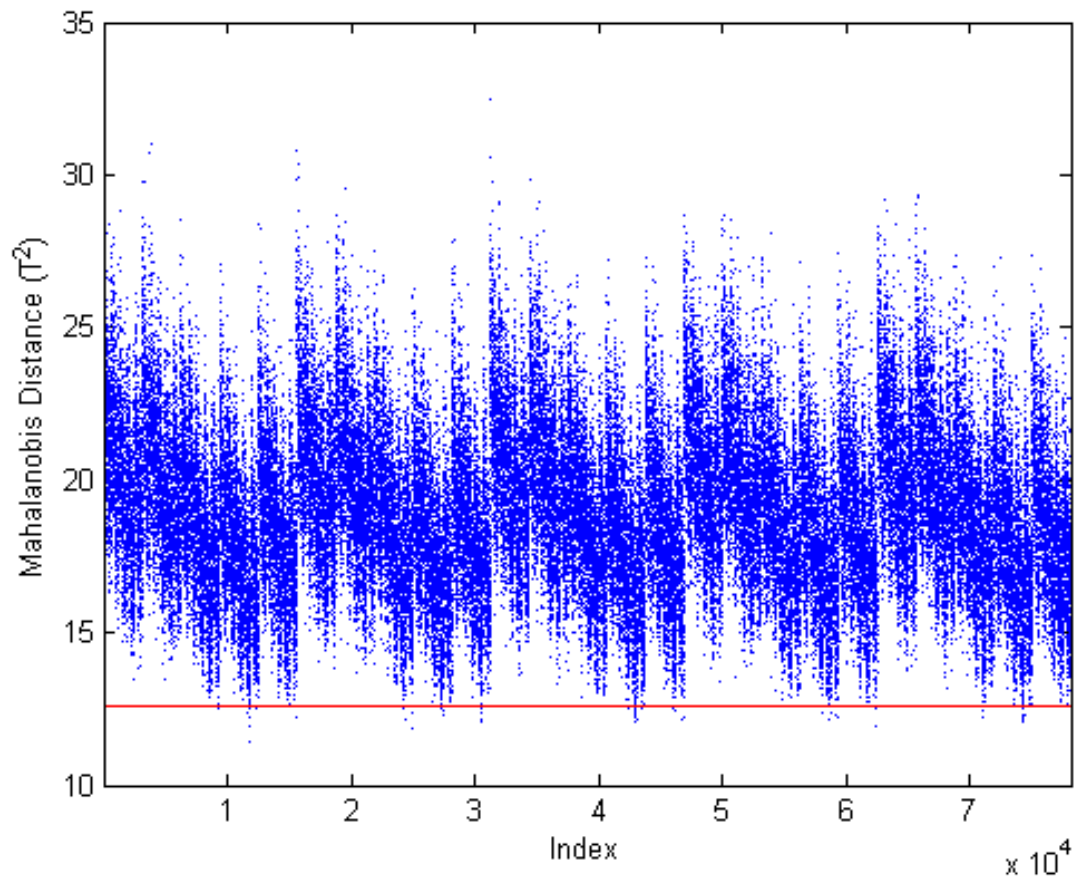
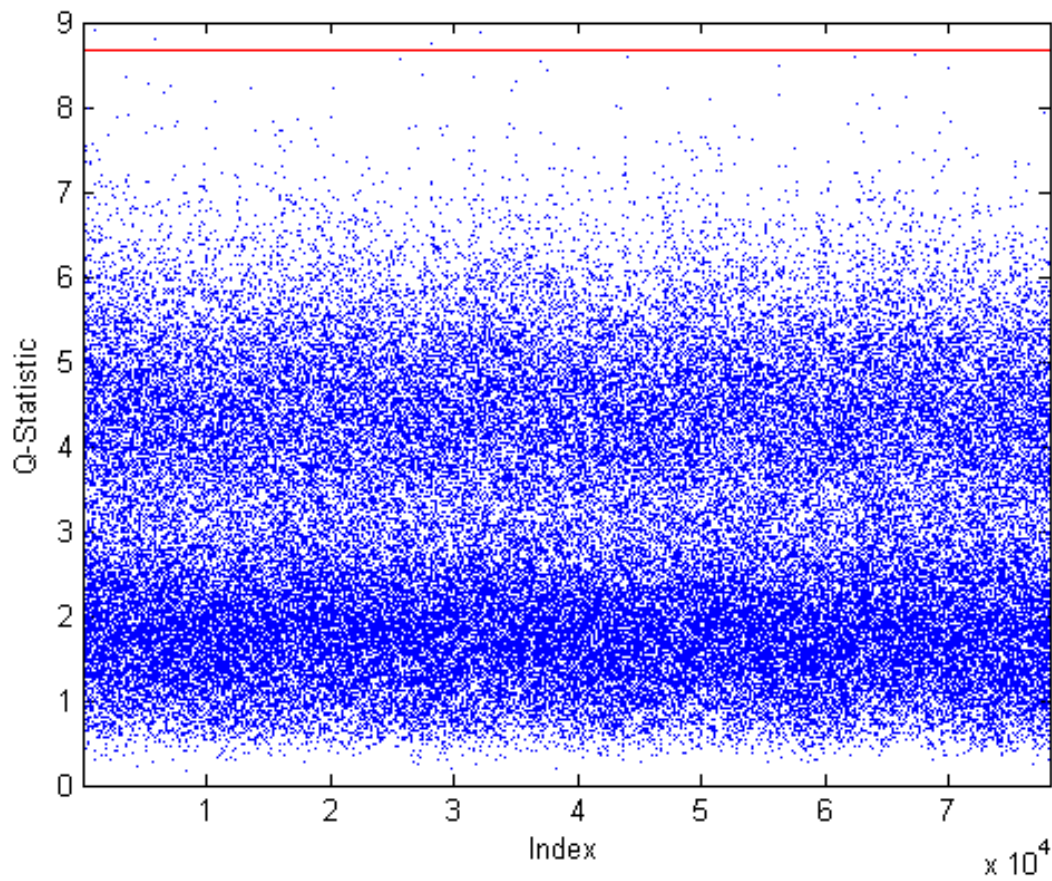**Figure 4.109. Reduced Faulty Case 1D Scores Plot for PC1 and PC3.** *Note: Only the faulty data are shown with the base case 95% confidence boundary displayed in red. There was a fault in PC1 scores.*
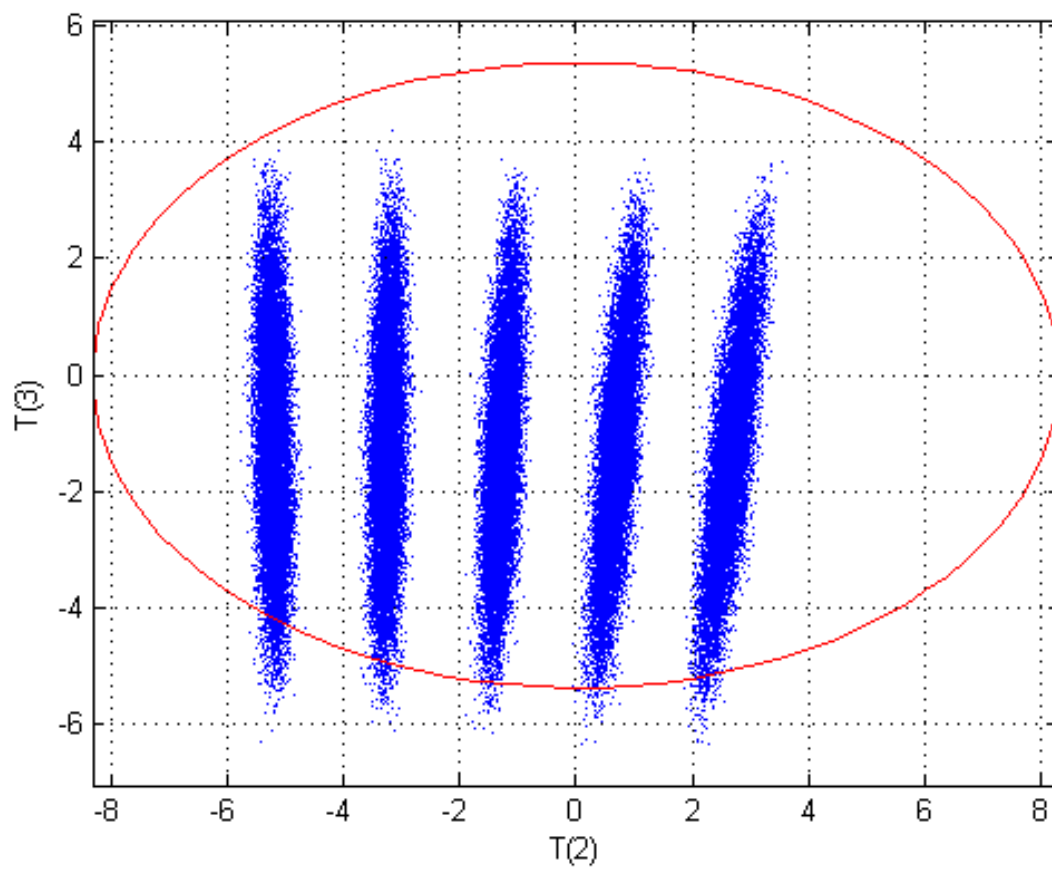
Figure 4.110. Reduced Faulty Case 1D Scores Plot for PC2 and PC3. *Note: Only the faulty data are shown with the base case 95% confidence boundary displayed in red. There was no detectable fault.*
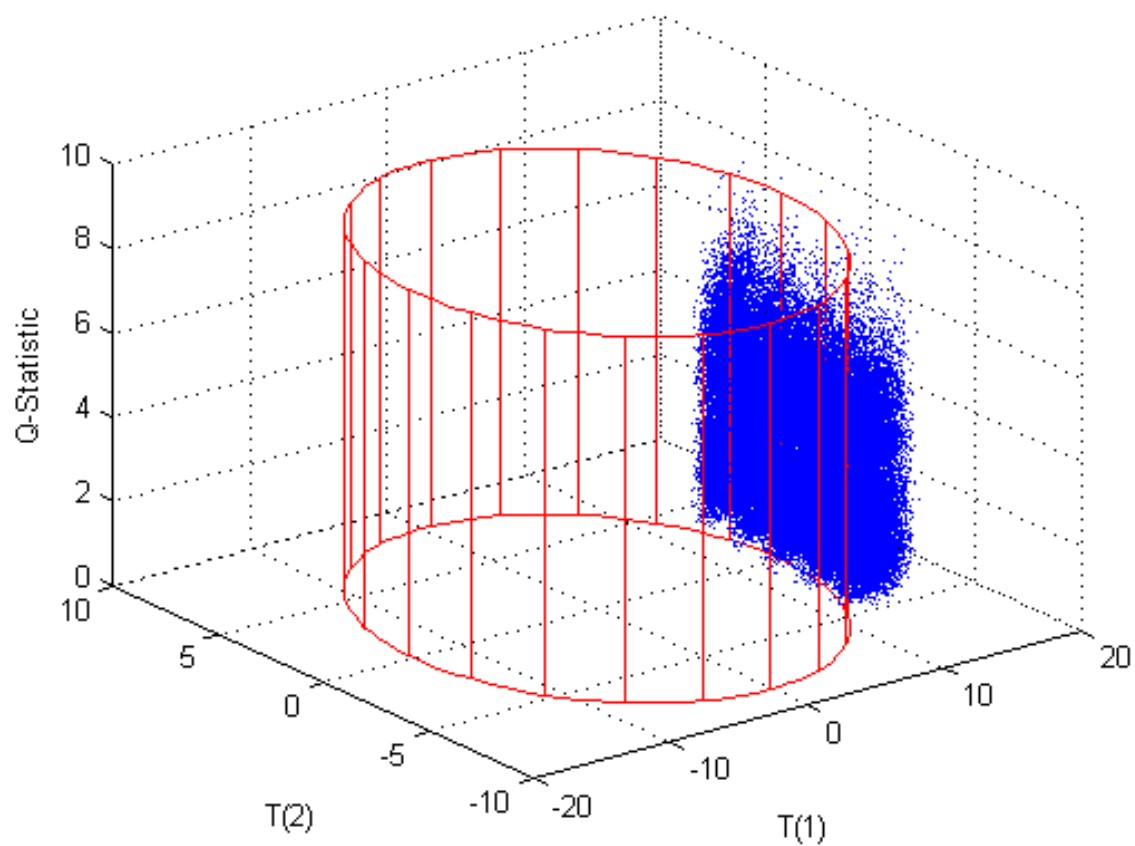
Figure 4.111. Reduced Faulty Case 1D 3D Scores Plot for PC1, PC2, and PC3. *Note: Only the faulty data are shown with the base case 95% confidence boundary displayed in red. There was a fault in PC1 scores.*

Figure 4.112. Reduced Faulty Case 1D Mahalanobis Distance Plot. *Note: Only the faulty data are shown with the base case 95% confidence boundary displayed in red. There was a detectable fault.*

Figure 4.113. Reduced Faulty Case 1D *Q*-Statistic Plot. *Note: Only the faulty data are shown with the base case 95% confidence boundary displayed in red. There was no detectable fault.*

Figure 4.114. Reduced Faulty Case 1D PC1, PC2, and Q-Statistic Plot. *Note: Only the faulty data are shown with the base case 95% confidence boundary displayed in red. There was a fault in PC1 scores.*

4.3.17.3 Reduced Case 4

For the fourth faulty case, inefficient operations of the re-extraction of uranium from the organic phase in Module 2 were investigated. Inefficient re-extraction would result in additional uranium being diverted to the organic waste stream. The reduced case was modeled the same as the original Case 4 which was modeled by changing the initial value of the column fractionation parameter for the uranyl nitrate in Module 2D, $K_{Mod2D,14}$, from 0.999 to 0.9. This was the fourth input variable [Xss(277)]. The results show that the fault in reduced Case 4 was clearly detectable in the Mahalanobis distance and may be detectable in the PC3 scores under certain operating conditions.

There was a slight shift in the PC1 scores and no change in the PC2 scores; the fault would not be detectable since all of the data points were still within the 95% confidence boundary for normal operation (Figure 4.115). The PC1 scores shift may be detectable using trending monitoring. There was a slightly negative shift in PC3 scores (Figures 4.116–4.118), but the fault may not be detectable depending on operating conditions since many of the data points were inside the 95% confidence boundaries. The PC3 scores shift may be detectable using trending monitoring. The fault in PC3 scores was expected because Xss(277) heavily loaded PC3 along with Xss(117). This resulted in an increase in the Mahalanobis distance (Figure 4.119). An increase in the Mahalanobis distance was expected since this was one of the input variables and the change was greater than the allowed variation of the base case. There was a no detectable shift in the Q-statistic (Figures 4.120–4.121).
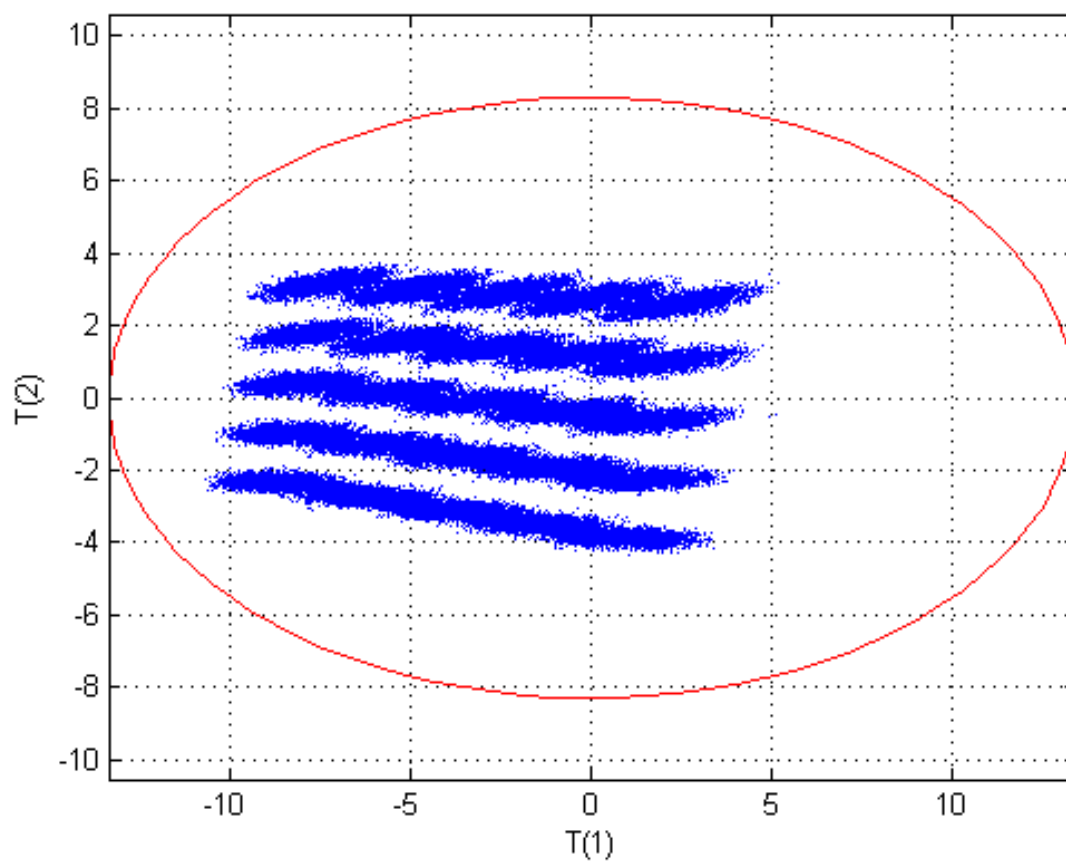
Figure 4.115. Reduced Faulty Case 4 Scores Plot for PC1 and PC2. *Note: Only the faulty data are shown with the base case 95% confidence boundary displayed in red. There was no detectable fault.*
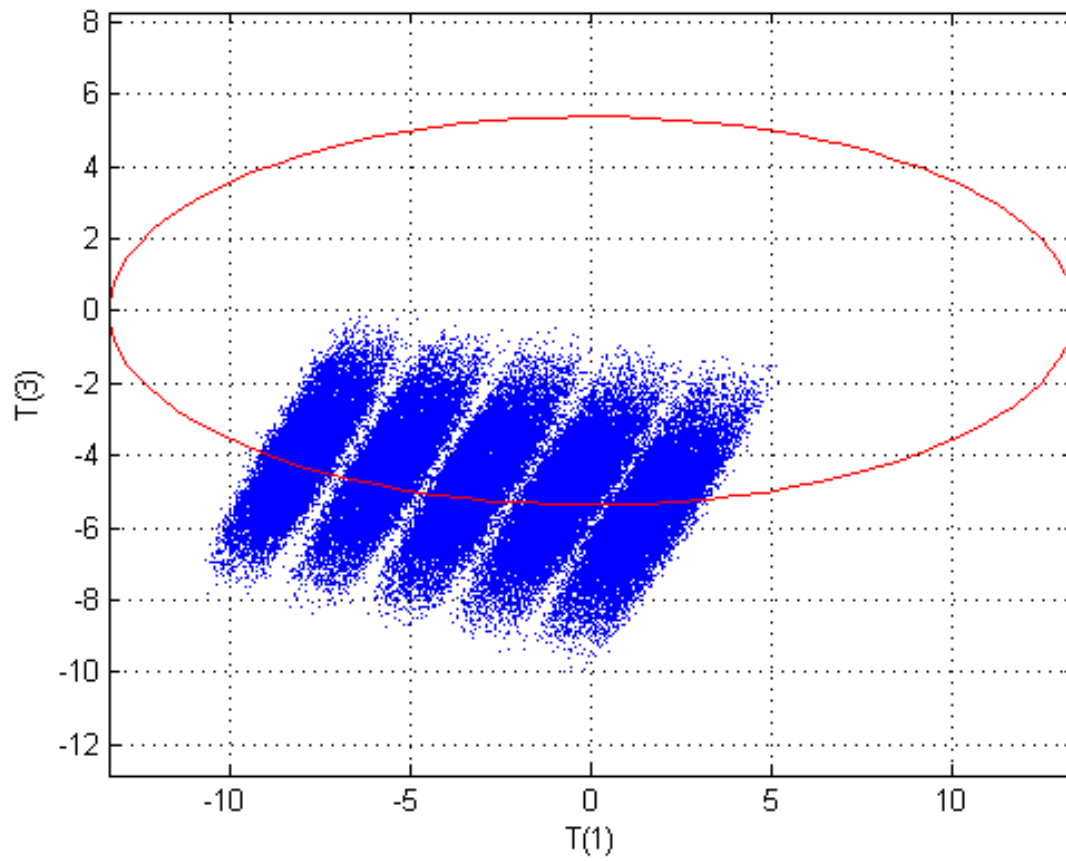
Figure 4.116. Reduced Faulty Case 4 Scores Plot for PC1 and PC3. *Note: Only the faulty data are shown with the base case 95% confidence boundary displayed in red. There was a shift in PC3 scores but the fault may not be detectable.*
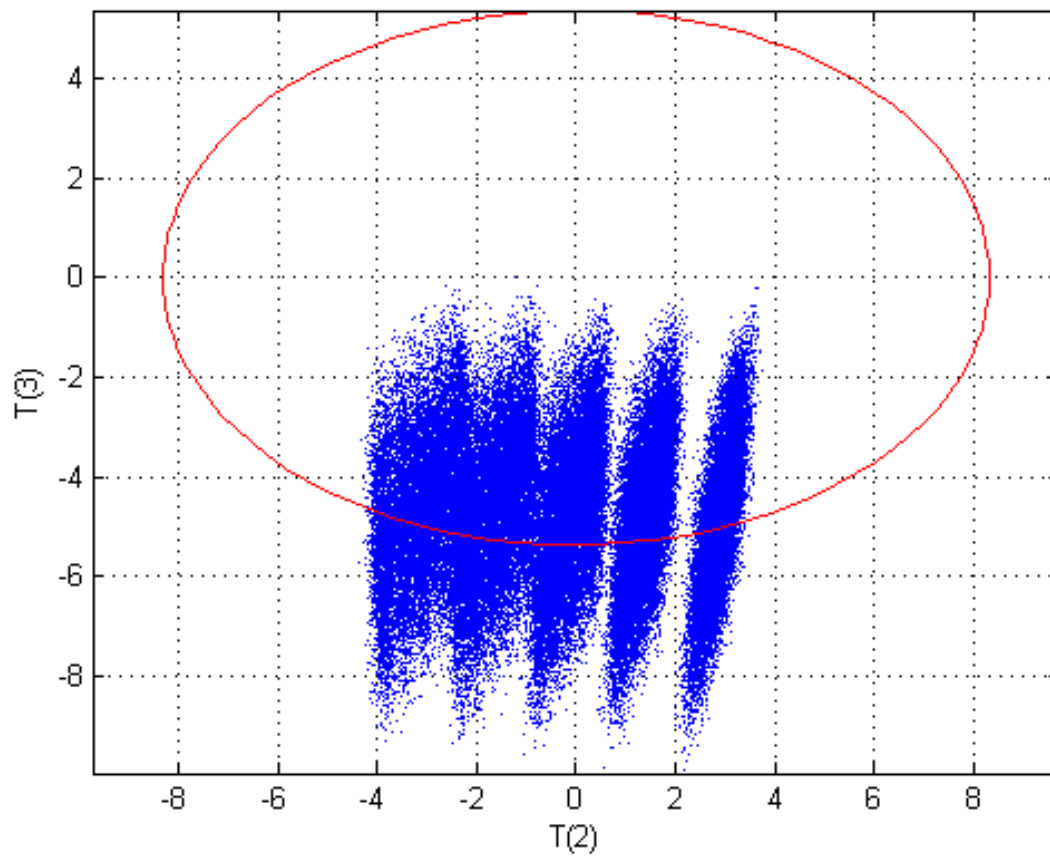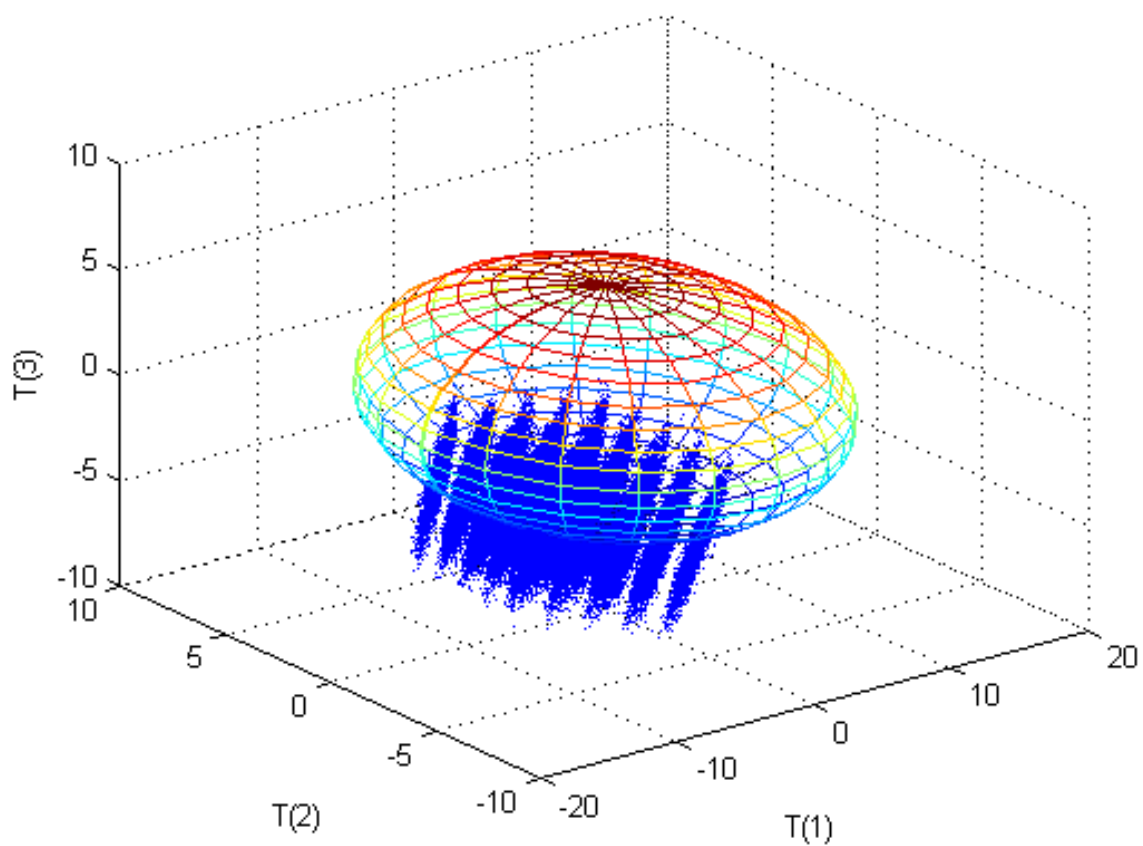
Figure 4.117. Reduced Faulty Case 4 Scores Plot for PC2 and PC3. *Note: Only the faulty data are shown with the base case 95% confidence boundary displayed in red. There was a shift in PC3 scores but the fault may not be detectable.*

Figure 4.118. Reduced Faulty Case 4 3D Scores Plot for PC1, PC2, and PC3. *Note: Only the faulty data are shown with the base case 95% confidence boundary displayed as an ellipsoid. There was a shift in PC3 scores but the fault may not be detectable.*
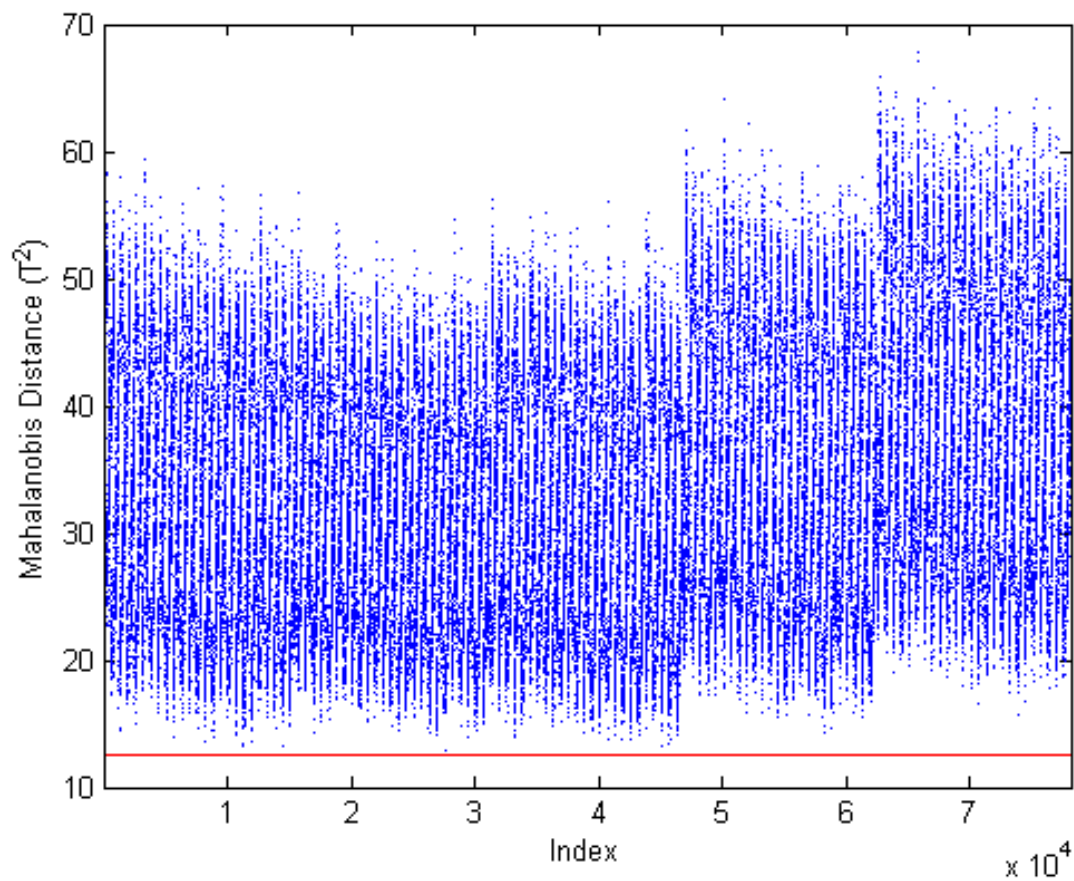
Figure 4.119. Reduced Faulty Case 4 Mahalanobis Distance Plot. *Note: Only the faulty data are shown with the base case 95% confidence boundary displayed in red. There was a shift but the fault may not be detectable.*
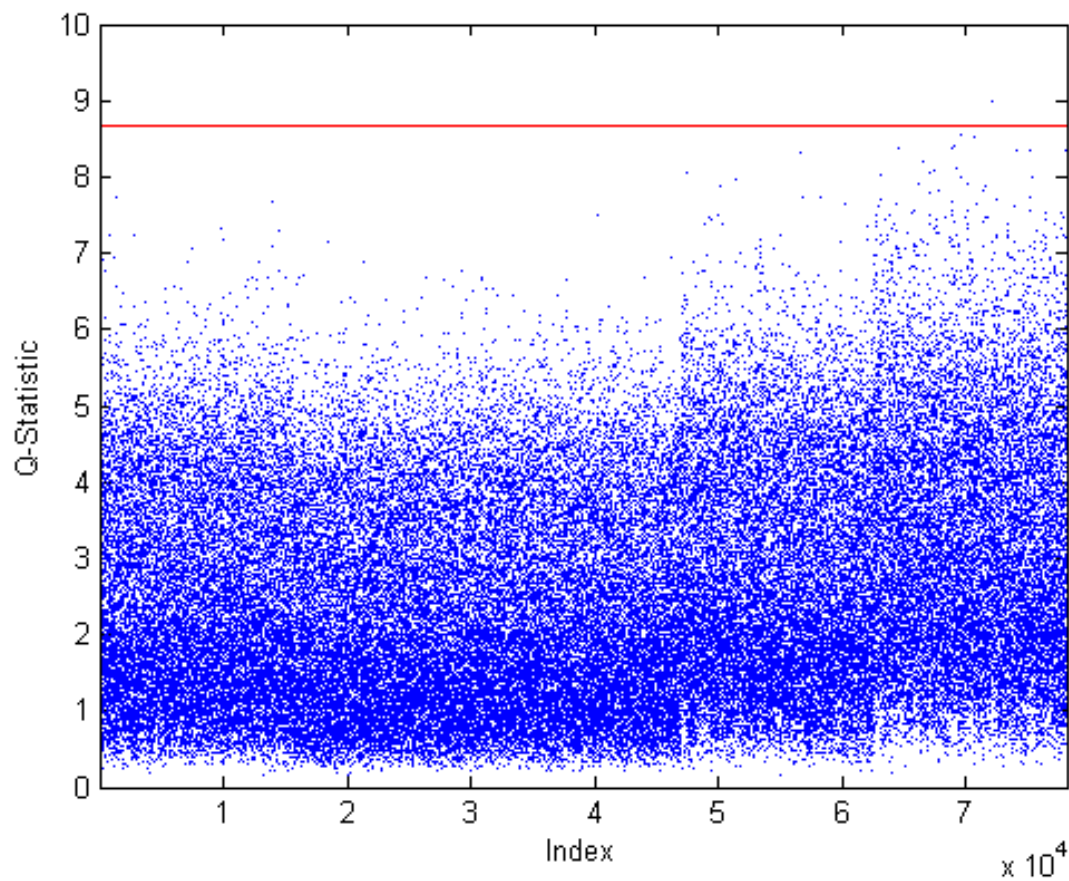
Figure 4.120. Reduced Faulty Case 4 *Q*-**Statistic Plot.** *Note: Only the faulty data are shown with the base case 95% confidence boundary displayed in red. There was not a detectable shift.*
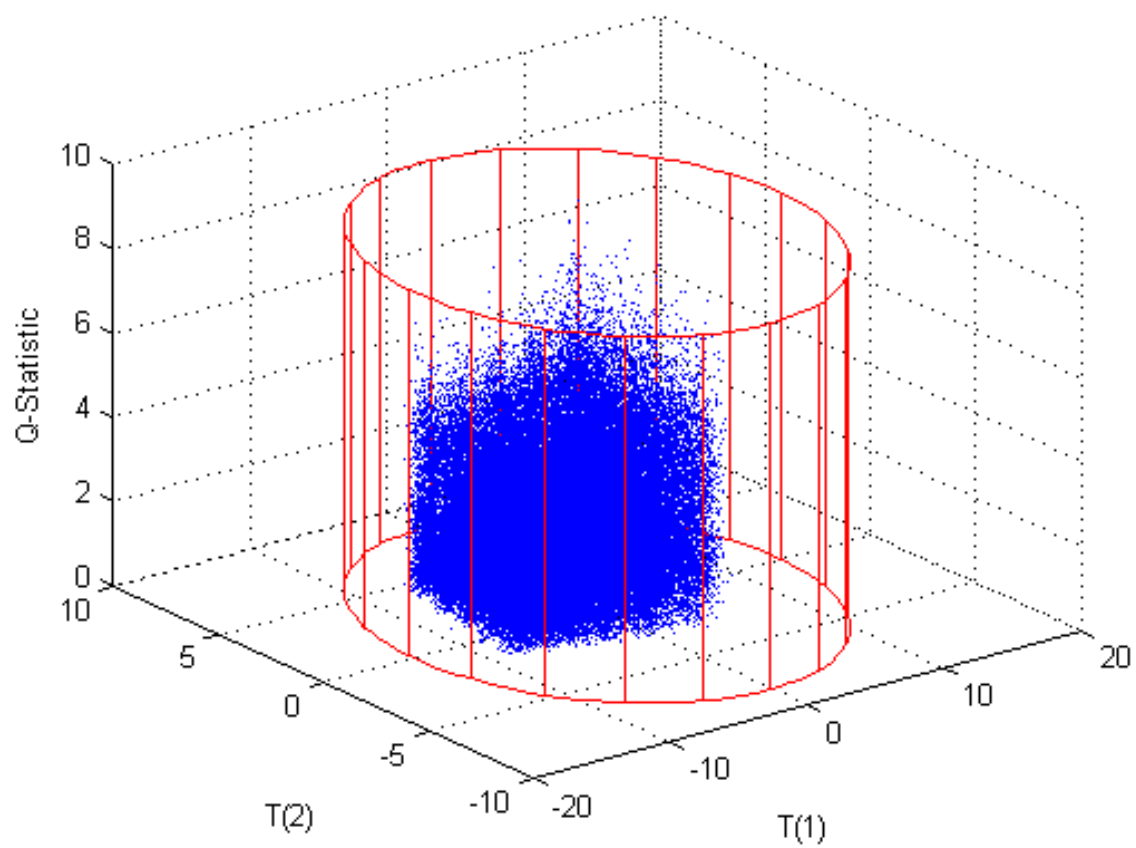
Figure 4.121. Reduced Faulty Case 4 PC1, PC2, and Q-Statistic Plot. *Note: Only the faulty data are shown with the base case 95% confidence boundary displayed in red. There was not a detectable shift.*

4.3.17.4 Reduced Case 11

For the eleventh faulty case, a percentage of the UF$_6$ product was diverted from the final mixer in Module 5. Streams 52 and 59 were pure UF$_6$ that were mixed to form the final product of the process. In this case, a new stream (61) was formed by diverting a percentage of Streams 52 and 59. Reduced Case 11 tested the diversion of 20% of the UF$_6$ product as was tested in the original faulty Case 11. The results show that the fault in this case was not detectable using the reduced case PC model until the final UF$_6$ product stream was scaled by a factor of 10. After the differential weighted scaling was applied, this fault was clearly detectable in the Q-statistic and may be detectable in the scores and Mahalanobis distance depending on operating conditions.

There was a slight shift in the scores plots (Figures 4.122–4.125), but the fault was not detectable under certain operating conditions since many of the data points were within the 95% confidence boundaries. The scores faults may be detectable using trend monitoring. The final output of the plant [Xss(273)] was a heavy contributor to both PC1 and PC3. There was also an increase in the Mahalanobis distance (Figure 4.126) which was expected since this fault may be outside normal operating conditions. There was an increase in the Q-statistic (Figures 4.127–4.128). The Q-statistic fault was expected since this changed the relative relationship between the state variables.
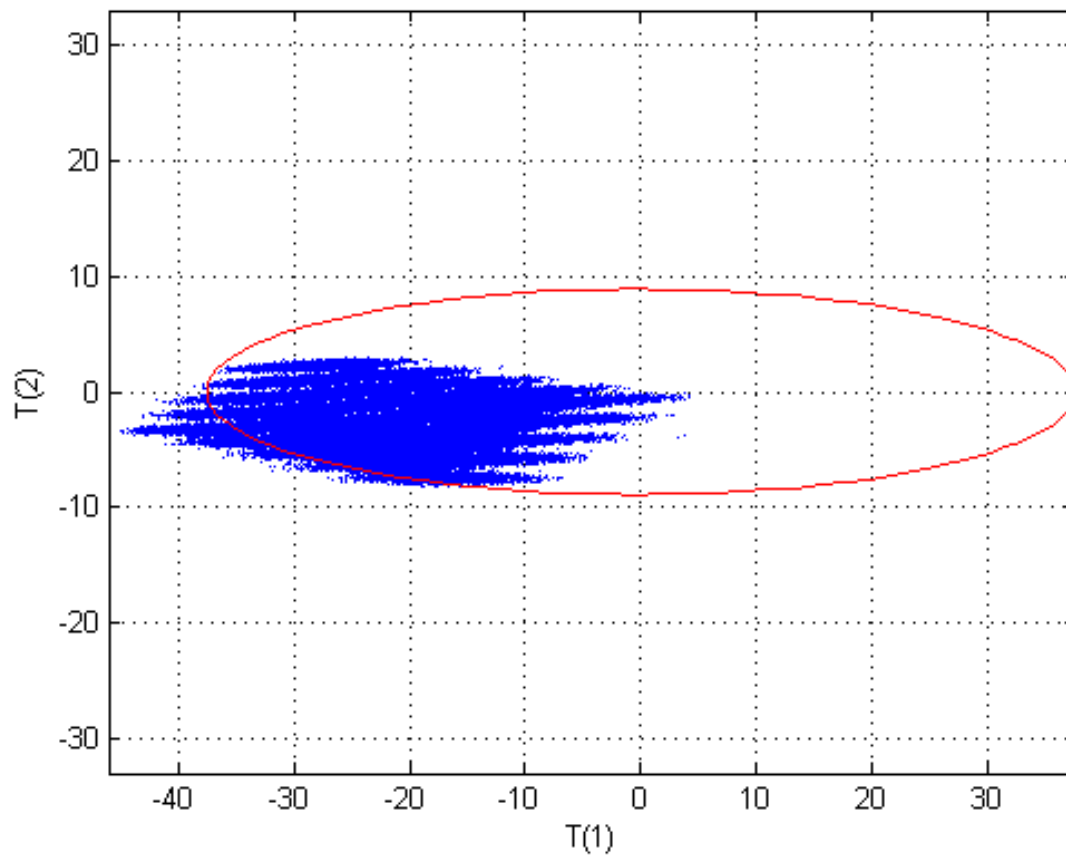
Figure 4.122. Reduced Faulty Case 11 Scores Plot for PC1 and PC2. *Note: Only the faulty data are shown with the base case 95% confidence boundary displayed in red. There was a shift in PC1 and PC2 scores but the fault may not be detectable depending on operating conditions.*

Figure 4.123. Reduced Faulty Case 11 Scores Plot for PC1 and PC3. *Note: Only the faulty data are shown with the base case 95% confidence boundary displayed in red. There was a shift in PC1 and PC3 scores but the fault may not be detectable depending on operating conditions.*
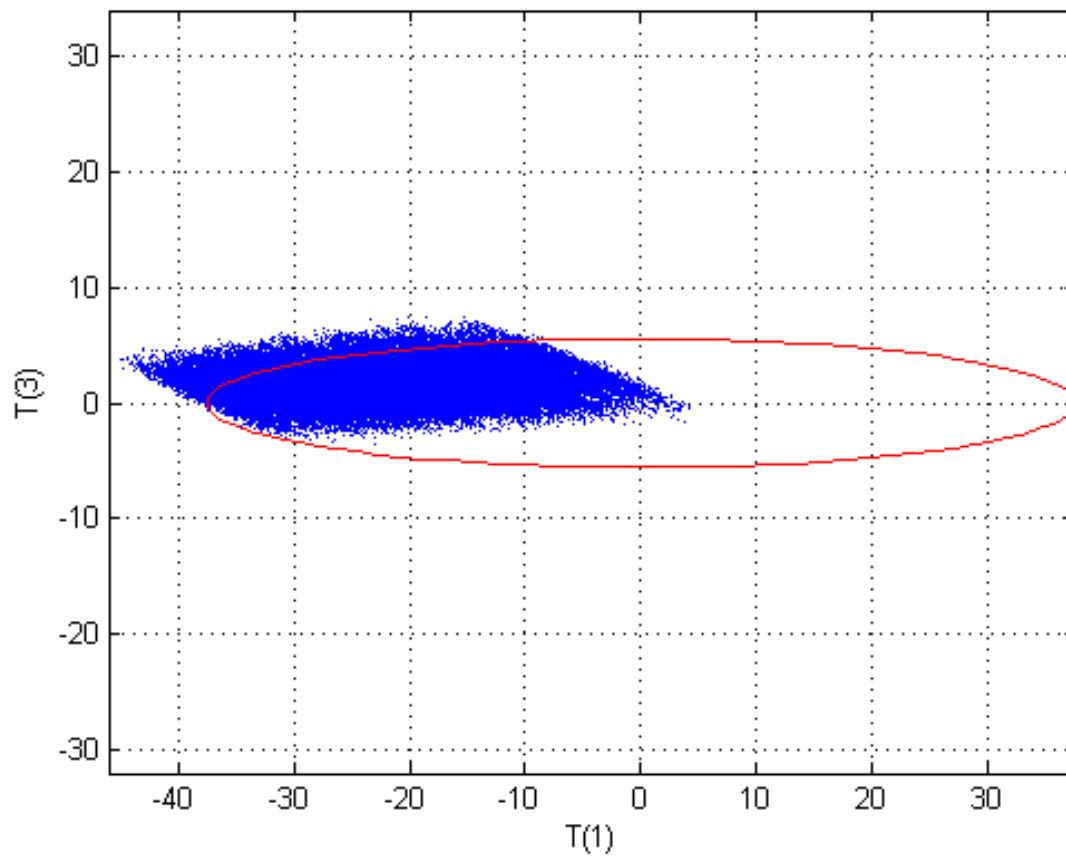
Figure 4.124. Reduced Faulty Case 11 Scores Plot for PC2 and PC3. *Note: Only the faulty data are shown with the base case 95% confidence boundary displayed in red. There was a shift in PC2 and PC3 scores but the fault may not be detectable depending on operating conditions.*
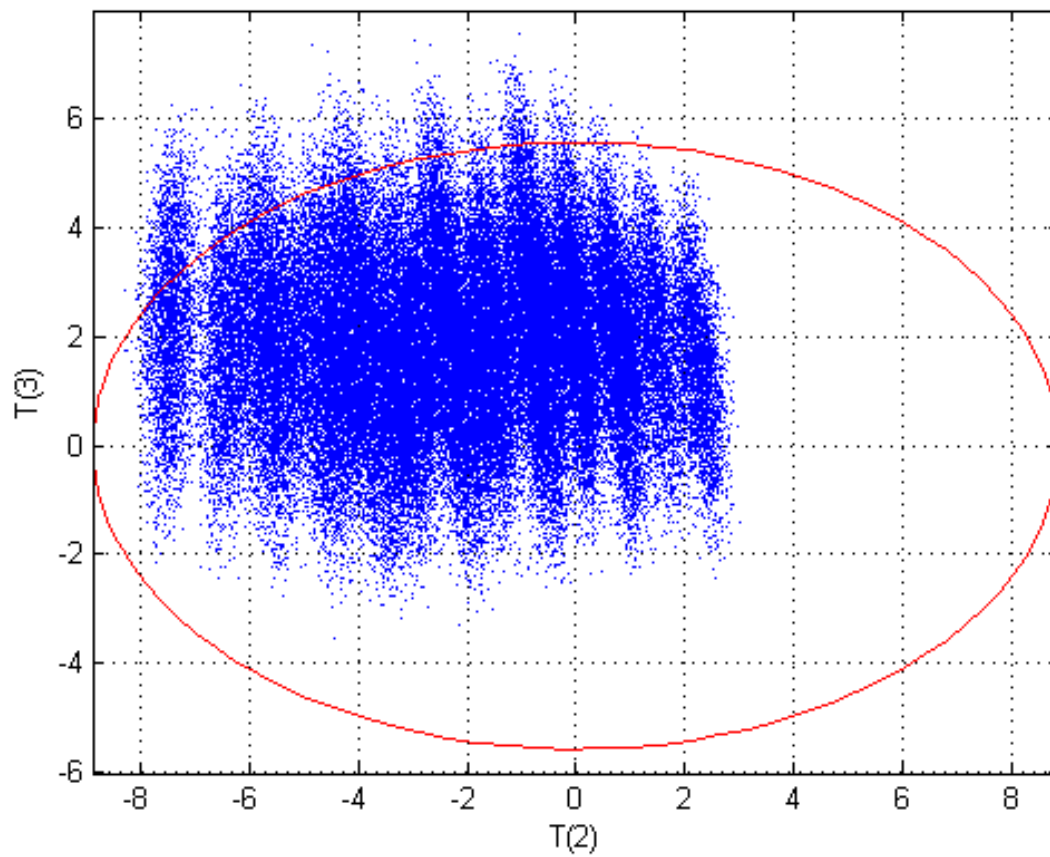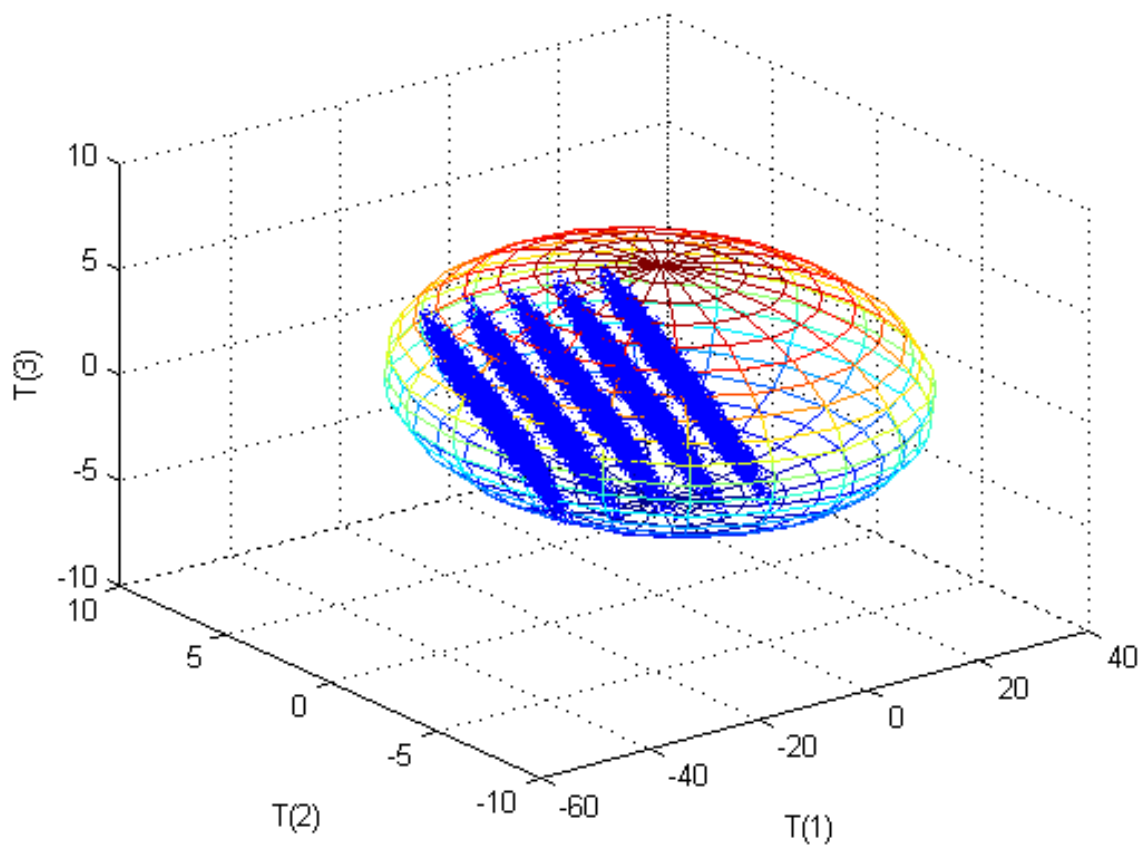
Figure 4.125. Reduced Faulty Case 11 3D Scores Plot for PC1, PC2, and PC3. *Note: Only the faulty data are shown with the base case 95% confidence boundary displayed as an ellipsoid. There was a shift in all three scores but the fault may not be detectable.*

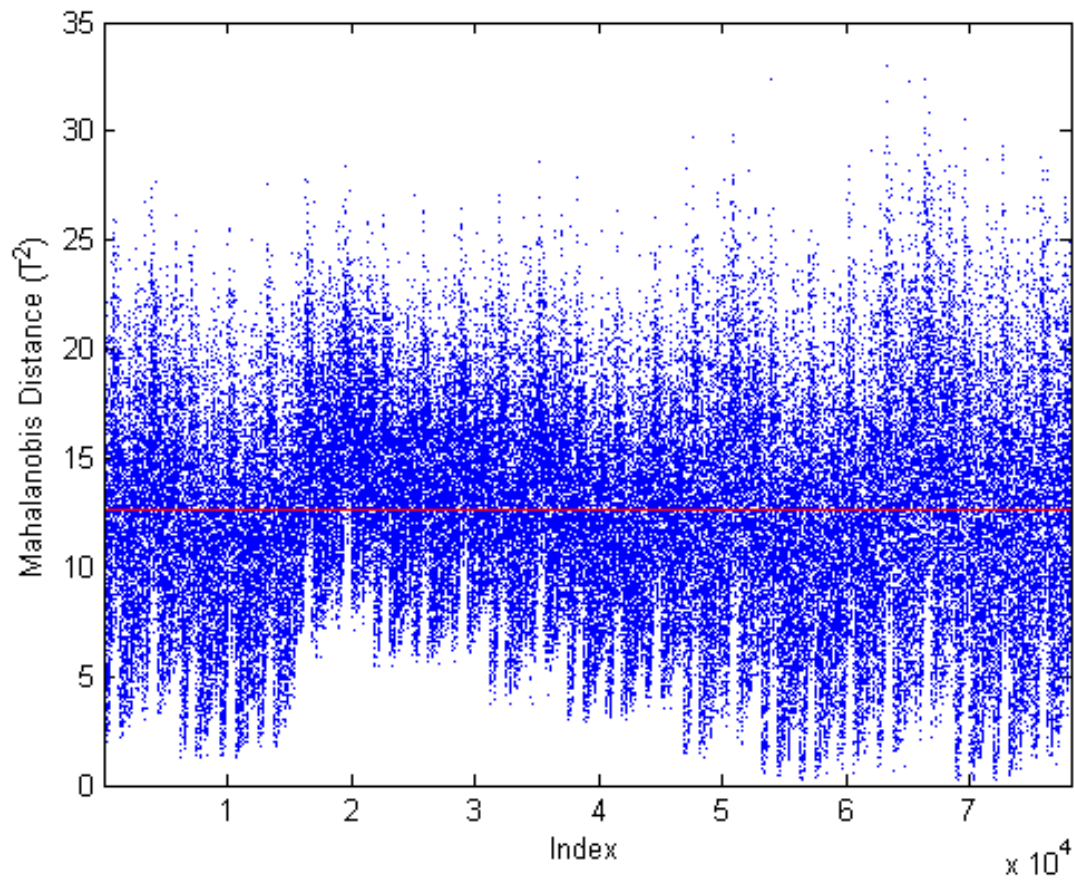**Figure 4.126. Reduced Faulty Case 11 Mahalanobis Distance Plot.** *Note: Only the faulty data are shown with the base case 95% confidence boundary displayed in red. There was a shift but the fault may not be detectable.*

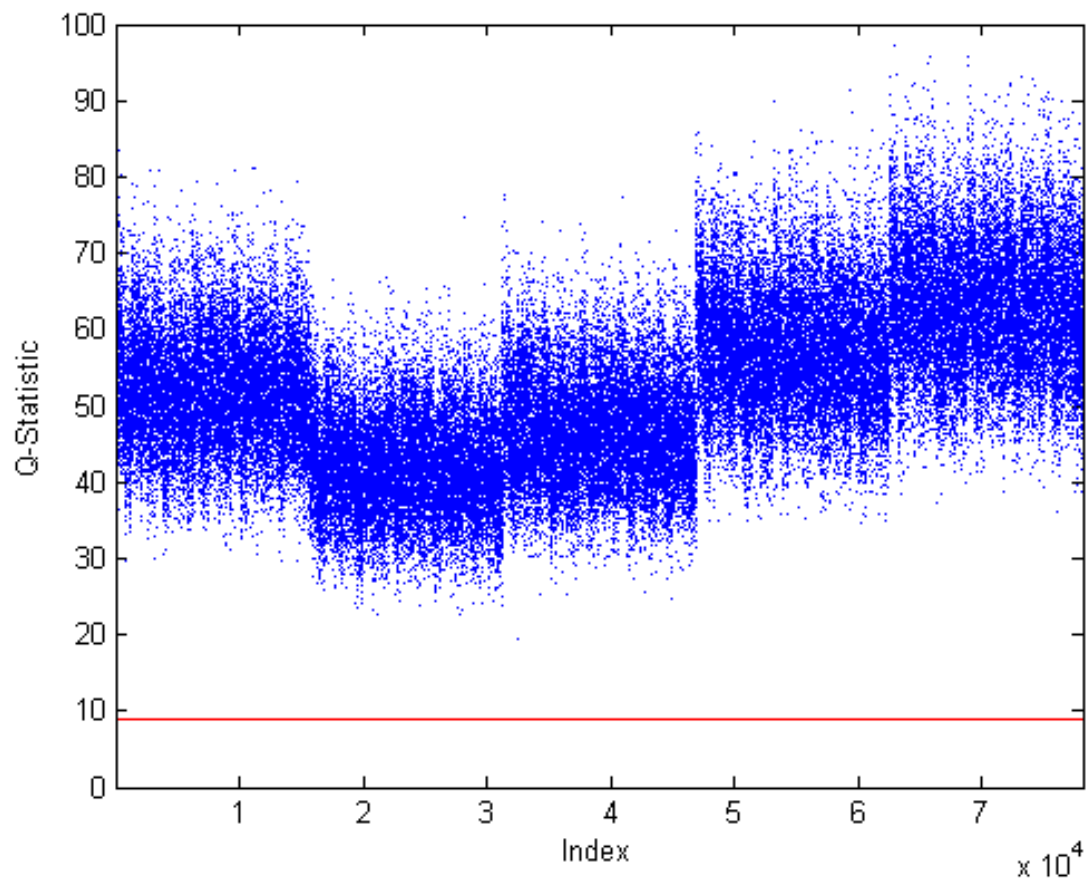**Figure 4.127. Reduced Faulty Case 11** Q**-Statistic Plot.** *Note: Only the faulty data are shown with the base case 95% confidence boundary displayed in red. There was a detectable fault.*
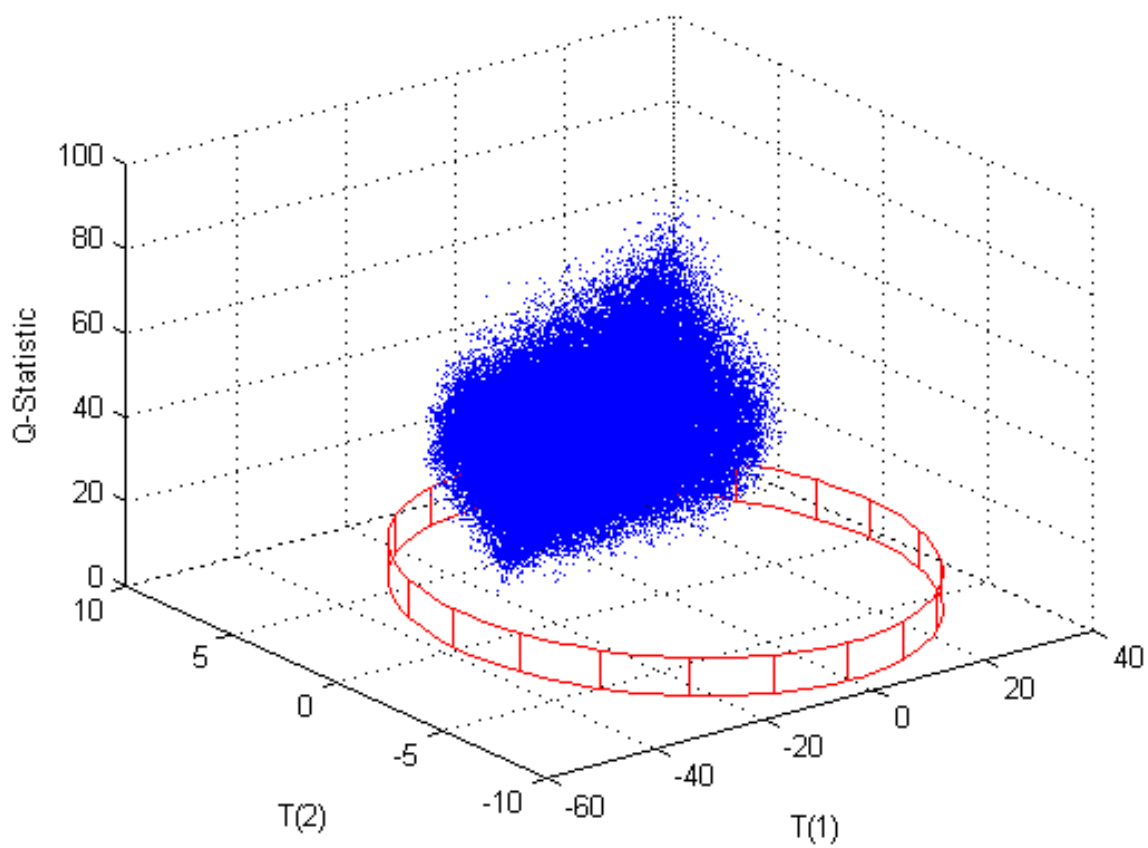
Figure 4.128. Reduced Faulty Case 11 PC1, PC2, and *Q*-Statistic Plot. *Note: Only the faulty data are shown with the base case 95% confidence boundary displayed in red. There was a detectable fault in the Q-statistic.*

4.3.17.5 Reduced Case Summary

For this reduced case monitoring framework, the original base case system was reduced from 273 state variables to 23 state variables. The only state variables retained for the reduced case were the uranium-bearing components in the product stream of each module and the uranium-bearing components in the waste streams from each module. A total of fourteen streams not including input streams are represented in the reduced case as opposed to sixty streams in the original case. Six principal components were retained for the reduced case PC model which retained approximately 92% of the original information. Three of the faulty cases were used to test the new reduced PC model for the detection of diversion of uranium in an NUCP. In each case, the fault was clearly detectable in at least one of the diagnostic plots. Based on these initial results, it is possible to detect diversion in an NUCP by monitoring only the uranium input, the final UF_6 product, the intermediate uranium-bearing products from each module, and the uranium-bearing waste streams. Therefore, option 2 is sufficient as a safeguards monitoring system to be applied with this detection framework.

4.3.18 Implementation of Monitoring Framework

Individually monitoring and analyzing the flow rates and uranium content of the recommended streams would be labor intensive and complicated since the limiting variation of each in combination with the others needs to be understood beforehand in order to properly interpret the monitored measurements. This consideration is behind the work reported in this dissertation. By subjecting all the measured values to a multivariate statistical analysis framework, deviations and the patterns of the deviations may be detectable and possible causes revealed can be followed up by the operator or IAEA inspector. Therefore, it is expected that the recommended streams would be monitored for flow rate and uranium content to provide the data for the monitoring and analysis framework but the individual measurements would not be analyzed independently.

Table 4.37 provides a lookup table to determine which type of fault may be occurring based on the results from the various diagnostic plots. If this framework was applied to an operating plant, the operator or in the case of safeguards applications, an IAEA inspector, would be monitoring the diagnostic plots each time new monitoring data was supplied (hourly, daily, etc.). The plots would include the 95% confidence boundary for normal operations at that particular plant and the recent operating data (data points representing the last few weeks or months of operations). A lookup table such as Table 4.37 can provide possible causes if new data points are outside the boundary or if new data points exhibit a trend of continuous migration from inside the boundary toward the boundary, and may end up crossing the boundary and ending up outside the boundary if the faulty continues. This table is based on the results of the faulty cases investigated in this work; additional faults could occur that may not be on the table or may have the same result as a different type of fault than is included in

Table 4.37. Lookup Table of Possible Faults Based on Results from PCA Diagnostic Plots*

Faults (Direction, Detectable)						Example
Q	T2	PC1 Scores	PC2 Scores	PC3 Scores	Possible Cause of Fault	Case
++++, Yes	++, Yes	---, Yes	+, No	0, No	Large increase in all flow rates	1A
++, Yes	~+, No	0, No	0, No	0, No	Slight increase in all flow rates	1B
0, No	~+, Not likely	-, No	0, No	0, No	Increase in $F_{1A,U}$ only slightly above normal	1C
0, No	+, Yes	-, Possibly	0, No	0, No	Increase in $F_{1A,U}$ above normal	1D
++, Possibly	~+, Possibly	+, No	+, No	-, Possibly	Inefficient re-extraction operations, reduce uranyl nitrate extraction in Module 2 resulting in more U in Module 2 waste	4
+++++, Yes	+, Yes	+, Possibly	-, Possibly	+, Yes	Slight diversion from the evaporator in Module 3	5
++, Yes	~+, Possibly	-, No	-, No	+, Possibly	Addition of uranyl nitrate to the precipitation process	6
++, Yes	0, No	0, No	0, No	0, No	Diversion of uranium in Module 5	9, 10, 11
++, Yes	+, Possibly	-, Possibly	+, No	-, No	Increased throughput of uranium and diverted a fraction of final product	12
++, Yes	~+, Possibly	+, No	+, No	-, Not likely	Multiple inefficient operations resulting more U in more than one waste stream	13
++++, Yes	+++, Yes	-, Possibly	+, Possibly	--, Yes	Inefficient dissolver operations resulting in a reduction of the amount of U_3O_8 converted to UN and more U in waste streams	3
++++, Yes	~+, Not likely	-, No	-, No	+, No	Inefficient separation downstream of the hydrofluorination reaction results in more U in Module 4 waste	8

*'Yes' indicates that all faulty data points were outside the confidence boundary while a 'no' indicates that there was no clearly detectable fault and most if not all of the data points were within the confidence boundary. 'Possibly' indicates that approximately 50% or more of the data points were outside the boundary while 'not likely' indicates that less than 50% of the data points were outside the boundary.

Table 4.37. Lookup Table of Possible Faults Based on Results from PCA Diagnostic Plots*
(continued)

Faults (Direction, Detectable)					Possible Cause of Fault	Example
Q	T2	PC1 Scores	PC2 Scores	PC3 Scores		Case
+++, Yes	~+, Possibly	+, No	-, No	+, Possibly	Decrease in impurities of uranium feed to plant	2
++, Yes	~+, Possibly	+, No	+, No	-, Not likely	Inefficient precipitation process operations resulted in less UN converted AUC and more U in waste streams	7
++++, Yes	++, Yes	-, Possibly	+, Possibly	--, Yes	Decrease the impurities in the uranium feed and reduce the amount of U_3O_8 converted to UN resulting in more U in waste streams	14

*'Yes' indicates that all faulty data points were outside the confidence boundary while a 'no' indicates that there was no clearly detectable fault and most if not all of the data points were within the confidence boundary. 'Possibly' indicates that approximately 50% or more of the data points were outside the boundary while 'not likely' indicates that less than 50% of the data points were outside the boundary.

the table. The person monitoring the new data would not only be looking for data points outside the boundary but also be watching if the data that are trending in one direction or another such that it may be approaching the confidence boundary but not yet outside the boundary. The table could possibly be used to determine the cause of the trend as well. It is also expected that data will occasionally be outside of the boundary, if this is only an occasional occurrence and the following few data points return within the boundary there is likely no cause for concern about an actual fault occurring.

Additionally, it is important that the system be allowed to return to steady-state following any upset conditions which might result in a false positive using the detection framework. Depending on the type of upset, the system may return to steady-state in a few hours or it may take more than a day. It is recommended that data only be recorded no more often than about every twelve hours in a conversion plant since the processing operations require several hours to complete. An additional consideration for implementation is that the "normal operation" model would need to be updated periodically as conditions within the plant change, particularly if a process is changed. If one of the processes is changed (i.e., more efficient equipment is installed) then the "normal operation" model would need to be changed with the new operation data to represent the new process.

Table 4.37 shows both the direction and the detectability of the possible faults. Direction refers to whether the fault in is in the positive or negative direction for the scores. The Q-statistic and Mahalanobis distance are positive valued and can only show an increase. Additionally, an indication of magnitude of the fault was provided by using multiple '+' or '-' signs. If there was no shift in the diagnostic plot then '0' was used. The detectability is given as 'yes', 'no', 'possibly', or 'not likely'. A 'yes' indicates that all faulty data points were outside the confidence boundary while a 'no' indicates that there was no clearly detectable fault and most if not all of the data points were within the confidence boundary. If 'possibly' or 'not likely' was listed then some of the data points were outside the boundary; 'possibly' indicates that approximately 50% or more of the data points were outside the boundary while 'not likely' indicates that less than 50% of the data points were outside the boundary.

The Mahalanobis distance is not independent of the scores and one would not expect to have a fault in the Mahalanobis distance without a clear fault or shift in all of the points in at least one of the scores. However in Case 1B, there was an increase in the number of data points above the Mahalanobis confidence boundary without a clear scores fault. The slight increase in the Mahalanobis distance was not truly a detectable fault and there was a only very slight shift in the PC1 scores. In this case, monitoring for a continuous shift in the trending pattern of the scores or the Q-statistic toward the boundary may be applicable.

Figures 4.129–4.131 provide examples of what actual diagnostic plots may look like. Figure 4.129 is a PC1 scores vs. PC2 scores plot based on Faulty Case 1A. The cluster of normal data (blue) are within the 95% confidence boundary and close to one another while the faulty data (green) are outside the boundary if the fault introduced is a step change from none to all over a short time span. Figure 4.130 is

a Mahalanobis distance plot based on Faulty Case 1A. The normal data (blue) are within the 95% confidence boundary while the faulty data (green) are outside the boundary. Figure 4.131 is a Q-statistic plot based on a slight increase over normal operation. The normal data (blue) are within the 95% confidence boundary while the faulty data (green) are outside the boundary. The Mahalanobis and Q-statistic plots also represent a step change for the fault because the faulty was introduced as a step change, instead of a trend. In regular operation, a fault may occur as a step fault, or it may manifest itself gradually as equipment deteriorate over time, or a deliberate fault is introduced slowly over time. Therefore, monitoring of the trending behavior of process operation is also applicable.
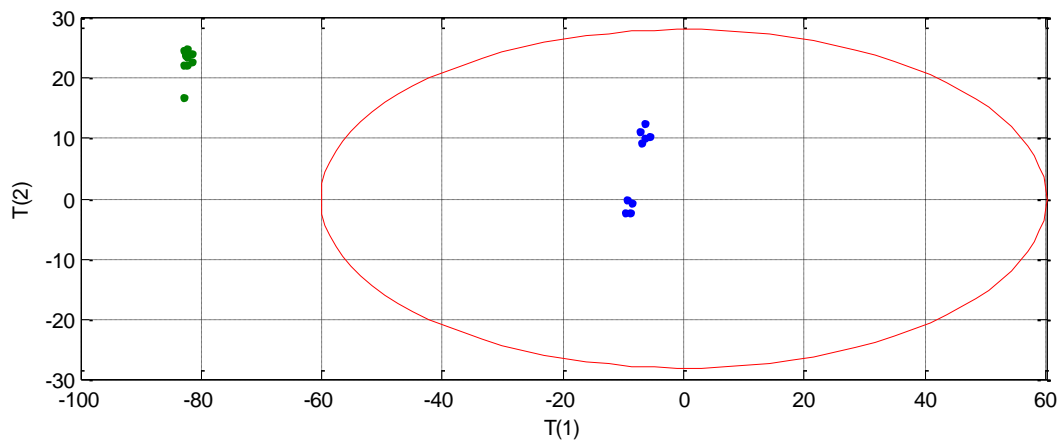

Figure 4.129. Example of PC1 vs. PC2 Scores for Implementation of the Monitoring Framework. *Note: The base case data are shown in blue while the faulty data are shown in green. The base case 95% confidence boundary displayed in red.*

Figure 4.130. Example Mahalanobis Distance Plot for Implementation of the Monitoring Framework. *Note: The base case data are shown in blue while the faulty data are shown in green. The base case 95% confidence boundary displayed in red.*

Figure 4.131. Example Case 14 *Q***-Statistic Plot for Implementation of the Monitoring Framework.** *Note: The base case data are shown in blue while the faulty data are shown in green. The base case 95% confidence boundary displayed in red.*
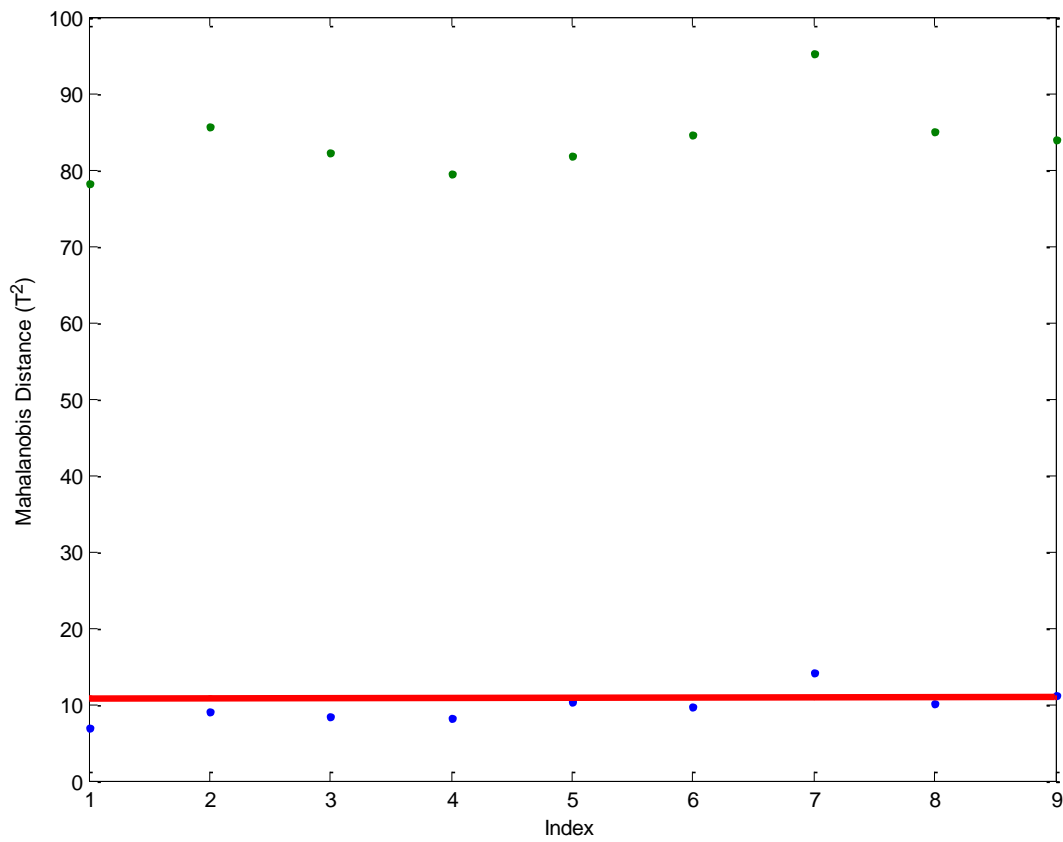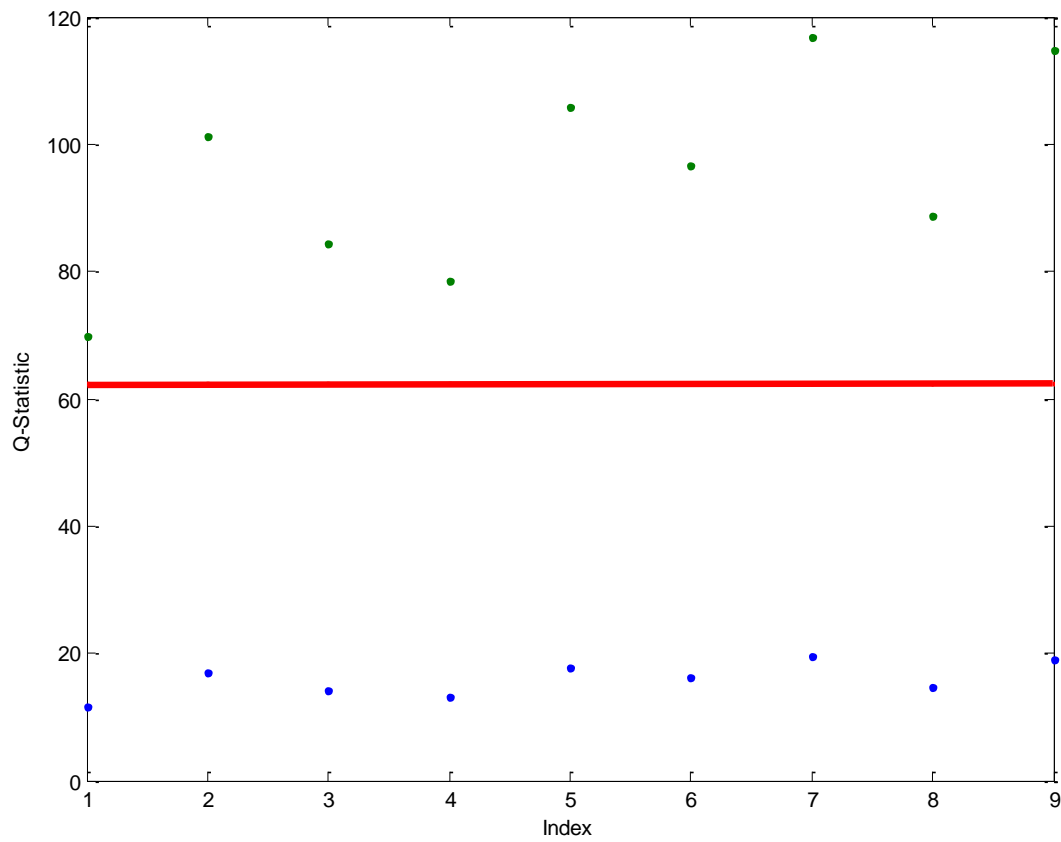
5. CONCLUSIONS AND RECOMMENDATIONS

The objective of this work was to develop a monitoring and data analysis framework using a multivariate statistical approach that would detect operational faults and/or the diversion of intermediate products such as UO_2, UF_4, and UF_6 in an NUCP. This was an initial effort to determine the feasibility of such approach for safeguards applications. The decision framework developed in this research has been shown to be able to detect various faults including the simulated diversion of material in the idealized NUCP. This study was developed for a 100 MTU/yr NUCP employing the wet solvent extraction method for the purification of uranium ore concentrate.

A workhorse in the multivariate statistical methodology was the PCA approach for the analysis of data, development of the base model from historical data, and evaluation of current and future operations. The PCA approach was implemented through the use of singular value decomposition of the data matrix. Component mole balances were used to model each of the process units in the NUCP. The decision framework could be used to determine whether or not a diversion of material has occurred at an NUCP as part of an IAEA safeguards system. The IAEA goal for NUCPs of this size is to have a 50% probability of detecting the diversion of 10 MTU over a period of one year; this was also used as the goal of detection for the monitoring framework. Therefore the detection goal of this effort was to be able to detect the diversion of 10% of the uranium fed to the plant.

An initial sensitivity analysis was performed on the relationship between the component molar flow rates (state variables) and the process parameters. The analysis results showed that the system was most sensitive to changes in the incoming flow rate of uranium. This was to be expected since all of the compounds of interest contain uranium and which values depend on the level of uranium in the incoming stream. This was a limited sensitivity analysis, and it is recommended that a complete sensitivity analysis be conducted to include all possible model parameters and input variables as part of the full development of this approach for safeguarding conversion plants.

Differential weighting of selected state variables was required during the data pre-processing step. The base case system was reduced in dimensionality from 273 state variables and seven input variables to five degrees of freedom using PCA. Heavy contributors to PC1 are the input uranium feed flow rate [Xss(274)] to Module 1 and the output uranium-bearing product flow rates from each of the five modules [Xss(64), Xss(111), Xss(163), Xss(218), and Xss(273)]. This correlation pattern is highly anticipated, since the molar flow rates of all uranium-bearing output streams should all be highly correlated to the main feed flow rate. The first principal component represented those state variables with the most variation in the data matrix. This makeup was expected for two reasons: (1) the first principal component represents 71.8% of the original data and (2) the uranium input flow rate to the process was the input variable that the uranium-bearing streams were most sensitive to as determined by the sensitivity analysis.

325

Fourteen faulty scenarios were developed to test the monitoring framework after the base case or "normal operating conditions" of the PCA model was established. The faulty cases tested the model's ability to detect an increase in total throughput or uranium throughput, an increase in uranium purity, inefficient operations in several of the processes, withdrawal of uranium at different points within the processes, addition of uranium to one of the processes, and a combination of faults. In each scenario, at least one of the diagnostic plots (scores, Mahalanobis distance, or Q-statistic) produced a detectable fault. The detection limit varied depending on the scenario, but it satisfied the limit stated above in most cases. Additional scaling may improve the detection limits in those cases where the fault was only detectable under certain operating conditions, such as Case 4.

Based on the results of this work, four safeguards monitoring schemes were recommended. At a minimum, the uranium feed to the plant must be monitored both for feed rate and uranium content as well as the final product from the plant. It is also recommended that all of the waste streams be monitored to detect excess uranium. However, if it is not reasonable to monitor all wastes then the waste streams that are most likely to contain diverted uranium must be monitored (Module 1 Stream 8, Module 2 Stream 20, Module 3 Stream 31, Module 4 Stream 43, and Module 5 Stream 50). Since the process operates serially where the product of one process becomes the feed to the next process, monitoring the feed, product, and all waste streams provides the minimum monitoring necessary to close the material balance and offer any certainty that uranium is not being diverted or additional uranium is not being fed to the plant.

The second option for monitoring that is recommended would be to add monitoring of the intermediate products throughout the process to the first option. These are the products from each module that becomes the feed to the next module: Module 1 Stream 12, Module 2 Stream 19, Module 3 Stream 30, and Module 4 Stream 44. Since there is normally some time lag between processes in actual plants, these would need to be monitored as the product of one process and then the feed to the next process. Monitoring both the rate and the uranium content would be necessary to determine that diversion of uranium had not occurred.

The third option for monitoring that could confirm that diversion had not occurred would be the monitoring of select intermediate streams. These streams could be correlated with the feed, product, and waste streams in that process area to determine that uranium was not diverted or added to the process. These streams are Module 1 Streams 1 and 4; Module 2 Stream 14; Module 3 Streams 22 and 27; Module 4 Streams 34, 39, and 42; and Module 5 Streams 46, 49, 52, 55, and 59.

The final level of monitoring that would be able to completely close the material balance and ensure that no additional uranium is fed to the process and that no uranium is diverted from the process would require monitoring all of the streams throughout the plant for both flow rate and uranium content. However, this would be too challenging to implement both from the perspective of the plant and the

costs required to purchase and install that number of monitoring points. Additionally, based on this research, it is likely unnecessary to monitor all of the streams in the plant.

Therefore, if not cost prohibitive, the second option would be the best safeguards monitoring system to be applied with this detection framework. This framework could also be applied to the less intrusive option 1 as well. However, the likelihood of detection is reduced as the number of monitoring points is reduced. Based on the initial results from the reduced case PC model, it is possible to detect diversion in an NUCP by monitoring only the uranium input, the final UF_6 product, the intermediate uranium-bearing products from each module, and the uranium-bearing waste streams. Therefore, option 2 is sufficient as a safeguards monitoring system to be applied with this detection framework.

Individually monitoring and analyzing the flow rates and uranium content of the recommended streams would be labor intensive and complicated since the limiting variation of each in combination with the others needs to be understood beforehand in order to properly interpret the monitored individual measurements. This consideration is behind the work reported in this dissertation. By subjecting all the measured values to a multivariate statistical analysis framework, deviations and the patterns of the deviations may be detectable and possible causes revealed can be followed up by the operator or IAEA inspector. Therefore, it is expected that the recommended streams would be monitored for flow rate and uranium content to provide the data for the monitoring and analysis framework but the individual measurements would not be analyzed independently.

The implementation of this monitoring and analysis framework in an operating plant would require monitoring the diagnostic plots each time new monitoring data was supplied (hourly, daily, etc.). The plots would include the 95% confidence boundary for normal operations based on that particular plant and the recent operating data (data points representing the last few weeks or months of operations). A lookup table such as Table 4.37 can provide possible causes if new data points are outside the boundary or if new data points exhibit a trend of continuous migration from inside the boundary toward crossing the boundary and ending up outside the boundary. The person monitoring the new data would not only be looking for data points outside the boundary but also be watching if the data that are trending in one direction or another such that it may be approaching the confidence boundary but not yet outside the boundary.

The following are recommendations for continuing this work in the future. These recommendations include research that is outside the scope of this effort.

- Complete sensitivity analysis of how all parameters and input variables affect the state variables.
- Update the detection framework to work for a less ideal case.
- Test the framework against real data.

- Test the limitations/uncertainty of the framework if data were unavailable by testing additional faulty cases and reducing the amount of the fault in the existing faulty cases to determine the detection limits.
- Identify the minimum number of streams that must be monitored to detect at least the high priority diversion scenarios (partially explored).
- Apply the monitoring approach to individual modules to see what faults can be detected.

LIST OF REFERENCES

Bakshi, B. R. 1998. "Multiscale PCA with Application to Multivariate Statistical Process Monitoring." *AIChE Journal.* **44** (7), 1596–1610.

Benedict, M., T. Pigford, and H. Levi. 1981. *Nuclear Chemical Engineering.* 2nd ed., McGraw-Hill, New York.

Boyer, B. D., D. M. Gordon, L. G. Fishbone, and J. R. Lemley. 2004. "International Safeguards Approach for Uranium Ore Concentrates to Uranium Hexafluoride Conversion Plants." *Proceedings 45th Annual Meeting of Institute of Nuclear Materials Management (INMM),* Orlando, July.

Brauner, N. and M. Shacham. 2000. "Considering precision of data in reduction of dimensionality and PCA." *Computers and Chemical Engineering.* **24**, 2603–2611.

Cochran, R. G. and N. Tsoulfanidis. 1990. *The Nuclear Fuel Cycle: Analysis and Management.* 2nd ed., American Nuclear Society, LaGrande Park.

Doo, J., D. Hurt, R. Fagerholm, and N. Tuley. 2003. "Safeguards Approach for Natural Uranium Conversion Plants." *Proceedings 44th Annual Meeting of Institute of Nuclear Materials Management (INMM),* Phoenix, July.

Elayat, H. A., H. Lambert, and W. J. O'Connell. 2004. "Systems Analysis of Safeguards Effectiveness in a Uranium Conversion Facility." *Proceedings 45th Annual Meeting of Institute of Nuclear Materials Management (INMM),* Orlando, July.

Faulkner, R. L., J. M. Begovich, J. J. Ferrada, R. D. Spence, J. M. Whitaker, W. J. Bicha, and L. G. Loden. 2004. "Oak Ridge Efforts to Enhance Conversion Plant Safeguards." *Proceedings 45th Annual Meeting of Institute of Nuclear Materials Management (INMM),* Orlando, July.

Ferrada, J. J. 2004. Personal communication to J. J. Ferrada, Oak Ridge National Laboratory, Oak Ridge, Tenn., April 30, 2004.

Himmelblau, D. M. 1967. *Basic Principles and Calculations in Chemical Engineering.* 59–62. 2nd ed., Prentice-Hall, New Jersey.

Hines, W. J., B. R. Upadhyaya, and J. J. Henkel. 2008. "Process Monitoring Techniques Applied to Safeguards." *Proceedings 49th Annual Meeting of Institute of Nuclear Materials Management (INMM),* Nashville, July.

Hotelling, H. 1933. "Analysis of a complex of statistical variables into principal components." *Journal of Educational Psychology.* **24**, 417–441 and 498–520.

Inoue, A. and T. Tsujino. 1984. "Dissolution rates of uranium oxide (U_3O_8) powders in nitric acid." *Industrial and Engineering Chemistry Process Design Development.* **23** (1), 122–125.

International Atomic Energy Agency (IAEA). September 1968. "The Agency's Safeguards Systems (1965, as Provisionally Extended in 1966 and 1968)," INFCIRC/66/Rev.2, http://www.iaea.org/Publications/Documents/Infcircs/Others/inf66r2.shtml.

International Atomic Energy Agency (IAEA). June 1972. "The Structure and Content of Agreements Between the Agency and States Required in Connection with the Treaty on the Non-Proliferation of Nuclear Weapons," INFCIRC/153 (corrected), http://www.fas.org/nuke/control/npt/text/inf153.html.

International Atomic Energy Agency (IAEA). June 2002. "IAEA Safeguards Glossary, 2001 Edition," http://www-pub.iaea.org/books/IAEABooks/6570/IAEA-Safeguards-Glossary-2001-Edition.

International Atomic Energy Agency (IAEA). August 2003. "Safeguards Techniques and Equipment, 2003 Edition," http://www-pub.iaea.org/MTCD/publications/PDF/NVS1-2003_web.pdf.

International Atomic Energy Agency (IAEA). July 2007. "IAEA Safeguards: Staying Ahead of the Game," www.iaea.org/Publications/Booklets/Safeguards3/safeguards0707.pdf.

Jackson, J. E. 2003. *A User's Guide to Principal Components*. 1st ed., Wiley-Interscience, New Jersey.

Jolliffe, I. T. 1986. *Principal Component Analysis.* 1st ed., Springer-Verlag, New York.

Kourti, T. 2002. "Process Analysis and Abnormal Situation Detection: From Theory to Practice." *IEEE Control Systems Magazine.* October 2002, 10–25.

Labaton, V. Y. and K. D. B. Johnson. 1959. "The Fluorides of Uranium—III: Kinetic Studies of the Fluorination of Uranium Tetrafluoride by Fluorine." *Journal of Inorganic Nuclear Chemistry.* **10**, 74–85.

MacGregor, J. F. and T. Kourti. 1995. "Statistical Process Control of Multivariate Processes." *Control Engineering Practice.* **3** (3), 403–414.

MATLAB® 2013a Documentation. 2013. http://www.mathworks.com/help/optim/ug/fsolve.html.

Martin, E. B., A. J. Morris, and J. Zhang. 1996. "Process performance monitoring using multivariate statistical process control." *IEE Proceedings-Control Theory and Applications.* **143** (2), 132–144.

Martin, E., J. Morris, and S. Lane. 2002. "Monitoring Process Manufacturing Performance." *IEEE Control Systems Magazine.* October 2002, 26–39.

Mellah, A., S. Chegrouche, and M. Barkat. 2007. "The precipitation of ammonium uranyl carbonate (AUC): Thermodynamic and kinetic investigations." *Hydrometallurgy.* **85**, 163–171.

McCabe, W. L., J. C. Smith, and P. Harriott. 1993. *Unit Operations of Chemical Engineering.* pp. 513. 5th ed., McGraw-Hill, New York.

Miller, M. C., M. M. Pickrell, D. H. Beddingfield, D. G. Langner, G. W. Eccleston. 2004. "Source Term Analysis in Support of Safeguards Approaches for Uranium Conversion Facilities." *Proceedings 45th Annual Meeting of Institute of Nuclear Materials Management (INMM),* Orlando, July.

Moghissi, A. A., H. W. Godbee, and S. A. Hobert. 1992. *Radioactive Waste Technology.* 1st ed., the American Society of Mechanical Engineers, New York.

Nicole, Ch., F. Patisson, D. Ablitzer, and J.-L. Houzelot. 1996. "A Thermogravimetric Study of the Kinetics of Hydrofluorination of Uranium Dioxide." *Chemical Engineering Science.* **51** (23), 5213–5222.

Pearson, K. 1901. "On lines and planes of closest fit to systems of points in space." *Philosophy Magazine.* **2**, 559–572.

Robel, M., M. J. Kristo, and M. A. Heller. 2009. "Nuclear Forensic Inferences Using Iterative Multidimensional Statistics." *Proceedings 50th Annual Meeting of Institute of Nuclear Materials Management (INMM),* Tucson, July.

Seader, J. D. and E. J. Henley. 1998. *Separation Process Principles.* pp. 242–246 and 514–519. John Wiley & Sons, Inc., New York.

Strang, G. 2006. *Linear Algebra and Its Applications.* 4th ed., Thomson, Brooks/Cole, Australia.

Valle, S., W. Li, and S. J. Qin. 1999. "Selection of the Number of Principal Components: The Variance of the Reconstruction Error Criterion with a Comparison to Other Methods." *Industrial and Engineering Chemistry Research.* **38**, 4389–4401.

Wang, T. 2006. "Multivariate Statistical Modeling and Data Analysis: Process Monitoring and Fault Detection." Chemical Engineering 561 Lecture Notes.

Yasuike, Y., Y. Ikeda, and Y. Takashima. 1995. "Kinetic Study on Dissolution of U_3O_8 Powders in Nitric Acid." *Journal of Nuclear Science and Technology.* **32**(6), pp. 596–598.

APPENDIX. DERIVATION OF THE KREMSER EQUATION

APPENDIX. DERIVATION OF THE KREMSER EQUATION

The following is the full derivation of the Kremser Equation to supplement the information provided in Section 3.2.2.6. This was adapted from Benedict, Pigford, and Levi 1981; McCabe, Smith, and Harriott 1993; and Seader and Henley (1998).

The Kremser Equation provides an algebraic solution for analyzing N ideal equilibrium stages connected with countercurrent flow. The Kremser Equation, also known as the Kremser Group Method, was originally designed for countercurrent gas absorption. It is a group method because it is an approximate calculation method to relate compositions of streams entering and exiting cascades to the number of equilibrium stages required but does not consider detailed changes in temperature, flow rates, and composition in the individual stages. The Kremser Equation can be applied to liquid-liquid separations such as the solvent extraction process in a natural uranium conversion plant. It assumes dilute solutions, so that solvent density is solution density.

This derivation starts with an extracting cascade where a feed solution containing one or more extractable components is contacted countercurrently with an organic solvent. Figure A.1 shows the nomenclature for the flow rates, concentrations, and stage numbers of the cascade with N ideal stages. It was assumed that equilibrium was reached between the aqueous and organic phases leaving each stage. Changes in the volume flow rates of the aqueous and organic phases were neglected.

A material balance on one of the extractable components in the section of the cascade below stage n is shown in Eq. (A.1).

$$Ey_0 + Fx_n = Ey_{n-1} + Fx_1 \qquad (A.1)$$

The input is equal to the output since there cannot be accumulation or depletion within the system. Equation (A.1) can be rewritten as Eq. (A.2).

$$y_{n-1} - y_0 = \frac{F}{E}(x_n - x_1) \qquad (A.2)$$

Concentrations in the organic and aqueous phases leaving a stage are related by the equilibrium relationship where D_n is the distribution coefficient at the conditions of the n-th stage.

$$y_n = D_n x_n \qquad (A.3)$$

Figure A.2 is the McCabe-Thiele diagram which provides a visual representation of Eqs. (A.2) and (A3). The material balance [Eq. (A.2)] is represented by the operating line that passes through the point (x_1, y_0) and has the slope E/F. The equilibrium relationship [Eq. (A.3)] is represented by the equilibrium line. When D is constant, the equilibrium line is a straight line. This would occur for the extraction of trace
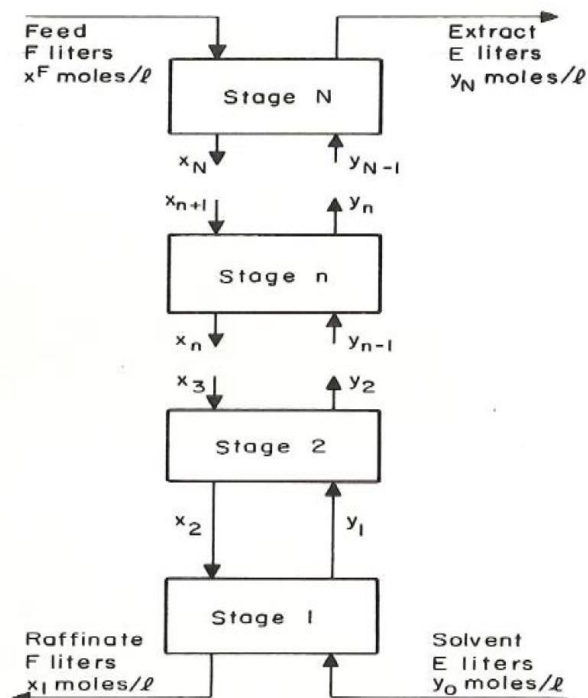
334

Figure A.1. Nomenclature for Cascade of Solvent Extraction Stages. (Source: Benedict, M., T. Pigford, and H. Levi. 1981. *Nuclear Chemical Engineering.* 2nd ed., McGraw-Hill, New York. Pg. 174.)
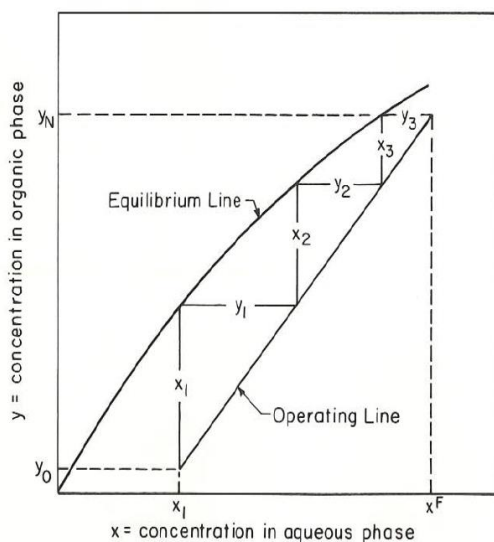

Figure A.2. Stage Concentration Diagram for Solvent Extraction Cascade. (Source: Benedict, M., T. Pigford, and H. Levi. 1981. *Nuclear Chemical Engineering.* 2nd ed., McGraw-Hill, New York. Pg. 174.)

quantities of solutes in the presence of non-extractable salting agents, with constant concentration of uncombined complexing agent. In general, D varies from stage to stage, resulting in a curved equilibrium line. Figure A.2 illustrates the equilibrium line typical for the extraction of a single component in the presence of a non-extractable salting agent.

The overall material balance for the cascade of solvent extraction stages (Figure A.1) can be written as shown in Eq. (A.4) because x^F is the virtual aqueous effluent concentration from stage $N + 1$.

$$Ey_0 + Fx^F = Ey_N + Fx_1 \tag{A.4}$$

By rearranging Eq. (A.4), it is apparent that the ratio of organic flow rate to aqueous flow rate is given by Eq. (A.5).

$$\frac{E}{F} = \frac{x^F - x_1}{y_N - y_0} \tag{A.5}$$

When the distribution coefficients are independent of stage number, meaning the distribution coefficients are constant, an equation can be derived for the analytical calculation of the number of stages. For any extractable component with a constant distribution coefficient, a constant extraction factor, β, can be defined as Eq. (A.6).

$$\beta \equiv \frac{DE}{F} \tag{A.6}$$

Equation (A.3) can be written for the constant distribution coefficient.

$$y_n = Dx_n \tag{A.7}$$

Equations (A.1) and (A.3) can be rewritten in terms of β.

$$Ey_0 + Fx_n = Ey_{n-1} + Fx_1 \tag{A.1}$$

Rearrange Eq. (A.7) for x_n.

$$x_n = \frac{y_n}{D} \tag{A.8}$$

Substitute for x_n in Eq. (A.1).

$$Ey_0 + F\frac{y_n}{D} = Ey_{n-1} + Fx_1 \tag{A.9}$$

Rearrange Eq. (A.9) to solve for y_n.

$$y_n = \frac{DE}{F}(y_{n-1} - y_0) + \frac{F\beta}{E}x_1 \tag{A.10}$$

Substitute D or β in Eq. (A. 10) as appropriate to obtain Eq. (A.11).

$$y_n = \beta(y_{n-1} - y_0) + Dx_1 \tag{A.11}$$

When $n = 1$, Eq. (A.11) becomes

$$y_1 = Dx_1 \tag{A.12}$$

When $n = 2$, Eq. (A.11) becomes

$$y_2 = \beta(y_1 - y_0) + Dx_1 \tag{A.13}$$

Equation (A.13) becomes Eq. (A.14) when Eq. (A.12) is substituted for y_1.

$$y_2 = (\beta + 1)Dx_1 - \beta y_0 \tag{A.14}$$

When $n = 3$, Eq. (A.11) becomes

$$y_3 = \beta(y_2 - y_0) + Dx_1 \tag{A.15}$$

Equation (A.15) becomes Eq. (A.16) when Eq. (A.14) is substituted for y_2.

$$y_3 = (1 + \beta + \beta^2)Dx_1 - (\beta + \beta^2)y_0 \tag{A.16}$$

Continuing in this way to stage N, Eq. (A.17) is obtained.

$$y_N = (1 + \beta + \ldots + \beta^{N-1})Dx_1 - (\beta + \cdots + \beta^{N-1})y_0 \tag{A.17}$$

Combining the series in Eq. (A.17) yields Eq. (A.18).

$$y_N = (1 + \beta + \ldots + \beta^{N-1})(Dx_1 - y_0) + y_0 \tag{A.18}$$

The series in Eq. (A.18) is a geometric series which can be written as shown in Eq. (A.19).

$$1 + \beta + \ldots + \beta^{N-1} = \frac{1 - \beta^N}{1 - \beta} \tag{A.19}$$

Substituting Eq. (A.19) into Eq. (A.18) and multiplying top and bottom by $(\beta - 1)$ gives Eq. (A.20) which is a form of the Kremser Equation.

$$y_N = \frac{\beta^N - 1}{\beta - 1}(Dx_1 - y_0) + y_0 \tag{A.20}$$

VITA

Jennifer LeAnn Ladd-Lively was born in Knoxville, Tennessee on February 25, 1980 to John and Edith Ladd. She was raised in Roane County, Tennessee. Jennifer graduated as valedictorian from Oliver Springs High School in May 1998. From there, she received an Associate of Science in Chemical Engineering from Roane State Community College in May 2000. After receiving her A.S., Jennifer transferred to Tennessee Technological University (TTU) in Cookeville, Tennessee where she received a Bachelor of Science in Chemical Engineering in May 2002 with a minor in chemistry and mathematics. Immediately after graduating, she entered graduate school at the University of Tennessee (UTK) in Knoxville, Tennessee. She was awarded a graduate fellowship from the United States Department of Energy Advanced Fuel Cycle Initiative (AFCI) program. Jennifer received a Master of Science in Chemical Engineering with a thesis entitled "Separation of Fluoride Residue Arising from Fluoride Volatility Recovery of Uranium from Spent Nuclear Fuel" under the guidance of Robert M. Counce, Ph.D. and Barry B. Spencer, Ph.D. in May 2004. After graduation, she was hired as a research engineer at Oak Ridge National Laboratory (ORNL). Jennifer continued her education at UTK by enrolling in evening classes while working at ORNL. She received a Doctor of Philosophy degree in Chemical Engineering from the University of Tennessee in December 2013. After completing her doctoral degree, Dr. Ladd-Lively plans to continue her current research and develop related research at ORNL.